



HAL
open science

Exploration and study of the impact of climate change on microbial mats in the Nouvelle-Aquitaine region

Camille Mazière

► **To cite this version:**

Camille Mazière. Exploration and study of the impact of climate change on microbial mats in the Nouvelle-Aquitaine region. Cellular Biology. Université de Pau et des Pays de l'Adour; Université de La Rochelle, 2021. English. NNT : 2021PAUU3032 . tel-03551876

HAL Id: tel-03551876

<https://theses.hal.science/tel-03551876>

Submitted on 2 Feb 2022

HAL is a multi-disciplinary open access archive for the deposit and dissemination of scientific research documents, whether they are published or not. The documents may come from teaching and research institutions in France or abroad, or from public or private research centers.

L'archive ouverte pluridisciplinaire **HAL**, est destinée au dépôt et à la diffusion de documents scientifiques de niveau recherche, publiés ou non, émanant des établissements d'enseignement et de recherche français ou étrangers, des laboratoires publics ou privés.

PhD

UNIVERSITE DE PAU ET DES PAYS DE L'ADOUR co-directed by
LA ROCHELLE UNIVERSITE
Collège STEE

Submitted and held on 2021, December 8th

by **Camille MAZIERE**

to obtain the degree of PhD
of the Université de Pau et des Pays de l'Adour

Speciality : Physiology and Biology of Organisms - Populations - Interactions

Exploration and study of the impact of climate change
on microbial mats in the Nouvelle-Aquitaine region

JURY MEMBERS

REPORTERS

- Claire HELLIO
- Pierre PEYRET

Professor, Université de Bretagne Occidentale
Professor, Université Clermont-Auvergne

REVIEWERS

- Rutger DE WIT
- Cristiana CRAVO-LAUREAU
- Cédric HUBAS

Research director, UMR CNRS MARBEC
Associate professor, Université de Pau et des Pays de l'Adour
Associate professor, HDR, Muséum national d'Histoire Naturelle

DIRECTORS

- Christine DUPUY
- Robert DURAN

Professor, La Rochelle Université
Professor, Université de Pau et des Pays de l'Adour



THÈSE

UNIVERSITE DE PAU ET DES PAYS DE L'ADOUR en codirection avec
LA ROCHELLE UNIVERSITE
Collège STEE

Présentée et soutenue le 8 décembre 2021

par **Camille MAZIERE**

pour obtenir le grade de docteur
de l'Université de Pau et des Pays de l'Adour

**Spécialité : Physiologie et Biologie des Organismes – Populations –
Interactions**

Exploration et étude de l'impact du changement
climatique sur les tapis microbiens en région Nouvelle-
Aquitaine

MEMBRES DU JURY

RAPPORTEURS

- Claire HELLIO
- Pierre PEYRET

Professeure, Université de Bretagne Occidentale
Professeur, Université Clermont-Auvergne

EXAMINATEURS

- Rutger DE WIT
- Cristiana CRAVO-LAUREAU
- Cédric HUBAS

Directeur de recherche, UMR CNRS MARBEC
MCF, HDR, Université de Pau et des Pays de l'Adour
MCF, HDR, Muséum national d'Histoire Naturelle

DIRECTEURS

- Christine DUPUY
- Robert DURAN

Professeure, La Rochelle Université
Professeur, Université de Pau et des Pays de l'Adour



*“Tampering can be dangerous. Nature can be vengeful.
We should have a great deal of respect for the planet on which we live.”*

Rossby, 1956

Acknowledgements

Je remercie en premier lieu mes rapporteurs de thèse, Claire Hellio et Pierre Peyret, ainsi que mes examinateurs, Rutger De Wit, Cristiana Cravo-Laureau et Cédric Hubas, pour avoir accepté d'évaluer mon travail de thèse.

J'adresse mes remerciements à Ryszard Lobinski, directeur de l'Institut des sciences analytiques et de physico-chimie pour l'environnement et les matériaux (IPREM), Olivier De Viron et Valérie Ballu, directeurs du laboratoire Littoral, Environnement et Sociétés (LIENSs) pour m'avoir accueillie au sein de leurs laboratoires et permis de réaliser ma thèse en co-direction.

Un grand merci à mes directeurs de thèse, Christine et Robert, pour votre confiance, votre soutien et pour avoir toujours répondu présent malgré la distance entre les deux laboratoires. Merci de m'avoir choisie pour réaliser cette thèse que j'ai adorée mener. Merci aussi d'avoir supporté mon obstination à vouloir finir toutes les manipulations et tout mettre dans cette thèse. Merci d'avoir autant fait confiance en mes choix, mes opinions et moi tout simplement. J'ai appris beaucoup de choses, professionnellement et humainement, ce qui m'a conforté dans mon choix de continuer dans la recherche.

Je tiens à remercier les personnes impliquées dans ce projet, Cédric Hubas, Cristiana Cravo-Laureau, Hélène Agogué et Christine Cagnon, pour votre aide et pour ce que j'ai appris grâce à vous. Je remercie Isabelle Lanneluc, Ingrid Fruitier et Sophie Sablé pour le prêt de matériel pour les manipulations EPS. Un grand merci à Edouard Metzger pour m'avoir appris à utiliser les sondes Unisense, à découper des carottes de sédiments et à utiliser un couteau à jointer correctement. Je remercie aussi Thomas Lacoue-Labarthe sans qui l'acidification en mésocosmes n'aurait pas eu lieu. Je suis vraiment très fière d'avoir pu collaborer avec autant de personnes avec des disciplines différentes des miennes qui, je pense, sera un grand atout dans ma future carrière.

J'aimerais remercier mes professeurs de l'UPPA de L3 et master qui m'ont permis de découvrir le monde des microorganismes après un grand moment d'incertitudes professionnelles et de m'épanouir dans une discipline qui me passionne et dans laquelle je veux continuer, l'écologie microbienne. Merci aux personnes qui m'ont encadrée lors de mes deux stages et qui m'ont donné envie de continuer dans la recherche, merci Anthony, Jean-Christophe, Claudia, Pierre et Lucie. Je tiens à remercier particulièrement Anthony qui m'a toujours soutenue et conseillée et qui m'a permis d'arriver où j'en suis. C'est toi qui m'as permis de faire un stage de M1 hyper intéressant avec des personnes supers, c'est aussi toi qui m'as conseillée pour mon stage de M2 et qui m'as parlé des thèmes de recherche de Pierre. Tu m'as toujours fait confiance, et encore aujourd'hui je suis contente de pouvoir travailler avec toi. Et oui ta lettre de recommandation m'a fait pleurer de joie ! J'espère qu'on continuera à travailler ensemble, ce sera un réel plaisir pour moi !

Je remercie Michel Jauffrais le propriétaire des marais salants. Je remercie aussi Emmanuel Dubillot et Nicolas Lachaussée pour leur aide dans la construction des mésocosmes. Maintenant je suis une pro du mésocosme, piscine, plomberie et perceuse. Merci à Anne pour m'avoir formée à mon arrivée au labo de Pau et être venue m'aider sur le terrain. Je tiens à remercier Florence et Claire G., Claire E., Bénédicte, Jérôme, Pierrick notamment pour m'avoir fait de la place dans la salle humide (la prochaine fois on essaie 8 mésocosmes ! ;)), Philippe pour tous les tubes de sels nutritifs mais aussi pour son aide dans le rangement des mésocosmes et les échantillonnages (et pour m'avoir prêté ton frigo), Armelle pour ton enthousiasme, ta bonne humeur et ton aide. Merci à François Rigal et Jean-Christophe Auguet pour leur aide en statistiques. Je tiens aussi à remercier Cyril Noël qui a pris beaucoup de temps à me former sur Samba, qui m'a permis de mieux comprendre la bioinformatique, et qui a aussi accepté de relire la partie bioinformatique de mon manuscrit. Je remercie aussi Dimitri Kalenitchenko, le nouveau de la team microbes du LIENSs, pour son aide en métagé.

Un grand merci à Martine pour son aide à chaque échantillonnage, sa joie et bonne humeur, pour avoir toujours trouvé du temps pour que tout se passe bien au labo et qu'on ne manque de rien, pour tout. Vivement la fin de la covid pour fêter ton départ. Profite bien de ta retraite tu le mérites amplement ! Grosse pensée à Christine, ma directrice, qui je pense a refait une thèse durant ma manip mésocosmes à ce moment-là et qui malgré cette période très compliquée était toujours là pour échantillonner. Je ne te remercierai jamais assez !

Je remercie Anaïs pour avoir été une stagiaire aussi assidue et qui m'a permis de finir de nombreuses manipulations. Je remercie aussi Maëlle Bodo que je n'ai pas personnellement encadrée mais qui a aussi effectué un travail exceptionnel sur mes échantillons.

Je remercie aussi les personnes de l'ADocs avec qui j'ai pu organiser un super Festival du Film *[pas trop]* Scientifique pour la fête de la Science. J'ai été ravie d'être Présidente de cette association.

Je remercie Marion, ma co-bureau de Pau qui est devenue maman d'un adorable petit bout de chou et qui a été une super élève très assidue à ma formation de bioinfo en faisant preuve d'une grande patience et d'une grande persévérance face à ces logiciels (mais pourquoi ça ne veut pas fonctionner ? :") () mais aussi envers moi ^^ Franchement tu as été tout de suite à l'aise ce qui m'a beaucoup impressionnée !

Merci à la famille Misère, vous allez me manquer Coco (alias Romain ou Romain alias Coco on ne sait plus trop) et Louis (alias M. Biscoto). On se retrouvera au QG « Chez Louise » (en vrai c'est quoi le nom de ce bar ^^). Romane, je suis contente de t'avoir rencontrée et je te souhaite de réussir pour la suite ! Merci à tous les 3 pour ces petits WE découvertes !

Alice, Alice... je ne t'ai rencontrée qu'il y a 3 ans mais j'ai l'impression que ça fait bien plus. Je veux te remercier pour tellement de choses professionnelles mais surtout humaines que je vais en oublier. Merci de m'avoir hébergée dans les moments difficiles, merci pour les supers journées coutures, merci pour ta joie et ton soutien, les tartines de fromage les soirs de terrain, merci à toi et Benoît pour les soirées jeux des sandwiches (tu excuseras ma

mémoire) et pour les burgers trop bons ! Je suis très heureuse de t'avoir rencontrée et c'est un « à bientôt » bien sûr !

Mery, toi aussi je te remercie énormément. Team microbio du LIENSs un jour, team microbio toujours ! On est restées tellement d'heures ensemble devant le cytomètre (devrais-je dire de nuits !) avec mes échantillons horribles et les caprices de cet appareil ^^ Il y a tellement de choses pour lesquelles j'aimerais te remercier toi aussi que je ne pourrais pas toutes les lister. Je suis très heureuse d'être ton amie et ce n'est pas un au revoir mais un à très bientôt ! Je n'oublierai jamais ce super colloque avec vous, Hélène, Mery et Mathieu (alias la team microbes).

Gros merci à Vincenounet ! Alala la boulangerie des Minimes et les burgers d'Aytré vont me manquer ! Et TONTON MABOUL (mon cœur saigne à cette idée). Merci Marine, d'avoir été présente lors du deuxième confinement, nos petites balades en bord de mer avec la petite boule de poil qui aime mâchouiller mes chaussettes vont me manquer (nos soirées ADocs moins ou sans ADocs plutôt ^^). A quand le prochain voyage Amélie ? Et Yannick j'attends encore que tu m'emmènes en Egypte ! ;) Merci à Clémence et Clément pour les soirées/goûters crêpes, vivement l'atelier cuisine ;).

J'adresse aussi mes remerciements à toutes les autres personnes avec qui j'ai passé des très bons moments, Kévin (la salchicha :)), Etienne, Kilian, Eva, Ivan, Joyce, Elise, Zeina, Magali, Sophie, Diva, Aurélien, Monia, Gauthier et Alice du Lasie.

Enfin j'aimerais remercier ma famille pour leur soutien depuis toujours dans mes choix d'études et de vie. Merci Papi et Mamie pour les sorties Oléron. Merci Papa et Maman de m'avoir toujours soutenue dans mon parcours et mes choix, merci Mathieu, merci Louloute pour ta joie, ta bonne humeur, ta « délicatesse » et ta très grande maturité pour ton âge. Je serai toujours contente de corriger ton espagnol même si tu finiras par m'apprendre des choses. Je serai toujours là si tu as besoin et pour que toi aussi tu puisses faire ce qui te plaît.

T'inquiète je viens bientôt te parler des « bactéries gentilles dans les marais salants de l'île de Ré » !

Enfin, j'adresse mes remerciements à toute personne ayant participé de près ou de loin à cette thèse et que je n'aurais pas citée.

List of abbreviations

A

A: adenine

AHM: aerobic heterotrophic microorganism

AMB: aerobic methanotrophic bacteria

ANME: anaerobic methanotrophic archaea

AOM: anaerobic oxidation of methane

APB: anoxygenic phototrophic bacteria

ATPase: ATP synthase

B

BChl: bacteriochlorophyll

C

C: cytosine or carbon

CaCO₃: calcium carbonate

CoB: coenzyme B

CH₄: methane

Chl: chlorophyll

[C₃H₆O₃]: complex carbon sources

[CH₂O]: organic matter

CoM: *coenzyme M*

CO₂: carbon dioxide

CO₃²⁻ : carbonate ion

CO(III): *cobalamin binding protein*

CODH-ACS: *Acetyl-CoA decarbonylase/synthase*

COI: cytochrome c oxydase subunit 1

Csma: *BChl a-binding protein*

D

DNA: deoxyribonucleic acid

dNTP: deoxyribonucleotide triphosphate

ddNTP: dye-labelled deoxyribonucleotide triphosphate

DOM: dissolved organic matter

dsrB: dissimilatory sulfite reductase beta subunit gene

E

e⁻: electron

Ech-H2ase: energy-converting hydrogenase

eDNA: environmental DNA

e.g.: *Exempli gratia*

EPS: extracellular polymeric substance

F

FAP: green filamentous anoxygenic phototroph

Fd: ferredoxin

FdhAB: formate dehydrogenase

Fe: Iron

Fe²⁺: ferrous ion

Fe³⁺: ferric ion

FeS: ferrous oxide

FeS₂: iron (II) disulfide

F420H₂: reduced coenzyme F420

FMO: Fenna-Matthews-Olsen protein

FpoA-O: F420H₂ dehydrogenase

FrhABG: coenzyme F420-reducing hydrogenase

Ftr: formylmethanofuran-tetrahydromethanopterin formyl-transferase

FwdA-F/FmdA-F: formylmethanofuran dehydrogenase

G

G: guanine

Ga: giga-annum

H

H⁺: hydrogen ion

H₂: dihydrogen

HCO₃⁻: bicarbonate ion

H₂CO₃: carbonic acid

HdrABC: soluble heterodisulfide reductase

HdrDE: membrane-bound heterodisulfide reductase

H4MPT: tetrahydromethanopterin

H₂O: water

H₂S: sulfur

H₂SO₄: sulfuric acid

I

i.e.: Id est

IPCC: intergovernmental panel on climate change

ITS: internal transcribed spacer

L

LC: light curve

LH: light-harvesting

M

Mch: methenyl-tetrahydromethanopterin cyclohydrolase

mcrA: methyl coenzyme-M reductase alpha subunit gene

McrABCDG methyl-coenzyme M reductase

Mer: 5,10-methylenetetrahydromethanopterin reductase

MFR: methanofuran

MP: methanophenazine

MTI and MTII: methyltransferase

Mtd: methylenetetrahydromethanopterin dehydrogenase

MtrA-H: tetrahydromethanopterin S-methyl-transferase

MvhAGD: F420-non-reducing hydrogenase

N

N: nitrogen

N₂: dinitrogen

NGS: next-generation sequencing

NH₄⁺: ammonium ion

nifH: iron protein subunit of nitrogenase gene

NO₂⁻: nitrite ion

NO₃⁻: nitrate ion

N₂O: nitrous oxide

O

OMZ: oxygen minimum zone

O₂: dioxygen

P

P: phosphorus

PAM: pulse amplitude modulated

PCR: polymerase chain reaction

PO₄²⁻: phosphate ion

ppm: parts per million

PS I or II: photosystem I or II

psu: practical salinity unit

PVC: PolyVinyl Chloride

R

RC: reaction center

RCP: representative concentration pathway

RNA: ribonucleic acid

Rnf: Na⁺-translocating ferredoxin:NAD⁺ oxidoreductase complex

(r)RNA: (ribosomal) ribonucleic acid

S

S₀: sulfur

S²⁻: disulfur ion

spp.: species

SO₄²⁻: sulfate ion

SOCB: sulfur-oxidizing chimiolithoautotroph bacteria

SRB: sulfate-reducer bacteria

SRM: sulfate-reducing microorganisms

SSU: small subunit

T

T: thymine

U

UV (-B): ultraviolet (-B)

List of figures

Chapter I: Introduction

Figure 1: Simulation of the average surface temperature modification of the Earth, predicted by the IPCC (2014).....	7
Figure 2: Simulation of the surface pH modification of the ocean, predicted by the IPCC (2014).....	9
Figure 3: Oceanic deoxygenation.....	11
Figure 4: Simulation of the average precipitation modification, predicted by the IPCC (2014).....	12
Figure 5: Simulation of the average sea level modification, predicted by the IPCC (2014)...	13
Figure 6: Microbial mats.....	17
Figure 7: Microbial mat and its role in biogeochemical cycles.....	19
Figure 8: Chlorosomes.....	29
Figure 9: Methanogenesis pathways.....	33
Figure 10: Cable bacteria metabolisms.....	38
Figure 11: Light, oxygen and sulfur gradients in a microbial mat.....	42

Chapter II: Experimental procedure

Figure 12: Location of the sampled salterns in Ré Island, France.....	55
Figure 13: Schematic representation of an exploited salt march.....	57
Figure 14: Seasonal sampling of microbial mats for one year.....	59
Figure 15: <i>In situ</i> sampling system of the microbial mat.....	60

Figure 16: Sampling <i>in situ</i> of the microbial mats for mesocosms experiment.....	62
Figure 17: Schematic representation of the experimental device with the control (C) and the acidification (A), warming (W) and mixed (WA) treatments.....	63
Figure 18: Schematic representation of the sampling scheme followed during the mesocosms experiment.....	65
Figure 19: Microprofilage system.....	68
Figure 20: Summary of the Illumina workflow.....	73
Figure 21: Schematic representation of the OTU assignment of a dataset using mothur approach.....	77
Figure 22: Summary of the SAMBA pipeline.....	81

Chapter III: Presentation of microbial mats of salterns of Ré Island

Article “New insights in bacterial and eukaryotic diversity of microbial mats inhabiting exploited and abandoned salterns at the Ré Island (France)” (accepted)

Fig. 1. Localisation of the sampling sites at the Ré Island (France).....	92
Fig. 2. Diversity indexes for bacterial (A, B) and eukaryotic (C, D) communities in the abandoned (red) and exploited (green) sites.....	94
Fig. 3. Bacterial community compositions at the phylum level in the abandoned and exploited sites.....	95
Fig. 4. Eukaryotic community compositions at the phylum level in the abandoned and exploited sites.....	96
Fig. 5. Comparison of bacterial and eukaryotic communities inhabiting the abandoned (red) and exploited (green) sites.....	97
Fig. 6. Comparison of bacterial (A) and eukaryotic (B) communities inhabiting the abandoned (red) and exploited (green) sites by linear discriminant analysis effect size (LEfSe).....	97

Fig. S1. Rarefaction curves of the observed bacterial ASVs (**A**) and observed eukaryotic ASVs (**B**) according to the number of sequences analysed.....103

Fig. S2. Relative abundances (%) of meiobenthic taxa inhabiting microbial mats in the abandoned and exploited salterns.....104

Chapter IV: Seasonal dynamic of the microbial mats of Ré Island

Figure 23: Collinearity between the physical-chemical parameters.....111

Figure 24: Principal component analysis (PCA) on the sample structure according to the non-correlated physical-chemical parameters.....112

Figure 25: Principal component analysis (PCA) on the sample structure according to the non-correlated physical-chemical parameters.....116

Figure 26: Prokaryotic abundance.....118

Figure 27: Meiofaunal groups and its abundance.....119

Chapter V: Impact of climate change on microbial mats

Article “Climate change effect on microbial mats structure modifies prokaryotic diversity and metabolism” (draft)

Figure 1: Principal coordinate analysis (PCA).....136

Figure 2: Bacterial production and heterotrophic prokaryotic biomass.....138

Figure 3: Indirect gradient analyses.....144

Figure 4: Indirect gradient analyses.....146

Figure S1: Nutrients variation.....149

Figure S2: Relative abundance of the phylum of the 100 most abundant bacterial ASVs.....150

Figure S3: Relative abundance of the phylum of the 100 most abundant archaeal ASVs.....150

Figure S4: Bacterial alpha diversity.....151

Figure S5: Archaeal alpha diversity.....	152
Figure 28: Nematodes abundance by binocular loupe.....	154
Figure 29: Domains identified with eukaryotic primers 515F and 951R.....	155
Figure 30: Relative abundance of eukaryotic phyla at different incubation time.....	158
Figure 31: Relative abundance of eukaryotic phyla at different incubation time.....	160
Figure 32: Principal coordinates analyses (PCoA).....	161

Chapter VI: Impact of climate change on phototrophic communities of microbial mats

Article “Climate change influences chlorophylls and bacteriochlorophylls metabolism in hypersaline microbial mat” (accepted)

Fig. 1. Schematic representation of the experimental device with the control (C) and the acidification (A), warming (W) and mixed (WA) treatments.....	168
Fig. 2. Temporal variation of the temperature (°C) (A), the pH (upH) (B), the salinity (psu) (C) and the dissolved oxygen (mg·L ⁻¹) (D) of the different treatments (control (C), acidification (A), warming (W) or warming and acidification mix (WA)).....	170
Fig. 3. Dynamics of microbial communities according to pigments composition and the sampling time (tX) (A). This figure was obtained thanks to analyze BCA combined with hierarchical cluster analysis with a Bray dissimilarity index and ward.D2 method.....	171
Fig. 4. Temporal variations of (A) the concentration of chlorophyll a (%) and (B) the concentration of chlorophyll derivatives (%).....	172
Fig. 5. Variation of the quantum efficiency of photosystem II ($\phi(II)^5$) in the different treatment.....	172
Fig. 6. Temporal variation of the carbohydrate concentration in the bound fraction of EPS (in $\mu\text{g}\cdot\text{g}^{-1}$ dry mass).....	173

Fig. 7. Normalized absorption spectra of different pigments of the microbial mats.....	173
Fig. A: Schematic representation of the sampling scheme followed during the mesocosms experiment.....	177
Fig. B: Physico-chemical parameters measured for each replicate of each treatment and at each sampling time.....	178
Fig. C: Redfield ratio determining (A) the limitation of nitrogen, (B) the limitation of phosphate and (C) the limitation of silicon in the mesocosms' water.....	184
Fig. D: Temporal variation of the pH (upH) of the water reserve of the different treatments (control (C), acidification (A), warming (W) or mix warming and acidification (WA)).....	185
Fig. E: Normalised signal recorded by the HPLC DAD detector at 665 nm.....	186

Chapter VII: Conclusions and perspectives

Figure 33: Graphical conclusion.....	195
---	-----

List of tables

Chapter I: Introduction

Table 1: Photosynthetic information about phototrophic communities of microbial mats.....45

Chapter II: Experimental procedure

Table 2: List of the different sampling carried out *in situ*.....61

Table 3: List of the different sampling carried out for the mesocosms analyses.....65

Table 4: Benefits and drawbacks of bioinformatics tools using OTU approaches.....78

Table 5: Programme and solvents used in HPLC analysis.....85

Chapter III: Presentation of microbial mats of salterns of Ré Island

Article “New insights in bacterial and eukaryotic diversity of microbial mats inhabiting exploited and abandoned salterns at the Ré Island (France)” (accepted)

Table S1. Data description during Qiime2 processing, richness and diversity indexes.....102

Chapter IV: Seasonal dynamic of the microbial mats of Ré Island

Table 6: Meteorological data measured by Météo France.....109

Table 7: Physical-chemical parameters measured during the seasonal sampling of the microbial mat in the non-exploited plot of the salt marsh.....110

Table 8: Physical-chemical parameters measured during the seasonal sampling of the microbial mat in the exploited plot of the salt marsh.....116

Table S9: Heterotrophic prokaryotic abundance.....120

Table S10: Meiofaunal abundance.....120
Table S11: Nutrient concentrations.....121

Chapter V: Impact of climate change on microbial mats

Table 12: Phyla and matching identified families.....158

Chapter VI: Impact of climate change on phototrophic communities of microbial mats

Article "Climate change influences chlorophylls and bacteriochlorophylls metabolism in hypersaline microbial mat" (accepted)

Table 1 Pigments identified by HPLC and its corresponding abbreviations.....170

Chapter VII: Conclusions and perspectives

List of annexes

Annexe 1: Sanger principle.

Annexe 2: Oxygen solubility at different temperatures and salinities of seawater.

Annexe 3: H₂S calibration protocol.

Annexe 4: Shotgun metagenomics.

Figure A4: *Summary of the metagenomics workflow.*

Annexe 5: Physical-chemical parameters measured in the mesocosms water.

Annexe 6: **Regional fact sheet (Introduction) and regional fact sheet of Europe** from the sixth assessment report of the Working Group I, “The Physical Science Basis” part, by the IPCC (2021).

Annexe 7: **Impact of Climate Change on Phototrophic Communities Inhabiting Microbial Mats (iPoster)**, World Microbe Forum online conference (international conference), virtual, 2021

Annexe 8: **Impact du changement climatique sur les communautés procaryotiques des tapis microbiens de l’île de Ré (Poster)**, Microbe 2021, 16^e Congrès National de la SFM (national conference), Nantes, France, 2021

Annexe 9: Abstract submitted for the « 10ème Colloque de l’Association Francophone d’Ecologie Microbienne » (national conference), virtual, 2021. Accepted for **oral presentation**.

Annexe 10: **Les Marais, entre Terre et Mer (Poster)**, Fête de la Science 2020 (local conference), La Rochelle, France, 2020

Annexe 11: **Biogeochemical interactions between iron and nutrient cycling in a saline inland lake (Poster)**, Goldschmidt 2021 (international conference), virtual, 2021

This poster was the result of a collaboration between the MESMIC project and me to perform vertical microprofiles during its sampling campaign.

Annexe 12: Exploration de tapis, article written by Marin Galilée for “l’Actualité Nouvelle-Aquitaine“, n°126, 2019

Annexe 13: Influence du changement climatique sur les tapis microbiens des marais salants / Influence of climate change on salt ponds microbial mats, front-page article of BOREA website, 2021.

Summary

General introduction.....	1
Chapter I: Introduction.....	4
1. <u>Climate change on marine ecosystems</u>	5
1.1 <u>Future climatic change in marine ecosystem</u>	5
1.1.1 <u>Ocean water warming</u>	6
1.1.2 <u>Ocean acidification</u>	7
a- <u>Actual marine carbon cycle and natural fluctuation of pH</u>	7
b- <u>Future ocean acidification</u>	8
1.1.3 <u>Other predicted effects</u>	9
a- <u>Ocean deoxygenation</u>	9
b- <u>Increase of extreme climatic events</u>	12
c- <u>Sea-level rise</u>	13
d- <u>Radiation effects</u>	14
1.2 <u>Climate change in Nouvelle-Aquitaine coasts (France)</u> ...	14
1.3 <u>Importance of studying climate change on microbial communities in the marine environment</u>	14
2. <u>Microbial mats</u>	16
2.1 <u>The prokaryotic populations: the major functional microbial groups composing the photoautotroph microbial mats</u>	18
2.1.1 <u>The prokaryotic oxygenic photolithoautotrophs</u>	20
2.1.2 <u>The aerobic heterotroph microorganisms</u>	22

2.1.3	<u>The sulfur-oxidizing chemolithoautotroph bacteria</u>	23
2.1.4	<u>The anoxygenic phototroph bacteria (purple and green)</u>	24
a-	<u>The purple bacteria</u>	26
b-	<u>Anoxygenic green bacteria</u>	28
c-	<u>Phototrophic Gemmatimonadetes bacteria</u>	31
2.1.5	<u>The sulfate-reducing microorganisms</u>	31
2.1.6	<u>The methanogens</u>	32
2.1.7	<u>The methylotrophs</u>	34
2.1.8	<u>The other metabolisms found on microbial mats</u>	36
a-	<u>Fermentation</u>	36
b-	<u>Diazotrophy</u>	36
c-	<u>Nitrification and denitrification</u>	37
d-	<u>Metal associated metabolisms</u>	37
2.2	<u>Eukaryotic communities</u>	39
2.3	<u>Viruses</u>	40
3.	<u>Adaptation of microbial mats in response to environmental changes</u>	41
3.1	<u>Physical-chemical microgradients within the microbial mats</u>	41
3.2	<u>Natural dynamics of the microbial mat in their environment</u>	43
3.3	<u>Microbial responses faced to climate change</u>	47
4.	<u>Techniques for studying microbial mats in microbial ecology</u>	48

4.1	<u>Cultivation approaches</u>	49
4.2	<u>Biogeochemical and microscopic methods</u>	49
4.3	<u>Molecular biology methods</u>	50
5.	<u>Objectives of the thesis</u>	53
Chapter II: Experimental procedure		54
1.	<u>Description of the salterns of Ré Island</u>	55
2.	<u>Microbial mats sampling in salt marshes</u>	58
2.1	<u>Description of the sampling sites</u>	58
2.1.1	<u>Site 1: a salt marsh with exploited and non exploited plots</u> ...	58
2.1.2	<u>Site 2: an exploited salt marsh</u>	59
2.1.3	<u>Site 3: an abandoned salt marsh</u>	59
2.2	<u>Sampling strategies</u>	60
3.	<u>Climatic change simulation on microbial mats in mesocosms</u>	61
3.1	<u>Microbial mats for mesocosms experiment</u>	61
3.2	<u>Mesocosms design</u>	62
3.3	<u>Simulated scenarios</u>	64
3.4	<u>Sampling strategy</u>	64
4.	<u>Physical-chemical parameters</u>	66
4.1	<u>Physical-chemical parameters of the water</u>	66
4.2	<u>Nutrients</u>	66

4.3	<u>Vertical microprofiling</u>	66
5.	<u>Analysis of diversity or/and abundances of organisms</u>	68
5.1	<u>Abundance of heterotrophic prokaryotes by flow cytometry</u>	68
5.2	<u>Abundance of meiofauna</u>	69
5.3	<u>Photosynthetic parameters (pulse amplitude modulated fluorometer)</u>	70
5.4	<u>Bacterial production</u>	71
6.	<u>Molecular biology analysis</u>	72
6.1	<u>DNA extraction</u>	72
6.2	<u>Illumina sequencing</u>	72
a-	<u>Bacterial sequences</u>	74
b-	<u>Archaeal sequences</u>	74
c-	<u>Eukaryotic sequences</u>	75
d-	<u>Dataset</u>	76
6.3	<u>Illumina sequencing data processing</u>	76
6.3.1	<u>Bioinformatic tools approach</u>	76
a-	<u>Operational Taxonomic Unit (OTU) approaches</u>	76
b-	<u>Amplicon Sequence Variant (ASV) approaches</u>	79
6.3.2	<u>QIIME 2: data processing of samples from the sites 2 and 3</u>	81
6.3.3	<u>SAMBA: data processing of the mesocosms' samples</u>	82
7.	<u>Biochemistry analyses</u>	82
7.1	<u>Extraction and determination of extracellular carbohydrate and protein polymeric substances (EPS)</u>	82

7.2	<u>Identification of pigments by HPLC</u>	84
8.	<u>Statistical analysis</u>	85
Chapter III: Presentation of microbial mats of salterns of Ré Island ..		88
1.	<u>Introduction</u>	89
2.	<u>New insights in prokaryotic and eukaryotic diversity of microbial mats inhabiting exploited and abandoned salterns at the Ré Island (France)</u>	90
	<i>Article “New insights in bacterial and eukaryotic diversity of microbial mats inhabiting exploited and abandoned salterns at the Ré Island (France)” (accepted)</i>	91
3.	<u>Conclusions and perspectives</u>	105
Chapter IV: Seasonal dynamic of the microbial mats of Ré Island ..		106
1.	Introduction	107
2.	Seasonal influence on the microbial mats of Ré Island in a non-exploited plot	108
2.1	<u>Environmental parameters</u>	108
2.2	<u>Biological parameters</u>	113
3.	<u>Impact of exploitation on the microbial mats of Ré Island</u>	114
4.	<u>Conclusions and perspectives</u>	119
5.	<u>Supplementary materials</u>	120

<u>Chapter V: Impact of climate change on microbial mats</u>	123
1. <u>Introduction</u>	124
2. <u>Impact of climate change on prokaryotic communities inhabiting microbial mats</u>	125
<i>Article “Climate change effect on microbial mats structure modifies prokaryotic diversity and metabolism” (draft)</i>	126
3. <u>Impact of climate change on eukaryotic communities inhabiting microbial mats</u>	153
4. <u>Conclusions and perspectives</u>	162
<u>Chapter VI: Impact of climate change on phototrophic communities of microbial mats</u>	164
1. <u>Introduction</u>	164
2. <u>Climate change influences chlorophylls and bacteriochlorophylls metabolism in hypersaline microbial mat</u>	165
<i>Article “Climate change influences chlorophylls and bacteriochlorophylls metabolism in hypersaline microbial mat” (accepted)</i>	166
3. <u>Conclusions and perspectives</u>	187
<u>Chapter VII: Conclusions and perspectives</u>	188
<u>References</u>	197
<u>Annexes</u>	

Life on Earth is facing unprecedented environmental changes, mainly due to the rapid increase in greenhouse gas emissions from human activities. Global average sea level has risen faster since 1900 than in any previous century for at least 3,000 years, and global ocean warming has occurred faster in the last century than since the end of the previous deglacial transition (about 11,000 years ago) (IPCC, 2021). The surface pH of the open ocean has risen over the past 50 million years and is currently as low as it has been in recent decades, which is unusual in the past 2 million years (IPCC, 2021). All these environmental modifications are called climate change.

Despite its buffering capacity, the ocean is one of the most affected compartments today. It plays an influential role in the climate system because ocean warming accounted for 91% of the heating (IPCC, 2021). Since the industrial revolution, the ocean's pH has decreased by 0.1 pH units, its temperature has increased between 0.68 and 1.01°C and its level has risen by an average of 0.20 m (IPCC, 2021, 2014). To establish the impacts of climate change as accurately as possible, local data are needed. In the Nouvelle-Aquitaine region, the most pessimistic scenario of the Intergovernmental Panel on Climate Change (IPCC) predicts ocean acidification of 0.4 to 0.45 pH units on average, combined with a surface water warming of 4°C by 2100 (IPCC, 2014). An increase of extreme climatic events and a sea-level rise of 0.6 to 0.7 are also predicted (IPCC, 2014).

Microorganisms are defined as 'the life support system of the biosphere' (Cavicchioli et al., 2019; Reinold et al., 2019). In the oceans, they accounted for 1×10^{29} cells (Flemming and Wuertz, 2019), dominating the metabolic activity, participating in several biogeochemical cycles, producing the half of the Earth's oxygen, sustaining the good functioning of the aquatic systems, being the basis of food webs and recycling of the organic matter. Little studies aim to understand how climate change affect microbial communities at the end of the century. To gain information on the effect of climate change on microbial communities, we believe that microbial mat, which is a structure that groups together numerous microorganisms and metabolisms making it a self-sufficient system, is a good model. Microbial mats play key roles

in the biogeochemical cycles of carbon, oxygen, sulphur, nitrogen, etc. In particular, they have been involved in the oxygenation of the atmosphere.

This thesis aims to determine the potential impacts of climate change on microbial mats in coastal environments of the Nouvelle-Aquitaine region. It is based on the most pessimistic predictions (RCP8.5 scenario) for the end of the century according to the IPCC report established in 2014 (IPCC, 2014).

The first chapter (state of art) aims to present the IPCC's predictions about the impact of climate change on the ocean, and more specifically on the coastal environments of the Nouvelle-Aquitaine region, as well as current knowledge of the impact on microorganisms. A description of the structure and functioning of microbial mats is also provided to better understand their composition, structure and functioning. The experimental approach, methods and devices used to carry out this study are described in the second chapter (methodology chapter).

The results of this thesis are presented in the next four chapters. The microbial mats in the salt marshes of the Ré Island have never been studied before. Thus, the third chapter aims to define and compare the microbial diversity present in two microbial mats, one from an exploited salt marsh and the other from a non-exploited salt marsh. This study also allows to choose the source of the mat to be sampled (exploited or not) for the simulation of climate change.

In the fourth chapter, we investigated the seasonal dynamic of microbial communities in a salt marsh. Indeed, as salt marshes are shallow environments and the region is defined by the alternation of marked seasons, the microbial mats already cope with environmental conditions comparable to those of climate change according to IPCC (2014). A comparison of microbial mats from exploited and non-exploited plots in the same salt marsh also allowed to determine the anthropogenic impact on these microbial communities over the seasons.

The impact of climate change on the microbial mats of the Ré Island salt marshes is studied in the fifth chapter with the simulation of the two parameters that will have the greatest impact on these environments, acidification and warming of the surface water, with the implementation of mesocosm experiments.

The sixth chapter focuses on the impact of climate change on phototrophic communities of microbial mats through the study of specific molecules produced, extracellular polymeric substances and pigments, as well as their photosynthetic capacity.

The last chapter summarises and discusses the main conclusions of this thesis, providing some perspectives.

Chapter I: Introduction

1. Climate change on marine ecosystems

Humans and their activities cause unprecedented changes in the climate and the environment at a world level. Climate is warming, extinctions of a lot of species occur, biodiversity is declining, pollution affects ecosystems and human health, and new risks are emerging like increase of the sea level, extreme climatic phenomenon, diseases and food insecurity. These changes have a global impact not only on ecosystems and communities but also to individuals. These global scale anthropogenic perturbations conducted the scientists to define a new geological period named “Anthropocene” (Crutzen, 2006).

One of the most impacted environments will be the marine environment. The oceans cover 70% of the Earth’s surface (Boyd et al., 2016; Raven and Falkowski, 1999) and are a principal component of the Earth functioning. This compartment has a crucial role in biogeochemical cycles, being responsible for more than 50% of the world’s oxygen production, a carbon sink, and transporting heat from the equator to the poles. Thus, the oceans are participating in the Earth’s climate regulation and the presence of seasons (Covey, 1995; Field, 1998; Forget and Ferreira, 2019; Gulev et al., 2013; IPCC, 2019). Human activities and survival are also dependant on the oceans: they provide food, medicine and recreation, but they are also used for the transport of most goods playing a pivotal role on the economy and employment (IPCC, 2019). Moreover, over 50 biogeographical provinces or biomes composed oceans’ ecosystems, from tropical to polar conditions (Longhurst, 2010), providing habitats for rich marine biodiversity.

1.1 Future climatic change in marine ecosystem

The Intergovernmental Panel on Climate Change (IPCC) is an intergovernmental body grouping several United Nations member countries. Its main activity is the preparation and divulgation of reports assessing the state of knowledge of climate change. The IPCC developed four scenarios named Representative Concentration Pathways (RCPs) (IPCC,

2014). They describe different pathways of greenhouse gas emissions and atmospheric concentrations, air pollutants and land use. The scenarios don't take account of possible changes in natural forcing. RCP2.6 is a stringent mitigation scenario, RCP4.5 and RCP6.0 are two intermediate scenarios and RCP8.5 is a scenario with very high greenhouse gas emissions. These scenarios predicted the future impact of climate change according to the data recording in 1850-1900.

1.1.1 Ocean water warming

The air temperature increases due to enhanced greenhouse effect (IPCC, 2014). This increase impacts the surface water temperature in the first instance and then the deep ocean temperature. The global surface temperature of the ocean is projected to exceed 2°C (relative to 1850-1900 temperatures) for the 22nd century according to RCP8.5 (IPCC, 2014) (**Fig. 1**).

The shallow aquatic environments like salt marshes will be very impacted because they receive surface ocean water with a temperature very close or equal to the surface temperature and the low depth contributes to warm this water.

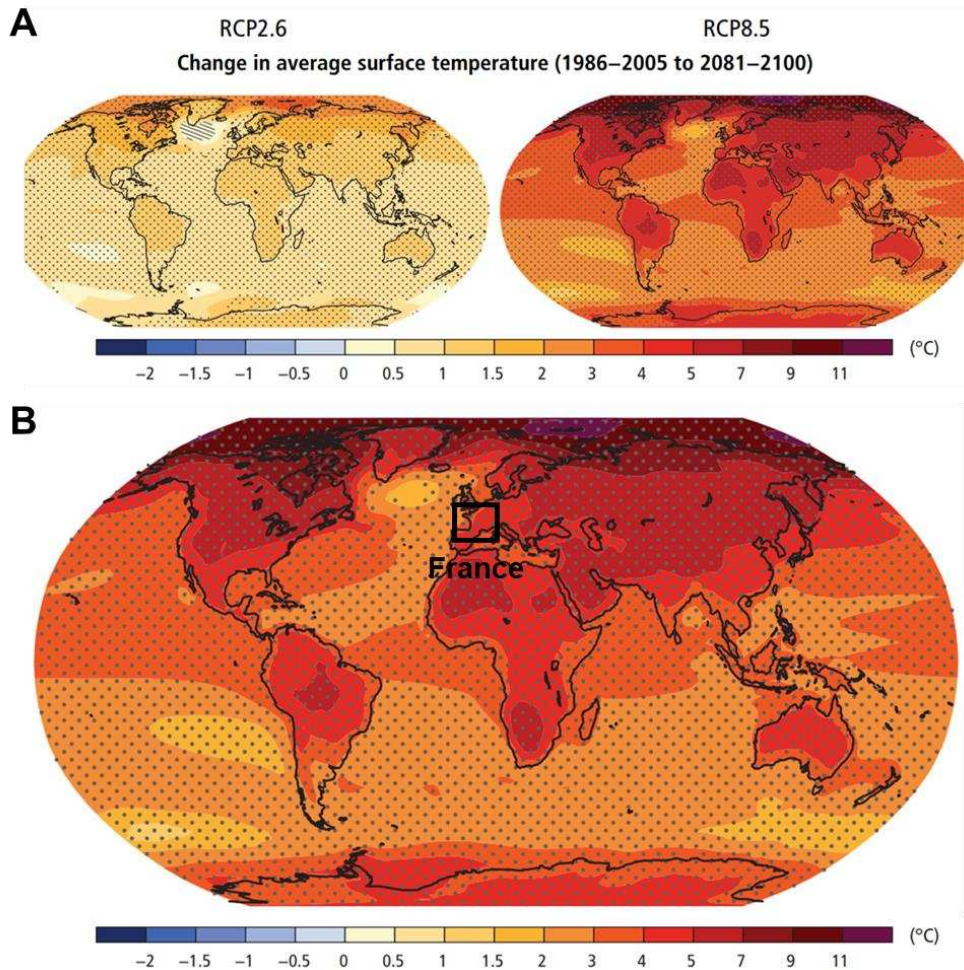


Figure 1: Simulation of the average surface temperature modification of the Earth, predicted by the IPCC (2014). **A)** Representation of two scenarios, RCP2.6 and RCP8.5, the less and the more pessimistic scenarios respectively, by the end of the century. **B)** Magnified representation of the RCP8.5 scenario by the end of the century. These figures are from the report of the IPCC (2014).

1.1.2 Ocean acidification

a- Actual marine carbon cycle and natural fluctuation of pH

The diffusion and mixing of atmospheric CO_2 across the surface water are the beginning of the ocean carbon cycle. This CO_2 becomes H_2CO_3 and rapidly HCO_3^- contributing to the reservoir of dissolved inorganic carbon. This process releases protons which contribute to ocean acidification (Hutchins and Fu, 2017).

Some of this dissolved inorganic carbon, fixed by photosynthetic microorganisms producing particulate and dissolved organic carbon, is then used in marine food webs. For

example, a major part of this organic carbon is respired by bacteria and became CO₂ again. Particulate organic carbon composes sinks, transferring this carbon from surface water into deeper water and marine sediments, and therefore sequestering CO₂ for several thousand years. Biomineralization is another way to enter the carbonate pump for surface ocean dissolved inorganic carbon. For example, the microorganisms like coccolithophores use it to build their calcium carbonate shells. Biocalcification acts as a source of CO₂ and contribute to ocean acidification (Hutchins and Fu, 2017).

Currently, the average pH of the seawater surface is about 8.1 (O'Brien et al., 2016) but natural fluctuations of pH occurred in the ocean. Some biological processes influence the seawater pH, such as photosynthesis tending to increase pH and respiration tending to decrease pH (Gao et al., 2012). Assimilation of some nutrients as nitrate or ammonia may also influence pH, but the production or consumption of hydrogen ions is low compared to changes due to photosynthetic carbon removal (Gao et al., 2012).

b- Future ocean acidification

The global carbon cycle is directly affected by anthropogenic actions *via* ocean acidification. It is the most directly quantifiable ecosystem impact. Since the industrial revolution, about a third of human CO₂ emissions in the atmosphere was absorbed by the ocean. This leads to a decrease of seawater pH by 0.1 unit which conducts the concentration of hydrogen ions to increase by 26% (Gao et al., 2012; O'Brien et al., 2016).

Global warming is predicted to release faster CO₂ into the atmosphere, increasing its concentration from 390 ppm to 700 ppm by 2100 (IPCC, 2014). This rise will conduct to a decrease of pH between 0.3 and 0.4 units (**Fig. 2**). Ocean acidification is associated with increasing concentrations of HCO₃⁻, CO₂ and H⁺ and decreasing concentrations of CO₃²⁻ and CaCO₃.

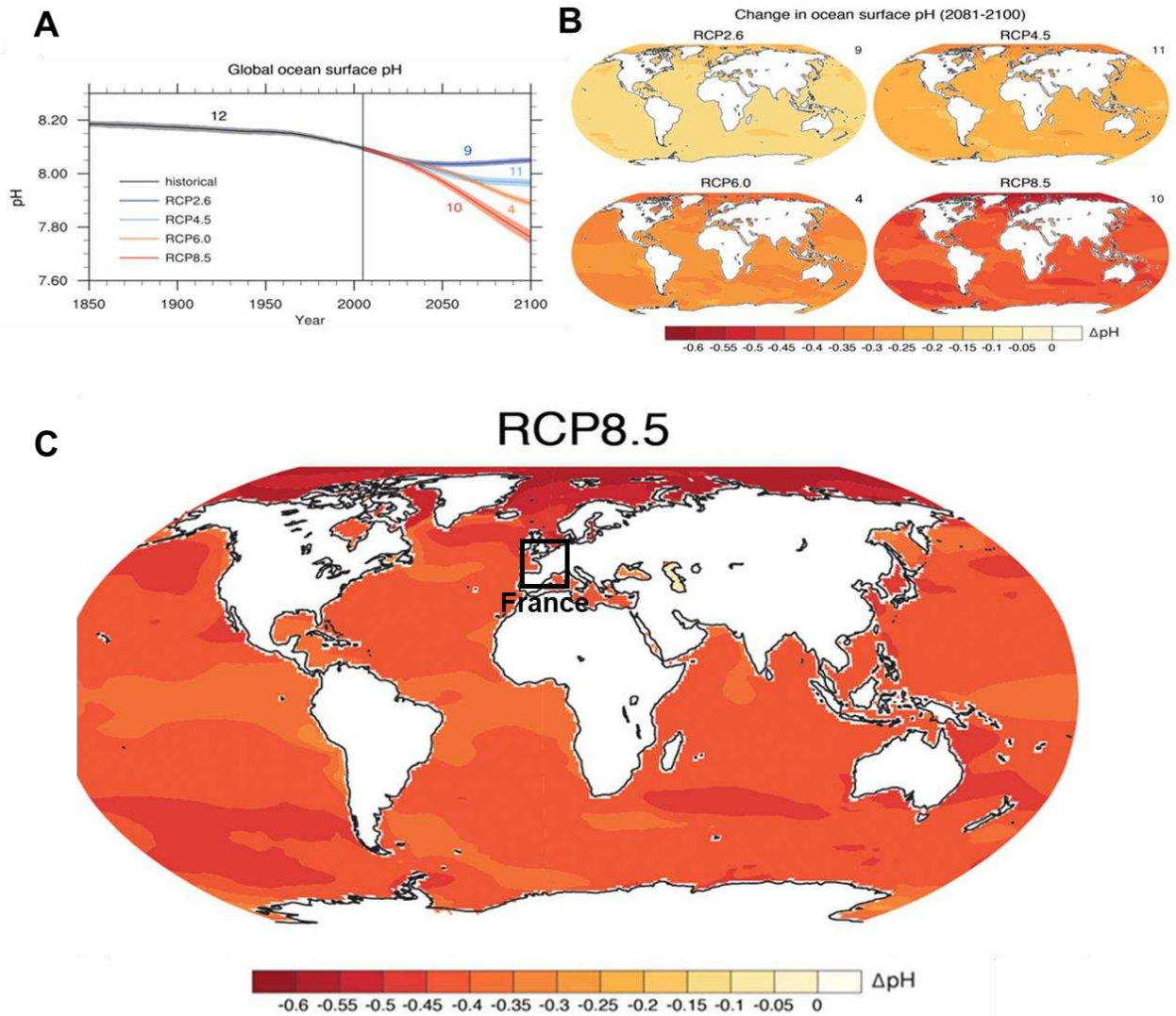


Figure 2: Simulation of the surface pH modification of the ocean, predicted by the IPCC (2014). **A)** Monitoring and predictions of the global surface pH by the end of the century according to four scenarios, RCP2.6, RCP4.5, RCP6.0 and RCP8.5 (from the less to the more pessimistic scenario). **B)** Representation of the four scenarios, RCP2.6 to RCP8.5, the less to the more pessimistic scenario respectively, by the end of the century. **C)** Magnified representation of the RCP8.5 scenario by the end of the century. These figures are from the report of the IPCC (2014).

1.1.3 Other predicted effects

a- Ocean deoxygenation

Ocean deoxygenation is the global loss of dissolved oxygen in Earth's ocean. It occurs in coastal waters, open oceans and semi-enclosed seas (Limburg et al., 2020). The oceans are estimated to have lost about 1%-2% of their oxygen since the middle of the 20th century

(Limburg et al., 2020; Oschlies et al., 2018; Schmidtko et al., 2017) and ocean models predicted a decline in the dissolved oxygen inventory of 1% to 7% by 2100 (Schmidtko et al., 2017).

Ocean deoxygenation in estuaries and coastal seas can be due to over-fertilization of water from agriculture and sewage, and the burning of fossil fuels which has historically been the main driver (Limburg et al., 2020). Moreover, climate warming is more and more an important factor participating in the decline in dissolved oxygen in the oceans, estuaries and seas (Limburg et al., 2020).

In the open ocean, oxygen-depleted waters named oxygen minimum zones (OMZs) are a natural phenomenon (Limburg et al., 2020; Oschlies et al., 2018). They are located several hundred meters below the ocean surface. Generally, they are not in touch with the sea bottom, but the combination of winds and ocean circulation can mix these layers, due for example, to upwelling (Limburg et al., 2020) (**Fig. 3**). In these OMZs, the low threshold of oxygen is often lethal for most organisms. The anaerobic remineralization processes consume fixed nitrogen while phosphate and iron release from sediments is increased (Oschlies et al., 2018) (**Fig. 3**). An excess in phosphate relative to fixed nitrogen is then observed. Following upwelling, this excess phosphate might stimulate nitrogen fixation into the surface waters, increasing the eutrophication and the oxygen consumption leading to a deoxygenation enhancement (Oschlies et al., 2018) (**Fig. 3**). Deoxygenation feedbacks can also arise the potent greenhouse gases, like nitrous oxide (N_2O) through nitrification and denitrification, from the ocean to the atmosphere that have ever been measured above (Arévalo-Martínez et al., 2015) (**Fig. 3**). The expansion of OMZs is predicted to have substantial biogeochemical, ecological, economic and eventual climatic impacts (Oschlies et al., 2018).

Hypoxia is the state of low oxygen at which physiological and ecological processes are altered. It is often defined as $2 \text{ mg}\cdot\text{L}^{-1} \text{ O}_2$ equivalent to $1.4 \text{ mL}\cdot\text{L}^{-1} \text{ O}_2$ or $63 \mu\text{mol}\cdot\text{L}^{-1} \text{ O}_2$ (Limburg et al., 2020). However, in reality, it depends on the organisms and processes where oxygen is required. For example, some species live in a low oxygen environment and only survive below

2 mg.L⁻¹ O₂. Hypoxia occurs when the rate of oxygen consumption exceeds its reload through photosynthesis and mixing of the water column (Limburg et al., 2020). Anoxia is defined as the absence of oxygen (or at concentrations below threshold detection) (Limburg et al., 2020).

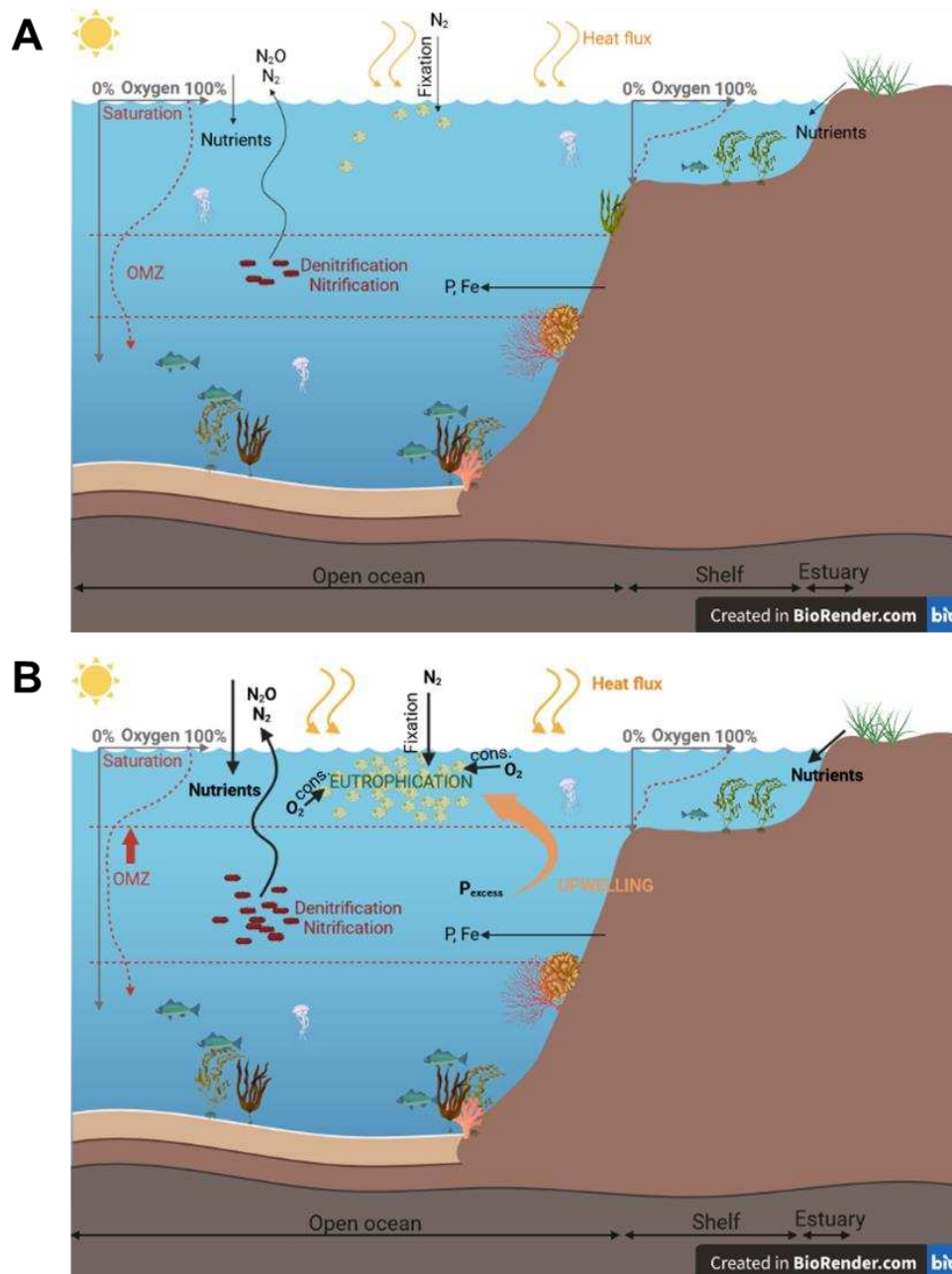


Figure 3: Oceanic deoxygenation. Schematic view of the drivers, processes and consequences of **A)** the current deoxygenation occurring in the ocean and **B)** the predicted deoxygenation in the future ocean. Based on Limburg *et al.* (2020) and Oschlies *et al.* (2018).

cons.: consumption

b- Increase of extreme climatic events

The IPCC (2014) predicts that extreme precipitation events will be more intense and heat waves will occur more often and longer. Occasional cold winter extremes will also be observed, but it is predicted to have more hot events and fewer cold events. The changes in precipitation will not be uniform on the Earth: in the high latitudes, the equatorial Pacific and in many mid-latitude wet regions would experience an increase in annual mean precipitation by the end of this century under RCP8.5 while in many mid-latitude and subtropical dry regions, mean precipitation would be decreased (**Fig. 4**) (IPCC, 2014). However, over most mid-latitude land and over wet tropical regions, extreme precipitation events would become more intense and more frequent (IPCC, 2014). Storms, coastal flooding, droughts and tsunamis would also become more frequent (IPCC, 2014).

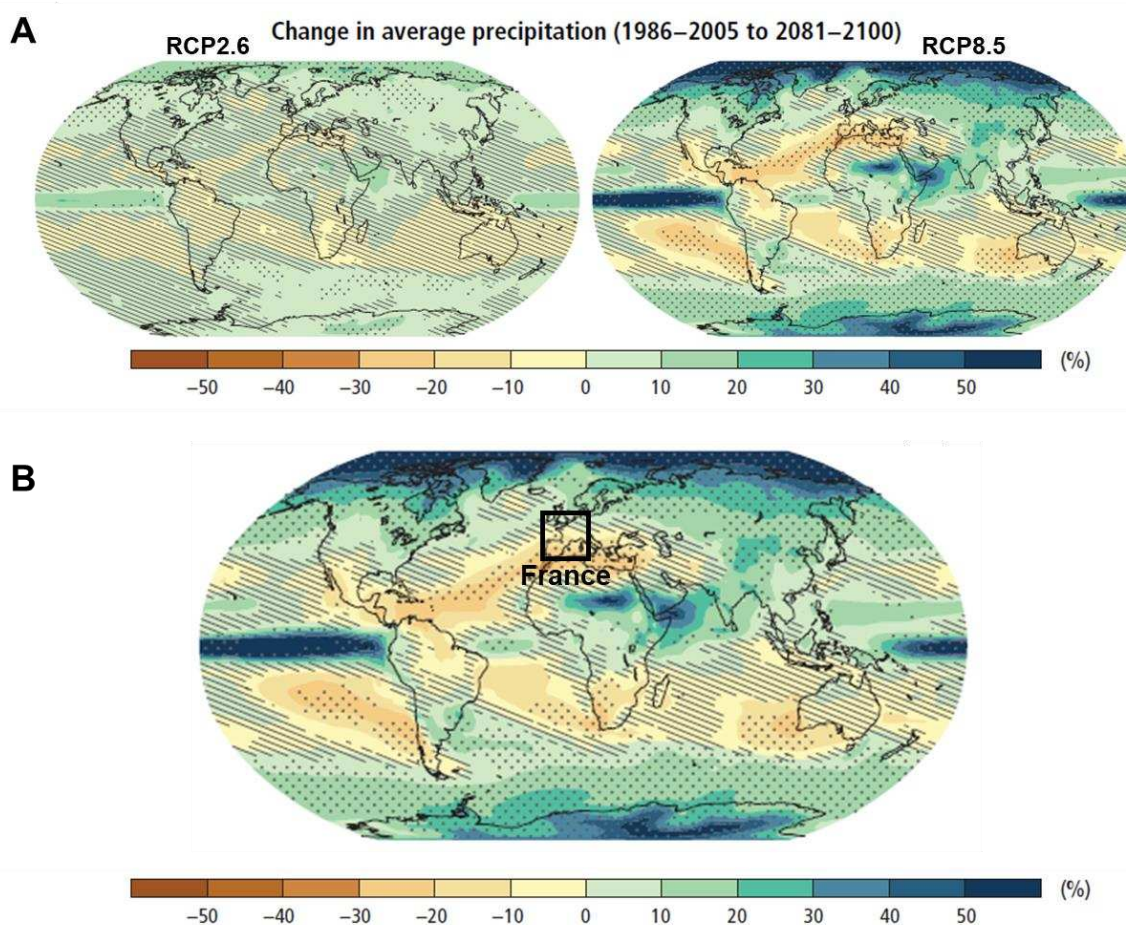


Figure 4: Simulation of the average precipitation modification, predicted by the IPCC (2014). A) Representation of two scenarios, RCP2.6 and RCP8.5, the less and the more pessimistic scenarios

respectively, by the end of the century. **B)** Magnified representation of the RCP8.5 scenario by the end of the century. These figures are from the report of the IPCC (2014).

c- Sea-level rise

The global mean sea level is predicted to continue to rise over the 21st century in more than 95% of the ocean area but this will not be uniform across regions (IPCC, 2014). About 70% of the global coastlines are projected to experience a relative sea-level change, between 0.26 to 0.55 m (RCP2.5) and 0.45 to 0.82 m (RCP8.5) for 2100 (**Fig. 5**) (IPCC, 2014).

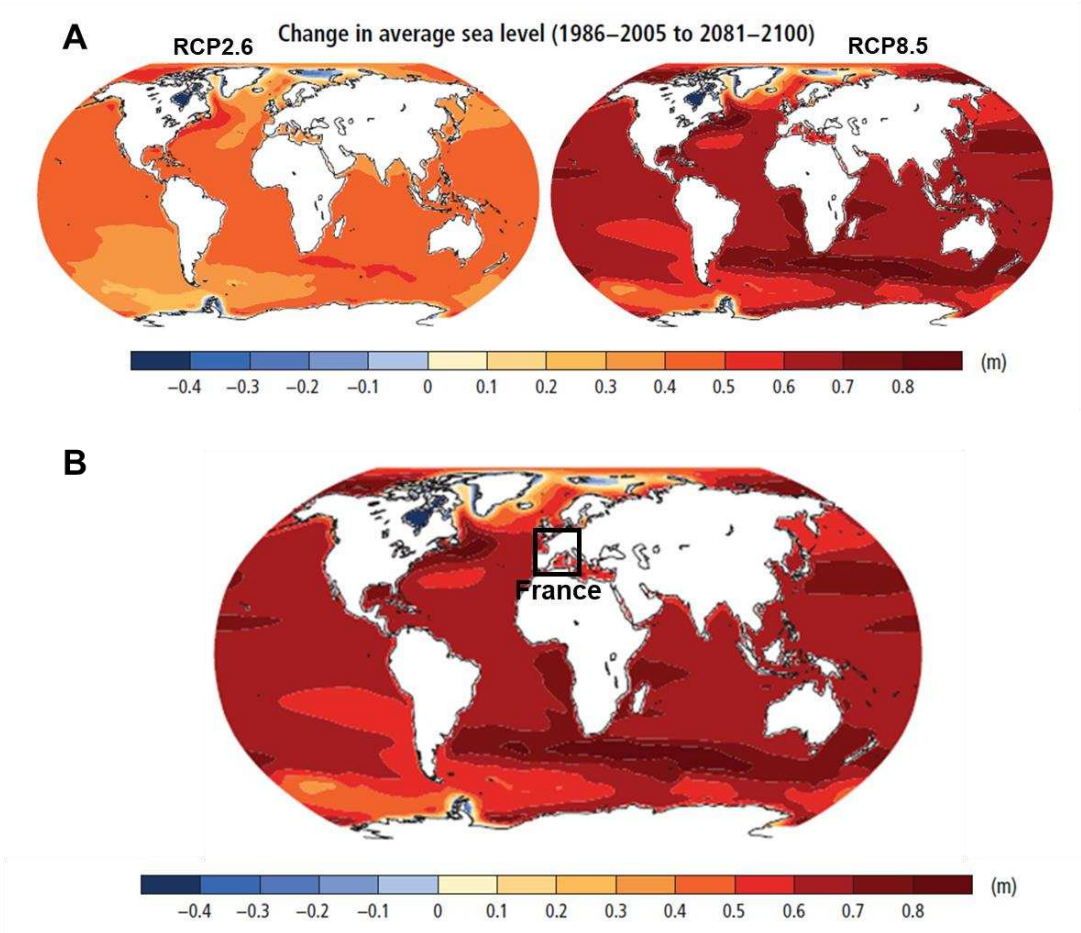


Figure 5: Simulation of the average sea level modification, predicted by the IPCC (2014). A) Representation of two scenarios, RCP2.6 and RCP8.5, the less and the more pessimistic scenarios respectively, by the end of the century. **B)** Magnified representation of the RCP8.5 scenario by the end of the century. These figures are from the report of the IPCC (2014).

d- Radiation effects

In the water column, the solar radiation penetration largely depends on the number of particles and dissolved organic matter (DOM), which may increase in various inland waters and coastal ecosystems due to an increase in rainfall (Gao et al., 2012).

The solar UV-B radiation is predicted to increase due to ozone depletion (Andrady et al., 2007). UV radiation reduces the CO₂ photosynthetic uptake and alters the ecosystems' productivity (Häder et al., 2011).

1.2 Climate change in Nouvelle-Aquitaine coasts (France)

The Nouvelle-Aquitaine region is an administrative French region. It is the largest region of France representing an eighth of the national territory with 84,061 km². The region is bordered by the Atlantic Ocean with a front of more than 900 km.

Locally, the predictions of IPCC are different from the global previsions and the impacts will not be the same. Even between the north and the south of the region, there will be various changes. By the end of the century, the average air temperature will increase between 3 and 4°C, the pH will decrease by 0.4 to 0.45 units pH, the sea-level average will rise by 0.5 m and the average precipitation will decrease by 10% (IPCC, 2014).

1.3 Importance of studying climate change on microbial communities in the marine environment

Global environmental change is predicted to affect severely aquatic ecosystems (Hutchins and Fu, 2017; Pajares et al., 2015). Climate change effects are very documented on animals and plants. By contrast, very few studies exist on their potential impact on microorganisms. While invisible to the naked eye, microorganisms are very abundant (10.2x10³⁰ bacteria and archaea cells) and diverse, underlying their importance in maintaining

a healthy global ecosystem (Cavicchioli et al., 2019; Flemming and Wuertz, 2019). They are defined as 'the life support system of the biosphere' allowing the macroscopic life directly or indirectly (Cavicchioli et al., 2019; Reinold et al., 2019) and play key roles in biogeochemical and nutrients cycling, global food web, plant and animal health, agriculture *etc.* Microorganisms are present in all environments where macroscopic life is observed, and they are the unique forms of life in other environments often called 'extreme environments' (Cavicchioli et al., 2019). Microbial organisms exist on Earth for at least 3.8 billion years, supposed to be the origin of life, and they will be likely present beyond any future extinction events (Cavicchioli et al., 2019). Microbial responses to environmental change are various due to their versatility and important diversity. Thus, microorganisms are major actors in the future climate change challenge. Only few studies have characterized the impact of climate change in microbial diversity and functioning (Cavicchioli et al., 2019; Dutta and Dutta, 2016; Walch, 2014). It is thus of paramount importance to gain insights on the resilience capacity of microbial community in response to these unprecedented changes.

Microorganisms are very abundant in our oceans: 4×10^{29} cells in the deep oceanic subsurface, 5×10^{28} cells in the upper oceanic sediment and 1×10^{29} cells in the oceans (Flemming and Wuertz, 2019). They are also the most abundant and diverse organisms in marine environments. They dominate the metabolic activity, with, for example, primary production of approximately half of the global primary production of the oceans (O'Brien et al., 2016). Marine microorganisms also play a central role in the carbon, oxygen, nitrogen, sulfur and nutrient cycles, as well as in the exchange of trace gases that have direct impacts on local climate (O'Brien et al., 2016). For example, cyanobacteria like *Synechococcus* and *Prochlorococcus*, contribute to fix 50% of the atmosphere carbon in marine systems and heterotrophic bacteria rapidly respire it. Marine phytoplankton is responsible for half of the global productivity (Field, 1998) in oceans. So, marine microorganisms participate in the key processes in the oceans and are crucial for the good functioning of the aquatic systems being

the basis of food webs with the recycling of the organic matter and being a considerable source of food to higher trophic levels.

Thus, marine microbial communities are expected to play a central role in the response of the ecosystem faced to environmental change because of their key functions in the oceans (Azam and Malfatti, 2007). Marine microbial communities possess important functional resilience due to their long evolutionary history in a constantly changing ocean environment (Hutchins and Fu, 2017). They also encounter environmental heterogeneity due to natural fluctuations to mean climate change, notably with the presence of seasons along the coast of temperate environments.

However, marine microbial microorganisms will deal with many rapidly simultaneous anthropogenic changes, and low knowledge has been acquired to predict how this combination of several factors in the short-term will modify the marine environment and how this will affect microbial and more generally, marine life. The comprehension of the microbial community responses face to environmental changes is very important to predict the effect of global changes in ecosystem functioning (Pajares et al., 2015). This will also allow to include microbial parameters to improve the current simulation models and make better predictions.

2. Microbial mats

Microbial mats exist on Earth for billions of years. The oldest observed were microbialites, the fossilized forms (Burne and Moore, 1987), in sedimentary rocks dating from 3.7 giga-annum (Ga) and 3.4 Ga, in West Australia (Allwood et al., 2006; Noffke et al., 2013; Nutman et al., 2016) and South Africa (Westall et al., 2006). Laminated microbial mats are considered like recent analogues of Precambrian stromatolites (**Fig. 6**). The microbial mats played a crucial role in Earth History because they participate in the composition and the modification of the atmosphere by producing O₂, H₂ et CH₄ (Hoehler et al., 2001).

The microbial mats are organo-sedimentary laminated structures of microorganisms (van Gernerden, 1993). These complex micro-scale ecosystems develop at the water-sediment interface of shallow environments as coastlines (Bolhuis and Stal, 2011), estuaries (Mir et al., 1991), lakes (Jørgensen and Cohen, 1977), deserts wadis (Abed et al., 2018b), hot springs (Dobretsov et al., 2011) or hypersaline environments like salt marshes (Fourçans et al., 2004; Giani et al., 1989). Diverse populations of prokaryotes are observed as well as some small eukaryotes (unicellular algae like diatoms) (Bolhuis and Stal, 2011; Franks and Stolz, 2009). The microbial mats' height varies from few millimetres to few centimetres. The sediment colonization depends mainly on environmental parameters (granulometry, sedimentation rate, erosion rate, water retention by capillarity, light penetration, presence of predators). Most of the time, the first millimetres are colonized by photoautotroph microorganisms like cyanobacteria and eukaryotic phyto-benthos defining the microbial mat as photosynthetic. They produce organic carbon which is then decomposed in the successive lower layers by different heterotrophic prokaryotes. This structure is characterised by strong vertical gradients of oxygen, sulfide, light and other electron acceptors, allowing the development of complex metabolite exchange networks (Pajares et al., 2015).

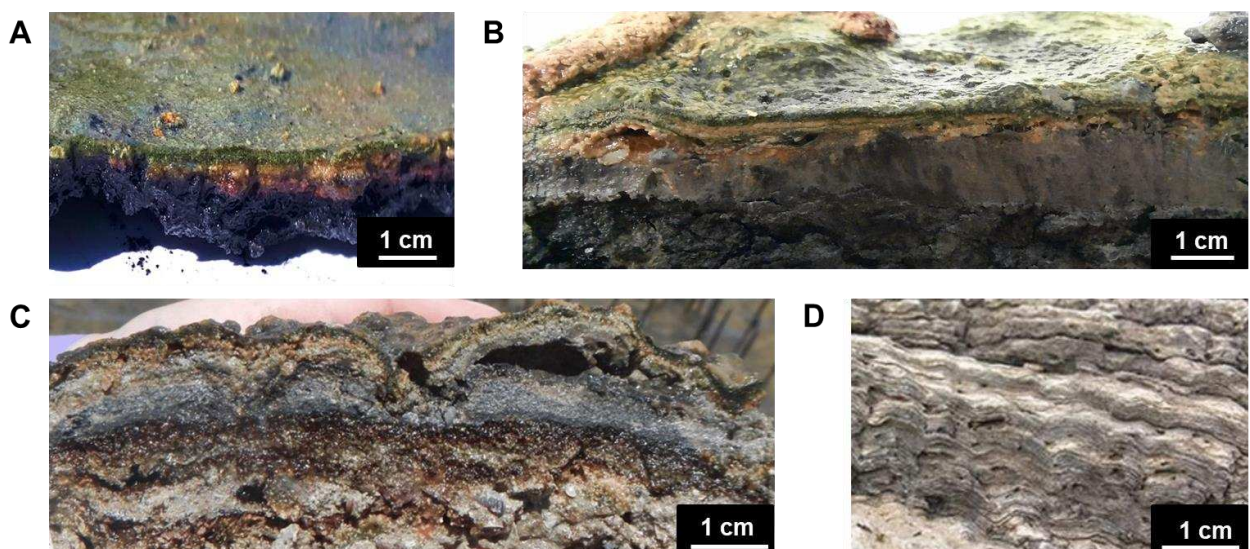


Figure 6: Microbial mats. Pictures of **A)** and **B)** microbial mats from non-exploited plots of a salt marsh, **C)** a mineralized microbial mat (Pace et al., 2021) and **D)** a microbialite (Bourillot, 2009).

Microbial mats are a key component of their ecosystem, and they contain a large diversity of microorganisms and metabolisms. Moreover, they are self-sustaining (Pajares et al., 2015) and very easy to sample. These particularities make them adequate models to represent microbial ecosystems. However, we must note that microbial mats are heterogeneous at the micro- (physical-chemical gradients) and larger scales (tide, precipitation, vegetation and bioturbation).

The microbial mats present a great diversity, therefore in this chapter, the principal microorganisms found in them will be introduced in the form of a list describing their characteristics, where they live and giving some examples of observed species.

2.1 The prokaryotic populations: the major functional microbial groups composing the photoautotroph microbial mats

In a microbial mat, the prokaryotic populations are mainly composed of bacteria which are extensively studied (Bolhuis and Stal, 2011). Less is known on the Archaeal populations (Thauer, 1998) but more and more studies are focusing on them. The microorganisms live close to each other representing a hot spot of exchange of nutrients, and carbon and energy sources, resulting in commingled biogeochemical cycles. Microorganisms are classified according to their major metabolism (**Fig. 7**).

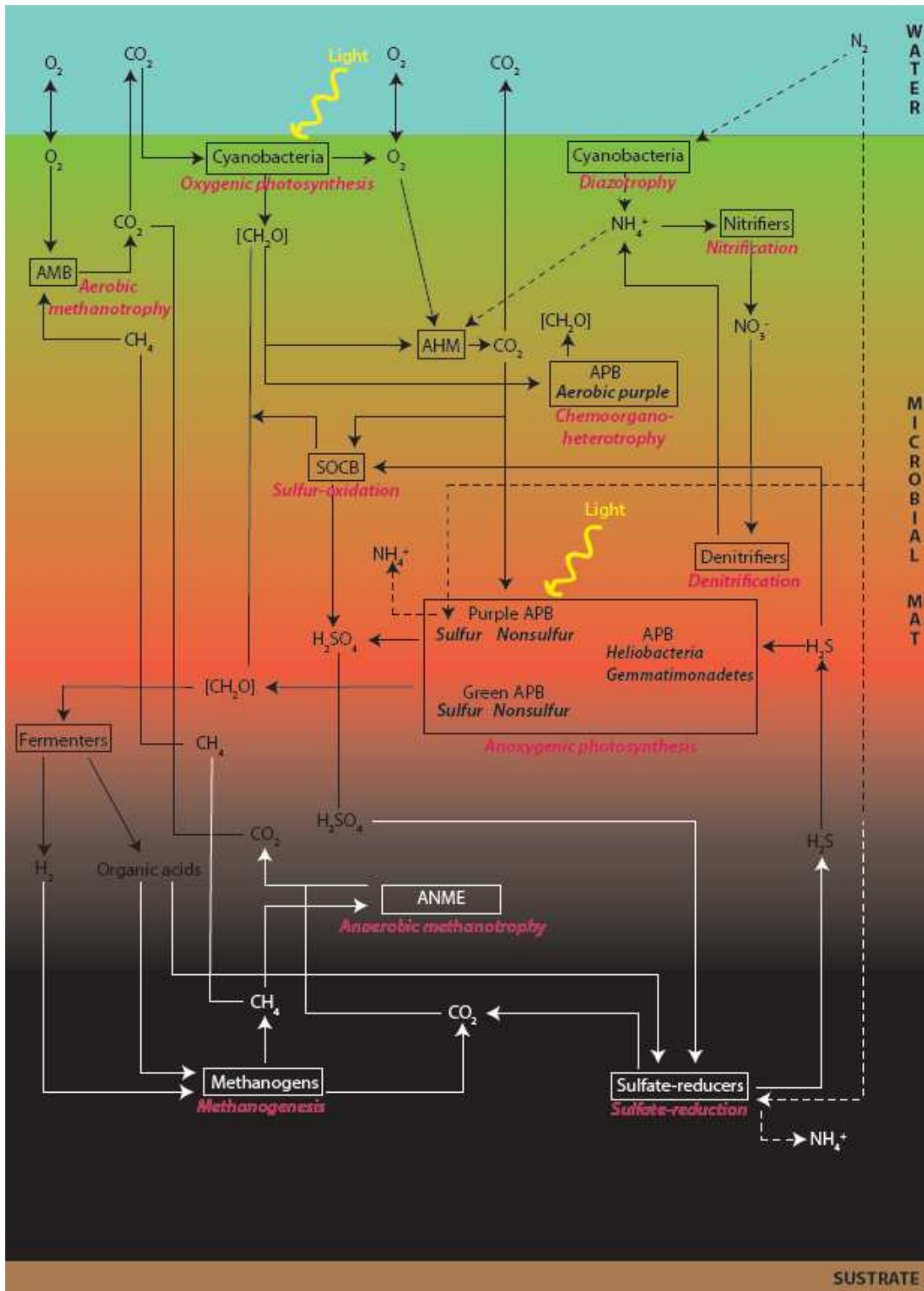


Figure 7: Microbial mat and its role in biogeochemical cycles. Schematic view of the major metabolisms and major microorganisms in a photosynthetic microbial mat. The green part is the oxic zone followed by the red and black parts corresponding to the anoxic zone. The black part is the sulfur-rich zone.

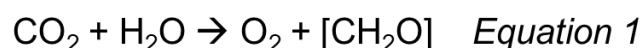
AMB: aerobic methanotrophic bacteria; AHM: aerobic heterotrophic microorganism; APB: anoxygenic phototrophic bacteria; SOCB: sulfur-oxidizing chemoautotrophic bacteria; ANME: anaerobic methanotrophic archaea.

2.1.1 The prokaryotic oxygenic photolithoautotrophs

The prokaryotic phototrophs are the major primary producers in microbial systems. They use light energy to fix inorganic carbon to organic carbon thanks to photosynthesis. This reaction is either oxygenic or anoxygenic. The latter is developed in another part of the manuscript (2.1.4).

Photosynthetic mats usually have an upper oxic green layer composed of oxygenic phototrophs which are at the basis of the food webs of the ecosystems (**Fig. 7**). Among them, cyanobacteria are the most productive. They are either filamentous or unicellular, being largely diverse. The more represented cyanobacterial genera in microbial mats are *Aphanothece*, *Chroococcus*, *Gloeocapsa*, *Halomicronema*, *Leptolyngbya*, *Microcoleus*, with *Microcoleus chthonoplastes* as the most abundant species in marine cyanobacterial microbial mat (van Gemerden, 1993), *Oscillatoria*, *Pleurocapsa*, *Spirulina* and *Synechocystis*.

The principal metabolism of these microorganisms is the oxygenic photosynthesis. This reaction consists of the reduction of the carbon dioxide into organic carbon, doing water protolysis thanks to light radiations of visible spectra, ended in oxygen production (**Equation 1**).



To perform this reaction, the cyanobacteria possess two membrane photosystems named PSI and PSII connected in series (Stal, 1995). They contain different pigments like chlorophyll *a*, carotenoids and phycobilins.

To do oxygenic photosynthesis, the cyanobacteria need CO₂ (carbon donor), light (energy source) and H₂O (electron source) which are generally present in most environments. However, many cyanobacterial species show a versatile metabolism (Stal, 1995). Some of them perform anoxygenic photosynthesis using sulfide as electron donor (Stal, 1995), sulfur fermentation/respiration (Stal, 1995) and nitrogen metabolism (Stal, 1995). They have been found in oxic and anoxic environments. Some species resist to desiccation growing in arid

environments such as deserts while other tolerate high salinity growing in hypersaline ponds (Stal, 1995).

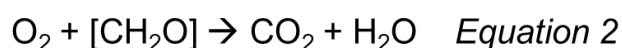
Phototrophic microorganisms are fundamental organisms in the functioning of microbial mats because they secrete extracellular polymeric substances (EPS), adhesive and protective, which form a matrix around the cells, a major component of microbial mats and remain crucial for their functioning (Decho, 1990; Fourçans et al., 2006; Hubas, 2018; Wieland et al., 2003). This matrix is generally composed of sugars, proteins, extracellular DNA and other molecules in smaller proportions (Fourçans et al., 2006; Hubas, 2018; Wieland et al., 2003). However, the composition varies depending on the physiological state of the organisms, the specific diversity, the growth stage of the mat and the physical-chemical conditions of the environment (Decho and Moriarty, 1990; Hubas, 2018; Reinold et al., 2019; Underwood et al., 2004). By binding to sedimentary particles, this matrix stabilises the microbial mat and prevents erosion phenomena (Decho, 1990), but it has many other essential roles such as nutrients supply by the sequestration and accumulation of dissolved and particulate nutrients coming from the water column that can be used by microorganisms, or it also helps microbial communication, or bring protection against UV radiations (Decho, 2000; Flemming and Wingender, 2010; Hubas, 2018).

The cyanobacteria are also responsible for the input of organic matter in the sediment ecosystem that becomes available for other microorganisms by different mechanisms: death or lysis of the cyanobacteria, glycolate excretion (lack of CO₂ induces photorespiration which excretes glycolate), excretion of fermentation products or extracellular polymeric substances (EPS) (Stal, 1995). They also participate in the enrichment of the sediments with dioxygen and nitrogen components. All these mechanisms lead to the delimitation of a rich oxic zone of nutrients allowing the development of other microorganisms. This layer is the most exposed in terms of environmental changes and disturbances.

2.1.2 The aerobic heterotrophic microorganisms

The aerobic heterotrophic microorganisms (AHMs) are observed in the oxic zone (Abed et al., 2018a). This group is highly diverse. In hypersaline microbial mats, AHMs identified were affiliated to the *Gammaproteobacteria*, *Bacteroidetes* and *Alphaproteobacteria* but also *Deltaproteobacteria*, *Planctomycetes*, *Spirochaetes*, *Acidobacteria*, *Deinococcus-Thermus*, *Marinobacter*, *Halomonas*, *Roseobacter*, *Rhodobacter* and *Alcanivorax* according to the culture method used (Raeid M.M. Abed et al., 2007; Jonkers and Abed, 2003).

These microorganisms use oxygen as an electron acceptor to degrade the organic carbon (**Equation 2**). The oxygen and organic matter used are produced by oxygenic phototrophs.



AHMs and cyanobacteria were shown to interact by the exchange of vitamins and other growth factors like nitrogen or carbon sources (Steppe et al., 1996). AHMs also produce CO₂ that can be used by cyanobacterial photosynthesis (Abed et al., 2018a). Aerobic respiration is as important as photosynthesis for the carbon budget within the mat.

During the daytime, the oxic part is saturated with photosynthetically produced oxygen whereas, during the night, anoxic conditions prevail due to continued respiration activities of AHMs (*i.e.*, on cyanobacterial fermentative products) and sulfide production. Respiration is supposed to be higher under the light because AHMs use the cyanobacterial soluble photosynthates.

AHMs activities have a key role because they decrease the oxygen concentration, which is toxic for the microorganisms located deeper in the mat. They also have an important role in the carbon cycling within cyanobacterial microbial mats (Raeid M.M. Abed et al., 2007), participating in the mineralisation of the carbon products of cyanobacteria. They are expected, with sulfate-reducing bacteria, to play a major role in organic carbon mineralization in the photic

zone of such mats, due to the changing diurnal oxic and anoxic conditions (Jonkers and Abed, 2003). Among AHMs, *Bacteroidetes* have been identified as specialists for the degradation of cyanobacterial dead cells (Raeid M.M. Abed et al., 2007). All AHMs metabolize cyanobacterial photosynthetic and fermentation products (Raeid M.M. Abed et al., 2007), some of them have also been observed to have a possible role in nitrogen cycling. Abed *et al.* (2018a) showed that the AHM community structure depends on the associated cyanobacterial species.

2.1.3 The sulfur-oxidizing chemolithoautotroph bacteria

The sulfur-oxidizing chemolithoautotroph bacteria (SOCBs) are also named colourless sulfur-oxidizing bacteria in opposition to the purple and green sulfur-oxidizing anoxygenic phototrophs (Franks and Stolz, 2009).

During the reduction of CO₂ to organic carbon, these microorganisms oxidize the sulfide, and other inorganic reduced sulfide forms, used as electron donors, to sulfate. This reaction is called sulfur oxidation. The terminal electron acceptors are the oxygen and the nitrate (van Gemerden, 1993), the last, could be stored intracellularly in some bacteria.

It is possible to distinguish four SOCB groups according to their carbon sources and the energy used (Robertson and Kuenen, 2006):

- The obligate chemolithoautotrophs such as *Thiomicrospira*, *Thiobacillus*, *Acidithiobacillus* and *Sulfolobus* use a mineral sulfur compound as an electron donor and fix carbon via the Calvin cycle. They can nevertheless become heterotrophs when environmental conditions are unfavourable, but this metabolism is secondary.

- The facultative chemolithoautotrophs can grow heterotrophically or mixotrophically.

- The chemolithoheterotrophs represented by some *Thiobacillus* and *Beggiatoa* do not fix mineral carbon and must have a source of organic carbon. They use reduced sulfur compounds as electron donors and energy sources.

- The heterotrophic chemoorganotrophs (some species of *Beggiatoa* spp., *Mecromonas*, *Thiobacterium* and *Thiotrix*) can oxidise sulfur compounds without apparent energy benefits.

These microorganisms are observed in sulfide-rich zones located at the oxic-anoxic zone interface of microbial mats. They are well-adapted to the nychthemeral cycle with properties of fluctuation of the oxygen-sulfide interface by vertical displacements (Fourçans et al., 2006). SOCBs compete with photosynthetic sulfur-oxidising bacteria.

The presence of SOCBs have been observed in microbial mats of various environments: surface sediments from coastal zones, hypersaline lake, cold seeps, mud volcanos *etc.* (de Beer et al., 2006; Hinck et al., 2007; Mills et al., 2004; Preisler et al., 2007). Studies on SOCBs have mainly focused on filamentous bacteria such as *Beggiatoa* spp., which is particularly present in microbial mats, *Thioploca* spp. and *Thiomargarita namibiensis* (Franks and Stolz, 2009; Hinck et al., 2007; Preisler et al., 2007). A competition between SOCBs and the anoxygenic phototrophic bacteria occur for the use of sulfide.

SOCBs are adapted to the nychthemeral cycles occurring on microbial mats and the geochemical variations associated (Møller et al., 1985; Nelson et al., 1986; Nelson and Castenholz, 1982). Their growth is favoured by the oxygen penetration beyond the zone where the photosynthetic activity is high (Jørgensen and Des Marais, 1986).

2.1.4 The anoxygenic phototrophic bacteria (purple and green)

The anoxygenic phototrophic bacteria (APBs) perform anaerobic photosynthesis by using the final products of the degradation of the organic matter as electron donors. In the microbial mats, they play an important role in the last steps of organic matter degradation. They also use as electron donors, reduced sulfur compounds such as sulfides from the respiration of sulfate, thiosulfate and elemental sulfur.

The APBs harvest light between 740–1020 nm allowing the coexistence of multiple anoxygenic phototrophs in the same environment. Within the microbial mats, they are located on the surface of the anoxic zone where the light radiation necessary for their photosynthetic metabolism still penetrates. These microorganisms are either green or purple, often competing for the same energy and electron sources. However, the wavelengths used are different because their pigments do not absorb light radiation of the same wavelength, leading to a stratification in the microbial mats with the purple bacteria above the green bacteria.

The earliest phototrophs were anaerobic (living in the absence of free oxygen) and anoxygenic (not producing oxygen) prokaryotes.

Commonly, the APBs are differentiated according to their heterotrophy potential and their oxygen tolerance into five groups: the purple sulfur bacteria, the purple nonsulfur bacteria, the green sulfur bacteria, the green nonsulfur bacteria and the heliobacteria. However, more recently, Madigan *et al.* (2017) share the APBs into six major groups: the purple bacteria (Proteobacteria) containing purple sulfur bacteria, purple nonsulfur bacteria and aerobic purple bacteria, green sulfur bacteria (*Chlorobi*), green nonsulfur bacteria which are also called the filamentous green bacteria (*Chloroflexi*), heliobacteria (*Firmicutes*), chloracidobacteria (*Acidobacteria*), and Gemmatimonas (*Gemmatimonadetes*) (George *et al.*, 2020; Madigan *et al.*, 2017).

This coloured stratification is sometimes observable with the naked eye, the pink layer is due to the presence of purple and the green layer above is due to the presence of green phototrophs (Franks and Stolz, 2009) (**Fig; 6, A**). In these shallow ecosystems, purple phototrophic sulfur-oxidizing bacteria are found more frequently than other phototrophic anoxygenic bacteria. Light radiation is quickly attenuated by the thickness of the sediments as well as by the presence of cyanobacteria and algae. These radiations allow the development of purple phototrophic sulfur-oxidizing bacteria whose pigments absorb at 800-850 nm (Jørgensen and Des Marais, 1986). In addition, green sulfur bacteria are not tolerant to oxygen

and are less adapted to fluctuations in oxygen gradients. So, they are less observed in microbial mats (van Gemerden, 1993).

a- The purple bacteria

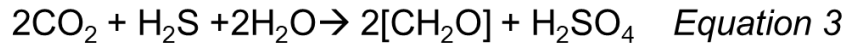
The purple bacteria are one of the major groups of photosynthetic microorganisms observed in aquatic and terrestrial environments. They are photoautotrophs only at low oxygen levels and their photosynthetic apparatus is down-regulated under higher oxygen levels and instead are chemophototrophs using organic carbon (Bauer et al., 2003; George et al., 2020; Madigan and Jung, 2009; Swingley et al., 2009). Purple bacteria are important in microbial mats because they consume the H₂S which is a toxic substance for other organisms, produce organic matter when they do photoautotrophy, and consume organic compounds, primarily non-fermentable organic compounds when they are photoheterotrophs (Madigan and Jung, 2009).

These bacteria are divided into three groups: the purple sulfur bacteria, the purple nonsulfur bacteria and the aerobic purple bacteria. Different types of phototrophic purple bacteria inhabit hypersaline coastal lagoons (Walter et al., 2021), salterns (Caumette et al., 1997; Hirschler-Réa et al., 2003) and salt lakes (Asao et al., 2011). Purple sulfur bacteria are different from nonsulfur bacteria on both metabolic and phylogenetic grounds, but species often coexist in illuminated anoxic habitats (Imhoff, 2017).

- **Purple sulfur bacteria:**

Purple sulfur bacteria are gram-negative prokaryotes belonging to the *Gammaproteobacteria* within the *Chromatiaceae* and *Ectothiorhodospiraceae* (Herbert et al., 2005; Imhoff, 2001; Imhoff et al., 2015).

These bacteria are strong photolithoautotrophs and use light energy to fix inorganic carbon to organic carbon thanks to the anoxygenic photosynthesis, using electron donors such as sulfides, polysulfides, elemental sulfur, thiosulfate, sulfite (**Equation 3**).



The purple sulfur bacteria convert energy by photophosphorylation like the other phototrophic prokaryotes, but only on anoxic conditions because pigment synthesis is repressed by molecular oxygen. So, to be successfully competitive, they need both light and anoxic conditions. They also perform limited photoheterotrophy and chemotrophy.

To process anoxygenic photosynthesis, the purple sulfur bacteria contain bacteriochlorophylls and carotenoids as photosynthetic pigments (Fenchel et al., 2012; Imhoff et al., 2015).

In mature microbial mats, the dominant purple sulfur bacterium is often *Thiocapsa roseopersicina* (van Gemerden, 1993; Visscher et al., 1990). This bacterium is both phototroph and chemotroph with sulfide and thiosulfate as sulfur source (de Wit and van Gemerden, 1987).

- **Purple nonsulfur bacteria :**

The purple nonsulfur bacteria are dispersed in Beta- (*Rhodofera*, *Rubrivivax*, etc.) and *Alphaproteobacteria* (*Rhodospirillum*, Rhodobacterales, Rhizobiales genera) (Imhoff et al., 2015). They are facultative phototrophs, and may be anaerobes and aerobes.

Purple nonsulfur bacteria are more versatile than purple sulfur bacteria. Under anaerobic conditions and in the presence of light, these bacteria are photoorganotrophs, using preferentially organic compounds as electron donors (Caumette et al., 2007). They are also capable of photolithotrophy using hydrogen or reduced sulfur compounds (Caumette et al., 2007; Guyoneaud et al., 2002), be autotrophs or heterotrophs, and live chemoorganoheterotrophic (Caumette et al., 2007). Purple non-sulfur bacteria distinguish from purple sulfur bacteria in that they do not oxidize sulfide to elemental sulfur (as intermediate).

- **The aerobic anoxygenic purple bacteria:**

The aerobic anoxygenic purple bacteria belong mostly to the *Alphaproteobacteria* within the order *Rhodobacterales*, in the *Roseobacter* clade (Yurkov and Beatty, 1998). However, one known representative is a *Betaproteobacteria*, *Roseateles depolymerans* (Suyama et al., 1999; Yurkov and Csotonyi, 2009; Yurkov, 2006) and another a *Gammaproteobacteria* with *Congregibacter litoralis* (Fuchs et al., 2007; Yurkov and Csotonyi, 2009). Unlike the other APBs, the aerobic anoxygenic purple bacteria require oxygen for their growth.

The aerobic anoxygenic purple bacteria possess bacteriochlorophyll *a* and carotenoids (George et al., 2020; Yurkov and Beatty, 1998), but bacteriochlorophyll can't be used for anaerobic photosynthetic growth by photoautotrophy (Sander and Dahl, 2009).

They are obligate heterotrophs for 80% (George et al., 2020; Yurkov and Csotonyi, 2009) with aerobic chemoorganotrophy as the preferred mode of growth (Sander and Dahl, 2009). However, some of these bacteria carry out photoheterotrophy only under aerobic conditions (Yurkov and Csotonyi, 2009), but the production of bacteriochlorophyll *a* only occurs in dark conditions, possibly to avoid the potential for oxidative damage caused by the excitation of chlorophyll intermediates (Beatty, 2002).

They are widely distributed in the oceans and they are key players in marine carbon cycle (Yurkov and Csotonyi, 2009). Several members of *Rhodobacterales*, such as *Loktanella*, are very present in developing mats while in low numbers in mature mats (Cardoso et al., 2019).

b- Anoxygenic green bacteria

Commonly, anoxygenic phototrophic green bacteria gathered the green sulfur bacteria (*Chlorobiaceae*) and the green nonsulfur bacteria (also called the filamentous anoxygenic phototrophs) (*Chloroflexaceae*) (Madigan et al., 2017) because there are very close phylogenetically. More recently Madigan *et al.* (2017) described other anoxygenic phototrophic bacteria called *Heliobacteria* (*Heliobacteriaceae*) among the green bacteria because they

share significant photochemical properties with green sulfur bacteria and are also green in colour (Madigan et al., 2017). Anoxygenic green bacteria are observed below the pink layer in the microbial mats but they don't constitute a lamination all by themselves (Martínez-Alonso et al., 2004).

The green sulfur and the green nonsulfur bacteria share similarities. Both contain chlorosomes, an organite where photosynthesis takes place only found in these bacteria (**Fig. 8**). Green sulfur phototrophs grow at low light intensities (Oelze and Golecki, 1995). Some species of these two communities also contain similar antenna pigments (bacteriochlorophylls *c*, *d* or *e*) located around chlorosomes. By contrast, *Heliobacteria* lack chlorosomes and have no discernible internal photosynthetic membrane system. However, they contain Bchl *g* as well as small amounts of chlorophyll *a* and chlorophyll *a* derivatives in the cytoplasmic membrane (Heinrich and Golbeck, 2007).

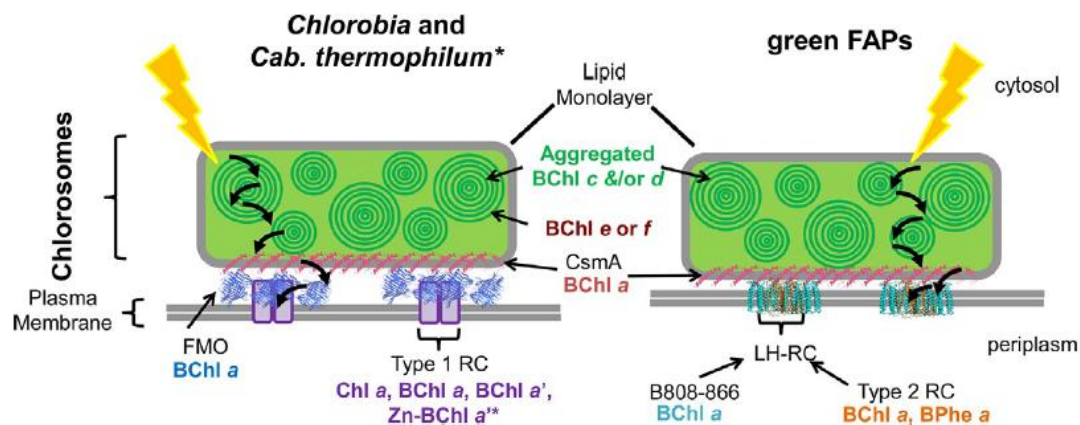


Figure 8: Chlorosomes. Schematic view of chlorosomes in *Chlorobia* and *Chloroacidobacterium* (*Cab.*) *thermophilum*, and in green filamentous anoxygenic phototrophs (FAPs). The “*” indicates a molecule found only in *Cab. thermophilum*. This figure is from Thweatt *et al.* (2019).

(*B*)Chl: (bacterio)chlorophyll; *CsmA*: BChl *a*-binding protein; *FMO*: Fenna-Matthews-Olsen protein; *LH*: light-harvesting; *RC*: reaction center.

The physiologies and habitats of green sulfur bacteria, green nonsulfur bacteria, and *Heliobacteria* are different (Madigan et al., 2017). All of them carry out photosynthesis only under anoxic conditions.

- **Green sulfur bacteria:**

The green sulfur bacteria belonging to *Chlorobia* are strict anaerobes and photolithoautotrophs. In the presence of CO₂ and sulfides, some simple organic compounds are photoassimilated. These bacteria utilize H₂S as an electron donor, which can tolerate this toxic molecule. Their presence has been ever observed in microbial mats (Martínez-Alonso et al., 2005; Roeselers et al., 2007).

- **Green nonsulfur bacteria:**

The green nonsulfur bacteria are also called green filamentous bacteria. They belong to *Chloroflexi* and have the capacity to move by sliding. These bacteria are facultative anaerobes and use oxygen as electron acceptor in darkness. Their growth is either photoautotrophic, or photoheterotrophic or chemotrophic (Kawai et al., 2021).

Some *Chloroflexi* bacteria also demonstrated a beneficial association with cyanobacteria in microbial mats from Guerrero Negro (Ley et al., 2006) reducing H₂S which is inhibitory for cyanobacterial oxygenic photosynthesis and using oxygen and organic carbon produced by cyanobacteria. Green nonsulfur bacteria are the main components of microbial mats forming in the outflows of alkaline hot springs or developing in shallow marine or hypersaline environments (Castenholz and Pierson, 1995; Madigan et al., 2017).

- **The Heliobacteria:**

The *Heliobacteria* are present in *Firmicutes* (Madigan et al., 2017) and are strict anaerobes.

This group includes phototrophic bacteria containing bacteriochlorophylls *g* which is unique and only found in this family (Madigan, 2006). The lack of differentiated photosynthetic internal membranes such as the membrane vesicles or lamellae of purple bacteria or the chlorosomes of green bacteria is also observed (Madigan, 2006). Their inability to fix CO₂ makes them incapable of autotrophy. Thus, they are photoheterotrophs, when grown under anoxic conditions and in the light, or fermentative anaerobes (chemotrophy) (Madigan, 2006).

Some Heliobacteria have been observed in microbial mats (Bryantseva et al., 2000; Kimble et al., 1995).

c- Phototrophic Gemmatimonadetes bacteria

The phototrophic *Gemmatimonadetes* phylum have been recently discovered, with the isolation of *Gemmatimonas aurantiaca* from wastewater (Zhang et al., 2003). They are phototrophs (Koblížek et al., 2020; Zeng and Koblížek, 2017). There is a lack of knowledge because few representatives are cultured (Zeng and Koblížek, 2017) but these bacteria have been found in microbial mats of salterns (Mazière et al., 2021).

2.1.5 The sulfate-reducing microorganisms

The sulfate-reducing bacteria belong mainly to the *Deltaproteobacteria* within the orders of *Desulfobacterales*, *Desulfovibrionales* and *Syntrophobacterales* (Castro et al., 2000; Muyzer and Stams, 2008; Plugge et al., 2011). They are also found in the phylum *Firmicutes* and within *Nitrospirae*. Sulfate-reducers are also present in the Archaea within the genera *Archeoglobus*, *Thermocladium* and *Caldivirga*. This ability to do sulfate respiration in some archaea is linked to a horizontal gene transfer (Karkhoff-Schweizer et al., 1995; Nelson et al., 1999; Wagner et al., 1998).

Sulfate-reducing microorganisms (SRMs) are observed in the anoxic zone below the APBs. Their activity leads to the precipitation of iron sulfide, recognizable in the microbial mat by its black colouring (Fourçans et al., 2004).

The metabolism of these microorganisms is chemolithotrophic with the anaerobic respiration using organic compounds as electron donors and carbon sources. Sulfate, sulfite, thiosulfate and sulfur are the electron acceptors leading to the formation of sulfide by dissimilatory respiration (Megonigal et al., 2014). Some SRMs perform aerobic respiration, supposed only for maintenance (Thauer et al., 2007). The substrates are often low molecular weight originating from the fermentation of organic matter, such as simple organic acids,

alcohols and hydrogen (Megonigal et al., 2014). More complex carbon sources can be used, such as long-chain fatty acids, sugars, aromatic compounds or hydrocarbons (Callaghan et al., 2008; Cravo-Laureau et al., 2005, 2004; Megonigal et al., 2014).



SRMs are responsible for 80% of carbon oxidation in coastal marine sediments (Canfield et al., 1993a, 1993b; Megonigal et al., 2014) and play a major role in the mineralization of organic matter in anoxic environments (Jørgensen, 1982; Jørgensen et al., 2019; Megonigal et al., 2014; Ollivier et al., 1994). Aerobic respiration of heterotrophic bacteria in the mat leads to oxygen depletion in the sediments, leading to anoxia of the microbial mat in depth. This area is also rich in organic matter, simple compounds originating from aerobic and anoxygenic degradation processes. Their sulfate reducing metabolism results in the production of sulfide and the formation of an associated gradient. These bacteria are not necessarily strict anaerobes (Camacho, 2009).

SRMs dominate anaerobic carbon consumption in marine microbial mats and are very well studied in hypersaline microbial mats (Cadena et al., 2018; Campbell et al., 2019; Caumette et al., 1994).

2.1.6 The methanogens

The methanogens are only represented by archaea belonging to the *Euryarchaeota* phylum (Liu, 2010), dispatched in seven orders. The *Methanobacteriales*, *Methanomicrobiales* and *Methanosarcinales* are common in anoxic environments (Liu, 2010). The *Methanococcales* are slightly halophilic marine methanogens and the *Methanopyrales* are hyperthermophilic with currently only one genus and one described species (Liu, 2010; Whitman and Jeanthon, 2006). The *Methanocellales* and *Methanomassiliicoccales* orders were described later (Paul et al., 2012; Sakai et al., 2008).

Three types of methanogenesis have been described. Hydrogenotrophic methanogenesis uses H_2 to produce CH_4 and CO_2 , acetoclastic methanogenesis uses acetate to produce CH_4 and CO_2 and methylotrophic methanogenesis uses methyl, methylamines, methyl-sulfides (Conrad, 2020) (**Fig. 9**). This last is commonly observed in saline environments and uses the « non-competitive » methanogenic substrates (Conrad, 2020).

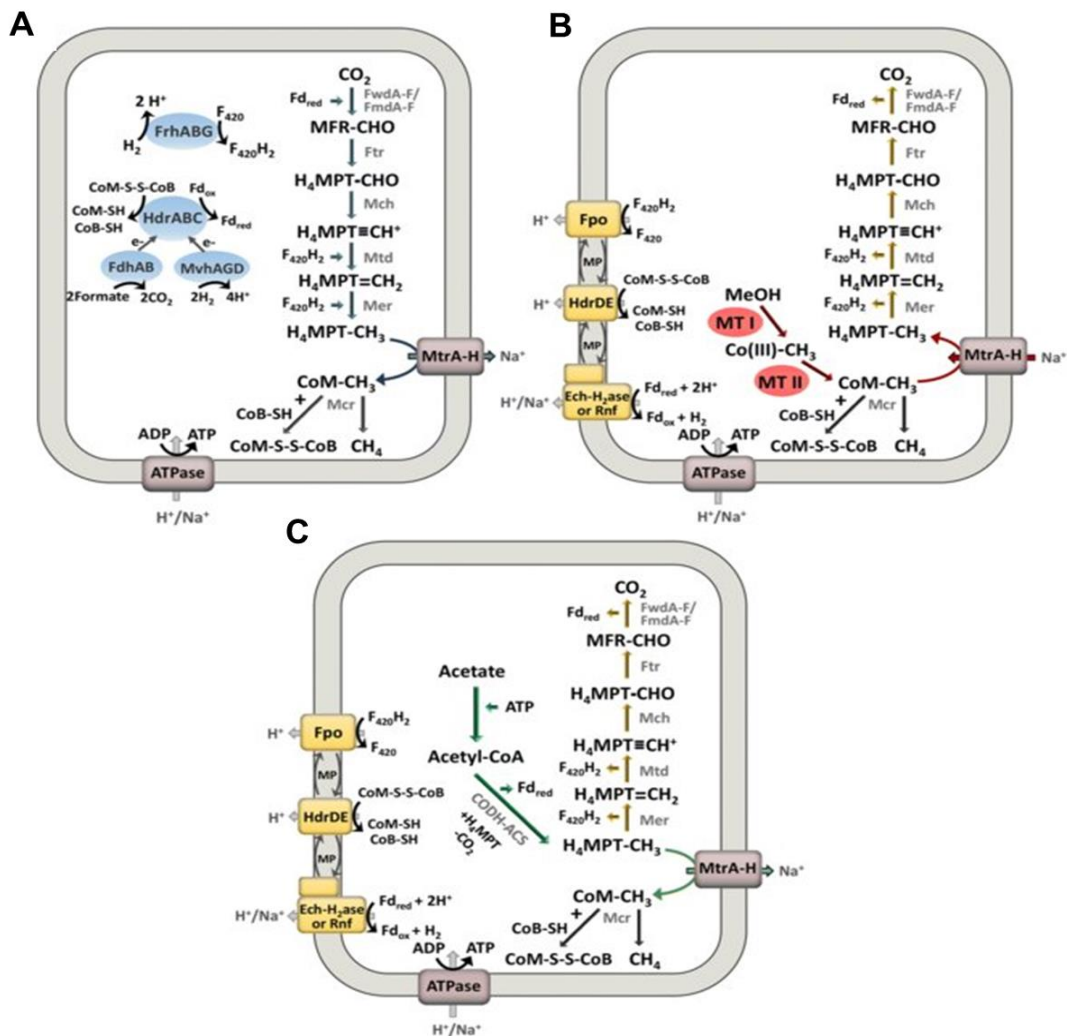


Figure 9: Methanogenesis pathways. A) Hydrogenotrophic, B) methylotrophic and C) acetoclastic methanogenesis pathways. This figure is from Kurth *et al.* (2020).

FwdA-F/FmdA-F: formylmethanofuran dehydrogenase, *Ftr*: formylmethanofuran-tetrahydromethanopterin formyl-transferase, *Mch*: methenyl-tetrahydromethanopterin cyclohydrolase, *Mtd*: methylenetetrahydromethanopterin dehydrogenase, *Mer*: 5,10-methylenetetrahydromethanopterin reductase, *MtrA-H*: tetrahydromethanopterin S-methyl-transferase, *McrABCDG* methyl-coenzyme M reductase, *FrhABG*: coenzyme F_{420} -reducing hydrogenase, *HdrABC*: soluble heterodisulfide reductase, *MvhAGD*: F_{420} -non-reducing hydrogenase, *FdhAB*: formate dehydrogenase, *FpoA-O*:

F420H2 dehydrogenase, HdrDE: membrane-bound heterodisulfide reductase, Ech-H2ase: energy-converting hydrogenase, Rnf: Na⁺-translocating ferredoxin:NAD⁺ oxidoreductase complex, ATPase: ATP synthase, CODH-ACS: Acetyl-CoA decarbonylase/synthase, MTI and MTII: methyltransferase, CoB: coenzyme B, CoM: coenzyme M, H4MPT: tetrahydromethanopterin, MFR: methanofuran, Fd: ferredoxin, F420H2: reduced coenzyme F420, MP: methanophenazine, CO(III): cobalamin binding protein.

The methanogens are strict anaerobes. These archaea dominate the last step of the organic matter degradation to form methane (CH₄) when the other electron acceptors are absent like O₂, NO₃⁻, Fe³⁺ and SO₄²⁻. They generally use simple carbon molecules with 1 or 2 carbon atoms like methanol, formate, acetate and methylamines. Some of them can use choline, glycine or betaine (Watkins et al., 2014, 2012) while others can do CO₂ respiration by using hydrogen as a electron donor.

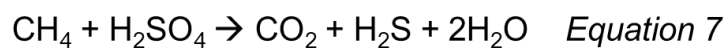
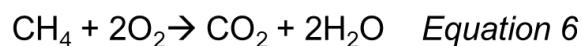
The methanogens are thermodynamically disadvantaged when they enter in competition with the sulfate-reducers for some substrates like acetate and hydrogen. In marine sediments where sulfate molecules are present, the methanogenesis persists by using substrates non-competitive like the methylamines, the dimethylsulfoniopropionates and the dimethylsulfides which are not preferentially used by the sulfate-reducers and which are present in high concentrations in microbial mats (Bolhuis and Stal, 2011). The hypersaline mats present high levels of methane production (Hoehler et al., 2001).

2.1.7 The methylotrophs

Methylotrophy is the ability to use reduced one-carbon compounds, such as methanol, as a single source of carbon and energy. Methylotrophic species have been characterized as belonging to *Alpha*-, *Beta*-, and *Gammaproteobacteria*, *Actinobacteria*, *Firmicutes*, *Verrucomicrobia*, and a *Candidatus* phylum NC10 (Chistoserdova et al., 2009).

The methylotrophs are separated into two groups: the methanotrophs, which metabolize methane as a sole carbon and energy source, and the non-methanotrophic methylotrophs that use methanol and other partially oxidized methane metabolites (Hanson

and Hanson, 1996). Methylotrophs should not be confused with methylophilic methanogens. The methanotrophs are composed of the aerobic methanotrophic bacteria (**Equation 6**) (Bürgmann, 2011; Knittel and Boetius, 2009) and the anaerobic methanotrophic archaea (ANME), which perform anaerobic oxidation of methane (AOM) (**Equation 7**) in the upper subsurface sediment, where sulfate but no oxygen is present (Knittel and Boetius, 2009; Krüger et al., 2003). The ANME belong to three distinct clusters of *Euryarchaeota* named ANME-1, -2, and -3 (Knittel and Boetius, 2009).



The methylophilic bacteria are chemolithoautotrophs (Franks and Stolz, 2009). Despite this, *Methylobacterium extorquens*, which is a pink-pigmented facultative methylophilic bacterium, possesses a genome with the complete information to do anoxygenic photosynthesis but no evidence of photosynthesis was done (Peyraud et al., 2011). *Methylobacterium radiotolerans* (previously called *Pseudomonas radiosa*) presents bacteriochlorophyll-protein complexes (Nishimura et al., 1989). *Paracoccus denitrificans* is an autotrophic methylophilic bacterium (Chistoserdova et al., 2009).

ANME perform different metabolisms according to the electron acceptor (Cui et al., 2015). The methylophilic bacteria have an important role in the carbon cycle but they also participate in the nitrogen cycle, some species being capable of nitrogen fixation, denitrification, or both (Chistoserdova, 2015). The methanotrophs have a major role in the natural capture of most of the methane, produced *via* methanogenesis, or non-biogenic methane.

The methylophilic bacteria have been ever observed in microbial mats (Buckley et al., 2008; Paul et al., 2017). Anaerobic oxidation of methane has been observed in sediments with methane concentrations like those observed in intertidal mat systems. In the Great Sippewissett Salt Marsh, both aerobic and anaerobic methanotrophs have a role in limiting

methane emissions from the mat system (Buckley et al., 2008). It seems that ANME-1 dominate in hypersaline environments (Cui et al., 2015).

2.1.8 The other metabolisms found on microbial mats

a- Fermentation

The fermentative bacteria perform the preliminary steps of organic matter degradation and provide substrates for sulfate-reducing bacteria. The ability to ferment is widespread among bacteria and archaea. Recent studies of the Elkhorn Slough microbial mats in Monterey Bay (USA) have shown that *Microcoleus* spp., the most abundant cyanobacterial group in this mat, was among the major fermenters (Burow et al., 2013). These cyanobacteria ferment photosynthate to organic acids, CO₂ and H₂ through multiple pathways and *Chloroflexi* microorganisms take up these organic acids for their growth (Burow et al., 2013). Fermentative and strictly anaerobic bacteria have also been shown to reduce nitrate into ammonium in sediments on the French Mediterranean coast resulting in the preservation of nitrogen in its biologically available form (Bonin et al., 1998).

b- Diazotrophy

The marine diazotrophs are essential microorganisms because they transfer the atmospheric nitrogen to bioavailable nitrogen in the biosphere (Boatman et al., 2017; LaRoche and Breitbarth, 2005; Tang et al., 2019; Zehr et al., 1995). Nitrogen is an essential element for life because it is then assimilated into amino acids and proteins to synthesize biomass (Cabello et al., 2009; Howarth, 2014). They fix dinitrogen (N₂) by reducing it into ammonium (NH₄⁺).

In most marine microbial mats, diazotrophic cyanobacteria commonly perform the fixation of N₂ and are essential to make available nitrogen for the microbial community (Bauersachs et al., 2011). On the southern North Sea, the filamentous non-heterocystous cyanobacterium *Lyngbya aestuarii* (previously assigned as *Oscillatoria*) is the most prominent

N₂-fixer in most intertidal microbial mats but many other unicellular, filamentous non-heterocystous and heterocystous cyanobacteria also supply nitrogen (Bauersachs et al., 2011; Severin and Stal, 2008). Other microorganisms also participate in the N₂ fixation. Some studies have shown that in intertidal microbial mats, sulfate-reducers and other heterotrophic bacteria have particular importance in the fixation of N₂ (Steppe and Paerl, 2002, 2005; Zehr et al., 1995). Purple sulfur bacteria have also been shown to make high rates of N₂ fixation in hypersaline microbial mats (Pinckney and Paerl, 1997).

c- Nitrification and denitrification

The nitrifying microorganisms are aerobes and chemolithoautotrophs oxidizing nitrogen (Franks and Stolz, 2009). Nitrification is an obligatory aerobic process.

Denitrifying bacteria are facultative aero-anaerobic heterotrophic bacteria that can use oxidized forms of nitrogen, often nitrate or nitrite, as a terminal electron acceptor and reduce it to dinitrogen.

d- Metal associated metabolisms

Other microbial metabolisms are present in microbial mats. Their abundance was less important than the other communities, but their presence was not less important. It is often metabolisms linked to metal, such as iron-oxidizing, iron-reducing microorganisms *etc.*

Cable bacteria have been notably observed in marine sediment (Geelhoed et al., 2020; Hermans et al., 2019). These bacteria are multicellular and filamentous bacteria belonging to the deltaproteobacterial family *Desulfobulbaceae* (Pfeffer et al., 2012). They transport electrons over centimetre distances (Nielsen et al., 2010; Risgaard-Petersen et al., 2012) allowing to couple the sulfide oxidation in deeper anoxic sediment layers with the reduction of oxygen or nitrate in the sediment-water surface, making them sulfur-oxidizing bacteria (Marzocchi et al., 2014; Nielsen et al., 2010) (**Fig. 10**). These bacteria are positioned vertically thanks to their motility (Bjerg et al., 2016; Malkin and Meysman, 2015). Cable bacteria and other sulfur-oxidizing bacteria, such as *Beggiatoa*, can co-occur suggesting competition for

the same ecological niches (Seitaj et al., 2015). However, the only source of H₂S for the *Beggiatoaceae* family is from sulfate-reduction, whereas cable bacteria can dissolve FeS (Seitaj et al., 2015; Sulu-Gambari et al., 2016). An seasonally alternance of *Beggiatoa* and cable bacteria have also been shown in a deep gully of a lake (Seitaj et al., 2015).

Cable bacteria oxidise sulfide and avoid euxinia in the upper layers (Seitaj et al., 2015). It also results in the release of protons and therefore a decrease in pH (Nielsen et al., 2010). This acidification leads to the FeS and CaCO₃ dissolution provoking the deposition of solid ferric iron minerals (Sulu-Gambari et al., 2016). This layer of ferric iron oxides may act as a firewall between the layers of oxygenic and anoxygenic phototrophs, protecting the cyanobacteria from sulfide and the purple sulfur bacteria from oxygen in microbial mats (Seitaj et al., 2015; Stal, 2001). Stal *et al.* (2019) developed the hypothesis that cable bacteria could participate to the construction of this solid layer (**Fig. 10**). Cable bacteria have been observed in photosynthetic biofilm (Malkin and Meysman, 2015), but to our knowledge, no one has been identified in microbial mats.

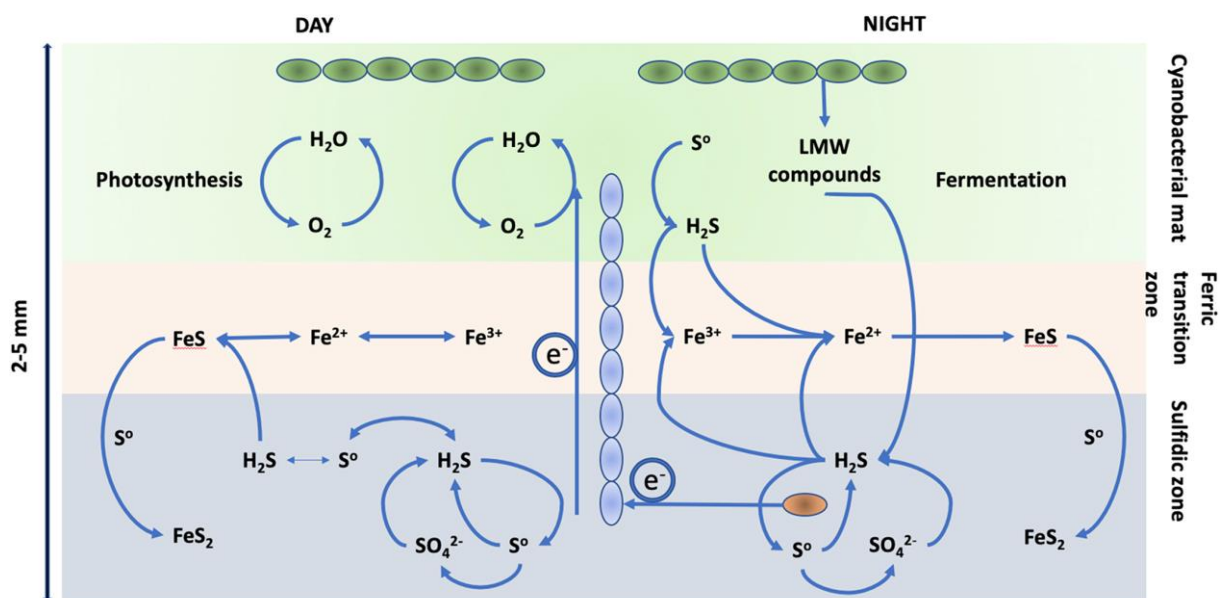


Figure 10: Cable bacteria metabolisms. Scheme of the cable bacteria metabolisms within a cyanobacterial mat and the hypothetical production of an iron 'firewall' between the oxygenic photosynthetic layer of cyanobacteria and the permanent anoxic sulfidic layer. This figure is from Stal *et al.* (2019).

2.2 Eukaryotic communities

Like for Bacteria and Archaea, there is a large diversity of eukaryotes colonizing microbial mats from different environments such as hot springs (Aguilera et al., 2010), polar regions (Jungblut et al., 2012), estuaries (Coull, 1999), hypersaline environments (Alexander et al., 2009; Elloumi et al., 2009) *etc.* Eukaryotes also live in several habitats with less favourable environmental conditions like extreme pH, temperature or pollution by metals (Aguilera et al., 2010; Cvitković et al., 2011). Temperature is one of the main factors determining the distribution and abundance of species due to its effect on enzymatic activities. In aquatic environments, eukaryotes are classified according to their size (macro-, meio-, micro-, nano-, pico-) or their type (auto-, phyto-, hetero-). For example, meiofauna includes eukaryotic organisms with a size comprise between 40 µm and 1 mm. It is a major part of marine mats and plays important roles in their ecosystem (Cvitković et al., 2011; El-Serehy et al., 2016; Franks and Stolz, 2009).

Eukaryotes in general have diverse lifecycles and include primary producers as well as primary and secondary consumers. Diatoms are often the dominant primary producers of the ecosystem with cyanobacteria (Jonkers and Abed, 2003). Several taxa have been observed in microbial mats including members of the *Bacillariophyta*, *Chlorophyta*, *Rhodophyta*, and *Euglenophyta* phyla as well as ciliates, amoebae and stramenopile (Aguilera et al., 2010).

Microbial mats are considered like a refugium for some eukaryotes reducing, for example, oxidative, osmotic, freeze-thaw, and dehydration stresses (Jungblut et al., 2012). The microbial mats are rich in inorganic nutrients (Bonilla et al., 2005), recycled organic matter and bacteria (Varin et al., 2010), providing food for eukaryotic heterotrophs such as ciliates and the metazoan microfauna. Saprophytic, phagotrophic, parasitic and predatory eukaryotes have been observed, increasing the nutrient and energy transfer within the mat and thus, increasing trophic complexity and potential resilience to environmental change (Duffy and Stachowicz, 2006). Grazing by meiofauna has a major role in the development of microbial mats (Fenchel, 1998; Stal, 2012). Microbial mats participated in the oxygenation of the Earth

leading to the appearance of grazers which then contributed to the rarefaction of microbial mats. Currently, it is therefore generally thought that microbial mats only thrive in environments that largely exclude grazing organisms (*e.g.*, extreme environments) to avoid grazing. But it seems that it is most probable that a balance between microbial mats and grazers occurs, grazing permitting to avoid the accumulation of cyanobacteria in microbial mats (Stal, 2012, 1995) and bacteria that could also produce EPS, limiting some grazers that would otherwise destroy mat integrity, as suggested for temperate regions (Stal, 2012).

2.3 Viruses

Viruses are diverse, abundant, and important ecological components of microbial communities, acting as key players in biodiversity and organic matter fluxes. In sediments, viruses have been described to affect prokaryotic host mortality, spatial distribution and biogeochemical cycles. Studies on the ecological role of viruses in ecosystems are few (Carreira et al., 2015).

Little is known about viruses (bacteriophages) in microbial mats but, they are observed and surely important factors for carbon and nutrient recycling and probably also contribute to genetic exchange and bacterial evolution in the mat (Brüssow et al., 2004). They control the development of microbial mats (Hennes et al., 1995) participating, for example, in the cellular lysis and recycling of bacteria, archaea, and microbial eukaryotes (Pedrós-Alió et al., 2000; Varin et al., 2010).

A higher amount of phages were observed in submerged marine cyanobacterial mats (Hennes and Suttle, 1995). *Alpha-*, *Beta-*, *Gammaproteobacteria* phages and cyanophages were observed in microbial mats (Varin et al., 2010).

3. Adaptation of microbial mats in response to environmental changes

Microbial mats are heterogeneous at the micro- and macroscopic scales. At the microscopic level, physical-chemical gradients of light (quantity and quality), temperature, oxygen, pH, redox potential, salinity and available electron acceptors in the water column and the sediment are observed and at a macroscopic scale, tide, precipitation, vegetation and bioturbation *etc.* Microbial mats also differ depending on the area, even comparing two mats a few square kilometres apart (Bolhuis et al., 2013) and the season (Cardoso et al., 2019; Desnues et al., 2007; Passarelli et al., 2015; Prieto-Barajas et al., 2017).

3.1 Physical-chemical microgradients within the microbial mats

Different metabolisms occur in the microbial mat, resulting in the establishment of vertical physical-chemical microgradients of oxygen, sulfur, hydrogen ions and other chemical species as well as light intensity and its spectrum (Jorgensen et al., 1983; Revsbech et al., 1983). The physical-chemical gradients also show strong variations during the nycthemeral cycle. This leads to changes in environmental conditions for mat microorganisms.

For example, during the day, the light radiation available at the surface for oxygenic phototrophs induces a significant production of oxygen (**Fig. 11**). This oxygen penetrates to the level of the first millimetre of the mat and then decreases sharply and disappears under the action of aerobic heterotrophic bacteria that consume it (**Fig. 11**). On the other hand, a sulfur gradient appears due to the reduction of sulfate by the sulfate-reducers at depth. This high concentration of sulfur disappears abruptly between the first and the second millimetre, under the action of sulfur-oxidizing bacteria, phototrophic or not (**Fig. 11**). The result is an anaerobic zone rich in sulfur separated from an aerobic zone. During the night, there is no light gradient, which means that there is no photosynthetic activity of the cyanobacteria, which leads to a rapid depletion of oxygen in the entire mat, which is therefore mainly anoxic (**Fig. 11**).

Anaerobic metabolisms of dissimilatory sulfate-reduction become dominant, the sulfide invades all the mat on the surface. The pH also shows variations during the day, increasing at the surface due to the high photosynthetic activity of the cyanobacteria and the low buffering capacity of the mat, then decreasing at depth.

These vertical microgradients lead to a stratification of the microbial mat, which provides the capacity to face the great variation of the physical-chemical parameters.

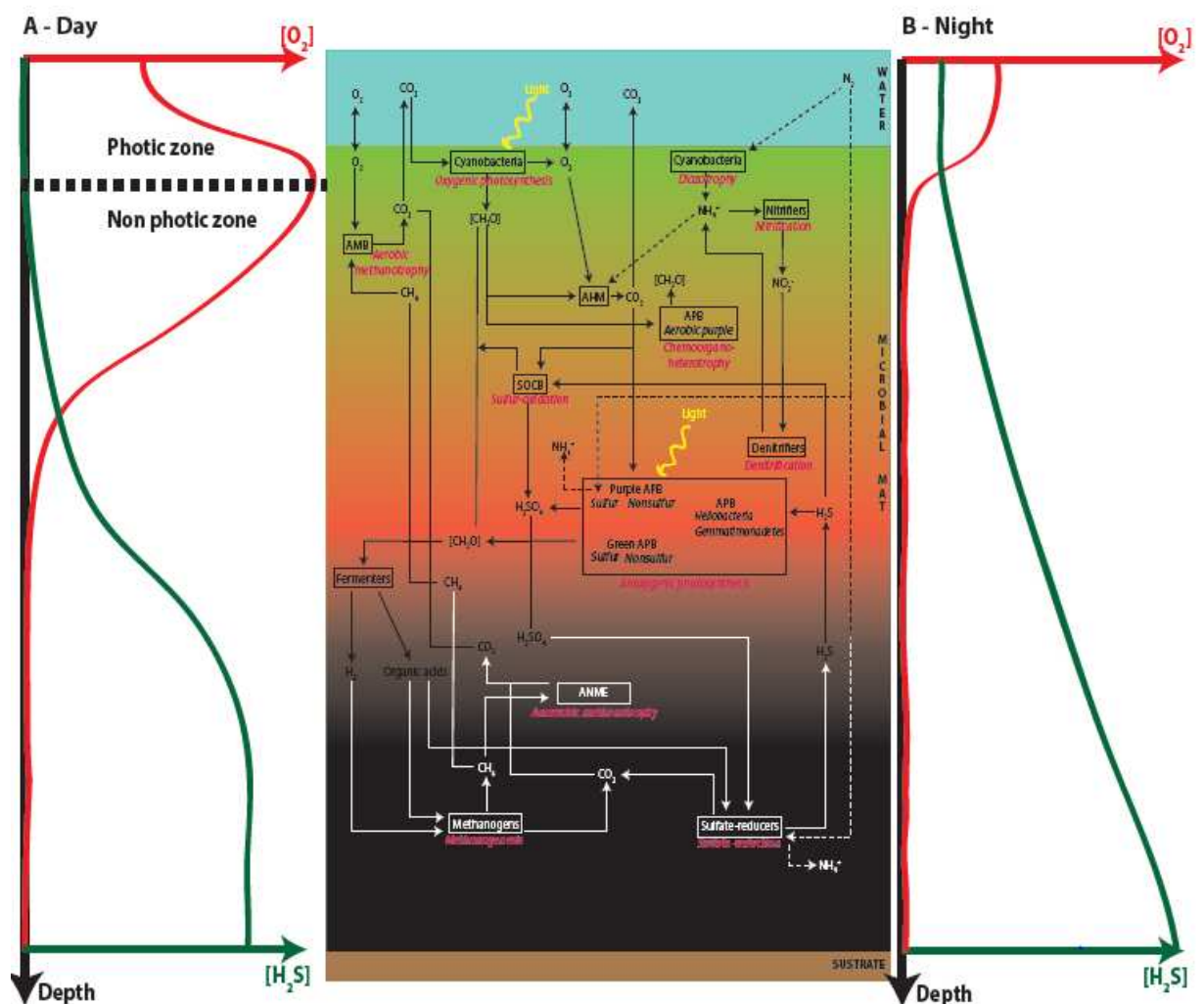


Figure 11: Light, oxygen and sulfur gradients in a microbial mat. Schematic view of these three gradients **A)** during the day and **B)** during the night. The schematic view at the middle represents a microbial mat during the day.

3.2 Natural dynamics of the microbial mat in their environment

The diversity and the composition of a microbial mat at the microscopic level are very influenced by its physical-chemical environment at the macroscopic level. The physical parameters are mainly defined by abiotic processes while the chemical processes are modified by microbial activities (Franks and Stolz, 2009). Each ecosystem has its defined parameters. Microbial mats face different natural and human modifications of environmental parameters occurring either in short-term (*e.g.*, daily variations, salt exploitation) or long-term (*e.g.*, climate change, recurrent pollution).

One of the major parameters driving the microbial mat organization is the light. Photoautotrophic communities' diversity and abundance depend largely on the amount of light (or light quantity) and the wavelengths (light quality) that is used by the light pigments and photosystems. The average amount of light that illuminates a surface on a sunny day is 1000 to 2000 $\mu\text{E}\cdot\text{m}^{-2}\cdot\text{s}^{-1}$ (Franks and Stolz, 2009). On the water column, the light is attenuated by the presence of particles and organisms and on the sediment, its depth penetration can be reduced depending on the sediment type. Most phototrophs are adapted to low light intensities. For cyanobacteria found in the microbial mats of Mellum Island in the North Sea, the optimum light intensity is 50 to 150 $\mu\text{E}\cdot\text{m}^{-2}\cdot\text{s}^{-1}$ (Stal et al., 1985). Purple sulfur bacteria from the same mats use from 5 to 10 $\mu\text{E}\cdot\text{m}^{-2}\cdot\text{s}^{-1}$ (Stal et al., 1985). Several strategies have been developed by microbial communities of mats to obtain the appropriate amount of light. *Cyanobacteria* produce carotenoids and other light attenuating products (*e.g.* scytonemin). (Hirschberg and Chamovitz, 1994; Palmisano et al., 1989; Rastogi et al., 2015). Some phototrophs are also specialized in the capture of rare photons in light-limited environments. For example, green sulfur bacteria containing bacteriochlorophyll *e* have been found at 100 m depth in the Black Sea (Manske et al., 2005). Geographic location is also important regarding the growing season of mats. Equatorial mats show little annual change, northern and southern latitudes are subject to seasonality, and arctic and antarctic systems are subject to month long extremes of constant light or darkness.

Moreover, in the same environment, the evolution of light harvesting structures and photosystems permit to the different phototrophic organisms to use different wavelengths of light. Cyanobacteria possess thylakoids with chlorophyll *a* (680 nm) and phycobilins (*e.g.*, phycoerythrin, phycocyanin), green anoxygenic phototrophs have chlorosomes with bacteriochlorophyll *c* (740 nm), *d* (725 nm) or *e* (714 nm), and purple anoxygenic phototrophs have intracytoplasmic membranes with bacteriochlorophyll *a* (800–890 nm) or bacteriochlorophyll *b* (1015 nm) (Frigaard, 2016; Madigan et al., 2000; Madigan and Jung, 2009; Scheer, 2006). Thus, a large variety of phototrophic microorganisms can coexist thanks to these different photosystems. Moreover, water is a natural attenuator of light, absorbing most of the infrared wavelengths in the first meter. The longer wavelengths penetrate further into shallow water sediments (Jørgensen and Des Marais, 1986), allowing the dominance of anoxygenic green and purple phototrophs in these layers. Flat laminated mats found in very shallow pools, lagoons, and salt marshes often have a distinct layer of anoxygenic purple.

On temperate coastal regions, seasons are one of the main drivers of environmental changes. Microbial mats have to face with high temperatures in summer and cold temperatures in winter, and a variation of the precipitation according to the season. These allow for a variation of the different other physical-chemical parameters, such as pH, nutrients availability and storage, salinity, dissolved oxygen *etc.* and therefore the modification of the structure of microbial mats (Cardoso et al., 2019; Desnues et al., 2007; Passarelli et al., 2015; Pierre et al., 2014). Anthropogenic impacts have also been reported to impact the structure of microbial mats like in salterns (Mazière et al., 2021).

Table 1: Photosynthetic information about phototrophic communities of microbial mats. This table resumes the reaction center and pigments present on each phototrophic community, the absorption wavelength, the electron donor and the performed metabolism. Modified from George *et al.* (2020).

PS: photosystem; Chl: chlorophyll; BChl: bacteriochlorophyll.

Microbial group	Reaction center	Photosynthetic pigments	Absorption wavelength
<i>Cyanobacteria</i> Prochlorophytes (also called type II <i>cyanobacteria</i>) Green algae	Types I and II	Chl <i>a</i> , Chl <i>b</i> and phycobilines	Chl <i>a</i> : ~ 430 nm and ~ 680 nm Chl <i>b</i> : ~ 460 nm and ~ 650 nm
Purple sulfur bacteria	Type II	BChl <i>a/b</i> , carotenoid pigments such as spirilloxanthin, spheroidene, lycopene, and rhodopsin	BChl <i>a</i> : ~ 800/ 815–960 nm. BChl <i>b</i> : a range of 835–850 and 1010–1040 nm
Purple non-sulfur bacteria	Type II	BChl <i>a/b</i> and carotenoid pigments such as spirilloxanthin, spheroidene, lycopene, and rhodopsin	BChl <i>a</i> : ~ 800/ 815–960 nm. BChl <i>b</i> : a range of 835–850 and 1010–1040 nm
Green sulfur bacteria	Type I	BChl <i>c, d</i> and <i>e</i> organized into chlorosomes. Carotenoid pigments such as chlorobactene, γ -carotene isorenieratene and derivatives (OH-chlorobactene and β -isorenieratene)	Bchl <i>c</i> : ~460, 730-760 nm, Bchl <i>d</i> : ~440, 720-750 nm, Bchl <i>e</i> : ~460, ~715 nm
Filamentous anoxygenic phototrophic bacteria	Type II	BChl <i>a</i> or <i>a</i> and <i>c/d</i> . Different carotenoid pigments such as carotene, β -carotene, OH- γ -caroteneglucoside ester, keto-OH- γ -carotene, keto-myxocoxanthin, myxobactene, methoxy-keto-myxocoxanthin, keto-myxocoxanthin glycoside ester are present depending on the family.	720–878 nm

<i>Heliobacteria</i>	Type I	BChl <i>g</i> . Carotenoid pigments such as 4,4' - diaponeurosporene, OH-diaponeurosporene glucoside esters.	<400, 780-850 nm
<i>Acidobacteria</i>	Type I	BChl <i>c</i> , BChl <i>aP</i> , Chl <i>aPD</i> and Zn-BChl <i>a'P</i> . Carotenoid pigments such as Echinenone, canthaxanthin, lycopene, γ and β - carotene may be present	Infrared light between 740–750 nm
<i>Gemmatimonadetes</i>	Type II	BChl <i>a</i>	BChl <i>a</i> : 816 and 866 nm

Salinity has been shown to be a major driver of the diversity and the structure of microbial mats (Ben Salem et al., 2019; Coull, 1999; Fei Xi et al., 2014). Richness and abundance of bacteria and eukaryotes decrease along an increased salinity gradient (Benlloch et al., 2002; Estrada et al., 2004; Nubel et al., 2000; Pedrós-Alió et al., 2000). Salinities above 100 psu led to the decrease of growth photosynthesis and oxygen consumption in microbial mats, suggesting a salt adaptation of the microorganisms and therefore a resilience accompanied by an adjustment of their diversity and function (Raeid M. M. Abed et al., 2007). Bolhuis et al., (2013) showed that salinity gradient in an intertidal environment impacted the composition of the primary producers of microbial mats with marine mats dominated by diatoms, intermediate brackish mats dominated by *Cyanobacteria* and freshwater mats dominated by *Cyanobacteria* and freshwater green algae. Other microbial activities have been shown to be modified by variations of the salinity, such as cyanobacterial nitrogenase transcription inhibited by increasing salinity (Severin et al., 2012). However, a more variable active diazotrophic community was observed in microbial mats which are naturally exposed to frequent salinity changes (Severin et al., 2012).

3.3 Microbial responses faced to climate change

Some studies have been performed on climate change on specific microbial communities, often evaluating the effect of one change (*e.g.*, acidification, warming...). The impact of climate change on microbial mats is still unknown. Temperature affects the composition, the photosynthetic performance, the growth, the biomass and the physiology of microphytobenthos (Cartaxana et al., 2015; Hancke and Glud, 2004). Sarmiento *et al.* (2010) showed that warming leads to the increase of heterotrophic bacterial respiration and production if enough resources are available. Grazers are affected by the increase of the bacterial losses and thus bacterial–grazer biomass flux within the microbial food web (Sarmiento et al., 2010). The increase of bacterial losses to grazing is observed at lower rates than bacterial production (decreasing the proportion of production removed by grazers) (Sarmiento et al., 2010). Thus, the abundance of heterotrophic bacteria on the oceans is supposed to increase and reinforce the already dominant role of microbes in the carbon cycle of a warmer ocean.

Acidification is thought to have effects mainly at the metabolic level, favouring the growth of some microorganisms (Baragi and Anil, 2016; Black et al., 2019; Hicks et al., 2011) but also increasing the energy cost for maintaining intracellular pH homeostasis and respiratory processes (Beardall et al., 2009; Black et al., 2019; Gao et al., 2012). Studies on diazotrophic cyanobacterium *Trichodesmium* have concluded that ocean acidification will enhance their growth and N₂ and CO₂ fixation, fundamentally altering the current marine nitrogen and carbon cycles and potentially driving some oceanic regimes towards phosphorus limitation (Hutchins et al., 2007; Shetye et al., 2013). But other diazotrophs are not favoured by seawater acidification such as *Nodularia spumigena* those cell division rates and nitrogen fixation rates are reduced (Czerny et al., 2009). The abundance of total heterotrophic bacteria did not differ in the mesocosms experiment under acidified conditions, whereas bacterial protein production increased (Grossart et al., 2006). Extracellular enzyme activities are also altered by an elevated level of pCO₂. Higher activity of bacterial protease, α-glucosidase and

β -glucosidase was observed by Grossart *et al.* (2006). Increased microbial polysaccharide degradation was also reported (Piontek *et al.*, 2009). One of the most probable consequences of this increased extracellular enzymes activity is the increase in the availability of simple carbon sources (Mangwani, 2015). Acidification and warming also affect the characteristics of EPS of diatoms and cyanobacteria with a modification of their composition (Li *et al.*, 2016; Ma *et al.*, 2019).

Microbial species composition of natural biofilm found in the Great Barrier Reef was modified under acidified conditions, with a decrease of *Alphaproteobacteria* and an increase of *Flavobacteriales* (Witt *et al.*, 2011). Witt *et al.* (2011) have also reported that carbon and nitrogen contents are increased and O₂ fluxes remained unchanged. They suggest that bacterial biofilm communities rapidly adapt and reorganize in response to acidified conditions to maintain activity such as oxygen production. The change in the structure communities of microbial biofilm is also supposed to affect grazers. Moreover, some effects have been seen at the metabolic level. Lidbury *et al.* (2012) observed that the content of the EPS matrix was modified with an increase of the uronic acid. Ahrendt *et al.* (2014) showed that elevated CO₂ levels did not alter the microbial diversity, community structure, or carbonate precipitation in the microbial mats. They also observed the enrichment of some key taxa, such as the sulfate-reducing bacteria *Deltasulfobacterales* (Ahrendt *et al.*, 2014).

4. Techniques for studying microbial mats in microbial ecology

Microbial ecology is the study of the ecology of microorganisms to understand their interaction with one another and with their environment. Several methods exist to study microorganisms: microbiological approaches and molecular biology approaches.

4.1 Cultivation approaches

Traditional cultivation techniques make it possible to describe the morphological, metabolic and physiological characteristics of microorganisms in a given ecosystem. This method allows to work on pure strains to study a microorganism and some of their functions precisely. The main limitation is that a small fraction of the various microorganisms in an environment has been isolated. Indeed, only 0.1 to 3% of the bacteria in a community would be cultivable under laboratory conditions (Amann et al., 1995), which is also the case for microorganisms from stratified microbial mats (Franks and Stolz, 2009). Another important limitation is that the physiological behaviour of microorganisms is different *in vitro* and *in vivo*. Finally, very little information on the interactions between various microorganism species is available using this type of approach. It is therefore essential to complement the data obtained from these microbiological culture techniques with broader studies involving other (or complementary) approaches.

4.2 Biogeochemical and microscopic methods

Biogeochemical approaches allow to characterize the functioning of microbial mats for example in their environment. In microbial mats, microsensors or microelectrodes have been used to detect the microvariations of several molecules such as O₂, S²⁻ or pH. These measures are very important to determine the structure and the functioning of microbial mats, *e.g.*, in characterizing the oxic-anoxic interface. Isotopic markings and some microprobes also measure the production/consumption rate of microbial activities.

Microscopy has also been used to characterize microbial mats structure with confocal or fluorescence microscopies. The determination and biomass estimation has also been done for some microorganisms with distinct morphologic characteristics, such as cyanobacteria (Solé et al., 2009).

However, these methods didn't allow to have access to the diversity of microorganisms.

4.3 Molecular biology methods

In 1977, ribosomal ribonucleic acid gene (*rRNA* gene) was defined as a marker gene for phylogenetic analysis (Woese and Fox, 1977). For prokaryotic communities, the *16S rRNA* gene, composing the 30S small subunit of a prokaryotic ribosome (SSU rRNA), was used. For eukaryotic communities, its homologue is the *18S rRNA* gene composing the 40S SSU ribosome. These two genes present several benefits: they are ubiquitous (*i.e.*, present in all prokaryotes or eukaryotes), preserved, divergent enough to distinguish taxa, one copy per genome, and have low evolutionary rate and low capacity for horizontal transfer (Normand et al., 2011). Moreover, an associated rich database named SILVA is often updated. However, the associated primers (*i.e.*, universal primers) amplify sequences from many taxa, but the taxonomic information they provide differs according to the target environment and the region of the gene to be amplified, especially when using short fragments (Soergel et al., 2012). Moreover, the *16S rRNA* gene is present until 15 copies in the genome of some prokaryotes (Rainey et al., 1996) and variabilities have been observed between these copies of the same genome (Yap et al., 1999). To counteract these drawbacks and complete the data, other very well-known marker genes can be used: ITS (internal transcribed spacer) for fungi (Schoch et al., 2012), *cytochrome c oxidase subunit 1* (COI) gene for animals (Hebert et al., 2003), prokaryotic functional genes like *dsrB* for sulfate-reducers (Müller et al., 2015; Pelikan et al., 2015), *mcrA* for methanogens (Luton et al., 2002; Yang et al., 2014), *nifH* for nitrogen-fixing bacteria (Gaby and Buckley, 2014; Turk et al., 2011), *etc.*

The sequencing consists of determining the sequence of the bases of all the DNA contained in the cells of an organism. In 1977, Sanger sequencing was the first approach allowing the determination of DNA nucleotide sequences (Sanger et al., 1977). This method comprises the following steps. A mix of the unknown sequence with nucleotides (dNTPs) and dye-labelled nucleotides (ddNTPs) is done. Each nucleotide, adenine (A), thymine (T), cytosine (C) or guanine (G) has an associated specific colour (*e.g.*, A in red, T in blue, C in

green and G in purple). Then, a polymerase chain reaction (PCR) is performed leading to the production of complementary sequences. When a ddNTP is randomly added to this sequence, the reaction is stopped. Several complementary sequences are therefore performed with different sizes. An electrophoresis migration is carried out on this mix allowing to determine the complementary sequence and then the unknown sequence (**Annexe 1**). The first genomes were sequenced with this method. It is currently the one that sequences the longest DNA sequence (up to 800 bases) and makes the fewest errors. However, Sanger sequencing only sequences a single DNA fragment at a time.

In 1987, environmental DNA (eDNA) was first mentioned (Lozano Mojica and Caballero, 2021; Ogram et al., 1987). Then, a lot of studies were carried out on microbial eDNA leading to the development of next-generation sequencing (NGS) technologies or high throughput sequencing in 2005. They allowed performing a cheaper and rapid sequencing of eDNA. In contrast to Sanger sequencing, NGS technologies sequence several DNA sequences at the same time. This led to the expansion of microbial ecology assessing biodiversity. NGS are omics approaches separated into two groups, metabarcoding and metagenomic approaches, and metatranscriptomic approaches (*e.g.*, RNA-seq).

Metabarcoding is a standard approach to describe microbial communities from DNA/RNA directly extracted from environmental samples. It consists of targeting a universal short section of DNA from a specific gene (a barcode) allowing the species identification, combined with high-throughput sequencing. It is divided into 4 steps, (i) DNA extraction from different types of samples, (ii) libraries preparation using specific preparation, (iii) sequencing, and (iv) bioinformatics analyses.

Several sequencing methods were developed to perform metabarcoding: sequencing by synthesis (Illumina), pyrosequencing (Roche 454), sequencing by ligation (SOLid Thermofisher) and detection of the H⁺ ions (Proton Thermofisher). They are based on 3 steps, (i) library preparation, (ii) clonal amplification and (iii) cyclic array sequencing. NGS technologies provide shorter lengths of the sequenced fragments than those obtained by the

Sanger sequencing. Moreover, despite the advantage of generating large libraries with these NGS technologies, many sources of bias have been identified. The diversity observed in analyses of high-throughput sequencing data is sensitive to biases caused by sample preparation, primer selection and the area of the gene that is targeted (Hong et al., 2009). It is also prone to chimeric sequence formation during the PCR step. Chimeras are hybrid products between several parent sequences that lead to misinterpreted new organisms. Sequence libraries vary greatly in quality and contain up to more than 45% chimeric sequences, which is one of the major biases within the libraries (Haas et al., 2011). In addition, the number of reads per sample is difficult to control (Gihring et al., 2012). High-throughput sequencing techniques offer a powerful method for community analysis, but data development and interpretation must be done with care to limit bias.

Shortly after the release of these technologies, third-generation sequencers appeared. They generate long reads of DNA without the amplification step of the fragment, leading to them also being called single-molecule sequencing. The most known technologies are Nanopore and PacBio. However, they still produce many sequencing errors.

Metagenomics methods target the entire genomic content of a sample. High throughput *16S rRNA* gene sequencing is sometimes mistakenly referred to as metagenomics but it is not a metagenomic method, because they target only a specific barcode. Shotgun metagenomics provides information on untargeted (“shotgun”) sequencing of all (“meta-”) microbial genomes “genomics” present in a sample, *i.e.*, on the total genomic DNA from all organisms in a sample (Quince et al., 2017). It allows to avoid the isolation and cultivation of microorganisms, the majority of which cannot be cultivated in the laboratory, or the amplification of targets region, doesn't take into account all the diversity, to study them. Shotgun metagenomic sequencing uses next-generation sequencing (NGS) technology to provide not only information on the taxonomic annotations of each organism but also the functional profiling, gene prediction and microbial interaction of the whole community.

5. Objectives of the thesis

In the current forecasting models the impact of climate change on microbial communities is neglected. The research presented here will help to refine them by including the share of microbial mats, particularly via their role in biogeochemical cycles. Moreover, it is necessary to study these phenomena at the local level because the forecasts are established globally but can change locally (IPCC, 2014).

The main goal of this thesis is to determine the impact of climate change on microbial mats from salterns in the Nouvelle-Aquitaine region (France) according to the most pessimistic predictions of the IPCC for 2100 (IPCC, 2014).

To do this, it is necessary to first do an inventory of the situation of the microbial mats in the Nouvelle-Aquitaine region, particularly we focalized on microbial mats from the island of Ré in order to establish the anthropic and seasonal impact on these structures. Indeed, it is possible that these microbial mats are already exposed to environmental conditions or stresses equivalent to those predicted for the end of the century. Thus, a seasonal monitoring of the microbial mats of the Ré Island was performed.

Then, a mesocosms study was performed to simulate the climate change on these microbial mats and determine how the microbial mats are impacted. The microbial mats in this study were collected in salt marshes, thus in shallow environments. The choice was made to simulate acidification and warming of the ocean surface, the two main parameters that will have a strong impact on these structures. The study presented in this manuscript is based on the previsions the most pessimists (RCP8.5) by the end of the century (2081-2100) (IPCC, 2014).

Chapter II: Experimental procedure

1. Description of the salterns of Ré Island

The microbial mats studied developed in three different solar salt marshes located in Ré Island (46°12'.29"N 1°30'.57"W) in the north of the Nouvelle-Aquitaine region (France) (**Fig. 12**). This region is submitted to a coastal temperate Aquitaine-type oceanic climate corresponding to an alternation of four seasons: winter, spring, summer and autumn. It is windy and marked by a high average amount of sunshine. The annual temperatures vary between 5°C in winter and 20°C in summer. Rainfall is moderate and does not exceed 1,200 mm per year. The autumn and winter are the wettest seasons while the spring and summer are drier seasons, sometimes leading to drought episodes during the summer.

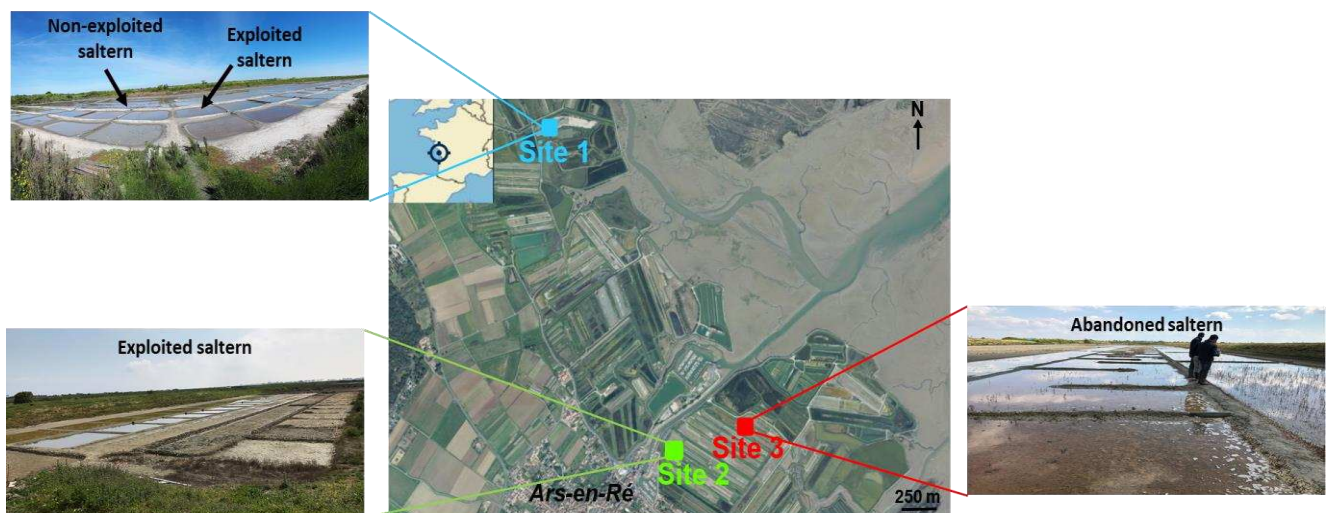


Figure 12: Location of the sampled salterns in Ré Island, France. The blue point represented site 1, a salt marsh with exploited and non-exploited plots, the green point represented site 2, an exploited salt marsh, and the red point represented site 3, an abandoned salt marsh. The pictures on the left and the right of the map were the salt marshes corresponding to each site.

The solar salt marshes of Ré Island are exploited to produce salt by natural evaporation of seawater over a series of ponds. First, the seawater is stored in the “vasais” plot where the mud is deposited by decantation (**Fig. 13**). After, it goes to the “cobier” plot for a second decantation of mud (**Fig. 13**). The seawater salinity is equal to 35 practical salinity units (psu) at this step. Then, the seawater arrived in the “fares” plots which are rectangular basins that allow for a significant increase in the salinity of the water (**Fig. 13**). They are followed by the “adernes” plots (**Fig. 13**). The seawater salinity continues to increase and is stored to fill the

next and last ponds. Finally, the salts are precipitated in the crystallizer ponds where the salinity can reach 350 psu (**Fig. 13**).

The water input depends on the saltern owner (named “saunier”). At the beginning of the spring, the salt marshes owners progressively empty the ponds. They clean them, one by one, scraping off the silt that has accumulated over the winter following the water circuit. Once a plot is cleaned, it is letting dry. In the meantime, the seawater has already started its circuit and is about to give the first salt. From the month of June and often until September, the days are exclusively reserved for the harvest of the salt. Every two days, the Coarse Salt is collected in the morning or the evening. The gathering of Flower of Salt is done every day scrapping the water surface. Winter is the period of rest for the salt marshes. It spends several months covered with water.

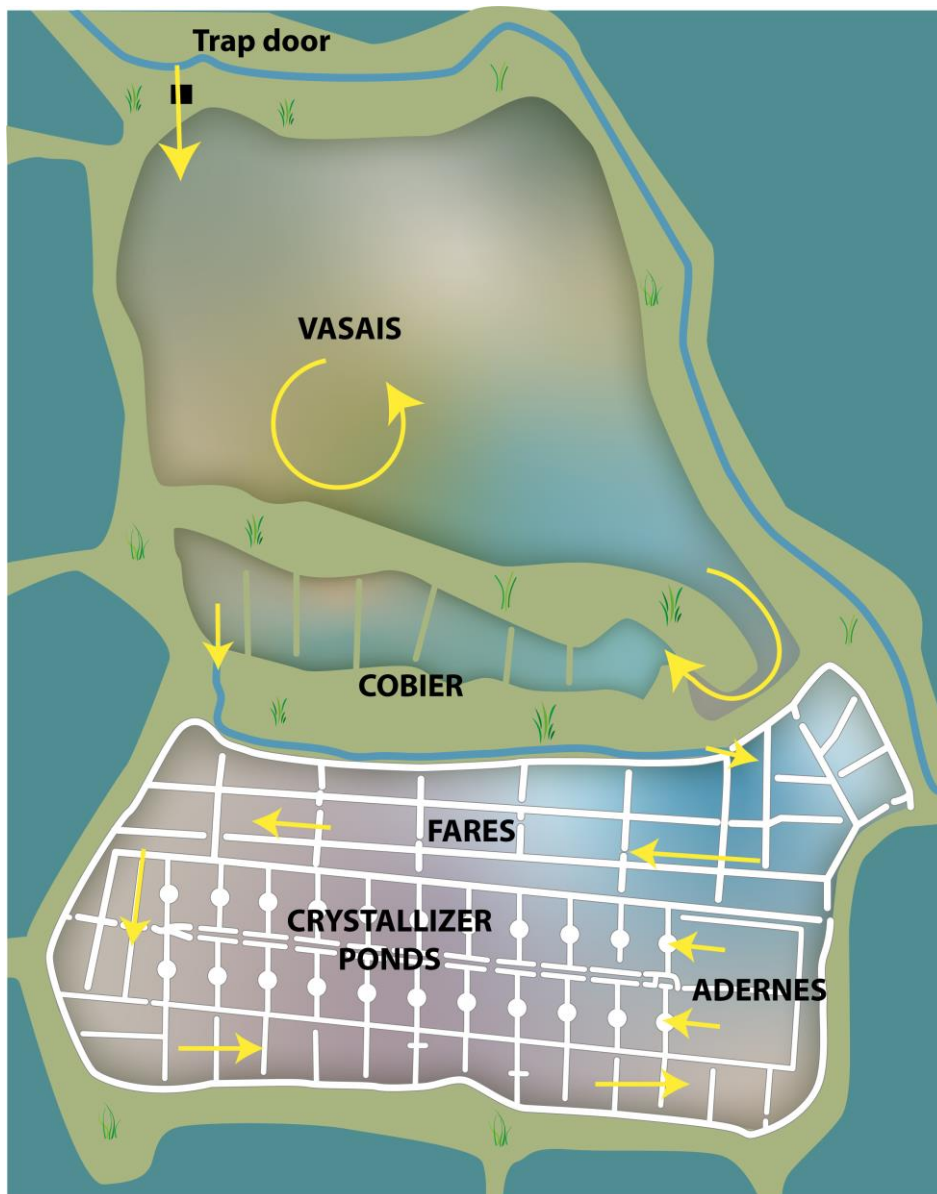


Figure 13: Schematic representation of an exploited salt march. The yellow arrows correspond to the seawater path (from a waterway connected to the ocean to the crystallizer ponds). Based on an illustration of Gildas Buron from the website <https://www.tradysel.com/fr/les-marais-salants/fonctionnement.html> (last view 21/08/28), modified by C. Mazière and T. Guyot.

Salt marshes can be into three statutes:

- **Exploited:** the different plots of the salterns are preserved as well as the precipitation gradient of the salt. The salt is harvested in the crystallizer ponds.
- **Non-exploited:** the different plots are maintained but no salt exploitation is carried out. The precipitation gradient of salt is not conserved. Only the water inlet and outlet are controlled.

- **Abandoned:** no maintenance of the plots occurs and there is no control of the seawater circulation.

2. Microbial mats sampling in salt marshes

2.1 Description of the sampling sites

Microbial mats were sampled in three salt marshes: a salt marsh with exploited and non-exploited plots (Site 1), an exploited salt marsh (Site 2) and an abandoned salt marsh (Site 3) (**Fig. 12**).

2.1.1 Site 1: a salt marsh with exploited and non exploited plots

To determine their natural environmental dynamics, microbial mats were monitored seasonally in a salt marsh located in Ars-en-Ré (46°13'29.9"N 1°31'07.5"W, Ré Island, France) (Site1, **fig. 12**). Exploited and non-exploited plots were studied.

The seasonal monitoring of the microbial mats of these two types of plots was processed seasonally on the 15th of July 2019, the 24th of October 2019, the 23rd of January 2020, the 19th of May 2020 and the 16th of July 2020 (**Fig. 14**).



Figure 14: Seasonal evolution of microbial mats for one year. The pictures represent the exploited and the non-exploited salt marsh plots according to the season, with the microbial mat observed within.

2.1.2 Site 2: an exploited salt marsh

Site 2 was a salt marsh where all the crystallizer ponds were exploited. It was located close to Ars-en-Ré (46°12'41.5"N 1°30'36.9"W) (Site 2, **fig. 12**). Three samplings of microbial mats were done on the 3rd of May 2017, two in the same basin and a third in a neighbouring basin.

2.1.3 Site 3: an abandoned salt marsh

The last studied salt marsh was abandoned crystallizer ponds for about 20 years, also located close to Ars-en-Ré (46°12'44.928"N 1°30'20.123"W) (Site 3, **fig. 12**). The samples were collected on the 26th of April 2017. Three replicates were collected as for the exploited site: two in the same basin and a third in a neighbouring basin

2.2 Sampling strategies

Microbial mats were sampled in independent biological triplicates using a PVC tube (15 cm diameter) as corer in each salt marshes for sites 2 and 3, and in each type of plot (exploited and non-exploited) in site 1. The first centimetre of each core was pushed out with a piston in order to collect the microbial mat (**Fig. 15**). After homogenisation by mixing, subsamples were dispatched in different tubes corresponding to different analyses (**Table 2**). The conditioning was done *in situ* and the samples were stored in the laboratory.

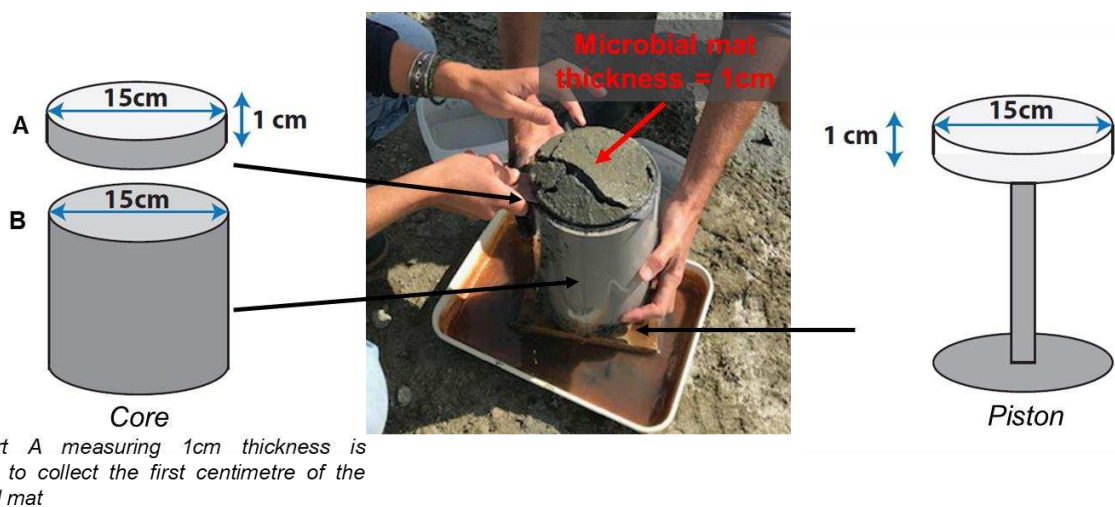


Figure 15: *In situ* sampling system of the microbial mat. The pictures represent the sampling of one centimetre thickness of the microbial mat. First, the core, with the part A above the part B, was sunk 10 cm deep on the sediment. Then, piston was placed below the core and the sediment was pushed out until the surface of the part A. This part of the core was removed, and the microbial mat was sampled.

Table 2: List of the different sampling carried out *in situ*. One part of the conditioning of the samples was achieved *in situ* and then finalized in the laboratory.

RT: room temperature; EPS: extracellular polymeric substances

Site	Sampled material	Analysis	Sampled volume	Conditioning		
				<i>In situ</i>	Laboratory	
2,3	Microbial mat	Illumina sequencing	2 mL	Liquid nitrogen	-80°C	
1	Microbial mat	Metagenomic	2 mL	Liquid nitrogen	-80°C	
1	Microbial mat	Flow cytometry	2 mL	In glutaraldehyde, liquid nitrogen	-80°C	
1	Microbial mat	EPS	5 mL	+4°C	Directly extracted, -20°C	
1	Surface water	EPS	5 mL	Filtration 0.22 µm (for extraction), +4°C	/	
1	Microbial mat	Porosity	30 mL	+4°C	-20°C	
1,2,3	Microbial mat	Meiofauna diversity and abundance	15 mL	RT in formol		
1	Surface water	Nutrients	nitrate, nitrite, ammonium, phosphate	15 mL	Filtration 0.22µm, +4°C	-20°C
			silicon	15 mL	Filtration 0.22µm, +4°C	+4°C

3. Climatic change simulation on microbial mats in mesocosms

3.1 Microbial mats for mesocosms experiment

Microbial mats for mesocosms experiment were sampled on the 30th of April 2019 on the non-exploited plot of site 1 located in Ars-en-Ré (46°13'29.9"N 1°31'07.5"W, Ré Island, France) (Site 1, **fig. 12**), because the mat was better structured than a mat from an exploited pond.

A plastic frame (48 cm x 33 cm) was sunken 3 cm deep into the microbial mat. The microbial mat within was cut into eight parts (**Fig. 16**). They were then placed on plastic boxes (48 cm x 33 cm) and transported to the laboratory at room temperature where they were put back in the water within three hours following the sampling (**Fig. 16**).

Microbial mats were also sampled *in situ* in independent biological triplicates using a PVC tube (15 cm diameter) as corer, like described in the part 2.2, to have *in situ* measure of each analysis.

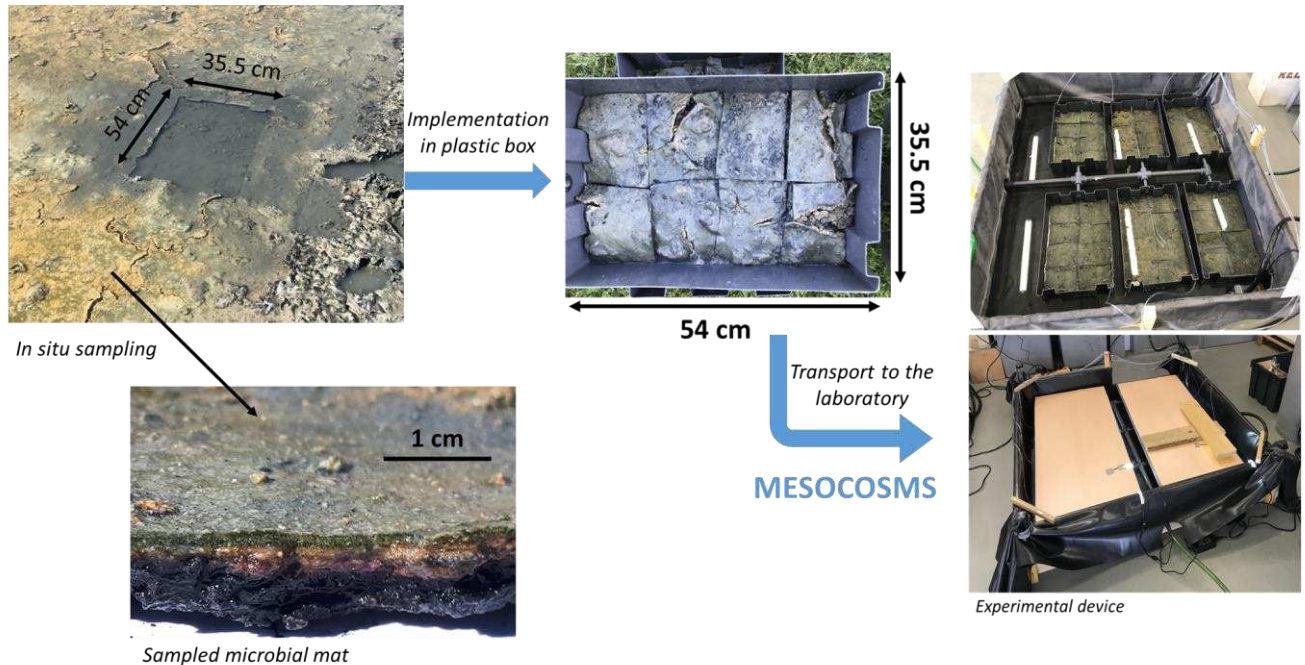


Figure 16: Sampling *in situ* of the microbial mats for mesocosms experiment. Microbial mats were placed in plastic boxes and transported to the laboratory for the mesocosms experiment.

3.2 Mesocosms design

Each plastic box with microbial mat represented a mesocosm (**Fig. 17**). The mesocosms were gathered in groups of six representing a condition (five replicates and a box for pulse amplitude modulated (PAM) measures). In these six mesocosms, incoming water was from a reserve and was distributed independently with stainless steel taps. This water corresponded to seawater filtered at 80 μm , passed under UV light and whose salinity was adjusted to 60 psu, corresponding to that measured *in situ*, with salt coming to the salt marshes of the Ré Island. At the opposite of the water inlet, a hole allowed the water outlet in a network of PVC tubes between all the replicates. This output allowed to maintain a stable water level at 3 cm above the mat (as *in situ*) and a natural supply of nutrients for the development of microbial mats. For each condition, a pool was constructed around the six plastic boxes where

water was maintained at the desired temperature with a pump (EHEIM universal 600, Germany) connected to a thermoregulating device (Teco®) to control the water temperature above the microbial mats. The microbial mats were illuminated twelve hours a day following the day/night cycle observed during the spring in France. To control the evaporation rate, the lights used were LED (TOP-24H company by SYLED, France). They provided white cold light colour and intensity of $11.8 \pm 0.9 \mu\text{mol.photons.m}^{-2}.\text{s}^{-1}$ (mean between the four treatments) (HOBO Pendant® Temperature/Light Data Logger, Onset Computer Corporation, USA) on the surface of the microbial mats.

Daily monitoring was done for the physical-chemical parameters (temperature (°C), pH, salinity (psu) and dissolved oxygen (mg.L^{-1})) with a multiparameter probe (pHenomenal® MU 6100H, VWR™, USA).

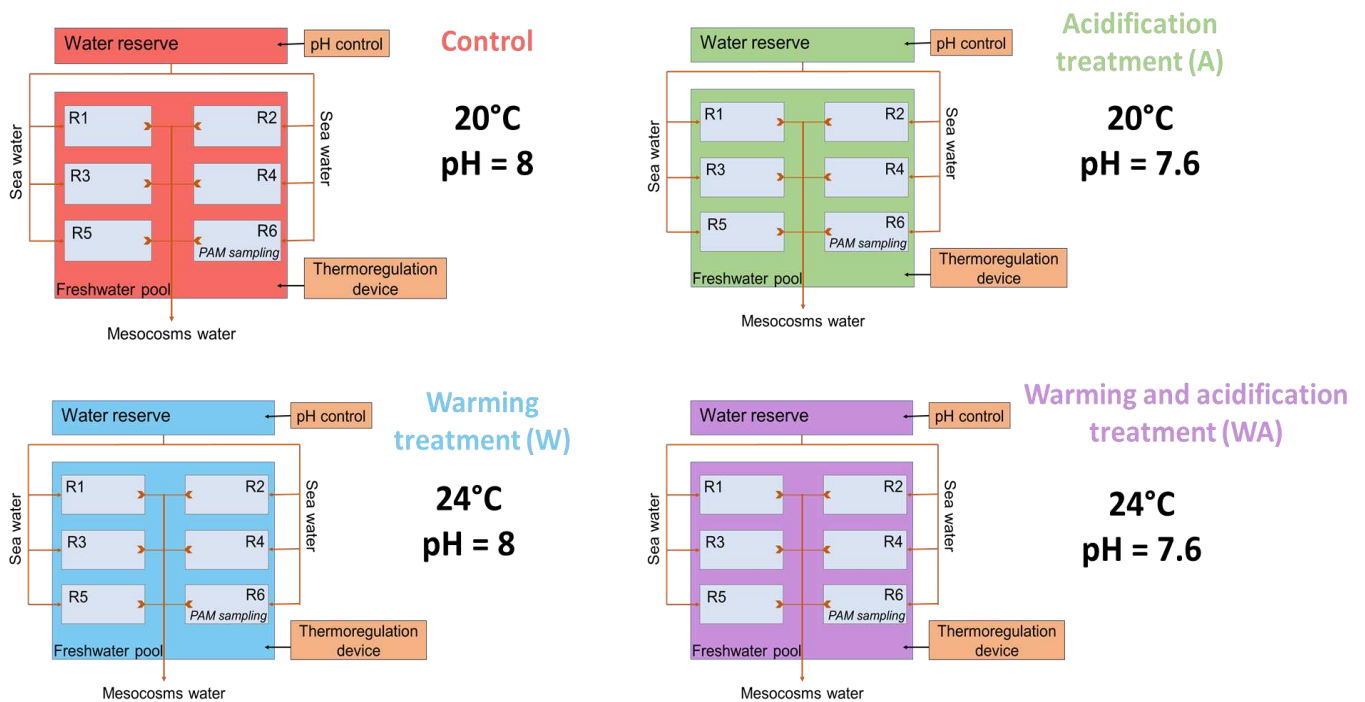


Figure 17: Schematic representation of the experimental device with the control (C) and the acidification (A), warming (W) and mixed (WA) treatments. The letter R represented the replicates. The first five are used for sampling and the sixth is dedicated to the fluorimetry measurements by pulse amplitude modulation (PAM).

3.3 Simulated scenarios

A stabilisation period of five weeks was applied to acclimate the microbial mats to their new environment (Gette-Bouvarot et al., 2015; Stauffert et al., 2013). The water temperature on the mesocosms was maintained at 20°C and the salinity of the incoming water was regulated in the water reserve to maintain salinity at 60 ± 2 psu in the mesocosms, reproducing *in situ* conditions. The implementation of different treatments occurred for seven additional weeks.

Four treatments were applied to the microbial mats. Each pool and its six mesocosms represented a condition. The first treatment was the control treatment (C) in which the parameters were not changed. The second treatment was the warming treatment (W) in which the temperature was increased by 0.5°C every two days for 2 weeks until reaching 24°C. The acidification treatment (A) represented the third condition. Water acidification was performed in the water reserve with the addition of CO₂ (IKS aquastar, iks ComputerSysteme GmbH, Germany), allowing a drop of initial water pH of 0.1 unit every four days for 2 weeks until reaching a decrease of the initial pH of the water reserve equal to 0.4 unit, *i.e.* 7.6. The water pH in the water reserve was precisely monitored with a pH probe (826 pH mobile, Ω Metrohm, Swiss) to adjust the values on IKS device. This probe was calibrated in standard solutions (pH 4, 7 and 10, HANNA® instruments, France). The fourth treatment combined warming and acidification treatments (WA). The mesocosms were then maintained with the stable treatments C, A, W, and WA for 5 further weeks.

3.4 Sampling strategy

A first sampling (noted t9) was performed after the stabilisation period of the microbial mats on the mesocosms, just before changing the environmental conditions. A second sampling (t16) was performed at the middle of the period of change and a third (t23) at the end (**Fig. 18**). After this period, sampling was performed every week (t30, t37, t44, t51 and t58)

(Fig. 18). For each sampling, ten 1 cm depth cores were collected with a 1 cm diameter cut-off syringe in each mesocosm and mixed together in order to obtain a homogeneous sample. After homogenisation by mixing, subsamples were dispatched in different tubes corresponding to different analyses (Table 3).

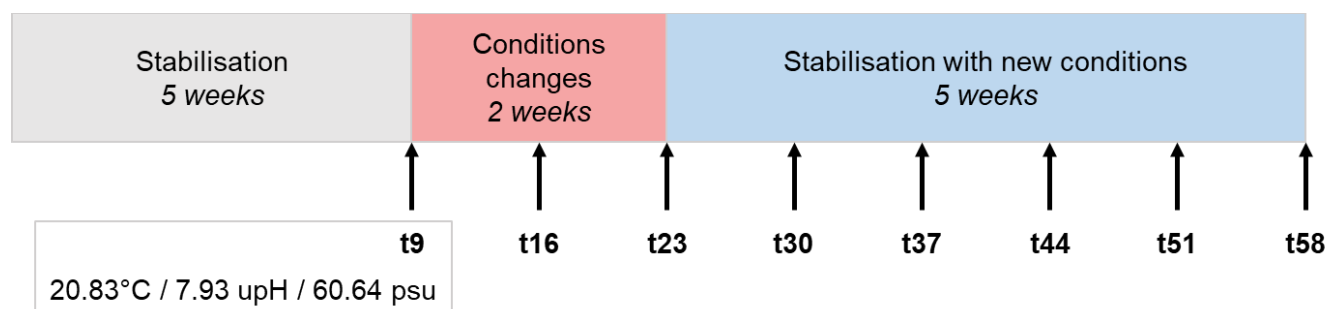


Figure 18: Schematic representation of the sampling scheme followed during the mesocosms experiment. A stabilisation period of 5 weeks was applied in order to adapt the microbial mats to their new environment. Then acidification and warming water were applied for 2 weeks followed by a stabilisation of these new conditions for 5 weeks. The sampling was represented by the letter t followed by a number indicates the sampling time.

Table 3: List of the different sampling carried out for the mesocosms analyses.

RT: room temperature; EPS: extracellular polymeric substances

Sampled material	Analysis	Sampled volume	Conditioning
Microbial mat	Illumina sequencing	2 mL	-80°C
Microbial mat	Flow cytometry	2 mL	-80°C in glutaraldehyde
Microbial mat	EPS	5 mL	Directly extracted, -20°C
Surface water	EPS	5 mL	Filtration 0.22 µm (for extraction), +4°C
Microbial mat	Pigment composition	1 mL	-20°C
Microbial mat	Porosity	30 mL	-20°C
Microbial mat	Meiofauna diversity and abundance	15 mL	RT in formol
Microbial mat	Bacterial production	1 mL	Directly analysed
Surface water	Bacterial production	1 mL	Filtration 0.22 µm (for extraction)
Surface water	Nutrients	nitrate, nitrite, ammonium, phosphate	Filtration 0.22µm, +4°C
		silicon	Filtration 0.22µm, +4°C

4. Physical-chemical parameters

4.1 Physical-chemical parameters of the water

The physical-chemical parameters (temperature (°C), salinity (practical salinity unit (psu)), pH, dissolved O₂ (mg.L⁻¹)) of the water were measured with a multi-parameter probe (pHenomenal® MU 6100H, VWRTM, USA) at each *in situ* plot type (exploited or non-exploited) of the site 1 and on the mesocosms, while only water salinity and temperature were measured in triplicate in each sampling plot of the sites 2 and 3 with a multiparameter probe (pHenomenal® MU 6100H, VWRTM, USA).

4.2 Nutrients

The nutrient analysis was done on the *in situ* samples from site 1 and on the mesocosms samples. Nutrient analysis was performed with a volume of 20 mL of *in situ* water or with 20 mL water from each mesocosm filtered at 0.22 µm (Millex® Syringe-driven Filter Unit sterile). Half of the volume was frozen at -20°C for nitrate, nitrite, ammonium, phosphate analysis while the other half was kept at 4°C for silicon analysis. Silicon, nitrate, nitrite and phosphate were measured by Segmented Continuous Flow Colorimetry (SFA) while ammonium was measured by SFA fluorimetry on an auto-analyser (SEAL AutoAnalyzer 3, SEAL analytical) as described by Aminot and K  rouel (2007).

4.3 Vertical microprofiling

Fine-scale vertical profiles of O₂, H₂S and pH distribution in the microbial mat were performed in a core sampled at each seasonal sampling date in the site 1 and transported until laboratory. These profiles were also done every week in the 6th replicate of each mesocosms treatment.

Fine-scale vertical profiles of O₂, H₂S and pH distribution in the microbial mat were obtained with Clark-type O₂ and H₂S microsensors (OX-50 and H₂S-50 (type II) respectively, Unisense, Denmark) and pH microelectrode (pH-500, Unisense, Denmark) connected to a microsensor multimeter (Unisense, Denmark) (**Fig. 19**). The sensors were manipulated thanks to a micromanipulator (Unisense, Denmark) controlled by a motor (Unisense, Denmark) (**Fig. 19**). The microsensor manipulator and the motor were connected to a computer and the measures were realised with SensorTrace Suite software (Unisense, Denmark) (**Fig. 19**).

The O₂ microsensor had an outside tip diameter of 40-60 µm, a stirring sensitivity inferior to 2% and a 90% response time less than 5s. It was linearly calibrated by a two-point calibration using readings of microsensor in the air-saturated overlying water (100% air saturation) and in the anoxic part of the mat (0% O₂). Dissolved O₂ concentrations of air saturated seawater at experimental temperatures and salinities were calculated according to Niels Ramsing and Jens Gundersen (*comm.pers.*, **annexe 2**).

The H₂S microsensor had an outside tip diameter of 40-60 µm, a stirring sensitivity inferior to 2% and a 90% response time less than 10s. During the manipulations of this thesis, only a calibration in fresh water was developed and described by Unisense. A protocol was therefore developed for calibration of the microprobes in seawater. A first solution (solution 1) was made with seawater bubbled with diazote, in order to remove all traces of oxygen, and Na₂S*9H₂O added to a final concentration of 10mM of S⁻² in anoxic condition. A second solution (solution 2) of non-bubbled seawater at pH = 4 with 12% TiCl₃ was made in parallel. Then, in several vacuum tubes filled with solution 2, increasing volumes of solution 1 were added in order to obtain a calibration range between 0 (tube only filled with solution 1) and 1000 µmol.L⁻¹ of S⁻². A new and simpler protocol was developed by Unisense in 2020 (**Annexe 3**).

The pH microelectrode had an outside tip diameter of 400-600 µm, a stirring sensitivity inferior to 2% and a 90% response time less than 20s. It was connected to an external reference. It was calibrated in standard solutions (pH 4, 7 and 10, HANNA® instruments, France).

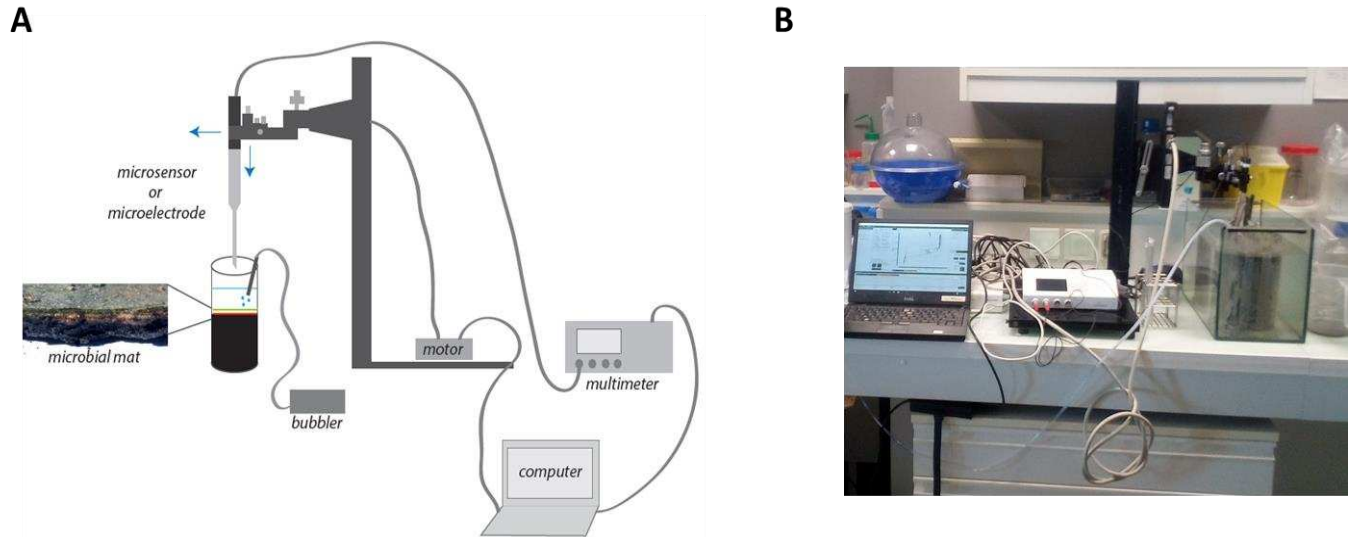


Figure 19: Microprofilage system. **A)** Schematic representation and **B)** photography of the vertical microprofilage system. The microbial mat is placed in a corer where oxygen saturation is maintained on the surface water with a bubbler. The microsensor (or microelectrode for pH) is placed above attached to a micromanipulator that can move vertically and horizontally, controlled by a motor. The microsensor (or microelectrode) is connected to a multimeter. A computer is connected to the multimeter to recover measure and to the motor to control its movement.

5. Analysis of diversity or/and abundances of organisms

5.1 Abundance of heterotrophic prokaryotes by flow cytometry

2 mL of sediment were sampled and immediately fixed with glutaraldehyde (final concentration of 2%). They were directly frozen in nitrogen liquid and maintained at -80°C until analysis. The analysis was done in the next three months after sampling (Lavergne et al., 2014). These analyses were performed for mesocosms' samples and *in situ* site 1 samples.

Abundance of the heterotrophic prokaryotes was performed according to Lavergne *et al.* (2014). A solution of sodium pyrophosphate (0.01M) was prepared and Tween 80 (0.1% final concentration) was added allowing the disaggregation of the attached cells. The samples were diluted successively until 1:2000 with a vortexing step between each dilution and incubated 30 min at 4°C. A mechanical extraction was applied by sonicating samples 30s at 60W (Sonifier®Cell Disruptor SLPe, BRANSON Ultrasonics Corporation, USA). A second

extraction was done in order to obtain a better yield (Lavergne et al., 2014) with the sample diluted at 1:2000. SYBR Green 1 (1:5000 final concentration) was then added to extracted samples and an incubation of 15 min in the dark was realized. The counting of the heterotrophic prokaryotic population was then performed thanks to a flow cytometer (BD FACSCanto™ II, BD Biosciences, USA) and the results were analysed with BD FACS DIVA software (BD Biosciences, USA). If necessary, a new dilution of the samples was done to avoid cytometer's saturation. The total abundance of heterotrophic prokaryotes and of each condition at a given time is equal to the mean of five replicates and was expressed as number of individuals per millilitre (mL) of fresh microbial mat.

5.2 Abundance of meiofauna

15 mL of sediment were sampled and fixed with 5 mL of 0.22 µm-filtered formol (12% of final concentration) and stored at room temperature. The day before counting the meiofauna, microbial mat was sieved through 50 µm and a coloration with Rose Bengal was done in order to colour the organic material.

For samples from sites 2 and 3, the formol was eliminated and a sample splitter (Motoda box as Rzeznik-Orignac et al., 2003) was used to obtain an aliquot containing at least 100 individual nematodes for abundance estimation. The abundance of other meiobenthic taxa (*i.e.*, copepods and ostracodes) was too low to be evaluated in split samples and, therefore, was quantified using whole samples. The observation was done under a binocular loupe (magnification x30, Zeiss).

For samples from site 1 and mesocosms experiment, the formol was eliminated and the meiofauna was diluted half, quarter, eighth and sixteenth. Specimens were counted and identified to the level of major taxonomic groups (*e.g.*, nematodes, copepods...) under binocular loupe (magnification x250, Zeiss).

The total meiofauna abundance of each sample is equal to the mean of the replicates and was expressed as number of individuals per cm³ of fresh microbial mat.

5.3 Photosynthetic parameters (pulse amplitude modulated fluorometer)

Chlorophyll fluorescence parameters were measured at 5 different locations of a core sampled in the 6th replicate of each mesocosms treatment using a fluorometer (Monitoring Pen, MP 100-E, Photon Systems Instruments, Czech Republic) illuminated with a blue LED emitter (455 nm). The samples were placed in the dark (for 5 min) before the measurement of Light Response Curves. Manufacturer predetermined LC3 protocol was used following manufacturer instructions. LC3 protocol was characterised by 7 steps of increasing light intensities (10, 20, 50, 100, 300, 500, 1000 $\mu\text{mol.photon.m}^{-2}.\text{s}^{-1}$) with an illumination duration of 60s. Minimum fluorescence level F_0^5 (Jesus et al., 2006) was obtained by using a non-actinic measuring light pulse (30 μs , 900 $\mu\text{mol.photon.m}^{-2}.\text{s}^{-1}$), which induced the minimal chlorophyll fluorescence (F_0^5). The samples were then subjected to a saturating light pulse (2,400 $\mu\text{mol.photon.m}^{-2}.\text{s}^{-1}$). This made it possible to measure the maximum fluorescence level F_m^5 (Jesus et al., 2006). All measurements were done in the same conditions and at the same time.

The data was then downloaded from the device to a computer using FluorPen software (v1.0.6.1, Photon Systems Instruments, Czech Republic) and all calculations and analyses were performed using R.Studio software (version 4.0.3[®] RStudio, Inc.). From the measured parameters the effective quantum yields of photosynthesis ($\phi(II)^5$) were calculated (Jesus et al., 2006) (**Equation 8**). They indicate the community's maximum potential for photosynthetic activity.

$$\phi(II)^5 = \frac{F_m^5 - F_0^5}{F_m^5} \quad (\text{Equation 8})$$

5.4 Bacterial production

Bacterial production was evaluated by the method of Garet and Moriarty (1996) modified by Pascal *et al.* (2009) This analysis was performed for mesocosms' samples. A slurry sediment was made with 1 mL of fresh microbial mat sampled in the mesocosms with the addition of mesocosms water filtered at 0.22 µm (1:1 vol/vol). For each sample, 30 µL of slurry sediment were sampled in a new tube and 20µL of ³H-Thymidine at a concentration of 0.74 MBq were added. Five replicates were done, triplicate to measure the bacterial production and two control tubes. The reaction in the control tubes was immediately stopped by adding 8 mL of cold ethanol (80%). The three other tubes were incubated for 1h at the mesocosms temperature. At the end of the incubation, the reaction was stopped by adding 8 mL of cold ethanol (80%). Afterwards, two washes with 80% cold ethanol by mixing and centrifugation (15 min, 4,500 g, +4°C) were performed. The slurries were then transferred with 2 mL of ice-cold TCA (5%, trichloroacetic acid) onto a polycarbonate filter (Nuclepore 0.2 µm, 25 mm, Millipore, NJ, USA). The filters were washed four times with 5% ice-cold TCA. Subsequently, the filters were transferred into scintillation vials containing 2 ml 0.5N chlorhydric acid and DNA was extracted 16 h at +95°C. Supernatant (0.5 mL) was transferred in a new scintillation vial with 5 mL of scintillation fluid (Ultima Gold, Perkin-Elmer, MA, USA). The amount of radioactivity in each vial was evaluated using a scintillation counter (Perkin-Elmer, USA).

Bacterial production was calculated using the equation (**Equation 9**) (Lavergne *et al.*, 2017):

$$BP = \frac{DPM \times F1}{T \times V \times SA} \quad (\text{Equation 9})$$

Where:

- BP is the bacterial production (nmol ³H-Thymidine.mL⁻¹ sediment.h⁻¹)
- DPM is the mean of the number of disintegration per minute between triplicate of measure
- F1 is the conversion factor 4.51x10⁻¹³ dpm.Ci⁻¹. It was evaluated experimentally to account for counter efficiency (Lavergne *et al.*, 2017)
- T is the incubation time (1h)
- V is the analysed volume of sediment (0.015 mL)
- SA is the specific activity (25,000 Ci.mol of ³H-Thymidine⁻¹)

- V_t is the total volume of sample (5.5 mL)

6. Molecular biology analysis

6.1 DNA extraction

At less 2 mL of microbial mat samples were ground in liquid nitrogen with a mortar and a pestle as previously described (Fourçans et al., 2008). Then, DNA was extracted from 0.25 g subsamples using the DNeasy® PowerSoil kit (Qiagen) according to the manufacturer's instructions, with a slight modification at the homogenization step, by using a Precellys homogenizer (Bertin Instruments).

6.2 Illumina sequencing

MiSeq Illumina sequencing was performed on the samples from the sites 2 and 3, and the mesocosms' samples. The Illumina sequencing principle is described in the **figure 20**.

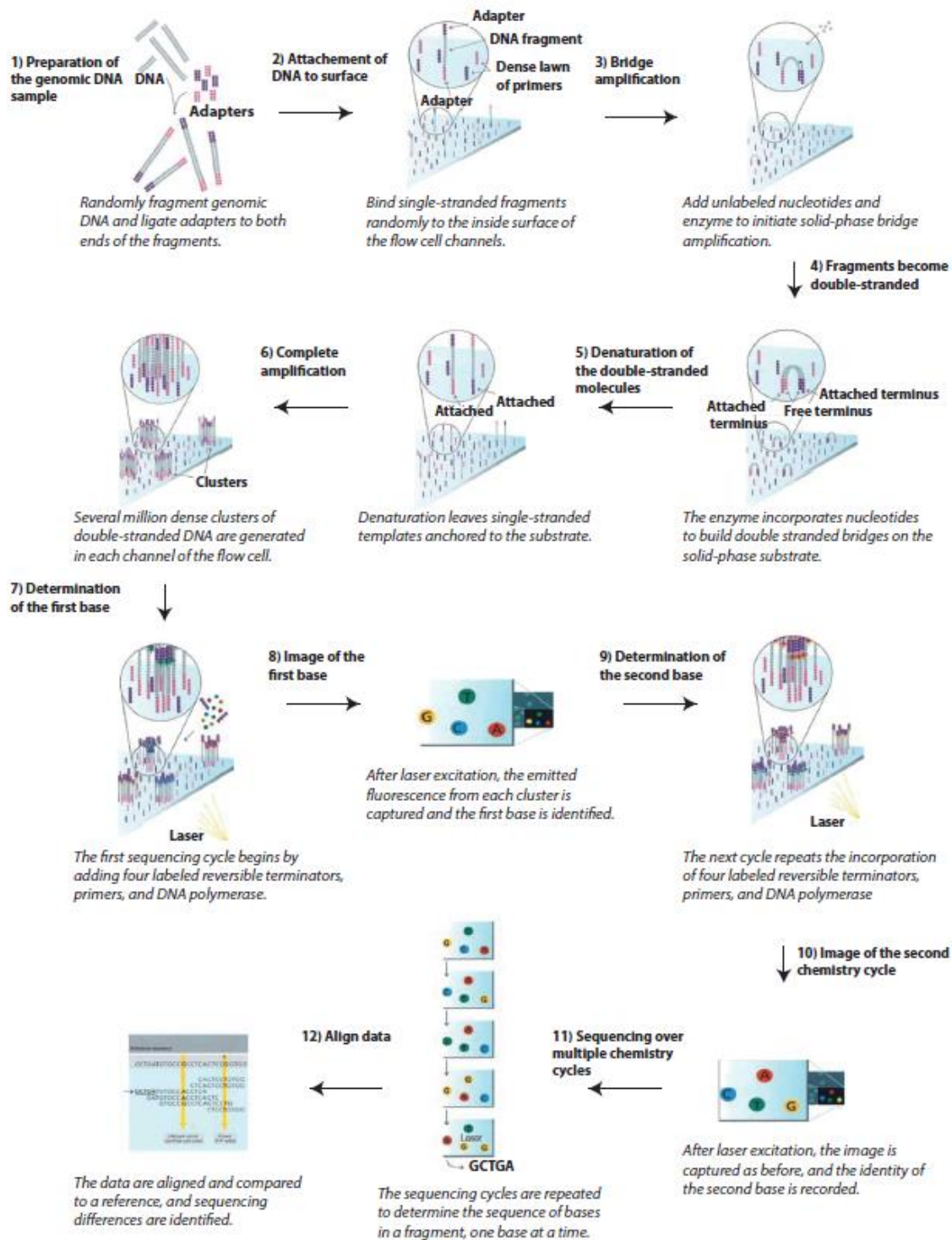


Figure 20: Summary of the Illumina workflow. Modified from the website https://www.illumina.com/documents/products/techspotlights/techspotlight_sequencing.pdf (last view: 21/08/24)

a- Bacterial sequences

For mesocosms' samples, the V3-V4 region of the bacterial 16S rRNA genes was amplified in triplicate using the primers 344F (5'-ACGGRAGGCAGCAG-3') and 801R_m (5'-ACCAGGGTATCTAATCCT-3') (Liu et al., 2007). PCR mix consisted in 12.5 μ L of AmpliTaq Gold[®] 360 master mix (Applied Biosystems), 1 μ L of each primer (10 μ M) and 1 μ L of genomic DNA, in a final volume of 25 μ L (adjusted with distilled water). All amplifications were performed on a Veriti 96 Well Thermal Cycler (Applied Biosystem) using the following PCR program: 10 min at 95°C, 30 cycles of 30 s at 95°C, 30 s at 63°C and 40 s at 72°C, and finally, 10 min at 72°C.

For the sites 2 and 3, the same region was amplified in triplicate using the same primer forward and a reverse primer a little different (801R, 5'-TACCAGGGTATCTAATCCT-3') (Liu et al., 2007). Polymerase chain reaction (PCR) mix consisted in 5 μ L of MTP Taq DNA polymerase (5 U/ μ L) with 1 μ L MTP Taq Buffer (10X) (Sigma-Aldrich), 1 μ L of dNTP (10 mM), 1.25 μ L of each primer (20 μ M) and 10 ng of genomic DNA, in a final volume of 50 μ L (adjusted with distilled water). All amplifications were performed on a Labcycler (SensoQuest) using the following PCR program: 2 min at 94°C, 30 cycles of 60 s at 94°C, 40 s at 65°C and 30 s at 72°C, and finally, 10 min at 72°C.

b- Archaeal sequences

The Illumina sequencing of the archaeal sequences was performed only the mesocosms' samples. The V4-V5 region of the archaeal 16S rRNA genes was amplified in triplicate performing a nested PCR. The first PCR was done using the primer 519F (5'-CAGCCGCCGCGGTAA-3') (Herfort et al., 2009) and the primer 915R (5'-GTGCTCCCCCGCCAATTCCT-3') (Casamayor et al., 2002) without Illumina tag. PCR mix consisted in 12.5 μ L of AmpliTaq Gold[®] 360 master mix (Applied Biosystems), 1 μ L of each primer (20 μ M) and 1 μ L of genomic DNA, in a final volume of 25 μ L (adjusted with distilled water). All these first amplifications were performed on a Labcycler (SensoQuest) using the

following PCR program: 10 min at 95°C, 35 cycles of 1 min at 95°C, 1 min at 62°C and 1 min 30 at 72°C, and finally, 10 min at 72°C. The second PCR was done on the PCR products of the first PCR using the same primers with Illumina tag. PCR mix consisted in 12.5 µL of AmpliTaq Gold® 360 master mix (Applied Biosystems), 1 µL of each primer (20 µM) and 1 µL of genomic DNA, in a final volume of 25 µL (adjusted with distilled water). All amplifications were performed on a Labcycler (SensoQuest) using the following PCR program: 10 min at 95°C, 35 cycles of 1 min at 95°C, 1 min at 58°C and 1 min 30 at 72°C, and finally, 10 min at 72°C.

c- Eukaryotic sequences

The V4 region of the 18S rRNA genes was amplified in triplicate performing a nested PCR for the mesocosms' samples. The first PCR was done using the universal primer 515F (5'-GTGYCAGCMGCCGCGGTA-3') (Caporaso et al., 2011) and the eukaryotic primer 951R (5'-TTGGYRAATGCTTTTCGC-3') (Lepère et al., 2016) without Illumina tag. PCR mix consisted in 12.5 µL of AmpliTaq Gold® 360 master mix (Applied Biosystems), 1 µL of each primer (20 µM) and 1 µL of genomic DNA, in a final volume of 25 µL (adjusted with distilled water). All these first amplifications were performed on a Labcycler (SensoQuest) using the following PCR program: 10 min at 95°C, 35 cycles of 30 s at 95°C, 30 s at 52.4°C and 45 s at 72°C, and finally, 10 min at 72°C. The second PCR was done on the PCR products of the first PCR using the same primers with Illumina tag. PCR mix consisted in 12.5 µL of AmpliTaq Gold® 360 master mix (Applied Biosystems), 1 µL of each primer (20 µM) and 1 µL of genomic DNA, in a final volume of 25 µL (adjusted with distilled water). All amplifications were performed on a Labcycler (SensoQuest) using the following PCR program: 10 min at 95°C, 35 cycles of 30 s at 95°C, 30 s at 58°C and 45 s at 72°C, and finally, 10 min at 72°C.

For the sites 2 and 3, the PCR was performed with the same primers. PCR mix consisted in 27.5 µL of AmpliTaq Gold® 360 master mix (Applied Biosystems), 1.1 µL of each primer (20 µM) and 5.5 µL of genomic DNA, in a final volume of 55 µL (adjusted with distilled water). All amplifications were performed on a Veriti 96 Well Thermal Cycler (Applied Biosystem) using the following PCR program: 10 min at 95°C, 35 cycles of 30 s at 95°C, 30 s

at 55°C and 45 s at 72°C, and finally, 10 min at 72°C. Illumina sequencing was performed by the NED team (UMR1388 GenPhySE) and the GeT core facility (Toulouse, France), using Illumina MiSeq technology.

d- Dataset

Illumina sequencing of the samples from the sites 2 and 3 was performed by the NED team (UMR1388 GenPhySE) and the GeT-PlaGe core facility (Toulouse, France), using Illumina MiSeq technology (paired-end, 2x300pb). For the mesocosms' samples, the Illumina sequencing was performed by the Genomer platform of Roscoff (France), using Illumina MiSeq technology (paired-end, 2x300pb).

The complete dataset of the sites 2 and 3 samples was deposited in the NCBI Sequence Read Archive (SRA) database under SRA accession number PRJNA627371 for eukaryotic dataset and PRJNA627173 for bacterial dataset.

For mesocosms, the complete dataset was deposited in the NCBI Sequence Read Archive (SRA) database under SRA accession number PRJNA771950.

6.3 Illumina sequencing data processing

6.3.1 Bioinformatic tools approach

Several bioinformatics tools exist to perform DNA analyses: mothur (Schloss et al., 2009), QIIME (Caporaso et al., 2010), FROGS (Escudié et al., 2018), QIIME 2 (Bolyen et al., 2019) and SAMBA (Noël et al., 2021).

a- Operational Taxonomic Unit (OTU) approaches

mothur, QIIME and FROGS are Operational Taxonomic Unit (OTU) approaches.

mothur is an open source and expandable software. It permits to trim, screen and align sequences, then assign sequences to OTUs and describe alpha- and beta-diversity of

sequencing data. mothur approach selects a random sequence and groups it with other sequences according to a similarity distance (e.g., 97%) to define an OTU (**Fig. 21**). However, if a second analysis is performed, the random sequence chosen can be different of the previous analysis and can have an assignment different leading to the definition of an OTU different of those previously defined (**Fig. 21**). So, the results were not replicable (**Table 4**).

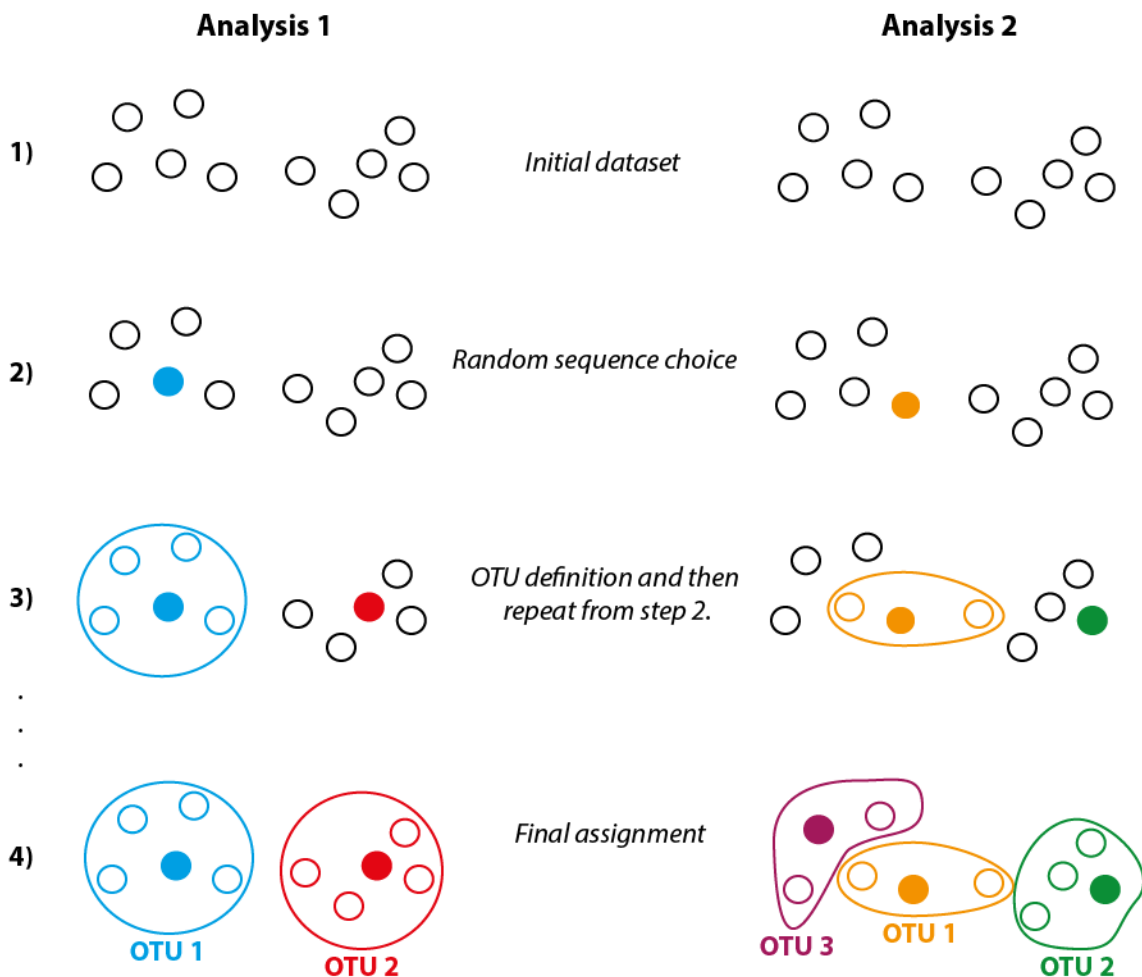


Figure 21: Schematic representation of the OTU assignment of a dataset using mothur approach.

The first analysis conducts to the random choice of the blue sequence. All sequences with a similarity distance less than or equal to 97% with the blue sequence were grouped with it to define the OTU 1. Then, a second random choice was done on the red sequence. All sequences with a similarity distance less than or equal to 97% with the red sequence were grouped with it to define the OTU 2.

The second analysis conducts to the random choice of the orange sequence, different of the blue sequence. Then, with the same process than the first analysis, 3 OTUs were defined on the dataset. The OTU 1 defined on the first analysis and the OTU defined on the second analysis can have a different

assignment. So, blue OTU 1 can be the specie A and orange OTU 1 can be the specie B leading to a different assignment of the OTU on the dataset leading to the non-replicability of this method.

Thus, mothur is not an accessible and reproducible tool. Since some years, the scientific community seeks to make findable, accessible, interoperable and reusable (FAIR) methods. QIIME (Quantitative Insights Into Microbial Ecology) is developed in this goal. It is an open-source bioinformatics pipeline for performing microbiome analysis from raw DNA sequencing data. QIIME allows users to process raw sequencing data generated on the Illumina or other platforms. This pipeline includes demultiplexing and quality filtering, OTU picking, taxonomic assignment, phylogenetic reconstruction, diversity analyses and visualizations. This pipeline does not select randomly a sequence to define an OTU. This pipeline chooses the most abundant sequence as reference sequence defining an OTU. So, this sequence will be the same in any analysis. Then the sequences were grouped according to their similarity. So, the results were replicable. The complexity of the tutorial was one of the major drawbacks (**Table 4**).

FROGS is Galaxy-supported pipeline. The clustering method uses Swarm (Mahé et al., 2014) and the chimera are removed using VSEARCH (Rognes et al., 2016). It uses the same process than QIIME, but it groups the sequences according to the distance. The major drawbacks of FROGS were its little flexibility in setting up the analysis and the lack of databases, notably for specific functional gene (*e.g.*, *mcrA* or *dsrB* databases) (**Table 4**).

Table 4: Benefits and drawbacks of bioinformatics tools using OTU approaches.

	Mothur	FROGS (on Galaxy)	QIIME
+	- Complete and easy to follow tutorial	- Easy to use	- Resource efficient - Short analysis time - Customizable pipeline - Statistical analysis facilitated but not advanced
-	- High RAM usage - Non-replicable result - Long analysis time	- Little flexibility in setting up the analysis	- Complex tutorial to follow - Need bioinformatics skills

b- Amplicon Sequence Variant (ASV) approaches

Amplicon Sequence Variant (ASV) approaches were introduced with QIIME 2. Since the 1st of January 2018, QIIME 2 has succeeded QIIME 1, which is no longer supported and developed nowadays (<http://qiime.org/>). QIIME 2 is a workflow where the raw sequences were demultiplexed and then filtered, denoised, merged and grouped in non-chimeric sequences with DADA2 (Callahan et al., 2016) followed by a singleton filtering. Then, this package performs a cluster of unique sequences to build ASVs, *i.e.*, as soon as a sequence is different from another one, it corresponds to a different ASV, contrary to OTUs which consists in a cluster of similar sequences. The use of ASVs is more appropriate for microbial ecology and ecotypes issues (Terrisse et al., 2017). It also presents other benefits: a step of filtration with phiX, a short time analysis, a customizable pipeline and facilitated statistical analyses but not advanced. However, QIIME 2 is a complex tutorial needing to have bioinformatics skills and the output format is specific to this pipeline (.qza and .qzv files).

SAMBA (Standardized and Automated MetaBarcoding Analyses workflow) is flexible, standardized, scalable, automated and reproducible workflow developed by SeBiMER, the IFREMER's Bioinformatics Core Facility, the French National Institute for Ocean Science. SAMBA is built using the NextFlow workflow manager (Di Tommaso et al., 2017). SAMBA is composed of three main parts (**Fig. 22**):

- data integrity checking: it allows to verify the integrity of the raw data (illumina sequencing on the same sequencer, presence of the same barcodes and primers forward and reverse sequences, *etc.*).
- bioinformatics processes: they are mainly based on the use of the next-generation microbiome bioinformatics platform QIIME 2 (Bolyen et al., 2019; version 2020.2) and on the approach of grouping sequences in ASV (Amplicon Sequence Variants) using DADA2 (Callahan et al., 2016). SAMBA also use dbOTU3, unlike QIIME2, that tends to reduce the diversity overestimation. ASVs are grouped according to their phylogeny and distribution. So, very similar sequences (different because of an error, a mutation

or just a slightly different 16S copy) are present in the same samples and with a difference in abundance are grouped in a "corrected ASV".

- statistical analyses: SAMBA performs extensive analyses of the alpha- and beta-diversity using homemade R scripts (written by C.Noël, SAMBA).

SAMBA offers a real alternative to the complex use of a suite of command line bioinformatics tools while providing access to state-of-the-art methods and tools in the field, making it a more FAIR tool than QIIME 2. The SAMBA source code, documentation and installation instructions are freely available at [SeBiMER GitHub](#).

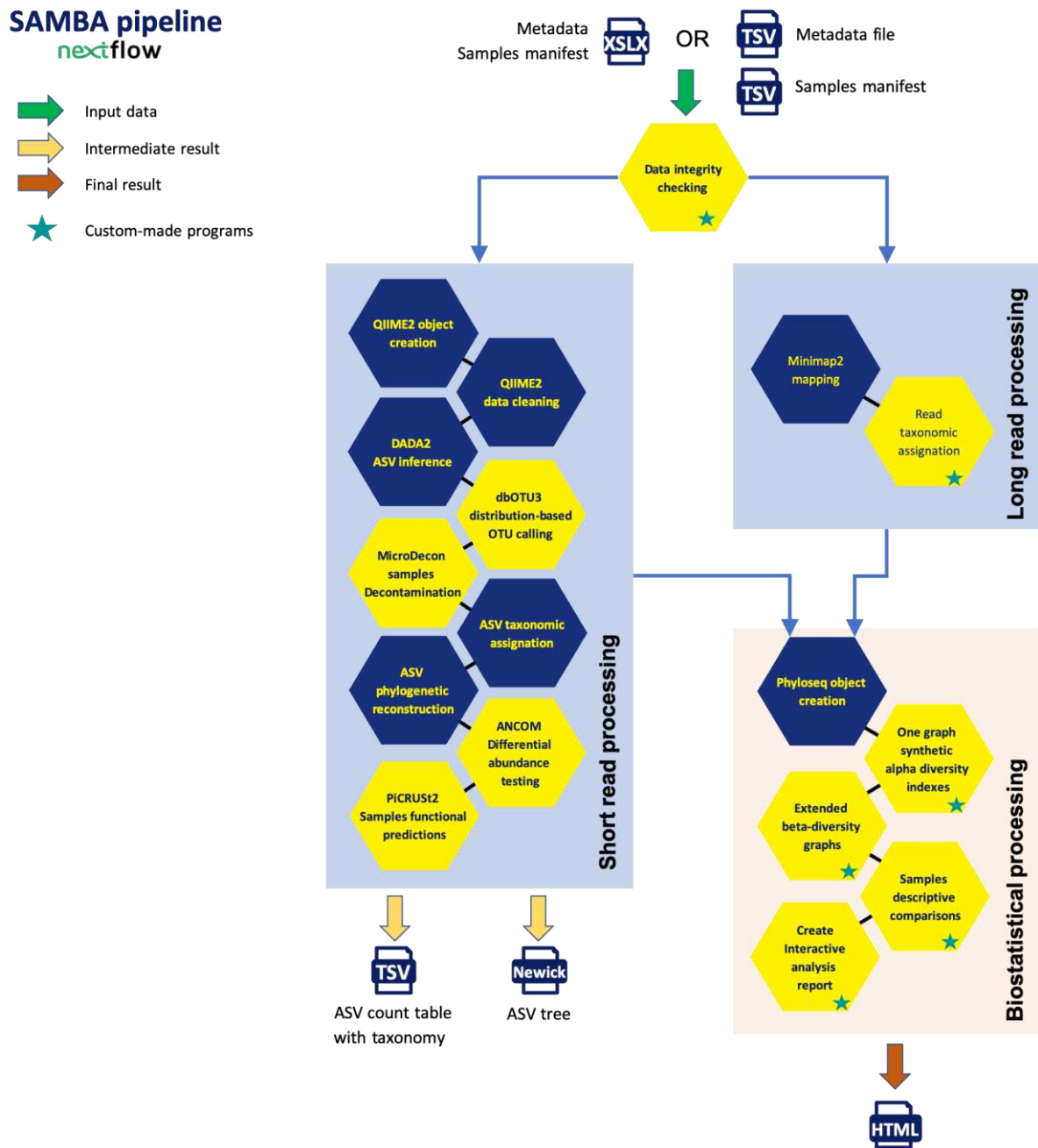


Figure 22: Summary of the SAMBA pipeline. This figure comes from the SAMBA website (<https://github.com/ifremer-bioinformatics/samba>, last view 21/08/28).

6.3.2 QIIME 2: data processing of samples from the sites 2 and 3

Bioinformatic processing for DNA sequences were performed using QIIME 2 2019.4 (Bolyen et al., 2019). The same process was followed for 16S (Bacteria) and 18S (Eukarya) rRNA gene sequences. The taxonomic affiliation was performed against the SILVA database

v132 (Quast et al., 2012; Yilmaz et al., 2013) with 97% of similarities. The non-affiliated sequences were excluded. The rarefaction normalized samples of different sample size by subsampling their size according to the smallest sample size. The BIOM file of the filtered rarefied sequences was done and converted in JSON file for further analyses.

6.3.3 SAMBA: data processing of the mesocosms' samples

SAMBA was selected for these DNA analyses instead of QIIME 2 because it presents several benefits: a verification of the raw data integrity and the use of dbOTU3 to produce ASVs. The pipeline was adapted to DNA sequences processing coming from mesocosms samples (site 1) (<https://github.com/ifremer-bioinformatics/samba>). These bioinformatic analyses were performed using SAMBA v3.0.0, Netxflow v20.10.0, QIIME 2 v2019.10.0, R v3.6.1, DESeq2 v1.26.0, metagenomeSeq v1.28.0, microbiome v1.8.0, phyloseq v1.30.0, vegan v2.5.6 and UpSetR v1.4.0. Bacterial, archaeal and eukaryotic datas were analysed separately. The taxonomic affiliation was performed against the SILVA database v138 (Quast et al., 2012; Yilmaz et al., 2013) with 99% of similarities.

7. Biochemical analyses

7.1 Extraction and determination of extracellular carbohydrate and protein polymeric substances (EPS)

The determination of the EPS for *in situ* samples of the site 1 and mesocosms' samples was performed following the same protocol adapted from Takahashi *et al.* (2009).

In a 15 mL Falcon® tube, 5 mL of microbial mat was mixed with an equivalent volume of seawater obtained by mixing surface water from each pond of the site 1 for *in situ* samples or, from the five sampled replicate of each treatment for mesocosms' samples. It was then filtered at 0.22 µm for each treatment. The tubes were subjected to mechanical agitation by

vortexing and by inversion at a rate of 40 oscillations.min⁻¹ for 1 h at 4°C in the dark. Then, they were centrifuged at 3500 g for 10 min at 4°C. The supernatant, containing the colloidal fraction, was recovered and stored at -20°C while the pellet, containing the bound fraction, was resuspended in 5 mL of seawater (again obtained by mixing water each pond of the site 1 for *in situ* samples or, from the five sampled replicate of each treatment for mesocosms' samples, and filtered at 0.22 µm). 1 g of Dowex resin (Dowex Marathon C, Na⁺, Sigma-Aldrich), was prepared according to the protocol of Takahashi *et al.* (2009). The tubes were again subjected to the same protocol to obtain the supernatant containing the fraction of bound EPS was recovered and stored at -20°C.

The carbohydrate concentration was performed according to Dubois' colorimetric method (Dubois *et al.*, 1956) while the protein concentration was performed according to the BiCinchoninic acid Assay (BCA) method using the Pierce™ Protein Assay Kit (Thermoscientific). A range of glucose (L-(-)-Glucose, 98%, Sigma-Aldrich) from 0 to 3 g.L⁻¹ and a range of bovine serum albumin (BSA) from 0 to 1 g.L⁻¹ were performed in seawater from the Ré Island hypersalinated at 60 psu and filtered at 0.22 µm. For carbohydrates, 100 µL of EPS sample were placed in a tube, then 100 µL of 5% phenol (Solid Phenol, Sigma-Aldrich, France) and 500 µL of 98% sulphuric acid (Sulphuric Acid 98%, Carlo-Erba Reagents, France) were added. The tubes were incubated for 30 min in the dark and at room temperature. A volume of 200 µL of the standard range and each triplicate sample was deposited in a 96-well microplate (Falcon® 96-well Clear Microplat, Thermo Fisher Scientific). The absorbance of each well was measured at 490 nm with a spectrophotometer (SPECTROstar® Nano, BMG LAB). For proteins, the reagent was prepared and stored in the dark at room temperature during the assay period. The assays were performed in 96-well microplates (Falcon® 96-well Clear Microplat, Thermo Fisher Scientific). 200 µL of reagents were placed in the wells and 25 µL standards or triplicate samples were added. The microplates were incubated for 30 min at 37°C, then the absorbance of each sample was measured at 562 nm by a spectrophotometer (SPECTROstar® Nano, BMG LAB). Two calibration curves were drawn from the standard

ranges and their respective abundances (corrected according to the kit indications for the BSA range), averaged over the duration of the experiment. They made it possible to determine the carbohydrate and protein concentrations. The latter were then related to the dry mass of the microbial mat.

7.2 Identification of pigments by HPLC

Lipophilic pigments were analysed by high performance liquid chromatography (HPLC). Microbial mats were incubated with 95% methanol (buffered with 2% ammonium acetate) during 15 min, at -20°C in the dark. Extracts were then filtered with 0.2 µm PTFE syringe filters and analysed within 16h using an Agilent 1260 Infinity HPLC composed of a quaternary pump (VL 400 bar), a UV-VIS photodiode array detector (DAD 1260 VL, 190–950 nm), a fluorescence detector (FLD 1260 excitation: 425 nm, emission: 655 nm), and a 100 µL automatic sample injector refrigerated at 4°C in the dark. Chromatographic separation was carried out using a C18 column for reverse phase chromatography (Supelcosil, 25 cm long, 4.6 mm inner diameter). The solvents used were: 0.5M ammonium acetate in methanol and water (85:15, v:v), acetonitrile and water (90:10, v:v), and 100% ethyl acetate. The solvent gradient was set according to Brotas and Plante-Cuny (2003), with a 0.5 mL.min⁻¹ flow rate (**Table 5**). Identification and calibration of the HPLC peaks were performed with ββ-carotene, canthaxanthin, chlorophyll *a*, chlorophyll *b*, chlorophyll *c*₂, diatoxanthin, diadinoxanthin, fucoxanthin and pheophytin *a* standards. We identified all detected peaks by their absorption spectra and relative retention times using the Agilent OpenLab software. Quantification was performed using standard calibration curves built with repeated injections of standards over a range of dilutions. Xanthophylls, carotens and chlorophyll *b* and *c* were quantified at 470 nm, chlorophyll *a* and their derivatives as well as pheopigments were quantified at 665 nm. The relative abundance of each pigment (%) was calculated from its respective concentration in the sample (µg.mg⁻¹).

Table 5: Programme and solvents used in HPLC analysis.

Time (min)	A (%)	B (%)	C (%)	Gradient system
0	60	40	0	Injection
2	0	100	0	Linear
7	0	80	20	Linear
17	0	50	50	Linear
21	0	30	70	Linear
28.5	0	30	70	Linear
29.5	0	100	0	Linear
30.5	60	40	0	Linear
35	60	40	0	Linear

Solvents composition

A: ammonium acetate with a concentration of 0.5 mol.L⁻¹ in a water and ethanol mix (85:15)

B: water and acetonitrile mix (90:10)

C: ethyl-acetate (100%)

8. Statistical analysis

All calculations and analyses were performed on R.Studio software (version 3.6.3[®] in the **chapter III** and then, version 4.0.3[®] RStudio, Inc.).

For comparative tests, the normality and homoscedasticity of the data were previously verified by carrying out a Shapiro test and a Bartlett test respectively.

To compare the physical-chemical parameters, meiofaunal abundance, diversity indices of two samples (*e.g.*, to compare the exploited and abandoned sites in the **chapter III** or the non-exploited and exploited plots in the **chapter IV**), a Student t-test was applied when the conditions of application (normality of data and variance independence) were verified, a Welch two sample t when the independence of variances was not verified and a Wilcoxon-Mann-

Whitney test if any condition was respected. The samples with measure in duplicate were not compared because of the non-robustness of the statistical tests.

For mesocosms, the physical-chemical parameters, the carbohydrates and proteins concentrations of each fraction, the photosynthetic parameters, the meiofaunal abundance and the diversity indices of each treatment were compared with each other at each sampling time. The normality and homoscedasticity of the data were previously verified by carrying out a Shapiro test and a Bartlett test respectively. If both conditions were met, the data were subjected to an analysis of variances (ANOVA). Otherwise, a Welch ANOVA was performed in the case of non-homogeneity of variances and a Kruskal-Wallis rank sum test in the case of non-normal data. If these tests were found to be significant ($p < 0.05$), then a pairwise comparison was performed using a Tukey test following the ANOVA, a Games-Howell test following a Welch ANOVA or a Nemenyi test following the Kruskal-Wallis test. These tests were also applied to compare triplicate measures between seasons in the **chapter IV**.

Permutational multivariate analysis of variance (PERMANOVA) was applied to determine the role of treatment and time in explaining the variance noted among the Bray–Curtis distance matrices (*adonis* function of the *vegan* package).

The collinearities between the environmental variables (temperature, pH, dissolved oxygen, salinity, phosphate, nitrate, nitrite, ammonium, silicon) were first tested with variance inflation factors (VIFs). The variables selection was based on the criterion $VIF < 5$. Then, a collinearity of up to 0.7 according to Spearman's rank correlation ($p < 0.05$) was performed. This process led to group the variables presenting collinearity and used the proxies for each group as explanatory variables.

A principal component analyses (PCA) was performed on the sample structure according to the non-correlated physical-chemical parameters transformed in Euclidian distances.

The principal coordinates analysis (PCoA) based on the Bray–Curtis distance matrices was used to analyse the beta diversity. The main contributor Amplicon Sequence Variants (ASVs) to the first two PCoA axes were determined by analysing correlations between these axes and each ASVs. The dendrogram of each replicate of the sites was also done with Bray-Curtis distance matrices (only in the **chapter III**). The contribution of each ASV explaining the differences between sites was defined by SIMPER (SIMilarity PERcentages) based on Bray-Curtis distance measure. Linear discriminant analysis effect size (LEfSe) (Segata et al., 2011) on the 50 more abundant ASVs was done on Galaxy web application to determine bacterial genera or eukaryotic families biomarkers of each site. The non-parametric Kruskal-Wallis sum-rank test ($\alpha = 0.05$) was performed to detect taxa with significant differential abundance. The biological consistency was investigated by performing a pairwise Wilcoxon test ($\alpha = 0.05$). A linear discriminant analysis (LDA) threshold score of 2.0 was applied. SIMPER analyses and LEfSe were applied only in the **chapter III**.

Alpha diversities indices were calculated according to the observed richness (based on presence/absence of ASVs), the Shannon diversity (ASVs richness and their evenness) and the Inverse Simpson index (giving more weight to common or dominant species).

A Between Class Analysis (BCA) combined with hierarchical cluster analysis with a Bray dissimilarity index and ward.D2 method was done on pigments proportions.

Chapter III: Presentation of
microbial mats of salterns of Ré
Island

1. Introduction

Hypersaline environments are characterised by salinity higher than that of seawater (by about 35 practical salinity units; psu), which develops when the supply of freshwater is dominated by water loss through evaporation (Paerl et al., 2003). These environments represent a significant surface area on a global scale, whether they are of natural origin (lakes, tidal basins, etc.) or artificial (for salt production) (Javor, 1989). Dammed salt marshes are artificial coastal hypersaline environments, created to gain land from the sea to develop economic production (Paticat, 2007). In France, their presence is observed along the Atlantic and Mediterranean coasts. This study focuses on the salt marshes of the Nouvelle-Aquitaine region, and more specifically those of Charente Maritime (17). In this department, they extend over 14,200 ha, including 5,700 ha on the territory of the Ré and Oléron Islands (Paticat, 2007). In the 19th century, 1,500 hectares of salt marshes were exploited, *i.e.*, 1/5 of the surface of the Ré Island. Currently, 460 ha were still used to produce marine salt leading to the production of 3,200 tonnes of salt (France3-regions, 2018, 2017), the other salt marshes being abandoned. In addition to their economic importance, salt marshes are refuges for many species, especially migratory birds (Rodrigues et al., 2011; Takekawa et al., 2015), and provide numerous cultural, provisioning, supporting and regulating ecosystem services (de Melo Soares et al., 2018), making them environments of high heritage and commercial value.

Although salt marshes appear, at first glance, to be unfavourable environments for life, they are nevertheless environments conducive to the development of a wide variety of microorganisms (Javor, 1989) which form microbial mats (Fourçans et al., 2004). Many studies have observed the structure, the diversity and the dynamics of microbial mats on salterns they represent interesting ecosystems adapted to fluctuating conditions (Caumette et al., 1994; Fourçans et al., 2008, 2004).

To the best of our knowledge, the microbial mats from salterns of Ré Island have not been studied yet. It is important to know the diversity and structure of these microbial mats in

order to determine their current microbial composition and structure, which will serve as a baseline for future studies. In the future, this will allow defining accurate prediction models to anticipate and better understand their response to climate change.

This chapter aims to compare microbial mats diversity coming from an exploited salt marsh and an abandoned salt marsh for 15 years. The sampling was done before the beginning of this thesis, in 2017. The results are presented in an article published in Microbiological Research (Volume 252, November 2021, DOI: 10.1016/j.micres.2021.126854) (Mazière et al., 2021).

2. New insights in prokaryotic and eukaryotic diversity of microbial mats inhabiting exploited and abandoned salterns at the Ré Island (France)



New insights in bacterial and eukaryotic diversity of microbial mats inhabiting exploited and abandoned salterns at the Ré Island (France)

Camille Mazière^{a,b}, H el ene Agogu e^b, Cristiana Cravo-Laureau^a, Christine Cagnon^a,
Isabelle Lanneluc^b, Sophie Sabl e^b, Ingrid Fruitier-Arnaudin^b, Christine Dupuy^b,
Robert Duran^{a,*}

^a Universit e de Pau et des Pays de l'Adour, E2S UPPA, CNRS, IPREM, Pau, France

^b UMR 7266 LIENSs (Littoral Environnement et Soci et es), CNRS - La Rochelle Universit e - 2, Rue Olympe de Gouges, 17000, LA ROCHELLE, France

ARTICLE INFO

Keywords:

Hypersaline environments
Marine solar salterns
Microbial diversity
Meiofaunal diversity
Human exploitation and perturbation

ABSTRACT

In order to understand the effect of human practices on microbial mats organisation, the study aimed to investigate the biodiversity within microbial mats from exploited and abandoned salterns. Despite several attempts, archaeal 16S rRNA gene fragment sequences were not obtained, indicating that microbial mats were probably dominated by Bacteria with very low abundance of Archaea (< 1%). Thus, the study compared the bacterial and meiofaunal diversity of microbial mats from abandoned and exploited salterns. The higher salinity (101 ± 3.7 psu vs. 51.1 ± 0.7 psu; Welch *t*-test $p < 0.05$) of the exploited site maintained lower bacterial diversity in comparison to the abandoned site where the salinity gradient was no longer maintained. However, the microbial mats exhibited similar bacterial class composition while the eukaryotic diversity was significantly higher in the exploited saltern. The abandoned saltern was dominated by sulfate-reducing bacteria and Nematoda, while the exploited saltern was characterized by the presence of halophilic bacteria belonging to *Marinobacter*, *Salinivibrio* and *Rhodohalobacter* genera, and the larger abundance of Hypotrichia (ciliates). Such bacterial and eukaryotic diversity difference might be explained by human actions for salt recovery in exploited salterns such as scraping the surface of microbial mat and increasing salinity renewing the microbial mat each year. Such action decreases the bacterial diversity changing the food web structure that favour the presence of a larger diversity of eukaryotic organisms. Our study provides new insights on microbial mat communities inhabiting salterns, especially the consequences of abandoning saltern exploitation.

1. Introduction

Microbial mats develop at the sediment/water interface in various habitats (Prieto-Barajas et al., 2018), including coastal areas (White et al., 2018,2021), sand beaches (Bolhuis and Stal, 2011), estuaries (Mir et al., 1991), lakes (J orgensen and Cohen, 1977), hot springs (Dobretsov et al., 2011), Andin glaciers (Fleming and Prufert-Bebout, 2010; Schmidt et al., 2017), polar region (Valdespino-Castillo et al., 2018), freshwater Lagunas (Falc on et al., 2020; Yanez-Montalvo et al., 2020), and salterns (Giani et al., 1989; Four ans et al., 2004; Kolesnikov et al., 2017). They are complex systems of multi-layered microbial communities vertically stratified where microorganisms are organized according to physical-chemical gradients of light, oxygen and sulfur (Caumette et al., 1994), playing an important role in the major biogeochemical cycles

(J orgensen and Cohen, 1977; Wieland et al., 2003; S anchez-Baracaldo et al., 2021). In microbial mats, different functional microbial groups with various metabolic capacities coexist at a microscale (van Gemerden, 1993). They experience daily fluctuations of environmental parameters resulting in variations of their vertical distribution (Four ans et al., 2006, 2008; Martinez et al., 2019). Therefore, microbial mats constitute an ideal model to study microbial interactions and their response to environmental changes.

Microbial mats developing in marine solar salterns are among the most studied (Oren, 2009) for examining microbial composition and their dynamics (Plominsky et al., 2018). Solar salterns, generally found in coastal regions, are man-made habitats for salt production through solar evaporation of seawater. Seawater evaporates through a series of shallow ponds, gradually increasing salinity constituting extreme

* Corresponding author at: B atiment IBEAS - Avenue de l'Universit e, BP 1155, 64013, PAU CEDEX, France.

E-mail address: robert.duran@univ-pau.fr (R. Duran).

<https://doi.org/10.1016/j.micres.2021.126854>

Received 5 June 2021; Received in revised form 9 August 2021; Accepted 21 August 2021

Available online 25 August 2021

0944-5013/  2021 Elsevier GmbH. All rights reserved.

hypersaline environments. The resulting brine, saturated with sodium chloride, reaches crystallizer ponds where salt deposits and is then collected by scraping the surface of the sediment. The salt production depends on physical-chemical processes and activities of the microbial mats developing in such extreme habitats, which could result in the production of several valuable chemicals by microorganisms with biotechnological potentials (Gómez-Villegas et al., 2018). Historically, several solar salterns have been exploited along the French Atlantic coast. Nowadays, many of these solar salterns have been abandoned because of loss of economic profitability. At the Ré Island (France), exploited and abandoned solar salterns coexist allowing the comparison of microbial mats developing under different saline fluctuating conditions but with similar environmental parameters. The salt production is artisanal, handwork following traditional practices with salt harvest by hands in summer. In winter the salterns are flooded with seawater, the exploitation starting in spring by increasing progressively the salinity, especially in crystallizer ponds where large variations in salinity are observed until reaching concentrations where salt precipitates. In contrast, the salinity variation is limited in the abandoned salterns because the water entry is no regulated. It has been demonstrated that the salinity fluctuations during salt production disturb the natural habitats (Tran et al., 2019), influencing the development and the structure of the microbial mats that also depend on the seasonal variations (Boujelben et al., 2012; Cardoso et al., 2019). Because only few studies have investigated abandoned salterns (Cvitković et al., 2011; Lee et al., 2020), the information on how the ecosystem is affected by the modifications of human practices is still scarce. The comparison of the diversity within microbial mats subjected to large saline variations (exploited saltern) with that of microbial mats inhabiting ponds where the saline variations are limited (abandoned saltern) within the same hydrological system will allow to describe the modifications of microbial communities in response to a drastic change on the human practices, which are affecting the salinity fluctuations. Understanding how the human practices affect the microbial community of microbial mats in solar salterns is of paramount importance providing useful information for the management of microbial communities in the context of global changes.

In this study, we investigated the diversity within microbial mats

from exploited and abandoned hypersaline ponds in salterns located at the Ré Island (France). We adopted a holistic view, investigating the microbial communities by 16S and 18S rRNA genes barcoding, completed by microscopic observations for the eukaryotic community, in order to describe the biodiversity in microbial mats and how it is affected by human-made drastic changes. Indeed, although bacterial communities inhabiting microbial mats have been widely studied (Fourçans et al., 2006, 2008; Bolhuis and Stal, 2011; Boujelben et al., 2012; Bolhuis et al., 2014; Stal et al., 2019), only few studies have reported on their eukaryotic community composition (Cvitković et al., 2011; Edgcomb et al., 2014), resulting in a lack of knowledge in the whole diversity of microbial mats. Our results bring new insights on microbial mats biodiversity modifications in response to a perturbation due to human activity.

2. Material and methods

2.1. Sampling site

The microbial mats were collected in crystallizer ponds of salterns located in two different sites, but within the same hydrological system, close to Ars-en-Ré (Ré Island, France; Fig. 1, the map was drawn with the R library gmap (Kahle and Wickham, 2013)), allowing the investigation of abandoning saltern exploitation considering similar physical-chemical parameters. The Abandoned site (46°12'44.928"N 1°30'20.123"W) located in an abandoned saltern for 15 years, and the Exploited site (46°12'41.5"N 1°30'36.9"W) located in an exploited saltern. The microbial mats were sampled in spring 2017. In each site, microbial mats were sampled in independent biological triplicates (R1, R2 and R3) corresponding to three distinct ponds (Fig. 1). Microbial mats were sampled using a PVC tube (15 cm diameter) as corer. From each core, the first 0.5 cm was pushed out, from the bottom to the up, with a piston in order to collect the microbial mat of the expected thickness. After homogenisation by mixing, subsamples for DNA microbial analysis were dispatched in 2 mL cryotubes flash frozen in liquid nitrogen and then stored at -80 °C. Meiofauna abundance and group composition were obtained from another core. Sediment (60 mL) was preserved in absolute ethanol (vol/vol).

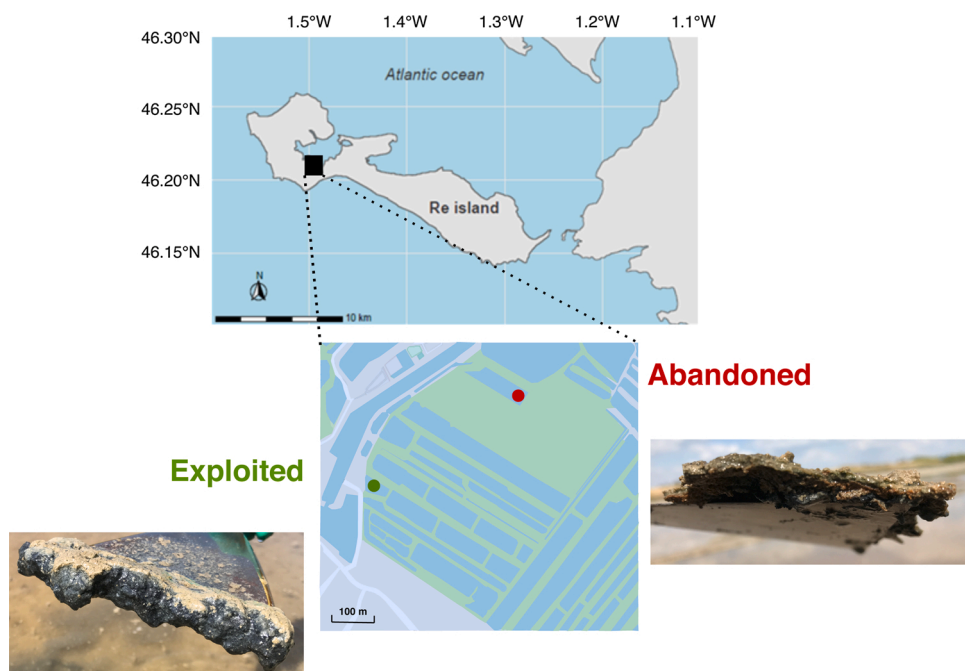


Fig. 1. Localisation of the sampling sites at the Ré Island (France). Microbial mats were sampled in abandoned (red point) and exploited (green point) sites in independent triplicates corresponding to three ponds in each site.

The water salinity (Practical Salinity Unit, psu corresponding to g/L) and the water temperature (°C) were measured in triplicate in each sampling spot with a multiparameter probe (pHénoménal® MU 6100H, VWR™, USA).

2.2. DNA extraction and Illumina sequencing

Microbial mat samples were ground in liquid nitrogen with a mortar and a pestle as previously described (Fourçans et al., 2008). Then, DNA was extracted from 0.25 g subsamples using the DNeasy® PowerSoil kit (Qiagen) according to the manufacturer's instructions, with a slight modification at the homogenization step, by using a Precellys homogenizer (Bertin Instruments).

The V3-V4 region of the bacterial 16S rRNA genes (460 bp) was amplified using the primers PCR1F_460 (5'-ACGGRAGGCAGCAG-3') and PCR1R_460 (5'-TACCAGGTATCTAATCCT-3') (Klindworth et al., 2013). The Primers 519 F (5'-GCCGCGCGGTA-3') and 915R (5'-GTGCTCCCCGCCAATTC-3') were used to amplify the V3-V5 region (400 pb) of the archaeal 16S rRNA gene (Hugoni et al., 2015). Polymerase chain reaction (PCR) mix consisted in 5 µL of MTP Taq DNA polymerase (5 U/µL) with 1 µL MTP Taq Buffer (10X) (Sigma-Aldrich), 1 µL of dNTP (10 mM), 1.25 µL of each primer (20 µM) and 10 ng of genomic DNA, in a final volume of 50 µL (adjusted with distilled water). All amplifications were performed on a Labcycler (SensoQuest) using the following PCR program: 2 min at 94 °C, 30 cycles of 60 s at 94 °C, 40 s at 65 °C for Bacteria (40 s at 57 °C for Archaea), and 30 s at 72 °C, and finally, 10 min at 72 °C.

The V4 region (390 bp) of the 18S rRNA genes was amplified using the universal primer 515 F (5'-GTGYCAGCMGCCGCGTA-3') (Caporaso et al., 2011) and the eukaryotic primer 951R (5'-TTGGYRAATGCTTTGCG-3') (Lepère et al., 2016). PCR mix consisted in 27.5 µL of AmpliTaq Gold® 360 master mix (Applied Biosystems), 1.1 µL of each primer (20 µM) and 5.5 µL of genomic DNA, in a final volume of 55 µL (adjusted with distilled water). All amplifications were performed on a Veriti 96 Well Thermal Cycler (Applied Biosystem) using the following PCR program: 10 min at 95 °C, 35 cycles of 30 s at 95 °C, 30 s at 55 °C and 45 s at 72 °C, and finally, 10 min at 72 °C.

All PCR were performed in triplicate for each sample and considered separately in order to obtain technical replicates in order to consider the PCR bias. Illumina sequencing was performed by the NED team (UMR1388 GenPhySE) and the GeT core facility (Toulouse, France), using Illumina MiSeq technology (paired-end 2 × 250 bp). The complete dataset was deposited in the NCBI Sequence Read Archive (SRA) database under SRA accession number PRJNA627371 for eukaryotic dataset and PRJNA627173 for bacterial dataset.

2.3. Sequence processing

Bioinformatic processing for DNA sequences were performed using QIIME 2 2019.4 (Bolyen et al., 2019). The same process was followed for 16S (Bacteria) and 18S (Eukaryote) rRNA gene sequences. Raw sequences were demultiplexed and then filtered, denoised, merged and grouped in non-chimeric sequences with DADA 2 (Callahan et al., 2016) followed by a singleton filtering. The taxonomic affiliation was performed against the Silva database v132 (Quast et al., 2012; Yilmaz et al., 2013) with 97 % of similarities in order to compare the biodiversity obtained in previous studies, as it is used in most studies exploring biodiversity in microbial mats (Cardoso et al., 2019; Sierra et al., 2020; Vogt et al., 2018). Additionally, Silva database allows to analyse the three domains of life (Bacteria, Archaea, and Eukarya) while the other databases (e.g. Greengenes, RDP) will not (Balvočiūtė and Huson, 2017). The non-affiliated sequences were excluded. The rarefaction was done at 5530 and 22,274 sequences per sample for bacteria and eukaryote respectively (Supplementary materials, Fig. S1.), which correspond to the lowest number of sequences considering the PCR replicates (data not shown).

2.4. Meiofauna characterization

Microbial mat was sieved through 50 µm before staining with rose Bengal and observation under a binocular loupe (magnification x30, Zeiss). A sample splitter (Motoda box as Rzeznik-Orignac et al., 2003) was used to obtain an aliquot containing at least 100 individual nematodes for abundance estimation. The abundance of other meiobenthic taxa (i.e. copepods and ostracodes) was too low to be evaluated in split samples and, therefore, was quantified using whole samples. Abundances were expressed as individuals per cubic centimetre (ind. cm⁻³).

2.5. Statistical analysis

Statistical analyses were performed using Rstudio software (R version 3.6.3, (2020–02-29), R Core Team, 2020). The water temperature between the two sites was compared with a Student *t*-test because the conditions of application (normality of data and variance independence) were verified and with a Welch two sample *t* for salinity because the independence of variances was not verified. Then, the difference in the relative microbial abundance was investigated between the abandoned and exploited sites. The biom file produced by the bioinformatic analysis and the table of environmental data were merged into a single R package using "phyloseq" (McMurdie and Holmes, 2013). The statistical analyses were performed on the average of the PCR triplicates (technical replicates) for each sample in order to consider the PCR bias. The alpha diversity was calculated by two indices, the richness (based on presence/absence of Amplicon Sequence Variants (ASVs)) and the Shannon index (according to the relative abundance of ASVs). The abundances were compared at different taxonomic levels with a Student *t*-test if the conditions of application (normality of data and variance independence) were verified, or with a Welch two sample *t* if the normality was verified but not the independence of variances and with a Wilcoxon-Mann-Whitney test if any condition was respected. The beta diversity between sites was then analysed with a principal coordinate analysis (PCoA) of Bray-Curtis distance matrices. A dendrogram of each replicate of the sites was also done with Bray-Curtis distance matrices. The contribution of each ASV explaining the differences between sites was defined by SIMPER (SIMilarity PERcentages) based on Bray-Curtis distance measure. Linear discriminant analysis effect size (LEfSe) (Segata et al., 2011) on the 50 more abundant ASVs was done on Galaxy web application to determine bacterial genera or eukaryotic families biomarkers of each site. The non-parametric Kruskal-Wallis sum-rank test ($\alpha = 0.05$) was performed to detect taxa with significant differential abundance. The biological consistency was investigated by performing a pairwise Wilcoxon test ($\alpha = 0.05$). A linear discriminant analysis (LDA) threshold score of 2.0 was applied.

3. Results and discussion

3.1. Description of the environmental parameters and the microbial mats

The water temperature and salinity were significantly higher in exploited site (25 ± 1 °C; 101 ± 3.7 psu) than in the abandoned site (23 ± 0.4 °C; 51.1 ± 0.7 psu) (Student *t*-test for temperature, $p < 0.05$; Welch two sample *t*-test for salinity, $p < 0.05$), while in both sites the water was at pH 8. Such results were expected as salinity increases in ponds for salt production without being subjected to desiccation, while seawater entering into the abandoned site maintains a lower salinity. The microbial mats showed different morphological aspects, particularly in their thickness that may be explained by the scraping during salt recovery, resulting in a thinner microbial mat in the exploited site. Also, it has been shown that salinity affect exopolysaccharide (EPS) production, that in turn might affect the mat structure and properties (Decho and Gutierrez, 2017). Such observation suggested that the environmental conditions may affect the microbial mats as observed in diverse coastal ecosystems including sediments (Pringault et al., 2008; Duran

et al., 2015), estuarine mudflats (Chronopoulou et al., 2013) and hypersaline microbial mats (Bordenave et al., 2004).

3.2. Microbial and meiofaunal community diversity in abandoned and exploited salterns

Despite several attempts, we were unable to obtain archaeal 16S rRNA gene fragment sequences. Although DNA extraction and PCR amplification bias cannot be excluded, this result was in accordance with previous studies showing that benthic mats in hypersaline ponds are dominated by bacteria and are even almost exclusively bacterial (Bolhuis and Stal, 2011; Bolhuis et al., 2014; Stal et al., 2019), with very low abundance of Archaea below 1%, especially within the upper part (0.5 cm) of the mat (Bolhuis and Stal, 2011) as analysed in this study. The flooding each winter, after salt recovery, induces the fluctuation of environmental parameters resulting on the renewing of the microbial mats that may also explain the fact that Archaea were not detected. Indeed, Archaea have been demonstrated to be sensitive to drastic modifications of environmental parameters (Zhao et al., 2020) probably preventing their development within microbial mats. Because Archaea have been shown to play a critical role in ecosystem function (Wong et al., 2017), further efforts with optimised molecular methods and tools will be beneficial to describe the archaeal diversity in microbial mats. Particularly, it is worth to note that our attempt to target Archaea was based on the utilisation of only a set of primers, several sets of primers have been developed allowing to extend the capacity to reveal Archaea

diversity (Bahram et al., 2019) that will help to detect Archaea in the microbial mats. Thus, our study focuses on the bacterial and eukaryotic components of the microbial mats inhabiting the abandoned and exploited saltern sites.

The composition of bacterial and eukaryotic communities was determined by high throughput sequencing in order to compare microbial mats of the abandoned salterns to that of exploited salterns. The number of raw sequences ranged between $30,243 \pm 4898$ (abandoned site) and $19,200 \pm 2626$ (exploited site) for Bacteria, and between $50,119 \pm 720$ (abandoned site) and $39,684 \pm 1408$ (exploited site) for Eukaryota (Supplementary materials, Table S1). After filtering, the rarefaction provided a random subsample of 5530 bacterial sequences and 22,274 eukaryotic sequences per sample (Supplementary materials, Table S1).

The bacterial richness observed for the microbial mats inhabiting the abandoned site was in the same range (between 200–700 ASVs) to that observed for other coastal ecosystems (Dillon et al., 2013; Cardoso et al., 2019). The bacterial Shannon indexes of the abandoned and the exploited sites (5.75 and 4.6, respectively) were higher than that reported for prokaryotic communities from solar salterns (Dillon et al., 2013) and spring coastal microbial mats (Cardoso et al., 2019) (Fig. 2).

For Bacteria, the richness and the Shannon index were significantly higher (Student *t*-test, $p < 0.05$) in the abandoned site (643 ± 60 ASVs and 5.73 ± 0.09) than in the exploited site (265 ± 75 ASVs and 4.77 ± 0.27 ; Fig. 2A, B). Interestingly, for Eukaryota, the opposite was observed, the richness and the Shannon index being significantly higher

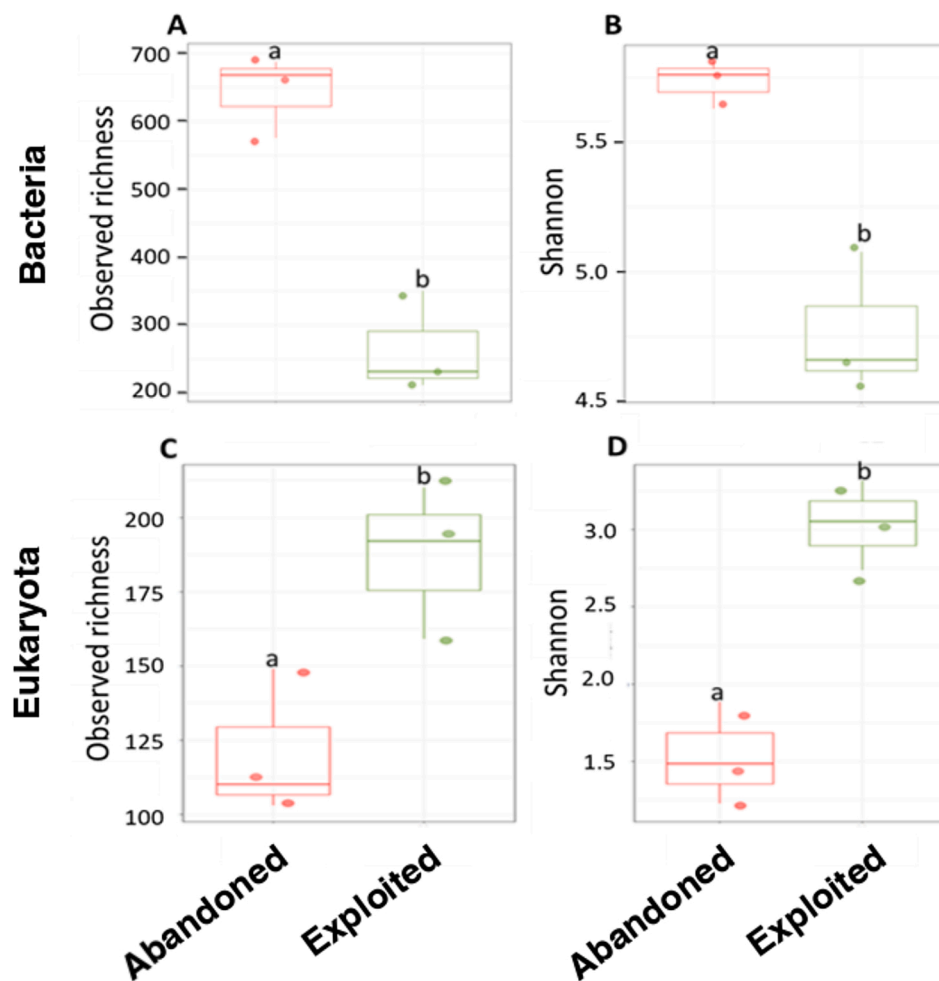


Fig. 2. Diversity indexes for bacterial (A, B) and eukaryotic (C, D) communities in the abandoned (red) and exploited (green) sites. The boxplots show observed richness (A, C) and Shannon (B, D) indexes determined at the ASV level from 16S (Bacteria) and 18S (Eukarya) rRNA gene sequences. Different letters indicate significant differences based on Student *t*-test at $p < 0.05$ ($n = 3$).

(Student *t*-test, $p < 0.05$) in the exploited site (187 ± 26 ASVs and 3.03 ± 0.29) than in the abandoned site (121 ± 25 ASVs and 1.53 ± 0.33 ; Fig. 2C, D). Such observation was consistent with previous reports indicating that salinity is a main driver for bacterial community diversity (Fei Xi et al., 2014; Jeanbille et al., 2016a; Ben Salem et al., 2019) and for the meiofaunal abundance and species composition (Coull, 1999). It has been demonstrated that the richness and abundance of bacteria and eukaryotes decrease along a gradient of salinity because the conditions become extreme with increasing salinity (Nubel et al., 2000; Pedrós-Alió et al., 2000; Benloch et al., 2002; Estrada et al., 2004). For eukaryotes, some populations have been reported dominant in high salt concentration (above seawater salinity, 35 psu) ecosystems (Eloumi et al., 2009). Interestingly, the eukaryotic diversity was higher in the more salted site (exploited) in our study.

The human actions for salt exploitation, which include regular scraping for salt recovery and microbial mat removal together with the fluctuations of environmental parameters (Wieland et al., 2003), are probably responsible for the decreased bacterial diversity observed in the exploited site in comparison to the abandoned site. Indeed, the abandoned site is not disturbed by human actions, which results to an ecosystem with weak fluctuations that is considered as an ecosystem with less selective pressure for bacterial communities (Graham et al., 2016). In contrast, the increasing of eukaryotic diversity with salinity has never been reported before for hypersaline environments (Pillay and Perissinotto, 2009; Heidelberg et al., 2013). Other factors have been reported to influence the composition of the eukaryotic population like hydrodynamic (Kapusta et al., 2005), sediment stability (Kapusta et al., 2005), sediment particle size (Coull, 1999), temperature (Coull, 1999; Kapusta et al., 2005), depth (Baguley et al., 2006), physical disturbance (Austen and Widdicombe, 2006), nutrient enrichment (Austen and Widdicombe, 2006) and long-term anthropogenic impacts (Boldina et al., 2014). Nevertheless, we assume that physical disturbance and long-term anthropogenic actions were the most probable factors driving eukaryotic communities in our study since salt workers in Ré Island follow a traditional exploitation removing the accumulated mud each winter as described for the Aveiro salterns (Rodrigues et al., 2011). More information about the physical-chemical parameters such as pH, dissolved oxygen concentration and water renewable rates will be necessary to determine the factor influencing the eukaryotic composition.

3.3. Bacterial and meiofaunal community composition of microbial mats inhabiting abandoned and exploited salterns

The first 0.5 cm of microbial mats from both sites were dominated by the same seven bacterial phyla with high abundance of Proteobacteria and Bacteroidetes (Fig. 3). This phyla composition was comparable to that of coastal microbial mats where Cyanobacteria, Proteobacteria and Bacteroidetes are dominant (Cardoso et al., 2019) as well as in most hypersaline microbial mats (Pal et al., 2020). Bacteroidetes and Proteobacteria, described as dominant phyla in the water and sediment of other salterns (Boujelben et al., 2012; Lee et al., 2020), are known to play important roles in carbon and nitrogen cycles (Bernhard et al., 2012; Wong et al., 2015). Only Gammaproteobacteria showed significant differences between the studied sites: they were significantly more abundant in the exploited site than in the abandoned site (Student *t*-test, $p < 0.05$). Such Gammaproteobacteria abundance discrepancy between both sites might be explained by the fact that Gammaproteobacteria class has been reported to be composed of pioneering microorganisms during the biofilm formation (Lee et al., 2008), which is in accordance with the fact that the microbial mat is renewed every year in the exploited site. Generally, Cyanobacteria are found dominant in microbial mat composition (Fourçans et al., 2004, 2006, 2008; Bolhuis and Stal, 2011; Boujelben et al., 2012; Bolhuis et al., 2014; Stal et al., 2019). Surprisingly, they accounted for less than 1% of the total phyla abundance in our study although that underestimation of Cyanobacteria cannot be excluded due to technical bias such as DNA extraction and primers efficiencies as previously reported (Fourçans et al., 2004).

Assuming that the physical-chemical parameters of the abandoned saltern, particularly the salinity, tend to be similar to those found at the near oceanic coast, we expect that the microbial mat composition will be close to that observed in microbial mats inhabiting such coastal areas. The microbial composition of the coastal sediment from Ré Island has not yet been described. However, Proteobacteria and Planctomycetes were found to be dominant in the first centimetre of sediments from Marennes-Oléron Bay, located about 50 km from Ré Island, while Bacteroidetes was the fourth dominant phylum (Lavergne, 2014), which differs from the bacterial phyla composition of microbial mats from both abandoned and exploited sites. Such observation suggested that the abandonment period (15 years) was not long enough for erasing the effect of saltern exploitation to reach the bacterial composition observed in coastal sediments, probably because the salinity in both abandoned and exploited sites exceeds regularly the seawater salinity (> 35 psu). To the best of our knowledge, only two studies have reported the

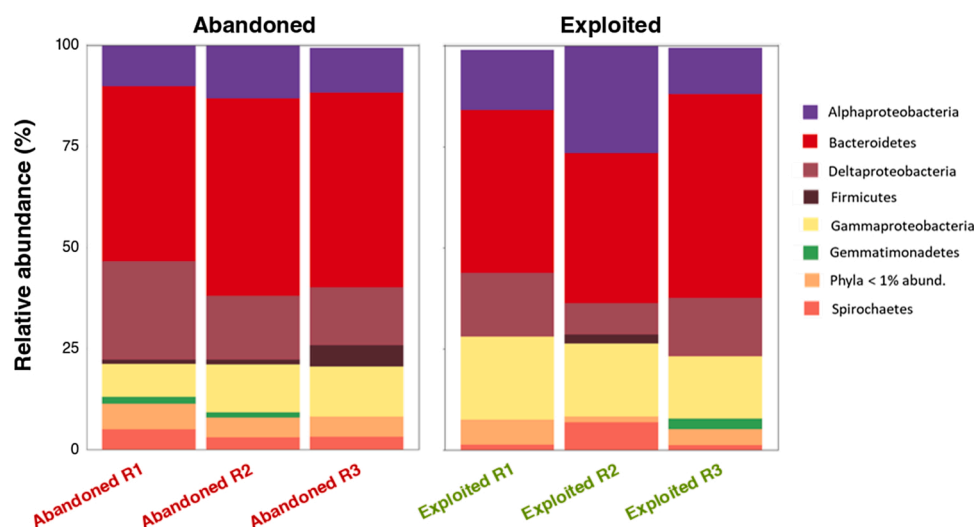


Fig. 3. Bacterial community compositions at the phylum level in the abandoned and exploited sites. The bar plots represent each replicate, presenting the phyla with a relative abundance above 1%. The class level within Proteobacteria phylum is shown.

reorganization of microbial communities after the abandonment of salterns exploitation (Bernhard et al., 2012; Lee et al., 2020). These studies concluded that the physical-chemical parameters were similar to that observed at the coast only one year after the natural collapse of embankments, but the bacterial composition remained different for more than 30 years (Bernhard et al., 2012; Lee et al., 2020). It is important to mention that in our study the salterns were still intact maintaining the salinity gradient, which drives bacterial community structure. Further long time-series analyses comparing microbial communities in different locations at Ré Island are still required to determine whether the microbial community reach the structure observed in the coast.

The eukaryotic community in the abandoned site was dominated by only three phyla (abundance above 1%) while the exploited site was characterized by a large eukaryotic diversity with six main phyla identified (Fig. 4). Metazoa dominated the eukaryotic community in the abandoned site, being significantly more abundant (Student *t*-test, $p < 0.05$) than in the exploited site (Fig. 4). The presence of Metazoa in both sites was not surprising since they are often found in marine sediments, which are usually dominated by Nematoda followed by Platyhelminthes and Arthropoda (Fonseca et al., 2014; López-Escardó et al., 2018). All the phyla identified have been ever seen in other exploited salterns (Feazel et al., 2008; Stock et al., 2012) and in abandoned salterns (Cvitković et al., 2011) but, to our knowledge, no studies compared the eukaryotic composition in these two types of salterns.

The more important eukaryotic diversity observed in the exploited site, in comparison to that of the abandoned site, might be explained by the human action of scratching the surface of the microbial mat, which probably prevents colonization by a single eukaryotic population.

Because it is known that molecular analysis has inherent bias derived from DNA extraction efficiency and primers specificity (Tedersoo et al., 2018), the eukaryotic diversity was completed by meiofaunal microscopic observations. The presence of Acari, Polychaeta, insect larvae and *Copepoda nauplii* was observed that were not detected by molecular analysis (Supplementary materials, Fig. S2). Consistently with the molecular analysis, Nematoda largely dominated (>99 %) the observable meiofaunal community of the abandoned site (Supplementary materials, Fig. S2). But, in contrast to the molecular analysis, Nematoda were also observed (around 69 %) together with adult Copepods (26 %), Acari (4%), insect larvae (2%) and Polychaeta (2%) in the exploited site (Supplementary materials, Fig. S2). Thus, we advocate that the combination of molecular techniques with microscopic observations will help to obtain a more comprehensive and accurate analysis of eukaryotes species diversity in the environmental samples.

3.4. Comparison of bacterial and meiofaunal communities from abandoned site and from exploited site

The comparison of the bacterial and eukaryotic communities between the abandoned site and the exploited site by principal coordinate analysis (PCoA) showed a clear separation between the sites along the PCo1 axis explaining around 47 % of the data distribution for the bacterial community (Fig. 5A) and 92 % for the eukaryotic community (Fig. 5B). Noteworthy, the PCoA analysis showed a heterogeneity within the exploited site with a dispersion of the triplicates along the PCo2 axis explaining around 21 % of the data distribution for bacteria (Fig. 5A) and around 5% for eukaryotes (Fig. 5B). However, cluster analysis based on Bray-Curtis distances confirmed that the bacterial and eukaryotic communities of the triplicates from the abandoned site were clustered together, clearly separated from the cluster formed by the bacterial and eukaryotic communities of the exploited site (Fig. 5C and D). The difference of the bacterial and eukaryotic communities between both sites was further confirmed by SIMPER analysis showing overall dissimilarity for bacterial community compositions (SIMPER: 50 %) as well as for eukaryotic community compositions (SIMPER: 72 %).

Accordingly, LEfSe analyses revealed taxa, bacterial and eukaryotic, differentially abundant between both sites (Fig. 6), which represent site-specific biomarkers as previously suggested in studies identifying environmental and contaminant microbial biomarkers (Segata et al., 2011; Jeanbille et al., 2016b). The abandoned site was characterized by 11 bacterial and 5 eukaryotic biomarkers (Fig. 6). Interestingly, ASVs related to *Loktanella* (Alphaproteobacteria) and Desulfobacterales, which are usually found in abandoned salterns and tidal flats (Lee et al., 2020), were identified among the bacterial biomarkers (Fig. 6A). The Desulfobacterales, sulfate reducing bacteria generally predominant in sulfate-rich sediment (Ruff et al., 2015), have been shown to influence the microbial re-colonization of abandoned salterns (Lee et al., 2020). Similarly, the Alphaproteobacteria *Loktanella*, has been described as a pioneer bacterium in marine biofilm formation (Lee et al., 2008). The identification of such biomarkers suggested that the bacterial community at the abandoned site was undergoing a re-organisation. Regarding the eukaryotic biomarkers, ASVs related to Arthropoda, Nematoda and Platyhelminthes belonging both to Metazoa as specific members of abandoned site (Fig. 6B). It is known that Nematoda dominate in marine sediments, followed by Platyhelminthes, Arthropoda and a random assemblage of Gastrotricha, Annelida, Mollusca... (Fonseca et al., 2014; López-Escardó et al., 2018). This observation was in accordance with our hypothesis that the microbial composition in the abandoned site would tend to be similar to that found on the coast.

According to the LEfSe analyses, the exploited site was characterized

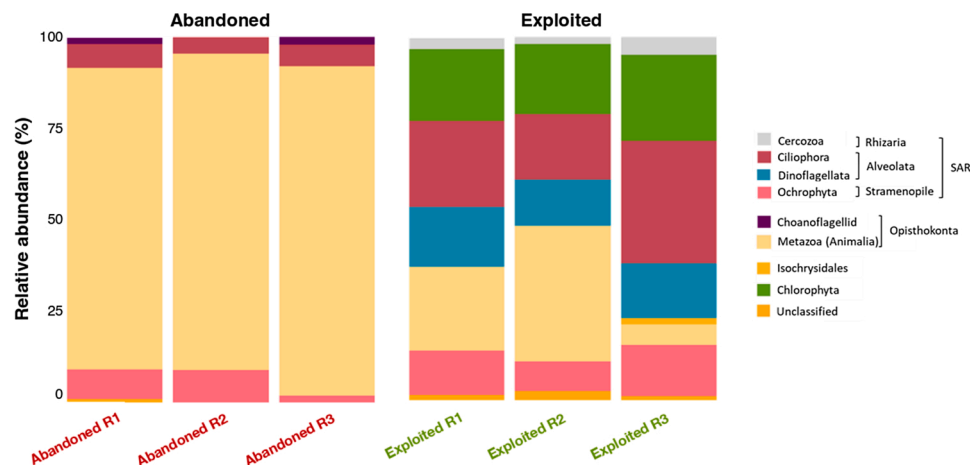


Fig. 4. Eukaryotic community compositions at the phylum level in the abandoned and exploited sites. The bar plots represent each replicate, presenting the phyla with a relative abundance above 1%.

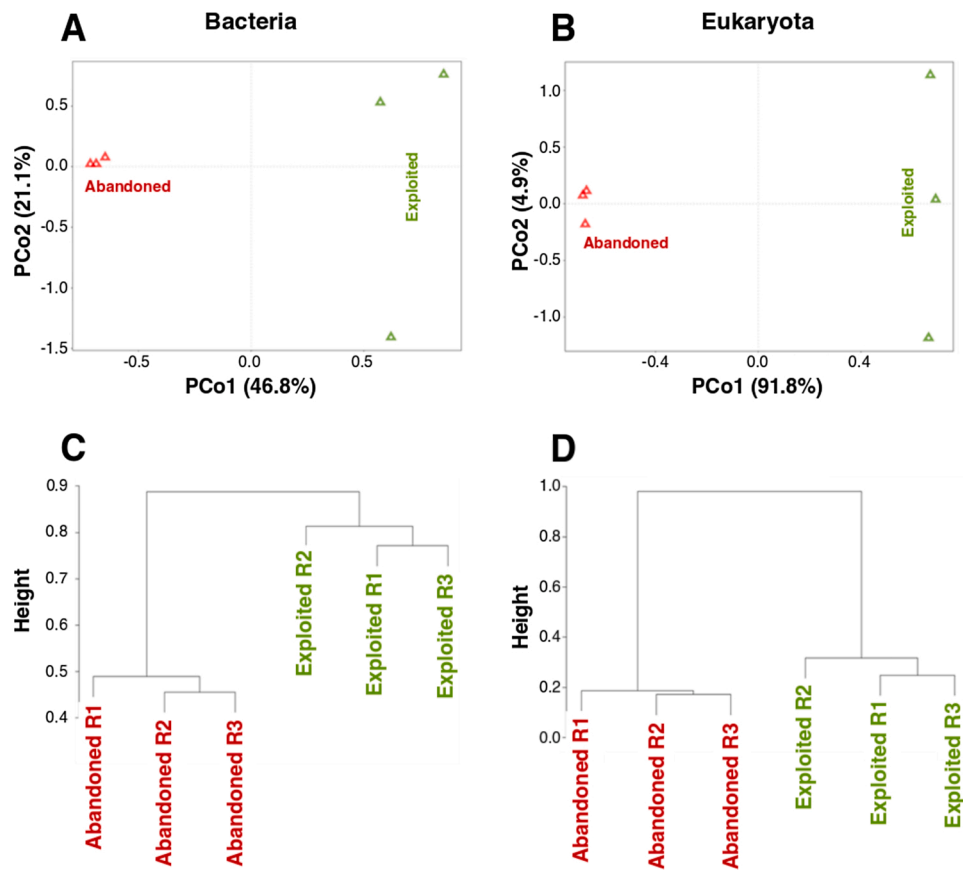


Fig. 5. Comparison of bacterial and eukaryotic communities inhabiting the abandoned (red) and exploited (green) sites. (A, B) Principal coordinate analysis (PCoA) comparing bacterial (A) and eukaryotic (B) communities. (C, D) Clustering analysis based on Bray-Curtis distances.

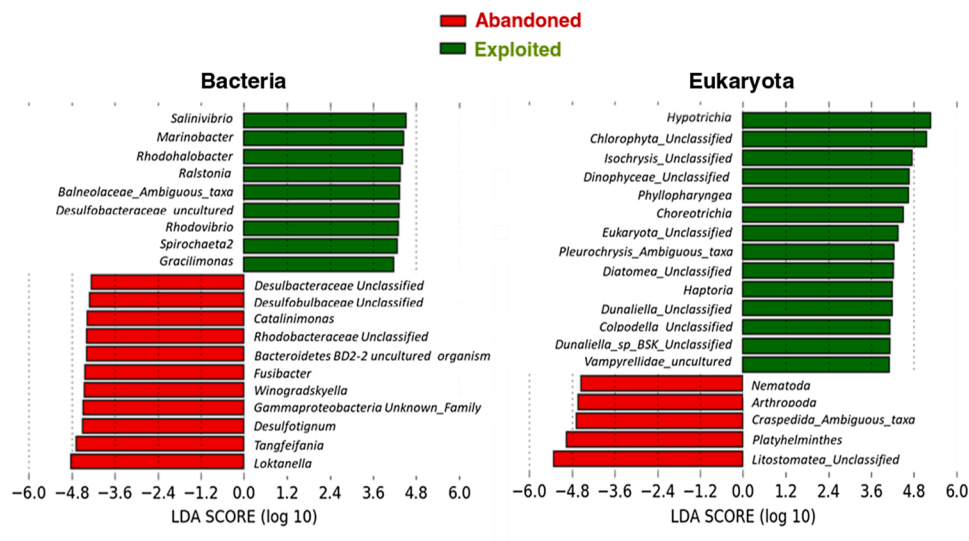


Fig. 6. Comparison of bacterial (A) and eukaryotic (B) communities inhabiting the abandoned (red) and exploited (green) sites by linear discriminant analysis effect size (LEfSe). The analysis was performed with the 50 more abundant bacterial and eukaryotic ASVs of each site.

by 9 bacterial and 14 eukaryotic biomarkers (Fig. 6). Consistent with the high salinity prevailing at the exploited site, ASVs related to halophilic bacterial genera were identified as biomarkers (Fig. 6A) such as *Marinobacter*, *Salinivibrio* and *Rhodohalobacter* that are usually found in hypersaline environments (Gorshkova, 2003; Duran, 2010; Kim et al., 2017; Xia et al., 2017; López-Hermoso et al., 2018; de la Haba et al., 2019). Such information showed the salinity impact of the microbial

mat organisation, further highlighting the differences the contrasted organization with the microbial mat from the abandoned salterns.

The specific eukaryotic ASVs identified in the exploited site were more diverse than that identified in the abandoned site. For example, ASVs related to the Ciliophora phylum were detected in both sites but the populations were different at the class and subclass levels (Fig. 6B). *Choreotrichia*, *Haptoria* and *Hypotrichia* sub-classes, and

Phylopharyngea class were found to be significantly more abundant in the exploited site, while ASVs related to Litostomatea class were significantly predominant in the abandoned site (Fig. 6B). Such observation was in accordance with previous report showing that members of the Ciliophora phylum (ciliates) were influenced by the salinity, their abundance and biomass increasing with salinity together with a modification in their composition (Nche-Fambo et al., 2016). Additionally, members of the Choreotrichia subclass have been reported dominant in saline environments with salinities reaching up to 64 psu (Nche-Fambo et al., 2016). The other ASVs found significantly dominant in the exploited site were related to eukaryotic phototrophs related to the Chlorophyta phylum (*Dunaliella*), Dinophyceae class (Dinoflagellates), Haptista phylum (*Isochrysis* and *Pleurochrysis*), and Diatomea (Fig. 6B), indicating that the exploited site was dominated by eukaryotic phototrophs in comparison to the abandoned site. In contrast, the abandoned site was characterized by the presence of ASVs related to Nematoda, Arthropoda, Platyhelminthes and Ciliophora (Litostomatea) phyla, and Craspedida order, which were found significantly abundant (Fig. 6B). Such differences in eukaryotic composition between both sites suggested an important influence of the salinity in the organization of eukaryotic community that in turn might provoke changes in the food web as previously reported along a salinity gradient (Pedrós-Alió et al., 2000). It is likely that the low diversity of preys on the abandoned site (bacteria and ciliates) favoured the development of Metazoa, explaining that Metazoa related ASVs (Nematoda, Arthropoda, and Platyhelminthes) were found significantly more abundant than in the exploited site. Indeed, the Metazoa related ASVs (Nematoda, Arthropoda, and Platyhelminthes) have been shown to be able to feed on bacteria (De Mesel et al., 2004; Feazel et al., 2008; Hubas et al., 2010), diatoms (Montagna, 1984), phytobenthos (algae and diatoms; Cowles et al., 1988), ciliates (Berk et al., 1977), and dinoflagellates (Cowles et al., 1988; Turner, 2004). In contrast, in the exploited site, the higher diversity of Ciliophora (ciliates) related ASVs together with large diversity of eukaryotic phototrophs (Diatoms, Dinoflagellata and Chlorophyta; (Cupp, 1943; Lewis and McCourt, 2004; Jordan, 2012) indicated a larger diversity of preys than in the abandoned site. The ciliates are well known as major predator for bacteria (Sherr and Sherr, 1987; Parry, 2004) but they can also feed flagellates and other ciliates (Bernard and Rassoulzadegan, 1990; Dolan and Coats, 1991). It is likely that the exploitation of the saltern resulted in more extreme conditions (higher salinity) reducing the bacterial diversity with concomitant modification in food web structure.

4. Conclusion

After stopping the exploitation of the salterns, the abandoned site was characterized by lower salinity with limited variations in comparison to the exploited site. Such conditions favoured the installation of a more diverse bacterial community in the abandoned site while the eukaryotic diversity was lower with the dominance of Nematoda. The presence of site specific ASVs, being significantly more abundant according to the site (biomarkers), suggested a re-organisation of the microbial mat in the abandoned site with a structure tending to get closer to that found in coastal areas. In contrast, the more extreme conditions at the exploited site, characterized by salinity variations, resulted in reduced bacterial diversity with a modification of the food web structure. The exploited site presented halophilic bacteria and a larger diversity of eukaryotic metabolisms. It is likely that the human exploitation of salterns constrains the microbial composition of the microbial mats, which undergo perceptible modifications several years after the abandonment of the salterns. A monitoring of the microbial mats during several years (at least 15 years) on the abandoned salterns is necessary to understand precisely how this structure could be resilient face to human activities.

CRedit authorship contribution statement

Camille Mazière: Conceptualisation, Investigation, Resources, Formal analysis, Writing – original draft. **Hélène Agogué:** Conceptualisation, Investigation, Formal analysis, Validation. **Cristiana Cravo-Laureau:** Conceptualisation, Investigation, Formal analysis, Writing – original draft. **Christine Cagnon:** Conceptualisation, Formal analysis, Validation. **Isabelle Lanneluc:** Conceptualisation, Sampling. **Sophie Sablé:** Conceptualisation, Sampling. **Ingrid Fruitier-Arnaudin:** Conceptualisation, Sampling. **Christine Dupuy:** Conceptualisation, Investigation, Resources, Formal analysis, Writing – original draft, Supervision, Project administration, Funding acquisition. **Robert Duran:** Conceptualisation, Investigation, Resources, Formal analysis, Writing – original draft, Supervision, Project administration, Funding acquisition.

Funding

C.M. was supported by a PhD grant from E2S-UPPA program and the Région Nouvelle-Aquitaine. We thank the funding support from the ACI U. La Rochelle and the European programme ERANETMED AQUASALT (NMED-0003–01).

Availability of data and material

Sequencing data has been deposited in sequence database.

Code availability

Not applicable

Declaration of Competing Interest

None declared.

Acknowledgements

The authors are grateful to Corentin Hervé, Nicolas Lachaussée, Philippe Pineau and the salterns owners Hélène and Tanguy Jouannet and the society Algorithme. We acknowledge the Molecular Core Facilities at LIENSs laboratory.

This work was performed in collaboration with the GeT core facility, Toulouse, France (<http://get.genotoul.fr>) supported by France Génomique National infrastructure, funded as part of “Investissement d’avenir” program managed by Agence Nationale pour la Recherche (contract ANR-10-INBS-09).

Appendix A. Supplementary data

Supplementary material related to this article can be found, in the online version, at doi:<https://doi.org/10.1016/j.micres.2021.126854>.

References

- Austen, M.C., Widdicombe, S., 2006. Comparison of the response of meio- and macrobenthos to disturbance and organic enrichment. *J. Exp. Mar. Biol. Ecol.* 330, 96–104.
- Baguley, J.G., Montagna, P.A., Hyde, L.J., et al., 2006. Metazoan meiofauna abundance in relation to environmental variables in the northern Gulf of Mexico deep sea. *Deep Sea Res Part Oceanogr Res Pap* 53, 1344–1362.
- Bahram, M., Anslan, S., Hildebrand, F., Bork, P., Tedersoo, L., 2019. Newly designed 16S rRNA metabarcoding primers amplify diverse and novel archaeal taxa from the environment. *Environ. Microbiol. Rep.* 11 (4), 487–494.
- Balvočiūtė, M., Huson, D.H., 2017. SILVA, RDP, Greengenes, NCBI and OTT — how do these taxonomies compare? *BMC Genomics* 18 (2), 114.
- Ben Salem, F., Ben Said, O., Cravo-Laureau, C., et al., 2019. Bacterial community assemblages in sediments under high anthropogenic pressure at Ichkeul Lake/Bizerte Lagoon hydrological system. Tunisia. *Environ. Pollut.* 252, 644–656.
- Benlloch, S., Lopez-Lopez, A., Casamayor, E.O., et al., 2002. Prokaryotic genetic diversity throughout the salinity gradient of a coastal solar saltern. *Environ. Microbiol.* 4, 349–360.

- Berk, S.G., Brownlee, D.C., Heinle, D.R., et al., 1977. Ciliates as a food source for marine planktonic copepods. *Microb. Ecol.* 4, 27–40.
- Bernard, C., Rassoulzadegan, F., 1990. (PDF) Bacteria or microflagellates as a major food source for marine ciliates: possible implications for the microzooplankton. *Res. Gate*. <https://doi.org/10.3354/meps064147>.
- Bernhard, A.E., Marshall, D., Yiannos, L., 2012. Increased variability of microbial communities in restored salt marshes nearly 30 years after tidal flow restoration. *Estuaries Coasts* 35, 1049–1059.
- Boldina, I., Beninger, P., Coz, M., 2014. Effect of long-term mechanical perturbation on intertidal soft-bottom meiofaunal community spatial structure. *J. Sea Res.* 85, 85–91.
- Bolhuis, H., Stal, L.J., 2011. Analysis of bacterial and archaeal diversity in coastal microbial mats using massive parallel 16S rRNA gene tag sequencing. *ISME J.* 5, 1701–1712.
- Bolhuis, H., Cretoiu, M.S., Stal, L.J., 2014. Molecular ecology of microbial mats. *FEMS Microbiol. Ecol.* 90, 335–350.
- Bolyen, E., Rideout, J.R., Dillon, M.R., et al., 2019. Reproducible, interactive, scalable and extensible microbiome data science using QIIME 2. *Nat. Biotechnol.* 37, 852–857.
- Bordenave, S., Fourçans, A., Blanchard, S., et al., 2004. Structure and functional analyses of bacterial communities changes in microbial mats following petroleum exposure. *Ophelia* 58, 195–203.
- Boujelben, I., Gomariz, M., Martínez-García, M., et al., 2012. Spatial and seasonal prokaryotic community dynamics in ponds of increasing salinity of Sfax solar saltern in Tunisia. *Antonie Van Leeuwenhoek* 101, 845–857.
- Callahan, B.J., McMurdie, P.J., Rosen, M.J., et al., 2016. DADA2: high-resolution sample inference from Illumina amplicon data. *Nat. Methods* 13, 581–583.
- Caporaso, J.G., Lauber, C.L., Walters, W.A., et al., 2011. Global patterns of 16S rRNA diversity at a depth of millions of sequences per sample. *Proc. Natl. Acad. Sci.* 108, 4516–4522.
- Cardoso, D.C., Cretoiu, M.S., Stal, L.J., et al., 2019. Seasonal development of a coastal microbial mat. *Sci. Rep.* 9, 9035.
- Caumette, P., Matheron, R., Raymond, N., et al., 1994. Microbial mats in the hypersaline ponds of Mediterranean salterns (Salins-de-Giraud, France). *FEMS Microbiol. Ecol.* 13, 273–286.
- Chronopoulou, P.-M., Fahy, A., Coulon, F., et al., 2013. Impact of a simulated oil spill on benthic phototrophs and nitrogen-fixing bacteria in mudflat mesocosms. *Environ. Microbiol.* 15, 242–252.
- Coull, B.C., 1999. Role of meiofauna in estuarine soft-bottom habitats* - Coull - 1999 - Australian Journal of Ecology - Wiley Online Library. *Aust. J. Ecol.* (24), 327–343.
- Cowles, T.J., Olson, R.J., Chisholm, S.W., 1988. Food selection by copepods: discrimination on the basis of food quality. *Mar. Biol.* 100, 41–49.
- Cupp, E.E., 1943. Marine Plankton Diatoms of the West Coast of North America.
- Cvitičević, I., Despalatović, M., Grubelić, I., et al., 2011. Spatio-temporal variability of meiofauna community structure in abandoned salina of velike soline and adjacent area (Mediterranean, Adriatic sea). *Fresenius Environ. Bull.* 20, 645–655.
- de la Haba, R.R., López-Hermoso, C., Sánchez-Porro, C., et al., 2019. Comparative genomics and Phylogenomic Analysis of the genus *Salinivibrio*. *Front. Microbiol.* 10 <https://doi.org/10.3389/fmicb.2019.02104>.
- De Mesel, I., Derycke, S., Moens, T., et al., 2004. Top-down impact of bacterivorous nematodes on the bacterial community structure: a microcosm study. *Environ. Microbiol.* 6, 733–744.
- Decho, A.W., Gutierrez, T., 2017. Microbial extracellular polymeric substances (EPSs) in ocean systems. *Front. Microbiol.* 8 (922).
- Dillon, J., Carlin, M., Gutierrez, A., et al., 2013. Patterns of microbial diversity along a salinity gradient in the Guerrero Negro solar saltern, Baja CA Sur. Mexico. *Front. Microbiol.* 4, 399.
- Dobretsov, S., Abed, R.M.M., Al Maskari, S.M.S., et al., 2011. Cyanobacterial mats from hot springs produce antimicrobial compounds and quorum-sensing inhibitors under natural conditions. *J. Appl. Phycol.* 23, 983–993.
- Dolan, J.R., Coats, D.W., 1991. A study of feeding in predacious ciliates using prey ciliates labeled with fluorescent microspheres. *J. Plankton Res.* 13, 609–627.
- Duran, R., 2010. Marinobacter. Volume 3: microbes and communities utilizing hydrocarbons, oils and lipids - chapter 5. In: Timmis, K.N. (Ed.), *Handbook of Hydrocarbon and Lipid Microbiology*, vol. 3. Springer, Berlin, Heidelberg, pp. 1725–1735.
- Duran, R., Bielen, A., Paradzik, T., et al., 2015. Exploring Actinobacteria assemblages in coastal marine sediments under contrasted Human influences in the West Istria Sea. Croatia. *Environ. Sci. Pollut. Res.* 22, 15215–15229.
- Edgcomb, V.P., Bernhard, J.M., Summons, R.E., Orsi, W., Beaudoin, D., Visscher, P.T., 2014. Active eukaryotes in microbialites from Highborne Cay, Bahamas, and Hamelin Pool (shark bay). Australia. *The ISME J.* 8 (2), 418–429.
- Elloumi, J., Guerrazi, W., Ayadi, H., et al., 2009. Abundance and biomass of prokaryotic and eukaryotic microorganisms coupled with environmental factors in an arid multi-pond solar saltern (Sfax, Tunisia). *J. Mar. Biol. Assoc. U.K.* 89, 243–253.
- Estrada, M., Henriksen, P., Gasol, J.M., et al., 2004. Diversity of planktonic photoautotrophic microorganisms along a salinity gradient as depicted by microscopy, flow cytometry, pigment analysis and DNA-based methods. *FEMS Microbiol. Ecol.* 49, 281–293.
- Falcón, L.I., Valdespino-Castillo, P.M., Alcántara-Hernández, R.J., Gómez-Acata, E.S., Yanez-Montalvo, A., Águila, B., 2020. Stromatolites in Crater-lake Alchichica and Bacalar Lagoon, Astrobiology and Cuatro Ciénegas Basin as an Analog of Early Earth. Springer, pp. 183–201.
- Feazel, L.M., Spear, J.R., Berger, A.B., et al., 2008. Eucaryotic diversity in a hypersaline microbial mat. *Appl. Environ. Microbiol.* 74, 329–332.
- Fei Xi, X., Wang, L., Jun Hu, J., et al., 2014. Salinity influence on soil microbial respiration rate of wetland in the Yangtze River estuary through changing microbial community. *J. Environ. Sci. China* 26, 2562–2570.
- Fleming, E.D., Prufert-Bebout, L., 2010. Characterization of cyanobacterial communities from high-elevation lakes in the Bolivian Andes. *J. Geophys. Res. Biogeosci.* 115 (G2).
- Fonseca, V.G., Carvalho, G.R., Nichols, B., et al., 2014. Metagenetic analysis of patterns of distribution and diversity of marine meiobenthic eukaryotes. *Glob. Ecol. Biogeogr.* 23, 1293–1302.
- Fourçans, A., de Oteyza T.G., Wieland, A., et al., 2004. Characterization of functional bacterial groups in a hypersaline microbial mat community (Salins-de-Giraud, Camargue, France). *FEMS Microbiol. Ecol.* 51, 55–70.
- Fourçans, A., Solé, A., Diestra, E., et al., 2006. Vertical migration of phototrophic bacterial populations in a hypersaline microbial mat from Salins-de-Giraud (Camargue, France). *FEMS Microbiol. Ecol.* 57, 367–377.
- Fourçans, A., Ranchou-Peyruse, A., Caumette, P., et al., 2008. Molecular analysis of the spatio-temporal distribution of sulfate-reducing Bacteria (SRB) in camargue (France) hypersaline microbial mat. *Microb. Ecol.* 56, 90–100.
- Giani, D., Seeler, J., Giani, L., et al., 1989. Marinobacter and physicochemistry in a saltern in the Bretagne (France) and in a laboratory scale saltern model. *FEMS Microbiol. Lett.* 62, 151–161.
- Gómez-Villegas, P., Vigarra, J., León, R., 2018. Characterization of fungi from hypersaline environments of solar salterns using morphological and molecular techniques. *Mar. Drugs* 16. <https://doi.org/10.3390/md16090332>.
- Gorshkova, N.M., 2003. Marinobacter excellens sp. nov., isolated from sediments of the Sea of Japan. *Int. J. Syst. Evol. Microbiol.* 53, 2073–2078.
- Graham, E.B., Crump, A.R., Resch, C.T., et al., 2016. Coupling spatiotemporal community assembly processes to changes in microbial metabolism. *Front. Microbiol.* 7 <https://doi.org/10.3389/fmicb.2016.01949>.
- Heidelberg, K.B., Nelson, W.C., Holm, J.B., et al., 2013. Characterization of eukaryotic microbial diversity in hypersaline Lake Tyrrell. Australia. *Front. Microbiol.* 4. <https://doi.org/10.3389/fmicb.2013.00115>.
- Hubas, C., Sachidhanandam, C., Rybarczyk, H., et al., 2010. Bacterivorous nematodes stimulate microbial growth and exopolymer production in marine sediment microcosms. *Mar. Ecol. Prog. Ser.* 419, 85–94.
- Hugoni, M., Domaizon, I., Taib, N., Biderre-Peti, C., Agogue, H., Galand, P.E., Debros, D., Mary, I., 2015. Temporal dynamics of active Archaea in oxygen-depleted zones of two deep lakes. *Env. Microbiol Rep* 7, 321–329.
- Jeanbille, M., Gury, J., Duran, R., et al., 2016a. Response of core microbial consortia to chronic hydrocarbon contaminations in coastal sediment habitats. *Front. Microbiol.* 7 <https://doi.org/10.3389/fmicb.2016.01637>.
- Jeanbille, M., Gury, J., Duran, R., et al., 2016b. Chronic polyaromatic hydrocarbon (PAH) contamination is a marginal driver for community diversity and prokaryotic predicted functioning in coastal sediments. *Front. Microbiol.* 7 <https://doi.org/10.3389/fmicb.2016.01303>.
- Jørgensen, B.B., Cohen, Y., 1977. Solar Lake (Sinai). 5. The sulfur cycle of the benthic cyanobacterial mats. *Limnol. Oceanogr.* 22, 657–666.
- Jordan, R.W., 2012. Haptophyta. *ELS. Cancer Epidemiol. Biomarkers Prev.*
- Kahle, D., Wickham, H., 2013. Ggmap: spatial Visualization with ggplot2. *R J.* 5, 144.
- Kapusta, S.C., Würdig, N.L., Bemvenuti, C.E., et al., 2005. Meiofauna structure in Tramandá-Armazém estuary (South of Brazil). *Acta. Limnol. Bras* 17, 349–359.
- Kim, J.-O., Lee, H.-J., Han, S.-I., et al., 2017. Marinobacter halotolerans sp. nov., a halophilic bacterium isolated from a saltern crystallizing pond. *Int. J. Syst. Evol. Microbiol.* 67, 460–465.
- Klindworth, A., Pruesse, E., Schweer, T., Peplies, J., Quast, C., Horn, M., Glöckner, F.O., 2013. Evaluation of general 16S ribosomal RNA gene PCR primers for classical and next-generation sequencing-based diversity studies. *Nucleic Acids Res.* 41 e1–e11.
- Kolesnikov, A.V., Danelian, T., Gommeaux, M., Maslov, A.V., Grazhdankin, D.V., 2017. Arumberiamorph structure in modern microbial mats: implications for Ediacaran palaeobiology. *Bulletin de la Société géologique de France* 188 (1-2), 5.
- Lavergne, C., 2014. Rôle (structure Et Fonction) Des Communautés Procarvotes (bactéries Et Archées) Dans Le Cycle De l'azote d'une Vasière Littorale Du Pertuis Charentais: Influence Des Facteurs Biotiques Et Abiotiques Par Une Approche Multi-échelle, 501.
- Lee, J.-W., Nam, J.-H., Kim, Y.-H., et al., 2008. Bacterial communities in the initial stage of marine biofilm formation on artificial surfaces. *J. Microbiol. Seoul Korea* 46, 174–182.
- Lee, H., Heo, Y.M., Kwon, S.L., et al., 2020. Recovery of the benthic bacterial community in coastal abandoned saltern requires over 35 years: a comparative case study in the Yellow Sea. *Environ. Int.* 135, 105412.
- Lepère, C., Domaizon, I., Hugoni, M., et al., 2016. Diversity and dynamics of active small microbial eukaryotes in the anoxic zone of a freshwater Meromictic Lake (Pavin, France). *Front. Microbiol.* 7 <https://doi.org/10.3389/fmicb.2016.00130>.
- Lewis, L.A., McCourt, R.M., 2004. Green algae and the origin of land plants. *Am. J. Bot.* 91, 1535–1556.
- López-Escardó, D., Paps, J., de Vargas, C., et al., 2018. Metabarcoding analysis on European coastal samples reveals new molecular metazoan diversity. *Sci. Rep.* 8, 9106.
- López-Hermoso, C., de la Haba, R.R., Sánchez-Porro, C., et al., 2018. *Salinivibrio kushneri* sp. nov., a moderately halophilic bacterium isolated from salterns. *Syst. Appl. Microbiol.* 41, 159–166.
- Martínez, J.N., Nishihara, A., Lichtenberg, M., Trampe, E., Kawai, S., Tank, M., Kühn, M., Hanada, S., Thiel, V., 2019. Vertical distribution and diversity of phototrophic bacteria within a hot spring microbial Mat (Nakabusa hot springs, Japan). *Microbes Environ.* 34 (4), 374–387.

- McMurdie, P.J., Holmes, S., 2013. Phyloseq: an R package for reproducible interactive analysis and graphics of microbiome census data. *Watson m* (ed.). *PLoS One* 8, e61217.
- Mir, J., Martnez-Alonso, M., Esteve, I., et al., 1991. Vertical stratification and microbial assemblage of a microbial mat in the Ebro Delta (Spain). *FEMS Microbiol. Lett.* 86, 59–68.
- Montagna, P.A., 1984. In situ measurement of meiobenthic grazing rates on sediment bacteria and edaphic diatoms. *Mar. Ecol. Prog. Ser.* 18, 119–130.
- Nche-Fambo, F.A., Tirok, K., Scharler, U.M., 2016. Hypersaline conditions cause distinct ciliate community structure in a South African estuarine lake system. *J. Plankton Res.* 38, 878–887.
- Nubel, U., Garcia-Pichel, F., Clavero, E., et al., 2000. Matching molecular diversity and ecophysiology of benthic cyanobacteria and diatoms in communities along a salinity gradient. *Environ. Microbiol.* 2, 217–226.
- Oren, A., 2009. Saltern evaporation ponds as model systems for the study of primary production processes under hypersaline conditions. *Aquat. Microb. Ecol.* 56, 193–204.
- Pal, S., Biswas, R., Misra, A., Sar, A., Banerjee, S., Mukherjee, P., Dam, B., 2020. Poorly known microbial taxa dominate the microbiome of hypersaline Sambhar Lake salterns in India. *Extremophiles* 24, 875–885.
- Parry, J.D., 2004. Protozoan grazing of freshwater biofilms. *Adv. Appl. Microbiol.* 54, 167–196. Elsevier.
- Pedros-Alio, C., Calderon-Paz, J.L., MacLean, M.H., et al., 2000. The microbial food web along salinity gradients. *FEMS Microbiol. Ecol.* 32, 143–155.
- Pillay, D., Perissinotto, R., 2009. Community structure of epibenthic meiofauna in the St. Lucia Estuarine Lake (South Africa) during a drought phase. *Estuar. Coast. Shelf Sci.* 81, 94–104.
- Plominsky, A.M., Henriquez-Castillo, C., Delherbe, N., et al., 2018. Distinctive archaeal composition of an artisanal crystallizer pond and functional insights into salt-saturated hypersaline environment adaptation. *Front. Microbiol.* 9 <https://doi.org/10.3389/fmicb.2018.01800>.
- Prieto-Barajas, C.M., Valencia-Cantero, E., Santoyo, G., 2018. Microbial mat ecosystems: structure types, functional diversity, and biotechnological application. *Electron. J. Biotechnol.* 31, 48–56.
- Pringault, O., Duran, R., Jacquet, S., et al., 2008. Temporal variations of microbial activity and diversity in marine tropical sediments (New Caledonia Lagoon). *Microb. Ecol.* 55, 247–258.
- Quast, C., Pruesse, E., Yilmaz, P., et al., 2012. The SILVA ribosomal RNA gene database project: improved data processing and web-based tools. *Nucleic Acids Res.* 41, D590–6.
- R Core Team, 2020. R: a Language and Environment for Statistical Computing. R Foundation for Statistical Computing, Vienna, Austria. URL <https://www.R-project.org/>. <https://www.R-project.org/>. Published.
- Rodrigues, C.M., Bio, A., Amat, F., et al., 2011. Artisanal salt production in Aveiro/Portugal - an ecofriendly process. *Aqua. Biosyst* 7, 3–14.
- Ruff, S.E., Biddle, J.F., Teske, A.P., et al., 2015. Global dispersion and local diversification of the methane seep microbiome. *Proc. Natl. Acad. Sci.* 112, 4015–4020.
- Rzeznik-Orignac, J., Fichet, D., Boucher, G., 2003. Spatio-temporal structure of the nematode assemblages of the Brouage mudflat (Marennes Oleron, France). *Estuar. Coast. Shelf Sci.* 58, 77–88.
- Sanchez-Baracaldo, P., Bianchini, G., Wilson, J.D., Knoll, A.H., 2021. Cyanobacteria and biogeochemical cycles through Earth history. *Trends Microbiol.*
- Schmidt, S., Darcy, J., Sommers, P., Gunawan, E., Knelman, J., Yager, K., 2017. Freeze-thaw revival of rotifers and algae in a desiccated, high-elevation (5500 meters) microbial mat, high Andes, Peru. *Extremophiles* 21 (3), 573–580.
- Segata, N., Izard, J., Waldron, L., et al., 2011. Metagenomic biomarker discovery and explanation. *Genome Biol.* 12, R60.
- Sherr, E.B., Sherr, B.F., 1987. High rates of consumption of bacteria by pelagic ciliates. *Nature* 325, 710–711.
- Sierra, M.A., Li, Q., Pushalkar, S., Paul, B., Sandoval, T.A., Kamer, A.R., Corby, P., Guo, Y., Ruff, R.R., Alekseyenko, A.V., Li, X., Saxena, D., 2020. The influences of bioinformatics tools and reference databases in analyzing the human oral microbial community. *Genes* 11 (8), 878.
- Stal, L.J., Bolhuis, H., Cretoiu, M.S., 2019. Phototrophic marine benthic microbiomes: the ecophysiology of these biological entities. *Environ. Microbiol.* 21, 1529–1551.
- Stock, A., Breiner, H.-W., Pachiadaki, M., et al., 2012. Microbial eukaryote life in the new hypersaline deep-sea basin Thetis. *Extremophiles* 16, 21–34.
- Tedersoo, L., Tooming-Klunderud, A., Anslan, S., 2018. PacBio metabarcoding of Fungi and other eukaryotes: errors, biases and perspectives. *New Phytol.* 217, 1370–1385.
- Tran, H.-T., Wang, H.-C., Hsu, T.-W., et al., 2019. Revegetation on abandoned salt ponds relieves the seasonal fluctuation of soil microbiomes. *BMC Genomics* 20. <https://doi.org/10.1186/s12864-019-5875-y>.
- Turner, J.T., 2004. The importance of small planktonic copepods and their roles in pelagic marine food webs. *Zool. Stud.* 13.
- Valdespino-Castillo, P.M., Cerqueda-Garca, D., Espinosa, A.C., Batista, S., Merino-Ibarra, M., Tas, N., Alcantara-Hernandez, R.J., Falcon, L.I., 2018. Microbial distribution and turnover in Antarctic microbial mats highlight the relevance of heterotrophic bacteria in low-nutrient environments. *FEMS Microbiol. Ecol.* 94 (9) [15129](https://doi.org/10.1111/1365-3113.15129).
- van Gemerden, H., 1993. Microbial mats: a joint venture. *Mar. Geol.* 113, 3–25.
- Vogt, J.C., Abed, R.M.M., Albach, D.C., Palinska, K.A., 2018. Bacterial and archaeal diversity in hypersaline cyanobacterial mats along a transect in the intertidal flats of the sultanate of Oman. *Microb. Ecol.* 75 (2), 331–347.
- White, R.A., Wong, H.L., Ruvindy, R., Neilan, B.A., Burns, B.P., 2018. Viral communities of Shark Bay Modern Stromatolites. *Front. Microbiol.* 9 (1223).
- White, R.A., Visscher, P.T., Burns, B.P., 2021. Between a rock and a soft place: the role of viruses in lithification of modern microbial mats. *Trends Microbiol.* 29 (3), 204–213.
- Wieland, A., Kuhl, M., McGowan, L., et al., 2003. Microbial mats on the Orkney Islands revisited: microenvironment and microbial community composition. *Microb. Ecol.* 46, 371–390.
- Wong, H.L., Smith, D.-L., Visscher, P.T., et al., 2015. Niche differentiation of bacterial communities at a millimeter scale in Shark Bay microbial mats. *Sci. Rep.* 5, 15607.
- Wong, H.L., Visscher, P.T., White, R.A., Smith, D.-L., Patterson, M.M., Burns, B.P., 2017. Dynamics of archaea at fine spatial scales in Shark Bay mat microbiomes. *Sci. Rep.* 7 (1), 46160.
- Xia, J., Xie, Z.-H., Dunlap, C.A., et al., 2017. *Rhodohalobacter halophilus* gen. nov., sp. nov., a moderately halophilic member of the family Balneolaceae. *Int. J. Syst. Evol. Microbiol.* 67, 1281–1287.
- Yanez-Montalvo, A., Gomez-Acata, S., Aguila, B., Hernandez-Arana, H., Falcon, L.I., 2020. The microbiome of modern microbialites in Bacalar Lagoon, Mexico. *PLoS one* 15 (3), e0230071.
- Yilmaz, P., Wegener Parfrey, L., Yarza, P., et al., 2013. The SILVA and “All-species living tree project (LTP)” taxonomic frameworks. *Nucleic Acids Res.* 42 <https://doi.org/10.1093/nar/gkt1209>.
- Zhao, J., Meng, Y., Drewer, J., Skiba, U.M., Prosser, J.I., Gubry-Rangin, C., 2020. Differential ecosystem function stability of ammonia-oxidizing archaea and bacteria following short-term environmental perturbation. *mSystems* 5, e00309–20.

Supplementary materials

New insights in bacterial and eukaryotic diversity of microbial mats inhabiting exploited and abandoned salterns at the Ré Island (France)

Camille Mazière^{a,b}, Hélène Agogué^b, Cristiana Cravo-Laureau^a, Christine Cagnon^a, Isabelle Lanneluc^b, Sophie Sablé^b, Ingrid Fruitier-Arnaudin^b, Christine Dupuy^b, Robert Duran^{a*}

^a Université de Pau et des Pays de l'Adour, E2S UPPA, CNRS, IPREM, Pau, France

^b UMR 7266 LIENSs (Littoral Environnement et Sociétés), CNRS - La Rochelle Université – 2, rue Olympe de Gouges, 17000 LA ROCHELLE, France

* Corresponding author: robert.duran@univ-pau.fr, +33 5 59 40 74 68, Bâtiment IBEAS - Avenue de l'Université, BP 1155 64013 PAU CEDEX

Table S1. Data description during Qiime2 processing, richness and diversity indexes.

<i>Saltern</i>	Bacteria						Eukaryota					
	Abandoned site			Exploited site			Abandoned site			Exploited site		
<i>Core replicate</i>	R1	R2	R3	R1	R2	R3	R1	R2	R3	R1	R2	R3
<i>Raw sequences count</i>	28,714	35,724	26,292	18,808	16,793	22,000	49,771	49,639	50,946	38,143	40,006	49,903
<i>Filtering sequences count</i>	13,085	16,583	11,789	10,128	9,208	11,940	31,289	33,330	35,047	24,434	25,563	24,636
<i>Rarefaction</i>	5,530						22,274					
<i>Observed richness</i>	687	668	575	350	212	232	149	103	110	192	159	210
<i>Shannon index</i>	5.76	5.81	5.63	5.07	4.58	4.66	1.88	1.48	1.23	3.05	2.74	3.32

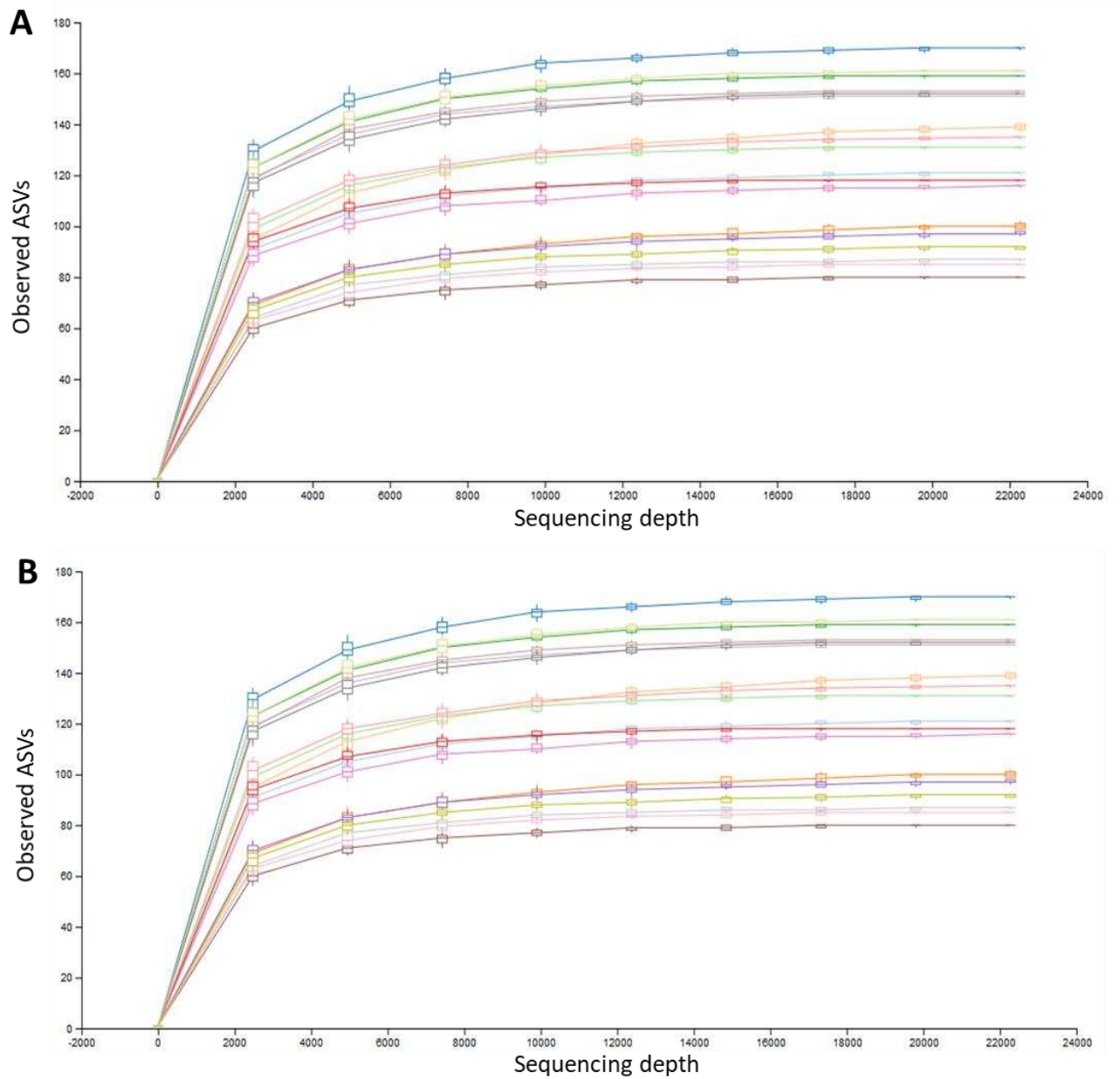


Fig. S1. Rarefaction curves of the observed bacterial ASVs (A) and observed eukaryotic ASVs (B) according to the number of sequences analysed. The number of observed ASVs is based on a 97% similarity threshold.

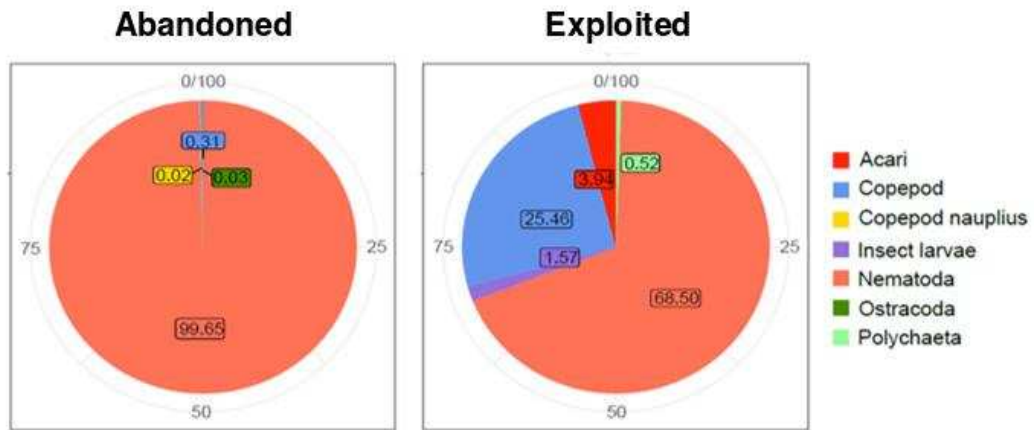


Fig. S2. Relative abundances (%) of meiobenthic taxa inhabiting microbial mats in the abandoned and exploited salterns. The meiobenthic taxa were identified and counted by microscopic observations.

3. Conclusions and perspectives

The bacterial and eukaryotic composition and diversity of microbial mats inhabiting exploited salterns were different to those of microbial mats from abandoned salterns. A higher diversity of bacteria occurred in the abandoned site while a higher eukaryotic diversity was observed in the exploited site revealing the anthropogenic impact on microbial mats structure.

A comparison with microbial mats coming from other Ré Island salt marshes will allow us to know whether microbial communities are commonly found in this area. The study of the impact of environmental changes, as well as the seasonal influence, will provide useful information to better understand not only the conditions in which these microbial mats currently live, but also their capacity to cope with environmental changes.

Chapter IV: Seasonal dynamic of the microbial mats of Ré Island

1. Introduction

Human activities have irreversibly transformed the Earth, leading to the advent of a new geological era called the Anthropocene (Crutzen, 2006; Lewis and Maslin, 2015). These transformations are referred as global change. Among them, environmental and climate changes are the main challenges for our society requiring collective global responses. However, the environmental consequences of global change at the local scale are various depending on the resilience and adaptation capacities of the area and the society. The study of global change is based on diagnoses of local territories proposing modelled scenarios such as those of the IPCC for 2100 (IPCC, 2014), representing thus a prospective approach.

In coastal areas of the Nouvelle-Aquitaine region, microbial mats are threatened mainly by climate change. However, microbial mats are subjected to variations of climatic conditions during the year (different seasons), which can represent those predicted by the IPCC for 2100. We assume that microbial mats own adapted populations to face such climatic conditions. It is therefore of paramount importance to follow the microbial mats dynamics during the year to identify the adapted populations and infer the potential consequences on their structure and function of climatic changes.

In this chapter, a seasonal monitoring of the dynamics of microbial mats was carried out in a specific environment that are the salt marshes of the Nouvelle-Aquitaine region. The exploitation of salt in salt marshes influences the structuring and development of the microbial mat resulting in a greater maturity in the non-exploited areas than in the exploited, thus probably leading to different dynamics in responses to environmental fluctuations (Mazière et al., 2021). Therefore, microbial mats from non-exploited plots will be used for mesocosms' experiment. The objective of this chapter is to determine if microbial mats from the non-exploited plot is submitted to natural physical-chemical parameters comparable with those of climate change predicted by the IPCC for 2100 (IPCC, 2014). It is also important to know how the salt exploitation impacts the microbial mats to make assumptions about their adaptability

to climate change because this environment is already perturbed and we can't forecast the climate change impact.

Seasons have been defined according to their climatological definition (*i.e.*, homogeneity in the average temperatures, rainfall, sunshine *etc*) found in a defined place. Sampling for the seasonal monitoring was performed in mid-July 2019 (summer), mid-October 2019 (fall), mid-January 2020 (winter), and mid-May 2020 (spring) and the last sampling in mid-July 2020 for summer to have a complete monitoring over one year.

2. Seasonal influence on the microbial mats of Ré Island in a non-exploited plot

The results presented below were preliminary results. The metagenomic analysis on the DNA (**Annexe 4**), the extracellular polymeric substances (EPS) extracted from the samples determination and quantification and the vertical profiles analysis are in progress. Some analyses were also planned to examine the composition in pigment and metabolites present in the microbial mats, but they can be not performed until now because of the health situation due to covid.

2.1 Environmental parameters

The air average temperature was significantly higher in July 2019 and July 2020 and lesser in January 2020 (Kruskal, $p < 0.05$) (**Table 6**). Its daily range average was significantly superior in July 2019, July 2020 and May 2020 than in October 2019 and January 2019 (Kruskal, $p < 0.05$) (**Table 6**). The January 2020 month was rainier than those of July 2019 and July 2020 (Kruskal, $p < 0.05$) (**Table 6**). No difference was observed on the wind speed (Welch, $p > 0.05$) (**Table 6**). No variability between July 2019 and July 2020 was noticed.

The air temperature average and its range, and average precipitation showed a marked between seasons with summer warmer with few precipitations than winter.

Table 6: Meteorological data measured by Météo France. The values correspond to the mean \pm standard deviation of daily measures on the month (July 2019, October 2019, January 2020, May 2020 or July 2020) in the station near to La Rochelle and the Ré Island (46°10'40"N 1°11'34"O).

	July 2019	October 2019	January 2020	May 2020	July 2020
Air average temperature	22.2 \pm 2.2 °C	15.5 \pm 1.7 °C	8.8 \pm 2.7 °C	16.8 \pm 3.1 °C	20.5 \pm 2.4 °C
Air temperature range	10.2 \pm 3.9 °C	5.4 \pm 2.2 °C	5.1 \pm 2.4 °C	9.9 \pm 4.4 °C	9.4 \pm 4.2 °C
Wind speed	4.9 \pm 1.1 m.s ⁻¹	4.8 \pm 1.3 m.s ⁻¹	5.4 \pm 1.8 m.s ⁻¹	5.1 \pm 1.4 m.s ⁻¹	5 \pm 0.8 m.s ⁻¹
Average daily precipitation	1.1 \pm 4.3 mm	3.8 \pm 5.6 mm	2.9 \pm 4.1 mm	2.7 \pm 8.2 mm	0.1 \pm 0.2 mm

The data below were measured in duplicate at two different hours during the sampling day (depending on the weather, the number of samplers, *etc.*). Therefore, no statistical analyses could be done. However, we chose to describe it because no data on water temperature, pH and dissolved oxygen occurring in the water of the salt marsh on the month were available.

When samples were taken in July 2019 in the non-exploited plot, the temperature of the water above the microbial mat varied between 20.8°C in the early morning and 31.6°C at midday, *i.e.*, an average of 26.2 \pm 3.8°C (**Table 7**). It decreased in October 2019 with an average of 13.9 \pm 0.6°C and reached its lowest value in winter with an average of 4.35 \pm 0.2°C, with small amplitudes, 1.6°C and 0.5°C respectively (**Table 7**). The water temperature increased again in May 2020 with values between 20.1°C and 22.6°C (average 21.35 \pm 0.9°C) (**Table 7**). The water in the plot in July 2020 was cooler than in July 2019 with an average of 24.9 \pm 0.4°C and a range of 1.2°C compared to 10.8°C in the previous year (**Table 7**). This seasonal variation in water temperature depends on the air temperature, which rises in summer to warm the water and falls in winter to cool it, and also depends on the wind allowing a more important evaporation. The variation in water temperature has an impact on salinity,

which increases evaporation as it warms. The latter reached $204 \pm \text{NA}$ psu during July 2019 sampling, then decreased to 40.1 ± 0.3 psu in October 2019 and 33 ± 0.14 psu in January 2020 before increasing again in the May 2020 to 109 ± 0.7 psu (**Table 7**). We can note, in July 2020, the salinity was 88.9 ± 2.3 psu, clearly below of those in July 2019 (**Table 7**).

The pH measured in July and October 2019 did not change much, 8.36 ± 0.25 and 8.42 ± 0.04 respectively. It had decreased in January 2020 to 8.05 ± 0.01 and then increased again in May 2020 when it reached its maximum at 8.9 ± 0.02 and decreased again in July 2020 to 8.57 ± 0.01 . The increase of pH was simultaneous with the increase of dissolved oxygen. During the day, microbial mat photosynthesis will increase with the solar irradiance, but also according to the seasons where summer is more illuminated than winter, leading to an increase of the photosynthetic efficiency producing oxygen (Jensen et al., 2011). This metabolism is known to increase the pH so in summer the production of oxygen and the pH will be superior to those in winter.

Table 7: Physical-chemical parameters measured during the seasonal sampling of the microbial mat in the non-exploited plot of the salt marsh. The sample name is composed by the date (month-year) followed by the type of site, NonEX for non-exploited plot. Two measures per sampling were done, corresponding to the parameters at the beginning and the end of the sampling.

Sample name	Water temperature (°C)	Salinity (psu)	Air temperature (°C)	Dissolved oxygen (mg.L ⁻¹)	pH	Water (cm)
07-19_NonEX	20.8	204	17.1	5	8.004	2.5
	31.6	NA	22.6	15.5	8.721	
10-19_NonEX	13.1	39.7	15.7	6.3	8.362	4
	14.7	40.5	15.4	6.82	8.478	
01-20_NonEX	4.1	32.8	4.5	12.8	8.04	1.5
	4.6	33.2	4.6	9.21	8.06	
05-20_NonEX	22.6	110.1	25.1	13.16	8.935	3
	20.1	108.1	26.2	13.42	8.87	
07-20_NonEX	24.3	84.8	21.2	12.45	8.551	0.4
	25.5	93	22.3	10.65	8.581	

The collinearities between the environmental variables (water temperature, salinity, air temperature, dissolved oxygen, pH, water height, phosphate, nitrate, nitrite, ammonium and silicon) were selected with a collinearity threshold of 0.7 according to Spearman's rank correlation ($p < 0.05$) (**Fig. 23**). This process led to group the variables presenting collinearity and used a proxy for each group as explanatory variables. Two correlated variables were removed, the water temperature correlated with the salinity and the silicon concentration, and the silicon concentration correlated with the water temperature.

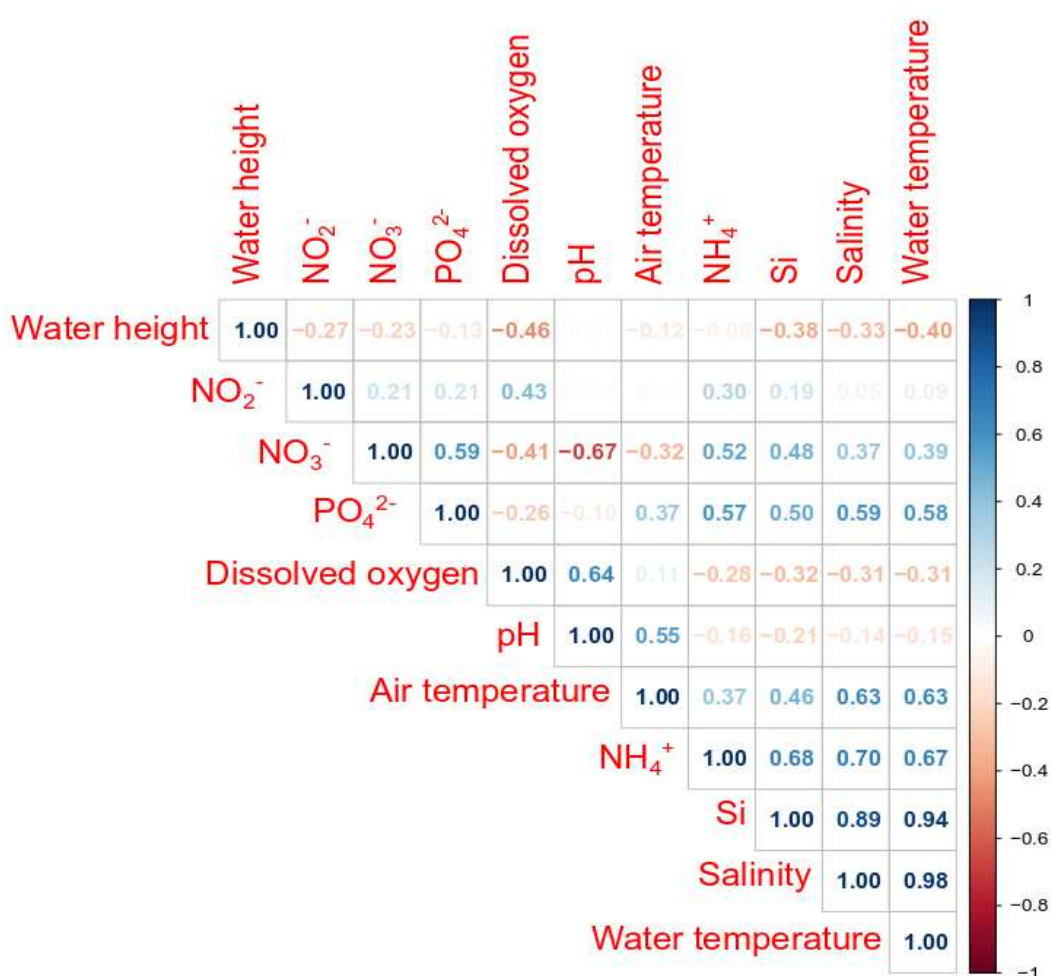


Figure 23: Collinearity between the physical-chemical parameters. The numbers are collinearity thresholds according to Spearman's rank correlation. NH₄⁺, NO₃⁻, NO₂⁻, PO₄²⁻ and Si corresponds to ammonium, nitrate, nitrite, phosphate and silicon.

The 4 seasons were significantly differentiated by the non-correlated physical-chemical parameters (PERMANOVA, $p < 0.05$). The two axes of the principal component analysis (PCA) done on the sample structure according to the non-correlated physical-chemical parameters explained a major part of the variability between samples (axis 1 explaining 52 % and axis 2 explaining 26 %). The samples of July 2019 were clearly different of the other samples by the axis 1 with a positive correlation with the salinity and the nutrients concentrations (**Fig. 24**). The samples of July 2020 were closed to the samples of May 2020 with a positive correlation with pH, air temperature and dissolved oxygen, by the axis 2, while samples of autumn and winter were negatively correlated with these parameters.

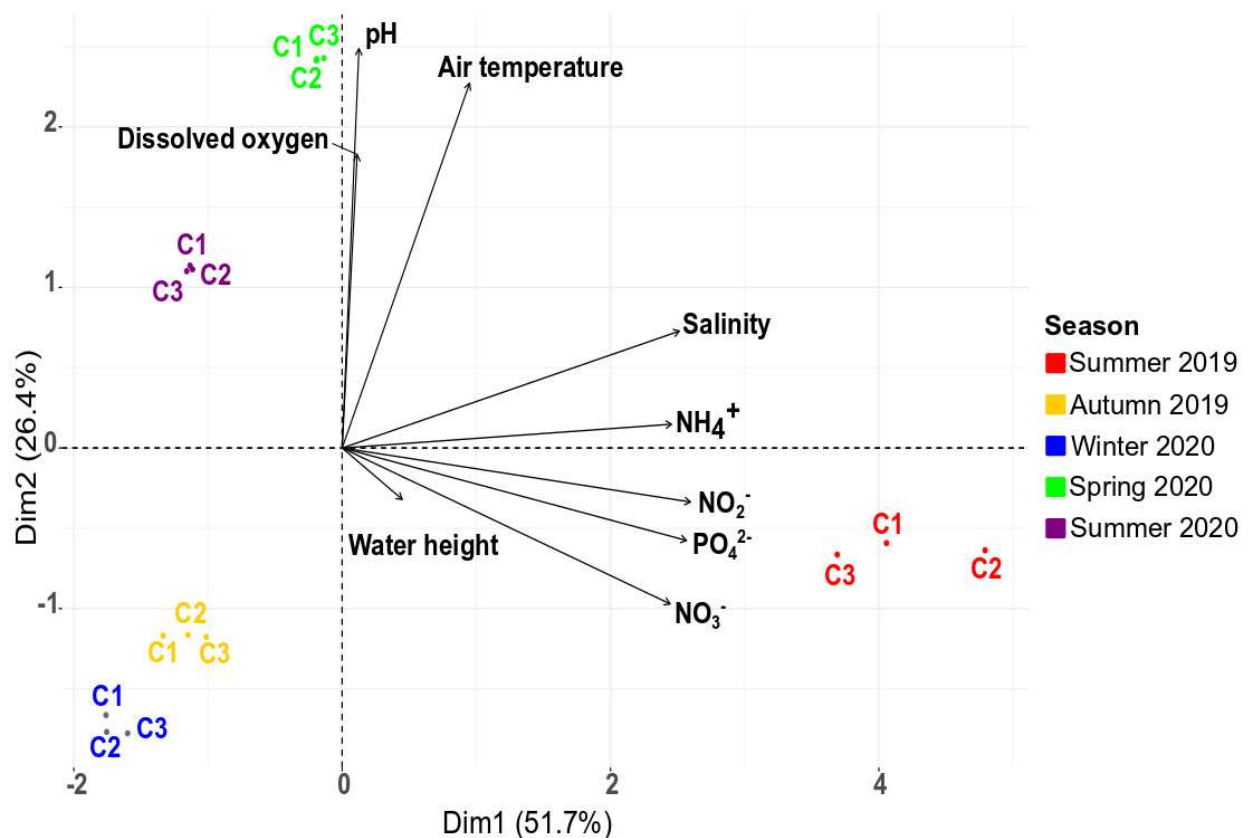


Figure 24: Principal component analysis (PCA) on the sample structure according to the non-correlated physical-chemical parameters. The seasons were represented by different colours. The letter C followed by a figure corresponds to a sampled core. NH_4^+ , NO_3^- , NO_2^- , PO_4^{2-} and Si corresponds to ammonium, nitrate, nitrite, phosphate and silicon.

2.2 Biological parameters

The heterotrophic prokaryotes increased from summer 2019 to winter 2020, with values included between $201.5 \times 10^8 \pm 46.2 \times 10^8$ cell.mL⁻¹ and $109.2 \times 10^9 \pm 38.1 \times 10^9$ cell.mL⁻¹, to decrease after until $285 \times 10^8 \pm 137.5 \times 10^8$ cell.mL⁻¹ in July 2020 (**Fig. 26, supplementary materials Table S9**). Regarding the meiofauna, only nematodes were observed in microbial mats of the non-exploited plot, except in spring and summer 2020 where copepods were also identified (1.07 ± 1.8 individuals.cm⁻³ (ind.cm⁻³) and 0.5 ± 0.8 ind.cm⁻³, respectively), but the number of nematodes were largely higher (**Fig. 27, supplementary materials Table S10**). During the sampling of July 2019, the number of nematodes was 115.7 ± 23.2 ind.cm⁻³. It was equal to 172.2 ± 105.5 ind.cm⁻³ in October 2019, 90.8 ± 77.3 ind.cm⁻³ in January 2020, 219 ± 159.4 ind.cm⁻³ in May 2020 and 163.7 ± 228.6 ind.cm⁻³ in July 2020(**Fig. 27, supplementary materials Table S10**). The triplicates presented a great dispersion.

Coastal microbial mats growth and activity were strongly dependent of the seasons (Cardoso et al., 2019). The development of these mats begins in early spring and mature until late summer (Cardoso et al., 2019). From autumn, the growth is stopped, and the microbial mat deteriorates by decomposition and erosion in winter (Cardoso et al., 2019). Surprisingly in the microbial mat studied, the number of heterotrophic prokaryotes increased in winter and decreased in summer. One hypothesis could be that the concentrations of nutrients could be more important favouring prokaryotic growth. However, in the non-exploited plot, the nutrients concentration was not superior in winter than in summer (**Supplementary materials Table S11**). A second hypothesis could be that the physical-chemical parameters, notably the light intensity, reduced the growth of phototrophs and promoted their decomposition (Cardoso et al., 2019). No data were obtained on the phototrophic communities (metagenomics is in progress and pigment composition could be not performed due to the covid health situation), but the green layer of oxygenic photosynthetic organisms was not observed in winter (**Chapter II, 2.1.1**). Therefore, the conditions occurring in winter could impact the phototrophic communities reducing their growth and favouring their decomposition,

thus increasing the nutrients concentrations and organic matter available for heterotrophic prokaryotes. The number of nematodes were higher in spring and autumn, and lower in summer and winter. The optimal environment (physical-chemical parameters and food availability) for their development occurred in spring but also in autumn where the environment was less selective. An increase in salinity was shown to affect the structure dynamics of meiofauna with a decrease of their richness and abundance (Broman et al., 2019; Estrada et al., 2004; Pedrós-Alió et al., 2000), explaining why the nematode abundance decrease in summer, but in winter the decrease of these organisms is certainly due to the lack of preys (*e.g.*, predation of photosynthetic/heterotrophic bacteria and diatoms) (Hubas et al., 2010) and the cold temperature.

3. Impact of exploitation on the microbial mats of Ré Island

The exploited and the non-exploited plots studied are from the salt marsh. They were maintained by the salt owner which controlled the output and input of water and the limitations of the plots were preserved. Only the salt recovery was different occurring exclusively in the exploited plot.

The two plots (exploited and non-exploited) and the seasons were significantly differentiated by the non-correlated physical-chemical parameters (PERMANOVA, $p < 0.05$). The interaction between both also explained this variability (PERMANOVA, $p < 0.05$). The two axes of the principal component analysis (PCA) done on the sample structure according to the non-correlated physical-chemical parameters explained a major part of the variability between samples (axis 1 explaining 45.2% and axis 2 explaining 24.6%). Exploited and non-exploited plots were separated by the axis 2 revealing the difference between the plots due to the physical-chemical parameters (**Fig. 25**). The samples of the two summers of the exploited plot were close and clearly separated from the others with a positive correlation with salinity (**Fig. 25**). Indeed, the salinity was higher in summer in the exploited plot (**Table 8**) because the

exploitation of salt occurring in this season led to high evaporation of seawater, due to a shallow depth of water leading to a significant heating of the water and therefore to a high salinity. The samples of winter and spring of both plots, and surprisingly of July 2020 of the non-exploited plot, were close, negatively correlated with the air temperature, salinity and the nitrite and nitrate concentrations (**Fig. 25**). The salinity was close to the seawater salinity in winter (**Table 8**) because the evaporation was not maintained due to cold temperatures, and it increased in spring because the owner restored the exploited parcel. The exploited plot presented a water temperature close to those measured in the non-exploited plot, except in July 2020 (**Table 8**). This is certainly because the non-exploited plot was maintained like the exploited plot, only salt recovery didn't occur. The dissolved oxygen and the pH were negatively correlated with the samples of both summers of the exploited plot (**Fig. 25**). Indeed, they were lower during this season (**Table 8**) because the salt recovery consists in scraping the surface of the microbial mat and therefore the photosynthetic oxygenic layer could not develop.

The samples of the non-exploited plot in summer were different from those of the exploited plot presented distinct physical-chemical parameters, therefore depending on the human exploitation.

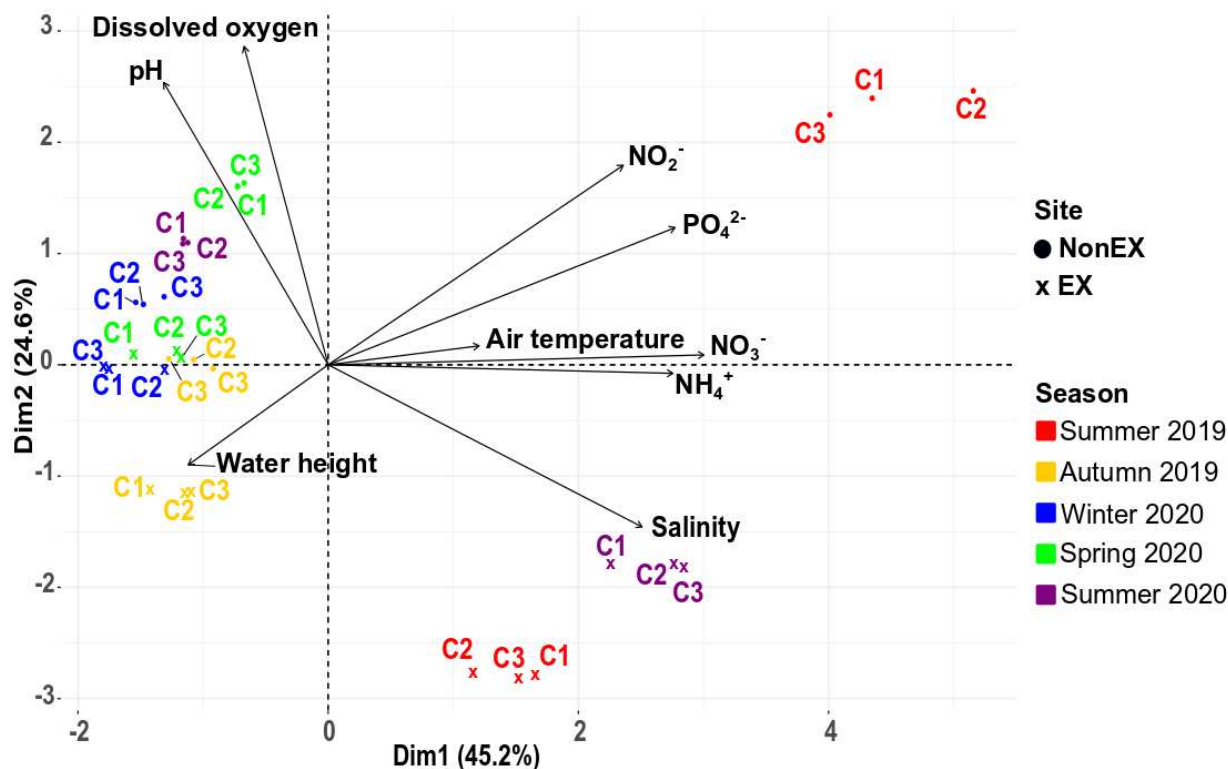


Figure 25: Principal component analysis (PCA) on the sample structure according to the non-correlated physical-chemical parameters. NH_4^+ , NO_3^- , NO_2^- , PO_4^{2-} and Si corresponds to ammonium, nitrate, nitrite, phosphate and silicon, respectively.

Table 8: Physical-chemical parameters measured during the seasonal sampling of the microbial mat in the exploited plot of the salt marsh. The sample name is composed by the date (month-year) followed by the type of site, EX for exploited plot. Two measures per sampling were done, corresponding to the parameters at the beginning and the end of the sampling.

Sample name	Water	Salinity	Air temperature	Dissolved	pH	Water
	temperature (°C)	(psu)	(°C)	oxygen (mg.L ⁻¹)		
07-19_EX	22.3	330	17.1	2.5	7.101	3
	34	NA	22.6	1.6	6.989	
10-19_EX	13.8	52.6	15	5.9	8.205	13
	14.9	55.3	14.8	3.85	7.9	
01-20_EX	3.7	25.6	4.5	8.99	7.99	8
	4.2	25.5	4.7	9	8.02	
05-20_EX	19.1	77.6	18.2	6.42	8.937	8

	23	77.3	26.2	6.54	8.85	
07-20_EX	26.1	278.8	21.2	4.49	7.174	2.7
	31.2	279.6	22.3	3.47	7.124	

The heterotrophic prokaryotes of the microbial mats of the exploited plot followed the same variation than those of the non-exploited plot: an increase from the July 2019 ($276.9 \times 10^7 \pm 122.3 \times 10^7$ cell.mL⁻¹) to the January 2020 ($298.8 \times 10^8 \pm 50.6 \times 10^8$ cell.mL⁻¹) and then a decrease until July 2020 ($363.7 \times 10^7 \pm 325.2 \times 10^7$ cell.mL⁻¹) (**Fig. 26**). However, it was lower than the heterotrophic prokaryotes of the non-exploited plot during the year (Wilcoxon test, $p < 0.05$) (**Fig. 26**). The decrease in prokaryotic abundance was certainly due to the human actions for salt exploitation, including regular scraping for salt recovery and microbial mat removal together, but also the fluctuations of environmental parameters which were more marked (Mazière et al., 2021; Wieland et al., 2003). We can suppose that both phototrophic and heterotrophic prokaryotes were impacted. In the non-exploited plot, only the input and output of seawater are controlled by the salt owner. Thus, the microbial mats could develop because it was not disturbed by human actions, resulting to an ecosystem with weak fluctuations that is considered as an ecosystem with less selective pressure for prokaryotic communities and therefore heterotrophic prokaryotes (Graham et al., 2016; Mazière et al., 2021).

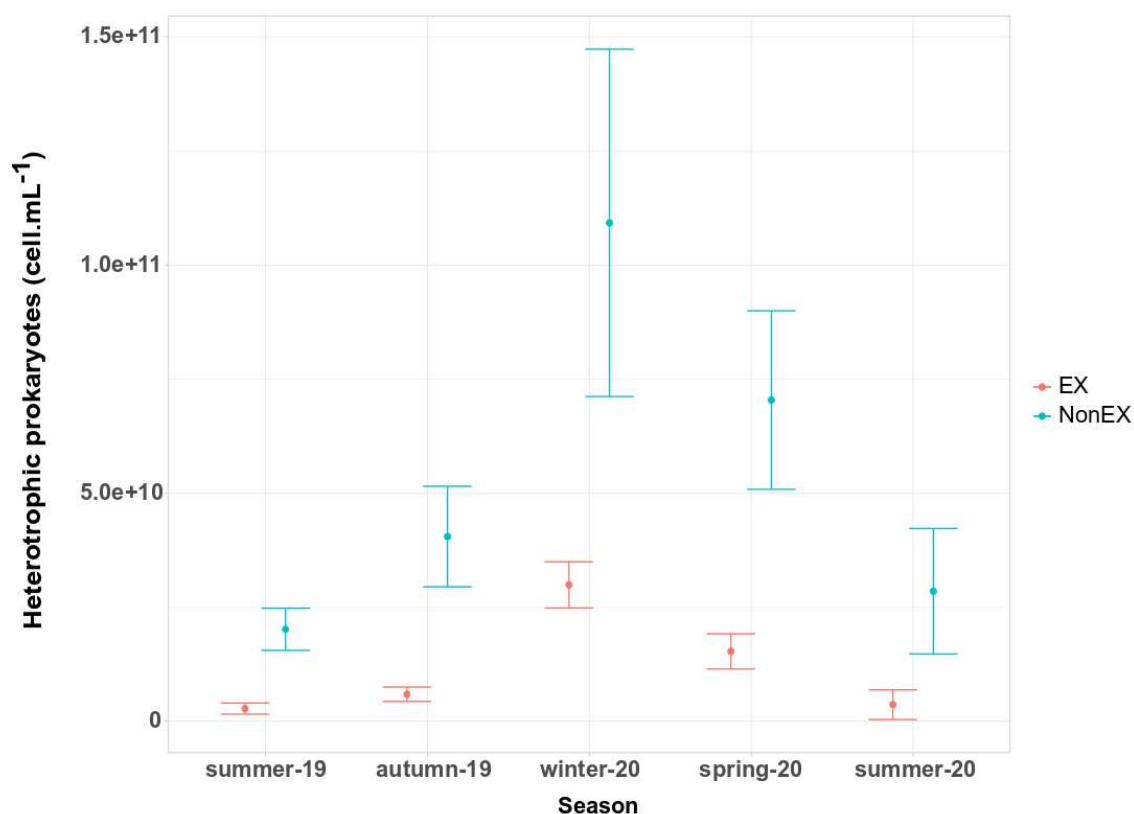


Figure 26: Prokaryotic abundance. The mean \pm standard deviation of the abundance of prokaryotes was represented during a seasonal monitoring of one year.

Regarding the meiofauna, the exploited plot presented nauplii of copepods in autumn 2019, winter and spring 2020, which were not observed in the non-exploited plot in any season (**Fig. 27, supplementary materials Table S10**). Copepods were observed in July 2019 and 2020, autumn 2019 and in winter 2020 while they were not present in the non-exploited plot. In Spring 2020, no difference was observed and in July 2020 no copepods were detected while they were distinguished in the non-exploited plot (**Fig. 27, supplementary materials Table S10**). The number of nematodes was on average higher in the non-exploited plot than in the exploited plot, but we can notice that in winter, spring and July 2020 it presented a great variability between cores in the non-exploited plot (**Fig. 27, supplementary materials Table S10**). Therefore, a greater diversity of groups occurred in the exploited plot than in the non-exploited plot. This has been demonstrated in other microbial mats of Ré Island salt marshes (Mazière et al., 2021).

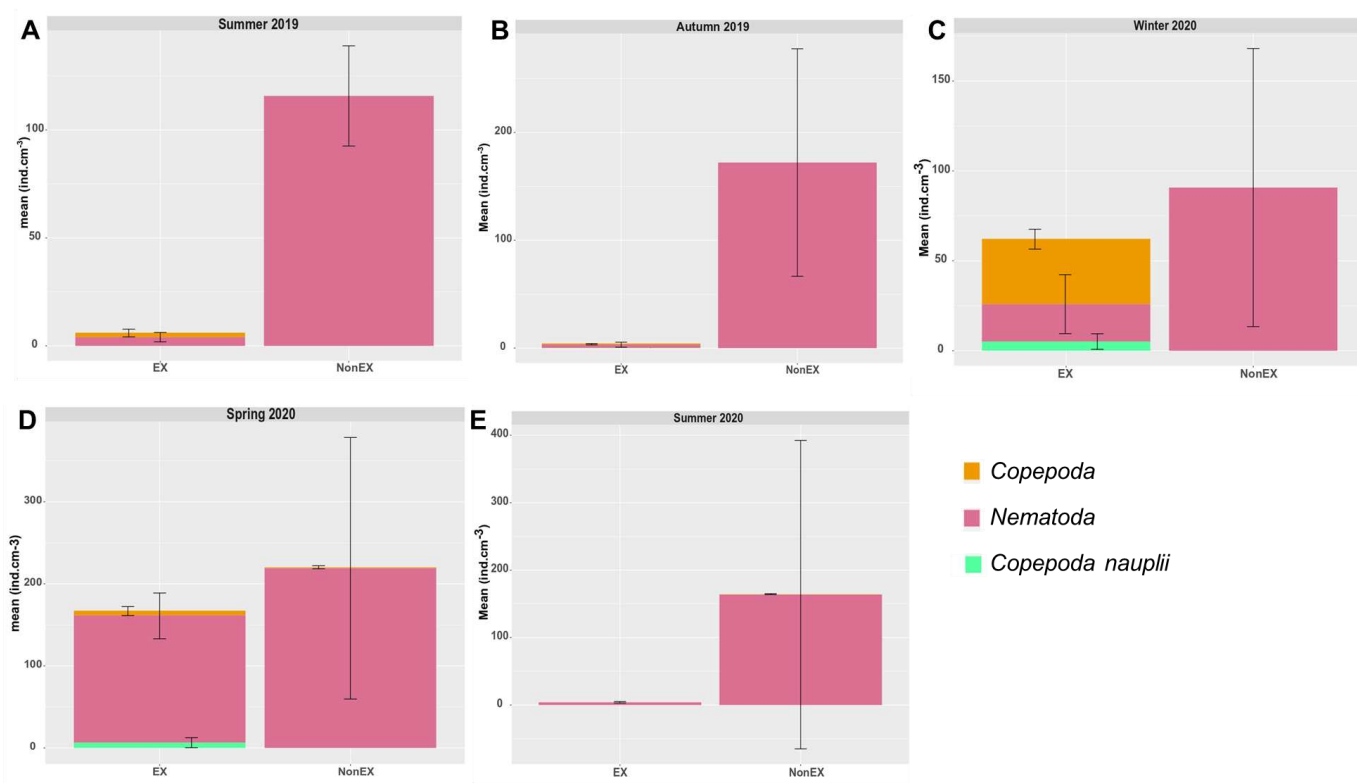


Figure 27: Meiofaunal groups and its abundance. These diagrams represent the mean \pm standard deviation of the abundance of each meiofaunal groups identified with a binocular loupe during a seasonal monitoring of one year.

4. Conclusions and perspectives

The microbial mats from the non-exploited plot face different seasons, with summer warmer and less rainy than winter, directly impacting the water temperature and thus the salinity. The air temperature and thus the water temperature showed a variation superior to 4°C during the year, and even during the day, with a range of 10°C during the sampling day of July 2019. The microbial mats collected for the mesocosms experiment were sampled in spring 2019, at an air temperature of 20°C. In summer, this temperature increased more than 4°C. Thus, these microbial mats already face to predicted temperature due to climate change which naturally occurs in summer in this environment. The water pH didn't decrease under the ocean pH (~8). Indeed, the pH predicted by the IPCC for 2100 (IPCC, 2014) never occurred. We can suppose that this parameter will have a great impact of microbial mats.

Salt exploitation impacts the environment of the microbial mats by causing greater evaporation of seawater leading to higher salinity. Salinity is one of the main drivers of microbial diversity and community structure. Thus, the prokaryotic abundance reduced and the diversity of the meiofauna increased, which has already been observed in other microbial mats in salt marshes on the Ré Island. This anthropogenic impact could reduce the metabolic diversity of the microbial mat, which would make it less resilient to climate change. Further metagenomic studies are underway to determine the prokaryotic and eukaryotic diversity and metabolisms potential in order to determine the dynamic over the seasons and how the anthropogenic impact is translated at the molecular level.

5. Supplementary materials

Table S9: Heterotrophic prokaryotic abundance. It was expressed in cellule per millimetre of microbial mat (cell.mL^{-1}).

	Heterotrophic prokaryotic abundance (cell.mL^{-1})	
	Exploited (EX)	Non-exploited (NonEX)
Summer 2019	$276.9 \times 10^7 \pm 122.3 \times 10^7$	$201.5 \times 10^8 \pm 46.2 \times 10^8$
Autumn 2019	$591.5 \times 10^7 \pm 158.5 \times 10^7$	$404.8 \times 10^8 \pm 110.2 \times 10^8$
Winter 2020	$298.8 \times 10^8 \pm 50.6 \times 10^8$	$109.2 \times 10^9 \pm 38.1 \times 10^9$
Spring 2020	$153.1 \times 10^8 \pm 38.5 \times 10^8$	$703.9 \times 10^8 \pm 195.6 \times 10^8$
Summer 2020	$363.7 \times 10^7 \pm 325.2 \times 10^7$	$285 \times 10^8 \pm 137.5 \times 10^8$

Table S10: Meiofaunal abundance. It was expressed by the number of individuals per cm^{-3} of microbial mat (ind.cm^{-3}).

	Nauplii of copepods (ind.cm^{-3})		Copepods (ind.cm^{-3})		Nematodes (ind.cm^{-3})	
	Exploited (EX)	Non-exploited (NonEX)	Exploited (EX)	Non-exploited (NonEX)	Exploited (EX)	Non-exploited (NonEX)
Summer 2019	0	0	2.1 ± 1.8	0	4.1 ± 2.2	115.7 ± 23.2
Autumn 2019	0.1 ± 0.1	0	1 ± 0.6	0	3.2 ± 2.3	172.2 ± 105.5
Winter 2020	5.1 ± 4.3	0	36.4 ± 5.5	0	20.8 ± 16.4	90.8 ± 77.3
Spring 2020	6.4 ± 6	0	5.7 ± 5.5	1.07 ± 1.8	155.2 ± 27.9	219 ± 159.4
Summer 2020	0	0	0	0.5 ± 0.8	4 ± 1.1	163.7 ± 228.6

Table S11: Nutrient concentrations. NH₄⁺, NO₃⁻, NO₂⁻, PO₄²⁻ and Si corresponds to ammonium, nitrate, nitrite, phosphate and silicon, respectively.

Season	Month	Plot	Core	NH ₄ ⁺	NO ₃ ⁻	NO ₂ ⁻	PO ₄ ²⁻	Si
Summer	07-2019	EX	C1	1.371	0.479	0.016	4.758	43.608
Summer	07-2019	EX	C2	0.677	0.434	0.019	5.03	43.645
Summer	07-2019	EX	C3	1.27	0.46	0.01	4.772	43.509
Summer	07-2019	NonEX	C1	2.116	0.847	0.31	71.764	47.661
Summer	07-2019	NonEX	C2	2.996	0.938	0.325	72.655	46.943
Summer	07-2019	NonEX	C3	1.548	0.919	0.263	75.96	46.751
Autumn	10-2019	EX	C1	0.743	0.18	0.031	0.476	37.793
Autumn	10-2019	EX	C2	1.092	0.225	0.027	0.135	33.273
Autumn	10-2019	EX	C3	1.157	0.226	0.027	0.151	37.138
Autumn	10-2019	NonEX	C1	0.319	0.238	0.019	7.341	2.244
Autumn	10-2019	NonEX	C2	0.602	0.25	0.018	7.556	2.166
Autumn	10-2019	NonEX	C3	0.834	0.3	0.003	6.736	1.988
Winter	01-2020	EX	C1	0.327	0.22	0.052	1.281	1.543
Winter	01-2020	EX	C2	0.904	0.269	0.05	1.352	1.559
Winter	01-2020	EX	C3	0.312	0.2	0.055	1.242	1.489
Winter	01-2020	NonEX	C1	0.702	0.133	0.033	0.305	2.054
Winter	01-2020	NonEX	C2	0.466	0.255	0.026	0.273	2.107
Winter	01-2020	NonEX	C3	0.607	0.259	0.041	0.44	2.057
Spring	05-2020	EX	C1	0.53	0.088	0.016	3.017	3.487
Spring	05-2020	EX	C2	1.03	0.097	0.027	1.81	3.338
Spring	05-2020	EX	C3	0.972	0.121	0.012	2.621	3.201
Spring	05-2020	NonEX	C1	1.189	0.117	0.047	2.627	30.787
Spring	05-2020	NonEX	C2	1.158	0.124	0.047	2.891	29.619
Spring	05-2020	NonEX	C3	1.249	0.103	0.052	3.608	29.274
Summer	07-2020	EX	C1	1.871	0.508	0.05	21.556	91.791
Summer	07-2020	EX	C2	2.558	0.51	0.048	24.554	92.229
Summer	07-2020	EX	C3	2.494	0.594	0.046	22.291	80.258

Summer	07-2020	NonEX	C1	0.485	0.099	0.041	0.484	38.734
Summer	07-2020	NonEX	C2	0.486	0.136	0.032	0.616	39.179
Summer	07-2020	NonEX	C3	0.404	0.149	0.03	0.326	38.633

Chapter V: Impact of climate change **on microbial mats**

1. Introduction

Little is known about the impacts of global changes on coastal microbial mats in the Nouvelle-Aquitaine region. However, climate change could affect their individual responses (such as survival, growth and reproduction), ecological interactions (such as trophic relationships and organism behaviour) and community characteristics (such as abundance, diversity, production and biomass) (Ingels et al., 2018). This knowledge must therefore be improved in order, for example, to implement strategies for mitigating the effects of global change.

Marine microorganisms will face several pressures in our future oceans. It is imperative that experimental approaches include multiple stressors in their designs to assess species, community, and ecosystem-level responses (Ingels et al., 2018). Therefore, to simulate climate change, mesocosms with microbial mats were set up. The microbial mats used in our study came from the non-exploited plot from salt marshes (the same as in **chapter IV**). These shallow environments will be mainly subjected to climate change resulting in an increase in ocean surface temperature of 4°C and its acidification of about 0.4 pH unit (IPCC, 2014). Indeed, four treatments were applied:

- control, where any parameter was changed,
- acidification, where the seawater was acidified by 0.4 (final value of 7.6),
- warming, where the seawater was warmed by 4°C (final value 24°C),
- both acidification and warming.

We assume that climate change will impact the diversity and structure of the communities present (bacteria, archaea, eukaryotes). DNA analysis with universal primers for each domain was therefore carried out to get an initial idea of the evolution of these communities in the face of the treatments imposed. Monitoring of the biomass of heterotrophs (prokaryotes, meiofauna), bacterial production and physical-chemical gradients was also carried out to complete these data.

This chapter aims to describe the impact of climate change on the bacterial, archaeal and eukaryotic diversity and composition of the microbial mats.

2. Impact of climate change on prokaryotic communities inhabiting microbial mats

This part is composed of a draft of a future paper named “Climate change effect on microbial mats structure modifies prokaryotic diversity and metabolism”.

Climate change effect on microbial mats structure modifies prokaryotic diversity and metabolism

C. Mazière^{1,2*}, R. Duran¹, C. Noël³, A. Baldy¹, E. Dubillot², T. Lacoue-Labarthe², P. Pineau², C. Cagnon¹, H. Agoué², C. Cravo-Laureau¹, C. Hubas⁴, C. Dupuy²

¹ Université de Pau et des Pays de l'Adour, E2S UPPA, CNRS, IPREM UMR 525 - Bât. IBEAS, BP1155, 64013 PAU cedex, France

² La Rochelle Université, CNRS, UMR 7266 LIENSs (Littoral Environnement et Sociétés) - 2, rue Olympe de Gouges, Bât. ILE, 17000 LA ROCHELLE, France

³ IFREMER - PDG-IRSI-SeBiMER, Plouzané, France

⁴ Muséum National d'Histoire Naturelle, UMR BOREA 8067, MNHN-IRD-CNRS-SU-UCN-UA - Station Marine de Concarneau, 29900 CONCARNEAU, France

* Corresponding author: camille.maziere@univ-pau.fr, +33 5 59 40 74 68, Bâtiment IBEAS – avenue de l'Université – 64013 Pau, France ; +33 5 46 50 76 31, Bâtiment Ile – 2, rue Olympe de Gouges – 17000 La Rochelle, France

1. Introduction

Climate change is predicted to severely affect marine ecosystems (Hutchins and Fu, 2017; Pajares et al., 2015). It will result in ocean acidification associated with ocean water warming caused by increasing levels of CO₂ in the atmosphere (Hutchins and Fu, 2017; IPCC, 2014). The Intergovernmental Panel on Climate Change (IPCC) predicts an increase in surface water temperature of 3 to 4 °C and ocean acidification of 0.4 to 0.45 pH units in its most pessimistic scenario (RCP 8.5) by the end of the century (IPCC, 2014) on France's Atlantic coasts. These unprecedented changes effects are well documented on animals and plants. By contrast, only few studies describe their potential impact on microorganisms, especially bacteria and archaea (Cavicchioli et al., 2019; Dutta and Dutta, 2016; Reinold et al., 2019). However, these organisms are very abundant on our oceans (4x10²⁹ cells in the deep oceanic subsurface, 5x10²⁸ cells in the upper oceanic sediment and 1x10²⁹ cells in the oceans) and

34 diverse, underlying their importance in maintaining a healthy global ecosystem (Cavicchioli et
35 al., 2019; Flemming and Wuertz, 2019). They dominate the metabolic activity, with, for
36 example, primary production of approximately half of the global primary production of the
37 oceans or the fixation of 50% of the carbon in marine ecosystems (O'Brien et al., 2016). Marine
38 prokaryotic microorganisms participate in the key processes in the ocean playing a central role
39 in the carbon, oxygen, nitrogen, sulfide and nutrient cycles, as well as in the exchange of trace
40 gases that have direct impacts on local climate (O'Brien et al., 2016). They are also crucial for
41 the good functioning of the aquatic systems being the basis of food webs with the recycling of
42 the organic matter and be a considerable source of food to higher tropic levels.

43 Microbial mats are complex vertical multilayered structures of microorganisms. Diverse
44 prokaryotic populations are observed within, mainly composed by bacteria which are well
45 studied (Bolhuis and Stal, 2011). The archaeal populations are less known but more and more
46 studies are interested on them. Microbial mats are observed at the water-sediment interface
47 of several shallow environments as deserts wadis (Abed et al., 2018), coastlines (Bolhuis and
48 Stal, 2011), estuaries (Mir et al., 1991), lakes (Jørgensen and Cohen, 1977), hot springs
49 (Dobretsov et al., 2011) or hypersaline environments like salt marshes (Fourçans et al., 2004;
50 Giani et al., 1989). This structure is characterised by the development of complex metabolite
51 exchange networks allowed by strong vertical microgradients of oxygen, sulfide, light and other
52 electron acceptors (Pajares et al., 2015). Microbial mats play important key roles in the marine
53 environment notably by participating in the biogeochemical cycles of oxygen, sulfide and
54 carbon. Despite the stratification, microbial mats are dynamic structures (Fourçans et al., 2008,
55 2006) with numerous microbial interactions, representing thus an ecosystem on its own
56 (Reinold et al., 2019).

57 Microbial mats in the salt marshes of Ré Island have been shown to be different
58 according to their environment (exploitation or no of the salt) (Mazière et al., 2021). Their
59 phototrophic communities were also affected by acidification at the metabolic level with the
60 increase of bound carbohydrates extracellular polymeric substances (EPS) and the change in

61 the pigment composition (Mazière et al., 2022). The impact of the climate change on diversity
62 and the composition of the prokaryotes of microbial mats is unknown but some studies have
63 been performed on biofilms. Microbial species composition of natural biofilm found in the Great
64 Barrier Reef was modified under acidified conditions, with a decrease of *Alphaproteobacteria*
65 and an increase of *Flavobacteriales* (Witt et al., 2011). They also suggested that bacterial
66 biofilm communities rapidly adapt and reorganize in response to acidified conditions to
67 maintain activity such as oxygen production.

68 Prokaryotic populations are highly adaptable to the changing physical-chemical
69 conditions of the environment (Fourçans et al., 2006) because they possess a remarkable
70 specific, metabolic and molecular diversity. This allows them to be major actors in the future
71 climate change challenge. This study aimed to understand the effect of climate change on the
72 diversity and the composition of the prokaryotic communities inhabiting microbial mats. Thus,
73 mesocosms were carried out to simulate acidification and/or warming on microbial mats
74 coming from a non-exploited salt marsh in Ré Island.

75

76 **2. Material and methods**

77

78 **2.1 Description of the sampled site**

79 Microbial mats were sampled in salterns located in Ars-en-Ré (46°13'29.9"N
80 1°31'07.5"W, Ré island, France) on a non-exploited pond the 30th of April 2019. They were
81 then placed on plastic boxes and transported to laboratory at room temperature. They were
82 recovered by 3 cm of water, as observed *in situ*, within three hours following the sampling. *In*
83 *situ* physico-chemical parameters (temperature, salinity, pH) of the water were measured with
84 a multi-parameter probe (pHenomenal® MU 6100H, VWRTM, USA) in order to apply them on
85 the mesocosms as control values. Samples were also taken to determine nutrient
86 concentrations in the pore water.

87

88 **2.2 Mesocosms design and implementation of different treatments**

89 Microbial mats were placed under controlled conditions in mesocosms where four
90 treatments were applied: 1/ control treatment (C), 2/ acidification treatment (A), 3/ warming
91 treatment (W) and 4/ warming and acidification treatment (WA). The mesocosms design and
92 the implementation of the different treatments were previously described (Mazière *et al.*, 2022).

93 One month of stabilisation was applied on the microbial mats. Samples of microbial mats
94 were collected at t9, after a 9-days period where the physical-chemical parameters of the
95 microbial mats on the mesocosms were followed to verify their stabilisation. Then the
96 environmental conditions were changed and the microbial mats were sampled, at t16 and t23,
97 respectively at the middle of the period of change and at the end, and then at every week (t30,
98 t37, t44, t51 and t58) (Mazière *et al.*, 2022). For each sampling, ten 1 cm depth cores were
99 collected with a 1 cm diameter cut-off syringe in each mesocosm and mixed together in order
100 to obtain a homogeneous sample. Five replicates for each treatment at each time were
101 obtained (160 samples).

102 **2.3 Nutrient concentrations**

103 Nutrient analysis was performed with a volume of 20 mL of water from each mesocosm
104 filtered at 0.22 µm (Millex® Syringe-driven Filter Unit; sterile). Half of the volume was frozen at
105 -20°C for nitrate, nitrite, ammonium, phosphate analysis while the other half was kept at 4°C
106 for silicon analysis. Silicon, nitrate, nitrite and phosphate were measured by Segmented
107 Continuous Flow Colorimetry (SFA) while ammonium was measured by SFA fluorimetry on an
108 auto-analyser (SEAL AutoAnalyzer 3, SEAL analytical) as described by Aminot and Kérouel
109 (2007).

110 **2.4 Diversity, abundance and production of prokaryotic communities**

111 **2.4.1 Abundance of heterotrophic prokaryotes by flow cytometer**

112 2 mL of sediment were sampled and immediately fixed with glutaraldehyde (final
113 concentration of 2%). They were directly frozen in nitrogen liquid and maintained at -80°C until

114 analysis. The analysis was done in the next three months after sampling (Lavergne et al.,
115 2014).

116 Abundance of the heterotrophic prokaryotes was performed according to Lavergne *et*
117 *al.* (Lavergne et al., 2014). A solution of sodium pyrophosphate (0.01M) was prepared and
118 Tween 80 (0.1% final concentration) was added allowing the disaggregation of the attached
119 cells. The samples were diluted successively until 1:2,000 with a vortexing step between each
120 dilution and incubated 30 min at 4°C. A mechanical extraction was applied by sonicating
121 samples 30s at 60W (Sonifier®Cell Disruptor SLPe, BRANSON Ultrasonics Corporation, USA).
122 A second extraction was done in order to obtain a better yield (Lavergne et al., 2014) with the
123 sample diluted at 1:2,000. SYBR Green 1 (1:5,000 final concentration) was then added to
124 extracted samples and an incubation of 15 min in the dark was realized. The counting of the
125 prokaryotic population was then performed thank to a flow cytometer (BD FACSCanto™ II, BD
126 Biosciences, USA) and the results were analysed with BD FACS DIVA software (BD
127 Biosciences, USA). If necessary, the sample was diluted again between 1:6,000 and 1:18,000
128 according to the cytometer saturation. The total abundance of heterotrophic prokaryotes and
129 of each condition at a given time is equal to the mean of five replicates and was expressed as
130 number of individuals per mL of fresh sediment microbial mat. It was converted in biomass by
131 a conversion factor of 7.6×10^{-8} .

132 **2.4.2 Bacterial production**

133 Bacterial production was evaluated by the method of Garet and Moriarty (1996)
134 modified by Pascal *et al.* (2009). A slurry sediment was made with 1mL of fresh microbial mat
135 sampled in the mesocosms with the addition of mesocosms water filtered at 0.22 (1:1 vol/vol).
136 For each sample, 30 µL of slurry sediment were sampled in a new tube and 20µL of ³H-
137 Thymidine at a concentration of 0.74 MBq were added. Five replicates were done, three
138 triplicate to measure the bacterial production and two control tubes. The reaction in the control
139 tubes were immediately stopped by adding 8 mL of cold ethanol (80%). The three other tubes
140 were incubated for 1h at the mesocosms temperature. At the end of the incubation, the reaction

141 was stopped by adding 8 mL of cold ethanol (80%). Afterwards, two washes with 80% cold
142 ethanol by mixing and centrifugation (15 min, 4,500 g, +4°C) were performed. The slurries
143 were then transferred with 2 mL of ice-cold TCA (5%, trichloroacetic acid) onto a polycarbonate
144 filter (Nuclepore 0.2 µm, 25 mm, Millipore, NJ, USA). The filters were washed four times with
145 5% ice-cold TCA. Subsequently, the filters were transferred into scintillation vials containing 2
146 ml 0.5N chlorhydric acid and DNA was extracted 16 h at +95°C. Supernatant (0.5 mL) was
147 transferred in a new scintillation vial with 5 mL of scintillation fluid (Ultima Gold, Perkin-Elmer,
148 MA, USA). The amount of radioactivity in each vial was evaluated using a scintillation counter
149 (Perkin-Elmer, USA).

150 Bacterial production was calculated using the equation (Equation 1) (Lavergne et al.,
151 2017):

$$152 \quad BP = \frac{DPM \times F1}{T \times V \times SA} \times Vt \quad (\text{Equation 1})$$

153 Where :

- 154 - BP is the bacterial production (nmol ³H-Thymidine.mL⁻¹ sediment.h⁻¹)
- 155 - DPM is the mean of the number of disintegrations per minutes between triplicate of
156 measure
- 157 - F1 is the conversion factor 4.51x10⁻¹³ dpm.Ci⁻¹. It was evaluated experimentally to
158 account for counter efficiency (Lavergne et al., 2017)
- 159 - T is the incubation time (1h)
- 160 - V is the analysed volume of sediment (0.015 mL)
- 161 - SA is the specific activity (25,000 Ci.mol of ³H-Thymidine⁻¹)
- 162 - Vt is the total volume of sample (5.5 mL)

163

164 **2.4.3 DNA diversity analysis**

165 **a- DNA extraction**

166 2 mL of sediment were sampled and directly frozen in nitrogen liquid. The matrix of the
167 samples was dense impeding a good extraction of the total DNA. So, before the extraction, a
168 step of homogenization and then of grinding with liquid nitrogen was added to destroy the
169 sample matrix (Fourçans et al., 2008). Subsamples of 0.25 g of grinded sample were done and

170 used for extraction. Then, DNA was extracted from 0.25 g subsamples using the DNeasy®
171 PowerSoil kit (Qiagen) according to the manufacturer's instructions, with a slight modification
172 at the homogenization step using Precellys homogenizer (Bertin Instruments).

173 **b- Illumina sequencing**

174 The V3-V4 region of the universal bacterial 16S rRNA genes was amplified in triplicate
175 using the primers 344F (5'-ACGGRAGGCAGCAG-3') and 801R_m (5'-
176 ACCAGGGTATCTAATCCT-3') (Liu et al., 2007). PCR mix consisted in 12.5 µL of AmpliTaq
177 Gold® 360 master mix (Applied Biosystems), 1 µL of each primer (10 µM) and 1 µL of genomic
178 DNA, in a final volume of 25 µL (adjusted with distilled water). All amplifications were performed
179 on a Veriti 96 Well Thermal Cycler (Applied Biosystem) using the following PCR program: 10
180 min at 95°C, 30 cycles of 30 s at 95°C, 30 s at 63°C and 40 s at 72°C, and finally, 10 min at
181 72°C.

182 The V4-V5 region of the universal archaeal 16S rRNA genes was amplified in triplicate
183 performing a nested PCR. The first PCR was done using the primer 519F without Illumina tag
184 (5'-CAGCCGCCGCGGTAA-3') (Herfort et al., 2009) and the primer 915R without Illumina tag
185 (5'-GTGCTCCCCCGCCAATTCCT-3') (Casamayor et al., 2002). PCR mix consisted in 12.5
186 µL of AmpliTaq Gold® 360 master mix (Applied Biosystems), 1 µL of each primer (20 µM) and 1
187 µL of genomic DNA, in a final volume of 25 µL (adjusted with distilled water). All these first
188 amplifications were performed on a Labcycler (SensoQuest) using the following PCR program:
189 10 min at 95°C, 35 cycles of 1 min at 95°C, 1 min at 62°C and 1 min 30 at 72°C, and finally,
190 10 min at 72°C. The second PCR was done on the PCR products of the first PCR using the
191 same primers with Illumina tag. PCR mix consisted in 12.5 µL of AmpliTaq Gold® 360 master
192 mix (Applied Biosystems), 1 µL of each primer (20 µM) and 1 µL of genomic DNA, in a final
193 volume of 25 µL (adjusted with distilled water). All amplifications were performed on a
194 Labcycler (SensoQuest) using the following PCR program: 10 min at 95°C, 35 cycles of 1 min
195 at 95°C, 1 min at 58°C and 1 min 30 at 72°C, and finally, 10 min at 72°C.

196 Illumina sequencing was performed by the Genomer platform of Roscoff, using Illumina
197 MiSeq technology. The complete dataset was deposited in the NCBI Sequence Read Archive
198 (SRA) database under SRA accession number PRJNA771950.

199 **c- Sequences treatments**

200 SAMBA (Standardized and Automated MetaBarcoding Analyses workflow) is a workflow
201 written by SeBIMER, the IFREMER's Bioinformatics Core Facility, the French National Institute
202 for Ocean Science (Noël et al., 2021). The pipeline was adapted to our DNA sequences
203 processing (<https://github.com/ifremer-bioinformatics/samba>). These bioinformatic analyses
204 were performed using SAMBA v3.0.0, Netxflow v20.10.0, QIIME 2 v2019.10.0, R v3.6.1,
205 DESeq2 v1.26.0, metagenomeSeq v1.28.0, microbiome v1.8.0, phyloseq v1.30.0, vegan
206 v2.5.6 and UpSetR v1.4.0. Bacterial, archaeal and eukaryotic data were analysed separately.

207 The taxonomic affiliation was performed against the Silva database v138 (Quast et al.,
208 2012; Yilmaz et al., 2013) with 99% of similarities.

209 **2.5 Statistical analysis**

210 All calculations and statistical analyses were performed on RStudio software (version
211 4.0.3[®] RStudio, R Core Team, 2020). The collinearities between the nine environmental
212 variables (temperature, pH, dissolved oxygen, salinity, phosphate, nitrate, nitrite, ammonium,
213 silicon) were first tested with variance inflation factors (VIFs). The variables selection was
214 based on the criterion $VIF < 5$. Then, a collinearity of up to 0.7 according to Spearman's rank
215 correlation ($p < 0.05$) was performed. This process led to group the variables presenting
216 collinearity and used the proxies for each group as explanatory variables. Seven variables
217 were thus selected (temperature, pH, dissolved oxygen, nitrate, nitrite, ammonium, silicon).
218 The principal coordinates analysis (PCoA) based on the Bray–Curtis distance matrices was
219 used to analyse the beta diversity. The main contributor Amplicon Sequence Variants (ASVs)
220 to the first two PCoA axes were determined by analysing correlations between these axes and
221 each ASVs. Alpha diversities indices were calculated according to the observed richness
222 (based on presence/absence of ASVs), the Shannon diversity (ASVs richness and their

223 evenness) and the Inverse Simpson index (giving more weight to common or dominant
224 species). Permutational multivariate analysis of variance (PERMANOVA) was applied to
225 determine the role of treatment and time in explaining the variance noted among the Bray–
226 Curtis distance matrices (*adonis* function of the *vegan* package). The differences between
227 treatments at a sampling time were performed with a post-hoc Tukey HSD test in the case of
228 an ANOVA, a Games-Howell test in the case of a Welch ANOVA or a Nemenyi test in the case
229 of a Kruskal Wallis test, according to a p -value of 0.05.

230

231 **3. Results and discussion**

232

233 **3.1 Characterisation of the physical-chemical environment of each treatment**

234 The physico-chemical environment occurring in this experiment has been already
235 described (Mazière et al., 2022). Briefly, the water temperature was increased by 4°C in the W
236 and WA treatments leading to an increase of the salinity (Mazière et al., 2022). The acidification
237 took place in the water reserves of the A and WA treatments but this decrease of pH was not
238 measured in the water of these mesocosms (Mazière et al., 2022). The dissolved oxygen
239 concentration was higher in these two last treatments (Mazière et al., 2022).

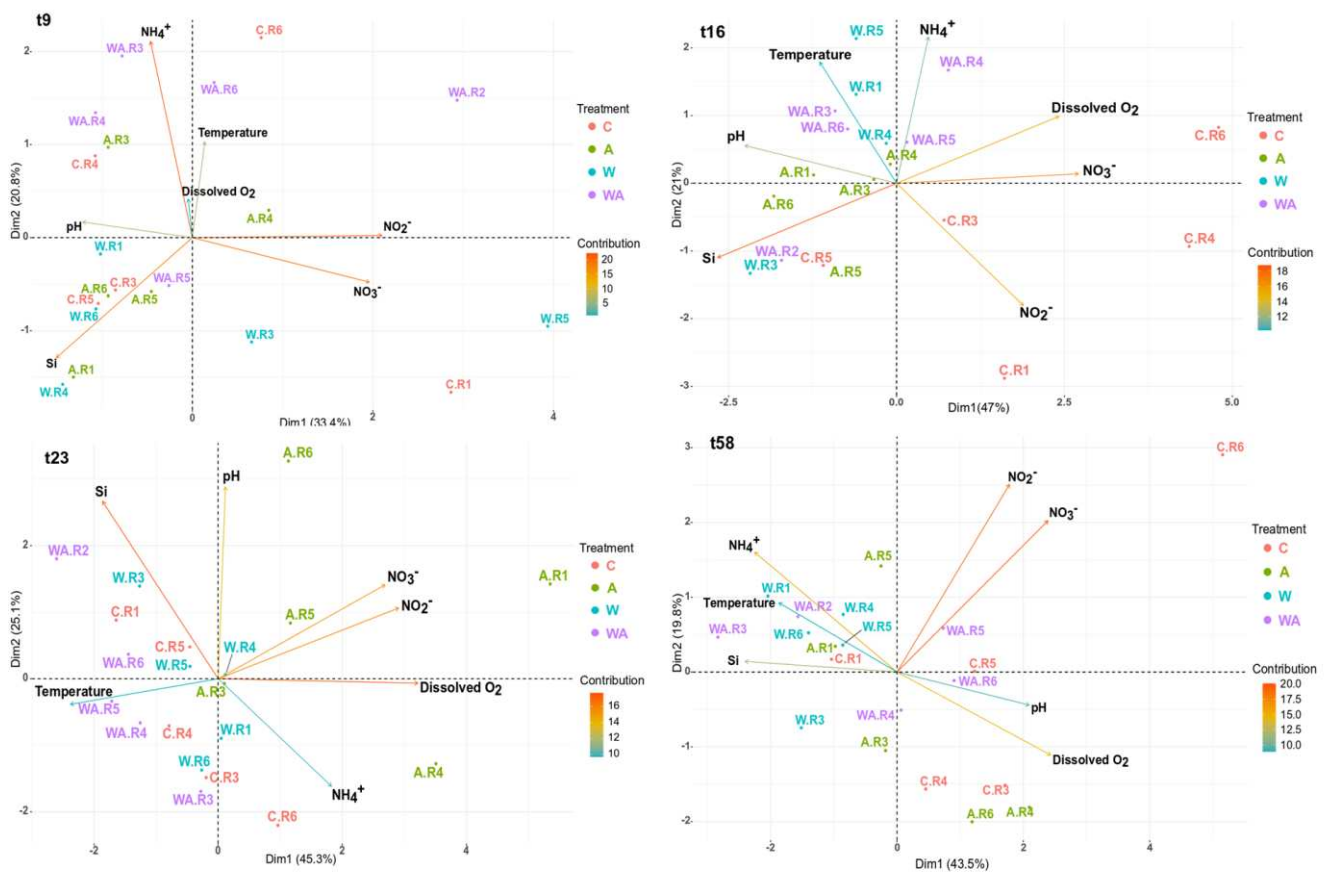
240 The treatment, the sampling time and the interaction between both affected
241 significantly the samples (PERMANOVA, $p < 0.05$). The nitrate concentration was higher at
242 t23 in the A treatment than in the C treatment (Kruskal, $p < 0.05$) (**Fig. S1**). The nitrite
243 concentration presented a significant difference only at t37 with the concentration in the C
244 treatment lower than the A treatment (Welch, $p < 0.05$) (**Fig. S1**). However, its concentration
245 tended to be higher in the A treatment than the 3 others at t23 and t37 (**Fig. S1**). No difference
246 was highlighted for ammonia concentration between treatment, except at t51 when it was lower
247 in the C treatment than in the WA treatment (Kruskal, $p < 0.05$), but the tendency of its nutritive
248 salt was to be higher in the W and WA treatments than the C and A treatments since t30 (**Fig.**
249 **S1**). The phosphate concentration was higher in the W treatment than the A treatment at t37
250 (Kruskal, $p < 0.05$) and in the W treatment than in the C treatment at t44 (ANOVA, $p < 0.05$) (**Fig.**

251 **S1**). No difference were reported for Si concentration between treatment, except at t44 where
252 its concentration was lower in the C treatment than in the W treatment (ANOVA, $p < 0.05$) (**Fig.**
253 **S1**). However, the silicon concentration tended to be higher in the W and WA treatments from
254 t37. The same trend was observed for phosphate concentration from t30 even if it tended to
255 be higher in the W treatment than the WA treatment at t37 and t44 (**Fig. S1**).

256 The two axes of the principal coordinate analysis (PCA) on the different sample
257 according to the physical-chemical parameters explained between 54.2% and 70.4% of the
258 variability (**Fig. 1**). The PCA showed that at t16, a separation between the C treatment and the
259 three other was observed by the axis 2 (**Fig. 1**). After one week of conditions change, the
260 temperature and the ammonium concentration were positively correlated with the W and WA
261 treatments but with low contributions, and only with temperature at t23 (**Fig. 1**). The A
262 treatment was positively correlated with the pH of the water (**Fig. 1**). The nitrite and nitrate
263 largely contributed to the differentiation of the C treatment with dissolved oxygen (**Fig. 1**). At
264 t23, at the end of the condition changes, the A treatment was separated from the other
265 treatments by the axis 2, with a positively correlation of nitrate and nitrite concentrations,
266 dissolved oxygen and pH. At t58, the W treatment was positively correlated with the
267 temperature and the WA treatment with temperature and pH (**Fig. 1**). The A treatment was not
268 correlated with pH et t58 (**Fig. 1**).

269 The W treatment was positively correlated with temperature during the first two weeks
270 of the experiment explaining by the water warming (**Fig. 1**). The A treatment differed from the
271 others at the beginning of the experiment, when the water acidification took place (**Fig. 1**).
272 When pH was decreased by 0.2 units pH, only this parameter was correlated with these
273 samples, but when it reached its final value (*i.e.*, 7.6), the A treatment was also positively
274 correlated with dissolved oxygen and nitrate and nitrite concentrations (**Fig. 1**). However at
275 t58, the nitrite and nitrate concentrations were negatively correlated with the A treatment (**Fig.**
276 **1**). The input of CO₂ favoured the oxygenic photosynthesis increasing the dissolved oxygen
277 concentration (Mazière et al., 2022). It is also known that acidification decreases nitrification

278 processes explaining the negative correlation with nitrates and nitrites which certainly
 279 accumulated (Beman et al., 2011; Wannicke et al., 2018). Surprisingly, the A treatment was
 280 not correlated with pH at t58 (Fig. 1). This was certainly explained by the fact that the pH in
 281 the mesocosms water was maintained at its initial value by the microbial mat (Mazière et al.,
 282 2022). Therefore, the A treatment communities have adapted to acidification. At t16 and t23,
 283 the WA treatment was correlated with temperature and at t58, with temperature and pH (Fig.
 284 1). Thus, this treatment reacted in the same way as W treatment in the beginning of the climate
 285 change simulation and then the acidification impact took place negatively correlated with those
 286 of the temperature.



287

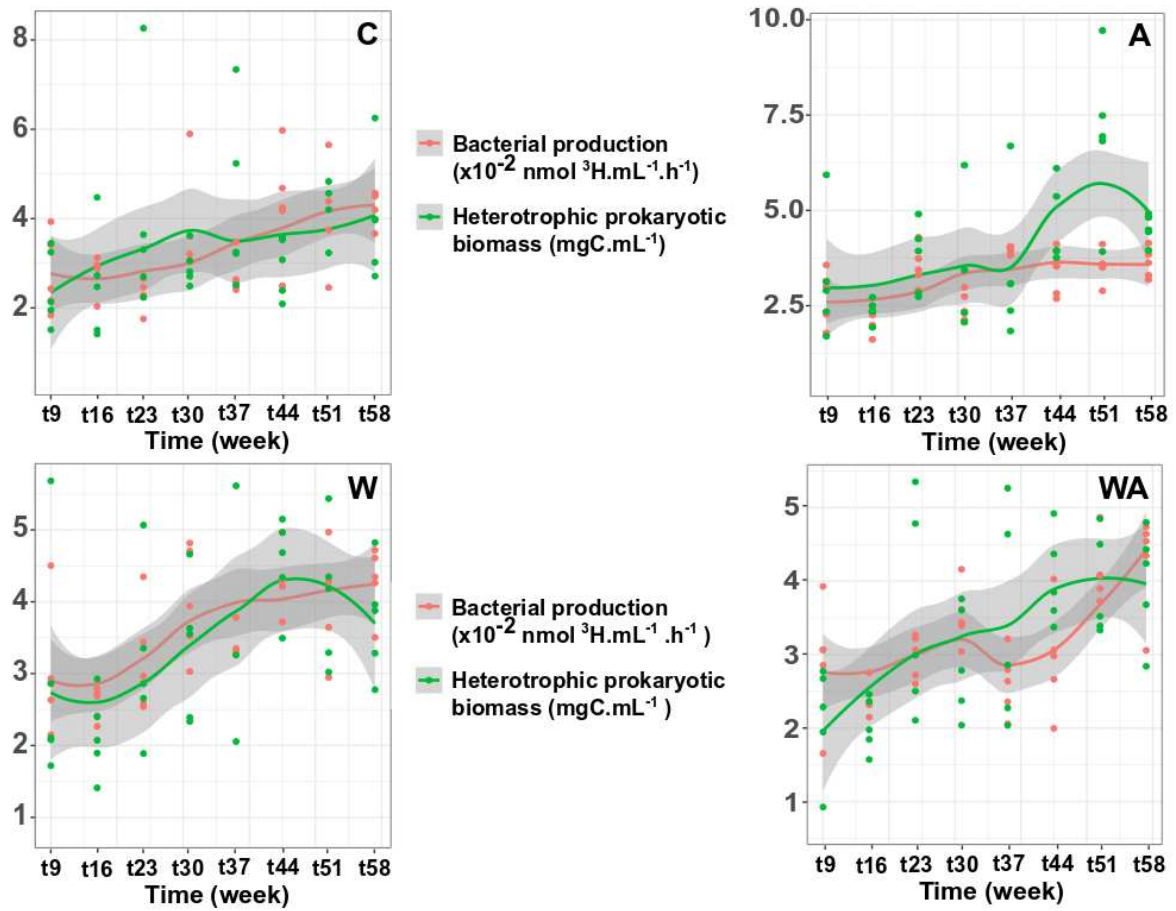
288 **Figure 1: Principal coordinate analysis (PCA)** on the sample structure according to the non-
 289 correlated physical-chemical parameters. At t16, W.R6 sample was not represented because
 290 the measures of the pH and the dissolved oxygen were not obtained.

291

3.2 Impact of climate change on the heterotrophic prokaryotic biomass and bacterial production

Climate change has been ever shown to impact the metabolism of the phototrophic communities of the microbial mats of Ré Island with the increase of the production of bound carbohydrates EPS (Mazière et al., 2022). A decrease of chlorophyll *a* concentration and an increase of chlorophyll derivatives proportion, which is supposed to be bacteriochlorophyll *c*, have been also observed, that probably indicate a change in either the pigment metabolism or the phototrophs' abundance (Mazière et al., 2022).

No statistical trend of the heterotrophic prokaryotic biomass or of the bacterial production was shown (**Fig. 2**). However, in the W and WA treatments, an increase of the bacterial production co-occurred with an increase of the heterotrophic prokaryotic biomass (**Fig. 2**). In the W treatment, a decrease of the heterotrophic prokaryotic biomass was observed at t51 and t58. At t44, the heterotrophic prokaryotic biomass was more important in the A and W treatments than in the C treatment (ANOVA; $p < 0.05$) and at t51, it was more important in the A treatment than in the other treatments (ANOVA; $p < 0.05$) (**Fig. 2**).



307

308 **Figure 2: Bacterial production and heterotrophic prokaryotic biomass.** The curves
 309 represented the bacterial production (in red) and the heterotrophic prokaryotic biomass (in
 310 green). The letters t followed by a number indicates the sampling time.

311

312 Heterotrophic prokaryotes grouped bacteria and archaea. Their biomass is controlled
 313 by grazing, viral lysis (top-down control) and also organic matter or nutrients availability
 314 (bottom-up control) (Boras et al., 2009; Gasol et al., 2002; Teira et al., 2019). In the W
 315 treatment, one or several of these factors were affected by warming because the heterotrophic
 316 prokaryotic biomass and the bacterial production increased (**Fig. 2**). However, from t51 the
 317 heterotrophic prokaryotic biomass decreased but the bacterial production was stable. This
 318 assumes either a decrease in the heterotrophic archaeal biomass, or an increase in the grazing
 319 or viral populations activity and/or a decrease in the organic matter or nutrients availability (**Fig.**
 320 **2**). In the A treatment, only the heterotrophic prokaryotic biomass increased without an
 321 increase of the bacterial production, supposing an increase of the heterotrophic archaea

322 biomass (**Fig. 2**). The WA treatment presented the same profile than the W treatment without
323 decreasing of the heterotrophic prokaryotic biomass (**Fig. 2**). So, warming and acidification
324 together increased the bacterial production and heterotrophic prokaryotic biomass.

325 These changes in the metabolism and growth indicate certainly a modification of the
326 diversity and/or the structure of the microbial mat.

327

328 **3.3 Prokaryotic structure of microbial mats faced to climate change**

329 A total of 17,666 bacterial ASVs dispatched within 49 phyla with 335 families and
330 12,090 archaeal ASVs dispatched within 13 phyla with 32 families were identified. The 100
331 most abundant bacterial ASVs identified belonged to *Bacteroidota*, *Chloroflexi*,
332 *Cloacimonadota*, *Desulfobacterota*, *Firmicutes*, *Gemmatimonadota*,
333 *Marinimicrobia_(SAR406_clade)*, *Patescibacteria*, *Planctomycatota*, *Proteobacteria* and
334 *Spirochaetota* (**Fig. S2**). For archaea, the 100 most abundant ASVs were reported between
335 *Asgardarchaeota*, *Crenarchaeota*, *Euryarchaeota*, *Halobacterota*, *Iainarchaeota*,
336 *Micrarchaeota*, *Nanoarchaeota* and *Thermoplasmatota* (**Fig. S3**).

337 Archaeal richness, Shannon diversity and Inverse Simpson indices were not different
338 between treatments during the experiment (**Fig. S5**). Bacterial richness presented also no
339 difference between the four treatments (**Fig. S4**). Therefore, the prokaryotic richness was the
340 same under the fourth treatments. However, the Shannon diversity of the bacterial
341 communities of the A treatment tends to be lower than the C treatment from t23 to the end of
342 the experiment (t58) (**Fig. S4**). It was significantly lower than the C treatment at t44 (ANOVA,
343 $p < 0.05$) and significantly higher in the W treatment than in the WA treatment at t16 (Kruskal,
344 $p < 0.05$) (**Fig. S4**). The Inverse Simpson index on bacteria was equal in all treatment (**Fig. S4**).
345 Nevertheless, in the A treatment it presented a trend to be lower than the other treatments
346 after t9 (**Fig. S4**). The reduction of the Shannon diversity, accompanied by a reduction of
347 richness, have been ever seen by Crummett (2020) on microbial communities of seawater

348 placed under climate change acidified conditions. These microorganisms coming from a region
349 that regularly experiences high pCO₂ and low pH meaning that microbial communities
350 supposed adapted to acidification is still sensitive to this parameter. The archaeal communities
351 diversity were not impacted by acidification or warming.

352 The treatment and the sampling time impacted significantly the ASVs composition
353 (PERMANOVA, $p < 0.05$). The interaction between both had no effect (PERMANOVA, $p > 0.05$).
354 The 2 axis of the principal coordinates analyses (PCoA) explained less than 50% of the
355 bacterial or archaeal diversity by the treatments and the families (**Fig. 3 and 4**). The same was
356 obtained with 3 axis. Therefore, it would say that treatment and families abundance were not
357 the only parameters explaining the variability of the bacterial or archaeal diversity. Time and
358 physical-chemical environment played certainly a great role. Bacterial structure differed
359 between the four treatments from t44 where treatment A clearly stood out (**Fig. 3**).

360 The ASVs explaining this difference belong to the families *Rhodothermaceae* and
361 *Rhodobacteraceae* at t44 and t51 (**Fig. 3**). From t51, *Rhodothermaceae* and *Chlorobiaceae*
362 were common to explain to the WA and A treatments (**Fig. 3**). The W treatment was more
363 explained by *Marinilabiliaceae* at t44 and t51 (**Fig. 3**). *Rhodothermaceae* family are
364 chemoheterotrophs aerobes (Park et al., 2014). In our study, two genera were identified,
365 *Salinibacter* and *Salisaeta*, isolated from high-salt environments and are considered as
366 halophiles (Park et al., 2014). *Rhodobacteraceae* is frequently found in marine environments
367 (Pujalte et al., 2014). The members of this family present a high phenotypic and ecologic
368 diversity with several metabolisms including the use of various organic and inorganic
369 compounds, sulfur oxidation, aerobic anoxygenic photosynthesis, carbon monoxide oxidation
370 and the production of secondary metabolites (Pujalte et al., 2014). Several genera from the
371 *Rhodobacteraceae* family found in the mesocosms of our study belong to the *Roseobacter*
372 genus (Pujalte et al., 2014), a versatile bacterial lineage (Newton et al., 2010). They are key
373 players in carbon and organic sulfur cycling (Newton et al., 2010). Some members of this
374 lineage have been characterized as ecological generalists (Moran et al., 2007; Newton et al.,

2010) that become dominant in a disturbed environment (Chen et al., 2021). Photoheterotrophic *Rhodobacteraceae* have been demonstrated to have a metabolic versatility conferring adaptation capacity to environmental changes, being more competitive resulting in the stability of the populations (Chen et al., 2021). Therefore in our study, this family, including *Roseobacter* genus, was favoured by acidification treatment (**Fig. 3**) certainly because the input of carbon in their environment favoured their metabolisms and thus, their competitiveness and abundance. The *Chlorobiaceae* are green sulfur bacteria comprised on the green anoxygenic phototroph bacteria (Madigan et al., 2017). The abundance of this family was positively correlated with the A and WA treatments at t51 and t58 (**Fig. 3**). A previous study of the pigment composition of the microbial mats of this experiment showed that the abundance of unknown chlorophyll derivatives were produced under acidification (Mazière et al., 2022). These molecules were supposed to be bacteriochlorophyll *c*, a pigment contained on green anoxygenic phototroph bacteria, presuming the increase of the relative abundance of these organisms or the occurrence of their metabolisms (Mazière et al., 2022). The indirect gradient analyses on bacterial ASVs confirmed that acidification favoured the development of the green anoxygenic bacteria, and more precisely of the green sulfur bacteria *Chlorobiaceae*. The W treatment was explained by *Marinilabiliaceae* with only *Anaerophaga* genus identified (**Fig. 3**). This microorganism is strictly anaerobic, chemoorganotroph and nonphotosynthetic, and has a fermentative metabolism (Whitman et al., 2015). A study in sulfidic arctic marine sediment has demonstrated that when cyanobacterial necromass was added to this sediment for mimicking fresh organic matter input, the initial hydrolysis and fermentation of mainly proteins, carbohydrates and lipids to diverse volatile fatty acids were done by several species including *Marinilabiliaceae* (Müller et al., 2018). Ocean warming is supposed to increase the development of cyanobacteria (Ma et al., 2019) but a previous study on pigment composition showed that relative abundance of chlorophyll *a*, the pigment contained in cyanobacteria, didn't increase and thus no augmentation of this population is supposed (Mazière et al., 2022). Nevertheless, another pigment defined as the chlorophyll derivative #6 was positively correlated with the W treatment at t51 and t58, but no identification was done on it (Mazière et

403 al., 2022). It can be supposed that this pigment was contained in a phototroph organism which
404 could belong to bacteria or eukaryota, and which abundance would be favoured with ocean
405 warming and would participate in the organic matter input used by *Marinilabiliaceae*.

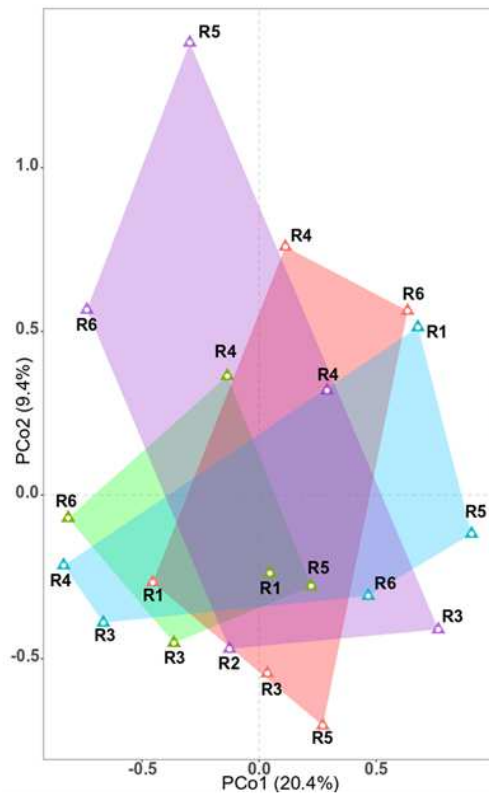
406 Archaeal structure clearly differed at t37 in the A treatment from the other treatments
407 under axis PCo1 explaining 18.2% of the variance (**Fig. 4**). However, from t23, this treatment
408 was explained by the presence of three families, *Micrarchaeales*, CG1-02-32-21 and
409 SCGC_AAA011-D5 (**Fig. 4**). Archaea are a great proportion of microbial biomass on Earth and
410 play major roles in biogeochemical cycles and in greenhouse gas emissions (Offre et al.,
411 2013). However, the impact of climate change on these microorganisms is less studied. In this
412 study, the families *Micrarchaeales* and CG1-02-32-21 belonging to the *Micrarchaeota* phylum
413 were found. These archaea belong to a lineage named DPANN for candidate divisions
414 “*Candidatus* Diapherotrites,” “*Candidatus* Parvarchaeota,” “*Candidatus* Aenigmarchaeota,”
415 “*Candidatus* Nanohaloarchaeota,” and phylum *Nanoarchaeota* (Kadnikov et al., 2020; Rinke
416 et al., 2013). This superphylum includes archaea with small cell and genome sizes with limited
417 metabolic capabilities (Kadnikov et al., 2020; Rinke et al., 2013). Among it, *Micrarchaeota* and
418 *Parvarchaeota*, are mentioned as Archaeal Richmond Mine Acidophilic Nanoorganisms
419 (ARMAN) (Baker et al., 2006). These microorganisms were observed to interact with
420 Thermoplasmatales cell with pili-like structures (Baker et al., 2010). The SCGC_AAA011-D5
421 family belongs to the *Nanoarchaeota* phylum (*Nanoarchaeia* class and *Woesearchaeales*
422 order). *Nanoarchaeota* are obligate symbionts/parasites with a highly reduced genome lacking
423 most primary biosynthetic and energetic functionalities (Munson-McGee et al., 2015; Wurch et
424 al., 2016). *Nanoarchaeum equitans* was the first discovered. This archaea possess one the
425 smallest archaeal genomes and grow attached to the surface of *Ignicoccus hospitalis*, its
426 archaeal host which supply nutrients to *N. equitans* (Huber et al., 2002; Waters et al., 2003).
427 The host organisms of *Nanoarchaeota* are diverse and not all identified (Clingenpeel et al.,
428 2013). They are found in a large variety of terrestrial or marine habitats like hyperthermophilic,
429 mesophilic and halophilic environments (Casanueva et al., 2008; Clingenpeel et al., 2013;

430 Flores et al., 2012; Hohn et al., 2002; McCliment et al., 2006). Acidification seems to favour
431 archaeal parasites of other archaea (**Fig. 4**). The host-parasite relationship can regulate
432 individuals and communities, impacting the structure and the diversity of an ecosystems.

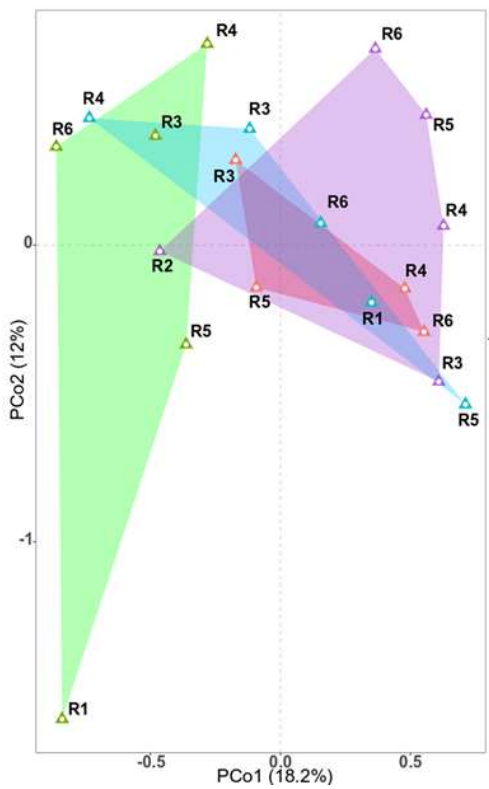
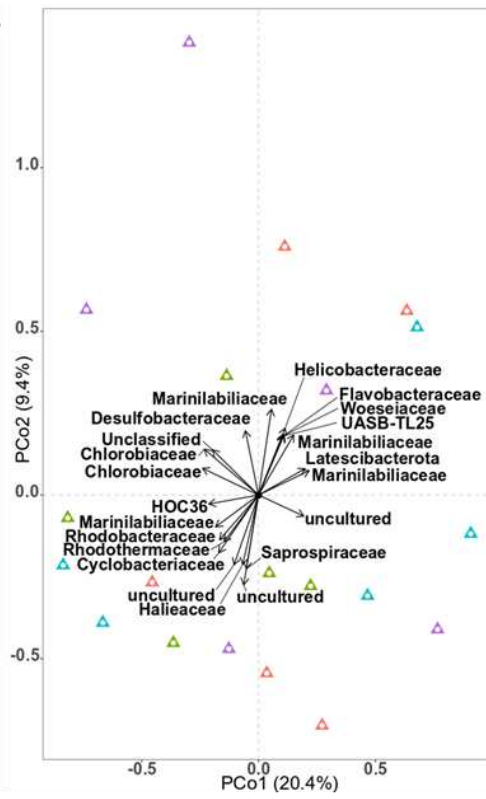
433

434

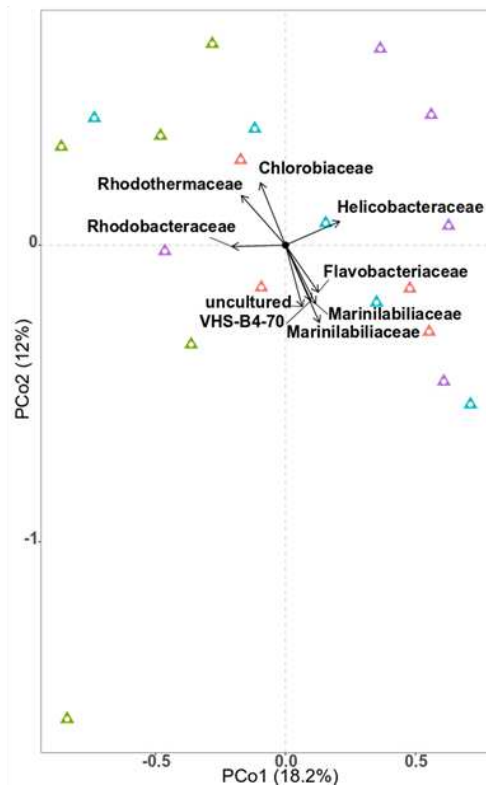
435

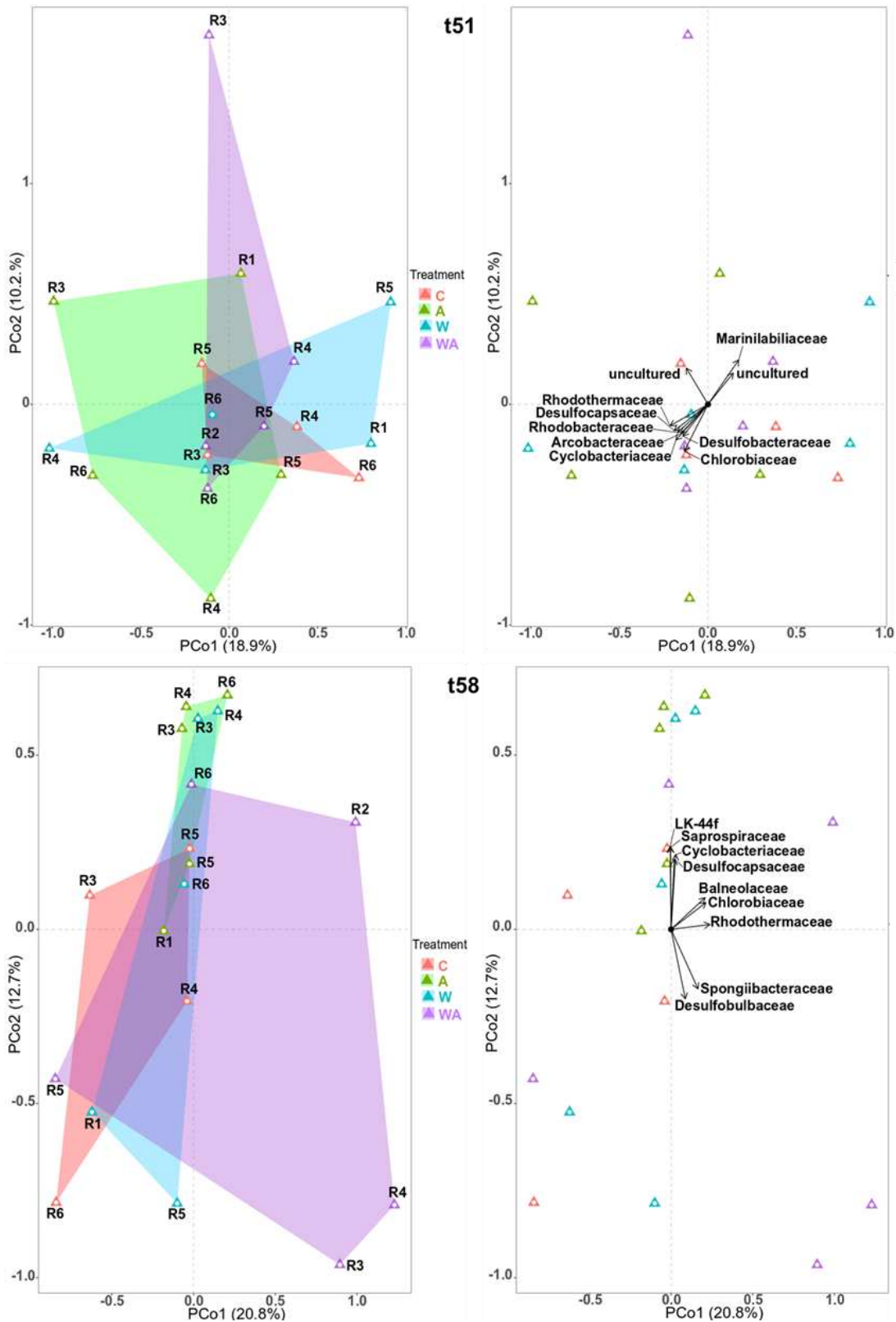


t37



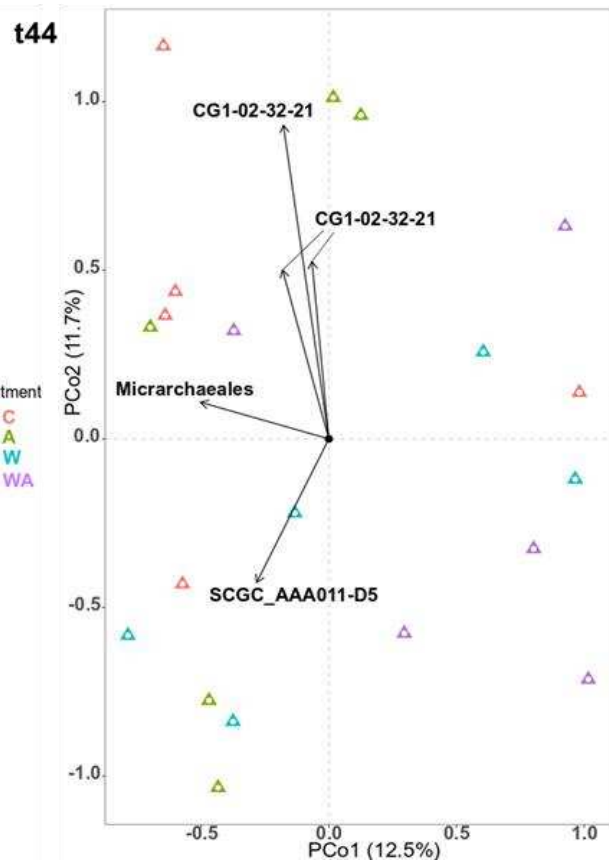
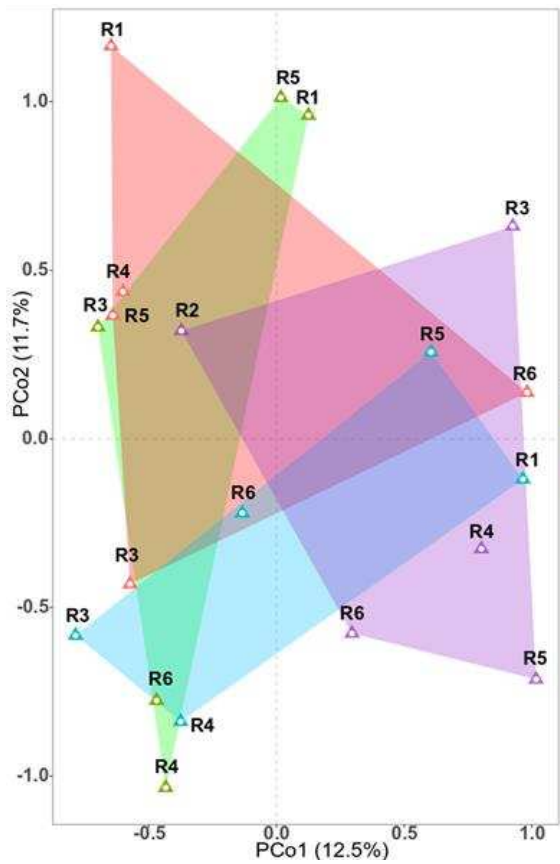
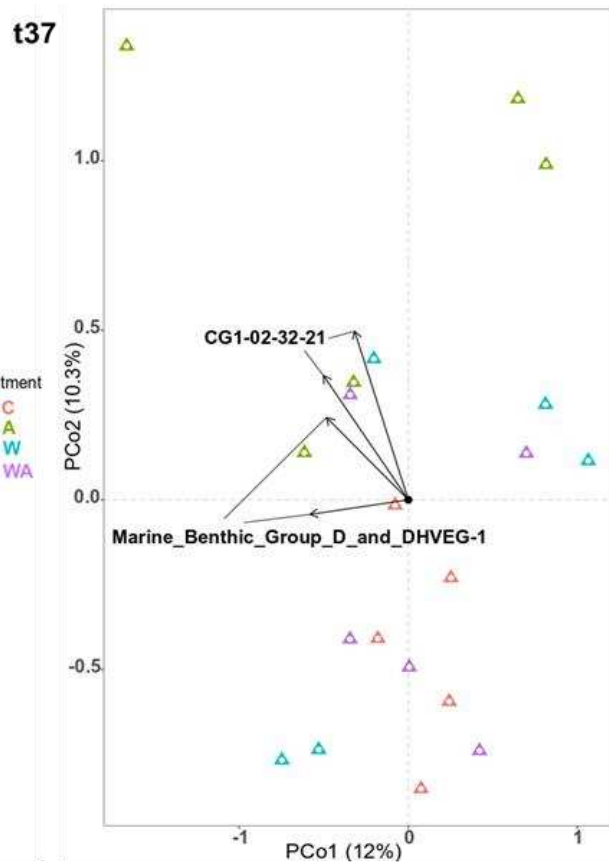
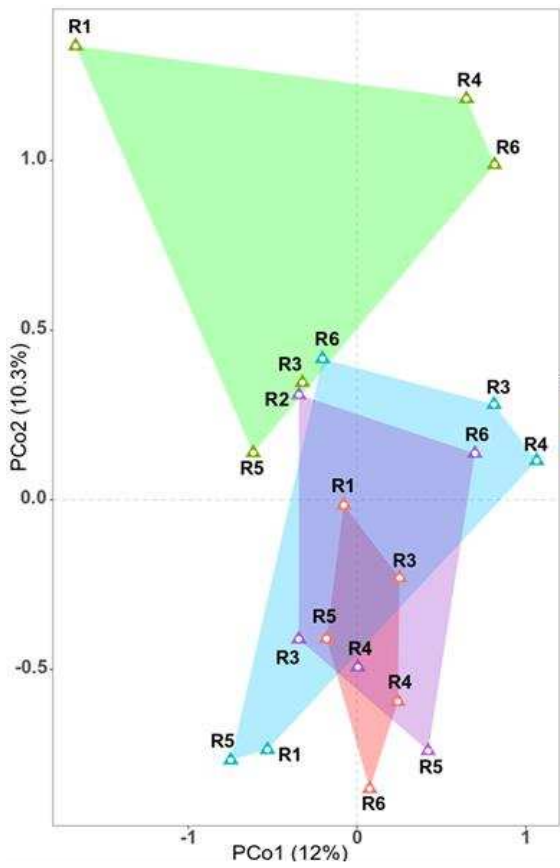
t44

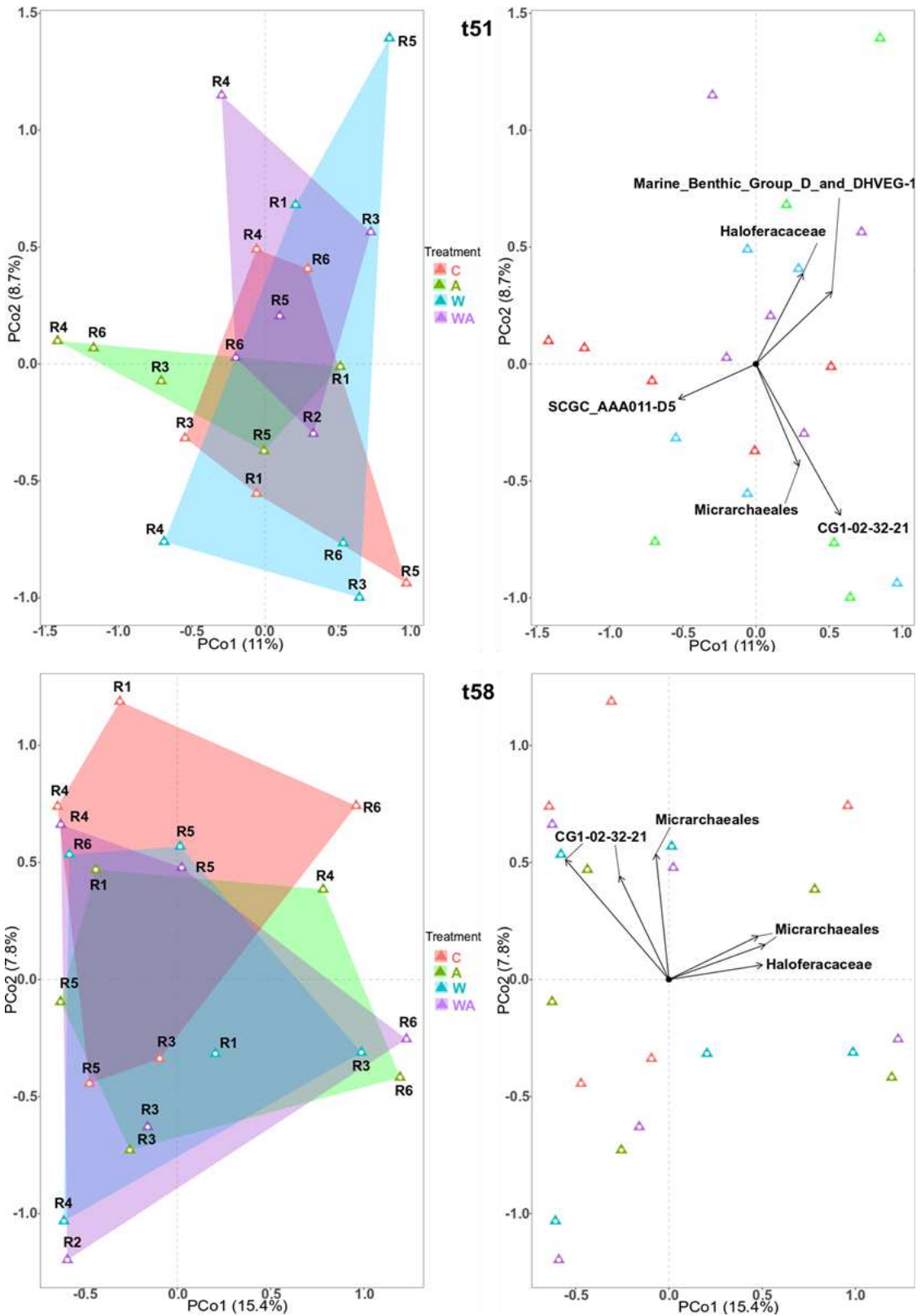




437

438 **Figure 3: Indirect gradient analyses** representing the bacterial diversity explained by the
 439 treatments themselves (graphics on the right) and by families (graphics on the left) along two
 440 axes, PCo1 and PCo2, for the bacterial 16S rRNA gene at t37, t44, t51 and t58. To simplify
 441 the data, only these four sampling times are represented to show the variability between
 442 samples. The triangles correspond to the replicates.





444

445 **Figure 4: Indirect gradient analyses** representing the diversity explained by the treatments
 446 themselves (graphics on the right) and by families (graphics on the left) along two axes, PCo1
 447 and PCo2, for the archaeal 16S rRNA gene at t37, t44, t51 and t58. To simplify the data, only
 448 these four sampling times are represented to show the variability between samples. The
 449 triangles correspond to the replicates.

450

451 **4. Conclusion**

452

453 The physical-chemical environment was modified by the different climate scenario applied.
454 The W treatment was differentiated from the others by its temperature. Surprisingly, the
455 variability of the A treatment was explained by the pH only during the change of conditions, the
456 first two weeks, and then it was correlated with the dissolved oxygen concentration, certainly
457 due to an increase of photosynthesis, and the nitrate and nitrite concentrations, certainly
458 correlated with a decrease of nitrification. The heterotrophic prokaryotic biomass and the
459 bacterial production increased in the W and WA treatments signified that temperature favour
460 the development of prokaryotes. However, at the end of the experiment, warming impacted
461 the archaeal heterotrophic biomass, or/and the top-down or bottom-up controls. The A
462 treatment increased the archaeal heterotrophic biomass. Moreover, these climate scenarios
463 modified the diversity and composition of prokaryotes in the microbial mats. The bacterial and
464 archaeal richness were not impacted by climate change scenarios, and only the Shannon
465 diversity changed because of acidification. The A treatment also modified the prokaryotic
466 composition with positive correlations with the *Rhodobacteraceae* and *Chlorobiaceae*
467 abundance, also found the WA treatment, certainly in favouring their metabolisms. Acidification
468 scenario also favoured *Micrarchaeales*, CG1-02-32-21 and SCGC_AAA011-D5 which are
469 parasites for other archaea. This study provided new insights on the prokaryotic compartment
470 in microbial mats face to climate change.

471

472

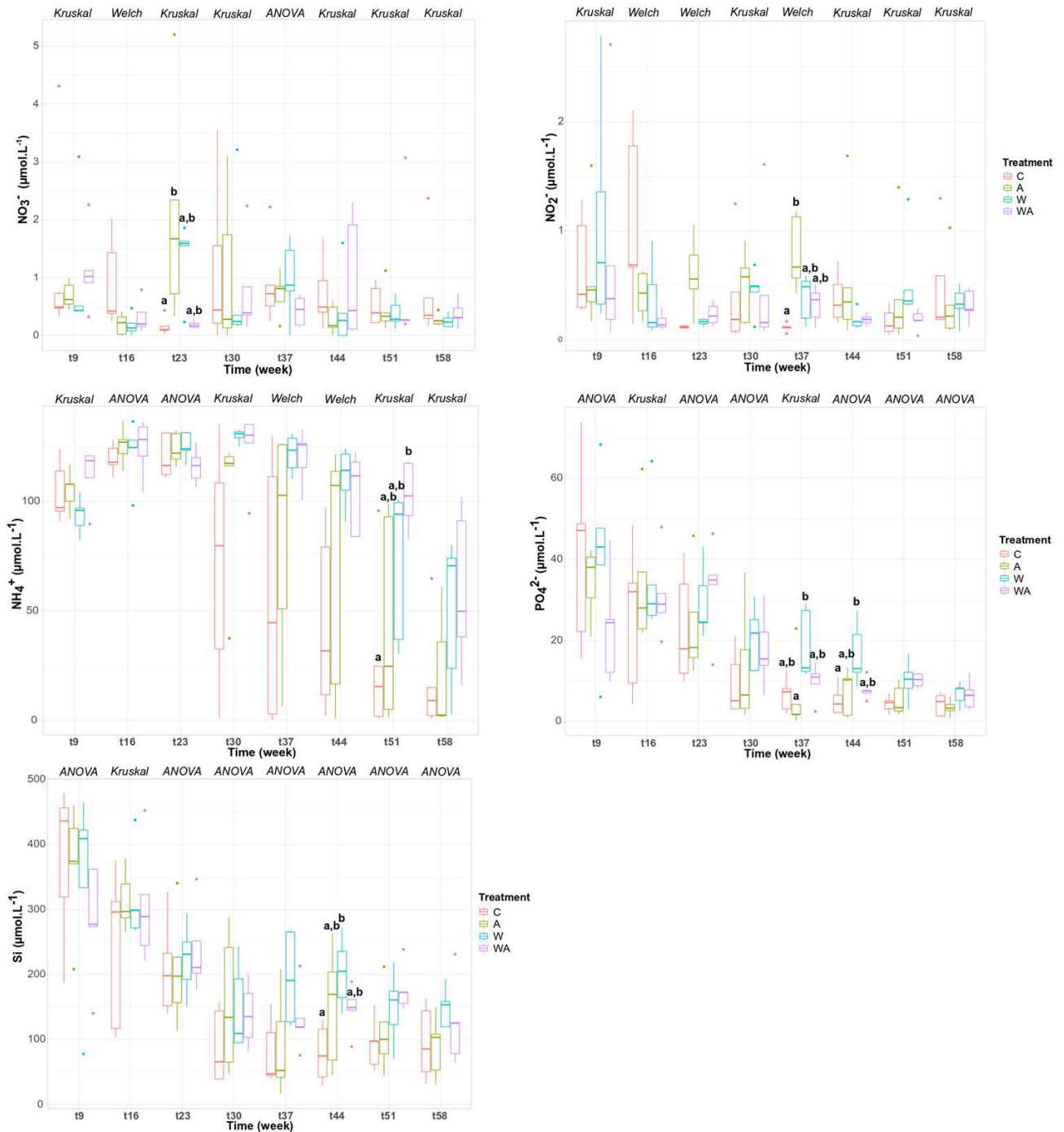
473

474

475

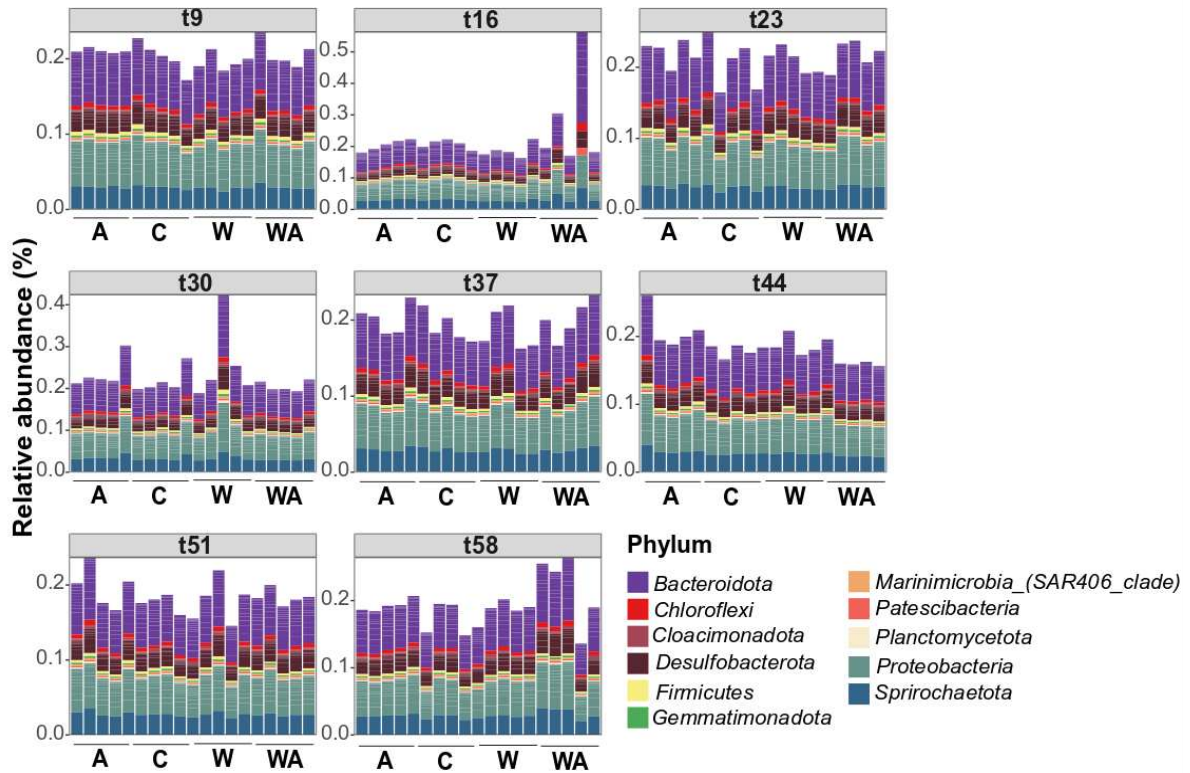
476
477
478

Supplementary materials of “Climate change effect on microbial mats structure modifies prokaryotic diversity and metabolism”



479

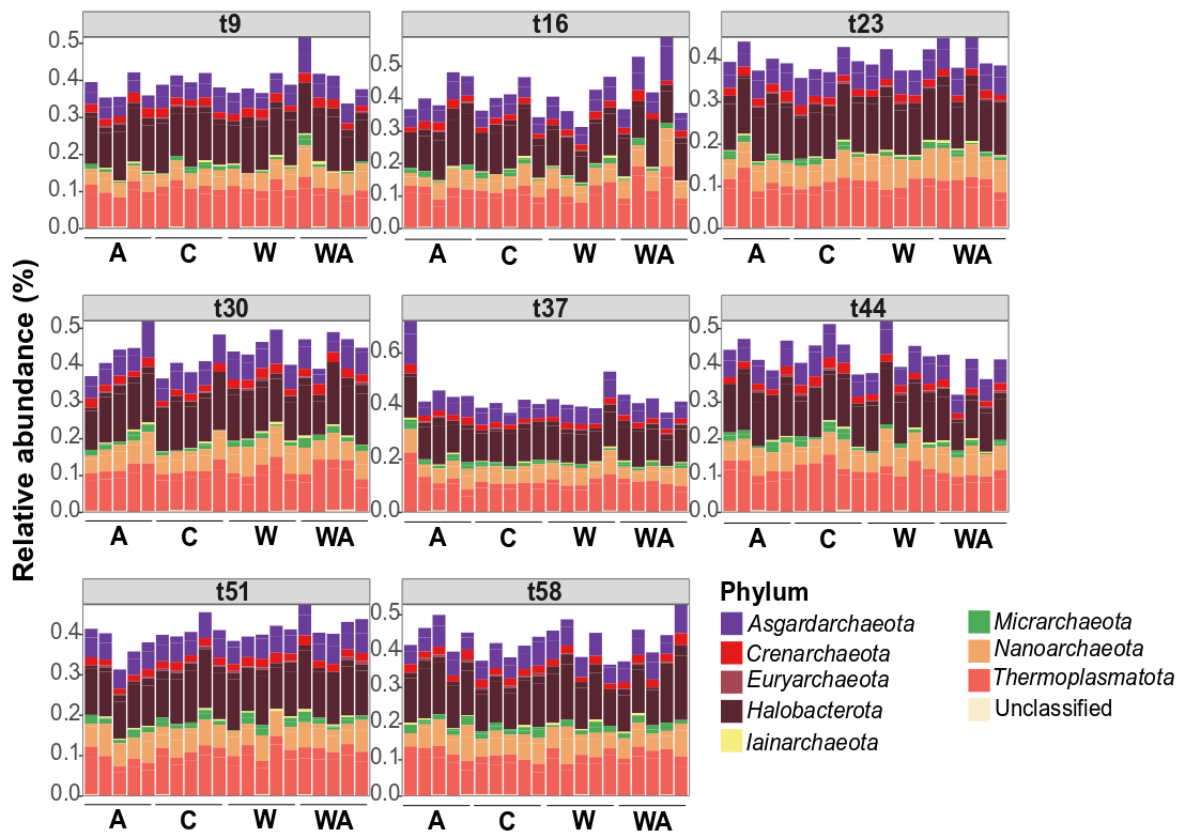
480 **Figure S1: Nutrients variation.** Boxplots of nitrite (NO_2^-), nitrate (NO_3^-), ammonium (NH_4^+),
481 phosphate (PO_4^{2-}) and silicon (Si). The letters t followed by a number indicates the sampling
482 time. The statistical test performed to show the differences between treatments at a sampling
483 time is indicated in italics above the figure. The letters indicated a significant difference ($p <$
484 0.05) found after a post-hoc Tukey HSD test in the case of an ANOVA, a Games-Howell test
485 in the case of a Welch ANOVA or a Nemenyi test in the case of a Kruskal Wallis test.



486

487 **Figure S2: Relative abundance of the phylum of the 100 most abundant bacterial ASVs.**

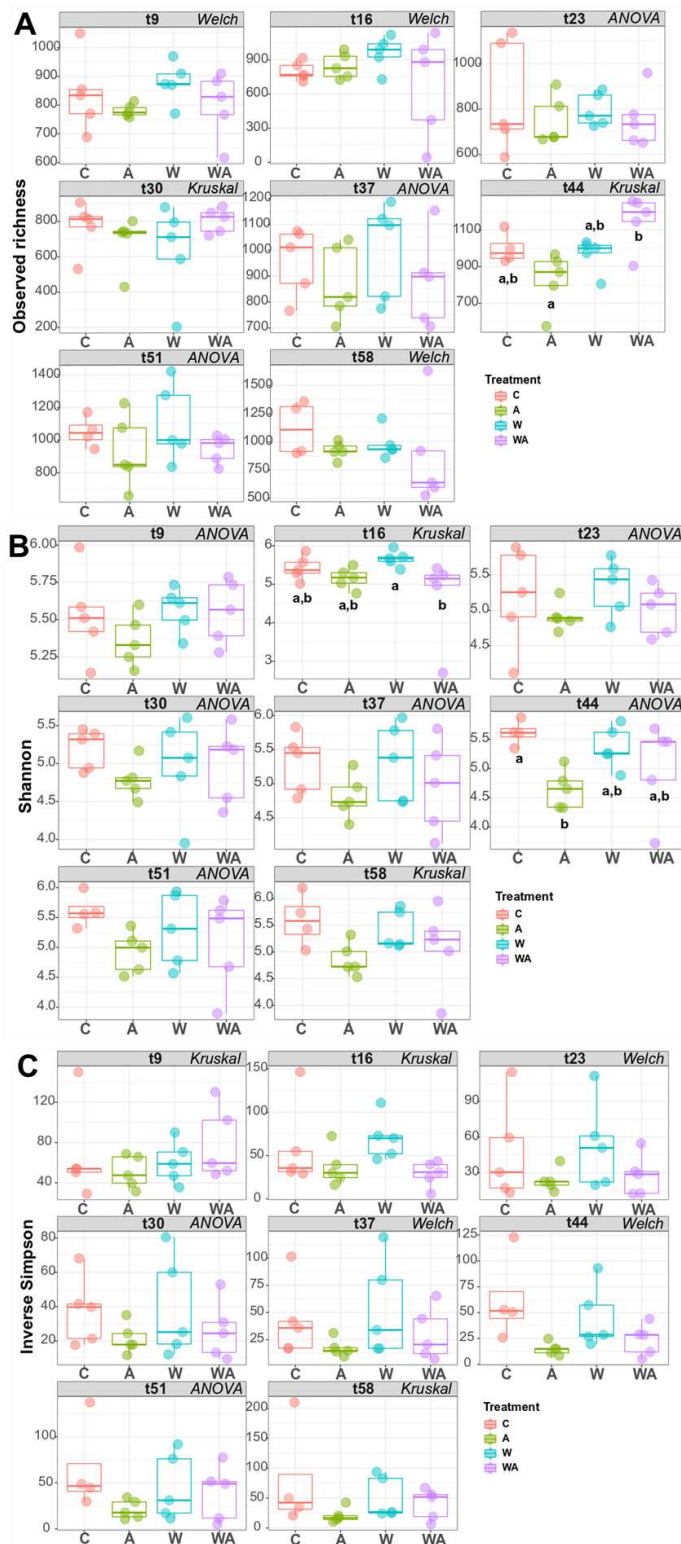
488 The letters t followed by a number indicates the sampling time.



489

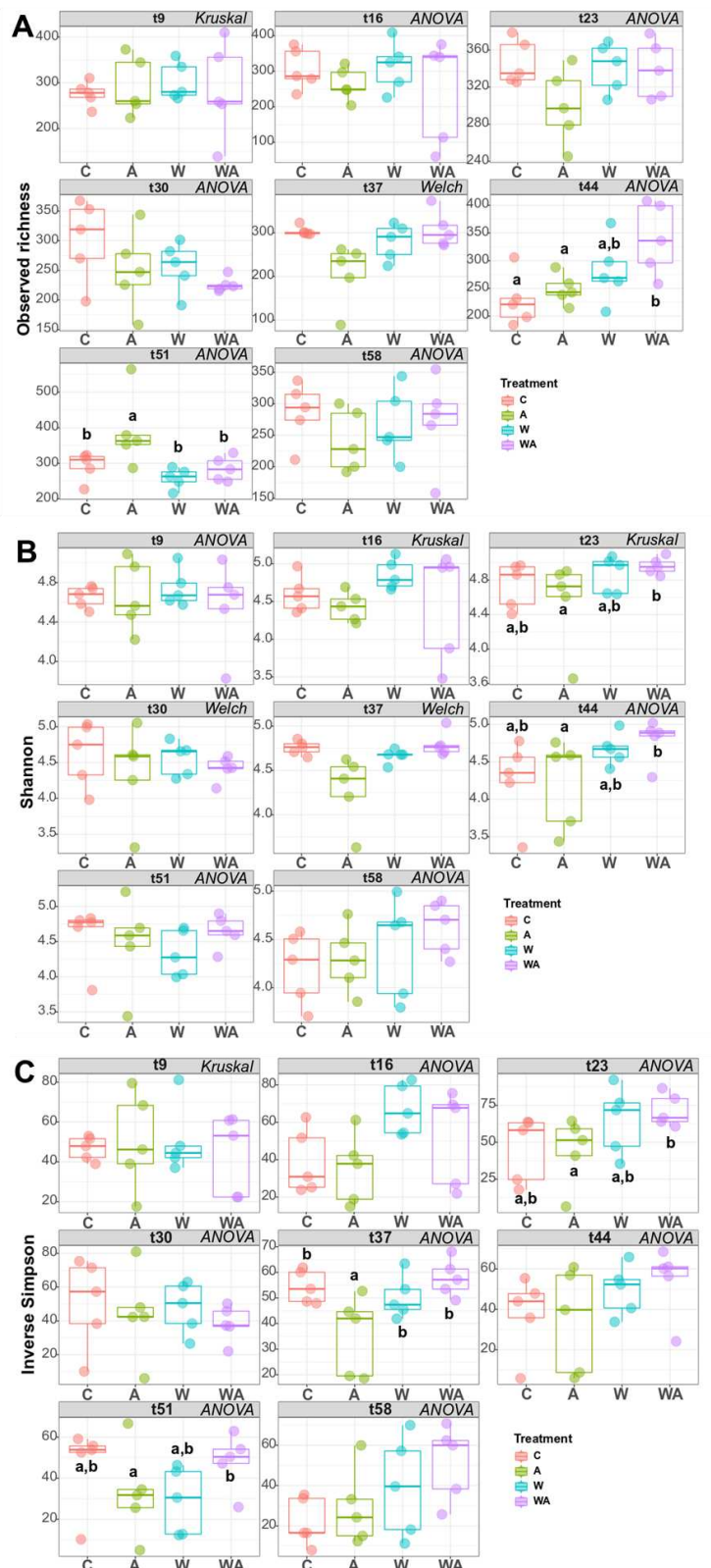
490 **Figure S3: Relative abundance of the phylum of the 100 most abundant archaeal ASVs.**

491 The letters t followed by a number indicates the sampling time.



492
 493
 494
 495
 496
 497
 498
 499
 500

Figure S4: Bacterial alpha diversity. Three indices were calculated: **A)** observed richness, **B)** Shannon diversity and **C)** Inverse Simpson index. The letters t followed by a number indicates the sampling time. The statistical test performed to show the differences between treatments at a sampling time is indicated in italics above the figure. The letters indicated a significant difference ($p < 0.05$) found after a post-hoc Tukey HSD test in the case of an ANOVA, a Games-Howell test in the case of a Welch ANOVA or a Nemenyi test in the case of a Kruskal Wallis test.



501

502 **Figure S5: Archaeal alpha diversity.** Three indices were calculated: **A)** observed richness,
 503 **B)** Shannon diversity and **C)** Inverse Simpson index. The letters t followed by a number
 504 indicates the sampling time. The statistical test performed to show the differences between
 505 treatments at a sampling time is indicated in italics above the figure. The letters indicated a
 506 significant difference ($p < 0.05$) found after a post-hoc Tukey HSD test in the case of an
 507 ANOVA, a Games-Howell test in the case of a Welch ANOVA or a Nemenyi test in the case of
 508 a KruskalWallis test.

3. Impact of climate change on eukaryotic communities inhabiting microbial mats

This part will be valued through the writing of a future paper. The determination of the meiofaunal abundance *in situ*, when the microbial mats were sampled, are in progress.

Meiofauna are major contributors to the chemical, physical and biological sediments properties and in benthic food webs (Ingels et al., 2018; Schratzberger and Ingels, 2018). They are also considered as important ecological components of benthic ecosystems (Ingels et al., 2018). Meiofaunal diversity and abundance in our mesocosms were first determined by binocular loupe. Only nematodes were observed. This is not surprising because nematodes with copepods are the most abundant metazoan meiofaunal organisms in marine sediments and nematodes have colonized every environment that can support meiofaunal life (Ingels et al., 2018).

The abundance of nematodes decreased over time in all treatments, but no difference was shown between the four treatments (ANOVA, Welch or Kruskal-Wallis; $p > 0.05$) (**Fig. 28**). However, the nematodes abundance in the C treatment tended to be higher than in the W treatment from t23 until the end of the experiment and also in the A treatment at t23, t44 and t58 (**Fig. 28**). Temperature didn't affect the nematodes communities certainly because they were ever submitted to fluctuations of temperature in their natural environment (**Chapter IV**). Moreover, temperature has never been shown to affect meiofaunal abundance, nematode abundance, nematode species richness, nematode diversity nor nematode evenness (Lee et al., 2017). No acidification of the water to a value of 7.6 was observed in the studied salterns (**Chapter IV**) explaining why this parameter impacted them. Other studies have also been shown that acidification of seawater affected the nematode abundance and reduced diversity of the nematodes (Lee et al., 2017; Widdicombe et al., 2009).

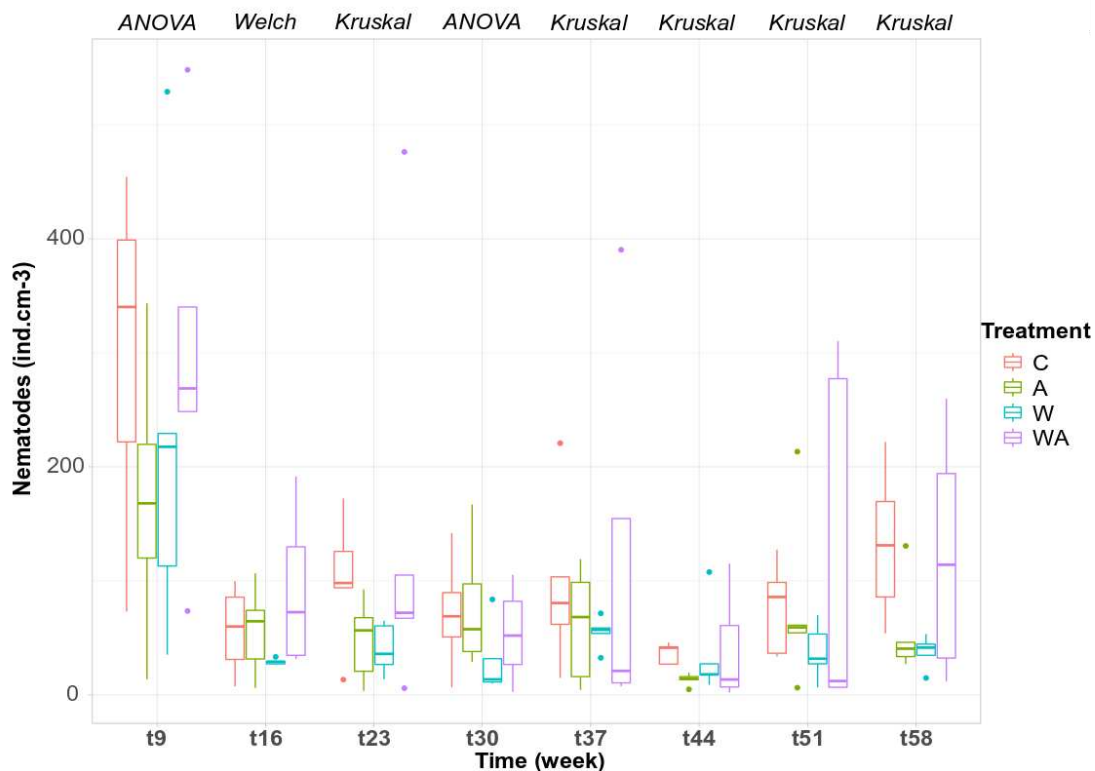


Figure 28: Nematodes abundance by binocular loupe. The results were presented by individuals per cubic centimetre of microbial mat. The letters t followed by a number indicates the sampling time.

To complete the study of eukaryotic organisms, a 18S rRNA gene analyse was performed. In fact, benthic protozoa or nanoflagellates and others are classically studied by using microscopy, but it is time consuming and it needs expert taxonomists to identify them (Fontaneto et al., 2009) and it is often difficult to separate them from the sediment matrix. It is also not possible to identify small sized groups (Fontaneto et al., 2009; Wright et al., 1996).

We identified 4816 sequences after affiliation with the SILVA databases. Bacteria represented 2871 sequences (59.6%), Archaea 224 sequences (4.7%) and 1490 sequences were unassigned (30.9%) (**Fig. 29**). Only 231 sequences belong to Eukarya (4.8%) (**Fig. 29**). “Universal” primers are not really universal because they are developed according to the known taxon (Normand et al., 2011). These universal primers used were certainly less specific because they were not developed for this type of environment. Therefore, it would be certainly interesting to develop primers for eukaryotes of hypersaline environments.

The samples C-R5 (control replicate n°5) at t23, C-R4 at t30 and A-R6 at t58 were left in the following analyses because the abundance of their identified ASVs present a problem of numeric conversion with R software. Its resolution is in progress.

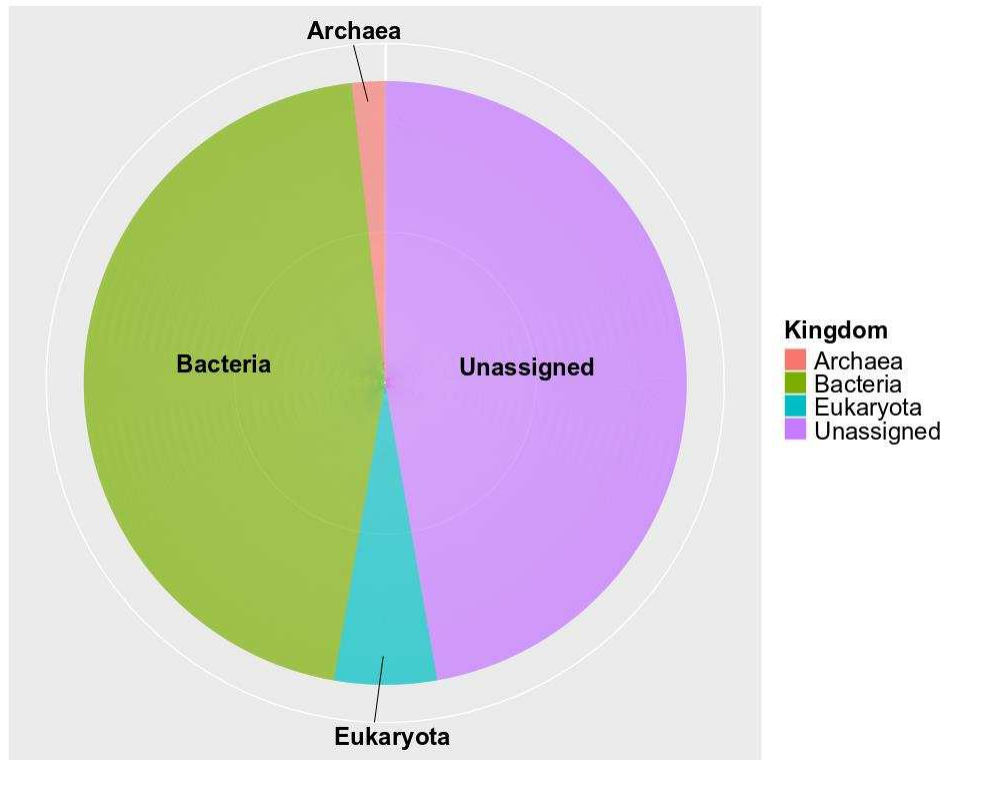


Figure 29: Domains identified with eukaryotic primers 515F and 951R. Bacteria represented 2871 sequences, Archaea 224 sequences, 1490 sequences were unassigned and 231 sequences belong to Eukarya.

A great diversity of eukaryotes was detected in the microbial mats with the 18S rRNA gene sequencing. A total of 38 families distributed in 22 phyla were identified (**Fig. 30, Table 12**): *Ameobozoa*, *Aphelidea*, *Apicomplexa*, *Arthropoda*, *Ascomycota*, *Basidiomycota*, *Bicosoecida*, *Breviatea*, *Cercozoa*, *Chlorophyta*, *Chytridiomycota*, *Ciliophora*, *Cryptomycota*, *Diatomea*, *Dinoflagellata*, *Holozoa*, *Labyrinthulomycetes*, LKM15, NAMA KO-1, *Nematozoa*, *Phragmoplastophyta*, *Prymnesiophyceae*. Several food regime were present: *Diatomea*, *Dinoflagellata* and *Chlorophyta* were phototrophs (Tragin and Vaultot, 2018), *Nematoda* and

Arthropoda have been shown to feed on bacteria (De Mesel et al., 2004; Feazel et al., 2008; Hubas et al., 2010), phytoplankton (Cowles et al., 1988; Montagna, 1984), ciliates (Berk et al., 1977) and dinoflagellates (Cowles et al., 1988; Turner, 2004), ciliates are a predator for bacteria (Parry, 2004; Sherr and Sherr, 1987) and flagellates and other ciliates (Bernard and Rassoulzadegan, 1990; Dolan and Coats, 1991), etc.

Chlorophyta and more precisely *Chlorophyceae* was clearly dominant at t9 in all treatments. However, along the experiment *Diatomea*, represented by *Bacillariophyceae* family, became more and more abundant until being dominant in the C treatment. The *Dinoflagellata* abundance also tended to decrease over time. *Chlorophyta*, *Diatomea* and *Dinoflagellata* are photosynthetic organisms composing a part of the phytobenthos (the other part being bacteria). The French Atlantic coast is an intense sink for atmospheric CO₂, primarily attributed to the photosynthesis (Takahashi et al., 2002). Therefore, participate in the carbon cycle in this region. These organisms are also a source of food for higher trophic levels. Two lineages composed the eukaryotic phytobenthos, the green and the red (Tragin and Vaultot, 2018). In marine waters, *Chlorophyta* is the major green algal group and contained chlorophyll *b* (Chl *b*) (Tomitani et al., 1999; Tragin and Vaultot, 2018). These organisms are found in small size fractions like picoplankton (cells from 0.2 to 2 µm) and nanoplankton (cells from 2 to 20 µm) (Tragin and Vaultot, 2018). *Diatomea* and *Dinoflagellata* composed the red lineage.

In oligotrophic lake littoral habitats, it has been observed that the enrichment in nitrogen (N) and phosphorus (P) favoured *Chlorophyta* and in the absence of it, *Bacillariophyta* relative abundance was greater than that of *Chlorophyta* and cyanobacteria (Oleksy et al., 2021). Indeed, the mesocosms impacted the N and P input which conducted to a shift in the phytobenthos communities. Indeed, the ammonium concentration decreased over the experiment in all treatments (Kruskal, $p < 0.05$) while nitrate and nitrite concentrations showed no difference. The phosphate concentration also decreased in all treatments (Kruskal or Welch, $p < 0.05$). Therefore, this decrease of the concentration of these two nutrients led to shift of the eukaryotic phototrophic communities in all treatment. The water input on the

mesocosms came from the ocean, close to the Ré Island. In spring 2019, when the mesocosms were performed, the nitrate, nitrite and phosphate concentrations were closed to 0 (*personal communication*, SOMLIT monitoring of the Atlantic French coastal ocean). The ammonium concentration was more variable, but its values were inferior to those observed in the mesocosms (*personal communication*, SOMLIT monitoring of the Atlantic French coastal ocean). The sediment and the microbial mats have certainly released these elements into the environment. The water in the plots of the salt marsh where the microbial mats were sampled did not have values similar to those observed in the ocean probably due to a nutrients enrichment in the plots preceding the crystallizer ponds. The decrease of nutrients corresponded certainly to the absence of this water enrichment of the plot. A comparison with the nutrients concentrations *in situ* and a monitoring of the metabolisms of nutrients, notably with marked nitrogen and phosphorus, will help to understand why their concentrations decreased along the experiment.

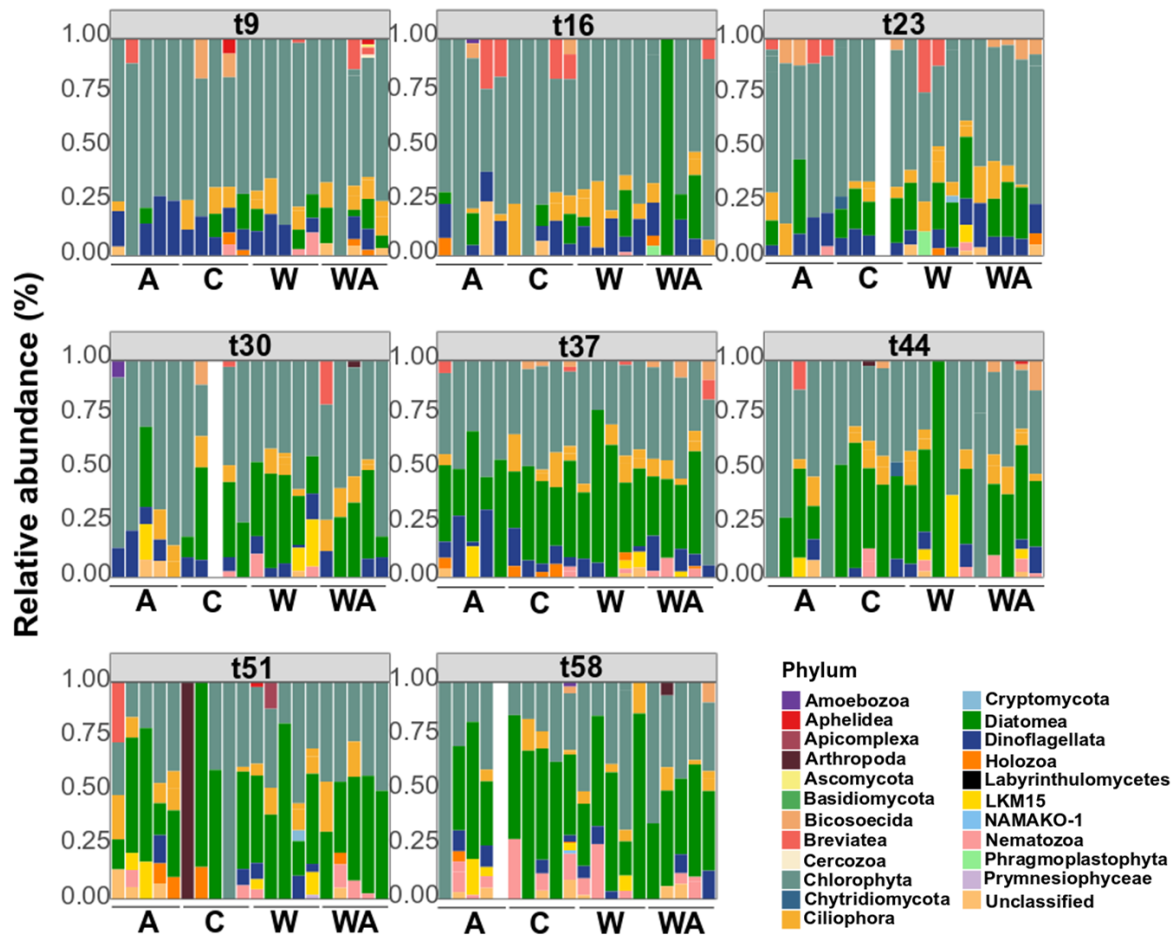


Figure 30: Relative abundance of eukaryotic phyla at different incubation time. The letters t followed by a number indicates the sampling time.

Table 12: Phyla and matching identified families.

Phylum	Family identified
<i>Ameoboza</i>	<i>Leptomyxida</i>
<i>Aphelidea</i>	<i>Aphelidea</i>
<i>Apicomplexa</i>	<i>Cryptosporida</i> <i>Cryptosporida</i>
<i>Arthropoda</i>	
<i>Ascomycota</i>	<i>Cladosporiaceae</i>
<i>Basidiomycota</i>	<i>Malasseziaceae</i>
<i>Bicosoecida</i>	<i>Bicocoecida</i>
<i>Breviatea</i>	<i>Breviatea</i>

<i>Cercozoa</i>	<i>Euglyphida</i>
<i>Chlorophyta</i>	<i>Chlorophyceae</i> <i>Trebouxiophyceae</i> <i>Ulvophyceae</i>
<i>Chytridiomycota</i>	<i>Chytridiaceae</i> <i>Olpidiaceae</i>
<i>Ciliophora</i>	<i>Armophorida</i> <i>Ciliophora</i> <i>Haptoria</i> <i>Heterotrichia</i> <i>Hypotrichia</i> <i>Nassophorea</i> <i>Oligophymenophorea</i> <i>Oligotrichia</i> <i>Oxytrichidae</i> <i>Phyllopharyngea</i> <i>Plagiopylea</i> <i>Protomatea</i>
<i>Cryptomycota</i>	<i>Incertae_Sedis</i>
<i>Diatomea</i>	<i>Bacillariophyceae</i>
<i>Dinoflagellata</i>	<i>Suessiaceae</i>
<i>Holozoa</i>	<i>Abeoformidae</i> <i>Capsasporidae</i> <i>Craspedida</i>
<i>Labyrinthulomycetes</i>	<i>Labyrinthulaceae</i>
LKM15	LKM15
NAMA KO-1	NAMA KO-1
<i>Nematozoa</i>	<i>Enoplida</i> <i>Monhysteria</i>
<i>Phragmoplastophyta</i>	<i>Magnoliophyta</i>
<i>Prymnesiophyceae</i>	<i>Isochrysidales</i>
<i>Unclassified</i>	

The observed richness and the Shannon diversity present no difference between the four treatments (ANOVA, Welch, Kruskal; $p > 0.05$) (**Fig. 31**). However, the Shannon diversity of the A treatment tended to be lower than the other treatments at t23, t30 and t37 (**Fig. 31**).

The 2 axes of the principal coordinates analyses (PCoA) explained between around 50% of the variance of the eukaryotic diversity explained by the treatments and the families (Fig. 32). The W treatment differed from the other only during the water warming (t16 and t23), positively explaining by *Bacillariophyceae* and negatively by *Chlorophyceae* (Fig. 32). Therefore, the increase of temperature impacted the eukaryotic communities and led to a dominance of *Bacillariophyceae* (Fig. 32).

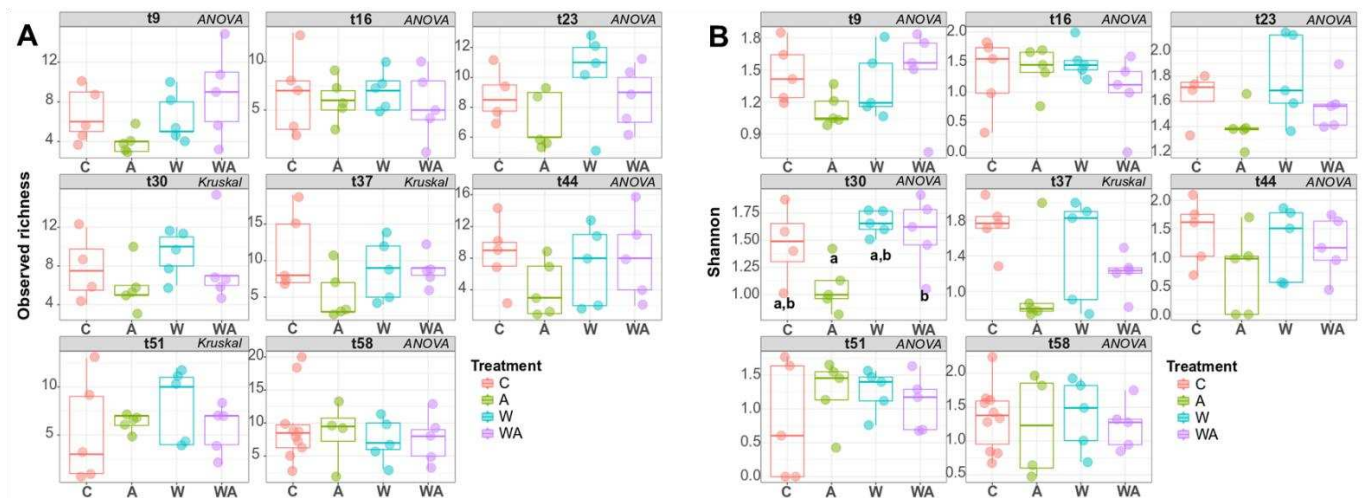


Figure 31: Relative abundance of eukaryotic phyla at different incubation time. The letters t followed by a number indicates the sampling time.

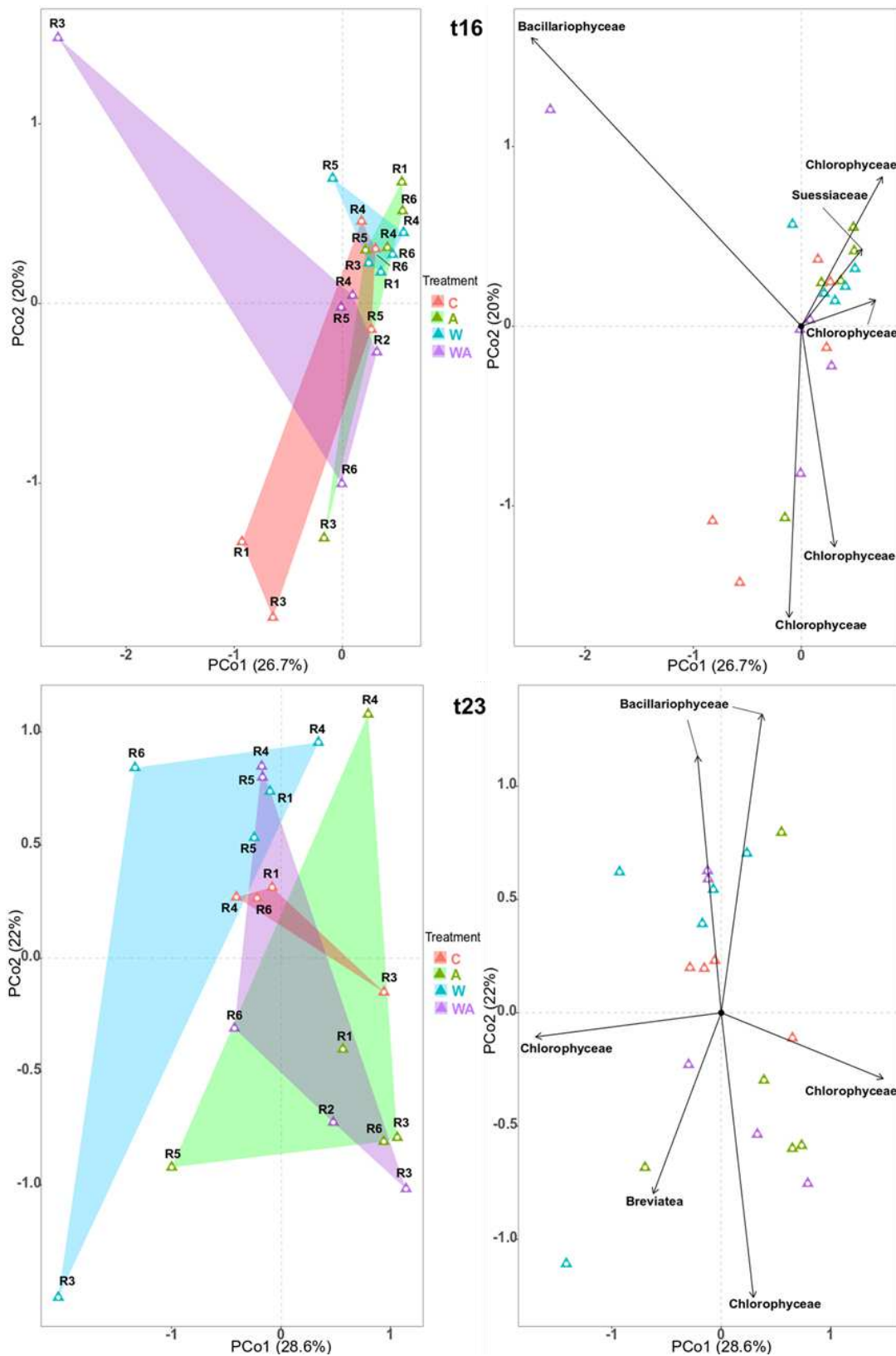


Figure 32: Principal coordinates analyses (PCoA) representing the eukaryotic diversity explained by the treatments themselves (graphics on the right) and by families (graphics on the left) along two axes, PCo1 and PCo2, for the eukaryotic 18Sr RNA gene at t16 and t23. The triangles correspond to the replicates.

The acidification of the seawater impacted the abundance of some eukaryotic organisms as related by Shannon diversity index. The eukaryotic structure was modified when the water was warmed. However, a shift in the eukaryotic phototrophs was observed in all treatments. The *Chlorophyceae* relative abundance decreased and those of *Bacillariophyceae* increased in all treatments. However, this change was more marked on the W treatment with maybe a change at the species level. The primers and the database used didn't allow to have a precision at this level, certainly because they are not adapted at this environment type. To improve these results, more specific primers could be used for *Chlorophyceae* and *Bacillariophyceae* (Moro et al., 2009). Despite these inherent biases of molecular analysis, we obtain first data on the impact of climate change on eukaryotic populations of microbial mats from Ré Island.

4. Conclusions and perspectives

The bacterial and archaeal diversity and general structure of the microbial mats were mainly impacted by acidification and the warming rather modified the eukaryotic communities. The determination of the microbial diversity *via* DNA sequencing allowed to know how the microbial composition of the microbial mats and how climate change can affect it. However, the universal primers used possess biases and didn't allow to correctly amplify some microorganisms, such as cyanobacteria, or were not done for this environment, such as the eukaryotic primers which amplified all the domains and resulted in very few amplified eukaryotic sequences. This is not surprisingly because "universal" primers were designed according to the known taxon (Normand et al., 2011) , so it would be interesting to develop primers for microbial mats from hypersaline environments. The functional diversity was also not described. Indeed, DNA analyses described only the microorganisms present but not the metabolisms occurring. The analysis of the fatty acids content was planned but the health situation due to covid prevented the development of the protocol for these samples and its

implementation. Vertical profiles were done to describe the physical-chemical gradients of oxygen, sulfur and pH occurring in the microbial mats in the four treatments, and their analysis is in progress.

**Chapter VI: Impact of climate
change on phototrophic
communities of microbial mats**

1. Introduction

Phototrophic communities are the major primary producers (Sørensen et al., 2005) found in microbial mats. They are fundamental organisms in the functioning of microbial mats participating in several biogeochemical cycles, such as carbon, oxygen, nitrogen, sulfide and nutrients cycles. Among them, some communities perform oxygenic photosynthesis, such as *Cyanobacteria*. This phylum produces organic carbon used by the lower heterotrophs of the microbial mats and secretes EPS that form an adhesive and protective matrix around the cells (Decho, 1990; Fourçans et al., 2006; Hubas, 2018; Wieland et al., 2003). Organisms performing anoxygenic photosynthesis are also observed, mainly belonging to the purple and green anoxygenic phototrophs. These communities are found in the upper layers of the microbial mats, in contact with the ocean's water, and are therefore the most exposed to environmental change and disturbances, and so to climate change.

DNA analyses underestimated the diversity of the phototrophs because the primers were not specific to these communities (Fourçans et al., 2004; Mazière et al., 2021). However, pigment analysis composition of the microbial mats allows a complementary approach to characterize the phototrophic communities present in microbial mats and the dynamic of the pigment production metabolism.

This chapter aims to describe the impact of climate change on the pigment composition and the photosynthetic efficiency of the microbial mats in response to ocean water warming and acidification. The results are presented in an article published in Science of Total Environment (STOTEN) (Volume 802, January 2022, DOI: 10.1016/j.scitotenv.2021.149787) (Mazière et al., 2022).

2. Climate change influences chlorophylls and bacteriochlorophylls metabolism in hypersaline microbial mat



Climate change influences chlorophylls and bacteriochlorophylls metabolism in hypersaline microbial mat

C. Mazière^{a,b,*}, M. Bodo^c, M.A. Perdrau^b, C. Cravo-Laureau^a, R. Duran^a, C. Dupuy^b, C. Hubas^c

^a Université de Pau et des Pays de l'Adour, E2S UPPA, CNRS, IPREM UMR 525, Bât. IBEAS, BP1155, 64013 Pau cedex, France

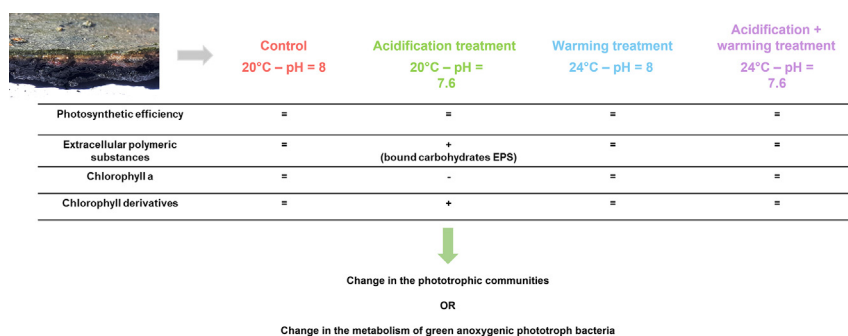
^b La Rochelle Université, CNRS, UMR 7266 LIENSs (Littoral Environnement et Sociétés), 2, rue Olympe de Gouges, Bât. ILE, 17000 La Rochelle, France

^c Muséum National d'Histoire Naturelle, UMR BOREA 8067, MNHN-IRD-CNRS-SU-UCN-UA, Station Marine de Concarneau, 29900 Concarneau, France

HIGHLIGHTS

- Higher chlorophyll derivatives concentration on acidification treatment
- Lower chlorophyll *a* concentration on acidification treatment
- Production of bound carbohydrates EPS on acidification treatment
- No impact of warming and acidification on mat photosynthetic efficiency

GRAPHICAL ABSTRACT



ARTICLE INFO

Article history:

Received 3 May 2021

Received in revised form 5 August 2021

Accepted 16 August 2021

Available online 24 August 2021

Editor: Jose Julio Ortega-Calvo

Keywords:

Hypersaline microbial mats

Ocean acidification

Mesocosms

Chlorophyll derivatives

Phototrophic communities

ABSTRACT

This study aimed to determine the effect of the climatic change on the phototrophic communities of hypersaline microbial mats. Ocean acidification and warming were simulated alone and together on microbial mats placed into mesocosms. As expected, the temperature in the warming treatments increased by 4 °C from the initial temperature. Surprisingly, no significance difference was observed between the water pH of the different treatments despite of a decrease of 0.4 unit pH in the water reserves of acidification treatments. The salinity increased on the warming treatments and the dissolved oxygen concentration increased and was higher on the acidification treatments. A total of 37 pigments were identified belonging to chlorophylls, carotenes and xanthophylls families. The higher abundance of unknown chlorophyll molecules called chlorophyll derivatives was observed in the acidification alone treatment with a decrease in chlorophyll *a* abundance. This change in pigmentary composition was accompanied by a higher production of bound extracellular carbohydrates but didn't affect the photosynthetic efficiency of the microbial mats. A careful analysis of the absorption properties of these molecules indicated that these chlorophyll derivatives were likely bacteriochlorophyll *c* contained in the chlorosomes of green anoxygenic phototroph bacteria. Two hypotheses can be drawn from these results: 1/ the phototrophic communities of the microbial mats were modified under acidification treatment leading to a higher relative abundance of green anoxygenic bacteria, or 2/ the highest availability of CO₂ in the environment has led to a shift in the metabolism of green anoxygenic bacteria being more competitive than other phototrophs.

© 2021 Elsevier B.V. All rights reserved.

1. Introduction

Since the industrial revolution, the atmospheric greenhouse gases concentration has increased sharply leading to a decrease in the pH of the surface ocean of about 0.1 pH unit (IPCC, 2014). In the coming

* Corresponding author at: Bâtiment IBEAS, avenue de l'Université, 64013 Pau, France; Bâtiment Ile, 2, rue Olympe de Gouges, 17000 La Rochelle, France.
E-mail address: camille.maziere@univ-pau.fr (C. Mazière).

decades, the ocean acidification will continue, associated with an ocean water warming caused by increasing levels of CO₂ in the atmosphere (Hutchins and Fu, 2017; IPCC, 2014). These climatic perturbations will alter the carbon and nutrients cycles on a global scale (Hutchins and Fu, 2017) and are expected to have a direct impact on all physical, chemical and biological parameters that govern marine organisms life (Hutchins and Fu, 2017). Organisms will be faced with unprecedented changes in future ocean conditions, particularly marine life will be severely affected. On France's Atlantic coasts, the Intergovernmental Panel on Climate Change (IPCC) predicts an increase in surface water temperature of 3 to 4 °C and ocean acidification of 0.4 to 0.45 pH units in its most pessimistic scenario (RCP 8.5) by the end of the century (IPCC, 2014).

Research on microorganisms facing climatic change is scarce compared to that on animals and plants (Cavicchioli et al., 2019; Dutta and Dutta, 2016; Reinold et al., 2019). Microbial mats play important key-roles in marine ecosystems, such as participating in the dynamics of carbon, nitrogen and oxygen cycles. They develop at the water-sediment interface in a large variety of environments including coastal beaches (Bolhuis and Stal, 2011), salterns (Fourçans et al., 2004), hot springs (Dobretsov et al., 2011) and many other coastal/marine environments. These are complex microbial structures containing a great diversity of microorganisms coexisting at microscale according to a vertical stratification due to light and microgradients of oxygen, pH and sulfurs (Fourçans et al., 2008; Jorgensen et al., 1983; Revsbech et al., 1983; van Gemerden, 1993). Despite the stratification, microbial mats are dynamic structures where the migration of microorganisms has been described according to the diel cycle (Fourçans et al., 2008, 2006). Numerous interactions occur in microbial mats representing thus an ecosystem on its own (Reinold et al., 2019). Microbial mats have a remarkable specific, metabolic and molecular diversity, making them highly adaptable to the changing physico-chemical conditions of the environment (Fourçans et al., 2006) as well as to contamination (Bordenave et al., 2008, 2004a, 2004b).

Autotrophic microorganisms are fundamental organisms in the functioning of microbial mats because they are the major primary producers. They can be chemotroph such as some Bacteroidetes but the major primary producers in photosynthetic microbial mats are the phototrophic microorganisms (Sørensen et al., 2005). Among them, Cyanobacteria produce organic carbon which is then decomposed in the successive lower layers by different heterotrophs. They also secrete adhesive and protective extracellular polymeric substances (EPS), that form a matrix around the cells (Decho, 1990; Fourçans et al., 2006; Hubas, 2018; Wieland et al., 2003). This matrix is generally composed of sugars, proteins, extracellular DNA and other molecules in smaller proportions (Fourçans et al., 2006; Hubas, 2018; Wieland et al., 2003). However, the composition varies depending on the physiological state of the organisms, the specific diversity, the growth stage of the mat and the physico-chemical conditions of the environment (Decho and Moriarty, 1990; Hubas, 2018; Reinold et al., 2019; Underwood et al., 2004). By binding to sedimentary particles, this matrix stabilises the microbial mat and prevents erosion phenomena (Decho, 1990), but it has many other essential roles such as nutrients supply, by the sequestration and accumulation of dissolved and particulate nutrients coming from the water column that can be used by microorganisms, it also helps microbial communication or bring protection against UV radiations (Decho, 2000; Flemming and Wingender, 2010; Hubas, 2018). EPS are therefore a major component of microbial mats and remain indispensable for their functioning.

Several studies have addressed the impact of climate change on photosynthetic marine microbial communities. Some authors have shown that temperature affects the composition, the photosynthetic performance as well as the growth, biomass and physiology of microphytobenthos (Cartaxana et al., 2015; Hancke and Glud, 2004). Acidification effects are thought to occur mainly at the metabolic level, favouring the growth of some microorganisms (Baragi and Anil, 2016; Black et al., 2019; Hicks et al., 2011) but also photorespiration in diatoms and increasing the number of proton pumps for maintaining intracellular pH homeostasis and respiratory processes (Beardall et al., 2009;

Black et al., 2019; Gao et al., 2012). Acidification and warming also affect the characteristics of EPS of diatoms and Cyanobacteria with a modification of their composition (Li et al., 2016; Ma et al., 2019).

Many studies have highlighted the impact of acidification and warming water separately but it is necessary to consider them together as they can act synergistically (Baragi et al., 2015; Baragi and Anil, 2016; Li et al., 2016). The aim of this study was to simulate an acidification and a water warming on microbial mats on mesocosms according to the RCP8.5 scenario of the IPCC for 2100. Here, the phototrophic microbial communities are described and their potential composition variation will be monitored.

2. Material and methods

2.1. Description of the sampled sites

Microbial mats for mesocosms experiment were sampled the 30th of April 2019 in salterns located in Ars-en-Ré (46°13'29.9"N 1°31'07.5"W, Ré island, France) on a non-exploited pond. The microbial mat, which had not been disturbed for at least three years, was more mature than a mat from an exploited pond. Undisturbed mats were then placed in plastic boxes and transported to laboratory at room temperature where they were put back in water within 3 h following the sampling. The water height was around 3 cm as observed *in situ*. *In situ* physico-chemical parameters (temperature, salinity, pH) of the water were measured with a multi-parameter probe (pHenomenal® MU 6100H, VWR™, USA) in order to apply them on the mesocosms as control values. Samples were also taken to determine nutrient concentrations in the pore water.

2.2. Mesocosm design

Microbial mats were separated into twenty-four plastic boxes (48 cm × 33 cm), each of them representing a mesocosm (Fig. 1). The mesocosms were gathered in groups of six representing a condition (five replicates and a box for pulse amplitude modulated (PAM) measures). In these six mesocosms, incoming water was from a reserve and was distributed individually with stainless steel taps. This water corresponded to seawater filtered at 80 μm, passed under UV light and whose salinity was adjusted to 60 psu with salt coming from the salt marshes of the Ré island. Opposite to the water inlet, a hole allowed the water outlet in a network of PVC tubes between all the replicates. The water was not recycled. This setup permitted to maintain a stable water level at 3 cm above the mat and to renew seawater and the supplying nutrients for the development of the microbial mats. For each condition, a pool was constructed around the six plastic boxes where water was maintained at the desired temperature with a pump (EHEIM universal 600, Germany) connected to a thermoregulating device (Teco®) to control the water temperature above the microbial mats. The microbial mats were illuminated 12 h a day following the day/night cycle observed during the spring. To control the evaporation rate, the lights used were LED (TOP-24H company by SYLED, France). They provided white cold light color and an intensity of $11.8 \pm 0.9 \mu\text{mol} \cdot \text{photons} \cdot \text{m}^{-2} \cdot \text{s}^{-1}$ (mean ± standard between the four treatments for a day) (HOBO Pendant® Temperature/Light Data Logger, Onset Computer Corporation, USA) on the surface of the microbial mats.

Daily monitoring was done for the physico-chemical parameters (temperature, pH, salinity and dissolved oxygen) thanks to a multiparameter probe (pHenomenal® MU 6100H, VWR™, USA).

2.3. Implementation of different treatments

A stabilisation period of five weeks was applied to acclimate the microbial mats to their new environment (Gette-Bouvarot et al., 2015; Stauffert et al., 2013). The water temperature on the mesocosms was maintained at 20 °C and the salinity of the incoming water was regulated in the water reserve to maintain a salinity at 60 ± 2 psu in the

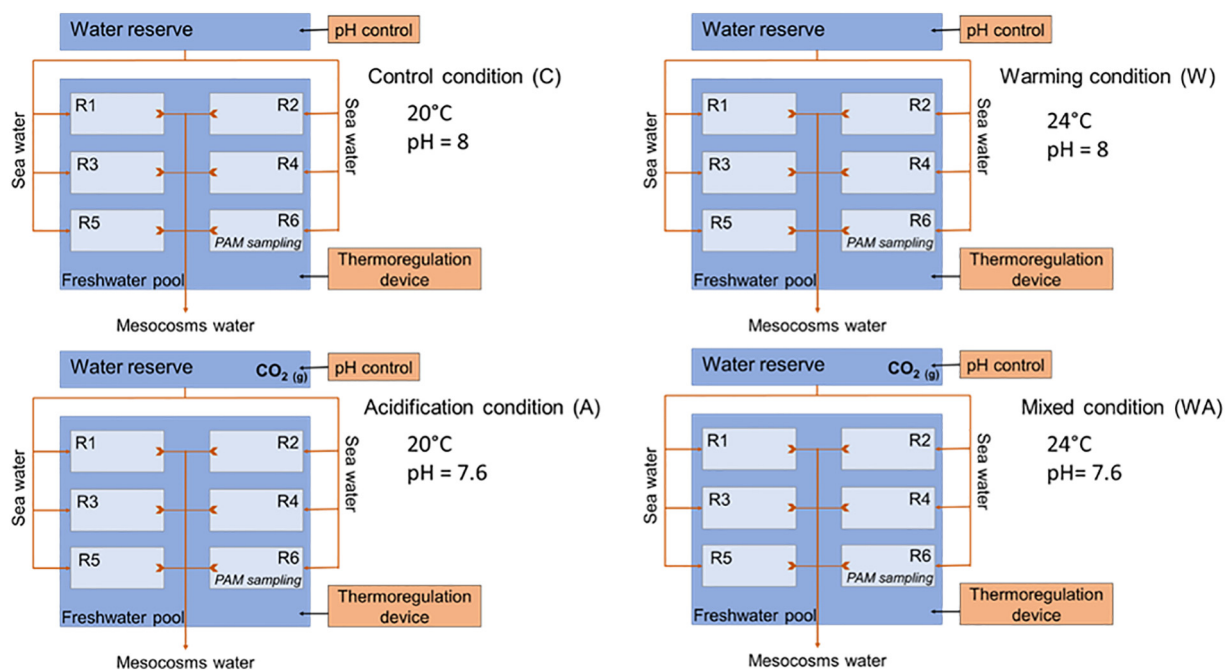


Fig. 1. Schematic representation of the experimental device with the control (C) and the acidification (A), warming (W) and mixed (WA) treatments. The replicates are represented by the letter R, the first five are used for sampling and the sixth is dedicated to the measurements of fluorimetry by pulse amplitude modulation (PAM).

mesocosms, reproducing *in situ* conditions. The implementation of different treatments occurred for seven additional weeks.

Four treatments were applied to the microbial mats. Each pool and its six mesocosms represented a treatment. The first treatment was the control treatment (C) in which the parameters were not changed. The second treatment was the warming treatment (W) in which the temperature was increased by 0.5 °C every two days for 2 weeks until reaching 24 °C. The acidification treatment (A) represented the third condition. The water acidification was performed in the water reserve by bubbling pure CO₂, allowing a drop of initial water pH of 0.1 unit every four days for 2 weeks until reaching a decrease of the initial pH of the water reserve equal to 0.4 unit, *i.e.* 7.6. The water pH in the water reserve was monitored with a continuous pH stat system (IKS aquastar, iks ComputerSysteme GmbH, Germany). Then the pH values of the pH stat system were adjusted twice a week from measurement using a pH meter (Metrohm, 826 pH mobile) with a glass electrode (Metrohm, electrode plus) calibrated on the total scale using Tris buffer solution (provided by Andrew Dickson, Scripps Institution Oceanography, San Diego). Every day, the pH values in the four treatments pools were also measured on the total scale. The fourth treatment combined warming and acidification treatments (WA). The mesocosms were then maintained under these treatments for 5 further weeks.

A first sampling (noted t₉) was performed after the stabilisation period of the microbial mats on the mesocosms, just before changing the environmental conditions. A second sampling (t₁₆) was performed at the middle of the period of change and a third (t₂₃) at the end (Supplementary materials, Fig. A). After this period, sampling was performed every week (t₃₀, t₃₇, t₄₄, t₅₁ and t₅₈) (Supplementary materials, Fig. A). For each sampling, ten 1 cm depth cores were collected with a 1 cm diameter cut-off syringe in each mesocosm and mixed together in order to obtain a homogeneous sample.

2.4. Nutrient concentrations

A volume of 20 mL of water from each mesocosm was filtered at 0.22 µm in order to perform a nutrient analysis. The same was done for *in situ* samples. Half of the volume was frozen at -20 °C while the other half was kept at 4 °C for silicon analysis. The samples were then analyzed

as described by Aminot and Kérouel (2007). Silicon, nitrate, nitrite and phosphate were measured by Segmented Continuous Flow Colorimetry (SFA) while ammonium was measured by SFA fluorimetry on an auto-analyzer (SEAL AutoAnalyzer 3, SEAL analytical) (Aminot and Kérouel, 2007).

2.5. Photosynthetic parameters

Chlorophyll fluorescence parameters were measured at 5 different locations of the core using a fluorometer (Monitoring Pen, MP 100-E, Photon Systems Instruments, Czech Republic) illuminated with a blue LED emitter (455 nm). The samples were placed in the dark (for 5 min) before the measurement of Light Response Curves. Manufacturer predetermined LC3 protocol was used following manufacturer instructions. LC3 protocol was characterized by 7 steps of increasing light intensities (10, 20, 50, 100, 300, 500, 1000 µmol·photon·m⁻²·s⁻¹) with an illumination duration of 60s. Minimum fluorescence level F₀⁵ (Jesus et al., 2006) was obtained by using a non actinic measuring light pulse (30 µs, 900 µmol·photon·m⁻²·s⁻¹), which induced the minimal chlorophyll fluorescence (F₀⁵). The samples were then subjected to a saturating light pulse (2400 µmol·photon·m⁻²·s⁻¹). This made it possible to measure the maximum fluorescence level F_m⁵ (Jesus et al., 2006). All measurements were done in the same conditions and at the same time.

The data was then downloaded from the device to a computer using FluorPen software (v1.0.6.1, Photon Systems Instruments, Czech Republic) and all calculations and analyses were performed using R-Studio software (version 4.0.3© RStudio, Inc.). From the measured parameters the effective quantum yields of photosynthesis (ϕ(II)⁵) were calculated (Jesus et al., 2006) (Eq. (1)). They indicate the community's maximum potential for photosynthetic activity.

$$\phi(II)^5 = \frac{F_m^5 - F_0^5}{F_m^5} \quad (1)$$

2.6. Pigment identification and quantification

Lipophilic pigments were analyzed by high performance liquid chromatography (HPLC). Microbial mats were incubated with 95% methanol

(buffered with 2% ammonium acetate) during 15 min, at -20°C in the dark. Extracts were then filtered with $0.2\ \mu\text{m}$ PTFE syringe filters and analyzed within 16 h using an Agilent 1260 Infinity HPLC composed of a quaternary pump (VL 400 bar), a UV-VIS photodiode array detector (DAD 1260 VL, 190–950 nm), a fluorescence detector (FLD 1260 excitation: 425 nm, emission: 655 nm), and a $100\ \mu\text{L}$ automatic sample injector refrigerated at 4°C in the dark. Chromatographic separation was carried out using a C18 column for reverse phase chromatography (Supelcosil, 25 cm long, 4.6 mm inner diameter). The solvents used were: 0.5 M ammonium acetate in methanol and water (85:15, v:v), acetonitrile and water (90:10, v:v), and 100% ethyl acetate. The solvent gradient was set according to Brotas and Plante-Cuny (2003), with a $0.5\ \text{mL}\ \text{min}^{-1}$ flow rate. Identification and calibration of the HPLC peaks were performed with $\beta\beta$ -carotene, canthaxanthin, chlorophyll *a*, chlorophyll *b*, chlorophyll *c2*, diatoxanthin, diadinoxanthin, fucoxanthin and pheophytin *a* standards. We identified all detected peaks by their absorption spectra and relative retention times using the Agilent OpenLab software. Quantification was performed using standard calibration curves built with repeated injections of standards over a range of dilutions. Xanthophylls, carotenes and chlorophyll *b* and *c* were quantified at 470 nm, chlorophyll *a* and their derivatives as well as pheopigments were quantified at 665 nm. The relative abundance of each pigment (%) was calculated from its respective concentration in the sample ($\mu\text{g}\cdot\text{mg}^{-1}$).

2.7. Extracellular polymeric substances (EPS) characterization

In a 15 mL Falcon® tube, 5 mL of microbial mat was mixed with an equivalent volume of seawater obtained by mixing water from the five sampled replicates and filtered at $0.22\ \mu\text{m}$ for each treatment. The tubes were subjected to mechanical agitation by vortexing and by inversion at a rate of 40 oscillations $\cdot\text{min}^{-1}$ for 1 h at 4°C in the dark. Then they were centrifuged at $3500g$ for 10 min at 4°C . The supernatant, containing the colloidal fraction, was recovered and stored at -20°C while the pellet, containing the bound fraction, was resuspended in 5 mL of seawater (again obtained by mixing water from the five sampled replicates and filtered at $0.22\ \mu\text{m}$ for each treatment). 1 g of Dowex resin (Dowex Marathon C, Na^{+} , Sigma-Aldrich), was prepared according to the protocol of Takahashi et al. (2009). The tubes were again subjected to the same protocol to obtain the supernatant containing the fraction of bound EPS was recovered and stored at -20°C .

The carbohydrate dosage was performed according to Dubois' colorimetric method (Dubois et al., 1956) while the protein dosage was performed according to the bicinchoninic acid assay (BCA) method using the Pierce™ Protein Assay Kit (ThermoFisher Scientific). A range of glucose (L-(-)-glucose, 98%, Sigma-Aldrich) from 0 to $3\ \text{g}\cdot\text{L}^{-1}$ and a range of bovine serum albumin (BSA) from 0 to $1\ \text{g}\cdot\text{L}^{-1}$ were performed in seawater from the Ré island hypersalinated at 60 psu and filtered at $0.22\ \mu\text{m}$. For carbohydrates, $100\ \mu\text{L}$ of EPS sample were placed in a tube, then $100\ \mu\text{L}$ of 5% phenol (Solid Phenol, Sigma-Aldrich, France) and $500\ \mu\text{L}$ of 98% sulfuric acid (Sulfuric Acid 98%, Carlo-Erba Reagents, France) were added. The tubes were incubated for 30 min in the dark and at room temperature. A volume of $200\ \mu\text{L}$ of the standard range and each triplicate sample was deposited in a 96-well microplate (Falcon® 96-well Clear Microplat, Thermo Fisher Scientific). The absorbance of each well was measured at 490 nm with a spectrophotometer (SPECTROstar® Nano, BMG LAB). For proteins, 225 mL of reagent was prepared and stored in the dark at room temperature during the assay period. The assays were performed in 96-well microplates (Falcon® 96-well Clear Microplat, Thermo Fisher Scientific). $200\ \mu\text{L}$ of reagent was placed in the wells and $25\ \mu\text{L}$ standards or triplicate samples were added. The microplates were incubated for 30 min at 37°C , then the absorbance of each sample was measured at 562 nm by a spectrophotometer (SPECTROstar® Nano, BMG LAB). Two calibration curves were drawn from the standard ranges and their respective abundances (corrected according to the kit indications for the BSA range), averaged over the duration of the experiment. They made it possible to determine

the carbohydrate and protein concentrations. The latter were then related to the dry mass of the microbial mat.

To determine the dry mass of the microbial mat, a volume of 30 mL of microbial mat was collected and weighed to obtain the fresh mass. The sample was then freeze-dried to remove water from the sample (Lyophilisateur Christ Alpha 1-4, Grosseron, France) and re-weighed to obtain the freeze-dried mass.

2.8. Data analysis

All calculations and analyses were performed on RStudio software (version 4.0.3© RStudio, Inc.). The mean of physico-chemical parameters, the carbohydrates and proteins concentrations of each fraction and the photosynthetic parameters of each treatment were compared with each other at each sampling time. The normality and homoscedasticity of the data were previously verified by carrying out a Shapiro test and a Bartlett test respectively. If both conditions were met, the data were subjected to an analysis of variances (ANOVA). Otherwise, a Welch ANOVA was performed in the case of non-homogeneity of variances and a Kruskal-Wallis rank sum test in the case of non-normal data. If these tests were found to be significant ($p < 0.05$), then a pairwise comparison was performed using a Tukey test following the ANOVA, a Games-Howell test following a Welch ANOVA or a Nemenyi test following the Kruskal-Wallis test.

A Between Class Analysis (BCA) combined with hierarchical cluster analysis with a Bray dissimilarity index and ward.D2 method was done on pigments proportions.

3. Results

3.1. Efficiency of the physico-chemical changes

As expected, the temperature in W and WA treatments increased well by 4°C from the initial temperature, the one maintained in C and A treatments ($23.89 \pm 0.49^{\circ}\text{C}$; $23.82 \pm 0.48^{\circ}\text{C}$; $20.32 \pm 0.36^{\circ}\text{C}$; $20.23 \pm 0.48^{\circ}\text{C}$; respectively) (Fig. 2, A; Supplementary materials, Fig. B). There was a delay of one week before reaching this increase after the change of state because this was the time needed to heat up all the water in the pool and then the mesocosms.

The pH of C and W treatments were stabilised after t37 at 7.94 ± 0.15 and 7.95 ± 0.09 , respectively (Fig. 2, B; Supplementary materials, Fig. B). The pH of A and WA treatments decreased until t44, then remaining stable at $\text{pH } 7.87 \pm 0.13$ and 7.86 ± 0.10 , respectively (Fig. 2, B; Supplementary materials, Fig. B). No significant difference between the four treatments was found at t9 (Kruskal, $p > 0.05$).

The salinity (Fig. 2, C; Supplementary materials, Fig. B) of C and A treatments remained stable at 60.87 ± 1.44 psu and 61.91 ± 1.79 psu, respectively. The salinity of the W treatment increased to a maximum mean value of 75.87 ± 4.84 psu after 40 days of incubation, and then decreased again to a final value of 67.35 ± 4.24 psu. The salinity of the WA treatment increased and reached its maximum value of 71.94 ± 6.55 psu on day 23 of the experiment and then decreased and remained at 66.13 ± 2.56 psu.

Dissolved oxygen remained stable between each treatment up to t16 (mean \pm standard deviation; $0.95 \pm 1.18\ \text{mg}\cdot\text{L}^{-1}$ for control, $0.61 \pm 1.15\ \text{mg}\cdot\text{L}^{-1}$ for pH, $0.60 \pm 0.46\ \text{mg}\cdot\text{L}^{-1}$ for W and $0.30 \pm 0.24\ \text{mg}\cdot\text{L}^{-1}$ for WA) (Fig. 2, D; Supplementary materials, Fig. B). From t23, the dissolved oxygen of the treatments increased linearly to t58 with a slope of $0.07\ \text{day}^{-1}$ ($R^2 = 0.45$, Student-test, $p < 0.05$) for A, $0.05\ \text{day}^{-1}$ ($R^2 = 0.39$, Student-test, $p < 0.05$) for W and $0.03\ \text{day}^{-1}$ ($R^2 = 0.19$, Student-test, $p < 0.05$) for WA. The A treatment had a final oxygen concentration of $5.95 \pm 1.63\ \text{mg}\cdot\text{L}^{-1}$, significantly higher (ANOVA, $p < 0.05$) than that of the other mesocosms by a factor of 1.6 for W, 2.2 for C and 2.4 for WA (mean \pm standard deviation).

The nutrients were analyzed thanks to the Redfield ratio calculations (Redfield, 1958). Only seven samples showed nitrogen limitation, notably four replicates of the A treatment at t30 and some samples showed a

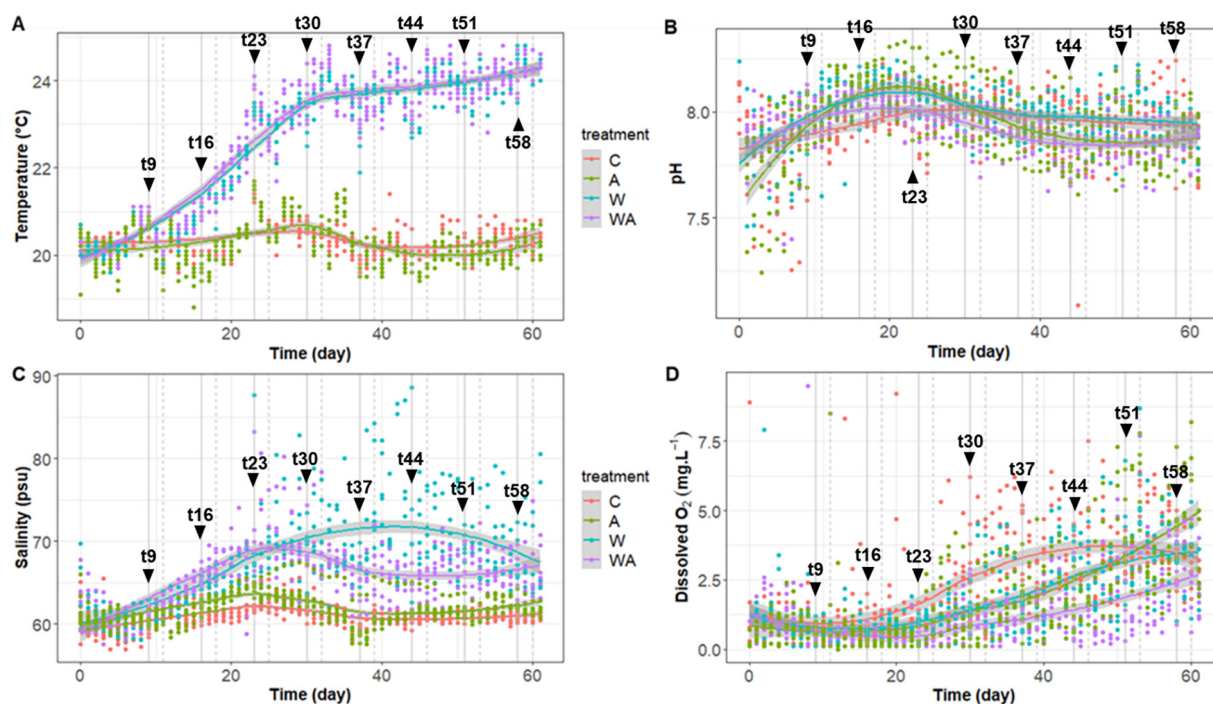


Fig. 2. Temporal variation of the temperature ($^{\circ}\text{C}$) (A), the pH (upH) (B), the salinity (psu) (C) and the dissolved oxygen ($\text{mg}\cdot\text{L}^{-1}$) (D) of the different treatments (control (C), acidification (A), warming (W) or warming and acidification mix (WA)). The points corresponded to the values measured for each sample. The curves represented local regressions, based on the k-nearest neighbors algorithm (*geom_smooth* function of the *ggplot2* package, loess method). The grey areas symbolised the 95% confidence intervals. The sampling days were represented by black arrows. The day 0 to day 8 corresponded to the stabilisation week.

limitation of silicon (Supplementary materials, Fig. B and C). Most of the samples showed phosphate limitation, but such phosphate limitation was also observed *in situ* (Supplementary materials, Fig. B and C).

3.2. Pigment composition

A total of 37 pigments were identified (Table 1). The analysis revealed the presence of several chlorophyll: chlorophyll *a* (Ca) and corresponding epimers and allomers, chlorophyll *b* (Cb) and chlorophyll *c2* (Cc2). Bacteriochlorophyll *a* (BCa) was identified as well as echinenone, oscillol diquinovoside, myxol quinovoside and zeaxanthin. Other pigments were identified including lutein, alloxanthin, carotenoids and

canthaxanthins and its isomers. Pigments corresponding to alteration products were also found: pyropheophytin, pheophytin *a*, pheophorbide *a* and chlorophyllide *a*. The presence of non-identified chlorophyll *a*-like molecules was also observed and hereby called chlorophyll derivatives (C deriv. #1-6).

3.3. Acidification changes the pigments dynamics

At t9, all treatments were placed under the same water temperature and pH. No difference between pigments were observed (Fig. 3, A) (ANOVA or Welch or Kruskal, $p > 0.05$).

The C treatment was different from the other treatments containing more myxol quinovoside and isomers 2 and 3 than A treatment at t37 and t44 (Kruskal, $p < 0.05$) and than the three other treatments at t51 (ANOVA, $p < 0.05$). It also contained more chlorophyll epimers at t58 than A, W and WA treatments (ANOVA, $p < 0.05$) (Fig. 3). The W treatment was differentiated from the A treatment with the presence of chlorophyll derivative #6 at t51 and t58 (Welch, $p < 0.05$) (Fig. 3). The concentration of chlorophyll *a* was around 4% at the beginning of the experiment (Fig. 4, A). It increased until t51 in all treatments except for A treatment and then decreased at t58 (Fig. 4, A). The A treatment slightly decreased at t58 and the proportion of chlorophyll *a* was lower in this treatment than in the C treatment (ANOVA, $p < 0.05$) at t51 and t58 (Fig. 4, A). Conversely, the proportion of chlorophyll derivatives (Fig. 4, B) was close to 0 at t9 for all treatments. It increased to t30, remained stable at t44 and then decreased again to t58 for the C, W and WA groups, while it increased to t44 before decreasing again to t58 for the A group (Fig. 4, B). The proportion of chlorophyll derivatives was significantly higher for the A treatment at t37, t44 and t51 (ANOVA and Welch, $p < 0.05$) (Fig. 4, B).

3.4. Comparison of the photosynthetic yields of the microbial mat in the different treatments

The quantum efficiency of photosystem II ($\phi(\text{II})^5$) indicated the photosynthetic efficiency of the mat. At t9, the quantum yields of the C and A

Table 1
Pigments identified by HPLC and its corresponding abbreviations.

Pigment	Notation
Alpha and beta cryptoxanthin	aCy; bCy
Alloxanthin	Al
Beta-beta carotene; beta-epsilon carotene	BB.Car; BE.Car
Unknown carotenoids	Car1; Car2
Chlorophyll <i>a</i> ; chlorophyll <i>a</i> allomers/epimers	Ca; Ca.allo; Ca.epi
Chlorophyll derivatives	C deriv. #1-6
Bacteriochlorophyll <i>a</i>	BCa
Chlorophyll <i>b</i>	Cb
Chlorophyll <i>c2</i>	Cc2
Chlorophyllide <i>a</i>	Cda
Canthaxanthin	Ct; Ct.iso
Echinenone	Ec
Fucoxanthin and isomers	F; F.iso1
Lutein and isomers	L; L.iso1; L.iso2
Myxol quinovoside and isomers	My.iso1; My.iso2; My.iso3; My.iso4
Oscillol diquinovoside	O
Pheophorbide	Pda.1
Pheophytin	Pha
Pyropheophytin	Pya
Zeaxanthin	Z

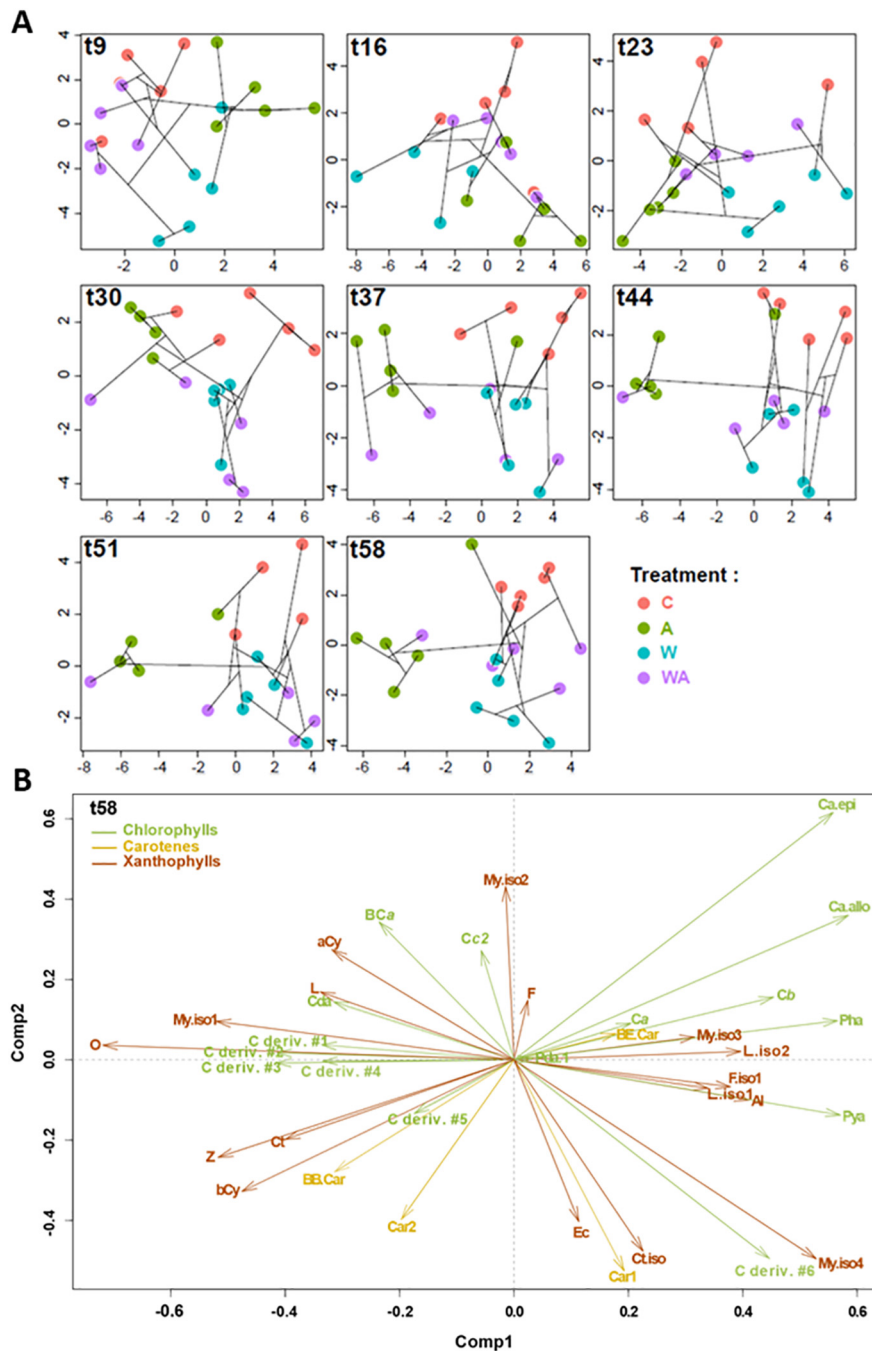


Fig. 3. Dynamics of microbial communities according to pigments composition and the sampling time (tX) (A). This figure was obtained thanks to analyze BCA combined with hierarchical cluster analysis with a Bray dissimilarity index and ward.D2 method. A representation more detailed with the different parameters was done at t58 (B). The correspondence between the abbreviations and the names of pigments is provided in Table 1.

treatments were close to 0, while those of the W and WA groups were 14 and 4.2 times more than C and A treatments respectively (Fig. 5). At t16 no significant difference was observed between all the quantum yields (ANOVA, $p > 0.05$) (Fig. 5). Other difference were observed between treatments during the experiment, but the kinetics obtained showed no real trend between treatments (Fig. 5), only WA treatment presented a quantum yields lower than C treatment at t37, t51 and t58 (ANOVA or Kruskal, $p < 0.05$) than W and A treatments at t37 and t58 (ANOVA, $p < 0.05$).

3.5. Acidification impacted the proportion of EPS

The A treatment was dissimilar from the other treatments, characterized by its higher concentrations of bound carbohydrates EPS.

The carbohydrates bound EPS concentration was notably more important in A treatment on three times: at t23, t37 and t58 (ANOVA, $p < 0.05$) (Fig. 6).

4. Discussion

The aim of the study was to simulate acidification and/or warming on microbial mats. The mesocosm system has the advantage to control the physico-chemical parameters allowing to simulate future conditions, which is impossible to achieve directly in the field; but the natural environment can never be mimicked perfectly (weather, daily or even seasonal variations in physico-chemical parameters, etc.). Although mesocosm system will never faithfully represent reality, it is a compromise

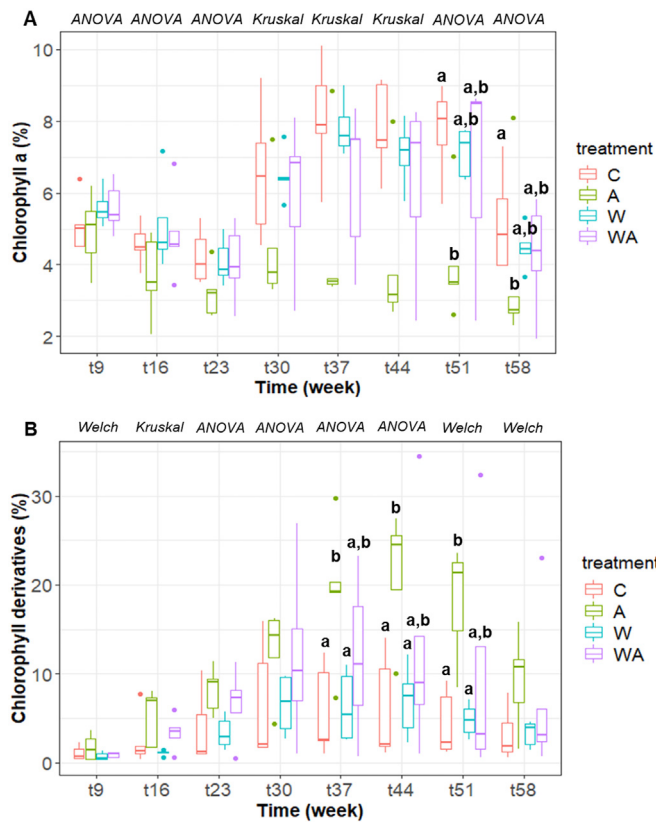


Fig. 4. Temporal variations of (A) the concentration of chlorophyll a (%) and (B) the concentration of chlorophyll derivatives (%). The letters t followed by a number indicates the sampling time. The statistical test performed to show the differences between treatments at a sampling time is indicated in italics above the figure. The letters indicated a significant difference ($p < 0.05$) found after a post-hoc Tukey HSD test in the case of an ANOVA, a Games-Howell test in the case of a Welch ANOVA or a Nemenyi test in the case of a Kruskal Wallis test.

often used to conduct experimental ecology studies (Cravo-Laureau and Duran, 2014). It is therefore advisable to remain vigilant so as not to extrapolate too generally the results obtained with *in situ* microbial mats. Given the diversity of structure and functioning of microbial mats

throughout the world, they may act differently in their natural environment. It should also be noted that this study was a simulation of the IPCC's most pessimistic predictions (RCP8.5) for 2100. The changes simulated only concerned the decrease in water pH and the increase in water temperature, but these are not the only parameters that are expected to vary in the future. Deoxygenation of the oceans, a succession of extreme weather events, and sea level rise in some regions are also foreseeable changes that have not been tested in this study. Moreover, they have been monitored over seven weeks, whereas variations in the natural environment are supposed to occur over several decades.

The renewal water in the mesocosm permitted to maintain a stable water level at 3 cm above the mat and a natural supply of nutrients for the development of microbial mats. Redfield ratio showed some limitation of nitrogen and/or phosphorus in the water under some conditions but previous studies have shown that microbial mats can develop in P- (Peimbert et al., 2012) and N-limited environment (Peimbert et al., 2012) (Supplementary materials, Fig. C).

Surprisingly, the decrease of pH under the A and WA treatments was not noticeable in the mesocosms (Fig. 2) although the pH in the respective water reserve decreased (Supplementary materials, Fig. D) at the expected pH 7.6 (the initial pH was 8). This phenomenon has been observed in other studies (Crawford et al., 2011; Ma et al., 2019). The most likely hypothesis is that the rate of CO₂ fixation by photosynthesis was higher in the A and WA treatments, which had the effect of increasing the pH. In our experiment, dissolved oxygen increased under A treatment after the third week. Moreover, many microbial species are able to use carbon concentration mechanisms (CCMs), storing high CO₂ concentrations before transport into the Rubisco compartments, which minimise photorespiration. These CCMs are found in oxygenic phototrophs like cyanobacteria or most of the phytoplankton (Ma et al., 2019). The CCMs have been proposed as mechanisms to prevent photosynthetic systems to directly detect ambient changes in CO₂ (Mackey et al., 2015). As a result, photosynthetic rates might not respond directly to ambient changes in CO₂ explaining the delay observed in the increase of dissolved oxygen in our experiment. Such observation is consistent with the fact that pH decreased from t23 while dissolved oxygen continued to increase (Fig. 2). Black et al. (2019) suggested that microphytobenthos use additional CO₂ due to acidification for photosynthesis until the maximum yield capacity has been reached. When the cells reached maximum intracellular CO₂ concentration through their CCMs, any additional CO₂ would

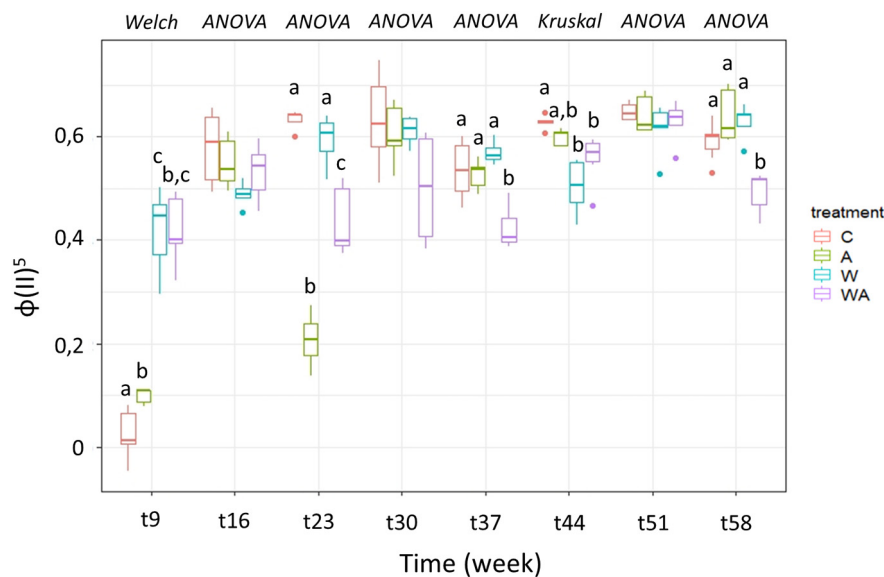


Fig. 5. Variation of the quantum efficiency of photosystem II ($\phi(II)^5$) in the different treatment. The letters t followed by a number indicates the sampling time. Above the figure was indicated in italics the test carried out for the comparison between treatments of the same week. The letters indicated a significant difference ($p < 0.05$) found after a post-hoc Tukey HSD test in the case of an ANOVA, a Games-Howell test in the case of a Welch ANOVA or a Nemenyi test in the case of a Kruskal Wallis test.

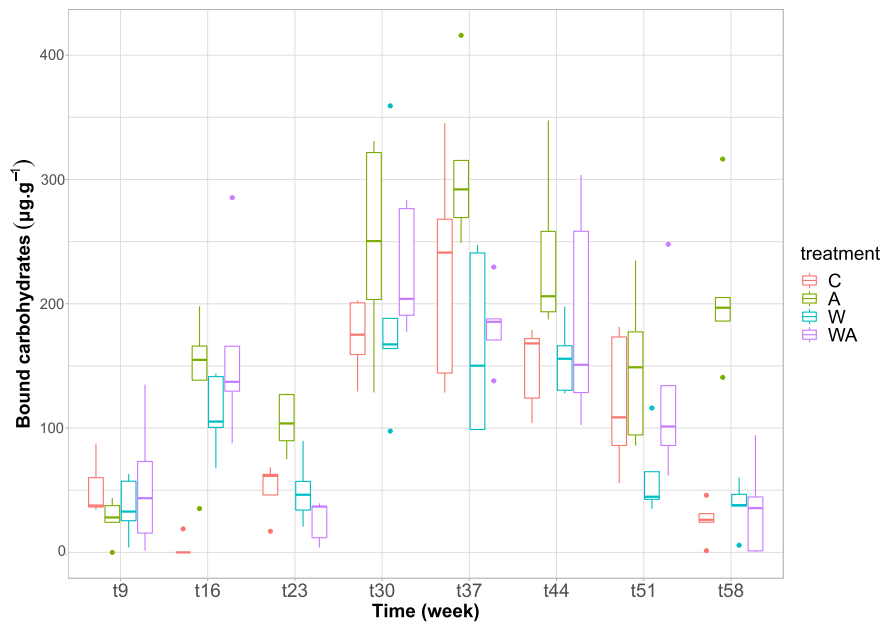


Fig. 6. Temporal variation of the carbohydrate concentration in the bound fraction of EPS (in $\mu\text{g}\cdot\text{g}^{-1}$ dry mass). The letters t followed by a number indicates the sampling time. The statistical test performed to show the differences between treatments at a sampling time is indicated in italics above the figure. The letters indicate a significant difference ($p < 0.05$) found after a post-hoc Tukey HSD test in the case of an ANOVA or a Games-Howell test in the case of a Welch ANOVA. Note: the ANOVA performed at t16 did not consider the C treatment because of the presence of outliers.

contribute to the decrease in pH. The pH of the WA treatment followed the same dynamic as observed for the A treatment. However, the dissolved oxygen concentration under WA treatment increased less than half in comparison to the A treatment (Fig. 2, D). The CO_2 absorption mechanisms may have been less efficient in WA treatment because temperature decreases the solubility of CO_2 (Wootton et al., 2008).

Numerous studies have shown that photosystem II is very sensitive to environmental stress (Murata et al., 2007; Nishiyama et al., 2008;

Wang et al., 2013). It is therefore important to focus on the quantum yield of photosystem II, which indicates the maximum photosynthetic activity potential of the communities. At t9, the quantum yield of photosystem II for the C and A treatments were close to 0 (Fig. 5), which indicated that the mats were not in good physiological condition when starting the experiment. Significantly lower quantum yields were observed under some treatments. At t23, under the A and the WA treatments an unexplained decrease of the quantum yield was observed

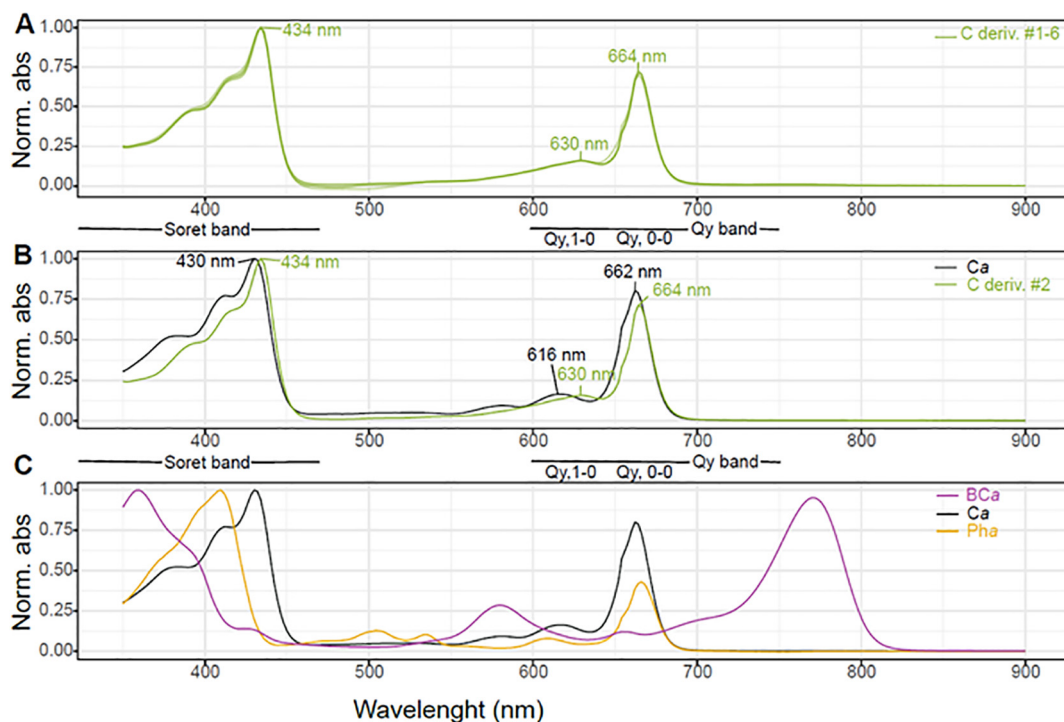


Fig. 7. Normalized absorption spectra of different pigments of the microbial mats. A: superimposed absorption spectra of the 6 detected chlorophyll derivatives (C deriv.). B: comparison between the absorption spectra of chlorophyll a (Ca) and C deriv. #2. C: comparison between the absorption spectra of Ca, pheophytin a (Pha) and bacteriochlorophyll a (BCa).

(Fig. 5). The WA treatment exhibited significantly lower quantum yield than the other treatments at t37, t51 and t58 (Fig. 5), suggesting that mats have more difficulty withstanding simultaneous acidification and heating. It was not surprising that there was no difference in quantum efficiency between A and C treatments (Fig. 5). Photosynthetic organisms have a high capacity to modify pH with evidence that pH is regulated at the water/cell interface (Black et al., 2019). Our fluorometer illuminated with a blue LED emitter (455 nm). Chlorophyll *a* fluorescence per unit concentration in cyanobacteria tends to be lower than in algae when it is excited with blue light. This leads to an erroneous biomass estimate of cyanobacteria. In their study, Simis et al. (2012) have sought the optimal excitation and emission pairs for the separation of cyanobacterial and algal Fv/Fm in communities. They demonstrate that the highest correlation between community and cyanobacterial variable fluorescence is obtained under orange-red excitation in the 590–650 nm range, exciting cyanobacterial phycobilipigments. No information was found about the other phototrophic communities.

The A treatment possessed more chlorophyll derivatives and lower chlorophyll *a* than the other treatments (Fig. 4). These chlorophyll derivatives molecules seemed to be bioindicators of a stress condition (water acidification). They were not identified by available standards. These molecules did not correspond to known metallised allomers or epimers of chlorophyll *a* (Ca), as revealed by their retention time (Supplementary materials, Fig. E). Based on their absorption spectra (Fig. 7), we can also rule out the hypothesis that these molecules correspond to demetallised derivatives of chlorophyll *a* such as pheophytin *a* or pheophorbide *a* or even to bacteriochlorophyll *a* (BCa).

We can assume that these molecules correspond to transmetalated Ca or BCa. Some microorganisms are known to possess bacteriochlorophyll those the central Mg ion is replaced by another metal, as observed for *Acidiphilium* where BCa possess a Zn central metal (Hiraishi and Shimada, 2001). This organism has been isolated from acidic mine ponds and it is supposed likely that pH constituted the evolutionary pressure responsible for the change of the central metal (Hiraishi and Shimada, 2001). Although this is an attractive hypothesis, it is highly unlikely that our pH treatment had the effect of promoting the synthesis of transmetalated BCa as Zn-BCa displays absorption features in the near infra-red range (Nagata et al., 2003) that were not observed here.

Chlorophylls and porphyrin derivatives generally have two major absorption bands (*i.e.* “red” (Q_y) and “blue” (Soret-) bands, Fig. 7) in the visible range, due to extended π -delocalization at the edge of cyclic porphyrin skeleton (Milenkovic et al., 2012). Two main Q-bands (Q_{y,0-0} and Q_{y,0-1}) are traditionally observed in the original Ca (or Mg-Ca) (Gerola et al., 2011). In our case, Ca wavelengths of maximum absorption λ_{\max} were respectively 665 (Q_{y,0-0}) and 615 nm (Q_{y,0-1}).

Based on these findings, the unidentified derivatives do not correspond to transmetalated Ca, although those absorption characteristics are close to the Mg-Ca molecule. As shown previously by Gerola et al. (2011), a hypsochromic (blue) shift of both Soret and Q_{y,0-0} bands must be expected with significant decreasing of λ_{\max} in Zn- and Cu-Ca in comparison to Mg-Ca. Such hypsochromic shifts were not observed in the unidentified derivatives spectra.

The only noticeable change corresponded to a decreased intensity (hypochromic effect) in the Q_{y,0-0} band in comparison with that of Mg-Ca and a bathochromic (red) shift in the Q_{y,0-1} (Fig. 7). These characteristics are similar to those of bacteriochlorophyll *c* (BCc) with a recorded λ_{\max} (630 nm) for Q_{y,0-1} close to the expected 623–629 nm (Goedheer, 1966; Oelze, 1985; Pierson and Castenholz, 1974). This pigment is typically found in the chlorosomes of green anoxygenic phototroph bacteria, including the green sulfur bacteria and the green non-sulfur bacteria (Frigaard et al., 2006; Scheer, 2006), which indicated that the pH conditions may have favoured the growth of these phototrophic bacteria.

Even moderate changes of both pH and temperature are relevant for bacterial community composition of microbial mats (Uribe-Lorío et al., 2019). A decrease in chlorophyll *a* has been observed under high CO₂ levels suggesting that the CO₂ input reduce CCMs and thus save

energy, particularly in pigment synthesis (Wang et al., 2019; Yue et al., 2019). In hot springs from Costa Rica, significant changes of microbial mat communities were observed with a significant increase of Chloroflexi (also named the green non-sulfur bacteria) abundance with decreasing pH and increasing temperature (Uribe-Lorío et al., 2019). Chloroflexi have been previously reported to be more abundant at decreased pH on sediment of hydrothermal CO₂ seeps in Papua New Guinea (Hassenrück et al., 2016) and in host-association with corals and sponges (Kandler et al., 2018; Morrow et al., 2015). Chlorobi, the green sulfur bacteria, have also been found to increase in abundance with acidification (Hassenrück et al., 2016). On their study, Hassenrück et al. (2016) supposed that in the sites characterized by low pH and high hydrothermal influence, including pronounced temperature increases, the Chloroflexi and Chlorobi replaced other microbial communities as major carbon degraders under anoxic conditions. Green anoxygenic bacteria participate on the carbon cycling and have been shown to fix CO₂ (Hug et al., 2013; Sirevåg, 2004). The phototrophic communities of the microbial mats could be modified under A treatment leading to a higher relative abundance of green anoxygenic bacteria. It is also possible that the presence of more CO₂ on the environment conducted to a shift on the metabolism of green anoxygenic phototrophic bacteria fixing the CO₂ and being more competitive with the other communities.

The bound carbohydrate EPS production was higher under the A treatment. EPS are essential for maintaining the physical properties and proper functioning of microbial mats, and are also involved in the adaptation of communities to their environment (Dupraz and Visscher, 2005; Hubas, 2018; Prieto-Barajas et al., 2018). Therefore, EPS are an essential element, even more when microorganisms are confronted with strong variations in physico-chemical parameters. It has been observed that the degradation of polysaccharides by bacterial extracellular enzymes is accelerated at low pH (Piontek et al., 2009). It can be supposed that microbial mats could therefore synthesize more carbohydrates to compensate for this degradation. Microbial mats in the W treatment did not show any variation in concentration, suggesting that temperature has no effect on this process. Those in the WA treatment also did not change suggesting that acidification and warming have probably antagonistic effects limiting the impact of acidification on EPS. However, Li et al. (2016) obtained contradictory results on three freshwater microalgae as they demonstrated that acidification and warming act synergistically. The variation of bound carbohydrate EPS suggest that microbial mats subjected to acidification modified their metabolism. Tan et al. (2019) have shown that a polar strain of *Chlorella* sp. modulates its metabolism under acidified conditions ($p\text{CO}_2 = 1000 \mu\text{atm}$), favouring its survival. They observed a decrease in the fluxes of glucose and sucrose, the main products of photosynthesis, under high $p\text{CO}_2$. Gong et al. (2020) also observed that the starch metabolism was modified by increasing the quantity of starch granules in another microalgae named *Symbiochlorum hainanensis*. These observations suggest that the organic carbon produced by photosynthesis in the microbial mats placed under the A treatment was redirected towards the synthesis of other carbohydrates which concentration had considerably increased.

5. Conclusion

The temperature in the warming treatments increased by 4 °C from the initial temperature as expected. Despite of a decrease of 0.4 unit pH in the water reserves of acidification treatments, no significance difference was observed between the water pH of the different treatments. The salinity increased on the warming treatments because of the water evaporation. The dissolved oxygen concentration increased and was higher on the acidification treatments, certainly due to an increase of the photosynthesis because of the carbon input.

In the acidification treatment, our results showed that the concentration of bound carbohydrates EPS increased. This indicated that the

metabolisms were modified to cope with the induced changes. In addition, the phototrophic communities of the microbial mats under the different treatments showed characteristic pigments. In particular, unknown chlorophyll derivatives were present under acidification and/or warming treatments. To the best of our knowledge the synthesis of such derivatives following an acidification or/and a warming experiment has never been reported before. These molecules were eventually identified as bacteriochlorophyll *c* and several possible isomers which suggest that experimentally induced climate change scenario may have favoured the increase of BCc contained on green anoxygenic phototroph bacteria.

The mesocosm experiment has shown that phototrophic communities of the microbial mats were able to adapt to the conditions defined by the IPCC (2014) regarding acidification and warming of surface water. The most probable explanation is that the studied microbial mats are already naturally confronted with environmental conditions (pH, light, temperature, salinity, etc.) that fluctuate with a great amplitude in salt marshes. They may therefore already be confronted with temperature and pH conditions predicted, for example, by the IPCC for 2100. Changes in their metabolism probably enabled them to maintain a high potential for photosynthetic activity when acidification took place. In the future, it would be interesting to observe if a difference in the phylogenetic composition of these communities occurred. This study provides new insights on the response of phototrophic communities of microbial mats in a context of climate change and permit to better understand their function in this ecosystem.

CRedit authorship contribution statement

C. Mazière: Conceptualization, Methodology, Validation, Formal analysis, Investigation, Writing – original draft. **M. Bodo:** Formal analysis, Investigation, Writing – review & editing. **M.A. Perdrau:** Formal analysis, Investigation, Writing – review & editing. **C. Cravo-Laureau:** Conceptualization, Investigation, Writing – review & editing, Funding acquisition. **R. Duran:** Conceptualization, Investigation, Writing – review & editing, Funding acquisition. **C. Dupuy:** Conceptualization, Investigation, Writing – review & editing, Funding acquisition. **C. Hubas:** Conceptualization, Formal analysis, Investigation, Writing – review & editing, Funding acquisition.

Declaration of competing interest

The authors declare that they have no known competing financial interests or personal relationships that could have appeared to influence the work reported in this paper.

Acknowledgements

C. Mazière was supported by a PhD grant from E2S-UPPA program and the Région Nouvelle-Aquitaine. We thank the funding support from the European programme ERANETMED AQUASALT (NMED-0003-01) and from the ACI politique d'établissement Université de La Rochelle.

The authors are grateful to the salterns owner Michel Jauffrais and Thomas Lacoue-Labarthe for his help in setting up the acidification treatment.

Appendix A. Supplementary data

Supplementary data to this article can be found online at <https://doi.org/10.1016/j.scitotenv.2021.149787>.

References

Aminot A., Kérouel R. 2007. Dosage automatique des nutriments dans les eaux marines. Quae. ed.

- Baragi, L.V., Anil, A.C., 2016. Synergistic effect of elevated temperature, pCO₂ and nutrients on marine biofilm. *Mar. Pollut. Bull.* 105, 102–109. <https://doi.org/10.1016/j.marpollbul.2016.02.049>.
- Baragi, L.V., Khandeparker, L., Anil, A.C., 2015. Influence of elevated temperature and pCO₂ on the marine periphytic diatom *Navicula distans* and its associated organisms in culture. *Hydrobiologia* 762, 127–142. <https://doi.org/10.1007/s10750-015-2343-9>.
- Beardall, J., Stojkovic, S., Larsen, S., 2009. Living in a high CO₂ world: impacts of global climate change on marine phytoplankton. *Plant Ecol. Divers.* 2, 191–205. <https://doi.org/10.1080/17550870903271363>.
- Black, J.G., Stark, J.S., Johnstone, G.J., McMinn, A., Boyd, P., McKinlay, J., Wotherspoon, S., Runcie, J.W., 2019. In-situ behavioural and physiological responses of Antarctic microphytobenthos to ocean acidification. *Sci. Rep.* 9, 1890. <https://doi.org/10.1038/s41598-018-36233-2>.
- Bolhuis, H., Stal, L.J., 2011. Analysis of bacterial and archaeal diversity in coastal microbial mats using massive parallel 16S rRNA gene tag sequencing. *ISME J.* 5, 1701–1712. <https://doi.org/10.1038/ismej.2011.52>.
- Bordenave, S., Fourçans, A., Blanchard, S., Goñi, M.S., Caumette, P., Duran, R., 2004a. Structure and functional analyses of bacterial communities changes in microbial mats following petroleum exposure. *Ophelia* 58, 195–203. <https://doi.org/10.1080/00785236.2004.10410227>.
- Bordenave, S., Goñi-urriza, M., Vilette, C., Blanchard, S., Caumette, P., Duran, R., 2008. Diversity of ring-hydroxylating dioxygenases in pristine and oil contaminated microbial mats at genomic and transcriptomic levels. *Environ. Microbiol.* 10, 3201–3211. <https://doi.org/10.1111/j.1462-2920.2008.01707.x>.
- Bordenave, S., Jézéquel, R., Fourçans, A., Budzinski, H., Merlin, F.X., Fourel, T., Goñi-Urriza, M., Guyoneaud, R., Grimaud, R., Caumette, P., Duran, R., 2004b. Degradation of the "Erika" oil. *Aquat. Living Resour.* 17, 261–267. <https://doi.org/10.1051/alr:2004027>.
- Brotas, V., Plante-Cuny, M.-R., 2003. The use of HPLC pigment analysis to study microphytobenthos communities. *Acta Oecol.* 24. [https://doi.org/10.1016/S1146-609X\(03\)00013-4](https://doi.org/10.1016/S1146-609X(03)00013-4).
- Cartaxana, P., Vieira, S., Ribeiro, L., Rocha, R., Cruz, S., Calado, R., Marques da Silva, J., 2015. Effects of elevated temperature and CO₂ on intertidal microphytobenthos. *BMC Ecol.* 15, 10. <https://doi.org/10.1186/s12898-015-0043-y>.
- Cavicchioli, R., Ripple, W.J., Timmis, K.N., Azam, F., Bakken, L.R., Baylis, M., Behrenfeld, M.J., Boetius, A., Boyd, P.W., Classen, A.T., Crowther, T.W., Danovaro, R., Foreman, C.M., Huisman, J., Hutchins, D.A., Jansson, J.K., Karl, D.M., Koskella, B., Mark Welch, D.B., Martiny, J.B.H., Moran, M.A., Orphan, V.J., Reay, D.S., Remais, J.V., Rich, V.I., Singh, B.K., Stein, L.Y., Stewart, F.J., Sullivan, M.B., van Oppen, M.J.H., Weaver, S.C., Webb, E.A., Webster, N.S., 2019. Scientists' warning to humanity: microorganisms and climate change. *Nat. Rev. Microbiol.* 17, 569–586. <https://doi.org/10.1038/s41579-019-0222-5>.
- Cravo-Laureau, C., Duran, R., 2014. Marine coastal sediments microbial hydrocarbon degradation processes: contribution of experimental ecology in the omics'era. *Front. Microbiol.* 5. <https://doi.org/10.3389/fmicb.2014.00039>.
- Crawford, K.J., Raven, J.A., Wheeler, G.L., Baxter, E.J., Joint, I., 2011. The response of *Thalassiosira pseudonana* to long-term exposure to increased CO₂ and decreased pH. *PLoS ONE* 6, e26695. <https://doi.org/10.1371/journal.pone.0026695>.
- Decho, A., 2000. Microbial biofilms in intertidal systems: an overview. *Cont. Shelf Res.* 20, 1257–1273. [https://doi.org/10.1016/S0278-4343\(00\)00022-4](https://doi.org/10.1016/S0278-4343(00)00022-4).
- Decho, A., 1990. Decho AW. Microbial exopolymer secretions in ocean environments: their role(s) in food webs and marine processes. *Oceanogr. Mar. Biol. Ann. Rev.* 28: 73–153. *Oceanogr. Mar. Biol. Annu. Rev.* 28, 73–154.
- Decho, A.W., Moriarty, D.J.W., 1990. Bacterial exopolymer utilization by a harpacticoid copepod: a methodology and results. *Limnol. Oceanogr.* 35, 1039–1049. <https://doi.org/10.4319/lo.1990.35.5.1039>.
- Dobretsov, S., Abed, R.M.M., Al Maskari, S.M.S., Al Sabahi, J.N., Victor, R., 2011. Cyanobacterial mats from hot springs produce antimicrobial compounds and quorum-sensing inhibitors under natural conditions. *J. Appl. Phycol.* 23, 983–993. <https://doi.org/10.1007/s10811-010-9627-2>.
- Dubois, Michel, Gilles, K.A., Hamilton, J.K., Rebers, P.A., Smith, Fred, 1956. Colorimetric method for determination of sugars and related substances. *Anal. Chem.* 28, 350–356. <https://doi.org/10.1021/ac60111a017>.
- Dupraz, C., Visscher, P.T., 2005. Microbial lithification in marine stromatolites and hypersaline mats. *Trends Microbiol.* 13, 429–438. <https://doi.org/10.1016/j.tim.2005.07.008>.
- Dutta, H., Dutta, A., 2016. The microbial aspect of climate change. *Energy Ecol. Environ.* 1, 209–232. <https://doi.org/10.1007/s40974-016-0034-7>.
- Flemming, H.-C., Wingender, J., 2010. The biofilm matrix. *Nat. Rev. Microbiol.* 8, 623–633. <https://doi.org/10.1038/nrmicro2415>.
- Fourçans, A., de Oteyza, T.G., Wieland, A., Solé, A., Diestra, E., van Bleijswijk, J., Grimalt, J.O., Kühl, M., Esteve, I., Muyzer, G., Caumette, P., Duran, R., 2004. Characterization of functional bacterial groups in a hypersaline microbial mat community (Salins-de-Giraud, Camargue, France). *FEMS Microbiol. Ecol.* 51, 55–70. <https://doi.org/10.1016/j.femsec.2004.07.012>.
- Fourçans, A., Ranchou-Peyruse, A., Caumette, P., Duran, R., 2008. Molecular analysis of the spatio-temporal distribution of sulfate-reducing bacteria (SRB) in Camargue (France) hypersaline microbial mat. *Microb. Ecol.* 56, 90–100. <https://doi.org/10.1007/s00248-007-9327-x>.
- Fourçans, A., Solé, A., Diestra, E., Ranchou-Peyruse, A., Esteve, I., Caumette, P., Duran, R., 2006. Vertical migration of phototrophic bacterial populations in a hypersaline microbial mat from Salins-de-Giraud (Camargue, France). *FEMS Microbiol. Ecol.* 57, 367–377. <https://doi.org/10.1111/j.1574-6941.2006.00124.x>.
- Frigaard, N.-U., Maqueo Chew, A.G., Maresca, J.A., Bryant, D.A., 2006. Bacteriochlorophyll biosynthesis in green bacteria. In: Grimm, B., Porra, R.J., Rüdiger, W., Scheer, H. (Eds.), *Chlorophylls and Bacteriochlorophylls, Advances in Photosynthesis and*

- Respiration. Dordrecht, Springer Netherlands, pp. 201–221 https://doi.org/10.1007/1-4020-4516-6_15.
- Gao, K., Helbling, E., Häder, D., Hutchins, D., 2012. Responses of marine primary producers to interactions between ocean acidification, solar radiation, and warming. *Mar. Ecol. Prog. Ser.* 470, 167. <https://doi.org/10.3354/meps10043>.
- Gerola, A.P., Tsubone, T.M., Santana, A., de Oliveira, H.P.M., Hioka, N., Caetano, W., 2011. Properties of chlorophyll and derivatives in homogeneous and microheterogeneous systems. *J. Phys. Chem. B* 115, 7364–7373. <https://doi.org/10.1021/jp201278b>.
- Gette-Bouvarot, M., Mermillod-Blondin, F., Lemoine, D., Delolme, C., Danjean, M., Etienne, L., Volatier, L., 2015. The potential control of benthic biofilm growth by macrophytes—a mesocosm approach. *Ecol. Eng.* 75, 178–186. <https://doi.org/10.1016/j.ecoleng.2014.12.001>.
- Goedheer, J.C., 1966. Visible absorption and fluorescence of chlorophyll and its aggregates in solution. *The Chlorophylls*. Elsevier, pp. 147–184 <https://doi.org/10.1016/B978-1-4832-3289-8.50012-6>.
- Gong, S., Jin, X., Xiao, Y., Li, Z., 2020. Ocean acidification and warming lead to increased growth and altered chloroplast morphology in the thermo-tolerant alga *Symbiodinium hainanensis*. *Front. Plant Sci.* 11. <https://doi.org/10.3389/fpls.2020.585202>.
- Hancke, K., Glud, R., 2004. Temperature effects on respiration and photosynthesis in three diatom-dominated benthic communities. *Aquat. Microb. Ecol.* 37, 265–281. <https://doi.org/10.3354/ame037265>.
- Hassenrück, C., Fink, A., Lichtschlag, A., Tegetmeyer, H.E., de Beer, D., Ramette, A., 2016. Quantification of the effects of ocean acidification on sediment microbial communities in the environment: the importance of ecosystem approaches. *FEMS Microbiol. Ecol.* 92. <https://doi.org/10.1093/femsec/fiw027>.
- Hicks, N., Bulling, M.T., Solan, M., Raffaelli, D., White, P.C., Paterson, D.M., 2011. Impact of biodiversity-climate futures on primary production and metabolism in a model benthic estuarine system. *BMC Ecol.* 11, 7. <https://doi.org/10.1186/1472-6785-11-7>.
- Hiraishi, A., Shimada, K., 2001. Aerobic anoxygenic photosynthetic bacteria with zinc-bacteriochlorophyll. *J. Gen. Appl. Microbiol.* 47, 161–180. <https://doi.org/10.2323/jgam.47.161>.
- Hubas, C., 2018. Biofilms, tapis et agrégats microbiens : vers une vision unificatrice (HDR (Habilitation à Diriger les Recherches)). Muséum National D'Histoire Naturelle <https://doi.org/10.5281/zenodo.3784703>.
- Hug, L.A., Castelle, C.J., Wrighton, K.C., Thomas, B.C., Sharon, I., Frischkorn, K.R., Williams, K.H., Tringe, S.G., Banfield, J.F., 2013. Community genomic analyses constrain the distribution of metabolic traits across the chloroflexi phylum and indicate roles in sediment carbon cycling. *Microbiome* 1, 22. <https://doi.org/10.1186/2049-2618-1-22>.
- Hutchins, D.A., Fu, F., 2017. Microorganisms and ocean global change. *Nat. Microbiol.* 2, 17058. <https://doi.org/10.1038/nmicrbiol.2017.58>.
- IPCC, 2014. *Climate Change 2014: Synthesis Report. Contribution of Working Groups I, II and III to the Fifth Assessment Report of the Intergovernmental Panel on Climate Change*. 169.
- Jesus, B., Perkins, R.G., Mendes, C.R., Brotas, V., Paterson, D.M., 2006. Chlorophyll fluorescence as a proxy for microphytobenthic biomass: alternatives to the current methodology. *Mar. Biol.* 150, 17–28. <https://doi.org/10.1007/s00227-006-0324-2>.
- Jørgensen, B.B., Revsbech, N.P., Cohen, Y., 1983. Photosynthesis and structure of benthic microbial mats: microelectrode and SEM studies of four cyanobacterial communities. *Limnol. Oceanogr.* 28, 1075–1093. <https://doi.org/10.4319/lo.1983.28.6.1075>.
- Kandler, N.M., Abdul Wahab, M.A., Noonan, S.H.C., Bell, J.J., Davy, S.K., Webster, N.S., Luter, H.M., 2018. In situ responses of the sponge microbiome to ocean acidification. *FEMS Microbiol. Ecol.* 94. <https://doi.org/10.1093/femsec/fiy205>.
- Li, W., Xu, X., Fujibayashi, M., Niu, Q., Tanaka, N., Nishimura, O., 2016. Response of microalgae to elevated CO₂ and temperature: impact of climate change on freshwater ecosystems. *Environ. Sci. Pollut. Res.* 23, 19847–19860. <https://doi.org/10.1007/s11356-016-7180-5>.
- Ma, J., Wang, P., Wang, X., Xu, Y., Paerl, H.W., 2019. Cyanobacteria in eutrophic waters benefit from rising atmospheric CO₂ concentrations. *Sci. Total Environ.* 691, 1144–1154. <https://doi.org/10.1016/j.scitotenv.2019.07.056>.
- Mackey, K., Morris, J., Morel, F., Kranz, S., 2015. Response of photosynthesis to ocean acidification. *Oceanography* 25, 74–91. <https://doi.org/10.5670/oceanog.2015.33>.
- Milenkovic, S.M., Zvezdanovic, J.B., Andelkovic, T.D., Markovic, D.Z., 2012. The identification of chlorophyll and its derivatives in the pigment mixtures: HPLC-chromatography, visible and mass spectroscopy studies. *Adv. Technol.* 9.
- Morrow, K.M., Bourne, D.G., Humphrey, C., Botté, E.S., Laffy, P., Zaneveld, J., Uthicke, S., Fabricius, K.E., Webster, N.S., 2015. Natural volcanic CO₂ seeps reveal future trajectories for host-microbial associations in corals and sponges. *ISME J.* 9, 894–908. <https://doi.org/10.1038/ismej.2014.188>.
- Murata, N., Takahashi, S., Nishiyama, Y., Allakhverdiev, S.I., 2007. Photoinhibition of photosystem II under environmental stress. *Biochim. Biophys. Acta BBA - Bioenerg. Struct. Funct. Photosyst.* 1767, 414–421. <https://doi.org/10.1016/j.bbabi.2006.11.019>.
- Nagata, M., Yoshimura, Y., Inagaki, J., Suemori, Y., Iida, K., Ohtsuka, T., Nango, M., 2003. Construction and photocurrent of light-harvesting polypeptides/zinc bacteriochlorophyll a complex in lipid bilayers. *Chem. Lett.* 32, 852–853. <https://doi.org/10.1246/cl.2003.852>.
- Nishiyama, Y., Allakhverdiev, S.I., Murata, N., 2008. Regulation by environmental conditions of the repair of photosystem II in cyanobacteria. In: Demmig-Adams, B., Adams, W.W., Mattoo, A.K. (Eds.), *Photoprotection, Photoinhibition, Gene Regulation, and Environment, Advances in Photosynthesis and Respiration*. Springer Netherlands, Dordrecht, pp. 193–203 https://doi.org/10.1007/1-4020-3579-9_13.
- Oelze, J., 1985. 9 Analysis of Bacteriochlorophylls**Dedicated to Prof. Dr. N. Pfennig on the occasion of his 60th birthday in recognition of his numerous contributions on the ecology and taxonomy of phototrophic bacteria. In: Bergan, T. (Ed.), *Methods in Microbiology*. Academic Press, pp. 257–284 [https://doi.org/10.1016/S0580-9517\(08\)70478-1](https://doi.org/10.1016/S0580-9517(08)70478-1).
- Peimbert, M., Alcaraz, L.D., Bonilla-Rosso, G., Olmedo-Alvarez, G., García-Oliva, F., Segovia, L., Eguarte, L.E., Souza, V., 2012. Comparative metagenomics of two microbial mats at Cuatro Ciénegas Basin I: ancient lessons on how to cope with an environment under severe nutrient stress. *Astrobiology* 12, 648–658. <https://doi.org/10.1089/ast.2011.0694>.
- Pierson, B.K., Castenholz, R.W., 1974. A phototrophic gliding filamentous bacterium of hot springs, *Chloroflexus aurantiacus*, gen. and sp. nov. *Arch. Microbiol.* 100, 5–24. <https://doi.org/10.1007/BF00446302>.
- Piontek, J., Lunau, M., Händel, N., Borchard, C., Wurst, M., Engel, A., 2009. Acidification increases microbial polysaccharide degradation in the ocean. *Biogeosci. Discuss.* 7. <https://doi.org/10.5194/bg-7-1615-2010>.
- Prieto-Barajas, C.M., Valencia-Cantero, E., Santoyo, G., 2018. Microbial mat ecosystems: structure types, functional diversity, and biotechnological application. *Electron. J. Biotechnol.* 31, 48–56. <https://doi.org/10.1016/j.ejbt.2017.11.001>.
- Redfield, A.C., 1958. *The biological control of chemical factors in the environment*. *Am. Sci.* 46, 230A–221.
- Reinold, Wong, MacLeod, Meltzer, Thompson, Burns, 2019. The vulnerability of microbial ecosystems in a changing climate: potential impact in Shark Bay. *Life* 9, 71. <https://doi.org/10.3390/life9030071>.
- Revsbech, N.P., Jørgensen, B.B., Blackburn, T.H., Cohen, Y., 1983. Microelectrode studies of the photosynthesis and O₂, H₂S, and pH profiles of a microbial mat. *Limnol. Oceanogr.* 28, 1062–1074. <https://doi.org/10.4319/lo.1983.28.6.1062>.
- Scheer, H., 2006. An overview of chlorophylls and bacteriochlorophylls: biochemistry, biophysics, functions and applications. In: Grimm, B., Porra, R.J., Rüdiger, W., Scheer, H. (Eds.), *Chlorophylls and Bacteriochlorophylls: Biochemistry, Biophysics, Functions and Applications, Advances in Photosynthesis and Respiration*. Springer Netherlands, Dordrecht, pp. 1–26 https://doi.org/10.1007/1-4020-4516-6_1.
- Simis, S.G.H., Huot, Y., Babin, M., Seppälä, J., Metsamaa, L., 2012. Optimization of variable fluorescence measurements of phytoplankton communities with cyanobacteria. *Photosynth. Res.* 112, 13–30. <https://doi.org/10.1007/s11220-012-9729-6>.
- Sirevåg, R., 2004. Carbon metabolism in green bacteria. In: Blankenship, R.E., Madigan, M.T., Bauer, C.E. (Eds.), *Anoxygenic Photosynthetic Bacteria, Advances in Photosynthesis and Respiration*. Kluwer Academic Publishers, Dordrecht, pp. 871–883 https://doi.org/10.1007/0-306-47954-0_40.
- Sørensen, K.B., Canfield, D.E., Teske, A.P., Oren, A., 2005. Community composition of a hypersaline endoevaporitic microbial mat. *Appl. Environ. Microbiol.* 71, 7352–7365. <https://doi.org/10.1128/AEM.71.11.7352-7365.2005>.
- Stauffert, M., Cravo-Laureau, C., Jezequel, R., Barantal, S., Cuny, P., Gilbert, F., Cagnon, C., Milioton, C., Amouroux, D., Mahdaoui, F., Bouysiere, B., Stora, G., Merlin, F., Duran, R., 2013. Impact of oil on bacterial community structure in bioturbated sediments. *PLoS One* 8, e65347. <https://doi.org/10.1371/journal.pone.0065347>.
- Takahashi, E., Ledauphin, J., Goux, D., Orvain, F., 2009. Optimising extraction of extracellular polymeric substances (EPS) from benthic diatoms: comparison of the efficiency of six EPS extraction methods. *Mar. Freshw. Res.* 60, 1201–1210. <https://doi.org/10.1071/MF08258>.
- Tan, Y.-H., Lim, P.-E., Beardall, J., Poong, S.-W., Phang, S.-M., 2019. A metabolomic approach to investigate effects of ocean acidification on a polar microalga *Chlorella* sp. *Aquat. Toxicol.* 217, 105349. <https://doi.org/10.1016/j.aquatox.2019.105349>.
- Underwood, G.J.C., Boulcott, M., Raines, C.A., Waldron, K., 2004. Environmental effects on exopolymer production by marine benthic diatoms: dynamics, changes in composition, and pathways of production. *J. Phycol.* 40, 293–304. <https://doi.org/10.1111/j.1529-8817.2004.03076.x>.
- Uribe-Lorio, L., Brenes-Guillén, L., Hernández-Ascencio, W., Mora-Amador, R., González, G., Ramírez-Umaña, C.J., Diez, B., Pedrós-Alió, C., 2019. The influence of temperature and pH on bacterial community composition of microbial mats in hot springs from Costa Rica. *MicrobiologyOpen* 8. <https://doi.org/10.1002/mbo3.893>.
- van Gemerden, H., 1993. Microbial mats: a joint venture. *Mar. Geol.* 113, 3–25. [https://doi.org/10.1016/0025-3227\(93\)90146-M](https://doi.org/10.1016/0025-3227(93)90146-M).
- Wang, S., Zhang, D., Pan, X., 2013. Effects of cadmium on the activities of photosystems of *Chlorella pyrenoidosa* and the protective role of cyclic electron flow. *Chemosphere* 93, 230–237. <https://doi.org/10.1016/j.chemosphere.2013.04.070>.
- Wang, X., Feng, X., Zhuang, Y., Lu, J., Wang, Y., Gonçalves, R.J., Li, X., Lou, Y., Guan, W., 2019. Effects of ocean acidification and solar ultraviolet radiation on physiology and toxicity of dinoflagellate *Karenia mikimotoi*. *Harmful Algae* 81, 1–9. <https://doi.org/10.1016/j.hal.2018.11.013>.
- Wieland, A., Kühl, M., McGowan, L., Fourçans, A., Duran, R., Caumette, P., Garcia de Oteyza, T., Grimalt, J.O., Solé, A., Diestra, E., Esteve, I., Herbert, R.A., 2003. Microbial mats on the Orkney Islands revisited: microenvironment and microbial community composition. *Microb. Ecol.* 46, 371–390. <https://doi.org/10.1007/s00248-002-0108-2>.
- Wootton, J.T., Pfister, C.A., Forester, J.D., 2008. Dynamic patterns and ecological impacts of declining ocean pH in a high-resolution multi-year dataset. *Proc. Natl. Acad. Sci.* 105, 18848–18853. <https://doi.org/10.1073/pnas.0810079105>.
- Yue, F., Gao, G., Ma, J., Wu, H., Li, X., Xu, J., 2019. Future CO₂-induced seawater acidification mediates the physiological performance of a green alga *Ulva linza* in different photoperiods. *PeerJ* 7. <https://doi.org/10.7717/peerj.7048>.

Supplementary materials of

Climate change influences chlorophylls and bacteriochlorophylls metabolism in hypersaline microbial mat

C. Mazière^{1,2*}, M. Bodo³, M. A. Perdrau², C. Cravo-Laureau¹, R. Duran¹, C. Dupuy², C. Hubas³

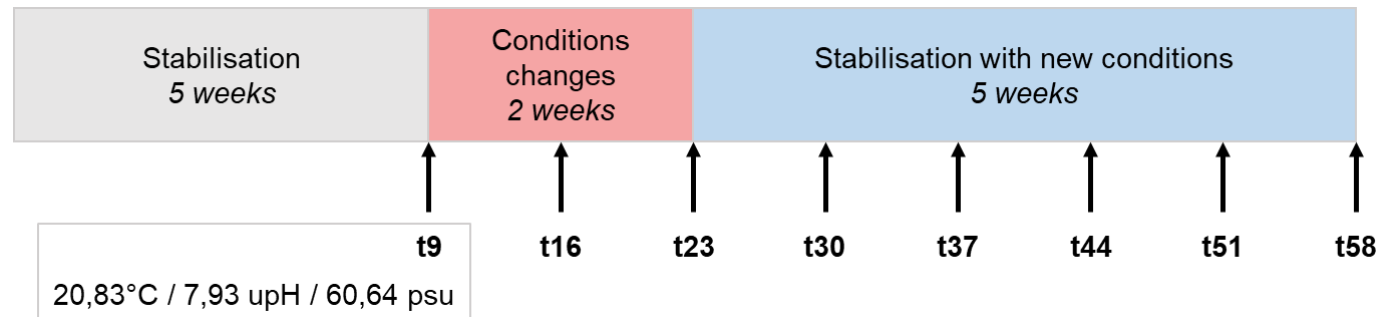


Fig. A: Schematic representation of the sampling scheme followed during the mesocosms experiment. A stabilisation period of 5 weeks was applied in order to adapt the microbial mats to their new environment. Then an acidification and a warmer water were done for 2 weeks followed by a stabilisation of these new conditions for 5 weeks. The sampling were represented by the letter t followed by a number indicates the sampling time.

Sample	Treatment	Time (week)	Replicate	Salinity (psu)	pH	Temperature (°C)	Dissolved O ₂ (mg.L ⁻¹)	Nitrate	Nitrite	Phosphate	Silicon	Ammonium
C-R1-P1	C	t9	R1	59.6	7.581	20.7	0.8	4.31	1.29	73.84	436.17	90.84
C-R1-P2	C	t16	R1	60.8	7.913	19.8	0.2	0.42	2.1	34.11	312.12	117.95
C-R1-P3	C	t23	R1	61.6	8.055	21.5	0.1	0.1	0.11	33.89	326.89	116.41
C-R1-P4	C	t30	R1	61.2	7.885	20.4	1.9	0	1.25	21.16	143.65	108.48
C-R1-P5	C	t37	R1	59	7.824	20.2	0.7	2.22	0.11	12.42	110.61	129.93
C-R3-P1	C	t9	R3	59.3	7.889	20.8	0.2	0.49	0.28	47.11	456.1	97.18
C-R3-P2	C	t16	R3	60.9	8.037	19.7	0.8	0.25	0.67	31.98	295.95	128.1
C-R3-P3	C	t23	R3	62.3	8.047	21.6	0.2	0.09	0.11	17.89	140.73	131.32
C-R3-P4	C	t30	R3	62.1	7.995	20.2	1.2	0.21	0.06	2.81	38.14	32.48
C-R3-P5	C	t37	R3	60.6	7.985	19.9	1.3	0.25	0.06	3.04	47.12	2.81
C-R3-P6	C	t44	R3	61.4	8.049	19.9	3.3	0.12	0.21	2.14	74.54	11.59
C-R3-P7	C	t51	R3	61.9	7.988	20	2.6	0.22	0.05	1.69	61.55	1.69
C-R3-P8	C	t58	R3	61.1	8.08	20.5	3.8	0.29	0.21	1.1	50.32	0.87
C-R4-P1	C	t9	R4	60.9	8.101	20.4	0.2	0.33	0.3	22.15	318.89	113.92
C-R4-P2	C	t16	R4	59.8	7.941	20.1	1.5	1.43	1.78	4.31	116.88	116.83
C-R4-P3	C	t23	R4	61.4	7.909	21.4	0.8	0.02	0.14	9.75	232.52	111.33
C-R4-P4	C	t30	R4	61.3	7.985	20.3	3.2	0.44	0.08	5.07	157.32	1.1
C-R4-P5	C	t37	R4	59	7.961	19.7	4.1	0.72	0.17	8.05	154.41	0.11
C-R4-P6	C	t44	R4	60.2	7.873	19.9	2.3	0.49	0.32	6.45	115.96	2.17
C-R4-P7	C	t51	R4	61.9	7.848	19.7	3	0.22	0.08	4.62	152.4	0.89
C-R4-P8	C	t58	R4	61.5	7.987	20.1	3.8	0.16	0.19	7.38	162.89	2.05
C-R5-P1	C	t9	R5	60.4	7.989	20.8	0.3	0.47	0.42	48.75	478.29	95.53
C-R5-P2	C	t16	R5	63.5	8.127	20	0.2	0.38	0.15	48.3	374.76	111.13
C-R5-P3	C	t23	R5	64.8	8.137	21.4	0.9	0.16	0.12	41.56	197.86	112.26
C-R5-P4	C	t30	R5	64.4	8.167	20.2	5.5	1.55	0.19	14.01	65.51	135.36
C-R5-P5	C	t37	R5	59.4	8.045	19.9	3.9	0.51	0.12	7.29	40.74	111.27
C-R5-P6	C	t44	R5	60.9	7.944	19.9	2.6	0.4	0.16	10.98	130.73	97.41
C-R5-P7	C	t51	R5	61.2	8.015	20.1	3.8	0.81	0.34	5.1	97.01	15.4
C-R5-P8	C	t58	R5	61.1	7.99	20.3	3.7	0.65	0.59	6.37	144.01	14.95

C-R6-P1	C	t9	R6	58.4	7.82	20.7	0.8	0.73	1.05	15.36	187.15	123.88
C-R6-P2	C	t16	R6	60.4	7.944	20.1	2	2.02	0.69	9.44	103.75	124.31
C-R6-P3	C	t23	R6	61.9	7.91	21.3	1.4	0.43	0.13	11.86	151.8	131.32
C-R6-P4	C	t30	R6	60.7	8.044	20.3	4.6	3.56	0.44	3.06	39.06	79.73
C-R6-P5	C	t37	R6	59.2	7.959	19.8	3	0.87	0.12	2.05	44.68	44.56
C-R6-P6	C	t44	R6	60.5	8.078	20.1	4.9	1.7	0.72	2.09	29.12	31.68
C-R6-P7	C	t51	R6	61.7	8.054	19.9	3.3	0.96	0.25	3.07	51.44	24.65
C-R6-P8	C	t58	R6	60.3	8.15	20.2	4.4	2.37	1.3	1.29	31.43	8.99
A-R1-P1	A	t9	R1	61.8	8.063	19.9	0.1	0.54	0.17	42.26	459.77	92.01
A-R1-P2	A	t16	R1	62.6	8.241	20.3	0.3	0.22	0.17	27.97	296.62	121.83
A-R1-P3	A	t23	R1	63.1	8.142	20.6	2.2	5.2	1.06	15.72	156.52	132.46
A-R1-P4	A	t30	R1	61.8	8.157	20.6	0.4	1.74	0.91	17.64	241.33	117.45
A-R1-P5	A	t37	R1	60.4	7.72	19.9	0.4	0.81	1.18	4.16	127.32	125.96
A-R1-P6	A	t44	R1	60.6	7.799	20.2	2.6	0	1.69	13.29	263.56	107.3
A-R1-P7	A	t51	R1	61.9	7.753	20.1	2	0.13	0.05	10.31	211.7	98.77
A-R1-P8	A	t58	R1	61.8	7.777	20.7	2.4	0.44	0.32	6.14	148.95	60.9
A-R3-P1	A	t9	R3	60.6	7.97	19.7	8.5	0.45	0.49	20.91	373.91	116.97
A-R3-P2	A	t16	R3	62.1	8.123	20.3	0.2	0.41	0.43	21.8	287.05	128.3
A-R3-P3	A	t23	R3	63.5	8.12	20.7	0.5	0.33	0.15	18.2	226.56	131.03
A-R3-P4	A	t30	R3	60.3	7.814	20	0.4	0.13	0.15	6.5	133.83	120.4
A-R3-P5	A	t37	R3	59.4	7.764	19.8	1.4	0.58	0.57	1.71	52.08	50.9
A-R3-P6	A	t44	R3	61.4	7.767	20.3	2.8	0.62	0.48	1.45	45.32	16.55
A-R3-P7	A	t51	R3	60.7	7.76	19.9	2.7	0.25	0.11	1.71	44.9	4.94
A-R3-P8	A	t58	R3	60.8	7.689	20.3	2.2	0.26	0.09	2.64	52.67	1.52
A-R4-P1	A	t9	R4	59.9	8.047	19.6	0.5	0.99	1.6	30.46	208.19	107.87
A-R4-P2	A	t16	R4	61.6	8.136	20.1	0.2	0.32	0.63	22.81	265.34	136.83
A-R4-P3	A	t23	R4	63.2	7.895	20.3	2.3	1.67	0.78	12.56	113.81	122.08
A-R4-P4	A	t30	R4	60.3	7.891	20.8	2.1	0.28	0.16	1.58	46.88	37.45
A-R4-P5	A	t37	R4	60.5	7.881	19.7	2.8	0.85	0.67	0.14	16.49	6.25
A-R4-P6	A	t44	R4	61.2	7.953	19.9	5.4	0.17	0.19	0.91	68.02	0.8
A-R4-P7	A	t51	R4	61.5	7.727	20.3	2.6	0.33	0.21	2.52	77.86	1.22
A-R4-P8	A	t58	R4	61.8	7.993	20	5	0.25	0.22	0.83	30.18	2.35

A-R5-P1	A	t9	R5	61.6	7.866	19.9	1.6	0.62	0.35	40.54	370.04	100.11
A-R5-P2	A	t16	R5	63	8.075	20.3	0.1	0	0.61	36.84	338.98	114.03
A-R5-P3	A	t23	R5	64.5	8.148	20.6	1	0.72	0.56	26.94	197.34	119.36
A-R5-P4	A	t30	R5	60.9	7.996	19.7	2.9	3.1	0.58	3.17	65.09	122.32
A-R5-P5	A	t37	R5	60.1	7.907	19.6	3	1.16	1.13	1.59	41.38	102.78
A-R5-P6	A	t44	R5	61.8	7.935	19.7	0.8	0.14	0.09	10.19	203.62	121.48
A-R5-P7	A	t51	R5	61.9	7.675	19.8	1.5	0.39	0.37	8.15	126.75	93.01
A-R5-P8	A	t58	R5	61.4	7.675	20.2	1.9	0.2	1.03	4.15	107.88	35.82
A-R6-P1	A	t9	R6	61.3	8.046	19.6	0.1	0.87	0.46	38.01	424.42	108.01
A-R6-P2	A	t16	R6	62.8	8.22	20.2	0.1	0.02	0.27	62.25	378.64	127.11
A-R6-P3	A	t23	R6	66.1	8.253	20.6	1.4	2.34	0.47	45.79	340.4	115.87
A-R6-P4	A	t30	R6	65.7	8.192	19.8	1.3	0	0.66	36.74	288.43	116.32
A-R6-P5	A	t37	R6	65.3	7.852	19.5	2.3	0.16	0.43	22.88	207.35	126.49
A-R6-P6	A	t44	R6	64.9	7.998	20.2	2.6	0.49	0.35	10.52	169.39	113.75
A-R6-P7	A	t51	R6	63.3	7.839	20.2	3	1.12	1.4	3.37	100.05	24.65
A-R6-P8	A	t58	R6	62.8	7.975	19.9	4.7	0.17	0.11	3.23	103.11	1.96
W-R1-P1	W	t9	R1	61.2	8.105	19.9	0.3	0.51	0.24	38.58	333.12	104.08
W-R1-P2	W	t16	R1	64.7	8.092	21.4	0.7	0.13	0.09	29.01	271.56	124.63
W-R1-P3	W	t23	R1	70.6	7.963	23	0.8	1.86	0.15	24.47	192.28	124.02
W-R1-P4	W	t30	R1	71.4	7.892	24.2	0.9	0.19	0.44	25.08	193.13	131.05
W-R1-P5	W	t37	R1	75.6	8.002	23.5	1.1	0	0.54	27.35	265.27	123.43
W-R1-P6	W	t44	R1	75.6	7.904	24	0.7	0	0.33	21.4	235.25	121.66
W-R1-P7	W	t51	R1	67.7	7.956	23.8	2.1	0.12	0.36	12.14	160.68	100.98
W-R1-P8	W	t58	R1	64.4	7.83	24.6	1.7	0.3	0.33	8.17	153.32	80.08
W-R3-P1	W	t9	R3	61.7	7.603	20	0.7	0.42	1.36	47.67	422.13	95.87
W-R3-P2	W	t16	R3	65.8	8.177	21.2	0.4	0	0.51	64.19	437.57	98.17
W-R3-P3	W	t23	R3	71.6	8.124	23.1	0.1	1.59	0.2	43.02	293.97	116.58
W-R3-P4	W	t30	R3	72.6	7.942	24	0.9	0.24	0.5	21.76	109.16	132.66
W-R3-P5	W	t37	R3	80.6	8.044	23.8	1.2	1.47	0.49	13.18	127.05	110.4
W-R3-P6	W	t44	R3	69.2	7.919	24	1.5	0	0.11	12.98	164.34	90.86
W-R3-P7	W	t51	R3	63.6	8.048	23.6	3.9	0.52	0.33	10.38	174.11	36.92
W-R3-P8	W	t58	R3	77.1	7.917	24.6	1.9	0.14	0.08	8.12	192.57	2.64

W-R4-P1	W	t9	R4	63.5	8.156	20	0.1	0.43	0.33	68.32	464.36	89.01
W-R4-P2	W	t16	R4	65.3	8.147	21.4	0.7	0.47	0.91	33.63	299.45	124.56
W-R4-P3	W	t23	R4	68	8.115	23	0.8	1.55	0.17	24.32	230.99	131.86
W-R4-P4	W	t30	R4	67.3	7.841	24.1	0.3	0.35	0.69	12.54	93.26	125.25
W-R4-P5	W	t37	R4	75.2	7.891	23.5	2.1	1.73	0.59	12.3	121.74	115.37
W-R4-P6	W	t44	R4	65	7.902	24.1	1	1.6	0.13	8.43	204.8	105.12
W-R4-P7	W	t51	R4	65.2	8.11	23.8	6.1	0.72	1.29	2.93	70.41	30.36
W-R4-P8	W	t58	R4	65.2	7.751	24.5	2.2	0.42	0.52	2.59	119.27	23.71
W-R5-P1	W	t9	R5	60.4	7.951	19.8	1	3.09	2.79	6	77.71	82.42
W-R5-P2	W	t16	R5	65.7	8.155	21.4	1.1	0.08	0.16	25.25	298.36	136.56
W-R5-P3	W	t23	R5	70.6	8.049	23.2	0.6	1.63	0.19	33.47	249.77	123.39
W-R5-P4	W	t30	R5	62	8.029	24.3	0.6	0.16	0.12	30.7	243.5	129.07
W-R5-P5	W	t37	R5	82.2	7.987	23.8	1	0.77	0.2	29.03	267.35	128.91
W-R5-P6	W	t44	R5	74	7.977	24.3	1.7	0.38	0.17	27.29	271.85	124.05
W-R5-P7	W	t51	R5	74.2	7.981	23.9	2.4	0.28	0.32	16.65	217.61	99.47
W-R5-P8	W	t58	R5	65.4	7.986	24.5	3.6	0.15	0.43	9.79	158.18	74.04
W-R6-P1	W	t9	R6	61.3	8.184	20.1	0.1	0.43	0.71	43.04	408.88	96.89
W-R6-P2	W	t16	R6	63.8	NA	20.6	NA	0.21	0.12	26.08	267.86	128.04
W-R6-P3	W	t23	R6	66.7	8.061	23	0.6	0.23	0.12	21.13	150.12	131.44
W-R6-P4	W	t30	R6	66.8	7.968	24.1	3.5	3.21	0.49	12.31	95.02	131.85
W-R6-P5	W	t37	R6	69.6	8.002	23.6	0.9	0.87	0.12	11.72	190.65	131.04
W-R6-P6	W	t44	R6	69.4	7.78	24.2	1.4	0.26	0.17	12.13	139.94	114.18
W-R6-P7	W	t51	R6	68.8	7.902	23.7	4.4	0.25	0.46	8.13	122.96	94.12
W-R6-P8	W	t58	R6	64.7	7.885	24.5	2.2	0.23	0.29	5.17	119.36	70.55
WA-R2-P1	WA	t9	R2	62.2	7.959	20.9	0.7	2.26	2.71	9.79	140.17	110.88
WA-R2-P2	WA	t16	R2	67.6	8.111	20.8	0.3	0.4	0.12	47.95	452.06	104.42
WA-R2-P3	WA	t23	R2	83.2	8.111	23.9	0.1	0.13	0.22	46.3	346.57	106.65
WA-R2-P4	WA	t30	R2	66.5	7.924	23.9	1.4	0.84	1.61	13.81	135.16	135.25
WA-R2-P5	WA	t37	R2	61.2	7.789	23.4	0.7	0.45	0.51	2.4	75.35	100.57
WA-R2-P6	WA	t44	R2	62.5	7.842	23.5	0.6	2.29	0.21	7.56	144.85	117.98
WA-R2-P7	WA	t51	R2	63.1	7.785	23.5	0.7	0.2	0.04	8.15	172.24	102.53

WA-R2-P8	WA	t58	R2	64.1	7.822	24.6	2.9	0.31	0.28	7.68	125.07	91.14
WA-R3-P1	WA	t9	R3	61.3	7.947	21.1	0.4	0.32	0.08	12.09	277.05	120.95
WA-R3-P2	WA	t16	R3	65.4	8.045	21	0.1	0.16	0.1	19.62	322.75	136.29
WA-R3-P3	WA	t23	R3	68.8	7.924	23.1	0.6	0.17	0.31	13.97	177.08	126.83
WA-R3-P4	WA	t30	R3	66.8	7.764	23.8	1.1	0.35	0.41	6.42	81.11	94.61
WA-R3-P5	WA	t37	R3	69	7.946	23.3	0.9	0.14	0.11	11.74	213.06	125.8
WA-R3-P6	WA	t44	R3	66	7.78	23.5	1.1	0.11	0.26	4.99	148.94	83.51
WA-R3-P7	WA	t51	R3	68.3	7.896	23.7	1.1	0.27	0.18	11.67	238.31	117.47
WA-R3-P8	WA	t58	R3	69.9	7.92	24.3	2.1	0.11	0.12	12	231	101.98
WA-R4-P1	WA	t9	R4	61	8.129	21	0.3	0.91	0.19	24.34	361.92	118.61
WA-R4-P2	WA	t16	R4	66.6	8.085	20.9	1	0.79	0.14	26.79	244.59	134.04
WA-R4-P3	WA	t23	R4	71.4	8.034	24.1	0.6	0.21	0.13	34.86	201.99	120.02
WA-R4-P4	WA	t30	R4	76.8	8.061	24.5	0.8	2.24	0.12	31.1	201.43	130.35
WA-R4-P5	WA	t37	R4	65.5	7.943	23.6	1.9	0.7	0.21	10.9	119.13	115.48
WA-R4-P6	WA	t44	R4	66.4	7.819	23.9	2.1	0.43	0.13	7.53	161.54	83.95
WA-R4-P7	WA	t51	R4	69.3	8.028	23.6	3.7	3.07	0.29	11.82	172.58	82.87
WA-R4-P8	WA	t58	R4	63.8	7.947	24.6	4.7	0.3	0.27	6.41	125.69	38.09
WA-R5-P1	WA	t9	R5	62.1	8.019	21	0.7	1.12	0.38	44.66	363.08	89.68
WA-R5-P2	WA	t16	R5	64.7	7.946	21.3	0.4	0.08	0.29	28.9	221.06	120.73
WA-R5-P3	WA	t23	R5	NA	7.997	23.1	0.1	0.14	0.16	33.71	210.61	110.68
WA-R5-P4	WA	t30	R5	69.8	7.832	24.2	0.8	0.39	0.16	22	170.61	126.73
WA-R5-P5	WA	t37	R5	66.4	7.932	23.2	0.8	0.64	0.43	14.57	132.41	132.92
WA-R5-P6	WA	t44	R5	64.2	7.705	23.5	1.2	1.91	0.19	6.97	88.95	111.66
WA-R5-P7	WA	t51	R5	64.6	7.869	23.7	0.5	0.27	0.18	10.29	146.97	118.11
WA-R5-P8	WA	t58	R5	62.6	7.948	24.2	3.9	0.72	0.45	2.99	64.09	49.8
WA-R6-P1	WA	t9	R6	60.5	7.873	20.9	0.3	1.02	0.68	25.13	273.39	120.84
WA-R6-P2	WA	t16	R6	65.2	8.038	21.2	0.1	0.2	0.2	31.53	288.94	128.31
WA-R6-P3	WA	t23	R6	69.9	8.058	23.8	0.1	0.29	0.37	36.1	251.7	116.45
WA-R6-P4	WA	t30	R6	66.4	7.865	24.4	0.1	0.16	0.09	15.39	103.28	135.38
WA-R6-P5	WA	t37	R6	62.9	7.815	23.9	0.9	0.18	0.37	9.2	118.28	126.52
WA-R6-P6	WA	t44	R6	65.5	7.725	24.2	0.1	0.09	0.16	12.11	188.69	122.67
WA-R6-P7	WA	t51	R6	67.4	7.768	24.2	1.2	0.26	0.24	8.78	155.27	93.56

WA-R6-P8	WA	t58	R6	65.1	7.912	24.7	4.6	0.47	0.48	3.59	78.29	15.98
----------	----	-----	----	------	-------	------	-----	------	------	------	-------	-------

Fig. B: Physico-chemical parameters measured for each replicate of each treatment and at each sampling time.

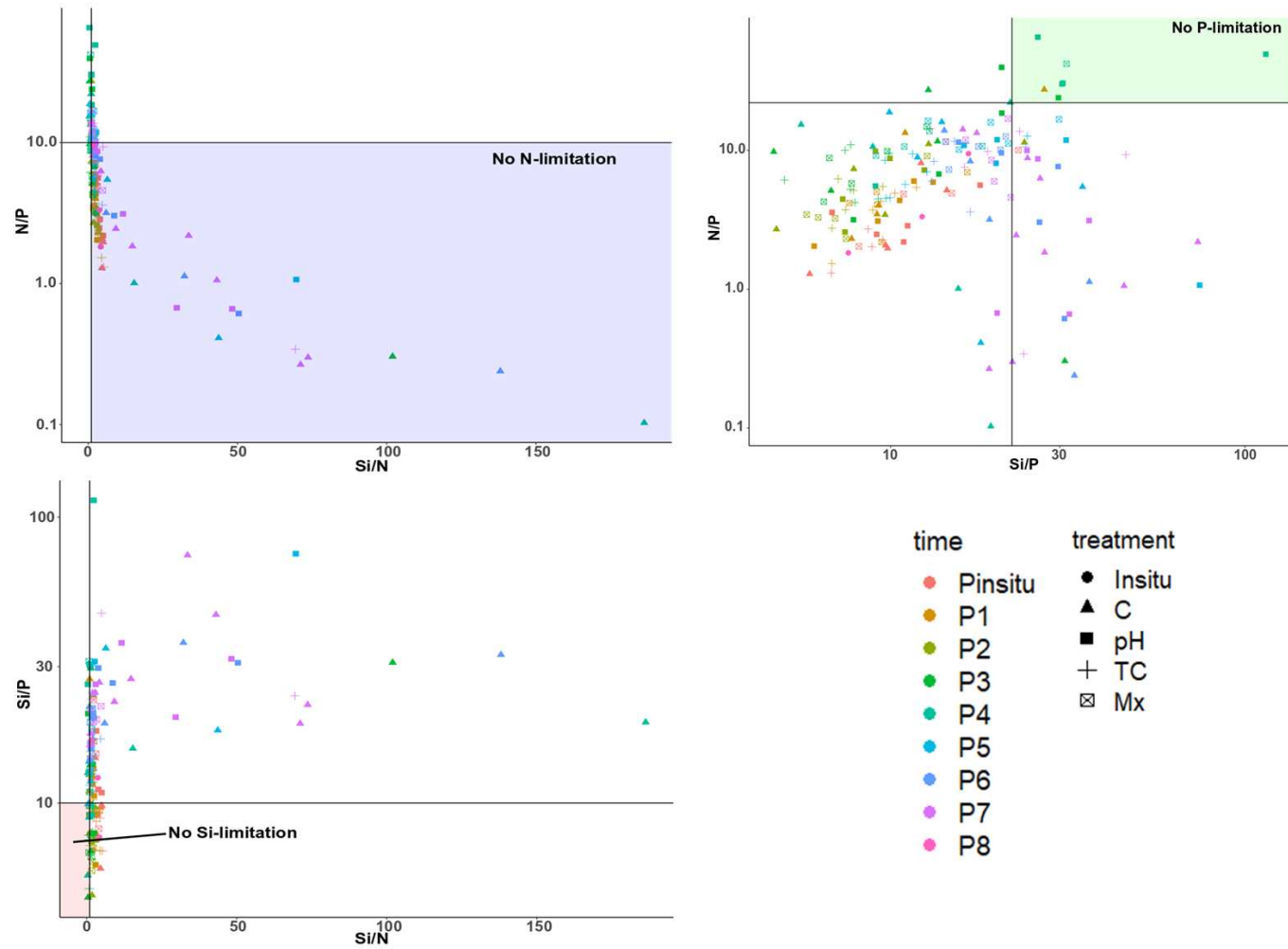


Fig. C: Redfield ratio determining (A) the limitation of nitrogen, (B) the limitation of phosphate and (C) the limitation of silicon in the mesocosms' water. The samples present in the coloured parts correspond to samples where no limitation of nitrogen, phosphate or silicon occurred.

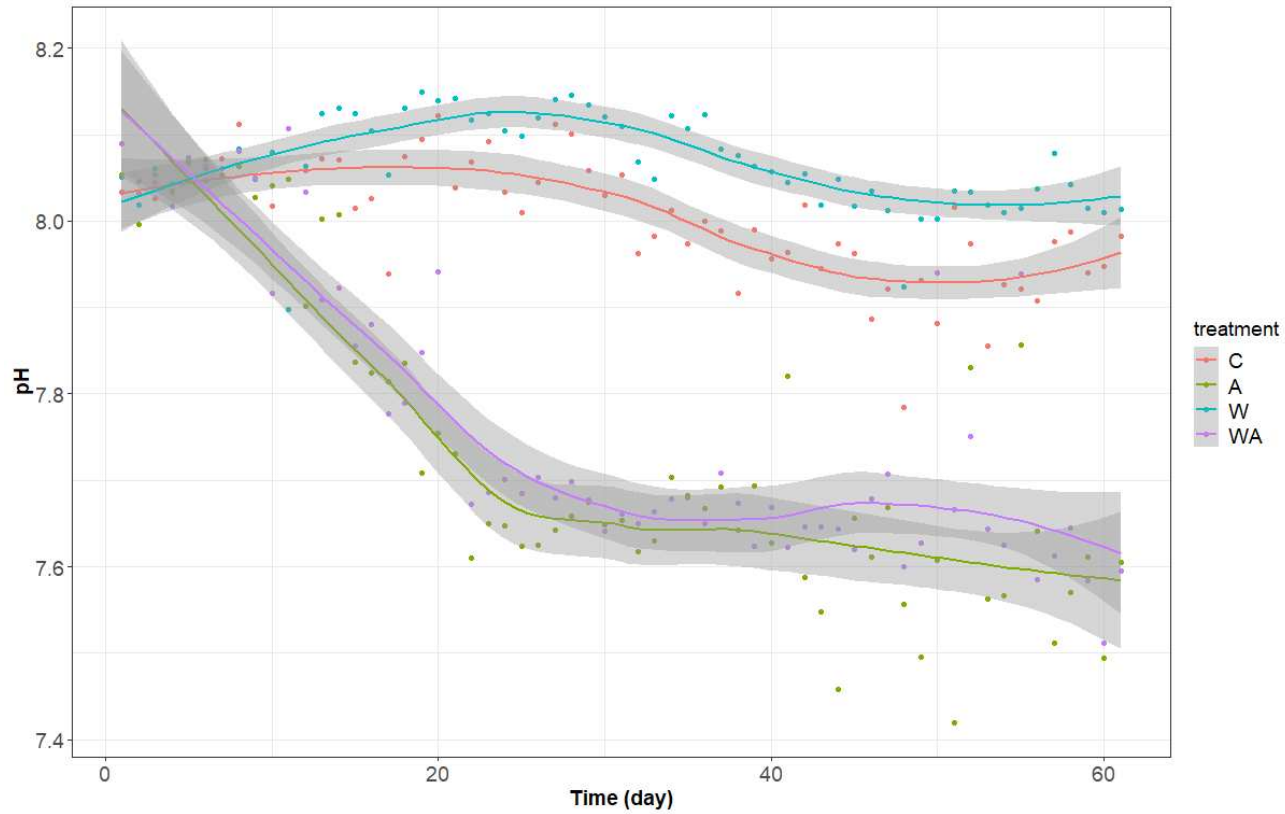


Fig. D: Temporal variation of the the pH (upH) of the water reserve of the different treatments (control (C), acidification (A), warming (W) or mix warming and acidification (WA)). The points correspond to the values measured for each sample. The curves represent local regressions, based on the k-nearest neighbors algorithm (*geom_smooth* function of the ggplot2 package, loess method). The grey areas symbolise the 95% confidence intervals. The day 0 to day 8 correspond to the stabilisation week.

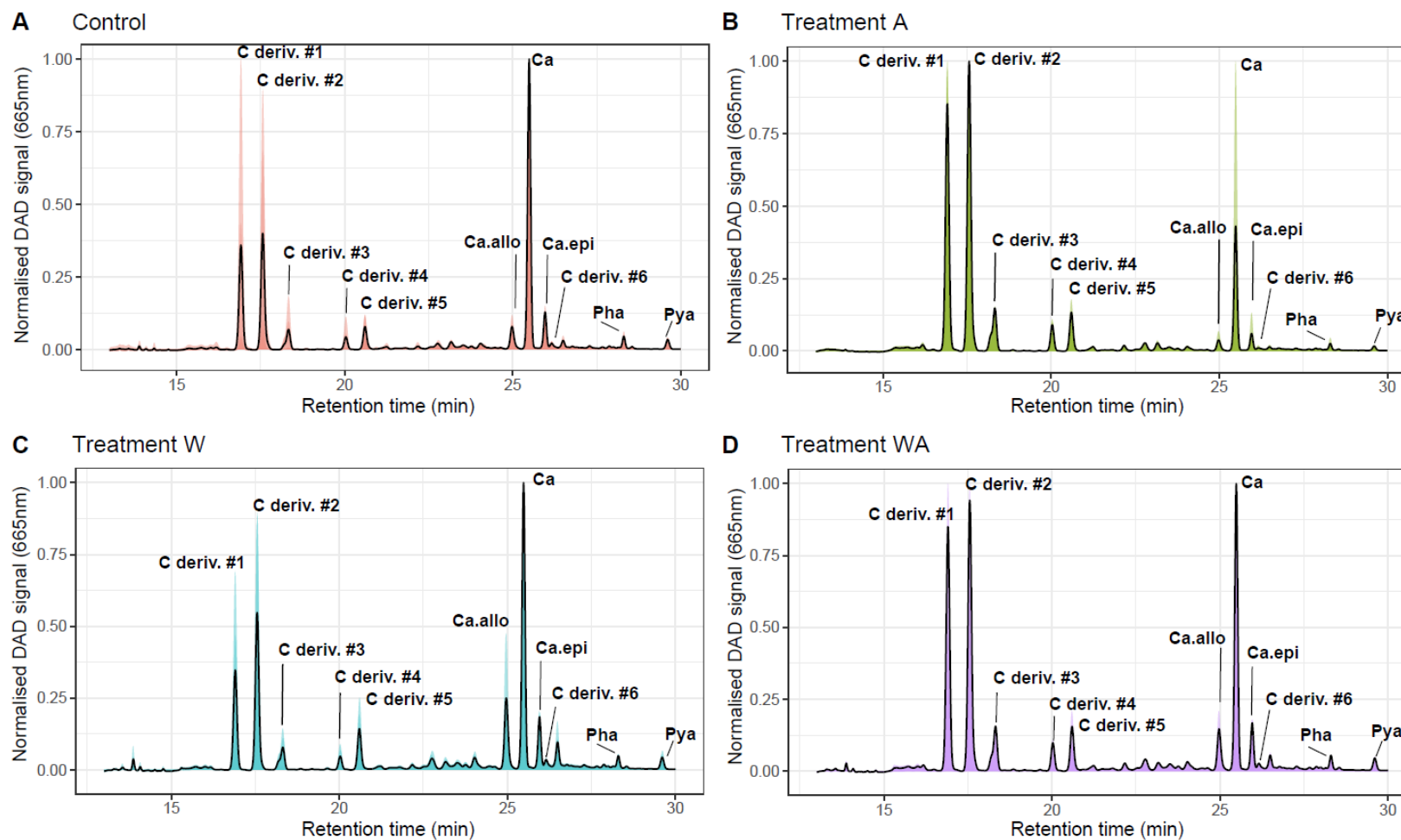


Fig. E: Normalised signal recorded by the HPLC DAD detector at 665 nm. Each panel represents an experimental treatment (Control, A= acidification, W=warming, WA = acidification and warming). All replicates (n=5 for each treatment) were superimposed and an average signal was calculated (black line). Chromatograms start at 13 min for better visualisation. No significant peaks were detected before this retention time at 665 nm.

3. Conclusions and perspectives

Ocean acidification simulated in mesocosms impacted the phototrophs of the microbial mats. A decrease of the chlorophyll *a* abundance and an increase of bound extracellular carbohydrates were observed, revealing an impact on oxygenic phototrophs, mostly represented by *Cyanobacteria*. In parallel, a decrease of unknown molecules, defined as chlorophyll derivatives, was reported. These molecules were supposed to be bacteriochlorophyll *c*, a pigment contained in the chlorosomes of green anoxygenic phototroph bacteria. These observations underlined either a modification of the phototrophic communities, with a higher relative abundance of green anoxygenic bacteria or a lower relative abundance of *Cyanobacteria*, or a change in the metabolism of these communities, producing more bacteriochlorophyll *c* and less chlorophyll *a*. These could result in anoxygenic photosynthesis more competitive than the oxygenic photosynthesis. The increase of bound carbohydrates EPS certainly pointed out the establishment of protection by *Cyanobacteria*, the first microorganisms of the microbial mats in contact with the seawater, face to acidification.

This study revealed that the phototrophs in microbial mats are affected by acidification but water warming had no effect, certainly because these communities already face these conditions in their natural environment. Moreover, water warming seemed to decrease the effect of acidification, when the microbial mats were exposed to both. However, climate change should be placed on a long-term that allows microbial communities to reach a point where resilience will not be more possible. It cannot be excluded that acidification will finally impact the phototrophic communities as demonstrated in this chapter. These changes in the abundance of some communities, or their metabolisms, probably result to a modification of the photosynthetic capacities of the microbial mats. In turn, such modification probably changes the biogeochemical cycles, as for instance the reduction of oxygen production when *Cyanobacteria* are impacted.

Chapter VII: Conclusions and perspectives

The different simulated climate scenarios impacted microbial mats through their diversity, structure and function (**Fig. 33**). Acidification alone impacted prokaryotic communities while temperature alone affected eukaryotic populations (**Fig. 33**). These two treatments together delayed the climate change impact (**Fig. 33**).

In situ monitoring of the diversity and structure of the microbial mats present in the salt marshes of the Ré Island has shown that some of the natural conditions they face are comparable to those predicted by the IPCC for 2100 (IPCC, 2014). For example, climate change is expected to cause surface water to warm by about 4°C (IPCC, 2014). However, the surface water temperatures to which the microbial mats are currently subjected can be similar or even higher than those predicted by the IPCC depending on the season: if the temperature is currently 20°C in spring, it will reach 24°C in 2100, which is already the case in summer at present. Therefore, microbial mats already have a natural resilience to variations in this parameter with amplitudes equal to or greater than 4°C. This is probably why few impacts were observed on the microbial mats on the Ré Island following the mesocosm study. However, even if the microbial mat can cope with temperatures of +4°C in 2100 in spring, this warming must be added to each season. Thus, a microbial mat that is "used to" temperatures of 20°C in spring will have to face 24°C in the same season at the end of the century, and this for each season. The temperature range, that the microbial mat will face, will thus be modified with a different intensity and frequency. It can be assumed that a microbial mat that is currently observed in spring will resemble one that is currently observed in summer in 2100. It will also be confronted with warmer temperatures that it may not have to deal with in summer.

As salt marshes are shallow environments, the water temperature is dependent on the air temperature. Daily variations can be very significant, sometimes exceeding ten degrees in this region (marked day/night difference). The surface water temperature in the mesocosms was maintained at a defined temperature (20°C or 24°C to simulate warming) and the mats present did not, therefore, face this daily temperature variation. It would be interesting to test the impact of this temperature amplitude through mesocosms. Indeed, the microbial mats were

able to adapt their functioning to the simulated warming because the temperature was constant, but perhaps some communities or metabolisms could have been affected, positively or negatively, if a simulation of the temperature variation had been implemented.

The choice of carrying out the water acidification was made in the water reserve distributing the seawater to the different mesocosms, instead of acidifying the mesocosm water directly. Indeed, the water in the salt marshes depends on the oceanic input according to the tides and this water reserve, therefore, represented "the ocean". We were able to see that the microbial mats could buffer the pH at its initial level despite the acidified water (Mazière et al., 2022). However, some improvements could be made to the system. A day/night pH monitoring could inform us on the daily pH variation, which perhaps at night would not be buffered anymore with the stop of phototrophic metabolisms, which would mean that the microbial communities would be directly in contact with acidified water. This could explain why, despite maintaining the pH in the system at initial levels, an increase in bound sugar EPS, supposed to have a protective role (Dupraz and Visscher, 2005; Hubas, 2018; Mazière et al., 2022; Prieto-Barajas et al., 2018), is observed. A continuous acidified seawater supply system, or a pre-reserve where the water is acidified, would also be of interest as the system tested was manual and there was a time interval before all newly arrived water was acidified. It could also have been envisaged to build a bell system where the concentration of greenhouse gases (the main ones being CO₂ and CH₄) would be increased but this method presents many biases including the time of exchange of gases between air and water, thus the time of acidification, and also the gases used since the two mentioned gases are not the only ones, it would thus be necessary to have a multiple gas diffusion system with very precise devices to control their concentration. Thus, the addition of CO₂ to the water is much simpler, but the addition of other gases could be considered. A degassing of the system can be assumed, so a perhaps more closed enclosure around the reserve could be considered to avoid too much degassing and save the gas used, but this poses the problem of exchange with atmospheric gases.

Seasonal monitoring has also shown that temperature and pH can vary according to the season, depending on natural phenomena such as precipitation, tides, *etc.* It would be interesting to simulate these environmental and climatic effects. In addition, other changes are predicted, such as rising sea levels, alternating extreme events, *etc.* This study should therefore be completed with these other parameters.

It is also important to note that the simulation of climate change on the microbial mats in this study lasted only 2 months. However, these changes have already started to take place (the 2014 IPCC report already mentioned climate change, confirmed by the 2021 report) and will continue to take place over several years. Thus, it is possible to imagine that microbial mats will be able to adapt better to climate change in their natural environment than over a smaller period like our experiment, or on the contrary that the combination of the different changed factors will affect them too much to change their structure and functioning and that they will reach their resilience point. It is very complicated to set up manipulations simulating climate change, partly because of the cost, time and personnel involved, and partly because, even if we were able to simulate the natural environment of the current and future microbial mat perfectly, the data for setting up the simulations are predictions and are constantly changing. However, these simulations are extremely important to clarify the data and to give an idea of the major impacts that could potentially take place.

Whatever the scenario, future microbial mats will be different from current mats because climate change is occurring and will continue. So-called "generalist" communities, *i.e.*, those that do not have a specific ecological niche and can adapt to different environmental conditions, will certainly not be affected, or will become more specialised. However, the so-called "specialist" communities, with a restricted ecological niche and evolving according to specific conditions with defined metabolisms, will be impacted because if their environment is modified (*i.e.*, their ecological niche) they will surely disappear, unable to adapt. However, in the same way, it may also favour the emergence of new specialist communities. It should also

be noted that a generalist population is in any case composed of specialist individuals because they can do whatever metabolism they want at any given time.

Regarding the methodology applied, the Illumina analyses carried out by targeting universal eukaryotic, bacterial and archaeal 16S rRNA genes showed numerous biases, such as the low amplification of cyanobacterial communities, despite the study of photosynthetic microbial mats, but they did provide a first general overview of the microbial communities present. The amplification of specific genes could be considered to target more specific communities, such as ITS (internal transcribed spacer) for fungi (Schoch et al., 2012), cytochrome *c* oxidase subunit 1 (COI) gene for animals (Hebert et al, 2003), prokaryotic functional genes like *dsrB* for sulphate-reducers (Müller et al., 2015; Pelikan et al., 2015), *mcrA* for methanogens (Luton et al., 2002; Yang et al., 2014), *nifH* for nitrogen-fixing bacteria (Gaby and Buckley, 2014; Turk et al., 2011), *etc.* However, the specific databases to these genes are often incomplete and not updated very often. It would be more interesting to carry out metagenomics to reconstruct the genomes present in the environment and to determine all the genes present, giving us information on the functions that may be carried out. This analysis should be combined with functional omics methods. RNA analysis and sequencing via cDNA could be considered but not all RNAs end up producing molecules. Metabolomic, proteomic or volatolomic studies would provide more precise information on the molecules metabolised. However, it must be borne in mind that this information is only valid at the time of sampling, as the functions of a cell change all the time. The combination of genomic and functional omics methods would provide information on the fundamental niche and the realised niche respectively. This would make it possible to determine which communities are generalists and which are specialists.

Recently, it has been observed that the microbial mats studied during this thesis are likely to precipitate carbonates. Dupraz *et al.* (2009) showed that this metabolism took place during the day thanks to the photosynthesis of oxygenic phototrophs (notably cyanobacteria) and thanks to sulfate reduction at night. In the microbial mats of the Ré Island in this study, the

precipitation layer would be located between the layer composed of anoxygenic phototroph bacteria and the layer of oxygenic phototrophs. Further analyses are underway. However, if this is demonstrated, the microbial mats could be considered as carbon sinks. It is possible to imagine that the addition of carbon to the medium would promote photosynthesis and thus precipitation. Nevertheless, we observed that acidification impacted the phototrophic communities of the microbial mats, leading either to a change in the community or to a metabolic modification potentially impacting photosynthesis in the long term. If the presence of oxygenic phototrophs or their photosynthesis decrease, it is quite possible that the precipitated carbon will be dissolved, leading to its release into the atmosphere. It would therefore be interesting to focus on this axis to determine the resilience point of carbon sequestration.

This experiment should be repeated on other microbial mats on the Ré Island and in the Nouvelle-Aquitaine region to better understand the impact of climate change because this region presents various environments, which suggests the presence of different microbial mats and therefore different behaviours. Seasonal monitoring should also be considered because, as shown in this thesis, the seasonality of environmental parameters impacts microbial mats and explain their behaviour in the face of climate change. Mats are very diverse around the world. It would therefore be interesting to extend this study to the global scale level.

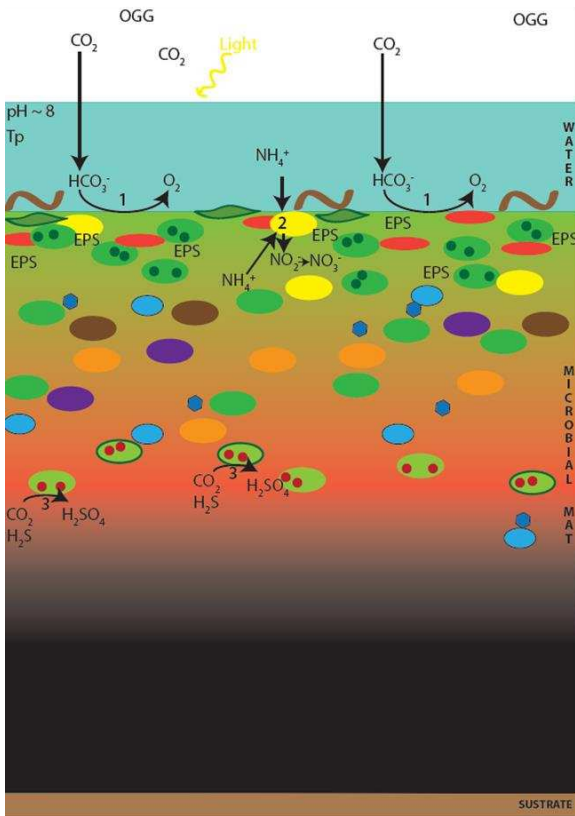
The interest of these studies and manipulations would ultimately be to find bioindicators, *i.e.*, living organisms, which, by their presence or absence, abundance or rarity, allow the degree of disturbance or pollution of an environment to be assessed. The determination of particular bioindicator molecules is to be considered, for example, acidification impacted the pigment composition, leading to the appearance of unknown molecules, probably bacteriochlorophyll *c* (Mazière et al., 2022).

In 2021, a new IPCC report (Working Group I Sixth Assessment Report, AR6-WGI) has been published where five climate change scenarios are defined. The least pessimists, SSP1-1.9 and SSP1-2.6, correspond to scenarios where greenhouse gas (GHG) emissions are very

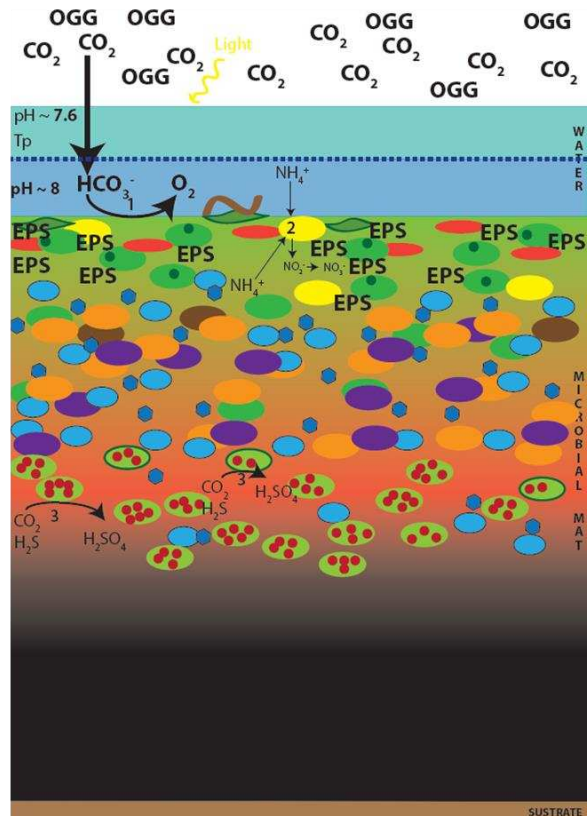
low (SSP1-1.9) and low (SSP1-2.6), and CO₂ emissions decline to net zero around or after 2050, followed by varying levels of net negative CO₂ emissions (IPCC, 2021). SSP2-4.5 is the intermediate scenario predicting that GHG emissions will be intermediate between the least and the most pessimistic scenarios and CO₂ emissions remain around current levels until the middle of the century (IPCC, 2021). The most pessimistic scenarios are SSP3-7.0 and SSP5-8.5 where high and very high GHG emissions occur, and CO₂ emissions are approximately double from the current levels by 2100 and 2050 (IPCC, 2021).

In Europe, IPCC (2021) predicts that temperature will rise in all areas with a rate higher than those of the global mean temperature changes (similar to past observations). Hot extremes, including marine heatwaves, will be more frequent and more intense and cold spells and frost days will be less observed (IPCC, 2021). The Nouvelle-Aquitaine region was classified into two zones defined by the IPCC in the AR6-WGI report: the western and central Europe (WCE) containing the north of the region, with the Ré Island, and the Mediterranean (MED) zone holding the south of the region (IPCC, 2021). The WCE is projected to face more pluvial flooding and extreme precipitation, river flooding, sea level rise and hydrological, agricultural and ecological droughts (IPCC, 2021). Along the French Atlantic coasts, coastal flooding is projected because of extreme sea level events more frequent and more intense and shorelines along sandy coasts will retreat throughout the 21st century (IPCC, 2021). These new predictions are more accurate than the previous ones, especially as they include a more detailed local view. It would therefore be interesting to test these new parameters in order to evaluate more precisely the impact of climate change on the microbial mats of the Nouvelle-Aquitaine region.

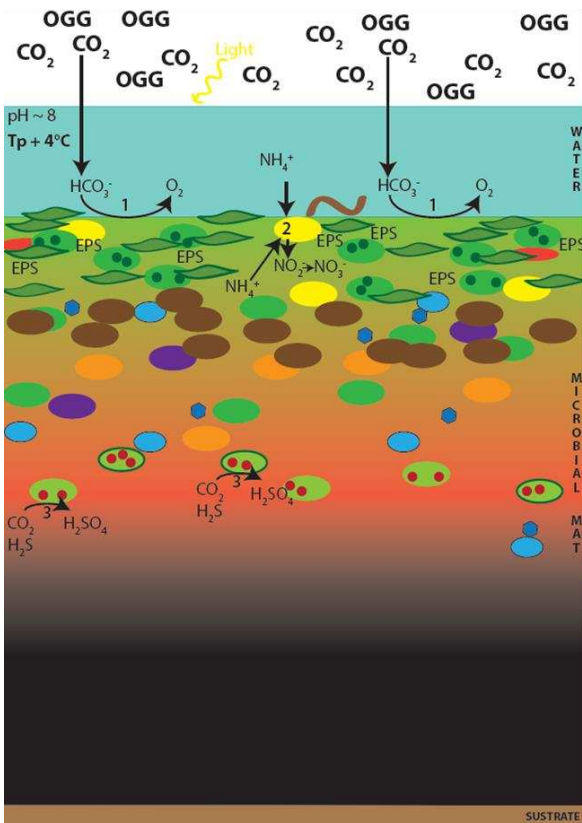
Actual



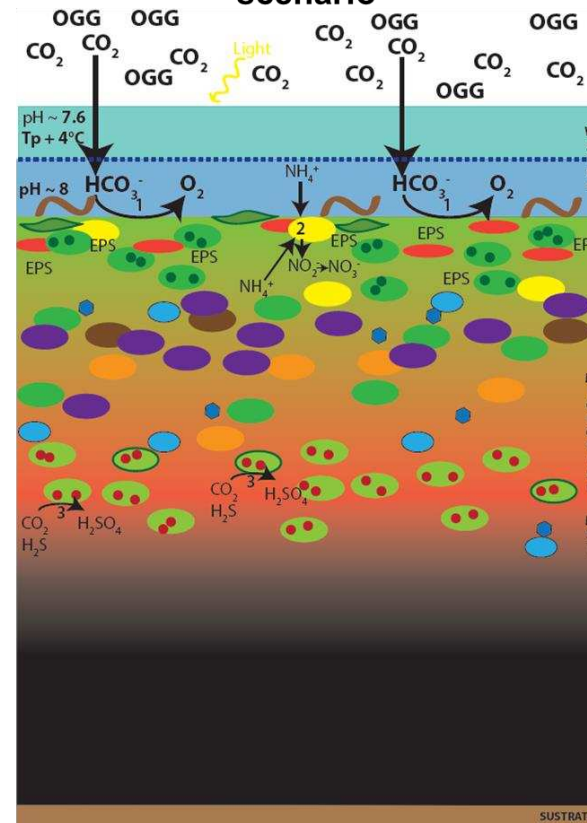
Acidification scenario



Warming scenario



Acidification and warming scenario



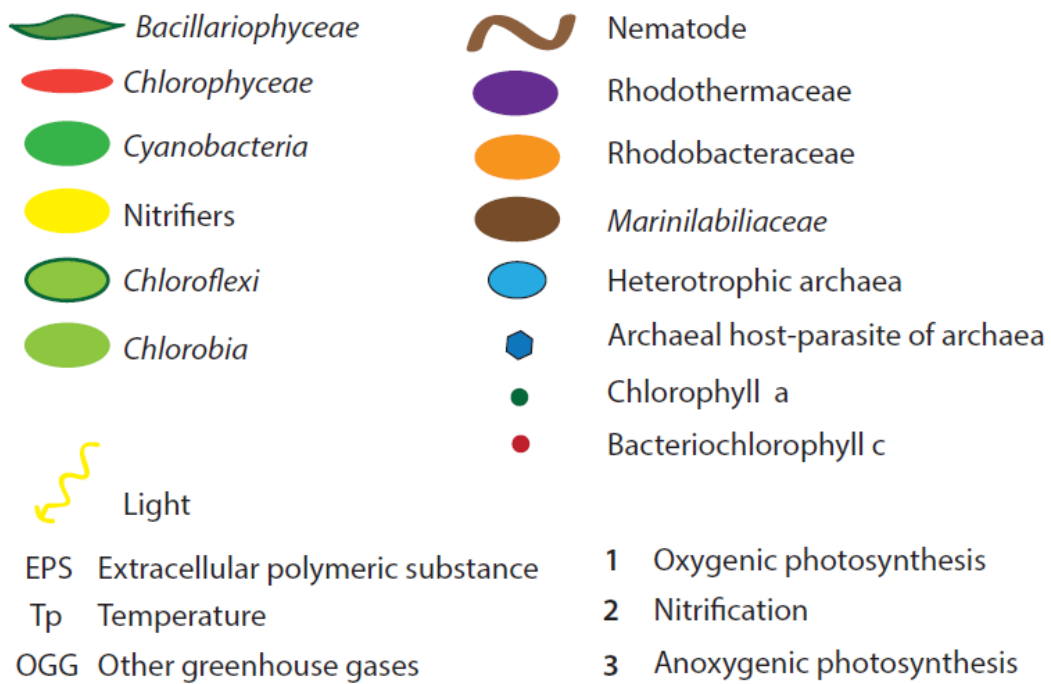


Figure 33: Graphical conclusion. The results of this thesis were represented in a schematic view. The actual microbial mat in its environment and the impact of the three climate scenarios (acidification, warming, both acidification and warming) are illustrated. For clarity, only the part of the microbial mat where an effect was observed is designed (*e.g.*, the communities and metabolisms not impacted are not present). Elements in bold signify that their quantity/presence were more important than in the actual scenario, and on the contrary, the small prints correspond to their diminution.

References

- Abed, Raeid M. M., Kohls, K., de Beer, D., 2007. Effect of salinity changes on the bacterial diversity, photosynthesis and oxygen consumption of cyanobacterial mats from an intertidal flat of the Arabian Gulf. *Environ. Microbiol.* 9, 1384–1392. <https://doi.org/10.1111/j.1462-2920.2007.01254.x>
- Abed, R.M.M., Kohls, K., Leloup, J., de Beer, D., 2018a. Abundance and diversity of aerobic heterotrophic microorganisms and their interaction with cyanobacteria in the oxic layer of an intertidal hypersaline cyanobacterial mat. *FEMS Microbiol. Ecol.* 94. <https://doi.org/10.1093/femsec/fix183>
- Abed, R.M.M., Palinska, K.A., Köster, J., 2018b. Characterization of Microbial Mats from a Desert Wadi Ecosystem in the Sultanate of Oman. *Geomicrobiol. J.* 35, 601–611. <https://doi.org/10.1080/01490451.2018.1435755>
- Abed, Raeid M.M., Zein, B., Al-Thukair, A., de Beer, D., 2007. Phylogenetic diversity and activity of aerobic heterotrophic bacteria from a hypersaline oil-polluted microbial mat. *Syst. Appl. Microbiol.* 30, 319–330. <https://doi.org/10.1016/j.syapm.2006.09.001>
- Aguilera, Á., Souza-Egipsy, V., González-Toril, E., Rendueles, O., Amils, R., 2010. Eukaryotic microbial diversity of phototrophic microbial mats in two Icelandic geothermal hot springs. *Int. Microbiol.* 29–40. <https://doi.org/10.2436/20.1501.01.108>
- Ahrendt, S., Mobberley, J., Visscher, P., Koss, L., Foster, J., 2014. Effects of Elevated Carbon Dioxide and Salinity on the Microbial Diversity in Lithifying Microbial Mats. *Minerals* 4, 145–169. <https://doi.org/10.3390/min4010145>
- Alexander, E., Stock, A., Breiner, H.-W., Behnke, A., Bunge, J., Yakimov, M.M., Stoeck, T., 2009. Microbial eukaryotes in the hypersaline anoxic L'Atalante deep-sea basin. *Environ. Microbiol.* 11, 360–381. <https://doi.org/10.1111/j.1462-2920.2008.01777.x>
- Allwood, A.C., Walter, M.R., Kamber, B.S., Marshall, C.P., Burch, I.W., 2006. Stromatolite reef from the Early Archaean era of Australia. *Nature* 441, 714–718. <https://doi.org/10.1038/nature04764>
- Amann, R.I., Ludwig, W., Schleifer, K.H., 1995. Phylogenetic identification and in situ detection of individual microbial cells without cultivation. *Microbiol. Rev.* 59, 143–169.
- Aminot, A., Kérouel, R., 2007. Dosage automatique des nutriments dans les eaux marines., Quae. ed.
- Andrady, A., Aucamp, P., Bais, A., Ballaré, C., Björn, L., Bornman, J., Caldwell, M., Cullen, A., de Gruijl, F., Erickson, D., Flint, S., Häder, D., Hamid, H., Ilyas, M., Kulandaivelu, G., Kumar, H., McKenzie, R., Longstreth, J., Lucas, R., Zepp, R., 2007. Environmental effects of ozone depletion: 2006 Assessment: Interactions of ozone depletion and climate change - Executive summary. *Photochem. Photobiol. Sci. Off. J. Eur. Photochem. Assoc. Eur. Soc. Photobiol.* 6, 212–7. <https://doi.org/10.1039/b700050m>
- Arévalo-Martínez, D.L., Kock, A., Löscher, C.R., Schmitz, R.A., Bange, H.W., 2015. Massive nitrous oxide emissions from the tropical South Pacific Ocean. *Nat. Geosci.* 8, 530–533. <https://doi.org/10.1038/ngeo2469>
- Asao, M., Pinkart, H.C., Madigan, M.T., 2011. Diversity of extremophilic purple phototrophic bacteria in Soap Lake, a Central Washington (USA) Soda Lake. *Environ. Microbiol.* 13, 2146–2157. <https://doi.org/10.1111/j.1462-2920.2011.02449.x>

- Azam, F., Malfatti, F., 2007. Microbial structuring of marine ecosystems. *Nat. Rev. Microbiol.* 5, 782–791. <https://doi.org/10.1038/nrmicro1747>
- Baker, B.J., Comolli, L.R., Dick, G.J., Hauser, L.J., Hyatt, D., Dill, B.D., Land, M.L., VerBerkmoes, N.C., Hettich, R.L., Banfield, J.F., 2010. Enigmatic, ultrasmall, uncultivated Archaea. *Proc. Natl. Acad. Sci.* 107, 8806–8811. <https://doi.org/10.1073/pnas.0914470107>
- Baker, B.J., Tyson, G.W., Webb, R.I., Flanagan, J., Hugenholtz, P., Allen, E.E., Banfield, J.F., 2006. Lineages of Acidophilic Archaea Revealed by Community Genomic Analysis. *Science* 314, 1933–1935. <https://doi.org/10.1126/science.1132690>
- Baragi, L.V., Anil, A.C., 2016. Synergistic effect of elevated temperature, pCO₂ and nutrients on marine biofilm. *Mar. Pollut. Bull.* 105, 102–109. <https://doi.org/10.1016/j.marpolbul.2016.02.049>
- Bauer, C., Elsen, S., Swem, L.R., Swem, D.L., Masuda, S., 2003. Redox and light regulation of gene expression in photosynthetic prokaryotes. *Philos. Trans. R. Soc. B Biol. Sci.* 358, 147–154. <https://doi.org/10.1098/rstb.2002.1189>
- Bauersachs, T., Compaoré, J., Severin, I., Hopmans, E.C., Schouten, S., Stal, L.J., Damsté, J.S.S., 2011. Diazotrophic microbial community of coastal microbial mats of the southern North Sea. *Geobiology* 9, 349–359. <https://doi.org/10.1111/j.1472-4669.2011.00280.x>
- Beardall, J., Stojkovic, S., Larsen, S., 2009. Living in a high CO₂ world: Impacts of global climate change on marine phytoplankton. *Plant Ecol. Divers.* 2, 191–205. <https://doi.org/10.1080/17550870903271363>
- Beatty, J.T., 2002. On the natural selection and evolution of the aerobic phototrophic bacteria. *Photosynth. Res.* 73, 109–114. <https://doi.org/10.1023/A:1020493518379>
- Beman, J.M., Chow, C.-E., King, A.L., Feng, Y., Fuhrman, J.A., Andersson, A., Bates, N.R., Popp, B.N., Hutchins, D.A., 2011. Global declines in oceanic nitrification rates as a consequence of ocean acidification. *Proc. Natl. Acad. Sci.* 108, 208–213. <https://doi.org/10.1073/pnas.1011053108>
- Ben Salem, F., Ben Said, O., Cravo-Laureau, C., Mahmoudi, E., Bru, N., Monperrus, M., Duran, R., 2019. Bacterial community assemblages in sediments under high anthropogenic pressure at Ichkeul Lake/Bizerte Lagoon hydrological system, Tunisia. *Environ. Pollut.* 252, 644–656. <https://doi.org/10.1016/j.envpol.2019.05.146>
- Benloch, S., Lopez-Lopez, A., Casamayor, E.O., Ovreas, L., Goddard, V., Daae, F.L., Smerdon, G., Massana, R., Joint, I., Thingstad, F., Pedrós-Alió, C., Rodríguez-Valera, F., 2002. Prokaryotic genetic diversity throughout the salinity gradient of a coastal solar saltern. *Environ. Microbiol.* 4, 349–360. <https://doi.org/10.1046/j.1462-2920.2002.00306.x>
- Berk, S.G., Brownlee, D.C., Heinle, D.R., Kling, H.J., Colwell, R.R., 1977. Ciliates as a food source for marine planktonic copepods. *Microb. Ecol.* 4, 27–40. <https://doi.org/10.1007/BF02010427>
- Bernard, C., Rassoulzadegan, F., 1990. (PDF) Bacteria or microflagellates as a major food source for marine ciliates: Possible implications for the microzooplankton [WWW Document]. ResearchGate. <http://dx.doi.org/10.3354/meps064147>
- Bjerg, J.T., Damgaard, L.R., Holm, S.A., Schramm, A., Nielsen, L.P., 2016. Motility of Electric Cable Bacteria. *Appl. Environ. Microbiol.* 82, 3816–3821. <https://doi.org/10.1128/AEM.01038-16>

- Black, J.G., Stark, J.S., Johnstone, G.J., McMinn, A., Boyd, P., McKinlay, J., Wotherspoon, S., Runcie, J.W., 2019. In-situ behavioural and physiological responses of Antarctic microphytobenthos to ocean acidification. *Sci. Rep.* 9, 1890. <https://doi.org/10.1038/s41598-018-36233-2>
- Boatman, T.G., Lawson, T., Geider, R.J., 2017. A Key Marine Diazotroph in a Changing Ocean: The Interacting Effects of Temperature, CO₂ and Light on the Growth of *Trichodesmium erythraeum* IMS101. *PLOS ONE* 12, e0168796. <https://doi.org/10.1371/journal.pone.0168796>
- Bolhuis, H., Fillinger, L., Stal, L.J., 2013. Coastal microbial mat diversity along a natural salinity gradient. *PLoS One* 8, e63166. <https://doi.org/10.1371/journal.pone.0063166>
- Bolhuis, H., Stal, L.J., 2011. Analysis of bacterial and archaeal diversity in coastal microbial mats using massive parallel 16S rRNA gene tag sequencing. *ISME J.* 5, 1701–1712. <https://doi.org/10.1038/ismej.2011.52>
- Bolyen, E., Rideout, J.R., Dillon, M.R., Bokulich, N.A., Abnet, C.C., Al-Ghalith, G.A., Alexander, H., Alm, E.J., Arumugam, M., Asnicar, F., Bai, Y., Bisanz, J.E., Bittinger, K., Brejnrod, A., Brislawn, C.J., Brown, C.T., Callahan, B.J., Caraballo-Rodríguez, A.M., Chase, J., Cope, E.K., Silva, R.D., Diener, C., Dorrestein, P.C., Douglas, G.M., Durall, D.M., Duvallet, C., Edwardson, C.F., Ernst, M., Estaki, M., Fouquier, J., Gauglitz, J.M., Gibbons, S.M., Gibson, D.L., Gonzalez, A., Gorlick, K., Guo, J., Hillmann, B., Holmes, S., Holste, H., Huttenhower, C., Huttley, G.A., Janssen, S., Jarmusch, A.K., Jiang, L., Kaehler, B.D., Kang, K.B., Keefe, C.R., Keim, P., Kelley, S.T., Knights, D., Koester, I., Kosciulek, T., Kreps, J., Langille, M.G.I., Lee, J., Ley, R., Liu, Y.-X., Lofffield, E., Lozupone, C., Maher, M., Marotz, C., Martin, B.D., McDonald, D., McIver, L.J., Melnik, A.V., Metcalf, J.L., Morgan, S.C., Morton, J.T., Naimey, A.T., Navas-Molina, J.A., Nothias, L.F., Orchanian, S.B., Pearson, T., Peoples, S.L., Petras, D., Preuss, M.L., Priesse, E., Rasmussen, L.B., Rivers, A., Robeson, M.S., Rosenthal, P., Segata, N., Shaffer, M., Shiffer, A., Sinha, R., Song, S.J., Spear, J.R., Swafford, A.D., Thompson, L.R., Torres, P.J., Trinh, P., Tripathi, A., Turnbaugh, P.J., Ul-Hasan, S., Hooft, J.J.J. van der, Vargas, F., Vázquez-Baeza, Y., Vogtmann, E., Hippel, M. von, Walters, W., Wan, Y., Wang, M., Warren, J., Weber, K.C., Williamson, C.H.D., Willis, A.D., Xu, Z.Z., Zaneveld, J.R., Zhang, Y., Zhu, Q., Knight, R., Caporaso, J.G., 2019. Reproducible, interactive, scalable and extensible microbiome data science using QIIME 2. *Nat. Biotechnol.* 37, 852–857. <https://doi.org/10.1038/s41587-019-0209-9>
- Bonilla, S., Villeneuve, V., Vincent, W., 2005. Benthic and planktonic algal communities in a High Arctic Lake: Pigment structure and contrasting responses to nutrient enrichment. *J. Phycol.* 41, 1120–1130. <https://doi.org/10.1111/j.1529-8817.2005.00154.x>
- Bonin, P., Omnes, P., Chalamet, A., 1998. Simultaneous occurrence of denitrification and nitrate ammonification in sediments of the French Mediterranean Coast. *Hydrobiologia* 389, 169–182. <https://doi.org/10.1023/A:1003585115481>
- Bourillot, R., 2009. Evolution des plates-formes carbonatées pendant la crise de salinité messinienne : de la déformation des évaporites aux communautés microbialithiques (sud-est de l'Espagne) (Thèse de doctorat). Dijon.
- Boyd, P.W., Cornwall, C.E., Davison, A., Doney, S.C., Fourquez, M., Hurd, C.L., Lima, I.D., McMinn, A., 2016. Biological responses to environmental heterogeneity under future ocean conditions. *Glob. Change Biol.* 22, 2633–2650. <https://doi.org/10.1111/gcb.13287>

- Broman, E., Raymond, C., Sommer, C., Gunnarsson, J.S., Creer, S., Nascimento, F.J.A., 2019. Salinity drives meiofaunal community structure dynamics across the Baltic ecosystem. *Mol. Ecol.* 28, 3813–3829. <https://doi.org/10.1111/mec.15179>
- Brotas, V., Plante-Cuny, M.-R., 2003. The use of HPLC pigment analysis to study microphytobenthos communities. *Acta Oecologica* 24. [https://doi.org/10.1016/S1146-609X\(03\)00013-4](https://doi.org/10.1016/S1146-609X(03)00013-4)
- Brüssow, H., Canchaya, C., Hardt, W.-D., 2004. Phages and the Evolution of Bacterial Pathogens: from Genomic Rearrangements to Lysogenic Conversion. *Microbiol. Mol. Biol. Rev.* 68, 560–602. <https://doi.org/10.1128/MMBR.68.3.560-602.2004>
- Bryantseva, I.A., Gorlenko, V.M., Tourova, T.P., Kuznetsov, B.B., Lysenko, A.M., Bykova, S.A., Garchenko, V.F., Mityushina, L.L., Osipov, G.A., 2000. *Hefiobacterium sulfidophilum* sp. nov. and *Hefiobacterium undosum* sp. nov.: Sulfide-oxidizing Heliobacteria from Thermal Sulfidic Springs 69, 10.
- Buckley, D.H., Baumgartner, L.K., Visscher, P.T., 2008. Vertical distribution of methane metabolism in microbial mats of the Great Sippewissett Salt Marsh. *Environ. Microbiol.* 10, 967–977. <https://doi.org/10.1111/j.1462-2920.2007.01517.x>
- Bürgmann, H., 2011. Methane Oxidation (Aerobic), in: Reitner, J., Thiel, V. (Eds.), *Encyclopedia of Geobiology*. Springer Netherlands, Dordrecht, pp. 575–578. https://doi.org/10.1007/978-1-4020-9212-1_139
- Burne, R., Moore, L., 1987. Microbialites: Organosedimentary Deposits of Benthic Microbial Communities. *Palaios* 2, 241–254. <https://doi.org/10.2307/3514674>
- Burow, L.C., Wobken, D., Marshall, I.P., Lindquist, E.A., Bebout, B.M., Prufert-Bebout, L., Hoehler, T.M., Tringe, S.G., Pett-Ridge, J., Weber, P.K., Spormann, A.M., Singer, S.W., 2013. Anoxic carbon flux in photosynthetic microbial mats as revealed by metatranscriptomics. *ISME J.* 7, 817–829. <https://doi.org/10.1038/ismej.2012.150>
- Cabello, P., Roldán, M.D., Castillo, F., Moreno-Vivián, C., 2009. Nitrogen Cycle, in: *Encyclopedia of Microbiology*. Elsevier, pp. 299–321. <https://doi.org/10.1016/B978-012373944-5.00055-9>
- Cadena, S., García-Maldonado, J.Q., López-Lozano, N.E., Cervantes, F.J., 2018. Methanogenic and Sulfate-Reducing Activities in a Hypersaline Microbial Mat and Associated Microbial Diversity. *Microb. Ecol.* 75, 930–940. <https://doi.org/10.1007/s00248-017-1104-x>
- Callaghan, A.V., Wawrik, B., Ní Chadhain, S.M., Young, L.Y., Zylstra, G.J., 2008. Anaerobic alkane-degrading strain AK-01 contains two alkylsuccinate synthase genes. *Biochem. Biophys. Res. Commun.* 366, 142–148. <https://doi.org/10.1016/j.bbrc.2007.11.094>
- Callahan, B.J., McMurdie, P.J., Rosen, M.J., Han, A.W., Johnson, A.J.A., Holmes, S.P., 2016. DADA2: High-resolution sample inference from Illumina amplicon data. *Nat. Methods* 13, 581–583. <https://doi.org/10.1038/nmeth.3869>
- Camacho, A., 2009. Sulfur Bacteria, in: *Encyclopedia of Inland Waters*. Elsevier, pp. 261–278. <https://doi.org/10.1016/B978-012370626-3.00128-9>
- Campbell, M.A., Coolen, M.J.L., Visscher, P.T., Bush, R., Burns, B.P., Grice, K., 2019. Sulfur Metabolising Bacteria within Hypersaline Microbial Mat Communities, in: 29th International Meeting on Organic Geochemistry. Presented at the 29th International Meeting on Organic

Geochemistry, European Association of Geoscientists & Engineers, Gothenburg, Sweden, pp. 1–2. <https://doi.org/10.3997/2214-4609.201902997>

Canfield, D.E., Jørgensen, B.B., Fossing, H., Glud, R., Gundersen, J., Ramsing, N.B., Thamdrup, B., Hansen, J.W., Nielsen, L.P., Hall, P.O.J., 1993a. Pathways of organic carbon oxidation in three continental margin sediments. *Mar. Geol.* 113, 27–40. [https://doi.org/10.1016/0025-3227\(93\)90147-N](https://doi.org/10.1016/0025-3227(93)90147-N)

Canfield, D.E., Thamdrup, B., Hansen, J.W., 1993b. The anaerobic degradation of organic matter in Danish coastal sediments: Iron reduction, manganese reduction, and sulfate reduction. *Geochim. Cosmochim. Acta* 57, 3867–3883. [https://doi.org/10.1016/0016-7037\(93\)90340-3](https://doi.org/10.1016/0016-7037(93)90340-3)

Caporaso, J.G., Kuczynski, J., Stombaugh, J., Bittinger, K., Bushman, F.D., Costello, E.K., Fierer, N., Peña, A.G., Goodrich, J.K., Gordon, J.I., Huttley, G.A., Kelley, S.T., Knights, D., Koenig, J.E., Ley, R.E., Lozupone, C.A., McDonald, D., Muegge, B.D., Pirrung, M., Reeder, J., Sevinsky, J.R., Turnbaugh, P.J., Walters, W.A., Widmann, J., Yatsunencko, T., Zaneveld, J., Knight, R., 2010. QIIME allows analysis of high-throughput community sequencing data. *Nat. Methods* 7, 335–336. <https://doi.org/10.1038/nmeth.f.303>

Caporaso, J.G., Lauber, C.L., Walters, W.A., Berg-Lyons, D., Lozupone, C.A., Turnbaugh, P.J., Fierer, N., Knight, R., 2011. Global patterns of 16S rRNA diversity at a depth of millions of sequences per sample. *Proc. Natl. Acad. Sci.* 108, 4516–4522. <https://doi.org/10.1073/pnas.1000080107>

Cardoso, D.C., Cretoiu, M.S., Stal, L.J., Bolhuis, H., 2019. Seasonal development of a coastal microbial mat. *Sci. Rep.* 9, 9035. <https://doi.org/10.1038/s41598-019-45490-8>

Carreira, C., Staal, M., Middelboe, M., Brussaard, C.P.D., 2015. Counting Viruses and Bacteria in Photosynthetic Microbial Mats. *Appl. Environ. Microbiol.* 81, 2149–2155. <https://doi.org/10.1128/AEM.02863-14>

Cartaxana, P., Vieira, S., Ribeiro, L., Rocha, R., Cruz, S., Calado, R., Marques da Silva, J., 2015. Effects of elevated temperature and CO₂ on intertidal microphytobenthos. *BMC Ecol.* 15, 10. <https://doi.org/10.1186/s12898-015-0043-y>

Casamayor, E.O., Massana, R., Benlloch, S., Øvreås, L., Díez, B., Goddard, V.J., Gasol, J.M., Joint, I., Rodríguez-Valera, F., Pedrós-Alió, C., 2002. Changes in archaeal, bacterial and eukaryal assemblages along a salinity gradient by comparison of genetic fingerprinting methods in a multipond solar saltern. *Environ. Microbiol.* 4, 338–348. <https://doi.org/10.1046/j.1462-2920.2002.00297.x>

Casanueva, A., Galada, N., Baker, G.C., Grant, W.D., Heaphy, S., Jones, B., Yanhe, M., Ventosa, A., Blamey, J., Cowan, D.A., 2008. Nanoarchaeal 16S rRNA gene sequences are widely dispersed in hyperthermophilic and mesophilic halophilic environments. *Extremophiles* 12, 651–656. <https://doi.org/10.1007/s00792-008-0170-x>

Castenholz, R.W., Pierson, B.K., 1995. Ecology of Thermophilic Anoxygenic Phototrophs, in: Blankenship, R.E., Madigan, M.T., Bauer, C.E. (Eds.), *Anoxygenic Photosynthetic Bacteria, Advances in Photosynthesis and Respiration*. Springer Netherlands, Dordrecht, pp. 87–103. https://doi.org/10.1007/0-306-47954-0_5

Castro, H.F., Williams, N.H., Ogram, A., 2000. Phylogeny of sulfate-reducing bacteria. *FEMS Microbiol. Ecol.* 31, 1–9. <https://doi.org/10.1111/j.1574-6941.2000.tb00665.x>

- Caumette, null, Imhoff, null, Suling, null, Matheron, null, 1997. *Chromatium glycolicum* sp. nov., a moderately halophilic purple sulfur bacterium that uses glycolate as substrate. Arch. Microbiol. 167, 11–18. <https://doi.org/10.1007/s002030050410>
- Caumette, P., Guyoneaud, R., Duran, R., Cravo-Laureau, C., Matheron, R., 2007. *Rhodobium pfennigii* sp. nov., a phototrophic purple non-sulfur bacterium with unusual bacteriochlorophyll *a* antennae, isolated from a brackish microbial mat on Rangiroa atoll, French Polynesia. Int. J. Syst. Evol. Microbiol. 57, 1250–1255. <https://doi.org/10.1099/ijs.0.64775-0>
- Caumette, P., Matheron, R., Raymond, N., Relexans, J.-C., 1994. Microbial mats in the hypersaline ponds of Mediterranean salterns (Salins-de-Giraud, France). FEMS Microbiol. Ecol. 13, 273–286. <https://doi.org/10.1111/j.1574-6941.1994.tb00074.x>
- Cavicchioli, R., Ripple, W.J., Timmis, K.N., Azam, F., Bakken, L.R., Baylis, M., Behrenfeld, M.J., Boetius, A., Boyd, P.W., Classen, A.T., Crowther, T.W., Danovaro, R., Foreman, C.M., Huisman, J., Hutchins, D.A., Jansson, J.K., Karl, D.M., Koskella, B., Mark Welch, D.B., Martiny, J.B.H., Moran, M.A., Orphan, V.J., Reay, D.S., Remais, J.V., Rich, V.I., Singh, B.K., Stein, L.Y., Stewart, F.J., Sullivan, M.B., van Oppen, M.J.H., Weaver, S.C., Webb, E.A., Webster, N.S., 2019. Scientists' warning to humanity: microorganisms and climate change. Nat. Rev. Microbiol. 17, 569–586. <https://doi.org/10.1038/s41579-019-0222-5>
- Chen, Y.-J., Leung, P.M., Wood, J.L., Bay, S.K., Hugenholtz, P., Kessler, A.J., Shelley, G., Waite, D.W., Franks, A.E., Cook, P.L.M., Greening, C., 2021. Metabolic flexibility allows bacterial habitat generalists to become dominant in a frequently disturbed ecosystem. ISME J. 15, 2986–3004. <https://doi.org/10.1038/s41396-021-00988-w>
- Chistoserdova, L., 2015. Methylophages in natural habitats: current insights through metagenomics. Appl. Microbiol. Biotechnol. 99, 5763–5779. <https://doi.org/10.1007/s00253-015-6713-z>
- Chistoserdova, L., Kalyuzhnaya, M.G., Lidstrom, M.E., 2009. The Expanding World of Methylophagic Metabolism. Annu. Rev. Microbiol. 63, 477–499. <https://doi.org/10.1146/annurev.micro.091208.073600>
- Clingenpeel, S., Kan, J., Macur, R., Woyke, T., Lóvalvo, D., Varley, J., Inskeep, W., Nealson, K., McDermott, T., 2013. Yellowstone Lake *Nanoarchaeota*. Front. Microbiol. 4, 274. <https://doi.org/10.3389/fmicb.2013.00274>
- Conrad, R., 2020. Importance of hydrogenotrophic, acetoclastic and methylophagic methanogenesis for methane production in terrestrial, aquatic and other anoxic environments: A mini review. Pedosphere 30, 25–39. [https://doi.org/10.1016/S1002-0160\(18\)60052-9](https://doi.org/10.1016/S1002-0160(18)60052-9)
- Coull, B.C., 1999. Role of meiofauna in estuarine soft-bottom habitats - Coull - 1999 - Australian Journal of Ecology - Wiley Online Library. Aust. J. Ecol. 24, 327–343.
- Covey, C., 1995. Global ocean circulation and equator-pole heat transport as a function of ocean GCM resolution. Clim. Dyn. 11, 425–437. <https://doi.org/10.1007/BF00209516>
- Cowles, T.J., Olson, R.J., Chisholm, S.W., 1988. Food selection by copepods: discrimination on the basis of food quality. Mar. Biol. 100, 41–49. <https://doi.org/10.1007/BF00392953>
- Cravo-Laureau, C., Grossi, V., Raphel, D., Matheron, R., Hirschler-Réa, A., 2005. Anaerobic n-Alkane Metabolism by a Sulfate-Reducing Bacterium, *Desulfatibacillum aliphaticivorans* Strain CV2803T. Appl. Environ. Microbiol. 71, 3458–3467. <https://doi.org/10.1128/AEM.71.7.3458-3467.2005>

- Cravo-Laureau, C., Matheron, R., Cayol, J.-L., Joulian, C., Hirschler-Réa, A., 2004. *Desulfatibacillum aliphaticivorans* gen. nov., sp. nov., an n-alkane- and n-alkene-degrading, sulfate-reducing bacterium. *Int. J. Syst. Evol. Microbiol.* 54, 77–83. <https://doi.org/10.1099/ijs.0.02717-0>
- Crummett, L.T., 2020. Acidification decreases microbial community diversity in the Salish Sea, a region with naturally high pCO₂. *PLOS ONE* 15, e0241183. <https://doi.org/10.1371/journal.pone.0241183>
- Crutzen, P.J., 2006. The “Anthropocene,” in: Ehlers, E., Krafft, T. (Eds.), *Earth System Science in the Anthropocene*. Springer, Berlin, Heidelberg, pp. 13–18. https://doi.org/10.1007/3-540-26590-2_3
- Cui, M., Ma, A., Qi, H., Zhuang, X., Zhuang, G., 2015. Anaerobic oxidation of methane: an “active” microbial process. *MicrobiologyOpen* 4, 1–11. <https://doi.org/10.1002/mbo3.232>
- Cvitković, I., Despalatović, M., Grubelić, I., Bogner, D., Nikolić, V., Žuljević, A., Antolić, B., Travizi, A., 2011. Spatio-temporal variability of meiofauna community structure in abandoned salina of velike soline and adjacent area (Mediterranean, Adriatic sea). *Fresenius Environ. Bull.* 20, 645–655.
- Czerny, J., Ramos, J., Riebesell, U., 2009. Influence of elevated CO₂ concentrations on cell division and nitrogen fixation rates in the bloom forming cyanobacterium *Nodularia spumigena*. *Biogeosciences* 6, 1865–1875. <https://doi.org/10.5194/bgd-6-4279-2009>
- de Beer, D., Sauter, E., Niemann, H., Kaul, N., Foucher, J.-P., Witte, U., Schlüter, M., Boetius, A., 2006. In situ fluxes and zonation of microbial activity in surface sediments of the Håkon Mosby Mud Volcano. *Limnol. Oceanogr.* 51, 1315–1331. <https://doi.org/10.4319/lo.2006.51.3.1315>
- de Melo Soares, R.H.R., de Assunção, C.A., de Oliveira Fernandes, F., Marinho-Soriano, E., 2018. Identification and analysis of ecosystem services associated with biodiversity of saltworks. *Ocean Coast. Manag.* 163, 278–284. <https://doi.org/10.1016/j.ocecoaman.2018.07.007>
- De Mesel, I., Derycke, S., Moens, T., Van der Gucht, K., Vincx, M., Swings, J., 2004. Top-down impact of bacterivorous nematodes on the bacterial community structure: a microcosm study. *Environ. Microbiol.* 6, 733–744. <https://doi.org/10.1111/j.1462-2920.2004.00610.x>
- de Wit, R., van Gemerden, H., 1987. Chemolithotrophic growth of the phototrophic sulfur bacterium *Thiocapsa roseopersicina*. *FEMS Microbiol. Ecol.* 3, 117–126. <https://doi.org/10.1111/j.1574-6968.1987.tb02347.x>
- Decho, A., 2000. Microbial biofilms in intertidal systems: an overview. *Cont. Shelf Res.* 20, 1257–1273. [https://doi.org/10.1016/S0278-4343\(00\)00022-4](https://doi.org/10.1016/S0278-4343(00)00022-4)
- Decho, A., 1990. Decho AW.. Microbial exopolymer secretions in ocean environments: their role(s) in food webs and marine processes. *Oceanogr Mar Biol Ann Rev* 28: 73-153. *Oceanogr. Mar. Biol. Annu. Rev.* 28, 73–154.
- Decho, A.W., Moriarty, D.J.W., 1990. Bacterial exopolymer utilization by a harpacticoid copepod: A methodology and results. *Limnol. Oceanogr.* 35, 1039–1049. <https://doi.org/10.4319/lo.1990.35.5.1039>
- Desnues, C., Michotey, V.D., Wieland, A., Zhizang, C., Fourçans, A., Duran, R., Bonin, P.C., 2007. Seasonal and diel distributions of denitrifying and bacterial communities in a hypersaline

- microbial mat (Camargue, France). *Water Res.* 41, 3407–3419. <https://doi.org/10.1016/j.watres.2007.04.018>
- Di Tommaso, P., Chatzou, M., Floden, E.W., Barja, P.P., Palumbo, E., Notredame, C., 2017. Nextflow enables reproducible computational workflows. *Nat. Biotechnol.* 35, 316–319. <https://doi.org/10.1038/nbt.3820>
- Dobretsov, S., Abed, R.M.M., Al Maskari, S.M.S., Al Sabahi, J.N., Victor, R., 2011. Cyanobacterial mats from hot springs produce antimicrobial compounds and quorum-sensing inhibitors under natural conditions. *J. Appl. Phycol.* 23, 983–993. <https://doi.org/10.1007/s10811-010-9627-2>
- Dolan, J.R., Coats, D.W., 1991. A study of feeding in predacious ciliates using prey ciliates labeled with fluorescent microspheres. *J. Plankton Res.* 13, 609–627. <https://doi.org/10.1093/plankt/13.3.609>
- Dubois, Michel., Gilles, K.A., Hamilton, J.K., Rebers, P.A., Smith, Fred., 1956. Colorimetric Method for Determination of Sugars and Related Substances. *Anal. Chem.* 28, 350–356. <https://doi.org/10.1021/ac60111a017>
- Duffy, J., Stachowicz, J., 2006. Why biodiversity is important to oceanography: Potential roles of genetic, species, and trophic diversity in pelagic ecosystem processes. *Mar. Ecol.-Prog. Ser. - MAR ECOL-PROGR SER* 311, 179–189. <https://doi.org/10.3354/meps311179>
- Dupraz, C., Visscher, P.T., 2005. Microbial lithification in marine stromatolites and hypersaline mats. *Trends Microbiol.* 13, 429–438. <https://doi.org/10.1016/j.tim.2005.07.008>
- Dutta, H., Dutta, A., 2016. The microbial aspect of climate change. *Energy Ecol. Environ.* 1, 209–232. <https://doi.org/10.1007/s40974-016-0034-7>
- Elloumi, J., Guermazi, W., Ayadi, H., Bouain, A., Aleya, L., 2009. Abundance and biomass of prokaryotic and eukaryotic microorganisms coupled with environmental factors in an arid multi-pond solar saltern (Sfax, Tunisia). *J. Mar. Biol. Assoc. U. K.* 89, 243–253. <https://doi.org/10.1017/S0025315408002269>
- El-Serehy, H.A., Al-Rasheid, K.A., Al-Misned, F.A., Al-Talasat, A.A.R., Gewik, M.M., 2016. Microbial–meiofaunal interrelationships in coastal sediments of the Red Sea. *Saudi J. Biol. Sci.* 23, 327–334. <https://doi.org/10.1016/j.sjbs.2016.01.023>
- Escudié, F., Auer, L., Bernard, M., Mariadassou, M., Cauquil, L., Vidal, K., Maman, S., Hernandez-Raquet, G., Combes, S., Pascal, G., 2018. FROGS: Find, Rapidly, OTUs with Galaxy Solution. *Bioinforma. Oxf. Engl.* 34, 1287–1294. <https://doi.org/10.1093/bioinformatics/btx791>
- Estrada, M., Henriksen, P., Gasol, J.M., Casamayor, E.O., Pedrós-Alió, C., 2004. Diversity of planktonic photoautotrophic microorganisms along a salinity gradient as depicted by microscopy, flow cytometry, pigment analysis and DNA-based methods. *FEMS Microbiol. Ecol.* 49, 281–293. <https://doi.org/10.1016/j.femsec.2004.04.002>
- Feazel, L.M., Spear, J.R., Berger, A.B., Harris, J.K., Frank, D.N., Ley, R.E., Pace, N.R., 2008. Eucaryotic Diversity in a Hypersaline Microbial Mat. *Appl. Environ. Microbiol.* 74, 329–332. <https://doi.org/10.1128/AEM.01448-07>
- Fei Xi, X., Wang, L., Jun Hu, J., Shu Tang, Y., Hu, Y., Hua Fu, X., Sun, Y., Fai Tsang, Y., Nan Zhang, Y., Hai Chen, J., 2014. Salinity influence on soil microbial respiration rate of wetland in

- the Yangtze River estuary through changing microbial community. *J. Environ. Sci. China* 26, 2562–2570. <https://doi.org/10.1016/j.jes.2014.07.016>
- Fenchel, T., 1998. Formation of laminated cyanobacterial mats in the absence of benthic fauna. *Aquat. Microb. Ecol.* 14, 235–240. <https://doi.org/10.3354/ame014235>
- Fenchel, T., King, G.M., Blackburn, T.H., 2012. Bacterial Metabolism, in: *Bacterial Biogeochemistry*. Elsevier, pp. 1–34. <https://doi.org/10.1016/B978-0-12-415836-8.00001-3>
- Field, C.B., 1998. Primary Production of the Biosphere: Integrating Terrestrial and Oceanic Components. *Science* 281, 237–240. <https://doi.org/10.1126/science.281.5374.237>
- Flemming, H.-C., Wingender, J., 2010. The biofilm matrix. *Nat. Rev. Microbiol.* 8, 623–633. <https://doi.org/10.1038/nrmicro2415>
- Flemming, H.-C., Wuertz, S., 2019. Bacteria and archaea on Earth and their abundance in biofilms. *Nat. Rev. Microbiol.* 17, 247–260. <https://doi.org/10.1038/s41579-019-0158-9>
- Flores, G.E., Shakya, M., Meneghin, J., Yang, Z.K., Seewald, J.S., Geoff Wheat, C., Podar, M., Reysenbach, A.-L., 2012. Inter-field variability in the microbial communities of hydrothermal vent deposits from a back-arc basin. *Geobiology* 10, 333–346. <https://doi.org/10.1111/j.1472-4669.2012.00325.x>
- Fontaneto, D., Kaya, M., Herniou, E.A., Barraclough, T.G., 2009. Extreme levels of hidden diversity in microscopic animals (Rotifera) revealed by DNA taxonomy. *Mol. Phylogenet. Evol.* 53, 182–189. <https://doi.org/10.1016/j.ympev.2009.04.011>
- Forget, G., Ferreira, D., 2019. Global ocean heat transport dominated by heat export from the tropical Pacific. *Nat. Geosci.* 12, 351–354. <https://doi.org/10.1038/s41561-019-0333-7>
- Fourçans, A., Oteyza, T.G. de, Wieland, A., Solé, A., Diestra, E., Bleijswijk, J. van, Grimalt, J.O., Köhl, M., Esteve, I., Muyzer, G., Caumette, P., Duran, R., 2004. Characterization of functional bacterial groups in a hypersaline microbial mat community (Salins-de-Giraud, Camargue, France). *FEMS Microbiol. Ecol.* 51, 55–70. <https://doi.org/10.1016/j.femsec.2004.07.012>
- Fourçans, A., Ranchou-Peyruse, A., Caumette, P., Duran, R., 2008. Molecular Analysis of the Spatio-temporal Distribution of Sulfate-reducing Bacteria (SRB) in Camargue (France) Hypersaline Microbial Mat. *Microb. Ecol.* 56, 90–100. <https://doi.org/10.1007/s00248-007-9327-x>
- Fourçans, A., Solé, A., Diestra, E., Ranchou-Peyruse, A., Esteve, I., Caumette, P., Duran, R., 2006. Vertical migration of phototrophic bacterial populations in a hypersaline microbial mat from Salins-de-Giraud (Camargue, France). *FEMS Microbiol. Ecol.* 57, 367–377. <https://doi.org/10.1111/j.1574-6941.2006.00124.x>
- France3-regions, 2018. Production de sel sur l'île de Ré: la récolte estivale s'annonce exceptionnelle [WWW Document]. Fr. 3 Nouv.-Aquitaine. URL <https://france3-regions.francetvinfo.fr/nouvelle-aquitaine/charente-maritime/production-sel-ile-re-recolte-estivale-s-annonce-exceptionnelle-1523924.html> (accessed 8.28.21).
- France3-regions, 2017. A la rencontre des sauniers, la fine fleur du sel [WWW Document]. Fr. 3 Nouv.-Aquitaine. URL <https://france3-regions.francetvinfo.fr/nouvelle-aquitaine/charente-maritime/rencontre-sauniers-fine-fleur-du-sel-1309343.html> (accessed 8.28.21).
- Franks, J., Stolz, J.F., 2009. Flat laminated microbial mat communities. *Earth-Sci. Rev.* 96, 163–172. <https://doi.org/10.1016/j.earscirev.2008.10.004>

- Frigaard, N.-U., 2016. Biotechnology of Anoxygenic Phototrophic Bacteria, in: Hatti-Kaul, R., Mamo, G., Mattiasson, B. (Eds.), *Anaerobes in Biotechnology, Advances in Biochemical Engineering/Biotechnology*. Springer International Publishing, Cham, pp. 139–154. https://doi.org/10.1007/10_2015_5006
- Fuchs, B.M., Spring, S., Teeling, H., Quast, C., Wulf, J., Schattenhofer, M., Yan, S., Ferreira, S., Johnson, J., Glöckner, F.O., Amann, R., 2007. Characterization of a marine gammaproteobacterium capable of aerobic anoxygenic photosynthesis. *Proc. Natl. Acad. Sci. U. S. A.* 104, 2891–2896. <https://doi.org/10.1073/pnas.0608046104>
- Gaby, J.C., Buckley, D.H., 2014. A comprehensive aligned *nifH* gene database: a multipurpose tool for studies of nitrogen-fixing bacteria. *Database J. Biol. Databases Curation* 2014, bau001. <https://doi.org/10.1093/database/bau001>
- Gao, K., Helbling, E., Häder, D., Hutchins, D., 2012. Responses of marine primary producers to interactions between ocean acidification, solar radiation, and warming. *Mar. Ecol. Prog. Ser.* 470, 167. <https://doi.org/10.3354/meps10043>
- Garet, M.J., Moriarty, D.J.W., 1996. Acid extraction of tritium label from bacterial DNA in clay sediment. *J. Microbiol. Methods* 25, 1–4. [https://doi.org/10.1016/0167-7012\(95\)00071-2](https://doi.org/10.1016/0167-7012(95)00071-2)
- Geelhoed, J.S., van de Velde, S.J., Meysman, F.J.R., 2020. Quantification of Cable Bacteria in Marine Sediments via qPCR. *Front. Microbiol.* 11, 1506. <https://doi.org/10.3389/fmicb.2020.01506>
- George, D.M., Vincent, A.S., Mackey, H.R., 2020. An overview of anoxygenic phototrophic bacteria and their applications in environmental biotechnology for sustainable Resource recovery. *Biotechnol. Rep.* 28, e00563. <https://doi.org/10.1016/j.btre.2020.e00563>
- Gette-Bouvarot, M., Mermillod-Blondin, F., Lemoine, D., Delolme, C., Danjean, M., Etienne, L., Volatier, L., 2015. The potential control of benthic biofilm growth by macrophytes—A mesocosm approach. *Ecol. Eng.* 75, 178–186. <https://doi.org/10.1016/j.ecoleng.2014.12.001>
- Giani, D., Seeler, J., Giani, L., Krumbein, W.E., 1989. Microbial mats and physicochemistry in a saltern in the Bretagne (France) and in a laboratory scale saltern model. *FEMS Microbiol. Lett.* 62, 151–161. <https://doi.org/10.1111/j.1574-6968.1989.tb03689.x>
- Gihring, T.M., Green, S.J., Schadt, C.W., 2012. Massively parallel rRNA gene sequencing exacerbates the potential for biased community diversity comparisons due to variable library sizes. *Environ. Microbiol.* 14, 285–290. <https://doi.org/10.1111/j.1462-2920.2011.02550.x>
- Graham, E.B., Crump, A.R., Resch, C.T., Fansler, S., Arntzen, E., Kennedy, D.W., Fredrickson, J.K., Stegen, J.C., 2016. Coupling Spatiotemporal Community Assembly Processes to Changes in Microbial Metabolism. *Front. Microbiol.* 7. <https://doi.org/10.3389/fmicb.2016.01949>
- Grossart, H.-P., Allgaier, M., Passow, U., Riebesell, U., 2006. Testing the effect of CO₂ concentration on the dynamics of marine heterotrophic bacterioplankton. *Limnol. Oceanogr.* 51, 1–11. <https://doi.org/10.4319/lo.2006.51.1.0001>
- Gulev, S.K., Latif, M., Keenlyside, N., Park, W., Koltermann, K.P., 2013. North Atlantic Ocean control on surface heat flux on multidecadal timescales. *Nature* 499, 464–467. <https://doi.org/10.1038/nature12268>
- Guyoneaud, R., Mouné, S., Eatock, C., Bothorel, V., Hirschler-Réa, A., Willison, J., Duran, R., Liesack, W., Herbert, R., Matheron, R., Caumette, P., 2002. Characterization of three spiral-

shaped purple nonsulfur bacteria isolated from coastal lagoon sediments, saline sulfur springs, and microbial mats: emended description of the genus *Roseospira* and description of *Roseospira marina* sp. nov., *Roseospira navarrensis* sp. nov., and *Roseospira thiosulfatophila* sp. nov. Arch. Microbiol. 178, 315–324. <https://doi.org/10.1007/s00203-002-0454-y>

Haas, B.J., Gevers, D., Earl, A.M., Feldgarden, M., Ward, D.V., Giannoukos, G., Ciulla, D., Tabbaa, D., Highlander, S.K., Sodergren, E., Methé, B., DeSantis, T.Z., Human Microbiome Consortium, Petrosino, J.F., Knight, R., Birren, B.W., 2011. Chimeric 16S rRNA sequence formation and detection in Sanger and 454-pyrosequenced PCR amplicons. Genome Res. 21, 494–504. <https://doi.org/10.1101/gr.112730.110>

Häder, D.-P., Helbling, E.W., Williamson, C.E., Worrest, R.C., 2011. Effects of UV radiation on aquatic ecosystems and interactions with climate change. Photochem. Photobiol. Sci. Off. J. Eur. Photochem. Assoc. Eur. Soc. Photobiol. 10, 242–260. <https://doi.org/10.1039/c0pp90036b>

Hancke, K., Glud, R., 2004. Temperature effects on respiration and photosynthesis in three diatom-dominated benthic communities. Aquat. Microb. Ecol. 37, 265–281. <https://doi.org/10.3354/ame037265>

Hanson, R.S., Hanson, T.E., 1996. Methanotrophic bacteria. Microbiol. Rev. 60, 439–471. <https://doi.org/10.1128/mr.60.2.439-471.1996>

Hebert, P.D.N., Ratnasingham, S., deWaard, J.R., 2003. Barcoding animal life: cytochrome *c* oxidase subunit 1 divergences among closely related species. Proc. Biol. Sci. 270 Suppl 1, S96–99. <https://doi.org/10.1098/rsbl.2003.0025>

Heinzel, M., Golbeck, J.H., 2007. Heliobacterial photosynthesis. Photosynth. Res. 92, 35–53. <https://doi.org/10.1007/s11120-007-9162-4>

Hennes, K.P., Suttle, C.A., 1995. Direct counts of viruses in natural waters and laboratory cultures by epifluorescence microscopy. Limnol. Oceanogr. 40, 1050–1055. <https://doi.org/10.4319/lo.1995.40.6.1050>

Hennes, K.P., Suttle, C.A., Chan, A.M., 1995. Fluorescently Labeled Virus Probes Show that Natural Virus Populations Can Control the Structure of Marine Microbial Communities. Appl. Environ. Microbiol. 61, 3623–3627. <https://doi.org/10.1128/aem.61.10.3623-3627.1995>

Herbert, R.A., Ranchou-Peyruse, A., Duran, R., Guyoneaud, R., Schwabe, S., 2005. Characterization of purple sulfur bacteria from the South Andros Black Hole cave system: highlights taxonomic problems for ecological studies among the genera *Allochromatium* and *Thiocapsa*. Environ. Microbiol. 7, 1260–1268. <https://doi.org/10.1111/j.1462-2920.2005.00815.x>

Herfort, L., Kim, J.-H., Coolen, M., Abbas, B., Schouten, S., Herndl, G., Sinninghe-Damste, J., 2009. Diversity of Archaea and detection of crenarchaeotal *amoA* genes in the river Rhine and Têt. Aquat. Microb. Ecol. - AQUAT MICROB ECOL 55, 189–201. <https://doi.org/10.3354/ame01294>

Hermans, M., Lenstra, W.K., Hidalgo-Martinez, S., van Helmond, N.A.G.M., Witbaard, R., Meysman, F.J.R., Gonzalez, S., Slomp, C.P., 2019. Abundance and Biogeochemical Impact of Cable Bacteria in Baltic Sea Sediments. Environ. Sci. Technol. 53, 7494–7503. <https://doi.org/10.1021/acs.est.9b01665>

- Hicks, N., Bulling, M.T., Solan, M., Raffaelli, D., White, P.C., Paterson, D.M., 2011. Impact of biodiversity-climate futures on primary production and metabolism in a model benthic estuarine system. *BMC Ecol.* 11, 7. <https://doi.org/10.1186/1472-6785-11-7>
- Hinck, S., Neu, T.R., Lavik, G., Mussmann, M., de Beer, D., Jonkers, H.M., 2007. Physiological Adaptation of a Nitrate-Storing *Beggiatoa* sp. to Diel Cycling in a Phototrophic Hypersaline Mat. *Appl. Environ. Microbiol.* 73, 7013–7022. <https://doi.org/10.1128/AEM.00548-07>
- Hirschberg, J., Chamovitz, D., 1994. Carotenoids in Cyanobacteria, in: Bryant, D.A. (Ed.), *The Molecular Biology of Cyanobacteria*. Springer Netherlands, Dordrecht, pp. 559–579. https://doi.org/10.1007/978-94-011-0227-8_18
- Hirschler-Réa, A., Matheron, R., Riffaud, C., Mouné, S., Eatock, C., Herbert, R.A., Willison, J.C., Caumette, P., 2003. Isolation and characterization of spirilloid purple phototrophic bacteria forming red layers in microbial mats of Mediterranean salterns: description of *Halorhodospira neutriphila* sp. nov. and emendation of the genus *Halorhodospira*. *Int. J. Syst. Evol. Microbiol.* 53, 153–163. <https://doi.org/10.1099/ijs.0.02226-0>
- Hoehler, T.M., Bebout, B.M., Des Marais, D.J., 2001. The role of microbial mats in the production of reduced gases on the early Earth. *Nature* 412, 324–327. <https://doi.org/10.1038/35085554>
- Hohn, M.J., Hedlund, B.P., Huber, H., 2002. Detection of 16S rDNA Sequences Representing the Novel Phylum “*Nanoarchaeota*”: Indication for a Wide Distribution in High Temperature Biotopes. *Syst. Appl. Microbiol.* 25, 551–554. <https://doi.org/10.1078/07232020260517698>
- Hong, S., Bunge, J., Leslin, C., Jeon, S., Epstein, S.S., 2009. Polymerase chain reaction primers miss half of rRNA microbial diversity. *ISME J.* 3, 1365–1373. <https://doi.org/10.1038/ismej.2009.89>
- Howarth, R., 2014. Nitrogen in Freshwater Systems and Estuaries Nitrogen, in: Reference Module in Earth Systems and Environmental Sciences. Elsevier. <https://doi.org/10.1016/B978-0-12-409548-9.09401-X>
- Hubas, C., 2018. Biofilms, tapis et agrégats microbiens : vers une vision unificatrice (HDR (Habilitation à Diriger les Recherches)). Muséum National D’Histoire Naturelle. <https://doi.org/10.5281/zenodo.3784703>
- Hubas, C., Sachidhanandam, C., Rybarczyk, H., Lubarsky, H., Rigaux, A., Moens, T., Paterson, D., 2010. Bacterivorous nematodes stimulate microbial growth and exopolymer production in marine sediment microcosms. *Mar. Ecol. Prog. Ser.* 419, 85–94. <https://doi.org/10.3354/meps08851>
- Huber, H., Hohn, M.J., Rachel, R., Fuchs, T., Wimmer, V.C., Stetter, K.O., 2002. A new phylum of Archaea represented by a nanosized hyperthermophilic symbiont. *Nature* 417, 63–67. <https://doi.org/10.1038/417063a>
- Hutchins, D.A., Fu, F., 2017. Microorganisms and ocean global change. *Nat. Microbiol.* 2, 17058. <https://doi.org/10.1038/nmicrobiol.2017.58>
- Hutchins, D.A., Fu, F.-X., Zhang, Y., Warner, M.E., Feng, Y., Portune, K., Bernhardt, P.W., Mulholland, M.R., 2007. CO₂ control of *Trichodesmium* N₂ fixation, photosynthesis, growth rates, and elemental ratios: Implications for past, present, and future ocean biogeochemistry. *Limnol. Oceanogr.* 52, 1293–1304. <https://doi.org/10.4319/lo.2007.52.4.1293>

Imhoff, J.F., 2017. Anoxygenic Phototrophic Bacteria from Extreme Environments, in: Hallenbeck, P.C. (Ed.), *Modern Topics in the Phototrophic Prokaryotes: Environmental and Applied Aspects*. Springer International Publishing, Cham, pp. 427–480. https://doi.org/10.1007/978-3-319-46261-5_13

Imhoff, J.F., 2001. True marine and halophilic anoxygenic phototrophic bacteria. *Arch. Microbiol.* 176, 243–254. <https://doi.org/10.1007/s002030100326>

Imhoff, J.F., Hiraishi, A., Siling, J., 2015. Anoxygenic Phototrophic Purple Bacteria, in: *Bergey's Manual of Systematics of Archaea and Bacteria*. American Cancer Society, pp. 1–23. <https://doi.org/10.1002/9781118960608.bm00002>

Ingels, J., dos Santos, G., Hicks, N., Vazquez, Y.V., Neres, P.F., Pontes, L.P., Amorim, M.N., Romn, S., Du, Y., Stahl, H., Somerfield, P.J., Widdicombe, S., 2018. Short-term CO₂ exposure and temperature rise effects on metazoan meiofauna and free-living nematodes in sandy and muddy sediments: Results from a flume experiment. *J. Exp. Mar. Biol. Ecol.*, IçIMCo, the 16th International Meiofauna Conference 502, 211–226. <https://doi.org/10.1016/j.jembe.2017.07.012>

IPCC, 2021. *Climate Change 2021: The Physical Science Basis. Contribution of Working Group I to the Sixth Assessment Report of the Intergovernmental Panel on Climate Change. Summary for Policymakers*, in: Masson-Delmotte, V., Zhai, P., Pirani, A., Connors, S.L., Pan, C., Berger, S., Caud, N., Chen, Y., Goldfarb, L., Gomis, M.I., Huang, M., Leitzell, K., Lonnoy, E., Matthews, J.B.R., Maycock, T.K., Waterfield, T., Yeleki, O., Yu, R., Zhou, B. (Eds.), *Sixth Assessment Report of the Intergovernmental Panel on Climate Change*.

IPCC, 2019. *IPCC Special Report on the Ocean and Cryosphere in a Changing Climate*, in: Prtner, H.-O., Roberts, D.C., Masson-Delmotte, V., Zhai, P., Tignor, M., Poloczanska, E., Mintenbeck, K., Alegria, A., Nicolai, M., Okem, A., Petzold, J., Rama, B., Weyer, N.M. (Eds.), *A Special Report of the Intergovernmental Panel on Climate Change*. p. 765.

IPCC, 2014. *Climate Change 2014: Synthesis Report. Contribution of Working Groups I, II and III to the Fifth Assessment Report of the Intergovernmental Panel on Climate Change*, in: The Core Writing Team, Pachauri, R.K., Meyer, L. (Eds.), *Climate Change 2014 Synthesis Report*. p. 169.

Javor, B., 1989. *Hypersaline Environments: Microbiology and Biogeochemistry*, Brock Springer Series in Contemporary Bioscience. Springer-Verlag, Berlin Heidelberg. <https://doi.org/10.1007/978-3-642-74370-2>

Jensen, S.I., Steunou, A.-S., Bhaya, D., Khl, M., Grossman, A.R., 2011. *In situ* dynamics of O₂, pH and cyanobacterial transcripts associated with CCM, photosynthesis and detoxification of ROS. *ISME J.* 5, 317–328. <https://doi.org/10.1038/ismej.2010.131>

Jesus, B., Perkins, R.G., Mendes, C.R., Brotas, V., Paterson, D.M., 2006. Chlorophyll fluorescence as a proxy for microphytobenthic biomass: alternatives to the current methodology. *Mar. Biol.* 150, 17–28. <https://doi.org/10.1007/s00227-006-0324-2>

Jonkers, H., Abed, R., 2003. Identification of aerobic heterotrophic bacteria from the photic zone of a hypersaline microbial mat. *Aquat. Microb. Ecol.* 30, 127–133. <https://doi.org/10.3354/ame030127>

Jrgensen, B.B., 1982. Ecology of the bacteria of the sulphur cycle with special reference to anoxic—oxic interface environments. *Philos Trans R Soc Lond B Biol Sci* 298, 543–561. <https://doi.org/10.1098/rstb.1982.0096>

- Jørgensen, B.B., Cohen, Y., 1977. Solar Lake (Sinai). 5. The sulfur cycle of the benthic cyanobacterial mats. *Limnol. Oceanogr.* 22, 657–666.
- Jørgensen, B.B., Des Marais, D.J., 1986. Competition for sulfide among colorless and purple sulfur bacteria in cyanobacterial mats. *FEMS Microbiol. Lett.* 38, 179–186. <https://doi.org/10.1111/j.1574-6968.1986.tb01727.x>
- Jørgensen, B.B., Findlay, A.J., Pellerin, A., 2019. The Biogeochemical Sulfur Cycle of Marine Sediments. *Front. Microbiol.* 10, 849. <https://doi.org/10.3389/fmicb.2019.00849>
- Jørgensen, B.B., Revsbech, N.P., Cohen, Y., 1983. Photosynthesis and structure of benthic microbial mats: Microelectrode and SEM studies of four cyanobacterial communities. *Limnol. Oceanogr.* 28, 1075–1093. <https://doi.org/10.4319/lo.1983.28.6.1075>
- Jungblut, A.D., Vincent, W.F., Lovejoy, C., 2012. Eukaryotes in Arctic and Antarctic cyanobacterial mats. *FEMS Microbiol. Ecol.* 82, 416–428. <https://doi.org/10.1111/j.1574-6941.2012.01418.x>
- Kadnikov, V.V., Mardanov, A.V., Beletsky, A.V., Karnachuk, O.V., Ravin, N.V., 2020. Microbial Life in the Deep Subsurface Aquifer Illuminated by Metagenomics. *Front. Microbiol.* 11. <https://doi.org/10.3389/fmicb.2020.572252>
- Karkhoff-Schweizer, R.R., Huber, D.P., Voordouw, G., 1995. Conservation of the genes for dissimilatory sulfite reductase from *Desulfovibrio vulgaris* and *Archaeoglobus fulgidus* allows their detection by PCR. *Appl. Environ. Microbiol.* 61, 290–296.
- Kawai, S., Martinez, J.N., Lichtenberg, M., Trampe, E., Köhl, M., Tank, M., Haruta, S., Nishihara, A., Hanada, S., Thiel, V., 2021. *In-Situ* Metatranscriptomic Analyses Reveal the Metabolic Flexibility of the Thermophilic Anoxygenic Photosynthetic Bacterium *Chloroflexus aggregans* in a Hot Spring Cyanobacteria-Dominated Microbial Mat. *Microorganisms* 9, 652. <https://doi.org/10.3390/microorganisms9030652>
- Kimble, L.K., Mandelco, L., Woese, C.R., Madigan, M.T., 1995. *Heliobacterium modesticaldum*, sp. nov., a thermophilic heliobacterium of hot springs and volcanic soils. *Arch Microbiol* 259–267.
- Knittel, K., Boetius, A., 2009. Anaerobic oxidation of methane: progress with an unknown process. *Annu. Rev. Microbiol.* 63, 311–334. <https://doi.org/10.1146/annurev.micro.61.080706.093130>
- Koblížek, M., Dachev, M., Bína, D., Nupur, P., Pivosz, K., Kaftan, D., 2020. Utilization of light energy in phototrophic *Gemmatimonadetes*. *J. Photochem. Photobiol. B* 213, 112085. <https://doi.org/10.1016/j.jphotobiol.2020.112085>
- Krüger, M., Meyerdierks, A., Glöckner, F.O., Amann, R., Widdel, F., Kube, M., Reinhardt, R., Kahnt, J., Böcher, R., Thauer, R.K., Shima, S., 2003. A conspicuous nickel protein in microbial mats that oxidize methane anaerobically. *Nature* 426, 878–881. <https://doi.org/10.1038/nature02207>
- Kurth, J., Op den Camp, H., Welte, C., 2020. Several ways one goal—methanogenesis from unconventional substrates. *Appl. Microbiol. Biotechnol.* 104. <https://doi.org/10.1007/s00253-020-10724-7>
- LaRoche, J., Breitbarth, E., 2005. Importance of the diazotrophs as a source of new nitrogen in the ocean. *J. Sea Res.* 53, 67–91. <https://doi.org/10.1016/j.seares.2004.05.005>

- Lavergne, C., Agogu , H., Leynaert, A., Raimonet, M., De Wit, R., Pineau, P., Br ret, M., Lachauss e, N., Dupuy, C., 2017. Factors influencing prokaryotes in an intertidal mudflat and the resulting depth gradients. *Estuar. Coast. Shelf Sci.* 189, 74–83. <https://doi.org/10.1016/j.ecss.2017.03.008>
- Lavergne, C., Beauguard, L., Dupuy, C., Courties, C., Agogu , H., 2014. An efficient and rapid method for the enumeration of heterotrophic prokaryotes in coastal sediments by flow cytometry. *J. Microbiol. Methods* 105, 31–38. <https://doi.org/10.1016/j.mimet.2014.07.002>
- Lee, M.R., Torres, R., Manr quez, P.H., 2017. The combined effects of ocean warming and acidification on shallow-water meiofaunal assemblages. *Mar. Environ. Res.* 131, 1–9. <https://doi.org/10.1016/j.marenvres.2017.09.002>
- Lep re, C., Domaizon, I., Hugoni, M., Vellet, A., Debroas, D., 2016. Diversity and Dynamics of Active Small Microbial Eukaryotes in the Anoxic Zone of a Freshwater Meromictic Lake (Pavin, France). *Front. Microbiol.* 7. <https://doi.org/10.3389/fmicb.2016.00130>
- Lewis, S.L., Maslin, M.A., 2015. Defining the Anthropocene. *Nature* 519, 171–180. <https://doi.org/10.1038/nature14258>
- Ley, R.E., Harris, J.K., Wilcox, J., Spear, J.R., Miller, S.R., Bebout, B.M., Maresca, J.A., Bryant, D.A., Sogin, M.L., Pace, N.R., 2006. Unexpected Diversity and Complexity of the Guerrero Negro Hypersaline Microbial Mat. *Appl. Environ. Microbiol.* 72, 3685–3695. <https://doi.org/10.1128/AEM.72.5.3685-3695.2006>
- Li, W., Xu, X., Fujibayashi, M., Niu, Q., Tanaka, N., Nishimura, O., 2016. Response of microalgae to elevated CO₂ and temperature: impact of climate change on freshwater ecosystems. *Environ. Sci. Pollut. Res.* 23, 19847–19860. <https://doi.org/10.1007/s11356-016-7180-5>
- Lidbury, I., Johnson, V., Hall-Spencer, J.M., Munn, C.B., Cunliffe, M., 2012. Community-level response of coastal microbial biofilms to ocean acidification in a natural carbon dioxide vent ecosystem. *Mar. Pollut. Bull.* 64, 1063–1066. <https://doi.org/10.1016/j.marpolbul.2012.02.011>
- Limburg, K.E., Breitbart, D., Swaney, D.P., Jacinto, G., 2020. Ocean Deoxygenation: A Primer. *One Earth* 2, 24–29. <https://doi.org/10.1016/j.oneear.2020.01.001>
- Liu, Y., 2010. Taxonomy of Methanogens, in: Timmis, K.N. (Ed.), *Handbook of Hydrocarbon and Lipid Microbiology*. Springer, Berlin, Heidelberg, pp. 547–558. https://doi.org/10.1007/978-3-540-77587-4_42
- Liu, Z., Lozupone, C., Hamady, M., Bushman, F.D., Knight, R., 2007. Short pyrosequencing reads suffice for accurate microbial community analysis. *Nucleic Acids Res.* 35, e120. <https://doi.org/10.1093/nar/gkm541>
- Longhurst, A.R., 2010. *Ecological Geography of the Sea*. Elsevier.
- Lozano Mojica, J.D., Caballero, S., 2021. Applications of eDNA Metabarcoding for Vertebrate Diversity Studies in Northern Colombian Water Bodies. *Front. Ecol. Evol.* 8, 522. <https://doi.org/10.3389/fevo.2020.617948>
- Luton, P.E., Wayne, J.M., Sharp, R.J., Riley, P.W., 2002. The *mcrA* gene as an alternative to 16S rRNA in the phylogenetic analysis of methanogen populations in landfill. *Microbiol. Read. Engl.* 148, 3521–3530. <https://doi.org/10.1099/00221287-148-11-3521>

- Ma, J., Wang, P., Wang, X., Xu, Y., Paerl, H.W., 2019a. Cyanobacteria in eutrophic waters benefit from rising atmospheric CO₂ concentrations. *Sci. Total Environ.* 691, 1144–1154. <https://doi.org/10.1016/j.scitotenv.2019.07.056>
- Ma, J., Wang, P., Wang, X., Xu, Y., Paerl, H.W., 2019b. Cyanobacteria in eutrophic waters benefit from rising atmospheric CO₂ concentrations. *Sci. Total Environ.* 691, 1144–1154. <https://doi.org/10.1016/j.scitotenv.2019.07.056>
- Madigan, M.T., 2006. The Family *Heliobacteriaceae*, in: Dworkin, M., Falkow, S., Rosenberg, E., Schleifer, K.-H., Stackebrandt, E. (Eds.), *The Prokaryotes*. Springer US, New York, NY, pp. 951–964. https://doi.org/10.1007/0-387-30744-3_31
- Madigan, M.T., Jung, D.O., 2009. An Overview of Purple Bacteria: Systematics, Physiology, and Habitats, in: Hunter, C.N., Daldal, F., Thurnauer, M.C., Beatty, J.T. (Eds.), *The Purple Phototrophic Bacteria, Advances in Photosynthesis and Respiration*. Springer Netherlands, Dordrecht, pp. 1–15. https://doi.org/10.1007/978-1-4020-8815-5_1
- Madigan, M.T., Jung, D.O., Woese, C.R., Achenbach, L.A., 2000. *Rhodoferox antarcticus* sp. nov., a moderately psychrophilic purple nonsulfur bacterium isolated from an Antarctic microbial mat. *Arch. Microbiol.* 173, 269–277. <https://doi.org/10.1007/s002030000140>
- Madigan, M.T., Schaaf, N.A.V., Sattley, W.M., 2017. The *Chlorobiaceae*, *Chloroflexaceae*, and *Heliobacteriaceae*, in: Hallenbeck, P.C. (Ed.), *Modern Topics in the Phototrophic Prokaryotes: Environmental and Applied Aspects*. Springer International Publishing, Cham, pp. 139–161. https://doi.org/10.1007/978-3-319-46261-5_4
- Mahé, F., Rognes, T., Quince, C., de Vargas, C., Dunthorn, M., 2014. Swarm: robust and fast clustering method for amplicon-based studies. *PeerJ* 2, e593. <https://doi.org/10.7717/peerj.593>
- Malkin, S.Y., Meysman, F.J.R., 2015. Rapid Redox Signal Transmission by “Cable Bacteria” beneath a Photosynthetic Biofilm. *Appl. Environ. Microbiol.* 81, 948–956. <https://doi.org/10.1128/AEM.02682-14>
- Mangwani, N., 2015. Ocean acidification and marine microorganisms: responses and consequences. *OCEANOLOGIA* 57. <https://doi.org/10.1016/j.oceano.2015.07.003>
- Manske, A.K., Glaeser, J., Kuypers, M.M.M., Overmann, J., 2005. Physiology and Phylogeny of Green Sulfur Bacteria Forming a Monospecific Phototrophic Assemblage at a Depth of 100 Meters in the Black Sea. *Appl. Environ. Microbiol.* 71, 8049–8060. <https://doi.org/10.1128/AEM.71.12.8049-8060.2005>
- Martínez-Alonso, M., Mir, J., Caumette, P., Gaju, N., Guerrero, R., Esteve, I., 2004. Distribution of phototrophic populations and primary production in a microbial mat from the Ebro Delta, Spain. *Int. Microbiol.* 7, 19–25.
- Martínez-Alonso, M., van Bleijswijk, J., Gaju, N., Muyzer, G., 2005. Diversity of anoxygenic phototrophic sulfur bacteria in the microbial mats of the Ebro Delta: a combined morphological and molecular approach. *FEMS Microbiol. Ecol.* 52, 339–350. <https://doi.org/10.1016/j.femsec.2004.11.021>
- Marzocchi, U., Trojan, D., Larsen, S., Louise Meyer, R., Peter Revsbech, N., Schramm, A., Peter Nielsen, L., Risgaard-Petersen, N., 2014. Electric coupling between distant nitrate reduction and sulfide oxidation in marine sediment. *ISME J.* 8, 1682–1690. <https://doi.org/10.1038/ismej.2014.19>

- Mazière, C., Agogué, H., Cravo-Laureau, C., Cagnon, C., Lanneluc, I., Sablé, S., Fruitier-Arnaudin, I., Dupuy, C., Duran, R., 2021. New insights in bacterial and eukaryotic diversity of microbial mats inhabiting exploited and abandoned salterns at the Ré Island (France). *Microbiol. Res.* 252, 126854. <https://doi.org/10.1016/j.micres.2021.126854>
- Mazière, C., Bodo, M., Perdrau, M.A., Cravo-Laureau, C., Duran, R., Dupuy, C., Hubas, C., 2022. Climate change influences chlorophylls and bacteriochlorophylls metabolism in hypersaline microbial mat. *Sci. Total Environ.* 802, 149787. <https://doi.org/10.1016/j.scitotenv.2021.149787>
- McCliment, E.A., Voglesonger, K.M., O'Day, P.A., Dunn, E.E., Holloway, J.R., Cary, S.C., 2006. Colonization of nascent, deep-sea hydrothermal vents by a novel Archaeal and Nanoarchaeal assemblage. *Environ. Microbiol.* 8, 114–125. <https://doi.org/10.1111/j.1462-2920.2005.00874.x>
- Megonigal, J.P., Hines, M.E., Visscher, P.T., 2014. Anaerobic Metabolism: Linkages to Trace Gases and Aerobic Processes, in: *Treatise on Geochemistry*. Elsevier, pp. 273–359. <https://doi.org/10.1016/B978-0-08-095975-7.00808-1>
- Mills, H.J., Martinez, R.J., Story, S., Sobecky, P.A., 2004. Identification of Members of the Metabolically Active Microbial Populations Associated with *Beggiatoa* Species Mat Communities from Gulf of Mexico Cold-Seep Sediments. *Appl. Environ. Microbiol.* 70, 5447–5458. <https://doi.org/10.1128/AEM.70.9.5447-5458.2004>
- Mir, J., MartÃ-nez-Alonso, M., Esteve, I., Guerrero, R., 1991. Vertical stratification and microbial assemblage of a microbial mat in the Ebro Delta (Spain). *FEMS Microbiol. Lett.* 86, 59–68. <https://doi.org/10.1111/j.1574-6968.1991.tb04795.x>
- Møller, M.M., Nielsen, L.P., Jørgensen, B.B., 1985. Oxygen Responses and Mat Formation by *Beggiatoa* spp. *Appl. Environ. Microbiol.* 50, 373–382. <https://doi.org/10.1128/aem.50.2.373-382.1985>
- Montagna, P.A., 1984. In situ measurement of meiobenthic grazing rates on sediment bacteria and edaphic diatoms. *Mar. Ecol. Prog. Ser.* 18, 119–130. <https://doi.org/10.3354/meps018119>
- Moran, M.A., Belas, R., Schell, M.A., González, J.M., Sun, F., Sun, S., Binder, B.J., Edmonds, J., Ye, W., Orcutt, B., Howard, E.C., Meile, C., Palefsky, W., Goesmann, A., Ren, Q., Paulsen, I., Ulrich, L.E., Thompson, L.S., Saunders, E., Buchan, A., 2007. Ecological Genomics of Marine Roseobacters. *Appl. Environ. Microbiol.* 73, 4559–4569. <https://doi.org/10.1128/AEM.02580-06>
- Moro, C., Crouzet, O., Rasconi, S., Thouvenot, A., Coffe, G., Batisson, I., Bohatier, J., 2009. New Design Strategy for Development of Specific Primer Sets for PCR-Based Detection of *Chlorophyceae* and *Bacillariophyceae* in Environmental Samples. *Appl. Environ. Microbiol.* 75, 5729–5733. <https://doi.org/10.1128/AEM.00509-09>
- Müller, A.L., Kjeldsen, K.U., Rattei, T., Pester, M., Loy, A., 2015. Phylogenetic and environmental diversity of DsrAB-type dissimilatory (bi)sulfite reductases. *ISME J.* 9, 1152–1165. <https://doi.org/10.1038/ismej.2014.208>
- Müller, A.L., Pelikan, C., de Rezende, J.R., Wasmund, K., Putz, M., Glombitza, C., Kjeldsen, K.U., Jørgensen, B.B., Loy, A., 2018. Bacterial interactions during sequential degradation of cyanobacterial necromass in a sulfidic arctic marine sediment. *Environ. Microbiol.* 20, 2927–2940. <https://doi.org/10.1111/1462-2920.14297>

- Munson-McGee, J.H., Field, E.K., Bateson, M., Rooney, C., Stepanauskas, R., Young, M.J., 2015. *Nanoarchaeota*, Their *Sulfolobales* Host, and *Nanoarchaeota* Virus Distribution across Yellowstone National Park Hot Springs. *Appl. Environ. Microbiol.* 81, 7860–7868. <https://doi.org/10.1128/AEM.01539-15>
- Muyzer, G., Stams, A.J.M., 2008. The ecology and biotechnology of sulphate-reducing bacteria. *Nat. Rev. Microbiol.* 6, 441–454. <https://doi.org/10.1038/nrmicro1892>
- Nelson, D.C., Castenholz, R.W., 1982. Light responses of *Beggiatoa*. *Arch. Microbiol.* 131, 146–155. <https://doi.org/10.1007/BF01053997>
- Nelson, D.C., Jørgensen, B.B., Revsbech, N.P., 1986. Growth Pattern and Yield of a Chemoautotrophic *Beggiatoa* sp. in Oxygen-Sulfide Microgradients. *Appl. Environ. Microbiol.* 52, 225–233. <https://doi.org/10.1128/aem.52.2.225-233.1986>
- Nelson, K.E., Clayton, R.A., Gill, S.R., Gwinn, M.L., Dodson, R.J., Haft, D.H., Hickey, E.K., Peterson, J.D., Nelson, W.C., Ketchum, K.A., McDonald, L., Utterback, T.R., Malek, J.A., Linher, K.D., Garrett, M.M., Stewart, A.M., Cotton, M.D., Pratt, M.S., Phillips, C.A., Richardson, D., Heidelberg, J., Sutton, G.G., Fleischmann, R.D., Eisen, J.A., White, O., Salzberg, S.L., Smith, H.O., Venter, J.C., Fraser, C.M., 1999. Evidence for lateral gene transfer between Archaea and bacteria from genome sequence of *Thermotoga maritima*. *Nature* 399, 323–329. <https://doi.org/10.1038/20601>
- Newton, R.J., Griffin, L.E., Bowles, K.M., Meile, C., Gifford, S., Givens, C.E., Howard, E.C., King, E., Oakley, C.A., Reisch, C.R., Rinta-Kanto, J.M., Sharma, S., Sun, S., Varaljay, V., Vila-Costa, M., Westrich, J.R., Moran, M.A., 2010. Genome characteristics of a generalist marine bacterial lineage. *ISME J.* 4, 784–798. <https://doi.org/10.1038/ismej.2009.150>
- Nielsen, L.P., Risgaard-Petersen, N., Fossing, H., Christensen, P.B., Sayama, M., 2010. Electric currents couple spatially separated biogeochemical processes in marine sediment. *Nature* 463, 1071–1074. <https://doi.org/10.1038/nature08790>
- Nishimura, Y., Mukasa, S., Iizuka, H., Shimada, K., 1989. Isolation and characterization of bacteriochlorophyll-protein complexes from an aerobic bacterium, *Pseudomonas radiosa*. *Arch. Microbiol.* 152, 1–5. <https://doi.org/10.1007/BF00447002>
- Noël, C., Quintric, L., Cormier, A., Leroi, L., Durand, P., 2021. SAMBA: Standardized and Automated MetaBarcoding Analyses workflow. <https://doi.org/10.48546/WORKFLOWHUB.WORKFLOW.156.1>
- Noffke, N., Christian, D., Wacey, D., Hazen, R.M., 2013. Microbially Induced Sedimentary Structures Recording an Ancient Ecosystem in the ca. 3.48 Billion-Year-Old Dresser Formation, Pilbara, Western Australia. *Astrobiology* 13, 1103–1124. <https://doi.org/10.1089/ast.2013.1030>
- Normand, P., Duran, R., Le Roux, X., Morris, C., Poggiale, J.-C., 2011. Biodiversité et fonctionnement des écosystèmes microbiens, in: *Ecologie Microbienne. Microbiologie Des Milieux Naturels et Anthropisés*. Presses Universitaires de Pau et des Pays de l'Adour.
- Nubel, U., Garcia-Pichel, F., Clavero, E., Muyzer, G., 2000. Matching molecular diversity and ecophysiology of benthic cyanobacteria and diatoms in communities along a salinity gradient. *Environ. Microbiol.* 2, 217–226. <https://doi.org/10.1046/j.1462-2920.2000.00094.x>
- Nutman, A.P., Bennett, V.C., Friend, C.R.L., Van Kranendonk, M.J., Chivas, A.R., 2016. Rapid emergence of life shown by discovery of 3,700-million-year-old microbial structures. *Nature* 537, 535–538. <https://doi.org/10.1038/nature19355>

- O'Brien, P.A., Morrow, K.M., Willis, B.L., Bourne, D.G., 2016. Implications of Ocean Acidification for Marine Microorganisms from the Free-Living to the Host-Associated. *Front. Mar. Sci.* 3, 14. <https://doi.org/10.3389/fmars.2016.00047>
- Oelze, J., Golecki, J.R., 1995. Membranes and Chlorosomes of Green Bacteria: Structure, Composition and Development, in: Blankenship, R.E., Madigan, M.T., Bauer, C.E. (Eds.), *Anoxygenic Photosynthetic Bacteria, Advances in Photosynthesis and Respiration*. Kluwer Academic Publishers, Dordrecht, pp. 259–278. https://doi.org/10.1007/0-306-47954-0_13
- Offre, P., Spang, A., Schleper, C., 2013. Archaea in biogeochemical cycles. *Annu. Rev. Microbiol.* 67, 437–457. <https://doi.org/10.1146/annurev-micro-092412-155614>
- Ogram, A., Sayler, G.S., Barkay, T., 1987. The extraction and purification of microbial DNA from sediments. *J. Microbiol. Methods* 7, 57–66. [https://doi.org/10.1016/0167-7012\(87\)90025-X](https://doi.org/10.1016/0167-7012(87)90025-X)
- Oleksy, I.A., Baron, J.S., Beck, W.S., 2021. Nutrients and warming alter mountain lake benthic algal structure and function. *Freshw. Sci.* 40, 88–102. <https://doi.org/10.1086/713068>
- Ollivier, B., Caumette, P., Garcia, J.-L., 1994. Anaerobic Bacteria from Hypersaline Environments. *MICROBIOL REV* 58, 12.
- Oschlies, A., Brandt, P., Stramma, L., Schmidtko, S., 2018. Drivers and mechanisms of ocean deoxygenation. *Nat. Geosci.* 11, 467–473. <https://doi.org/10.1038/s41561-018-0152-2>
- Pace, A., Bourillot, R., Vennin, E., Dupraz, C., Braissant, O., Duteil, T., Bundeleva, I., Patrier, P., Sanajofre, P., Yokoyama, Y., Visscher, P., 2021. Modèle de minéralisation et diagenèse des tapis microbiens stromatolithiques hypersalins en domaine restreint, comparaison avec les microbialithes anciens.
- Paerl, H.W., Steppe, T.F., Buchan, K.C., Potts, M., 2003. Hypersaline Cyanobacterial Mats as Indicators of Elevated Tropical Hurricane Activity and Associated Climate Change. *AMBIO J. Hum. Environ.* 32, 87–90. <https://doi.org/10.1579/0044-7447-32.2.87>
- Pajares, S., Souza, V., Eguiarte, L.E., 2015. Multivariate and Phylogenetic Analyses Assessing the Response of Bacterial Mat Communities from an Ancient Oligotrophic Aquatic Ecosystem to Different Scenarios of Long-Term Environmental Disturbance. *PLOS ONE* 10, e0119741. <https://doi.org/10.1371/journal.pone.0119741>
- Palmisano, A.C., Summons, R.E., Cronin, S.E., Des Marais, D.J., 1989. Lipophilic Pigments from Cyanobacterial (blue-Green Algal) and Diatom Mats in Hamelin Pool, Shark Bay, Western Australia. *J. Phycol.* 25, 655–661. <https://doi.org/10.1111/j.0022-3646.1989.00655.x>
- Park, S., Akira, Y., Kogure, K., 2014. The Family Rhodothermaceae, in: Rosenberg, E., DeLong, E.F., Lory, S., Stackebrandt, E., Thompson, F. (Eds.), *The Prokaryotes*. Springer Berlin Heidelberg, Berlin, Heidelberg, pp. 849–856. https://doi.org/10.1007/978-3-642-38954-2_141
- Parry, J.D., 2004. Protozoan Grazing of Freshwater Biofilms, in: *Advances in Applied Microbiology*. Elsevier, pp. 167–196. [https://doi.org/10.1016/S0065-2164\(04\)54007-8](https://doi.org/10.1016/S0065-2164(04)54007-8)
- Pascal, P.-Y., Dupuy, C., Richard, P., Mallet, C., telet, E.A. du C., Niquilb, N., 2009. Seasonal variation in consumption of benthic bacteria by meio- and macrofauna in an intertidal mudflat. *Limnol. Oceanogr.* 54, 1048–1059. <https://doi.org/10.4319/lo.2009.54.4.1048>
- Passarelli, C., Meziane, T., Thiney, N., Boeuf, D., Jesus, B., Ruivo, M., Jeanthon, C., Hubas, C., 2015. Seasonal variations of the composition of microbial biofilms in sandy tidal flats: Focus

of fatty acids, pigments and exopolymers. *Estuar. Coast. Shelf Sci.* 153, 29–37. <http://dx.doi.org/10.1016/j.ecss.2014.11.013>

Paticat, F., 2007. Flux et usages de l'eau de mer dans les marais salés endigués Charentais : Cas du marais salé endigué de l'île de Ré.

Paul, B.G., Ding, H., Bagby, S.C., Kellermann, M.Y., Redmond, M.C., Andersen, G.L., Valentine, D.L., 2017. Methane-Oxidizing Bacteria Shunt Carbon to Microbial Mats at a Marine Hydrocarbon Seep. *Front. Microbiol.* 0. <https://doi.org/10.3389/fmicb.2017.00186>

Paul, K., Nonoh, J.O., Mikulski, L., Brune, A., 2012. “*Methanoplasmatales*,” *Thermoplasmatales*-Related Archaea in Termite Guts and Other Environments, Are the Seventh Order of Methanogens. *Appl. Environ. Microbiol.* 78, 8245–8253. <https://doi.org/10.1128/AEM.02193-12>

Pedrós-Alió, C., Calderón-Paz, J.I., MacLean, M.H., Medina, G., Marrasé, C., Gasol, J.M., Guixa-Boixereu, N., 2000. The microbial food web along salinity gradients. *FEMS Microbiol. Ecol.* 32, 143–155. <https://doi.org/10.1111/j.1574-6941.2000.tb00708.x>

Pelikan, C., Herbold, C., Hausmann, B., Müller, A., Pester, M., Loy, A., 2015. Diversity analysis of sulfite- and sulfate-reducing microorganisms by multiplex *dsrA* and *dsrB* amplicon sequencing using new primers and mock community-optimized bioinformatics. *Environ. Microbiol.* 18. <https://doi.org/10.1111/1462-2920.13139>

Peyraud, R., Schneider, K., Kiefer, P., Massou, S., Vorholt, J.A., Portais, J.-C., 2011. Genome-scale reconstruction and system level investigation of the metabolic network of *Methylobacterium extorquens* AM1. *BMC Syst. Biol.* 5, 189. <https://doi.org/10.1186/1752-0509-5-189>

Pfeffer, C., Larsen, S., Song, J., Dong, M., Besenbacher, F., Meyer, R.L., Kjeldsen, K.U., Schreiber, L., Gorby, Y.A., El-Naggar, M.Y., Leung, K.M., Schramm, A., Risgaard-Petersen, N., Nielsen, L.P., 2012. Filamentous bacteria transport electrons over centimetre distances. *Nature* 491, 218–221. <https://doi.org/10.1038/nature11586>

Pierre, G., Zhao, J.-M., Orvain, F., Dupuy, C., Klein, G.L., Graber, M., Maugard, T., 2014. Seasonal dynamics of extracellular polymeric substances (EPS) in surface sediments of a diatom-dominated intertidal mudflat (Marennes–Oléron, France). *J. Sea Res., Trophic significance of microbial biofilm in tidal flats* 92, 26–35. <https://doi.org/10.1016/j.seares.2013.07.018>

Pinckney, J.L., Paerl, H.W., 1997. Anoxygenic photosynthesis and nitrogen fixation by a microbial mat community in a bahamian hypersaline lagoon. *Appl. Environ. Microbiol.* 63, 420–426. <https://doi.org/10.1128/aem.63.2.420-426.1997>

Piontek, J., Lunau, M., Händel, N., Borchard, C., Wurst, M., Engel, A., 2009. Acidification increases microbial polysaccharide degradation in the ocean. *Biogeosciences Discuss.* 7. <https://doi.org/10.5194/bg-7-1615-2010>

Plugge, C., Zhang, W., Scholten, J., Stams, A., 2011. Metabolic Flexibility of Sulfate-Reducing Bacteria. *Front. Microbiol.* 2, 81. <https://doi.org/10.3389/fmicb.2011.00081>

Preisler, A., de Beer, D., Lichtschlag, A., Lavik, G., Boetius, A., Jørgensen, B.B., 2007. Biological and chemical sulfide oxidation in a *Beggiatoa* inhabited marine sediment. *ISME J.* 1, 341–353. <https://doi.org/10.1038/ismej.2007.50>

- Prieto-Barajas, C.M., Alfaro-Cuevas, R., Valencia-Cantero, E., Santoyo, G., 2017. Effect of seasonality and physicochemical parameters on bacterial communities in two hot spring microbial mats from Araró, Mexico. *Rev. Mex. Biodivers.* 88, 616–624. <https://doi.org/10.1016/j.rmb.2017.07.010>
- Prieto-Barajas, C.M., Valencia-Cantero, E., Santoyo, G., 2018. Microbial mat ecosystems: Structure types, functional diversity, and biotechnological application. *Electron. J. Biotechnol.* 31, 48–56. <https://doi.org/10.1016/j.ejbt.2017.11.001>
- Pujalte, M.J., Lucena, T., Ruvira, M.A., Arahál, D.R., Macián, M.C., 2014. The Family *Rhodobacteraceae*, in: Rosenberg, E., DeLong, E.F., Lory, S., Stackebrandt, E., Thompson, F. (Eds.), *The Prokaryotes*. Springer Berlin Heidelberg, Berlin, Heidelberg, pp. 439–512. https://doi.org/10.1007/978-3-642-30197-1_377
- Quast, C., Pruesse, E., Yilmaz, P., Gerken, J., Schweer, T., Yarza, P., Peplies, J., Glöckner, F.O., 2012. The SILVA ribosomal RNA gene database project: improved data processing and web-based tools. *Nucleic Acids Res.* 41, D590–D596. <https://doi.org/10.1093/nar/gks1219>
- Quince, C., Walker, A.W., Simpson, J.T., Loman, N.J., Segata, N., 2017. Shotgun metagenomics, from sampling to analysis. *Nat. Biotechnol.* 35, 833–844. <https://doi.org/10.1038/nbt.3935>
- Rainey, F.A., Ward-Rainey, N.L., Janssen, P.H., Hippe, H., Stackebrandt, E., 1996. *Clostridium paradoxum* DSM 7308T contains multiple 16S rRNA genes with heterogeneous intervening sequences. *Microbiol. Read. Engl.* 142 (Pt 8), 2087–2095. <https://doi.org/10.1099/13500872-142-8-2087>
- Rastogi, R.P., Sonani, R.R., Madamwar, D., 2015. Cyanobacterial Sunscreen Scytonemin: Role in Photoprotection and Biomedical Research. *Appl. Biochem. Biotechnol.* 176, 1551–1563. <https://doi.org/10.1007/s12010-015-1676-1>
- Raven, J.A., Falkowski, P.G., 1999. Oceanic sinks for atmospheric CO₂. *Plant Cell Environ.* 22, 741–755. <https://doi.org/10.1046/j.1365-3040.1999.00419.x>
- Reinold, Wong, MacLeod, Meltzer, Thompson, Burns, 2019. The Vulnerability of Microbial Ecosystems in A Changing Climate: Potential Impact in Shark Bay. *Life* 9, 71. <https://doi.org/10.3390/life9030071>
- Revsbech, N.P., Jørgensen, B.B., Blackburn, T.H., Cohen, Y., 1983. Microelectrode studies of the photosynthesis and O₂, H₂S, and pH profiles of a microbial mat. *Limnol. Oceanogr.* 28, 1062–1074. <https://doi.org/10.4319/lo.1983.28.6.1062>
- Rinke, C., Schwientek, P., Sczyrba, A., Ivanova, N.N., Anderson, I.J., Cheng, J.-F., Darling, A., Malfatti, S., Swan, B.K., Gies, E.A., Dodsworth, J.A., Hedlund, B.P., Tsiamis, G., Sievert, S.M., Liu, W.-T., Eisen, J.A., Hallam, S.J., Kyrpides, N.C., Stepanauskas, R., Rubin, E.M., Hugenholtz, P., Woyke, T., 2013. Insights into the phylogeny and coding potential of microbial dark matter. *Nature* 499, 431–437. <https://doi.org/10.1038/nature12352>
- Risgaard-Petersen, N., Revil, A., Meister, P., Nielsen, L.P., 2012. Sulfur, iron-, and calcium cycling associated with natural electric currents running through marine sediment. *Geochim. Cosmochim. Acta* 92, 1–13. <https://doi.org/10.1016/j.gca.2012.05.036>
- Robertson, L., Kuenen, J.G., 2006. The Colorless Sulfur Bacteria, in: *The Prokaryotes: Prokaryotic Physiology and Biochemistry*. pp. 985–1011. https://doi.org/10.1007/0-387-30742-7_31

- Rodrigues, C.M., Bio, A., Amat, F., Vieira, N., 2011. Artisanal salt production in Aveiro/Portugal - an ecofriendly process. *Saline Syst.* 7, 3. <https://doi.org/10.1186/1746-1448-7-3>
- Roeselers, G., Norris, T.B., Castenholz, R.W., Rysgaard, S., Glud, R.N., Kühl, M., Muyzer, G., 2007. Diversity of phototrophic bacteria in microbial mats from Arctic hot springs (Greenland). *Environ. Microbiol.* 9, 26–38. <https://doi.org/10.1111/j.1462-2920.2006.01103.x>
- Rognes, T., Flouri, T., Nichols, B., Quince, C., Mahé, F., 2016. VSEARCH: a versatile open source tool for metagenomics. *PeerJ* 4, e2584. <https://doi.org/10.7717/peerj.2584>
- Rzeznik-Orignac, J., Fichet, D., Boucher, G., 2003. Spatio-temporal structure of the nematode assemblages of the Brouage mudflat (Marennes Oléron, France). *Estuar. Coast. Shelf Sci.* 58, 77–88. [https://doi.org/10.1016/S0272-7714\(03\)00061-1](https://doi.org/10.1016/S0272-7714(03)00061-1)
- Sakai, S., Imachi, H., Hanada, S., Ohashi, A., Harada, H., Kamagata, Y. 2008, 2008. *Methanocella paludicola* gen. nov., sp. nov., a methane-producing archaeon, the first isolate of the lineage ‘Rice Cluster I’, and proposal of the new archaeal order *Methanocellales* ord. nov. *Int. J. Syst. Evol. Microbiol.* 58, 929–936. <https://doi.org/10.1099/ijs.0.65571-0>
- Sander, J., Dahl, C., 2009. Metabolism of Inorganic Sulfur Compounds in Purple Bacteria, in: Hunter, C.N., Daldal, F., Thurnauer, M.C., Beatty, J.T. (Eds.), *The Purple Phototrophic Bacteria, Advances in Photosynthesis and Respiration*. Springer Netherlands, Dordrecht, pp. 595–622. https://doi.org/10.1007/978-1-4020-8815-5_30
- Sanger, F., Nicklen, S., Coulson, A.R., 1977. DNA sequencing with chain-terminating inhibitors. *Proc. Natl. Acad. Sci. U. S. A.* 74, 5463–5467.
- Sarmiento, H., Montoya, J.M., Vázquez-Domínguez, E., Vaqué, D., Gasol, J.M., 2010. Warming effects on marine microbial food web processes: how far can we go when it comes to predictions? *Philos. Trans. R. Soc. B Biol. Sci.* 365, 2137–2149. <https://doi.org/10.1098/rstb.2010.0045>
- Scheer, H., 2006. An Overview of Chlorophylls and Bacteriochlorophylls: Biochemistry, Biophysics, Functions and Applications, in: Grimm, B., Porra, R.J., Rüdiger, W., Scheer, H. (Eds.), *Chlorophylls and Bacteriochlorophylls: Biochemistry, Biophysics, Functions and Applications, Advances in Photosynthesis and Respiration*. Springer Netherlands, Dordrecht, pp. 1–26. https://doi.org/10.1007/1-4020-4516-6_1
- Schloss, P.D., Westcott, S.L., Ryabin, T., Hall, J.R., Hartmann, M., Hollister, E.B., Lesniewski, R.A., Oakley, B.B., Parks, D.H., Robinson, C.J., Sahl, J.W., Stres, B., Thallinger, G.G., Van Horn, D.J., Weber, C.F., 2009. Introducing mothur: Open-Source, Platform-Independent, Community-Supported Software for Describing and Comparing Microbial Communities. *Appl. Environ. Microbiol.* 75, 7537–7541. <https://doi.org/10.1128/AEM.01541-09>
- Schmidtko, S., Stramma, L., Visbeck, M., 2017. Decline in global oceanic oxygen content during the past five decades. *Nature* 542, 335–339. <https://doi.org/10.1038/nature21399>
- Schoch, C.L., Seifert, K.A., Huhndorf, S., Robert, V., Spouge, J.L., Levesque, C.A., Chen, W., Consortium, F.B., 2012. Nuclear ribosomal internal transcribed spacer (ITS) region as a universal DNA barcode marker for Fungi. *Proc. Natl. Acad. Sci.* 109, 6241–6246. <https://doi.org/10.1073/pnas.1117018109>
- Schratzberger, M., Ingels, J., 2018. Meiofauna matters: The roles of meiofauna in benthic ecosystems. *J. Exp. Mar. Biol. Ecol.*, IçIMCo, the 16th International Meiofauna Conference 502, 12–25. <https://doi.org/10.1016/j.jembe.2017.01.007>

- Segata, N., Izard, J., Waldron, L., Gevers, D., Miropolsky, L., Garrett, W.S., Huttenhower, C., 2011. Metagenomic biomarker discovery and explanation. *Genome Biol.* 12, R60. <https://doi.org/10.1186/gb-2011-12-6-r60>
- Seitaj, D., Schauer, R., Sulu-Gambari, F., Hidalgo-Martinez, S., Malkin, S.Y., Burdorf, L.D.W., Slomp, C.P., Meysman, F.J.R., 2015. Cable bacteria generate a firewall against euxinia in seasonally hypoxic basins. *Proc. Natl. Acad. Sci.* 112, 13278–13283. <https://doi.org/10.1073/pnas.1510152112>
- Severin, I., Confurius-Guns, V., Stal, L.J., 2012. Effect of salinity on nitrogenase activity and composition of the active diazotrophic community in intertidal microbial mats. *Arch. Microbiol.* 194, 483–491. <https://doi.org/10.1007/s00203-011-0787-5>
- Severin, I., Stal, L.J., 2008. Light dependency of nitrogen fixation in a coastal cyanobacterial mat. *ISME J.* 2, 1077–1088. <https://doi.org/10.1038/ismej.2008.63>
- Sherr, E.B., Sherr, B.F., 1987. High rates of consumption of bacteria by pelagic ciliates. *Nature* 325, 710–711. <https://doi.org/10.1038/325710a0>
- Shetye, S., Sudhakar, M., Jena, B., Mohan, R., 2013. Occurrence of Nitrogen Fixing Cyanobacterium *Trichodesmium* under Elevated pCO₂ Conditions in the Western Bay of Bengal. *Int. J. Oceanogr.* 2013. <https://doi.org/10.1155/2013/350465>
- Soergel, D.A.W., Dey, N., Knight, R., Brenner, S.E., 2012. Selection of primers for optimal taxonomic classification of environmental 16S rRNA gene sequences. *ISME J.* 6, 1440–1444. <https://doi.org/10.1038/ismej.2011.208>
- Solé, A., Diestra, E., Esteve, I., 2009. Confocal laser scanning microscopy image analysis for cyanobacterial biomass determined at microscale level in different microbial mats. *Microb. Ecol.* 57, 649–656. <https://doi.org/10.1007/s00248-008-9463-y>
- Stal, L.J., 2012. Cyanobacterial Mats and Stromatolites, in: Whitton, B.A. (Ed.), *Ecology of Cyanobacteria II*. Springer Netherlands, Dordrecht, pp. 65–125. https://doi.org/10.1007/978-94-007-3855-3_4
- Stal, L.J., 2001. Coastal microbial mats: the physiology of a small-scale ecosystem. *South Afr. J. Bot.* 67, 399–410. [https://doi.org/10.1016/S0254-6299\(15\)31156-X](https://doi.org/10.1016/S0254-6299(15)31156-X)
- Stal, L.J., 1995. Physiological ecology of cyanobacteria in microbial mats and other communities. *New Phytol.* 131, 1–32. <https://doi.org/10.1111/j.1469-8137.1995.tb03051.x>
- Stal, L.J., Bolhuis, H., Cretoiu, M.S., 2019. Phototrophic marine benthic microbiomes: the ecophysiology of these biological entities. *Environ. Microbiol.* 21, 1529–1551. <https://doi.org/10.1111/1462-2920.14494>
- Stal, L.J., van Gemerden, H., Krumbein, W.E., 1985. Structure and development of a benthic marine microbial mat. *FEMS Microbiol. Ecol.* 1, 111–125. <https://doi.org/10.1111/j.1574-6968.1985.tb01138.x>
- Stauffert, M., Cravo-Laureau, C., Jezequel, R., Barantal, S., Cuny, P., Gilbert, F., Cagnon, C., Militon, C., Amouroux, D., Mahdaoui, F., Bouyssiere, B., Stora, G., Merlin, F., Duran, R., 2013. Impact of Oil on Bacterial Community Structure in Bioturbated Sediments. *PloS One* 8, e65347. <https://doi.org/10.1371/journal.pone.0065347>
- Steppe, T., Paerl, H., 2002. Potential N₂ fixation by sulfate-reducing bacteria in a marine intertidal microbial mat. *Aquat. Microb. Ecol. - AQUAT MICROB ECOL* 28, 1–12. <https://doi.org/10.3354/ame028001>

- Steppe, T.F., Olson, J.B., Paerl, H.W., Litaker, R.W., Belnap, J., 1996. Consortial N₂ fixation: a strategy for meeting nitrogen requirements of marine and terrestrial cyanobacterial mats. *FEMS Microbiol. Ecol.* 21, 149–156. [https://doi.org/10.1016/S0168-6496\(96\)00047-5](https://doi.org/10.1016/S0168-6496(96)00047-5)
- Steppe, T.F., Paerl, H.W., 2005. Nitrogenase Activity and *nifH* Expression in a Marine Intertidal Microbial Mat. *Microb. Ecol.* 49, 315–324. <https://doi.org/10.1007/s00248-004-0245-x>
- Sulu-Gambari, F., Seitaj, D., Meysman, F.J.R., Schauer, R., Polerecky, L., Slomp, C.P., 2016. Cable Bacteria Control Iron–Phosphorus Dynamics in Sediments of a Coastal Hypoxic Basin. *Environ. Sci. Technol.* 50, 1227–1233. <https://doi.org/10.1021/acs.est.5b04369>
- Suyama, T., Shigematsu, T., Takaichi, S., Nodasaka, Y., Fujikawa, S., Hosoya, H., Tokiwa, Y., Kanagawa, T., Hanada, S., 1999. *Roseateles depolymerans* gen. nov., sp. nov., a new bacteriochlorophyll *a*-containing obligate aerobe belonging to the beta-subclass of the Proteobacteria. *Int. J. Syst. Bacteriol.* 49 Pt 2, 449–457. <https://doi.org/10.1099/00207713-49-2-449>
- Swingley, W.D., Blankenship, R.E., Raymond, J., 2009. Evolutionary Relationships Among Purple Photosynthetic Bacteria and the Origin of Proteobacterial Photosynthetic Systems, in: Hunter, C.N., Daldal, F., Thurnauer, M.C., Beatty, J.T. (Eds.), *The Purple Phototrophic Bacteria, Advances in Photosynthesis and Respiration*. Springer Netherlands, Dordrecht, pp. 17–29. https://doi.org/10.1007/978-1-4020-8815-5_2
- Takahashi, E., Ledauphin, J., Goux, D., Orvain, F., 2009. Optimising extraction of extracellular polymeric substances (EPS) from benthic diatoms: Comparison of the efficiency of six EPS extraction methods. *Mar. Freshw. Res.* 60, 1201–1210. <http://dx.doi.org/10.1071/MF08258>
- Takahashi, T., Sutherland, S.C., Sweeney, C., Poisson, A., Metzl, N., Tilbrook, B., Bates, N., Wanninkhof, R., Feely, R.A., Sabine, C., Olafsson, J., Nojiri, Y., 2002. Global sea–air CO₂ flux based on climatological surface ocean pCO₂, and seasonal biological and temperature effects. *Deep Sea Res. Part II Top. Stud. Oceanogr., The Southern Ocean I: Climatic Changes in the Cycle of Carbon in the Southern Ocean* 49, 1601–1622. [https://doi.org/10.1016/S0967-0645\(02\)00003-6](https://doi.org/10.1016/S0967-0645(02)00003-6)
- Takekawa, J.Y., Ackerman, J.T., Brand, L.A., Graham, T.R., Eagles-Smith, C.A., Herzog, M.P., Topping, B.R., Shellenbarger, G.G., Kuwabara, J.S., Mruz, E., Piotter, S.L., Athearn, N.D., 2015. Unintended Consequences of Management Actions in Salt Pond Restoration: Cascading Effects in Trophic Interactions. *PLOS ONE* 10, e0119345. <https://doi.org/10.1371/journal.pone.0119345>
- Tang, W., Wang, S., Fonseca-Batista, D., Dehairs, F., Gifford, S., Gonzalez, A.G., Gallinari, M., Planquette, H., Sarthou, G., Cassar, N., 2019. Revisiting the distribution of oceanic N₂ fixation and estimating diazotrophic contribution to marine production. *Nat. Commun.* 10, 831. <https://doi.org/10.1038/s41467-019-08640-0>
- Terrisse, F., Cravo-Laureau, C., Noël, C., Cagnon, C., Dumbrell, A.J., McGenity, T.J., Duran, R., 2017. Variation of Oxygenation Conditions on a Hydrocarbonoclastic Microbial Community Reveals *Alcanivorax* and *Cycloclasticus* Ecotypes. *Front. Microbiol.* 8, 1549. <https://doi.org/10.3389/fmicb.2017.01549>
- Thauer, R.K., 1998. Biochemistry of methanogenesis: a tribute to Marjory Stephenson:1998 Marjory Stephenson Prize Lecture. *Microbiology* 144, 2377–2406. <https://doi.org/10.1099/00221287-144-9-2377>

- Thauer, R.K., Stackebrandt, E., Hamilton, W.A., 2007. Energy metabolism and phylogenetic diversity of sulphate-reducing bacteria, in: Barton, L.L., Hamilton, W.A. (Eds.), *Sulphate-Reducing Bacteria*. Cambridge University Press, Cambridge, pp. 1–38. <https://doi.org/10.1017/CBO9780511541490.002>
- Thweatt, J.L., Canniffe, D.P., Bryant, D.A., 2019. Biosynthesis of chlorophylls and bacteriochlorophylls in green bacteria, in: *Advances in Botanical Research*. Elsevier, pp. 35–89. <https://doi.org/10.1016/bs.abr.2019.03.002>
- Tomitani, A., Okada, K., Miyashita, H., Matthijs, H.C., Ohno, T., Tanaka, A., 1999. Chlorophyll *b* and phycobilins in the common ancestor of cyanobacteria and chloroplasts. *Nature* 400, 159–162. <https://doi.org/10.1038/22101>
- Tragin, M., Vaulot, D., 2018. Green microalgae in marine coastal waters: The Ocean Sampling Day (OSD) dataset. *Sci. Rep.* 8, 14020. <https://doi.org/10.1038/s41598-018-32338-w>
- Turk, K.A., Rees, A.P., Zehr, J.P., Pereira, N., Swift, P., Shelley, R., Lohan, M., Woodward, E.M.S., Gilbert, J., 2011. Nitrogen fixation and nitrogenase (*nifH*) expression in tropical waters of the eastern North Atlantic. *ISME J.* 5, 1201–1212. <https://doi.org/10.1038/ismej.2010.205>
- Turner, J.T., 2004. The Importance of Small Planktonic Copepods and Their Roles in Pelagic Marine Food Webs. *Zool. Stud.* 13.
- Underwood, G.J.C., Boulcott, M., Raines, C.A., Waldron, K., 2004. Environmental Effects on Exopolymer Production by Marine Benthic Diatoms: Dynamics, Changes in Composition, and Pathways of Production. *J. Phycol.* 40, 293–304. <https://doi.org/10.1111/j.1529-8817.2004.03076.x>
- van Gernerden, H., 1993. Microbial mats: A joint venture. *Mar. Geol.* 113, 3–25. [https://doi.org/10.1016/0025-3227\(93\)90146-M](https://doi.org/10.1016/0025-3227(93)90146-M)
- Varin, T., Lovejoy, C., Jungblut, A.D., Vincent, W.F., Corbeil, J., 2010. Metagenomic profiling of Arctic microbial mat communities as nutrient scavenging and recycling systems. *Limnol. Oceanogr.* 55, 1901–1911. <https://doi.org/10.4319/lo.2010.55.5.1901>
- Visscher, P.T., Nijburg, J.W., van Gernerden, H., 1990. Polysulfide utilization by *Thiocapsa roseopersicina*. *Arch. Microbiol.* 155, 75–81. <https://doi.org/10.1007/BF00291278>
- Wagner, M., Roger, A.J., Flax, J.L., Brusseau, G.A., Stahl, D.A., 1998. Phylogeny of Dissimilatory Sulfite Reductases Supports an Early Origin of Sulfate Respiration. *J. Bacteriol.* 180, 2975–2982.
- Walch, D.A., 2014. Consequences of climate change on microbial life in the ocean [WWW Document]. *Microbiol. Soc.* URL <https://microbiologysociety.org/publication/past-issues/water/article/consequences-of-climate-change-on-microbial-life-in-the-ocean-water.html> (accessed 10.6.21).
- Walter, J.M., de Oliveira, L.S., Tschoeke, D.A., Meirelles, P.M., Neves, M.H.C.B., Batista, D., Carvalho, A.P., Santos Costa, R.D., Dobretsov, S., Coutinho, R., Swings, J., Thompson, C.C., Thompson, F.L., 2021. Metagenomic Insights Into Ecosystem Function in the Microbial Mats of a Large Hypersaline Coastal Lagoon System. *Front. Mar. Sci.* 8, 1089. <https://doi.org/10.3389/fmars.2021.715335>
- Wannicke, N., Frey, C., Law, C.S., Voss, M., 2018. The response of the marine nitrogen cycle to ocean acidification. *Glob. Change Biol.* 24, 5031–5043. <https://doi.org/10.1111/gcb.14424>

- Waters, E., Hohn, M.J., Ahel, I., Graham, D.E., Adams, M.D., Barnstead, M., Beeson, K.Y., Bibbs, L., Bolanos, R., Keller, M., Kretz, K., Lin, X., Mathur, E., Ni, J., Podar, M., Richardson, T., Sutton, G.G., Simon, M., Söll, D., Stetter, K.O., Short, J.M., Noordewier, M., 2003. The genome of *Nanoarchaeum equitans*: Insights into early archaeal evolution and derived parasitism. *Proc. Natl. Acad. Sci.* 100, 12984–12988. <https://doi.org/10.1073/pnas.1735403100>
- Watkins, A.J., Roussel, E.G., Parkes, R.J., Sass, H., 2014. Glycine Betaine as a Direct Substrate for Methanogens (*Methanococoides* spp.). *Appl. Environ. Microbiol.* 80, 289–293. <https://doi.org/10.1128/AEM.03076-13>
- Watkins, A.J., Roussel, E.G., Webster, G., Parkes, R.J., Sass, H., 2012. Choline and N,N-dimethylethanolamine as direct substrates for methanogens. *Appl. Environ. Microbiol.* 78, 8298–8303. <https://doi.org/10.1128/AEM.01941-12>
- Westall, F., Vries, S.T. de, Nijman, W., Rouchon, V., Orberger, B., Pearson, V., Watson, J., Verchovsky, A., Wright, I., Rouzaud, J.-N., Marchesini, D., Severine, A., 2006. The 3.466 Ga “Kitty’s Gap Chert,” an early Archean microbial ecosystem. [https://doi.org/10.1130/2006.2405\(07\)](https://doi.org/10.1130/2006.2405(07))
- Whitman, W.B., Jeanthon, C., 2006. Methanococcales, in: Dworkin, M., Falkow, S., Rosenberg, E., Schleifer, K.-H., Stackebrandt, E. (Eds.), *The Prokaryotes: Volume 3: Archaea. Bacteria: Firmicutes, Actinomycetes*. Springer, New York, NY, pp. 257–273. https://doi.org/10.1007/0-387-30743-5_13
- Whitman, W.B., Rainey, F., Kämpfer, P., Trujillo, M., Chun, J., DeVos, P., Hedlund, B., Dedysh, S. (Eds.), 2015. *Bergey’s Manual of Systematics of Archaea and Bacteria*, 1st ed. Wiley. <https://doi.org/10.1002/9781118960608>
- Widdicombe, S., Dashfield, S.L., McNeill, C.L., Needham, H.R., Beesley, A., McEvoy, A., Øxnevad, S., Clarke, K.R., Berge, J.A., 2009. Effects of CO₂ induced seawater acidification on infaunal diversity and sediment nutrient fluxes. *Mar. Ecol. Prog. Ser.* 379, 59–75. <https://doi.org/10.3354/meps07894>
- Wieland, A., Kühl, M., McGowan, L., Fourçans, A., Duran, R., Caumette, P., Garcia de Oteyza, T., Grimalt, J.O., Solé, A., Diestra, E., Esteve, I., Herbert, R.A., 2003. Microbial Mats on the Orkney Islands Revisited: Microenvironment and Microbial Community Composition. *Microb. Ecol.* 46, 371–390. <https://doi.org/10.1007/s00248-002-0108-2>
- Witt, V., Wild, C., Anthony, K.R.N., Diaz-Pulido, G., Uthicke, S., 2011. Effects of ocean acidification on microbial community composition of, and oxygen fluxes through, biofilms from the Great Barrier Reef. *Environ. Microbiol.* 13, 2976–2989. <https://doi.org/10.1111/j.1462-2920.2011.02571.x>
- Woese, C.R., Fox, G.E., 1977. Phylogenetic structure of the prokaryotic domain: The primary kingdoms. *Proc. Natl. Acad. Sci.* 74, 5088–5090. <https://doi.org/10.1073/pnas.74.11.5088>
- Wright, S., Thomas, D., Marchant, H., Higgins, H., Mackey, M., Mackey, D., 1996. Analysis of phytoplankton of the Australian sector of the Southern Ocean: comparisons of microscopy and size frequency data with interpretations of pigment HPLC data using the “CHEMTAX” matrix factorisation program. *Mar. Ecol. Prog. Ser.* 144, 285–298. <https://doi.org/10.3354/meps144285>
- Wurch, L., Giannone, R.J., Belisle, B.S., Swift, C., Utturkar, S., Hettich, R.L., Reysenbach, A.-L., Podar, M., 2016. Genomics-informed isolation and characterization of a symbiotic

- Nanoarchaeota* system from a terrestrial geothermal environment. Nat. Commun. 7, 12115. <https://doi.org/10.1038/ncomms12115>
- Yang, S., Liebner, S., Alawi, M., Ebenhöf, O., Wagner, D., 2014. Taxonomic database and cut-off value for processing *mcrA* gene 454 pyrosequencing data by MOTHUR. J. Microbiol. Methods 103, 3–5. <https://doi.org/10.1016/j.mimet.2014.05.006>
- Yap, W.H., Zhang, Z., Wang, Y., 1999. Distinct types of rRNA operons exist in the genome of the actinomycete *Thermomonospora chromogena* and evidence for horizontal transfer of an entire rRNA operon. J. Bacteriol. 181, 5201–5209. <https://doi.org/10.1128/JB.181.17.5201-5209.1999>
- Yilmaz, P., Wegener Parfrey, L., Yarza, P., Gerken, J., Priesse, E., Quast, C., Schweer, T., Peplies, J., Ludwig, W., Glöckner, F., 2013. The SILVA and “All-species living tree project (LTP)” taxonomic frameworks. Nucleic Acids Res. 42. <https://doi.org/10.1093/nar/gkt1209>
- Yurkov, V., Csotonyi, J.T., 2009. New Light on Aerobic Anoxygenic Phototrophs, in: Hunter, C.N., Daldal, F., Thurnauer, M.C., Beatty, J.T. (Eds.), The Purple Phototrophic Bacteria, Advances in Photosynthesis and Respiration. Springer Netherlands, pp. 31–55. https://doi.org/10.1007/978-1-4020-8815-5_1
- Yurkov, V.V., 2006. Aerobic Phototrophic Proteobacteria, in: Dworkin, M., Falkow, S., Rosenberg, E., Schleifer, K.-H., Stackebrandt, E. (Eds.), The Prokaryotes. Springer New York, New York, NY, pp. 562–584. https://doi.org/10.1007/0-387-30745-1_23
- Yurkov, V.V., Beatty, J.T., 1998. Aerobic Anoxygenic Phototrophic Bacteria. Microbiol. Mol. Biol. Rev. 62, 695–724.
- Zehr, J.P., Mellon, M., Braun, S., Litaker, W., Steppe, T., Paerl, H.W., 1995. Diversity of heterotrophic nitrogen fixation genes in a marine cyanobacterial mat. Appl. Environ. Microbiol. 61, 2527–2532. <https://doi.org/10.1128/aem.61.7.2527-2532.1995>
- Zeng, Y., Koblížek, M., 2017. Phototrophic *Gemmatimonadetes*: A New “Purple” Branch on the Bacterial Tree of Life, in: Hallenbeck, P.C. (Ed.), Modern Topics in the Phototrophic Prokaryotes: Environmental and Applied Aspects. Springer International Publishing, Cham, pp. 163–192. https://doi.org/10.1007/978-3-319-46261-5_5
- Zhang, H., Sekiguchi, Y., Hanada, S., Hugenholtz, P., Kim, H., Kamagata, Y., Nakamura, K. 2003, 2003. *Gemmatimonas aurantiaca* gen. nov., sp. nov., a Gram-negative, aerobic, polyphosphate-accumulating micro-organism, the first cultured representative of the new bacterial phylum *Gemmatimonadetes* phyl. nov. Int. J. Syst. Evol. Microbiol. 53, 1155–1163. <https://doi.org/10.1099/ijs.0.02520-0>

La vie sur Terre est confrontée à des changements environnementaux sans précédent, principalement en raison de l'augmentation rapide des émissions de gaz à effet de serre dues aux activités humaines. Le niveau moyen mondial des mers s'est élevé plus rapidement depuis 1900 qu'au cours de tout autre siècle précédent depuis au moins 3000 ans, et le réchauffement mondial des océans s'est produit plus rapidement au cours du siècle dernier que depuis la fin de la précédente transition déglaciaire (il y a environ 11000 ans) (GIEC, 2021). Le pH de surface de l'océan a augmenté au cours des 50 derniers millions d'années et est actuellement aussi bas qu'il l'a été au cours des dernières décennies, ce qui est inhabituel au cours des 2 derniers millions d'années (GIEC, 2021). Toutes ces modifications environnementales sont appelées changement climatique.

Malgré son pouvoir tampon, l'océan est aujourd'hui l'un des compartiments les plus touchés. Il joue un rôle influent dans le système climatique puisque le réchauffement des océans est responsable de 91% du réchauffement global (GIEC, 2021). Depuis la révolution industrielle, le pH de l'océan a diminué de 0,1 unité de pH, sa température a augmenté entre 0,68 et 1,01°C et son niveau s'est élevé en moyenne de 0,20 m (GIEC, 2021, 2014). Pour établir les impacts du changement climatique de la manière la plus précise possible, des données locales sont nécessaires. En région Nouvelle-Aquitaine, le scénario le plus pessimiste du Groupe d'experts intergouvernemental sur l'évolution du climat (GIEC) prévoit une acidification des océans de 0,4 à 0,45 unité de pH en moyenne, associée à un réchauffement des eaux de surface de 4°C d'ici 2100 (GIEC, 2014). Une augmentation des événements climatiques extrêmes et une élévation du niveau de la mer de 0,6 à 0,7 m sont également prévues (GIEC, 2014).

Les micro-organismes sont définis comme " le support de vie de la biosphère " (Cavicchioli et al., 2019 ; Reinold et al., 2019). Dans les océans, ils représentaient 1×10^{29} cellules (Flemming et Wuertz, 2019), dominant l'activité métabolique, participant à plusieurs cycles biogéochimiques, produisant la moitié de l'oxygène de la Terre, assurant le bon fonctionnement des systèmes aquatiques et étant à la base des réseaux alimentaires et du

recyclage de la matière organique. Peu d'études visent à comprendre comment le changement climatique affectera les communautés microbiennes à la fin du siècle. Pour obtenir des informations sur l'effet du changement climatique sur les communautés microbiennes, nous pensons que le tapis microbien, qui est une structure regroupant de nombreux microorganismes et métabolismes, ce qui en fait un système autosuffisant, est un bon modèle. Les tapis microbiens jouent un rôle clé dans les cycles biogéochimiques du carbone, de l'oxygène, du soufre, de l'azote, *etc.* Ils ont été notamment impliqués dans l'oxygénation de l'atmosphère.

Cette thèse vise à déterminer les impacts potentiels du changement climatique sur les tapis microbiens des milieux côtiers de la région Nouvelle-Aquitaine. Elle se base sur les prédictions les plus pessimistes (scénario RCP8.5) pour la fin du siècle selon le rapport du GIEC établi en 2014 (GIEC, 2014).

Le premier chapitre (état de l'art) vise à présenter les prédictions du GIEC concernant l'impact du changement climatique sur l'océan, et plus particulièrement sur les milieux côtiers de la région Nouvelle-Aquitaine, ainsi que les connaissances actuelles de l'impact sur les microorganismes. Une description de la structure et du fonctionnement des tapis microbiens y est également faite afin de mieux comprendre leur composition, leur structure et leur fonctionnement. L'approche expérimentale, les méthodes et les dispositifs utilisés pour réaliser cette étude sont décrits dans le deuxième chapitre (chapitre méthodologie).

Les résultats de cette thèse sont présentés dans les quatre chapitres suivants. Les tapis microbiens des marais salants de l'île de Ré n'ont jamais été étudiés auparavant. Ainsi, le troisième chapitre vise à définir et à comparer la diversité microbienne présente dans deux tapis microbiens, l'un provenant d'un marais salé exploité et l'autre d'un marais salé non exploité. Cette étude permet également de choisir la source du tapis à échantillonner (exploité ou non) pour la simulation du changement climatique.

Dans le quatrième chapitre, nous avons étudié la dynamique saisonnière des communautés microbiennes dans un marais salant. En effet, les marais salants étant des

milieux peu profonds et la région étant définie par l'alternance de saisons marquées, les tapis microbiens font déjà face à des conditions environnementales comparables à celles du changement climatique selon le GIEC (2014). La comparaison des tapis microbiens de parcelles exploitées et non exploitées d'un même marais salant a également permis de déterminer l'impact anthropique sur ces communautés microbiennes au fil des saisons.

L'impact du changement climatique sur les tapis microbiens des marais salants de l'île de Ré est étudié dans le cinquième chapitre avec la simulation des deux paramètres qui auront le plus d'impact sur ces milieux, l'acidification et le réchauffement des eaux océaniques de surface, avec la mise en place d'expériences en mésocosmes.

Le sixième chapitre se concentre sur l'impact du changement climatique sur les communautés phototrophes des tapis microbiens à travers l'étude des molécules spécifiques produites, des substances polymériques extracellulaires et des pigments, ainsi que leur capacité photosynthétique.

Le dernier chapitre résume et discute les principales conclusions de cette thèse, en offrant quelques perspectives.

Les différents scénarios climatiques simulés ont eu un impact sur les tapis microbiens en termes de diversité, de structure et de fonction. L'acidification seule a eu un impact sur les communautés procaryotiques, tandis que la température seule a affecté les populations eucaryotiques. Ces deux traitements combinés ont retardé l'impact du changement climatique.

Le suivi *in situ* de la diversité et de la structure des tapis microbiens présents dans les marais salants de l'île de Ré a montré que certaines des conditions naturelles auxquelles ils sont confrontés sont comparables à celles prévues par le GIEC pour 2100 (GIEC, 2014). Par exemple, le changement climatique devrait entraîner un réchauffement des eaux de surface d'environ 4°C (GIEC, 2014). Cependant, les températures des eaux de surface auxquelles les tapis microbiens sont actuellement soumis peuvent être similaires ou même supérieures à celles prédites par le GIEC en fonction de la saison : si la température est actuellement de 20°C au printemps, elle atteindra 24°C en 2100, ce qui est déjà le cas en été actuellement. Les tapis microbiens présentent donc déjà une résilience naturelle aux variations de ce paramètre avec des amplitudes égales ou supérieures à 4°C. C'est probablement pour cela que peu d'impacts ont été observés sur les tapis microbiens de l'île de Ré suite à l'étude en mésocosmes. Cependant, même si le tapis microbien peut supporter des températures de +4°C en 2100 au printemps, ce réchauffement doit être ajouté à chaque saison. Ainsi, un tapis microbien "habitué" à des températures de 20°C au printemps devra faire face à 24°C à la même saison à la fin du siècle, et ce pour chaque saison. La gamme de températures à laquelle le tapis microbien sera confronté sera donc modifiée avec une intensité et une fréquence différentes. On peut supposer qu'un tapis microbien observé actuellement au printemps ressemblera à celui observé actuellement en été en 2100. Il sera également confronté à des températures plus chaudes auxquelles il n'a peut-être pas à faire face en été actuellement.

Les marais salants étant des milieux peu profonds, la température de l'eau dépend de la température de l'air. Les variations journalières peuvent être très importantes, dépassant parfois dix degrés dans cette région (différence jour/nuit marquée). La température de l'eau de

surface dans les mésocosmes était maintenue à une température définie (20°C ou 24°C pour simuler un réchauffement) et les tapis présents n'étaient donc pas confrontés à cette variation de température journalière. Il serait intéressant de tester l'impact de cette amplitude de température à travers les mésocosmes. En effet, les tapis microbiens ont pu adapter leur fonctionnement au réchauffement simulé car la température était constante, mais peut-être que certaines communautés ou métabolismes auraient pu être affectés, positivement ou négativement, si une simulation de la variation de température avait été mise en place.

Le choix de réaliser l'acidification de l'eau a été fait dans la réserve d'eau distribuant l'eau de mer aux différents mésocosmes, au lieu d'acidifier directement l'eau des mésocosmes. En effet, l'eau des marais salants dépend de l'apport océanique en fonction des marées et cette réserve d'eau représentait donc " l'océan ". Nous avons pu constater que les tapis microbiens pouvaient tamponner le pH à son niveau initial malgré une eau acidifiée (Mazière et al., 2022). Cependant, certaines améliorations pourraient être apportées au système. Un suivi du pH jour/nuit pourrait nous informer sur la variation quotidienne du pH, qui peut-être la nuit ne serait plus tamponné avec l'arrêt des métabolismes phototrophes, ce qui signifierait que les communautés microbiennes seraient directement en contact avec l'eau acidifiée. Cela pourrait expliquer pourquoi, malgré le maintien du pH du système à son niveau initial, on observe une augmentation des sucres de la fraction d'EPS liées, censés avoir un rôle protecteur (Dupraz et Visscher, 2005 ; Hubas, 2018 ; Mazière et al., 2022 ; Prieto-Barajas et al., 2018). Un système d'approvisionnement en eau de mer acidifiée en continu, ou une pré-réserve où l'eau est acidifiée, serait également intéressant car le système testé était manuel et il y avait un intervalle de temps avant que toute l'eau nouvellement arrivée soit acidifiée. Il aurait également pu être envisagé de construire un système de cloche où la concentration des gaz à effet de serre (les principaux étant le CO₂ et le CH₄) serait augmentée mais cette méthode présente de nombreux biais dont le temps d'échange des gaz entre l'air et l'eau, donc le temps d'acidification, et aussi les gaz utilisés puisque les deux gaz mentionnés ne sont pas les seuls, il faudrait donc avoir un système de diffusion de plusieurs gaz avec des dispositifs

très précis pour contrôler leur concentration. Ainsi, l'ajout de CO₂ à l'eau est beaucoup plus simple, mais l'ajout d'autres gaz pourrait être envisagé. On peut aussi supposer un dégazage du système, donc une enceinte peut-être plus fermée autour de la réserve pourrait être envisagée pour éviter un dégazage trop important et économiser le gaz utilisé, mais cela pose un problème d'échange avec les gaz atmosphériques.

Le suivi saisonnier a également montré que la température et le pH peuvent varier selon la saison, en fonction de phénomènes naturels tels que les précipitations, les marées, *etc.* Il serait intéressant de simuler ces effets environnementaux et climatiques. De plus, d'autres changements sont prévus, comme l'élévation du niveau de la mer, l'alternance d'événements extrêmes, *etc.* Cette étude devrait donc être complétée avec ces autres paramètres.

Il est également important de noter que la simulation des changements climatiques sur les tapis microbiens dans cette étude n'a duré que 2 mois. Cependant, ces changements ont déjà commencé à se produire (le rapport 2014 du GIEC mentionnait déjà le changement climatique, confirmé par le rapport 2021) et continueront à se produire pendant plusieurs années. Ainsi, il est possible d'imaginer que les tapis microbiens pourront mieux s'adapter au changement climatique dans leur environnement naturel que sur une période plus courte comme notre expérience, ou au contraire que la combinaison des différents facteurs modifiés les affectera trop pour modifier leur structure et leur fonctionnement et qu'ils atteindront leur point de résilience. Il est très compliqué de mettre en place des manipulations simulant le changement climatique, d'une part en raison du coût, du temps et du personnel impliqués, et d'autre part parce que, même si nous étions capables de simuler parfaitement l'environnement naturel du tapis microbien actuel et futur, les données permettant de mettre en place les simulations sont des prédictions et changent constamment. Cependant, ces simulations en laboratoire sont extrêmement importantes pour clarifier les données et donner une idée des impacts majeurs qui pourraient potentiellement avoir lieu.

Quel que soit le scénario, les tapis microbiens du futur seront différents des tapis actuels car le changement climatique est en cours et va se poursuivre. Les communautés dites "généralistes", c'est-à-dire celles qui n'ont pas de niche écologique spécifique et qui peuvent s'adapter à différentes conditions environnementales, ne seront certainement pas affectées, ou se spécialiseront davantage. En revanche, les communautés dites "spécialistes", ayant une niche écologique restreinte et évoluant selon des conditions spécifiques avec des métabolismes définis, seront impactées car si leur environnement est modifié (c'est-à-dire leur niche écologique), elles disparaîtront sûrement, incapables de s'adapter. Cependant, de la même manière, cela peut aussi favoriser l'émergence de nouvelles communautés de spécialistes. Il faut également noter qu'une population généraliste est de toute façon composée d'individus spécialistes car ils peuvent faire le métabolisme qu'ils veulent à tout moment.

Concernant la méthodologie appliquée, les analyses Illumina réalisées en ciblant les gènes universels de l'ARNr 16S bactériens et archéens, et eukaryotes (gène de l'ARNr 18S) ont montré de nombreux biais, comme la faible amplification des communautés cyanobactériennes, malgré l'étude des tapis microbiens photosynthétiques, mais elles ont permis d'obtenir un premier aperçu général des communautés microbiennes présentes. L'amplification de gènes spécifiques pourrait être envisagée pour cibler des communautés plus spécifiques, comme l'ITS (internal transcribed spacer) pour les champignons (Schoch et al., 2012), le gène de la sous-unité 1 de la cytochrome *c* oxydase (COI) pour les animaux (Hebert et al., 2003), les gènes fonctionnels procaryotes comme *dsrB* pour les sulfato-réducteurs (Müller et al., 2015 ; Pelikan et al., 2015), *mcrA* pour les méthanogènes (Luton et al., 2002 ; Yang et al., 2014), *nifH* pour les bactéries fixatrices d'azote (Gaby et Buckley, 2014 ; Turk et al., 2011), etc. Cependant, les bases de données spécifiques à ces gènes sont souvent incomplètes et peu mises à jour. Il serait plus intéressant de réaliser de la métagénomique pour reconstruire les génomes présents dans l'environnement et déterminer l'ensemble des gènes présents, nous donnant des informations sur les fonctions qui peuvent

être réalisées. Cette analyse devrait être combinée avec des méthodes omiques fonctionnelles. L'analyse et le séquençage des ARN via l'ADNc pourraient être envisagés mais tous les ARN ne finissent pas par produire des molécules. Des études métabolomiques, protéomiques ou volatolomiques fourniraient des informations plus précises sur les molécules métabolisées. Il faut cependant garder à l'esprit que ces informations ne sont valables qu'au moment du prélèvement, car les fonctions d'une cellule changent en permanence. La combinaison des méthodes génomiques et omiques fonctionnelles permettrait d'obtenir des informations sur la niche fondamentale et la niche réalisée respectivement. Il serait ainsi possible de déterminer quelles communautés sont généralistes et lesquelles sont spécialisées.

Récemment, il a été observé que les tapis microbiens étudiés au cours de cette thèse sont susceptibles de précipiter les carbonates. Dupraz *et al.* (2009) ont montré que ce métabolisme avait lieu le jour grâce à la photosynthèse oxygénique de phototrophes (notamment des cyanobactéries) et grâce à la réduction des sulfates la nuit. Dans les tapis microbiens de l'île de Ré étudiés dans cette étude, la couche de précipitation serait située entre la couche composée de bactéries phototrophes anoxygéniques et la couche de phototrophes oxygéniques. Des analyses complémentaires sont en cours. Cependant, si cela est démontré, les tapis microbiens pourraient être considérés comme des puits de carbone. On peut imaginer que l'ajout de carbone dans le milieu favoriserait la photosynthèse et donc la précipitation. Néanmoins, nous avons observé que l'acidification avait un impact sur les communautés phototrophes des tapis microbiens, conduisant soit à un changement de la communauté, soit à une modification métabolique pouvant impacter la photosynthèse à long terme. Si la présence de phototrophes oxygénés ou leur photosynthèse diminue, il est tout à fait possible que le carbone précipité soit dissous, conduisant à sa libération dans l'atmosphère. Il serait donc intéressant de se concentrer sur cet axe pour déterminer le point de résilience de la séquestration du carbone.

Cette expérience devrait être répétée sur d'autres tapis microbiens sur l'île de Ré et dans la région Nouvelle-Aquitaine pour mieux comprendre l'impact du changement climatique car cette région présente des environnements variés, ce qui suggère la présence de différents tapis microbiens et donc de différents comportements. Un suivi saisonnier doit également être envisagé car, comme le montre cette thèse, la saisonnalité des paramètres environnementaux a un impact sur les tapis microbiens et explique leur comportement face au changement climatique. Les tapis sont très diversifiés à travers le monde. Il serait donc intéressant d'étendre cette étude au niveau de l'échelle globale.

L'intérêt de ces études et manipulations serait finalement de trouver des bioindicateurs, c'est-à-dire des organismes vivants, qui, par leur présence ou leur absence, leur abondance ou leur rareté, permettent d'évaluer le degré de perturbation ou de pollution d'un environnement. La détermination de molécules bioindicatrices particulières est à envisager, par exemple, l'acidification a eu un impact sur la composition des pigments, entraînant l'apparition de molécules inconnues, probablement la bactériochlorophylle *c* (Mazière et al., 2022).

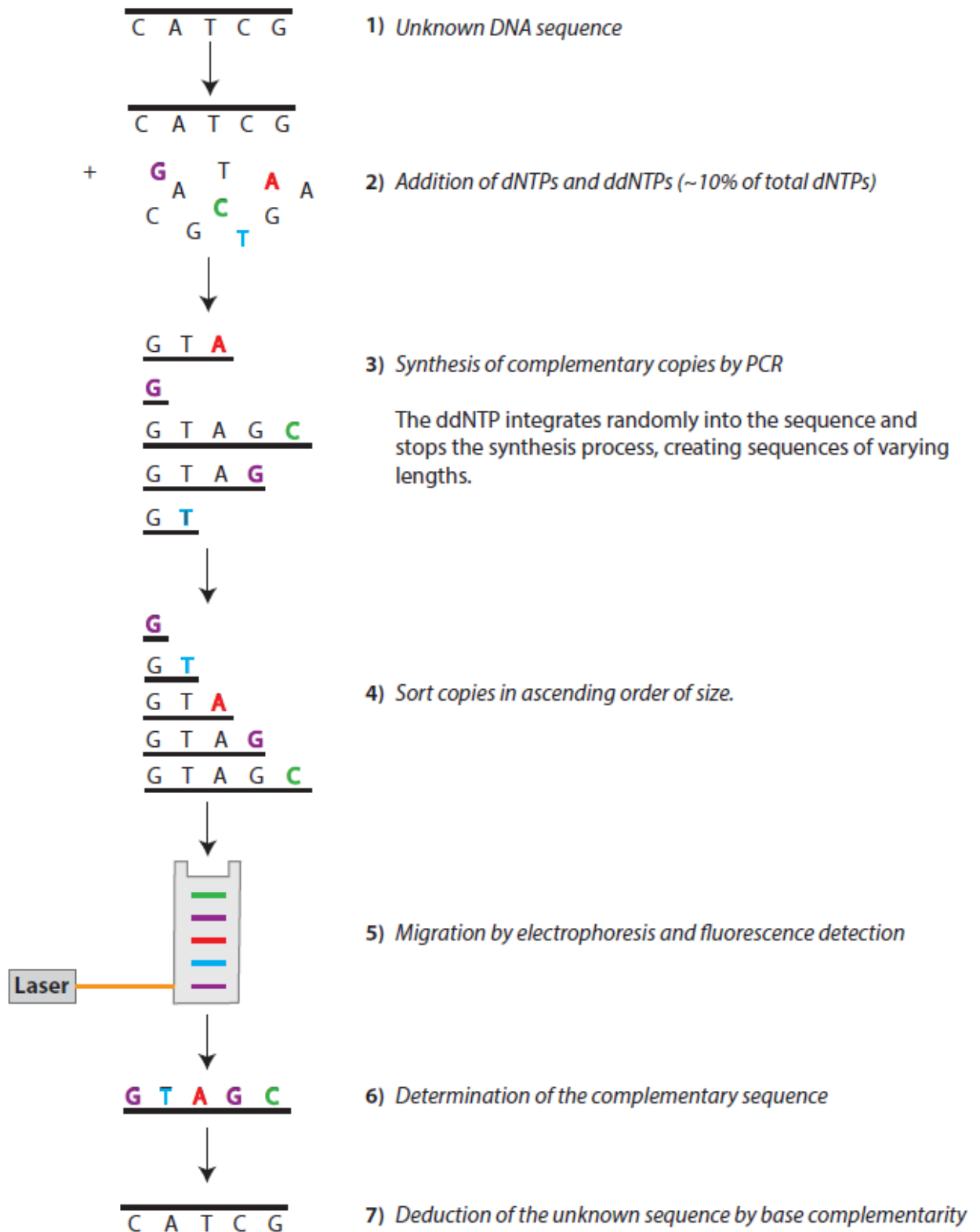
En 2021, un nouveau rapport du GIEC (Groupe de travail I - Sixième rapport d'évaluation, AR6-WGI) a été publié dans lequel cinq scénarios de changement climatique sont définis. Les moins pessimistes, SSP1-1.9 et SSP1-2.6, correspondent à des scénarios où les émissions de gaz à effet de serre (GES) sont très faibles (SSP1-1.9) et faibles (SSP1-2.6), et où les émissions de CO₂ diminuent jusqu'à devenir nulles vers ou après 2050, suivies de niveaux variables d'émissions nettes négatives de CO₂ (GIEC, 2021). SSP2-4.5 est le scénario intermédiaire qui prévoit que les émissions de GES seront intermédiaires entre le scénario le moins pessimiste et le plus pessimiste et que les émissions de CO₂ resteront autour des niveaux actuels jusqu'au milieu du siècle (GIEC, 2021). Les scénarios les plus pessimistes sont SSP3-7.0 et SSP5-8.5, dans lesquels les émissions de GES sont élevées et très élevées, et les émissions de CO₂ doublent approximativement par rapport aux niveaux actuels en 2100 et 2050 (GIEC, 2021).

En Europe, le GIEC (2021) prévoit que la température augmentera dans toutes les régions à un rythme supérieur à celui des changements de la température moyenne mondiale (similaire aux observations passées). Les extrêmes de chaleur, y compris les vagues de chaleur marines, seront plus fréquents et plus intenses et les périodes de froid et les jours de gel seront moins observés (IPCC, 2021). La région Nouvelle-Aquitaine a été classée en deux zones définies par le GIEC dans le rapport AR6-WGI : l'Europe occidentale et centrale (WCE) contenant le nord de la région, avec l'île de Ré, et la zone méditerranéenne (MED) contenant le sud de la région (GIEC, 2021). L'Europe occidentale et centrale devrait être confrontée à davantage d'inondations pluviales et de précipitations extrêmes, d'inondations fluviales, d'élévation du niveau de la mer et de sécheresses hydrologiques, agricoles et écologiques (GIEC, 2021). Le long des côtes atlantiques françaises, les inondations côtières devraient être plus fréquentes et plus intenses en raison d'événements extrêmes liés au niveau de la mer, et les rivages des côtes sableuses reculeront tout au long du 21^e siècle (GIEC, 2021). Ces nouvelles prédictions sont plus précises que les précédentes, d'autant plus qu'elles incluent une vision locale plus détaillée. Il serait donc intéressant de tester ces nouveaux paramètres afin d'évaluer plus précisément l'impact du changement climatique sur les tapis microbiens de la région Nouvelle-Aquitaine.

Annexes

Annexe 1: Sanger principle.

dNTPs: deoxyribonucleotide triphosphate (A, T, C or G); ddNTPs: dideoxyribonucleotide triphosphate with a fluorochrome



Annexe 2: Oxygen solubility at different temperatures and salinities of seawater.



DATA-TABLE 8 *by Niels Ramsing & Jens Gundersen*

Oxygen solubility at different temperatures and salinities of seawater

Units: $\mu\text{mol/l}$

Salinity (%)	Temperature (°C)																				
	0.0	5.0	10.0	15.0	20.0	25.0	30.0	35.0	40.0	45.0	50.0	55.0	60.0	65.0	70.0	75.0	80.0	85.0	90.0	95.0	100.0
0.0	456.6	398.9	352.6	314.9	283.9	257.9	235.9	217.0	200.4	185.6	172.2	159.9	148.3	137.2	126.5	115.9	105.5	95.1	84.7	74.5	64.3
5.0	441.1	385.9	341.6	305.5	275.7	250.7	229.5	211.3	195.3	181.0	168.1	156.2	145.0	134.2	123.8	113.6	103.4	93.3	83.2	73.2	63.3
10.0	426.1	373.3	330.8	296.2	267.6	243.7	223.3	205.7	190.3	176.6	164.1	152.6	141.7	131.3	121.2	111.3	101.4	91.6	81.7	71.9	62.2
15.0	411.7	361.1	320.5	287.3	259.9	236.8	217.3	200.4	185.5	172.3	160.2	149.1	138.6	128.5	118.7	109.0	99.4	89.8	80.2	70.7	61.2
20.0	397.7	349.3	310.4	278.6	252.3	230.2	211.4	195.1	180.8	168.0	156.4	145.6	135.5	125.7	116.2	106.8	97.5	88.1	78.8	69.4	60.2
25.0	384.1	337.9	300.7	270.2	244.9	223.7	205.6	190.0	176.2	163.9	152.7	142.3	132.4	123.0	113.7	104.6	95.5	85.4	77.3	68.2	59.2
30.0	371.0	326.9	291.2	262.0	237.8	217.4	200.1	185.0	171.7	159.9	149.0	139.0	129.4	120.3	111.3	102.5	93.6	84.8	75.9	67.0	58.2
35.0	358.4	316.2	282.0	254.1	230.9	211.3	194.6	180.1	167.4	155.9	145.5	135.7	126.5	117.7	109.0	100.4	91.8	83.2	74.5	65.8	57.2
40.0	346.2	305.8	273.2	246.4	224.1	205.4	189.3	175.4	163.1	152.1	142.0	132.6	123.7	115.1	106.7	98.3	90.0	81.6	73.1	64.7	56.3
45.0	334.4	295.8	264.6	238.9	217.6	199.6	184.2	170.8	159.0	148.3	138.6	129.5	120.9	112.6	104.4	96.3	88.2	80.0	71.8	63.5	55.3
50.0	323.0	286.1	256.3	231.7	211.3	194.0	179.2	166.3	154.9	144.7	135.3	126.5	118.2	110.1	102.2	94.3	86.4	78.5	70.5	62.4	54.4
55.0	311.9	276.7	248.2	224.7	205.1	188.5	174.3	161.9	151.0	141.1	132.1	123.6	115.5	107.7	100.0	92.4	84.7	77.0	69.2	61.3	53.5
60.0	301.3	267.7	240.4	217.9	199.1	183.2	169.6	157.7	147.1	137.6	128.9	120.7	112.9	105.4	97.9	90.5	83.0	75.5	67.9	60.2	52.6
65.0	291.0	258.9	232.8	211.3	193.3	178.1	165.0	153.5	143.4	134.2	125.8	117.9	110.4	103.1	95.8	88.6	81.4	74.1	66.6	59.2	51.7
70.0	281.0	250.4	225.5	204.9	187.7	173.0	160.5	149.5	139.8	130.9	122.8	115.2	107.9	100.8	93.8	86.8	79.8	72.6	65.4	58.1	50.8
75.0	271.4	242.2	218.4	198.7	182.2	168.2	156.1	145.6	136.2	127.7	119.9	112.5	105.5	98.6	91.8	85.0	78.2	71.2	64.2	57.1	50.0
80.0	262.2	234.2	211.5	192.6	176.8	163.4	151.9	141.7	132.7	124.6	117.0	109.9	103.1	96.4	89.9	83.3	76.6	69.9	63.0	56.1	49.1
85.0	253.2	226.6	204.8	186.8	171.7	158.8	147.7	138.0	129.3	121.5	114.2	107.3	100.8	94.3	88.0	81.6	75.1	68.5	61.8	55.1	48.3
90.0	244.5	219.1	198.3	181.1	166.7	154.3	143.7	134.4	126.0	118.5	111.5	104.9	98.5	92.3	86.1	79.9	73.6	67.2	60.7	54.1	47.5
95.0	236.2	211.9	192.1	175.6	161.8	150.0	139.8	130.8	122.8	115.6	108.8	102.4	96.3	90.2	84.3	78.2	72.1	65.9	59.6	53.1	46.6
100.0	228.1	205.0	186.0	170.3	157.1	145.8	136.0	127.4	119.7	112.7	106.2	100.0	94.1	88.3	82.5	76.6	70.7	64.6	58.4	52.2	45.8
105.0	220.3	198.2	180.2	165.1	152.5	141.7	132.3	124.0	116.7	109.9	103.6	97.7	92.0	86.3	80.7	75.0	69.3	63.4	57.4	51.2	45.1
110.0	212.7	191.7	174.5	160.1	148.0	137.7	128.7	120.8	113.7	107.2	101.2	95.4	89.9	84.4	79.0	73.5	67.9	62.1	56.3	50.3	44.3
115.0	205.4	185.4	169.0	155.2	143.7	133.8	125.2	117.6	110.8	104.5	98.7	93.2	87.9	82.6	77.3	72.0	66.5	60.9	55.2	49.4	43.5
120.0	198.4	179.3	163.6	150.5	139.5	130.0	121.8	114.5	108.0	102.0	96.4	91.0	85.9	80.8	75.7	70.5	65.2	59.8	54.2	48.5	42.8
125.0	191.6	173.4	158.5	146.0	135.4	126.3	118.4	111.5	105.2	99.4	94.1	88.9	83.9	79.0	74.0	69.0	63.9	58.6	53.2	47.7	42.1
130.0	185.0	167.7	153.4	141.5	131.4	122.8	115.2	108.5	102.5	97.0	91.8	86.9	82.0	77.3	72.5	67.6	62.6	57.5	52.2	46.8	41.3
135.0	178.7	162.2	148.6	137.2	127.6	119.3	112.1	105.7	99.9	94.6	89.6	84.8	80.2	75.6	70.9	66.2	61.3	56.4	51.2	46.0	40.6
140.0	172.8	156.9	143.9	133.1	123.8	115.9	109.0	102.9	97.3	92.2	87.4	82.9	78.4	73.9	69.4	64.8	60.1	55.3	50.3	45.1	39.9
145.0	166.6	151.7	139.4	129.0	120.2	112.7	106.0	100.2	94.9	90.0	85.4	80.9	76.6	72.3	67.9	63.5	58.9	54.2	49.3	44.3	39.2
150.0	160.9	146.7	134.9	125.1	116.7	109.5	103.2	97.5	92.4	87.7	83.3	79.0	74.9	70.7	66.5	62.2	57.7	53.1	48.4	43.5	38.6
155.0	155.4	141.9	130.7	121.3	113.3	106.4	100.3	95.0	90.1	85.6	81.3	77.2	73.2	69.1	65.1	60.9	56.6	52.1	47.5	42.7	37.9
160.0	150.1	137.2	126.5	117.6	110.0	103.4	97.6	92.5	87.8	83.4	79.3	75.4	71.5	67.6	63.7	59.6	55.4	51.1	46.6	42.0	37.2
165.0	144.9	132.7	122.5	114.0	106.7	100.5	94.9	90.0	85.5	81.4	77.4	73.6	69.9	66.1	62.3	58.4	54.3	50.1	45.7	41.2	36.6
170.0	139.9	128.3	118.7	110.5	103.6	97.6	92.3	87.6	83.4	79.4	75.6	71.9	68.3	64.7	61.0	57.2	53.2	49.1	44.9	40.5	36.0
175.0	135.1	124.1	114.9	107.2	100.6	94.9	89.8	85.3	81.2	77.4	73.8	70.2	66.8	63.3	59.7	56.0	52.1	48.2	44.0	39.7	35.3
180.0	130.5	120.0	111.3	103.9	97.6	92.2	87.4	83.1	79.1	75.5	72.0	68.6	65.2	61.9	58.4	54.8	51.1	47.2	43.2	39.0	34.7
185.0	126.0	116.0	107.8	100.8	94.8	89.6	85.0	80.9	77.1	73.6	70.3	67.0	63.8	60.5	57.1	53.7	50.1	46.3	42.4	38.3	34.1
190.0	121.7	112.2	104.3	97.7	92.0	87.0	82.7	78.7	75.2	71.8	68.6	65.4	62.3	59.2	55.9	52.6	49.1	45.4	41.6	37.6	33.5
195.0	117.5	108.5	101.0	94.7	89.3	84.6	80.4	76.7	73.2	70.0	66.9	63.9	60.9	57.9	54.7	51.5	48.1	44.5	40.8	36.9	32.9
200.0	113.5	104.9	97.8	91.8	86.7	82.2	78.2	74.6	71.4	68.3	65.3	62.4	59.5	56.6	53.6	50.4	47.1	43.6	40.0	36.3	32.4

Annexe 3: H₂S calibration protocol. This protocol was developed by UNISENSE A/S. This document is from https://www.unisense.com/calibration_kits/ (last view: 2021/10/24).

H₂S sensor calibration kit

For H₂S and SULF sensors

Manual



Contents

1	WARRANTY AND LIABILITY	3
1.1	NOTICE TO PURCHASER.....	3
1.2	WARNING	3
1.3	WARRANTY AND LIABILITY	3
2	SUPPORT, ORDERING, AND CONTACT INFORMATION	3
3	CONTENT OF THE CALIBRATION KIT	3
4	PRINCIPLE OF CALIBRATION	4
5	CORRECTION FOR SALINITY	4
6	CALIBRATION PROCEDURE	6
6.1	PREPARATION OF THE H ₂ S CALIBRATION SOLUTION	6
6.2	PREPARATION OF THE HYDROGEN SULFIDE SENSOR	7
6.3	CALIBRATING MOST HYDROGEN SULFIDE SENSORS	7
6.3.1	<i>Obtaining the low calibration point</i>	7
6.3.1.1	Using the Unisense Calibration Chamber	7
6.3.1.2	Using the Calibration Cap.....	7
6.3.2	<i>Obtaining the high calibration point</i>	7
6.4	CALIBRATING HYDROGEN SULFIDE SENSORS WITH PIERCING NEEDLE	8
6.4.1	<i>Obtaining the low calibration point</i>	8
6.4.2	<i>Obtaining the high calibration point</i>	8
6.5	CALIBRATING HYDROGEN SULFIDE SENSORS FOR THE MICRORESPIRATION SYSTEM	8
6.5.1	<i>Obtaining the high calibration point</i>	8
6.5.2	<i>Obtaining the low calibration point</i>	9
6.5.2.1	Using the Unisense Cal300 Calibration Chamber	9
6.5.2.2	Using a Microrespiration Chamber	9
6.6	NOTES AND RECOMMENDATIONS	9
7	CALIBRATING AT OTHER CONCENTRATIONS	10
8	SPECIFICATIONS	10
9	APPENDIX 1: CALCULATION OF THE CORRECTION FACTOR FOR SALINITY	11
10	TABLE 1. CORRECTION FACTORS FOR CALCULATING VIRTUAL CONCENTRATION	12

1 Warranty and liability

1.1 Notice to Purchaser

This product is for research use only. Not for use in human diagnostic or therapeutic procedures.

1.2 Warning

Microsensors have very pointed tips and must be handled with care to avoid personal injury and only by trained personnel. Unisense A/S recommends users to attend instruction courses to ensure proper use of the products.

1.3 Warranty and Liability

The H₂S Calibration Kit is guaranteed to give the concentration indicated on the package label until expiry as indicated on the package label. The warranty does not include replacement necessitated by accident, neglect, misuse, unauthorized repair, or modification of the product. In no event will Unisense A/S be liable for any direct, indirect, consequential or incidental damages, including lost profits, or for any claim by any third party, arising out of the use, the results of use, or the inability to use this product.

2 Support, ordering, and contact information

If you wish to order additional products or if you encounter any problems and need scientific or technical assistance, please do not hesitate to contact our sales and support team. We will respond to your inquiry within one working day.

E-mail: sales@unisense.com

Unisense A/S

Tueager 1

DK-8200 Aarhus N, Denmark

Tel: +45 8944 9500

Fax: +45 8944 9549

Further documentation and support are available at our website: www.unisense.com.

3 Content of the calibration kit

Item	Number
Exetainer with ZnS suspension - H ₂ S stock solution	10
Exetainer with HCl (pH = 2.1) and glass beads - Mixing vial	10
Calibration cap with O-ring and 3 cm Viton tubing	1
10 ml syringe	1
1 ml syringe	2
80 x 2.1 mm needle (green)	1
30 x 0.6 mm needle (blue)	1
50 x 1.2 mm needle (red)	1



Figure 1: Calibration kit contents: A: Calibration kit box with Exetainers, B: 80 x 2.1 mm needle (green), C: 1 ml syringes, D: 10 ml syringe, E 50 x 1.2 mm needle (red), F: 30 x 0.6 mm needle (blue), G: Calibration Cap with tubing, H: O-ring.

4 Principle of calibration

Unisense Hydrogen Sulfide sensors (H_2S and SUF) respond linearly to H_2S concentrations within their linear range (see specifications for your sensor at <https://www.unisense.com/H2S>). Therefore, a two-point calibration is sufficient. One calibration point is the signal for zero H_2S , which can be water equilibrated with atmospheric air, and the other calibration point is the signal for one known H_2S concentration.

In this calibration kit, the sulfide is shipped in the form of zinc sulfide precipitate (ZnS) which is insoluble in water (Solubility product = ca. 2×10^{-25}). During the calibration procedure, ZnS is injected into a dilute HCl ($pH = 2.1$). This causes the ZnS to dissolve and H_2S is formed quantitatively.

H_2S will react slowly with O_2 if this is present. To minimize this, the ZnS suspension and the dilute HCl are anoxic when dispensed into the Exetainers. However, during storage and handling a small amount of O_2 will enter the solution. Therefore, the calibration must be performed relatively rapid, as described below, to keep this reaction at a negligible level.

5 Correction for salinity

During calibration, a relationship between sensor signal and concentrations is established. However, the sensor responds to the partial pressure of H_2S which at a given concentration varies with salinity. Therefore, a correction for salinity must be applied.

Henry's law describes how partial pressure depends on the concentration and solubility of a gas:

$$\text{Partial pressure} = \frac{\text{Concentration}}{\text{Solubility}} \quad (\text{Equation 1})$$

The calibration solution, prepared as described in section 6.1 below, will have the H₂S concentration stated on the package label. The solubility of H₂S will decrease with increasing salinity. Therefore, at a given concentration, the partial pressure will increase with increasing salinity. As the sensor responds to partial pressure, the sensor signal will increase as well when salinity increases at a constant H₂S concentration. The conversion of sensor signal to concentration must, therefore, take the relationship between salinity and solubility into account.

The salinity in the calibration solution (0.36‰) corresponds to freshwater. If measuring at other salinities, a correction must be made. This correction is done by assuming a H₂S concentration different from that given on the package label. This *Virtual concentration* is the one that, at the measuring salinity, gives the same partial pressure of H₂S as that in the calibration solution. If the measuring salinity is higher than that in the calibration solution, the *Virtual concentration* will be lower than that given on the package label. The reason is that when salinity is higher than in the calibration solution, a lower H₂S concentration is needed to give the same partial pressure as that in the calibration solution (see Henry's law above).

The *Virtual concentration* is calculated as (see Appendix 1):

$$Conc. (Virtual) = Conc. (Kit) \times \frac{Sol.(Virtual)}{Sol.(Kit)} \quad (\text{Equation 2})$$

⇕

$$Conc. (Virtual) = Conc. (Kit) \times Corr. factor \quad (\text{Equation 3})$$

where *Conc. (Virtual)* is the *Virtual concentration*, *Conc. (kit)* is the H₂S concentration given on the calibration box label, *Sol. (Virtual)* is the solubility of H₂S at the measurement salinity and temperature, *Sol. (Kit)* is the solubility of H₂S at the salinity in the calibration solution and the measurement temperature, and *Corr. factor* is the correction factor. Note that calibration and measurements must be carried out at the same temperature.

The *Virtual concentration*, calculated from Equation 3, is the concentration that must be entered as the *Known value* (μmol/L) in the SensorTrace software.

Example:

Measure at 30‰ and 20°C.

Calibrate at 20°C.

Concentration of H₂S in the calibration solution (*Conc. (Kit)*) = 104.3 μM

Correction factor (*Corr. factor*, Table 1) = 0.871

Virtual H₂S concentration (*Conc. (Virtual)*) = 104.3 μM × 0.871 = 91.2 μM

In this example a concentration of 91.2 μM will give the same sensor signal as the concentration of 104.3 μM in the calibration solution due to the difference in solubility of H₂S at the two salinities. Therefore, 91.2 μM is the value to be entered as the *Known value* in the SensorTrace software.

6 Calibration procedure

For calibrating the H₂S sensor, a low and a high calibration point are needed. Note that piercing needle sensors and microrespiration sensors will not fit the calibration cap and must be calibrated as described in section 6.4. and 6.5 This calibration kit is not for calibrating High Range H₂S sensors that work in the mM range.

6.1 Preparation of the H₂S calibration solution

1. Mount the 50 x 1.2 mm needle (red) on one 1 ml syringe, mount the 30 x 0.6 mm needle (blue) on the other 1 ml syringe, and mount the 80 x 2.1 mm needle (green) on the 10 ml syringe.
2. Adjust the temperature of the Exetainers with ZnS and HCl to the wanted calibration temperature (see note A, section 6.6).
3. Shake the Exetainer with the ZnS precipitate vigorously for 30 seconds (see note B, section 6.6).
4. Open the Exetainer with the ZnS precipitate.
5. Aspirate ca. 0.3 ml with the 1 ml syringe with the red needle, turn the needle upwards, tap it gently to get the bubbles to the top and eject these.
6. Empty the syringe and aspirate 1 ml ZnS suspension and eject this back into the Exetainer with the needle immersed. Repeat this three times before filling the syringe.
7. Adjust the volume in the syringe to exactly 1.0 ml.
8. Insert the blue needle, mounted on the second 1 ml syringe, through the septum of the Exetainer with HCl. Leave the tip of the needle right below the septum.
9. Insert the red needle, mounted on the syringe with ZnS, fully into the HCl Exetainer and inject the ZnS. The excess liquid is pushed into the empty syringe (See note C, section 6.6).
10. Remove first the ZnS syringe, then the syringe with the excess liquid.
11. Shake the Exetainer vigorously for 10 seconds.
12. Leave the Exetainer for 15 minutes for the formation of H₂S from ZnS to complete.



Figure 2: Sulfide sensor with the calibration cap mounted. Calibration solution is injected with the 10 ml syringe.

6.2 Preparation of the hydrogen sulfide sensor

IMPORTANT:

- The pre-polarization period of the H₂S sensor must have been completed before doing the calibration. See the H₂S sensor manual for details: <https://www.unisense.com/manuals/>
- The temperature of the low and high calibration solutions must be the same.
- Perform the calibration at the same temperature as the measurements if possible. The UniAmp series of amplifiers has a built-in temperature compensation within ±3°C of the calibration temperature.
- If doing the low calibration point with the calibration cap, make sure to do this before the high calibration point to avoid carry over from the H₂S standard.

6.3 Calibrating most hydrogen sulfide sensors

6.3.1 Obtaining the low calibration point

6.3.1.1 Using the Unisense Calibration Chamber

1. Place the sensor with the protection tube in sulfide free water (see the H₂S microsensor manual (<https://www.unisense.com/manuals/>))
2. Allow the sensor to respond and stabilize and record the calibration value in SensorTrace (see the SensorTrace manual for details: <https://www.unisense.com/manuals/>)

6.3.1.2 Using the Calibration Cap

1. Mount the calibration cap on the protection tube with the H₂S sensor (Figure 2). Make sure that the O-ring is in place at the bottom of the calibration cap creating a seal between this and the protection tube.
2. Fill the 10 ml syringe with sulfide free water.
3. Inject this water into the calibration cap until the sensor tip is immersed at least 2-3 cm.
4. Allow the sensor to respond and stabilize. Then record the calibration value in SensorTrace (see the SensorTrace manual for details: <https://www.unisense.com/manuals/>)

6.3.2 Obtaining the high calibration point

1. Mount the calibration cap, if not already mounted, as described above in 6.3.1.2.
2. Open the Exetainer with the H₂S calibration solution prepared as above in 6.1.
3. Aspirate ca. 10 ml of the H₂S calibration solution with the syringe and needle.
4. Keep the syringe vertical and avoid mixing of the calibration solution with the air bubble inside.
5. Remove the needle and attach the 10 ml syringe to the calibration cap tubing.
6. Inject the calibration solution slowly until the sensor tip is immersed at least 2-3 cm.
7. Allow the sensor to respond and stabilize. Then record the calibration value in SensorTrace (see the SensorTrace manual for details: <https://www.unisense.com/manuals/>) (See note D, section 6.6). If the response is much slower than expected, the ZnS may not have been converted fully into H₂S (See note E, section 6.6)
8. Remove the H₂S calibration solution with the syringe.
9. Wash the calibration cap and protection tube carefully, removing all the H₂S calibration solution using the 10 ml syringe.

6.4 Calibrating hydrogen sulfide sensors with piercing needle

Sensor of the piercing needle type (SULF-NP & H₂S-NP) cannot be calibrated using the calibration cap. Therefore, the calibration done by inserting the needle directly into sulfide free water and the calibration solution.

Pay attention to the general information in section 6.1 and 6.2, the Notes and recommendations in section 6.6, and follow the procedure below.

6.4.1 Obtaining the low calibration point

1. Place the sensor in sulfide free water.
2. Allow the sensor to respond and stabilize. Then record the calibration value in SensorTrace (see the SensorTrace manual for details: <https://www.unisense.com/manuals/>)

6.4.2 Obtaining the high calibration point

1. Open the Exetainer with the H₂S calibration solution.
2. Insert the needle of the sensor fully into the H₂S calibration solution.
 - a. Use a clamp to hold the sensor stable to avoid handling noise
3. Allow the sensor to respond and stabilize and record the calibration value in SensorTrace (see the SensorTrace manual for details: <https://www.unisense.com/manuals/>) (See note D, section 6.6). If the response is much slower than expected, the ZnS may not have been converted fully into H₂S (See note E, section 6.6)
4. Remove the sensor and rinse the needle thoroughly.

6.5 Calibrating hydrogen sulfide sensors for the Microrespiration system

Sensors of the Microrespiration type (OX-MR) cannot be calibrated using the calibration cap. Instead it is recommended to follow the procedure outlined below. Pay attention to the general information in section 6.1 and 6.2, the Notes and recommendations in section 6.6, and follow the procedure below



Figure 3: H₂S sensor in the Microrespiration guide.

6.5.1 Obtaining the high calibration point

1. Prepare the H₂S calibration solution as described in section 6.1.
2. Aspirate 5 ml of the H₂S calibration solution with the syringe and needle. Do this slowly to avoid bubble formation.
3. Dispense the H₂S calibration solution into a microrespiration chamber. Place the needle at the bottom of the chamber, filling from below, to avoid bubbles and splashing.
4. Mount the lid in the microrespiration chamber making sure that no air bubbles are trapped.
5. Place the microrespiration chamber in the stirrer rack.
6. Place the H₂S sensor in the stirrer rack with its plastic tip in the opening of the lid.
7. Insert the sensor into the chamber.
8. Allow the sensor to respond and stabilize and record the calibration value in SensorTrace (see the SensorTrace manual for details: <https://www.unisense.com/manuals/>).
9. Retract the sensor tip and remove the sensor from the stirrer rack.

6.5.2 Obtaining the low calibration point

6.5.2.1 Using the Unisense Cal300 Calibration Chamber

1. Place the sensor in the Cal300 Calibration Chamber containing H₂S free water (see the H₂S microsensor manual (<https://www.unisense.com/manuals/>)).
 - The H₂S sensor must be mounted in the blue Microrespiration guide and the tip must be retracted.
 - Temperature of the water must be the same as where the measurements are done.
2. Allow the sensor to respond and stabilize and record the calibration value in SensorTrace (see the SensorTrace manual for details: <https://www.unisense.com/manuals/>)

6.5.2.2 Using a Microrespiration Chamber

1. Prepare a volume of H₂S free water at the same temperature as the H₂S calibration solution used in 6.5.1.
2. Transfer this water to a microrespiration chamber and mount the lid.
3. Place the microrespiration chamber in the stirrer rack
4. Place the H₂S sensor in the stirrer rack with its plastic tip in the opening of the lid.
5. Insert the sensor into the chamber.
6. Allow the sensor to respond and stabilize and record the calibration value in SensorTrace (see the SensorTrace manual for details: <https://www.unisense.com/manuals/>) (See note D, section 6.6). If the response is much slower than expected, the ZnS may not have been converted fully into H₂S (See note E, section 6.6)
7. Retract the sensor tip and remove the sensor from the stirrer rack.

6.6 Notes and recommendations

- A. Perform the calibration at the same temperature as the measurements if possible. The UniAmp series of amplifiers has a built in temperature compensation within $\pm 3^{\circ}\text{C}$ of the calibration temperature.
- B. It is important to shake the ZnS suspension very well and obtain a homogenous distribution of the precipitate. If not, the aliquot of suspension transferred to the HCl Exetainer will not contain the correct amount of ZnS and the final H₂S concentration will be wrong.
- C. Injection of the H₂S containing water is done with the needle inserted fully while the blue needle on the empty syringe is inserted just below the septum. Thereby the injected H₂S containing water will not be lost.
- D. The calibration point should be saved within ca. 30-60 seconds after injecting the H₂S calibration solution. The period between injection and saving the calibration point should be long enough to obtain almost full response which depends on the sensor response time. Furthermore, it should not be longer than needed because the H₂S calibration solution will be contaminated with O₂ during handling, and consumption of H₂S due to reaction with O₂ will occur. This reaction is slow but can be seen as a slow decrease in signal over a few minutes.
- E. If the sensor signal keeps rising for several minutes, the formation of H₂S from ZnS may not have been completed. Leave the sensor in the H₂S until the signal is stable. For the next calibration, extend the time for the ZnS to be converted to H₂S (Section 6.1)

7 Calibrating at other concentrations

It is possible to obtain a lower concentration than that obtained using the standard procedure in section. This may be done either injecting less than 1.0 ml or by diluting the calibration solution obtained using the standard procedure in section.

Dilution of the solution made in section 6.1.

1. Prepare two Mixing Exetainers.
2. Transfer 1.0 ml the ZnS suspension into the first Mixing Exetainer as described above in section 6.1.
3. After shaking the Exetainer vigorously to obtain a homogenous distribution of H₂S, open the Exetainer and aspirate a volume with a syringe.
4. Inject a known volume into the second Exetainer with the blue needle on a syringe inserted just below the septum to collect the excess liquid (this volume of this syringe must be sufficient to accept all the excess liquid).
5. Shake the Exetainer vigorously.

Now the sensor may be calibrated, as described above for the different types of sensors, using the calibration solution in the second Exetainer.

The concentration of H₂S in the second Exetainer may be calculated as:

$$\text{Final conc. } (\mu\text{M}) = \text{Inj. vol. (ml)}/\text{Exetainer vol. (ml)} \times \text{Certified conc. } (\mu\text{M})$$

where *Final conc. (μM)* is the concentration obtained in the second Exetainer, *Inj. vol (ml)* is the volume injected transferred from the first to the second the Exetainer, *Exetainer vol. (μM)* is the volume of the second Exetainer and *Certified conc. (μM)* is the H₂S concentration obtained when following the standard procedure in section. The *Certified conc.* and the *Exetainer volume* are shown on the label on the calibration kit box.

Please note that when injecting less than the full volume of a syringe, the accuracy of the injection will become lower. Therefore, always use a syringe with a full volume that is close the amount to be injected. E.g. if 3 ml is injected with a 10 ml syringe the accuracy is low.

8 Specifications

- Volume of ZnS suspension in Exetainer¹: 12.5 ml
- Volume of HCl (pH = 2.1) in Exetainer¹: 12.5 ml
- Lifetime of the calibration kit: See label on the calibration box
- Concentration of H₂S in calibration solution²: See label on the calibration box

¹The zinc sulfide suspension and the HCl solution are made anoxic with Ar bubbling before these liquids are dispensed into the Exetainers.

²The actual concentration of H₂S in the final calibration solution is determined from measurements with a H₂S sensor calibrated with a certified calibration gas. The number of this certificate is specified on the calibration kit box. The H₂S concentration in the final calibration solution, following the procedure in section 6.1, is specified in the label on the calibration kit box.

9 Appendix 1: Calculation of the correction factor for salinity

The relationship between partial pressure, concentration and solubility for a gas is given by Henrys law:

$$\text{Part. press.} = \text{Conc.}/\text{Sol.}$$

where Part. press. is partial pressure of H₂S, Conc. is the molar concentrations of H₂S, Sol. is the molar solubility of H₂S at the given temperature and salinity.

In the calibration solution:

$$\text{Part.press (Kit)} = \frac{\text{Conc. (Kit)}}{\text{Sol. (Kit)}}$$

During measurement at a different salinity:

$$\text{Part.press (Meas)} = \frac{\text{Conc. (Meas)}}{\text{Sol. (Meas)}}$$

The aim is to calculate which concentration at the measuring salinity that will give the same partial pressure as in the calibration solution. The partial pressure at the measurement salinity and that at the calibration salinity are thus set to be equal:

$$\begin{aligned} & \Downarrow \\ & \text{Part.press (Meas)} = \text{Part.press (Kit)} \\ & \Downarrow \\ & \frac{\text{Conc. (Meas)}}{\text{Sol. (Meas)}} = \frac{\text{Conc. (Kit)}}{\text{Sol. (Kit)}} \\ & \Downarrow \\ & \text{Conc. (Meas)} = \frac{\text{Conc. (Kit)} \times \text{Sol. (Meas)}}{\text{Sol. (Kit)}} \\ & \Downarrow \\ & \text{Conc. (Meas)} = \text{Conc. (Kit)} \times \frac{\text{Sol. (Meas)}}{\text{Sol. (Kit)}} \\ & \Downarrow \\ & \text{Conc. (Meas)} = \text{Conc. (Kit)} \times \text{Corr. factor} \end{aligned}$$

Example

Concentration calculated based on the calibration = 100 μM

Conditions at measuring: Temperature = 20°C, Salinity = 32‰ => Correction factor = 0.863 (Table 1)

True concentration at 20°C, 32‰ = 100 μM x 0.863 = 86.3 μM

10 Table 1. Correction factors for calculating virtual concentration

Temp (°C)	Salinity (‰)																				
	0	2	4	6	8	10	12	14	16	18	20	22	24	26	28	30	32	34	36	38	40
-1	1.001	0.993	0.985	0.978	0.970	0.962	0.954	0.946	0.939	0.931	0.924	0.916	0.909	0.902	0.895	0.887	0.880	0.873	0.866	0.859	0.852
0	1.001	0.993	0.985	0.977	0.969	0.962	0.954	0.946	0.938	0.931	0.923	0.916	0.908	0.901	0.894	0.887	0.879	0.872	0.865	0.858	0.851
1	1.001	0.993	0.985	0.977	0.969	0.961	0.953	0.946	0.938	0.930	0.923	0.915	0.908	0.900	0.893	0.886	0.879	0.871	0.864	0.857	0.850
2	1.001	0.993	0.985	0.977	0.969	0.961	0.953	0.945	0.938	0.930	0.922	0.915	0.907	0.900	0.892	0.885	0.878	0.871	0.863	0.856	0.849
3	1.001	0.993	0.985	0.977	0.969	0.961	0.953	0.945	0.937	0.929	0.922	0.914	0.907	0.899	0.892	0.884	0.877	0.870	0.862	0.855	0.848
4	1.002	0.993	0.985	0.977	0.969	0.961	0.953	0.945	0.937	0.929	0.921	0.914	0.906	0.898	0.891	0.883	0.876	0.869	0.862	0.854	0.847
5	1.002	0.993	0.985	0.977	0.968	0.960	0.952	0.944	0.936	0.928	0.921	0.913	0.905	0.898	0.890	0.883	0.875	0.868	0.861	0.853	0.846
6	1.002	0.993	0.985	0.976	0.968	0.960	0.952	0.944	0.936	0.928	0.920	0.912	0.905	0.897	0.889	0.882	0.874	0.867	0.860	0.853	0.845
7	1.002	0.993	0.985	0.976	0.968	0.960	0.952	0.943	0.935	0.927	0.920	0.912	0.904	0.896	0.889	0.881	0.874	0.866	0.859	0.852	0.844
8	1.002	0.993	0.984	0.976	0.968	0.959	0.951	0.943	0.935	0.927	0.919	0.911	0.903	0.896	0.888	0.880	0.873	0.865	0.858	0.851	0.843
9	1.002	0.993	0.984	0.976	0.967	0.959	0.951	0.943	0.935	0.926	0.918	0.911	0.903	0.895	0.887	0.880	0.872	0.864	0.857	0.850	0.842
10	1.002	0.993	0.984	0.976	0.967	0.959	0.951	0.942	0.934	0.926	0.918	0.910	0.902	0.894	0.886	0.879	0.871	0.864	0.856	0.849	0.841
11	1.002	0.993	0.984	0.976	0.967	0.959	0.950	0.942	0.934	0.925	0.917	0.909	0.901	0.894	0.886	0.878	0.870	0.863	0.855	0.848	0.840
12	1.002	0.993	0.984	0.975	0.967	0.958	0.950	0.941	0.933	0.925	0.917	0.909	0.901	0.893	0.885	0.877	0.869	0.862	0.854	0.847	0.839
13	1.002	0.993	0.984	0.975	0.967	0.958	0.950	0.941	0.933	0.924	0.916	0.908	0.900	0.892	0.884	0.876	0.869	0.861	0.853	0.846	0.838
14	1.002	0.993	0.984	0.975	0.966	0.958	0.949	0.941	0.932	0.924	0.916	0.908	0.899	0.891	0.883	0.876	0.868	0.860	0.852	0.845	0.837
15	1.002	0.993	0.984	0.975	0.966	0.957	0.949	0.940	0.932	0.923	0.915	0.907	0.899	0.891	0.883	0.875	0.867	0.859	0.851	0.844	0.836
16	1.002	0.993	0.984	0.975	0.966	0.957	0.948	0.940	0.931	0.923	0.915	0.906	0.898	0.890	0.882	0.874	0.866	0.858	0.850	0.843	0.835
17	1.002	0.993	0.983	0.975	0.966	0.957	0.948	0.940	0.931	0.922	0.914	0.906	0.897	0.889	0.881	0.873	0.865	0.857	0.850	0.842	0.834
18	1.002	0.992	0.983	0.974	0.965	0.957	0.948	0.939	0.930	0.922	0.914	0.905	0.897	0.889	0.880	0.872	0.864	0.856	0.849	0.841	0.833
19	1.002	0.992	0.983	0.974	0.965	0.956	0.947	0.939	0.930	0.921	0.913	0.905	0.896	0.888	0.880	0.872	0.864	0.856	0.848	0.840	0.832
20	1.002	0.992	0.983	0.974	0.965	0.956	0.947	0.938	0.930	0.921	0.912	0.904	0.896	0.887	0.879	0.871	0.863	0.855	0.847	0.839	0.831
21	1.002	0.992	0.983	0.974	0.965	0.956	0.947	0.938	0.929	0.920	0.912	0.903	0.895	0.886	0.878	0.870	0.862	0.854	0.846	0.838	0.830
22	1.002	0.992	0.983	0.974	0.964	0.955	0.946	0.937	0.929	0.920	0.911	0.903	0.894	0.886	0.877	0.869	0.861	0.853	0.845	0.837	0.829
23	1.002	0.992	0.983	0.973	0.964	0.955	0.946	0.937	0.928	0.919	0.911	0.902	0.893	0.885	0.877	0.868	0.860	0.852	0.844	0.836	0.828
24	1.002	0.992	0.983	0.973	0.964	0.955	0.946	0.937	0.928	0.919	0.910	0.901	0.893	0.884	0.876	0.867	0.859	0.851	0.843	0.835	0.827
25	1.002	0.992	0.983	0.973	0.964	0.955	0.945	0.936	0.927	0.918	0.910	0.901	0.892	0.884	0.875	0.867	0.858	0.850	0.842	0.834	0.826
26	1.002	0.992	0.982	0.973	0.964	0.954	0.945	0.936	0.927	0.918	0.909	0.900	0.891	0.883	0.874	0.866	0.857	0.849	0.841	0.833	0.825
27	1.002	0.992	0.982	0.973	0.963	0.954	0.945	0.935	0.926	0.917	0.908	0.900	0.891	0.882	0.874	0.865	0.857	0.848	0.840	0.832	0.824
28	1.002	0.992	0.982	0.973	0.963	0.954	0.944	0.935	0.926	0.917	0.908	0.899	0.890	0.881	0.873	0.864	0.856	0.847	0.839	0.831	0.823
29	1.002	0.992	0.982	0.972	0.963	0.953	0.944	0.935	0.925	0.916	0.907	0.898	0.889	0.881	0.872	0.863	0.855	0.846	0.838	0.830	0.822
30	1.002	0.992	0.982	0.972	0.963	0.953	0.944	0.934	0.925	0.916	0.907	0.898	0.889	0.880	0.871	0.863	0.854	0.845	0.837	0.829	0.821

Calculated from: Morse, J. W., F. J. Millero, J. C. Cornwell, and D. Rickard. 1987. The chemistry of the hydrogen sulfide and iron sulfide systems in natural waters.

Earth-Science Rev. 24: 1–42. [https://doi.org/10.1016/0012-8252\(87\)90046-8](https://doi.org/10.1016/0012-8252(87)90046-8)

Annexe 4: Shotgun metagenomics.

Shotgun metagenomics analysis was performed on *in situ* samples coming from the seasonal monitoring of the site 1.

This analysis provides information on untargeted (“shotgun”) sequencing of all (“meta-”) microbial genomes “genomics” present in a sample, *i.e.*, on the total genomic DNA from all organisms in a sample (Quince et al., 2017). It permits to avoid the isolation and cultivation of microorganisms, the majority of which cannot be cultivated in the laboratory, or the amplification of targets region, doesn't take into account all the diversity, to study them.

Shotgun metagenomic sequencing uses **next-generation sequencing (NGS)** technology to provide not only information on the taxonomic annotations of each organism but also the functional profiling, gene prediction and microbial interaction of the whole community.

1. Sequencing

DNA was sent after its extraction (Chapter II) to Novogene where shotgun metagenomics analysis was then performed. It comprises 5 steps (Quince et al., 2017) (**Annexe 4**):

- 1) collection, processing and sequencing of the samples,
- 2) preprocessing of the sequencing reads,
- 3) sequence analysis to profile taxonomic, functional and genomic features of the microbiome,
- 4) statistical and biological post-processing analysis,
- 5) validation.

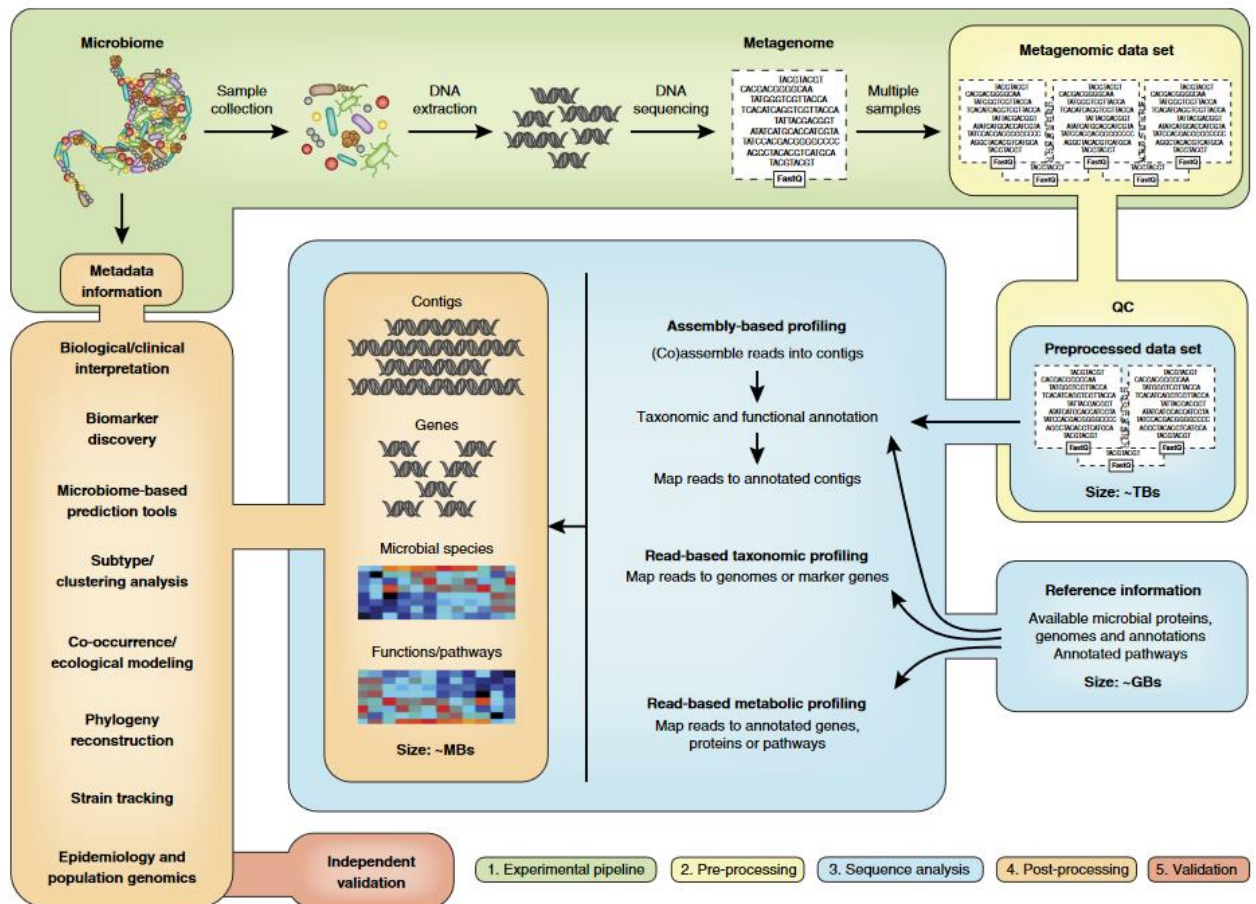


Figure A4: Summary of the metagenomics workflow. Based on Quince *et al.*, (2017).

2. Metagenomics data treatment

Anvi'o (an analysis and visualization platform for 'omics data) is an open-source, community-driven analysis and visualization platform for microbial 'omics. It brings together many aspects of today's cutting-edge strategies including genomics, metagenomics, metatranscriptomics, pangenomics, metapangenomics, phylogenomics, and microbial population genetics in an integrated and easy-to-use fashion through extensive interactive visualization capabilities.

Anvi'o workflow was used and adapted for the process of raw metagenomic datas obtained for the seasonal monitoring samples.

Annexe 5: Physical-chemical parameters measured in the mesocosms water. Temperature (°C), salinity (psu), pH, dissolved oxygen (dissolved O₂; mg.L⁻¹), and nitrate (NO₃⁻), nitrite (NO₂⁻), phosphate (PO₄²⁻), silicon (Si) and ammonium (NH₄⁺) concentrations were measured in the mesocosms' water at each sampling time during the climate change simulation. Four treatments were applied: C for control, A for acidification, W for warming and WA for acidification and warming. The letters t followed by a number indicates the sampling time and the letters R followed by a number the replicate

ample name	Treatment	Time	Replicate	Temperature (°C)	Salinity (psu)	pH	Dissolved O ₂ (mg.L ⁻¹)	NO ₃ ⁻ (μmol.L ⁻¹)	NO ₂ ⁻ (μmol.L ⁻¹)	PO ₄ ²⁻ (μmol.L ⁻¹)	Si (μmol.L ⁻¹)	NH ₄ ⁺ (μmol.L ⁻¹)
C.R1	C	t9	R1	20.7	59.6	7.581	0.8	4.31	1.29	73.84	436.17	90.84
C.R1	C	t16	R1	19.8	60.8	7.913	0.2	0.42	2.1	34.11	312.12	117.95
C.R1	C	t23	R1	21.5	61.6	8.055	0.1	0.1	0.11	33.89	326.89	116.41
C.R1	C	t30	R1	20.4	61.2	7.885	1.9	0	1.25	21.16	143.65	108.48
C.R1	C	t37	R1	20.2	59	7.824	0.7	2.22	0.11	12.42	110.61	129.93
C.R1	C	t44	R1	20.1	60	7.087	3.3	0.95	0.51	4.26	42.26	79.18
C.R1	C	t51	R1	20	61.8	7.904	2.8	0.39	0.13	6.91	97.94	95.74
C.R1	C	t58	R1	20.8	60.6	7.765	1.7	0.35	0.19	4.88	85.34	64.75
C.R3	C	t9	R3	20.8	59.3	7.889	0.2	0.49	0.28	47.11	456.1	97.18
C.R3	C	t16	R3	19.7	60.9	8.037	0.8	0.25	0.67	31.98	295.95	128.1
C.R3	C	t23	R3	21.6	62.3	8.047	0.2	0.09	0.11	17.89	140.73	131.32
C.R3	C	t30	R3	20.2	62.1	7.995	1.2	0.21	0.06	2.81	38.14	32.48
C.R3	C	t37	R3	19.9	60.6	7.985	1.3	0.25	0.06	3.04	47.12	2.81
C.R3	C	t44	R3	19.9	61.4	8.049	3.3	0.12	0.21	2.14	74.54	11.59
C.R3	C	t51	R3	20	61.9	7.988	2.6	0.22	0.05	1.69	61.55	1.69
C.R3	C	t58	R3	20.5	61.1	8.08	3.8	0.29	0.21	1.1	50.32	0.87
C.R4	C	t9	R4	20.4	60.9	8.101	0.2	0.33	0.3	22.15	318.89	113.92
C.R4	C	t16	R4	20.1	59.8	7.941	1.5	1.43	1.78	4.31	116.88	116.83
C.R4	C	t23	R4	21.4	61.4	7.909	0.8	0.02	0.14	9.75	232.52	111.33
C.R4	C	t30	R4	20.3	61.3	7.985	3.2	0.44	0.08	5.07	157.32	1.1
C.R4	C	t37	R4	19.7	59	7.961	4.1	0.72	0.17	8.05	154.41	0.11

C.R4	C	t44	R4	19.9	60.2	7.873	2.3	0.49	0.32	6.45	115.96	2.17
C.R4	C	t51	R4	19.7	61.9	7.848	3	0.22	0.08	4.62	152.4	0.89
C.R4	C	t58	R4	20.1	61.5	7.987	3.8	0.16	0.19	7.38	162.89	2.05
C.R5	C	t9	R5	20.8	60.4	7.989	0.3	0.47	0.42	48.75	478.29	95.53
C.R5	C	t16	R5	20	63.5	8.127	0.2	0.38	0.15	48.3	374.76	111.13
C.R5	C	t23	R5	21.4	64.8	8.137	0.9	0.16	0.12	41.56	197.86	112.26
C.R5	C	t30	R5	20.2	64.4	8.167	5.5	1.55	0.19	14.01	65.51	135.36
C.R5	C	t37	R5	19.9	59.4	8.045	3.9	0.51	0.12	7.29	40.74	111.27
C.R5	C	t44	R5	19.9	60.9	7.944	2.6	0.4	0.16	10.98	130.73	97.41
C.R5	C	t51	R5	20.1	61.2	8.015	3.8	0.81	0.34	5.1	97.01	15.4
C.R5	C	t58	R5	20.3	61.1	7.99	3.7	0.65	0.59	6.37	144.01	14.95
C.R6	C	t9	R6	20.7	58.4	7.82	0.8	0.73	1.05	15.36	187.15	123.88
C.R6	C	t16	R6	20.1	60.4	7.944	2	2.02	0.69	9.44	103.75	124.31
C.R6	C	t23	R6	21.3	61.9	7.91	1.4	0.43	0.13	11.86	151.8	131.32
C.R6	C	t30	R6	20.3	60.7	8.044	4.6	3.56	0.44	3.06	39.06	79.73
C.R6	C	t37	R6	19.8	59.2	7.959	3	0.87	0.12	2.05	44.68	44.56
C.R6	C	t44	R6	20.1	60.5	8.078	4.9	1.7	0.72	2.09	29.12	31.68
C.R6	C	t51	R6	19.9	61.7	8.054	3.3	0.96	0.25	3.07	51.44	24.65
C.R6	C	t58	R6	20.2	60.3	8.15	4.4	2.37	1.3	1.29	31.43	8.99
A.R1	A	t9	R1	19.9	61.8	8.063	0.1	0.54	0.17	42.26	459.77	92.01
A.R1	A	t16	R1	20.3	62.6	8.241	0.3	0.22	0.17	27.97	296.62	121.83
A.R1	A	t23	R1	20.6	63.1	8.142	2.2	5.2	1.06	15.72	156.52	132.46
A.R1	A	t30	R1	20.6	61.8	8.157	0.4	1.74	0.91	17.64	241.33	117.45
A.R1	A	t37	R1	19.9	60.4	7.72	0.4	0.81	1.18	4.16	127.32	125.96
A.R1	A	t44	R1	20.2	60.6	7.799	2.6	0	1.69	13.29	263.56	107.3
A.R1	A	t51	R1	20.1	61.9	7.753	2	0.13	0.05	10.31	211.7	98.77
A.R1	A	t58	R1	20.7	61.8	7.777	2.4	0.44	0.32	6.14	148.95	60.9
A.R3	A	t9	R3	19.7	60.6	7.97	8.5	0.45	0.49	20.91	373.91	116.97
A.R3	A	t16	R3	20.3	62.1	8.123	0.2	0.41	0.43	21.8	287.05	128.3
A.R3	A	t23	R3	20.7	63.5	8.12	0.5	0.33	0.15	18.2	226.56	131.03

A.R3	A	t30	R3	20	60.3	7.814	0.4	0.13	0.15	6.5	133.83	120.4
A.R3	A	t37	R3	19.8	59.4	7.764	1.4	0.58	0.57	1.71	52.08	50.9
A.R3	A	t44	R3	20.3	61.4	7.767	2.8	0.62	0.48	1.45	45.32	16.55
A.R3	A	t51	R3	19.9	60.7	7.76	2.7	0.25	0.11	1.71	44.9	4.94
A.R3	A	t58	R3	20.3	60.8	7.689	2.2	0.26	0.09	2.64	52.67	1.52
A.R4	A	t9	R4	19.6	59.9	8.047	0.5	0.99	1.6	30.46	208.19	107.87
A.R4	A	t16	R4	20.1	61.6	8.136	0.2	0.32	0.63	22.81	265.34	136.83
A.R4	A	t23	R4	20.3	63.2	7.895	2.3	1.67	0.78	12.56	113.81	122.08
A.R4	A	t30	R4	20.8	60.3	7.891	2.1	0.28	0.16	1.58	46.88	37.45
A.R4	A	t37	R4	19.7	60.5	7.881	2.8	0.85	0.67	0.14	16.49	6.25
A.R4	A	t44	R4	19.9	61.2	7.953	5.4	0.17	0.19	0.91	68.02	0.8
A.R4	A	t51	R4	20.3	61.5	7.727	2.6	0.33	0.21	2.52	77.86	1.22
A.R4	A	t58	R4	20	61.8	7.993	5	0.25	0.22	0.83	30.18	2.35
A.R5	A	t9	R5	19.9	61.6	7.866	1.6	0.62	0.35	40.54	370.04	100.11
A.R5	A	t16	R5	20.3	63	8.075	0.1	0	0.61	36.84	338.98	114.03
A.R5	A	t23	R5	20.6	64.5	8.148	1	0.72	0.56	26.94	197.34	119.36
A.R5	A	t30	R5	19.7	60.9	7.996	2.9	3.1	0.58	3.17	65.09	122.32
A.R5	A	t37	R5	19.6	60.1	7.907	3	1.16	1.13	1.59	41.38	102.78
A.R5	A	t44	R5	19.7	61.8	7.935	0.8	0.14	0.09	10.19	203.62	121.48
A.R5	A	t51	R5	19.8	61.9	7.675	1.5	0.39	0.37	8.15	126.75	93.01
A.R5	A	t58	R5	20.2	61.4	7.675	1.9	0.2	1.03	4.15	107.88	35.82
A.R6	A	t9	R6	19.6	61.3	8.046	0.1	0.87	0.46	38.01	424.42	108.01
A.R6	A	t16	R6	20.2	62.8	8.22	0.1	0.02	0.27	62.25	378.64	127.11
A.R6	A	t23	R6	20.6	66.1	8.253	1.4	2.34	0.47	45.79	340.4	115.87
A.R6	A	t30	R6	19.8	65.7	8.192	1.3	0	0.66	36.74	288.43	116.32
A.R6	A	t37	R6	19.5	65.3	7.852	2.3	0.16	0.43	22.88	207.35	126.49
A.R6	A	t44	R6	20.2	64.9	7.998	2.6	0.49	0.35	10.52	169.39	113.75
A.R6	A	t51	R6	20.2	63.3	7.839	3	1.12	1.4	3.37	100.05	24.65
A.R6	A	t58	R6	19.9	62.8	7.975	4.7	0.17	0.11	3.23	103.11	1.96
W.R1	W	t9	R1	19.9	61.2	8.105	0.3	0.51	0.24	38.58	333.12	104.08

W.R1	W	t16	R1	21.4	64.7	8.092	0.7	0.13	0.09	29.01	271.56	124.63
W.R1	W	t23	R1	23	70.6	7.963	0.8	1.86	0.15	24.47	192.28	124.02
W.R1	W	t30	R1	24.2	71.4	7.892	0.9	0.19	0.44	25.08	193.13	131.05
W.R1	W	t37	R1	23.5	75.6	8.002	1.1	0	0.54	27.35	265.27	123.43
W.R1	W	t44	R1	24	75.6	7.904	0.7	0	0.33	21.4	235.25	121.66
W.R1	W	t51	R1	23.8	67.7	7.956	2.1	0.12	0.36	12.14	160.68	100.98
W.R1	W	t58	R1	24.6	64.4	7.83	1.7	0.3	0.33	8.17	153.32	80.08
W.R3	W	t9	R3	20	61.7	7.603	0.7	0.42	1.36	47.67	422.13	95.87
W.R3	W	t16	R3	21.2	65.8	8.177	0.4	0	0.51	64.19	437.57	98.17
W.R3	W	t23	R3	23.1	71.6	8.124	0.1	1.59	0.2	43.02	293.97	116.58
W.R3	W	t30	R3	24	72.6	7.942	0.9	0.24	0.5	21.76	109.16	132.66
W.R3	W	t37	R3	23.8	80.6	8.044	1.2	1.47	0.49	13.18	127.05	110.4
W.R3	W	t44	R3	24	69.2	7.919	1.5	0	0.11	12.98	164.34	90.86
W.R3	W	t51	R3	23.6	63.6	8.048	3.9	0.52	0.33	10.38	174.11	36.92
W.R3	W	t58	R3	24.6	77.1	7.917	1.9	0.14	0.08	8.12	192.57	2.64
W.R4	W	t9	R4	20	63.5	8.156	0.1	0.43	0.33	68.32	464.36	89.01
W.R4	W	t16	R4	21.4	65.3	8.147	0.7	0.47	0.91	33.63	299.45	124.56
W.R4	W	t23	R4	23	68	8.115	0.8	1.55	0.17	24.32	230.99	131.86
W.R4	W	t30	R4	24.1	67.3	7.841	0.3	0.35	0.69	12.54	93.26	125.25
W.R4	W	t37	R4	23.5	75.2	7.891	2.1	1.73	0.59	12.3	121.74	115.37
W.R4	W	t44	R4	24.1	65	7.902	1	1.6	0.13	8.43	204.8	105.12
W.R4	W	t51	R4	23.8	65.2	8.11	6.1	0.72	1.29	2.93	70.41	30.36
W.R4	W	t58	R4	24.5	65.2	7.751	2.2	0.42	0.52	2.59	119.27	23.71
W.R5	W	t9	R5	19.8	60.4	7.951	1	3.09	2.79	6	77.71	82.42
W.R5	W	t16	R5	21.4	65.7	8.155	1.1	0.08	0.16	25.25	298.36	136.56
W.R5	W	t23	R5	23.2	70.6	8.049	0.6	1.63	0.19	33.47	249.77	123.39
W.R5	W	t30	R5	24.3	62	8.029	0.6	0.16	0.12	30.7	243.5	129.07
W.R5	W	t37	R5	23.8	82.2	7.987	1	0.77	0.2	29.03	267.35	128.91
W.R5	W	t44	R5	24.3	74	7.977	1.7	0.38	0.17	27.29	271.85	124.05
W.R5	W	t51	R5	23.9	74.2	7.981	2.4	0.28	0.32	16.65	217.61	99.47

W.R5	W	t58	R5	24.5	65.4	7.986	3.6	0.15	0.43	9.79	158.18	74.04
W.R6	W	t9	R6	20.1	61.3	8.184	0.1	0.43	0.71	43.04	408.88	96.89
W.R6	W	t16	R6	20.6	63.8	NA	NA	0.21	0.12	26.08	267.86	128.04
W.R6	W	t23	R6	23	66.7	8.061	0.6	0.23	0.12	21.13	150.12	131.44
W.R6	W	t30	R6	24.1	66.8	7.968	3.5	3.21	0.49	12.31	95.02	131.85
W.R6	W	t37	R6	23.6	69.6	8.002	0.9	0.87	0.12	11.72	190.65	131.04
W.R6	W	t44	R6	24.2	69.4	7.78	1.4	0.26	0.17	12.13	139.94	114.18
W.R6	W	t51	R6	23.7	68.8	7.902	4.4	0.25	0.46	8.13	122.96	94.12
W.R6	W	t58	R6	24.5	64.7	7.885	2.2	0.23	0.29	5.17	119.36	70.55
WA.R2	WA	t9	R2	20.9	62.2	7.959	0.7	2.26	2.71	9.79	140.17	110.88
WA.R2	WA	t16	R2	20.8	67.6	8.111	0.3	0.4	0.12	47.95	452.06	104.42
WA.R2	WA	t23	R2	23.9	83.2	8.111	0.1	0.13	0.22	46.3	346.57	106.65
WA.R2	WA	t30	R2	23.9	66.5	7.924	1.4	0.84	1.61	13.81	135.16	135.25
WA.R2	WA	t37	R2	23.4	61.2	7.789	0.7	0.45	0.51	2.4	75.35	100.57
WA.R2	WA	t44	R2	23.5	62.5	7.842	0.6	2.29	0.21	7.56	144.85	117.98
WA.R2	WA	t51	R2	23.5	63.1	7.785	0.7	0.2	0.04	8.15	172.24	102.53
WA.R2	WA	t58	R2	24.6	64.1	7.822	2.9	0.31	0.28	7.68	125.07	91.14
WA.R3	WA	t9	R3	21.1	61.3	7.947	0.4	0.32	0.08	12.09	277.05	120.95
WA.R3	WA	t16	R3	21	65.4	8.045	0.1	0.16	0.1	19.62	322.75	136.29
WA.R3	WA	t23	R3	23.1	68.8	7.924	0.6	0.17	0.31	13.97	177.08	126.83
WA.R3	WA	t30	R3	23.8	66.8	7.764	1.1	0.35	0.41	6.42	81.11	94.61
WA.R3	WA	t37	R3	23.3	69	7.946	0.9	0.14	0.11	11.74	213.06	125.8
WA.R3	WA	t44	R3	23.5	66	7.78	1.1	0.11	0.26	4.99	148.94	83.51
WA.R3	WA	t51	R3	23.7	68.3	7.896	1.1	0.27	0.18	11.67	238.31	117.47
WA.R3	WA	t58	R3	24.3	69.9	7.92	2.1	0.11	0.12	12	231	101.98
WA.R4	WA	t9	R4	21	61	8.129	0.3	0.91	0.19	24.34	361.92	118.61
WA.R4	WA	t16	R4	20.9	66.6	8.085	1	0.79	0.14	26.79	244.59	134.04
WA.R4	WA	t23	R4	24.1	71.4	8.034	0.6	0.21	0.13	34.86	201.99	120.02
WA.R4	WA	t30	R4	24.5	76.8	8.061	0.8	2.24	0.12	31.1	201.43	130.35
WA.R4	WA	t37	R4	23.6	65.5	7.943	1.9	0.7	0.21	10.9	119.13	115.48

WA.R4	WA	t44	R4	23.9	66.4	7.819	2.1	0.43	0.13	7.53	161.54	83.95
WA.R4	WA	t51	R4	23.6	69.3	8.028	3.7	3.07	0.29	11.82	172.58	82.87
WA.R4	WA	t58	R4	24.6	63.8	7.947	4.7	0.3	0.27	6.41	125.69	38.09
WA.R5	WA	t9	R5	21	62.1	8.019	0.7	1.12	0.38	44.66	363.08	89.68
WA.R5	WA	t16	R5	21.3	64.7	7.946	0.4	0.08	0.29	28.9	221.06	120.73
WA.R5	WA	t23	R5	23.1	NA	7.997	0.1	0.14	0.16	33.71	210.61	110.68
WA.R5	WA	t30	R5	24.2	69.8	7.832	0.8	0.39	0.16	22	170.61	126.73
WA.R5	WA	t37	R5	23.2	66.4	7.932	0.8	0.64	0.43	14.57	132.41	132.92
WA.R5	WA	t44	R5	23.5	64.2	7.705	1.2	1.91	0.19	6.97	88.95	111.66
WA.R5	WA	t51	R5	23.7	64.6	7.869	0.5	0.27	0.18	10.29	146.97	118.11
WA.R5	WA	t58	R5	24.2	62.6	7.948	3.9	0.72	0.45	2.99	64.09	49.8
WA.R6	WA	t9	R6	20.9	60.5	7.873	0.3	1.02	0.68	25.13	273.39	120.84
WA.R6	WA	t16	R6	21.2	65.2	8.038	0.1	0.2	0.2	31.53	288.94	128.31
WA.R6	WA	t23	R6	23.8	69.9	8.058	0.1	0.29	0.37	36.1	251.7	116.45
WA.R6	WA	t30	R6	24.4	66.4	7.865	0.1	0.16	0.09	15.39	103.28	135.38
WA.R6	WA	t37	R6	23.9	62.9	7.815	0.9	0.18	0.37	9.2	118.28	126.52
WA.R6	WA	t44	R6	24.2	65.5	7.725	0.1	0.09	0.16	12.11	188.69	122.67
WA.R6	WA	t51	R6	24.2	67.4	7.768	1.2	0.26	0.24	8.78	155.27	93.56
WA.R6	WA	t58	R6	24.7	65.1	7.912	4.6	0.47	0.48	3.59	78.29	15.98

Annexe 6: Regional fact sheet (Introduction) and regional fact sheet of Europe from the sixth assessment report of the Working Group I, “The Physical Science Basis” part, by the IPCC (2021).

Regional fact sheet - Introduction

Purpose

- Regional fact sheets are an outreach product that is fully traceable to the [IPCC Working Group I Sixth Assessment Report: \(AR6-WGI\)](#).
- The fact sheets constitute an entry point for regionalized information in the Chapters, the Technical Summary and the Interactive Atlas.
- The content is not exhaustive but represents most of the high level key messages assessed in the WGI Report region by region.
- As the scope of the IPCC Working Group I is to assess the physical science of climate change, the fact sheets are focused on the relevant regional climatic information.

Disclaimer

The regional fact sheets were built based on the Final Governmental Distribution of the Report which is the most updated version prior to the approval of the Summary For Policymakers. They are subject to revisions following the SPM approval, copy-editing, and layout.

Icons



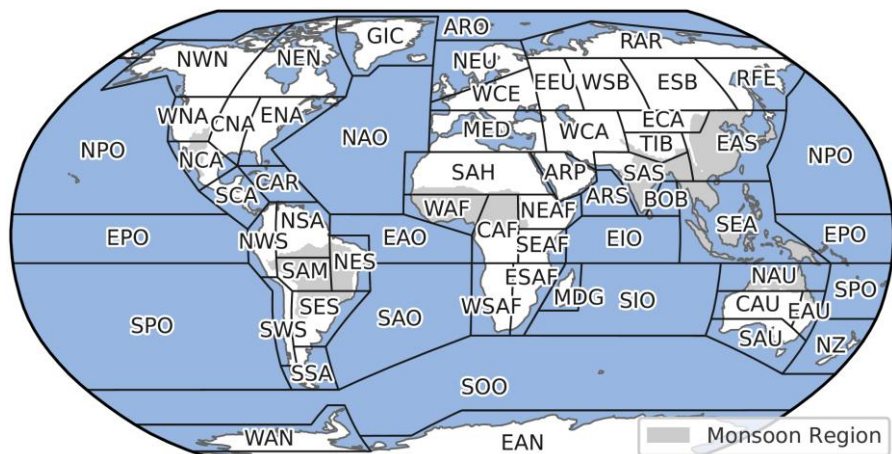
The blue font in the statements is used to highlight if the changes are **observed**, **attributed to climate change** or **projected**.

Attribution statements are provided when the studies are available in the scientific publications. Not being mentioned does not mean that the change is not attributable to climate change.

Regions

The fact sheets provide key statements for 11 regions that combine sub-sets of the AR6 reference regions

- Africa
- Asia
- Australasia
- Central and South America
- Europe
- Mountains
- North and Central America
- Ocean
- Polar regions
- Small Islands
- Urban areas



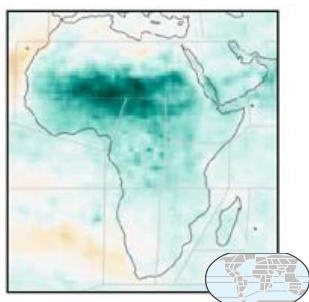
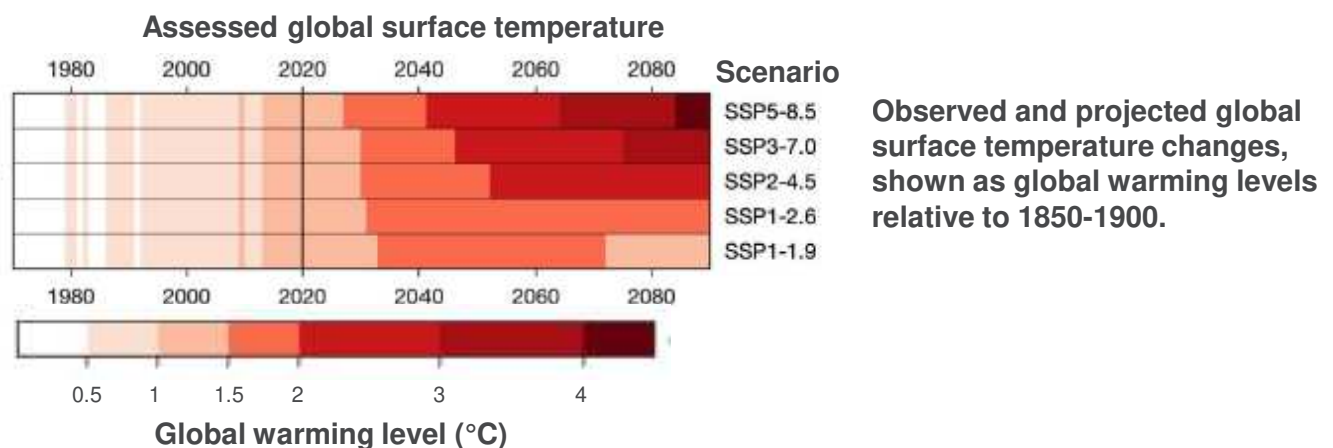
- Some subregions are duplicated to represent all the relevant areas for specific climate phenomena. For example, the Mediterranean subregion is included both in Africa and Europe fact sheets.
- For more information about the reference regions, see the description of the AR6 reference regions and the typological regions in the Interactive Atlas GitHub repository (<https://github.com/IPCC-WG1/Atlas/tree/devel/reference-regions>)

Definitions

- **Climatic impact-drivers (CIDs):** Climatic impact-drivers are physical climate system conditions (e.g., means, events, extremes) that affect an element of society or ecosystems. Depending on system tolerance, CIDs and their changes can be detrimental, beneficial, neutral or a mixture of each across interacting system elements and regions. See also Risk, Hazard and Impacts (Glossary).
- **Meteorological drought:** A period with an abnormal precipitation deficit (Glossary).
- **Agricultural and ecological drought:** Depending on the affected biome: a period with abnormal soil moisture deficit, which results from combined shortage of precipitation and excess evapotranspiration, and during the growing season impinges on crop production or ecosystem function in general. (Glossary).
- **Fire weather:** Weather conditions conducive to triggering and sustaining wildfires, usually based on a set of indicators and combinations of indicators including temperature, soil moisture, humidity, and wind. Fire weather does not include the presence or absence of fuel load. (Glossary).

Links between scenarios, global warming levels and time horizons

- **Scenarios:** Five illustrative scenarios that cover the range of possible future development of anthropogenic drivers of climate change found in the literature are used consistently across this report. They start in 2015, and include scenarios with high and very high greenhouse gas (GHG) emissions (SSP3-7.0 and SSP5-8.5), and intermediate GHG emissions (SSP2-4.5) and with low and very low GHG emissions (SSP1-2.6, SSP1-1.9). (TS.1.3.1).
- **Global warming levels:** Quantifying geographical response patterns at global warming levels, such as 1.5 or 2°C above the 1850-1900 period, is a useful approach to quantify changes in mean climate, extremes and climatic impact-drivers. Global Warming Levels are used in this Report, and across the Working Groups, as a dimension of integration independent of the timing when the warming is reached and of the emissions scenario that led to the warming (TS.1.3.2).











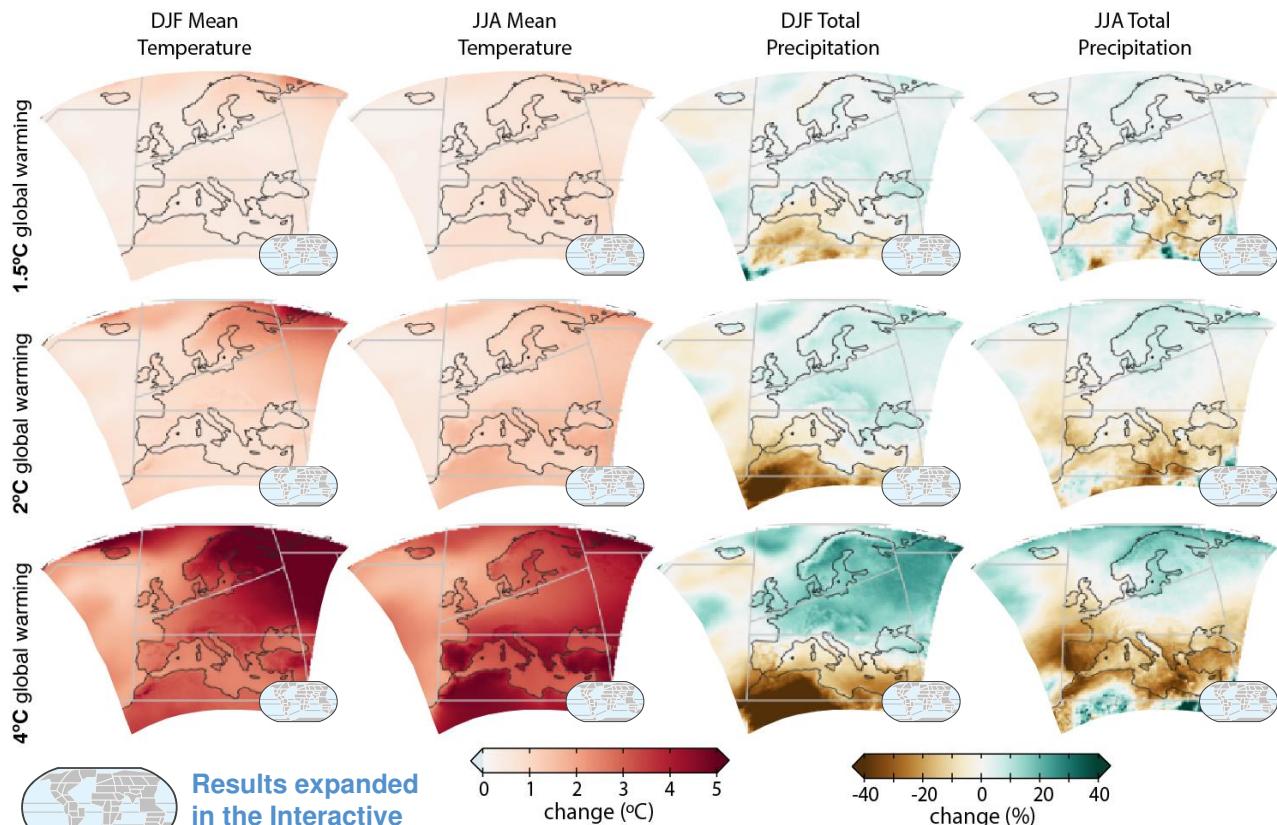
Most of the maps of the fact sheets are provided by the Interactive Atlas, a novel AR6 Working Group I tool that allows for a flexible spatial and temporal analysis of both data-driven climate change information and assessment findings in the report. **Link:** <https://interactive-atlas.ipcc.ch/>

The icon in the bottom right corner is a hyperlink that leads to the displayed map in the Interactive Atlas

Regional fact sheet - Europe

Common regional changes

-  Regardless of future levels of global warming, temperatures **will rise** in all European areas at a rate exceeding global mean temperature changes, **similar to past observations** (*high confidence*).
-  The frequency and intensity of hot extremes, including marine heatwaves, **have increased** in recent decades and **are projected** to keep increasing regardless of the greenhouse gas emissions scenario. Critical thresholds relevant for ecosystems and humans **are projected to be exceeded** for global warming of 2°C and higher (*high confidence*).
-  The frequency of cold spells and frost days **will decrease** under all the greenhouse gas emissions scenarios in this report and all time horizons, **similar to past observations**. (*high confidence*)
-  Despite strong internal variability, **observed** trends in European mean and extreme temperatures cannot be explained without accounting for anthropogenic factors. Before the 1980s, warming by greenhouse gases **was** partly offset by anthropogenic aerosol emissions. Reduced aerosol influence in the recent decades **has led to** an observable positive trend in shortwave radiation. (*high confidence*)
-  **Observations** have a seasonal and regional pattern consistent with **projected** increase of precipitation in winter in Northern Europe. A precipitation decrease **is projected** in summer in the Mediterranean extending to northward regions. Extreme precipitation and pluvial flooding **are projected** to increase at global warming levels exceeding 1.5°C in all regions except the Mediterranean. (*high confidence*)
-  Regardless of level of global warming, relative sea level **will rise** in all European areas except the Baltic Sea, at a rate close to or exceeding global mean sea level. Changes **are projected** to continue beyond 2100. Extreme sea level events **will become** more frequent and more intense, leading to more coastal flooding. Shorelines along sandy coasts **will retreat** throughout the 21st century (*high confidence*).
-  Strong declines in glaciers, permafrost, snow cover extent, and snow seasonal duration at high latitudes/altitudes **are observed** and **will continue** in a warming world (*high confidence*).
-  Multiple climatic impact-drivers **have already** changed concurrently over recent decades. The number of climatic impact-driver changes **is expected** to increase with increasing global warming (*high confidence*).



Projected changes in seasonal (Dec–Feb, DJF, and Jun–Aug, JJA) mean temperature and precipitation at 1.5°C, 2°C, and 4°C global warming relative to 1995–2014.

Based on EURO CORDEX (40 models) using the SSP5-8.5 scenario to compute the warming levels.

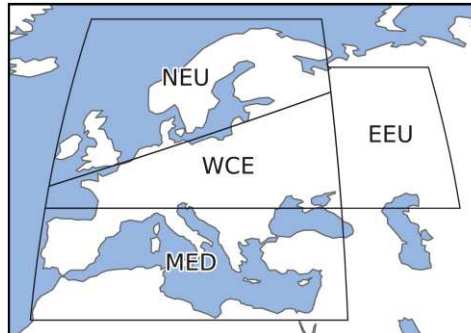
 **Results expanded in the Interactive Atlas (active links)**
interactive-atlas.ipcc.ch

Northern Europe (NEU)

- **Observed** increase in pluvial flooding **attributed** to human influence and **projected** to further increase at global warming of 1.5°C (*medium confidence*) and 2°C and above (*high confidence*).
- **Projected** decrease in river flood at global warming of 2°C and above (*medium confidence*).
- **Projected** increase in severe wind storms at global warming of 2°C and above (*medium confidence*).

Western & Central Europe (WCE)

- **Projected** increase in pluvial flooding at global warming of 1.5°C (*medium confidence*) and 2°C and above (*high confidence*).
- **Observed** increasing trend in river flooding and **projected** further increase at 2°C and above of global warming (*high confidence*).
- **Projected** increases in hydrological, agricultural and ecological droughts at mid-century warming levels of 2°C or above, regardless of the greenhouse gas emissions scenario (*medium confidence*).



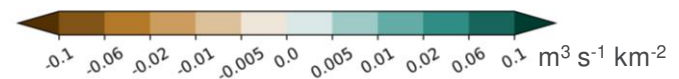
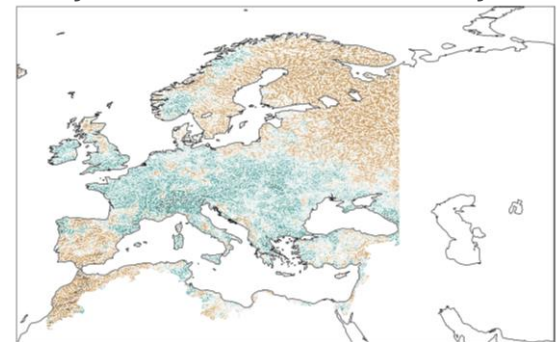
Eastern Europe (EEU)

- **Projected** increase in pluvial flooding at global warming of 1.5°C (*medium confidence*) and 2°C and above (*high confidence*).
- **Projected** decrease in river flood at global warming of 2°C and above (*medium confidence*).
- **Projected** increase in fire weather at global warming of 2°C and above (*medium confidence*).

Mediterranean (MED)

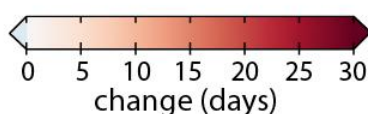
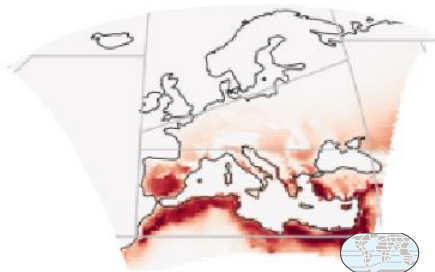
- **Observed** increase in hydrological and agricultural and ecological droughts (*medium confidence*), **projected** increase in aridity and fire weather conditions at global warming of 2°C and above (*high confidence*).
- **Projected** combination of climatic impact-driver changes (warming, temperature extremes, increase in droughts and aridity, precipitation decrease, increase in fire weather, mean and extreme sea levels, snow cover decrease, and wind speed decrease) by mid-century and at global warming of at least 2°C and above (*high confidence*).

Change in river discharge per unit catchment area corresponding to the return period of 100 years for the mid-21st century

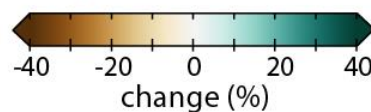
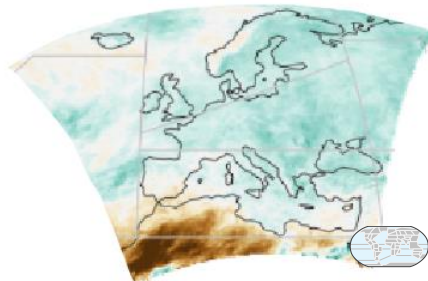


Projected changes for 2041–2060 relative to 1995–2014

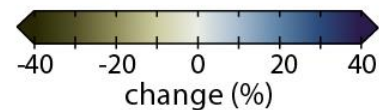
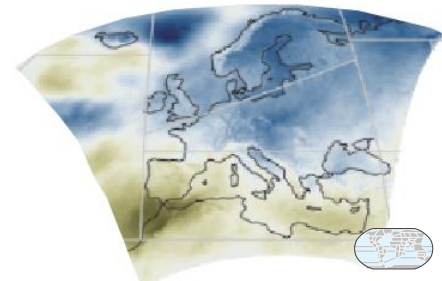
JJA Days with Daily Maximum Temperature above 35°C



DJF Maximum Annual 1-day precipitation (RX1 day)



Standardized Precipitation Index (SPI-6) drought indicator




Links for further details:

Common Changes: TS.4.3.1, TS.4.3.2.5, 11.3.4, 11.9, 12.4.5, Atlas.8.2, Atlas.8.4

Sub-regions: TS.4.3.2.5, 11.9, Tables 11.16–18, 12.4.5, Atlas.8.2, Atlas.8.4


Annexe 7: Impact of Climate Change on Phototrophic Communities Inhabiting Microbial Mats (iPoster), World Microbe Forum online conference (conférence internationale), virtual, 2021



Impact of Climate Change on Phototrophic Communities Inhabiting Microbial Mats

C. Mazière (1,2), M-A. Perdrau (2), M. Bodo (3), C. Cravo-Laureau (1), C. Hubas (3), C. Dupuy (2), R. Duran (1)

(1) UMR 5254 IPREM (Inst. des Sci. Analytiques et de Physico-chimie pour l'Environnement et les Matériaux), CNRS, Pau, France
 (2) UMR 7266 LIENSs (Littoral Environnement et Sociétés), CNRS, La Rochelle, France
 (3) UMR BOREA 8067 Muséum Natl. d'Histoire Naturelle, MNHN-IRD-CNRS-SU-UCN-UA, Concarneau, France



Context

Climate change

The Intergovernmental Panel on Climate Change (IPCC, 2014) predicts that marine systems will face many environmental pressures in 2100, in particular rising temperature and ocean acidification.

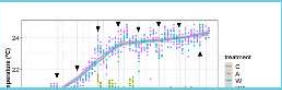
The most pessimistic scenario (RCP 8.5) for 2100 in Nouvelle-Aquitaine region was (Fig.1).

OPEN

The efficiency of the physicochemical changes

Water temperature

Increased surface water temperature of 4 °C in W and WA treatments reached (Fig.7)



OPEN

Acidification changes the pigments dynamics

Pigment identification and quantification


Lipophilic pigments were analyzed by high-performance liquid chromatography (Agilent 1260 Infinity HPLC). Identification and calibration of the HPLC peaks were performed with different pigment standards. Quantification was performed using standard calibration curves built with repeated injections of

OPEN

Comparison of photosynthetic yields

Photosynthetic parameters measurement

Chlorophyll fluorescence parameters were measured using a fluorometer (Monitoring Pen, MP 100-E, Photon Systems Instruments, Czech Republic) illuminated with a blue LED emitter (455 nm).




OPEN

Experimental design


Description of the sampled site

Microbial mats for mesocosms experiment were sampled in spring 2019 in salterns located in Ars-en-Ré (46°13'29.9"N 1°31'07.5"W, Ré Island, France) (Fig.2) on a non-exploited pond (Fig.3)



OPEN

Conclusion



	Control 20°C - pH = 8	Microcosm 20°C - pH = 7.6	Microcosm 24°C - pH = 8	Microcosm 24°C - pH = 7.6
Photosynthetic efficiency	+	+	+	+
Extracellular polymeric substances	+	+	+	+
Chlorophyll a	+	+	+	+

OPEN

Acidification impacts the proportion of EPS

Extracellular Polymeric Substances (EPS) characterization

Microbial mats EPS were extracted on two fractions (bound and colloidal) following Lavergne (2014) protocol.

The carbohydrates were dosed according to Dubois' colorimetric method (Dubois *et al.*, 1956) while the

OPEN

AUTHOR INFORMATION
ABSTRACT
REFERENCES
CONTACT AUTHOR

Annexe 8: Impact du changement climatique sur les communautés procaryotiques des tapis microbiens de l'île de Ré (Poster), Microbe 2021, 16^e Congrès National de la SFM (national conference), Nantes, France, 2021

Impact du changement climatique sur les communautés procaryotiques des tapis microbiens de l'île de Ré

Camille Mazière^{1,2} (camille.maziere@univ-pau.fr), Alice Baldy¹, Martine Bréret², Philippe Pineau², Emmanuel Dubillot², Cyril Noël³, Thomas Lacoue-Labarthe², Cédric Hubas⁴, Hélène Agogue², Cristiana Cravo-Laureau¹, Christine Cagnon¹, Robert Duran¹, Christine Dupuy²

¹ Université de Pau et des Pays de l'Adour, E2S UPPA, CNRS, IPREM, Pau, France ² UMR 7266 LIENSs (Littoral Environnement et Sociétés), CNRS, La Rochelle, France ³ IFREMER - PDG-IRSI-SeBIMER, Plouzané, France ⁴ UMR BOREA 8067 Muséum Natl. d'Histoire Naturelle, MNHN-IRD-CNRS-SU-UCN-UA, Concarneau, France

Tapis microbien

- Association microbienne complexe
- Développement à l'interface eau-sédiment
- Structure verticale stratifiée
- Différents métabolismes
- Micro-gradients
- Rôles-clés écosystèmes

↳ Bon modèle d'étude

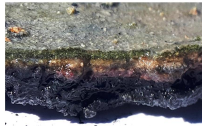


Fig. 1 : Photographie du tapis microbien prélevé pour l'étude

Changement climatique

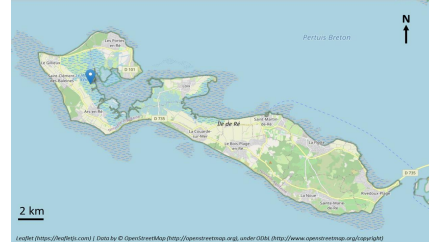


Fig. 2 : Site d'étude

Région Nouvelle-Aquitaine - Ile de Ré

- Réchauffement de l'eau de surface (+4°C) (GIEC, 2014)
- Acidification de 0,4 unité pH (GIEC, 2014)

Impact de l'acidification sur les communautés phototrophes (Mazière *et al.*, 2021).

Quel est l'impact du changement climatique sur les communautés procaryotiques de ces tapis microbiens ?

Matériel et méthodes

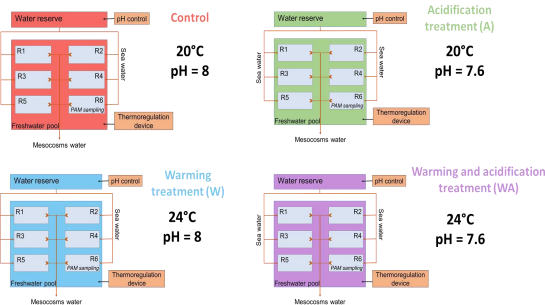


Fig. 3 : Représentation schématique des mésocosmes.

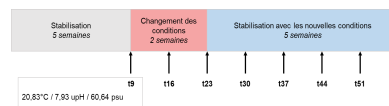


Fig. 4 : Échantillonnage durant l'expérience.

Etude en mésocosmes

- 4 traitements
- 8 échantillonnages sur 2 mois
- Extraction ADN : bactéries, archées
- Comptage cytométrie en flux
- Détermination production bactérienne

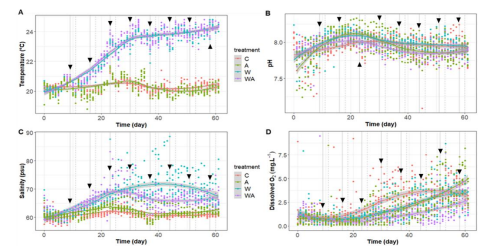


Fig. 5 : Suivi des paramètres physico-chimiques.

W et WA : augmentation de la température de 4°C → augmentation salinité
A et WA : acidification de 0,4 unité pH dans réserves d'eau → non visible dans les mésocosmes. Augmentation en oxygène dissous.

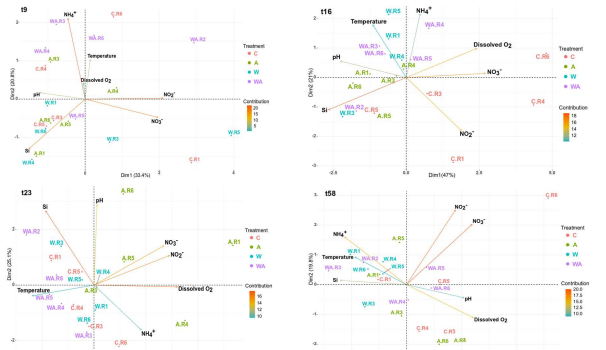


Fig. 6 : Analyse en composantes principales (PCA) de la structure des échantillons en fonction des paramètres physico-chimiques non corrélés.

▶ A t58, l'oxygène dissous et le pH sont corrélés positivement avec le traitement A, avec une plus forte contribution du premier paramètre. La température est corrélée positivement avec la traitement W.

W : augmentation de la production bactérienne corrélée à une augmentation de la population procaryotique.

A : augmentation de la population procaryotique sans augmentation de la production bactérienne → augmentation du nombre d'archées

WA : même profil que W

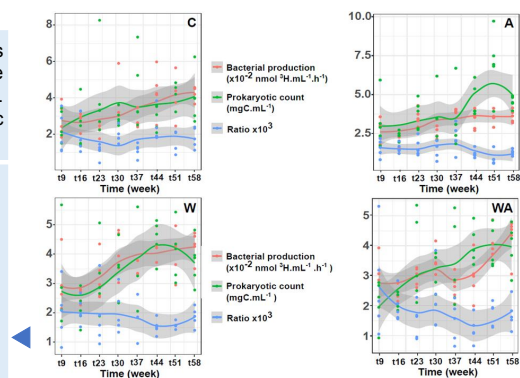


Fig. 8 : Evolution de la production bactérienne, du nombre de procaryotes et de leur ratio au cours de l'expérience.

Alpha-diversité : Diversités bactérienne et archéenne stables (richesse observée) mais structure bactérienne inférieure dans le traitement acidification après t23 (diversité de Shannon). Pas de différence de diversité de Shannon observée pour les archées.

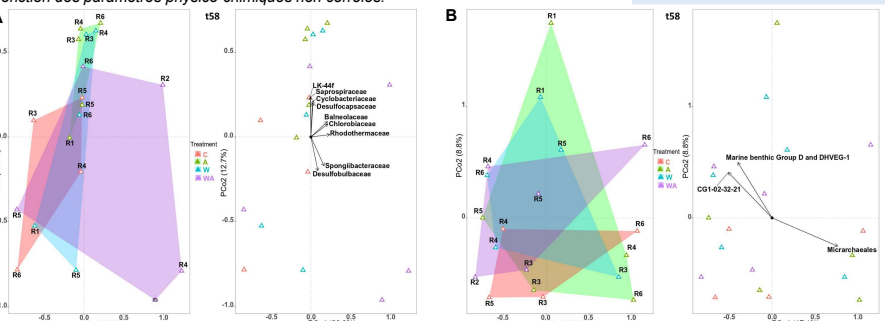


Fig. 7 : Analyse en coordonnées principales (PCoA) montrant la structure des bactéries (A) et des archées (B) selon les différents traitements.

La structure des communautés archéennes n'est pas différente entre les traitements, alors que celle des bactéries se distingue dans le traitement A par la présence de 4 bactéries plus dominantes que dans les autres traitements.

Conclusions

- Modifications des conditions bien atteintes.
- L'oxygène dissous contribue plus à la différenciation du traitement A que le pH.
- L'acidification n'affecte pas la production bactérienne contrairement au réchauffement de l'eau et des 2 combinés. L'acidification conduit à une augmentation de la population archéenne.
- Pas de modification de la structure de la communauté archéenne. L'acidification modifie la structure bactérienne du tapis microbien.

Remerciements

Nous remercions M. Jauffrais, le propriétaire des marais salants, ainsi que N. Lachaussée.

Références

IPCC, 2014. Climate Change 2014: Synthesis Report. Contribution of Working Groups I, II and III to the Fifth Assessment Report of the Intergovernmental Panel on Climate Change, in: The Core Writing Team, Pachauri, R.K., Meyer, L. (Eds.), Climate Change 2014: Synthesis Report. p. 169.

Mazière, C., Bodo, M., Pedrau, M.A., Cravo-Laureau, C., Duran, R., Dupuy, C., Hubas, C., 2021. Climate change influences chlorophylls and bacteriochlorophylls metabolism in hypersaline microbial mat. Sci. Total Environ. 802, 149787. <https://doi.org/10.1016/j.scitotenv.2021.149787>



Annexe 9: Abstract submitted for the « 10ème Colloque de l'Association Francophone d'Ecologie Microbienne » (national conference), virtual, 2021. Accepted for **oral presentation**.

Impact du changement climatique sur les tapis microbiens de l'île de Ré (France)

Camille Mazière^{1,2} (camille.maziere@univ-pau.fr), Alice Baldy¹, Cyril Noël³, Philippe Pineau², Emmanuel Dubillot², Christine Cagnon¹, Hélène Agogué², Cédric Hubas⁴, Thomas Lacoue-Labarthe², Cristiana Cravo-Laureau¹, Robert Duran¹, Christine Dupuy²

¹ Université de Pau et des Pays de l'Adour, E2S UPPA, CNRS, IPREM, Pau, France

² UMR 7266 LIENSs (Littoral Environnement et Sociétés), CNRS, La Rochelle, France

³ IFREMER - PDG-IRSI-SeBiMER, Plouzané, France

⁴ UMR BOREA 8067 Muséum Natl. d'Histoire Naturelle, MNHN-IRD-CNRS-SU-UCN-UA, Concarneau, France

Introduction et objectifs

Le groupe d'experts intergouvernemental sur l'évolution du climat (GIEC, 2014) prévoit que les systèmes marins seront parmi les zones les plus affectées par le changement climatique. Elles feront face à de nombreuses pressions environnementales, en particulier l'augmentation de la température et l'acidification des océans. Les sédiments marins jouent un rôle important dans la transformation de la matière organique et dans la dynamique des cycles biogéochimiques tels que le carbone, l'azote et l'oxygène. Dans les zones côtières, les tapis microbiens assurent ces rôles clefs. Les impacts du changement climatique sur les écosystèmes marins sont beaucoup étudiés au niveau mondial mais très peu au niveau local. Ils sont notamment méconnus en région Nouvelle-Aquitaine. Il est primordial de connaître les modifications, structurales et fonctionnelles, et la dynamique des communautés microbiennes en réponse au changement climatique. Notre étude vise à définir l'impact de du réchauffement et de l'acidification du milieu marin sur les tapis microbiens de l'île de Ré.

Matériel et méthodes

Des tapis microbiens prélevés dans des marais salants non exploités de l'île de Ré ont été placés dans des mésocosmes en laboratoire. Une augmentation de la température de l'eau et une diminution de son pH ont été simulés durant 8 semaines d'après les prévisions RCP8.5 pour 2100 du GIEC (2014). Un suivi quotidien des paramètres physico-chimiques et des

prélèvements hebdomadaires du tapis ont été réalisés afin de suivre sa dynamique fonctionnelle et de caractériser la modification de sa diversité.

Résultats, discussion et conclusion

Malgré son acidification, un maintien du pH de l'eau des mésocosmes est observé. Une augmentation de la température est bien réalisée. Des premiers résultats ont montré que l'acidification impactait la concentration de pigments inconnus, vraisemblablement de la bactériochlorophylle *c*, qui augmente alors que la concentration en chlorophylle *a* diminue. De plus, les substances extracellulaires polymériques sucrées liées augmentent, jouant certainement un rôle de protection. Le traitement acidification affecte donc la communauté phototrophe microbienne. Cela pourrait potentiellement impacter d'autres communautés au sein du tapis microbien et donc son fonctionnement entier.

Annexe 10: Les Marais, entre Terre et Mer (Poster), Fête de la Science 2020 (local conference), La Rochelle, France, 2020

Annexe 11: Biogeochemical interactions between iron and nutrient cycling in a saline inland lake (Poster), Goldschmidt 2021 (international conference), virtual, 2021

This poster was the result of a collaboration between the MESMIC project and me to perform vertical microprofiles during its sampling campaign.

Les Marais, entre Terre et Mer

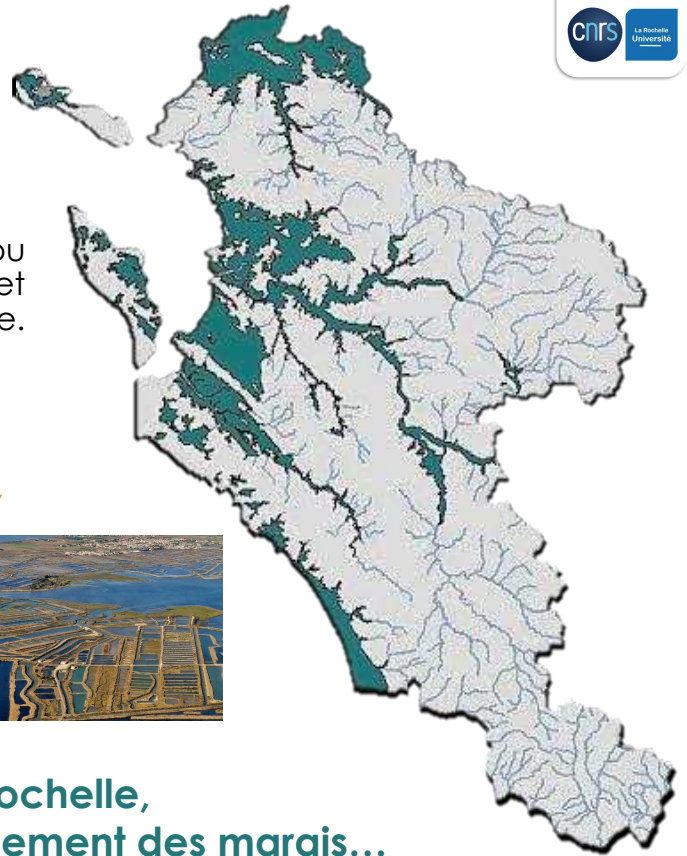
Camille Mazière^{1,2} et Raphaël Moncelon^{1,3}

¹ LIENSs (Littoral Environnement et Sociétés) UMR CNRS 7266, Université de La Rochelle, LA ROCHELLE
² IPREM (Institut des Sciences Analytiques et de Physico-chimie pour l'Environnement et les Matériaux) UMR CNRS 5254, Université de Pau et des Pays de l'Adour (UPPA/E2S), PAU
³ LPG-BIAF (Laboratoire de Planétologie et Géodynamique, étude des Bio-Indicateurs Actuels et Fossiles), UMR CNRS 6112, Université d'Angers, ANGERS

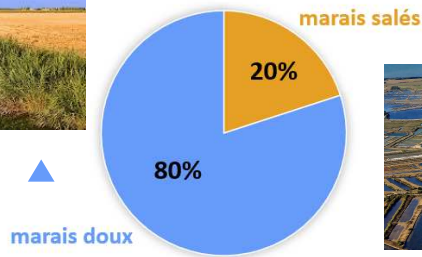


Les marais ...

Zones humides terrestres, périodiquement ou continuellement inondées par une eau stagnante et peu profonde, d'origine naturelle ou anthropique.



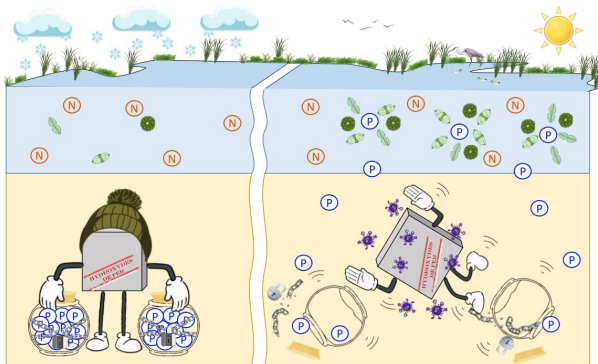
Répartition des différents types de marais en Charente Maritime



Des travaux de recherche menés à La Rochelle, pour comprendre et prédire le fonctionnement des marais...

Avec la thèse de Raphaël Moncelon « Structure et fonctionnement des marais de la Charente-Maritime : vers un développement d'un indicateur de fonctionnement trophique et son application à la gestion des zones humides. »

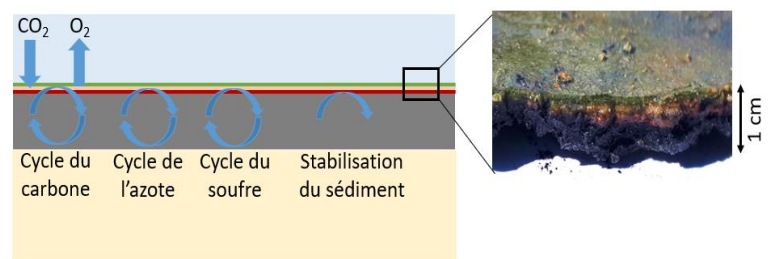
Image de présentation à la MT180 2020.



Dans le cas des marais doux, la croissance du phytoplancton dépend de la libération de nutriments par le sédiment lors du processus de minéralisation de la matière organique.

Avec la thèse de Camille Mazière, « Exploration et exploitation des tapis microbiens en région Nouvelle-Aquitaine. »

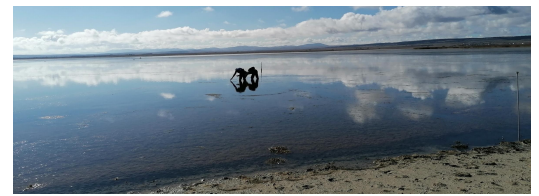
Les marais salants abritent des structures microbiennes au niveau de la surface du sédiment : les tapis microbiens. Ces derniers jouent un rôle important dans les cycles biogéochimiques essentiels au fonctionnement de l'écosystème.



Biogeochemical interactions between iron and nutrient cycling in a saline inland lake

R. Margalef-Marti^{1*}, M. Sebilo^{1,2}, S. Bendaha¹, A. Thibault De Chanvalon¹, I. Gonzalez-Alvarez¹, C. Mazière^{1,3}, M. Guibert¹, E. Tessier¹, B. Lauga¹ and D. Amouroux¹

¹ Université de Pau et des Pays de l'Adour, E2S UPPA, CNRS, IPREM, Pau, France; ² Sorbonne Université, CNRS, IEES, Paris, France; ³ La Rochelle Université, CNRS, LIENSs, La Rochelle, France; *rosanna.margalef-marti@univ-pau.fr



REDOX REACTIONS INVOLVING Fe, S AND N

In aquatic ecosystems Fe can be linked to S and N biogeochemical cycles through biotic and abiotic redox reactions that can take place simultaneously (Fig. 1). These processes will depend on several environmental parameters such as salinity.

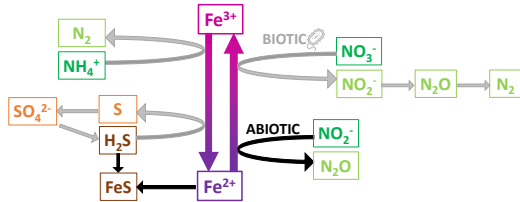


Fig. 1. Simplified scheme of S and N cycling processes involving Fe reduction and oxidation

OBJECTIVES

This study aims to determine the impact of Fe redox reactions on S and N cycling processes in a saline lake. To reach the goal, surface water, porewater and sediment samples will be characterized chemically and isotopically.

GALLOCANTA LAKE SAMPLING

Gallocanta lake (GL) is located in NE Spain, in a semi-arid climate region. It is endorheic, alkaline and saline. Its average water depth is ca. 50-70 cm but it can dry depending on evaporation, rainfall and groundwater table. Migrating crane are present in GL from October to March. Two sampling campaigns have been performed in GL to study Fe and nutrient cycling and check seasonal variations (November 2020 and June 2021). Sediment and surface water samples were obtained from three points (Fig. 2, Table 1). Here we report preliminary results for the characterization of porewater (PW) obtained from sediment (Fig. 3).

Table 1. Sampling campaigns.

November 2020	June 2021
Point A + B	Point A + B + C
3 sediment core (13 cm) / point	1 sediment core (25 cm) / point
Surface water EC: A = 17, B = 20 mS/cm	Surface water EC: A = 17, B = 16, C = 42 mS/cm



Fig. 3. Sediment core sample processing

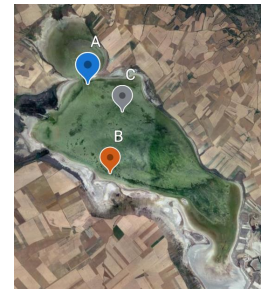


Fig. 2. Map of the three sampling points in GL, NE Spain (40°58'00"N 1°29'50"E)

Fe, S AND N CYCLING IN POREWATER OF GALLOCANTA LAKE

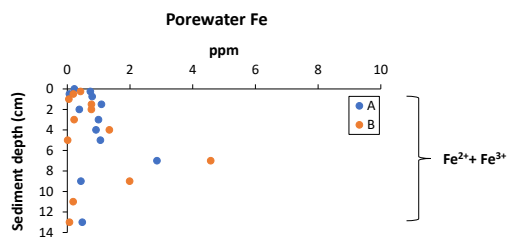


Fig. 4. Dissolved Fe in PW of GL (sites A and B, average 3 cores, November 2020)

- Fe in PW reached up to 5 ppm at 7 cm depth.
- No difference was observed between sites A and B.
- In **June 2021**, ferrozine analysis proved the presence of dissolved Fe²⁺ (up to 3 ppm).

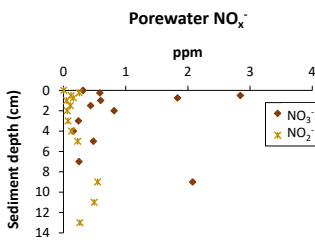


Fig. 6. Dissolved NO_x⁻ in PW of GL (site B, average 3 cores, November 2020)

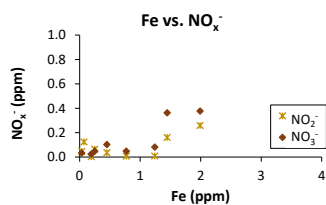


Fig. 7. Relationship between NO_x⁻ and Fe in PW of GL (site B, November 2020)

- NO₃⁻ showed higher concentration than NO₂⁻ in November 2020. Both compounds showed a negligible concentration in **June 2021** (increased NO_x⁻ reduction in spring).
- Similar Fe and NO₃⁻/NO₂⁻ evolution suggest the occurrence of biotic denitrification and/or chemodenitrification.

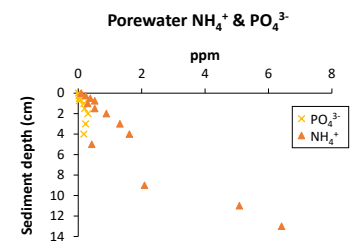


Fig. 8. Dissolved NH₄⁺ and PO₄³⁻ in PW of GL (site B, average 3 cores, November 2020)

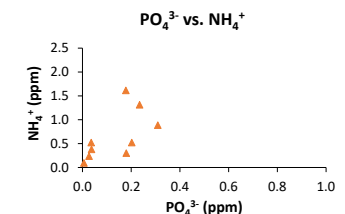


Fig. 9. Relationship between NH₄⁺ and PO₄³⁻ in PW of GL (site B, November 2020)

- The strong increase of NH₄⁺ concentration with depth and the lack of correlation between NH₄⁺ and PO₄³⁻ seems to indicate additional reactions to organic matter mineralization such as DNRA.

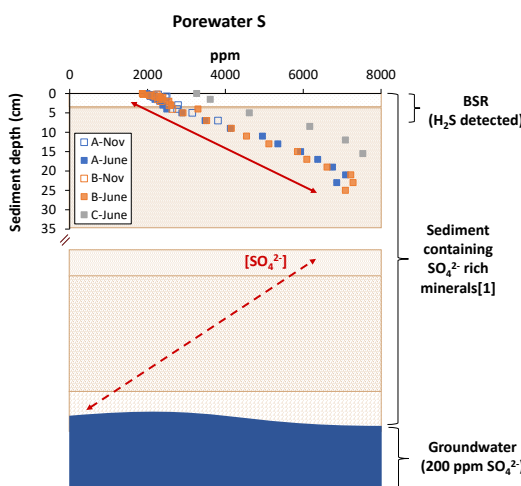


Fig. 5. Dissolved S (SO₄²⁻) in PW of GL (sites A, B and C, November 2020 and June 2021)

- High SO₄²⁻ content in PW of GL is likely due to minerals dissolution.
- Higher SO₄²⁻ content was observed in site C compared to A and B.
- H₂S was detected in the top 5 cm of sediment (microprofile), suggesting that SO₄²⁻ might decrease due to bacterial reduction (BSR).
- H₂S could be oxidized by Fe(III) reduction.

CONCLUSIONS

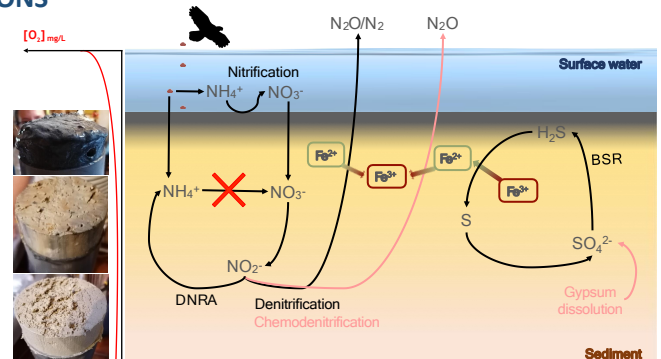


Fig. 10. Interactions between Fe, S and N cycles in GL

REFERENCES

[1] Comin et al., 1990. Hydrobiologia 197: 51-66.

ACKNOWLEDGEMENTS

This study has been financed by E2S (Université de Pau et Pays de l'Adour, Pau, France) through the MeSMic project.

Fe, S and N biogeochemical cycles are active in porewater of GL. Some specific processes have been hypothesized according to concentration data (Fig. 10). Further metagenomic and isotopic ($\delta^{34}\text{S}$ and $\delta^{15}\text{N}$) characterisation of the samples will allow to verify the occurrence of these reactions.

Annexe 12: Exploration de tapis, article written by Martin Galilée for “l’Actualité Nouvelle-Aquitaine“, n°126, 2019

Exploration de tapis

Par Martin Galilée

Camille Mazière étudie les tapis microbiens en Nouvelle-Aquitaine. Ce sont des assemblages de micro-organismes stratifiés verticalement, des lasagnes de microbiologie, contenant bactéries, virus, archées et méiofaune – animaux de 42 µm à 1 mm. On les trouve dans certains écosystèmes comme les côtes, les sources hydrothermales ou les zones polaires. Ceux de Camille Mazière proviennent des marais salants de l’île de Ré, choisie pour ses beaux tapis microbiens observés en 2017, une fierté locale trop peu valorisée. Leur épaisseur varie de quelques millimètres à quelques centimètres. «Sur le terrain, c’est vraiment comme un tapis. On peut le soulever, le prendre dans la main et ça fait une plaque», témoigne la chercheuse. Dans ses échantillons se succèdent quatre couches de couleur : vert, blanc, rouge puis noir. «Les micro-organismes sont en quelque sorte rangés selon les gradients biogéochimiques qui se forment. Le tapis microbien joue un rôle environnemental important dans les cycles du carbone, de l’oxygène, de l’azote et du soufre. L’oxygène est présent au-dessus et absent en-dessous, et inversement pour le soufre». Camille Mazière conduit son doctorat en co-direction entre deux laboratoires CNRS, avec Robert Duran de l’Institut des sciences analytiques et de physico-chimie pour l’environnement et les matériaux de Pau (Iprem, UMR 5254) et Christine Dupuy du laboratoire Littoral, environnement et sociétés de La Rochelle (Lienss, UMRi 7266). Elle est financée à parts égales par la région Nouvelle-Aquitaine et l’université de Pau et des pays de l’Adour. «À Pau se trouve toute l’expertise sur les micro-organismes et la biologie moléculaire. À La Rochelle, la spécialité est le milieu marin et la méiofaune. J’y trouve le savoir-faire nécessaire pour réaliser mes expériences, construire mes mésocosmes», explique-t-elle.

Compter les brouteurs

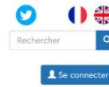
Ses mésocosmes, intermédiaires entre macrocosmes et microcosmes, sont des boîtes de plastique, petits mondes isolés dans lesquels elle cultive le tapis microbien. «La plus grosse partie de mon travail de thèse consiste à simuler les changements climatiques les plus pessimistes prévus par le GIEC pour 2100 et à observer si les tapis microbiens vont s'adapter ou disparaître.» Elle acidifie donc l'eau de 0,4 unités pH et augmente sa température de 4°C pour deux mois d'observations comparées, carottages, mesures du pH et sondages de l'oxygène et du sulfure à toutes les profondeurs. Les procaryotes sont comptés au cytomètre en flux, la méiofaune étudiée à la loupe binoculaire, et l'ADN extrait des échantillons pour déterminer la variété du vivant : bactéries (dont les cyanobactéries), virus, archées, microfaune (dont les petits brouteurs), microflore (euglènes), méiofaune, etc. En 1971, Terry Pratchett publiait *Le Peuple du tapis*. Camille Mazière saura bientôt s'il survivra jusqu'à la fin du siècle.



Annexe 13: Influence du changement climatique sur les tapis microbiens des marais salants / Influence of climate change on salt ponds microbial mats, front-page article of BOREA website, 2021.



Laboratoire de biologie des organismes et des écosystèmes aquatiques



Accueil Laboratoire- Recherche- Annuaire- Programmes Publications- Actualités- Archives-

Actualités / Articles à la Une / Influence du changement climatique sur les tapis microbiens des marais salants / influence of climate change on salt ponds microbial mats

Articles à la une 15 oct 2021

Influence du changement climatique sur les tapis microbiens des marais salants / Influence of climate change on salt ponds microbial mats



Mazière Camille, Maëlle Bodo, Marie Anais Perdrau, Cristiana Cravo-Laureau, Robert Duran, Christine Dupuy, et Cédric Hubas. 2022. « **Climate Change Influences Chlorophylls And Bacteriochlorophylls Metabolism in Hypersaline Microbial Mat** ». *Science Of The Total Environment*, 802: 149787. <https://doi.org/10.1016/j.scitotenv.2021.149787>

Cette étude visait à déterminer l'effet du changement climatique sur les communautés phototrophes des tapis microbiens des marais salants. Parmi les paramètres testés (diminution du pH, augmentation de la température et combinaison des deux), la diminution du pH dans l'eau de mer a induit une modification de la composition pigmentaire des tapis microbiens qui se traduit par une baisse significative de la quantité relative de chlorophylle a et une augmentation des bactériochlorophylles. La baisse de pH favoriserait donc la photosynthèse anoxygénique (C-à-d, qui ne produit pas d'oxygène), dans ces écosystèmes. Pour autant, ces communautés microbiennes sont naturellement confrontées à des conditions environnementales (pH, lumière, température, salinité, etc.) qui fluctuent, parfois à l'échelle d'une journée, bien au-delà de ce que prévoit le GIEC pour 2100. C'est probablement la raison pour laquelle les capacités photosynthétiques des microorganismes oxygéniques n'ont pas été altérées au cours de cette expérience. Cette étude représente une étape préliminaire dans la compréhension de l'impact à long terme du changement climatique sur les communautés microbiennes des marais salants.

Contact BOREA : Cédric Hubas, maître de conférences MNHN, cedric.hubas@mnhn.fr

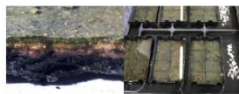
Légendes photos :

Illustration de couverture : Photographie de la zone d'étude : un marais salant de l'île de Ré où se développent des tapis microbiens / Photography of the studied area: a salt marsh in Ré Island where microbial mats are observed. © Alice Baldy et Camille Mazière

Photo 1 : Photographie d'un tapis microbien prélevé dans un marais salant de l'île de Ré / Photography of a microbial mat sampled in a salt marsh of Ré Island. © Alice Baldy et Camille Mazière

Photo 2 : Photographie des mésocosmes où a été simulé le changement climatique (acidification et réchauffement de l'eau) sur les tapis microbiens (sans le système lumineux) / Photography of the mesocosms' system where climate change (ocean acidification and warming) was simulated on microbial mats, without the light system. © Cristiana Cravo-Laureau et Camille Mazière

Article en ligne



Cédric HUBAS

MNHN Station marine
Concarneau

Maître de Conférences

SOMAGUA

Muséum National
d'Histoire Naturelle
(MNHN)

Publié le 15 oct 2021

Mis à jour le 15 oct 2021

Tweets de @LABR_BOREA

Laboratoire BOREA a retweeté

Benoît Wiese @BenoitWiese

Merci Marc! Moi je de @Piracetam pour ce séminaire être plus @LABR_BOREA « La production d'organes qui tire plus de 30 milliards de tonnes de carbone par an »

[boreamaths.fr/actualite/MC3...](https://www.boreamaths.fr/actualite/MC3...)

23h

Laboratoire BOREA a retweeté

Maria & Liborace @Maria_Liborace

Étude sur la contamination des saumons par le chlorocène dans le Pacifique de la région

Ce polluant provient de la terre pose une difficulté supplémentaire au développement des filices de stockage et de rétention des algues

• @difo @MDEBESOT

8 oct 2021

Laboratoire BOREA @LABR_BOREA

Offre stage M2 Evaluation de l'effet du séquençage du génome sur l'évolution des traits de sélectivité et de sélectivité intracellulaire vs sélectivité dans deux autres organismes - programme de recherche FFRABE (diplo-licence)

@Uneorale_Care

@LABR_BOREA @Maranda

[boreamaths.fr/actualite/MC3...](https://www.boreamaths.fr/actualite/MC3...)

8 oct 2021

8 oct 2021

8 oct 2021

8 oct 2021

8 oct 2021

8 oct 2021

8 oct 2021

8 oct 2021

8 oct 2021

8 oct 2021

8 oct 2021

8 oct 2021

8 oct 2021

8 oct 2021

8 oct 2021

8 oct 2021

8 oct 2021

8 oct 2021

8 oct 2021

8 oct 2021

8 oct 2021

8 oct 2021

8 oct 2021

8 oct 2021

8 oct 2021

8 oct 2021

8 oct 2021

8 oct 2021

8 oct 2021

8 oct 2021

8 oct 2021

8 oct 2021

8 oct 2021

8 oct 2021

8 oct 2021

8 oct 2021

8 oct 2021

8 oct 2021

8 oct 2021

8 oct 2021

8 oct 2021

Laboratoire de Biologie des Organismes et des Ecosystèmes Aquatiques
MNHN, CNRS 8067, SU, IRD 207, UCN, UA
43 rue Cuvier, CP 26
75231 Paris Cedex 05, France
Téléphone secrétariat : 01.40.79.80.83
0034.2020 - Laboratoire BOREA
SE CONNECTER - PLAN DU SITE - MENTIONS LEGALES



Headline paper 15 Oct 2021

Influence du changement climatique sur les tapis microbiens des marais salants / Influence of climate change on salt ponds microbial mats



Mazière Camille, Maëlle Bodo, Marie Anaïs Perdrau, Cristiana Cravo-Laureau, Robert Duran, Christine Dupuy, et Cédric Hubas. 2022. « **Climate Change Influences Chlorophylls And Bacteriochlorophylls Metabolism In Hypersaline Microbial Mat** ». *Science Of The Total Environment*, 802: 149787. <https://doi.org/10.1016/j.scitotenv.2021.149787>

This study aimed to determine the effect of climate change on the phototrophic communities of salters microbial mats. Among the parameters tested (decrease in pH, increase in temperature and a combination of both), the decrease in pH in seawater induced a modification of the pigment composition of the microbial mats, which resulted in a significant decrease in the relative quantity of chlorophyll a and an increase in bacteriochlorophylls. The drop in pH would therefore favor anoxygenic photosynthesis (i.e., which does not produce oxygen) in these ecosystems. However, these microbial communities are naturally confronted with environmental conditions (pH, light, temperature, salinity, etc.) that fluctuate, sometimes on a daily basis, well beyond IPCC predictions for 2100. This probably explains why the photosynthetic capacities of oxygenic microorganisms were not altered during this experiment. This study represents a preliminary step in understanding the long-term impact of climate change on salt ponds microbial communities.

BOREA contact: Cédric Hubas, assistant professor MNHN, cedric.hubas@mnhn.fr

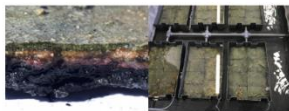
Photo titles :

Main ill.: Photographie de la zone d'étude : un marais salant de l'île de Ré où se développent des tapis microbiens / Photography of the studied area: a salt marsh in Ré Island where microbial mats are observed. © Alice Baldy et Camille Mazière

Photo 1 : Photographie d'un tapis microbien prélevés dans un marais salant de l'île de Ré / Photography of a microbial mat sampled in a salt marsh of Ré Island. © Alice Baldy et Camille Mazière

Photo 2 : Photographie des mésocosmes où a été simulé le changement climatique (acidification et réchauffement de l'eau) sur les tapis microbiens (sans le système lumineux) / Photography of the mesocosms' system where climate change (ocean acidification and warming) was simulated on microbial mats, without the light system. © Cristiana Cravo-Laureau et Camille Mazière

[Link article](#)



Cédric HUBAS
 MNHN Paris

Assistant professor
 SOMAQUA
 The French National
 Museum of Natural History
 (MNHN)

Published on 15 Oct 2021
 Updated on 15 Oct 2021

Tweets de @UMR_BOREA

Laboratoire BOREA a retweeté
 Benoît Mirou @BenoitMirou

Merci Moriz! Merci de @Pinelcra pour ce séminaire intéressant @UMR_BOREA : « Le pyrénoïde: un organelle qui fixe plus de 30 milliards de tonnes de carbone par an » borea.mnhn.fr/fr/actualite/C3...

14 oct 2021

Laboratoire BOREA a retweeté

Mers & littoraux @Mers_Littoraux
 Etude sur la contamination des sargasses par le chloroforme dans le Parc marin de Martinique

Ce polluant provenant de la terre pose une difficulté supplémentaire au développement des filières de stockage et de valorisation des algues

infos: bit.ly/3818j97n



8 oct 2021

Laboratoire BOREA @UMR_BOREA

Offre stage M2: Evaluation de l'état physiologique du fibreuse #Fibromon serratus on secteurs intertidal vs subtidal dans deux sites normands - programme de recherche FEAMP @goudbouq @Université_Coan @UMR_BOREA #Normandie borea.mnhn.fr/fr/actualite/C3...



Intégrer Voir sur Twitter

The Intergovernmental Panel on Climate Change (IPCC, 2014) predicts that marine ecosystems will face many environmental pressures by 2100, in particular ocean acidification and warming. In coastal areas, microbial mats play key roles in the transformation of organic matter and the dynamics of biogeochemical cycles. The impacts of climate change on marine ecosystems have been widely studied at the global level but very little at the local level. They are particularly poorly understood in the Nouvelle-Aquitaine region (France). It is essential to understand the structural and functional modifications and dynamics of microbial communities in response to climate change. This thesis aims to define the impact of ocean warming and acidification on the microbial mats of Ré Island. First, a study of this microbial structure was performed *in situ*, in several types of salt marshes and according to the seasons, allowing to select the most suitable area to collect microbial mat and the season of sampling. The selected microbial mats were then maintained in mesocosms at laboratory. An increase in water temperature and a decrease in water pH were simulated for 8 weeks according to the most pessimistic predictions (RCP8.5) of the IPCC (2014) for 2100. Daily monitoring of physical-chemical parameters and weekly sampling of the microbial mat were performed to follow the functional dynamics and characterise the diversity changes. Acidification impacted the diversity and functioning of the microbial mats, particularly on the phototrophic communities. It has contributed to a decrease in prokaryotic diversity and an increase in some archaea that parasitise other archaea. The warming of the water had rather an effect on eukaryotic communities, with a change in *Chlorophyceae* and *Diatomea* abundance. The combination of these two conditions had less impact than the conditions alone suggesting a mitigating effect between them. However, in their current natural environment, these microbial mats already face temperatures higher or equal to those simulated, which is not the case for the pH reaching a final value of 7.6. Thus, these microorganisms are certainly already adapted and resilient to the simulated temperature, explaining little impact observed with this parameter, whereas acidification affects were more visible.

Keywords: microbial mats, salterns, climate change, ocean acidification, ocean warming.

Le groupe d'experts intergouvernemental sur l'évolution du climat (GIEC, 2014) prévoit que les écosystèmes marins feront face à de nombreuses pressions environnementales d'ici 2100, en particulier l'acidification et le réchauffement océaniques. Dans les zones côtières, les tapis microbiens jouent des rôles clés dans la transformation de la matière organique et la dynamique des cycles biogéochimiques. Les impacts du changement climatique sur les écosystèmes marins ont été très largement étudiés au niveau mondial mais très peu au niveau local. Ils sont particulièrement méconnus en région Nouvelle-Aquitaine (France). Il est essentiel de comprendre les modifications et les dynamiques structurales et fonctionnelles des communautés microbiennes en réponse au changement climatique. Cette thèse a pour but de définir l'impact du réchauffement et de l'acidification de l'océan sur les tapis microbiens de l'île de Ré. Dans un premier temps, une étude de cette structure microbienne a été réalisée *in situ*, dans plusieurs types de marais salants et en fonction des saisons. Cela a permis de choisir la zone de provenance du tapis microbien et la saison de prélèvement les plus adéquates. Ensuite, les tapis microbiens choisis ont été échantillonnés et placés dans des mésocosmes en laboratoire. Une augmentation de la température et une diminution du pH de l'eau ont été simulés durant 8 semaines selon les prédictions les plus pessimistes (RCP8.5) du GIEC (2014) pour 2100. Un suivi journalier des paramètres physico-chimiques et un échantillonnage hebdomadaire du tapis microbien ont été effectués afin de suivre les dynamiques fonctionnelles et de caractériser la modification de sa diversité. L'acidification a impacté la diversité et le fonctionnement des tapis microbiens, notamment des communautés phototrophes. Il a notamment contribué à la diminution de la diversité procaryotique et à l'augmentation de certaines archées parasites d'autres archées. Le réchauffement de l'eau a plutôt affecté les communautés eucaryotes, avec une modification de l'abondance de *Chlorophyceae* et des *Diatomea*. La combinaison de ces deux conditions a eu moins d'impact que les conditions seules suggérant un effet atténuant entre elles. Cependant, dans leur environnement naturel actuel, ces tapis microbiens font déjà face à des températures supérieures ou égales à celles simulées, ce qui n'est pas le cas concernant le pH atteignant une valeur finale de 7,6. Ainsi, ces microorganismes sont certainement déjà adaptés et résilients face à la température simulée, expliquant pourquoi ce paramètre a peu d'impact, alors que l'acidification les affecte plus.

Mots-clés : tapis microbien, marais salants, changement climatique, acidification océanique, réchauffement océanique.

ECOLE DOCTORALE :
Collège Sciences et Technologies pour l'Energie et l'Environnement (STEE)

INSTITUT DES SCIENCES ANALYTIQUES ET DE PHYSICO-CHIMIE POUR L'ENVIRONNEMENT ET
LES MATERIAUX (IPREM) AND LITTORAL, ENVIRONNEMENT ET SOCIETES (LIENSs)